UCL

New insights into pain mechanisms through the study of genes associated with monogenic pain disorders

A thesis submitted for the degree of Doctor of Philosophy
to University College London

Ayako Matsuyama

Wolfson Institute for Biomedical Research
University College London
2017

DECLARATION

I, Ayako Matsuyama, confirm that the work presented in this thesis is my own. I confirm that where information has been derived from other sources, this has been indicated in the thesis.

ABSTRACT

Pain is an intrinsic mechanism that promotes our survival by helping us to avoid injuries. However, chronic pain remains a significant clinical burden and is poorly treated. The development of new analgesic drugs may significantly improve quality of life for chronic pain patients. This thesis investigates the mechanisms of pain sensation and also suggests some novel analgesic drug targets by using molecular, genetic, and transgenic approaches.

Firstly, a novel function of sodium channel $Na_v1.7$ is explored. Microarray data showed that gene expression profiles are dramatically altered in dorsal root ganglia from $Na_v1.7$ null mice. These changes were confirmed by real-time qRT-PCR. Altered expression of preproenkephalin (*Penk*) and carcinoembryonic antigen-related cell adhesion molecule 10 (*Ceacam10*) may contribute to the pain insensitive phenotype seen in $Na_v1.7$ nulls. The gene expression changes were further explored using *in vitro* cell based assays, showing a potential role of sodium ions in controlling transcription of *Penk*.

Secondly, we study a family with six members affected with a pain insensitive phenotype characterized by multiple painless bone fractures and frequent painless lesions caused by burning stimuli. A novel point mutation in *ZFHX2*, encoding a putative transcription factor expressed in small diameter sensory neurons, was identified. By analysing *Zfhx2* knockout and BAC transgenic mice bearing the orthologous mutation, we confirm that ZFHX2 is crucial for normal pain perception. We study how the mutation disrupts ZFHX2 function, resulting in altered downstream expression of pain-related genes.

Thirdly, a patient with small fibre neuropathy and erythromelalgia-like symptoms was genetically analysed. Using exome sequencing and detailed bioinformatics analyses, I have shortlisted three missense mutations in the genes *CWC22*, *TMEM8B* and *ATL3* that are potentially pathogenic.

By studying genes mutated in families with rare inherited pain disorders this thesis broadens our understanding of pain sensation and highlights new routes to develop better analgesic drugs.

CONTENTS

LIST OF FIGURES

LISTS OF TABLES

ABBREVIATIONS

Atl1	Atlastin GTPase 1
Atl3	Atlastin GTPase 3
CCI	Chronic constriction injury
Ceacam10	Carcinoembryonic antigen-related cell adhesion molecule 10
CFA	Complete Freund's adjuvant
CIP	Congenital insensitivity to pain
CNS	Central nervous system
Cre	Cyclization recombinase protein
Ct	Cycle threshold
Cwc22	CWC22 spliceosome associated protein
DNA	Deoxyribonucleic acid
dNTPs	Deoxyribonucleotide triphosphate
DRG	Dorsal root ganglia
EM	Erythromelalgia
FEP	Familial episodic pain syndrome
IASP	International Association for the Study of Pain
IEM	Inherited primary erythromelalgia
KO	Knockout
mRNA	Messenger RNA
NGF	Nerve growth factor
PAG	Periaqueductal grey
PCR	Polymerase chain reaction
Penk	Preproenkephalin
PEPD	Paroxysmal extreme pain disorder
PNS	Peripheral Nervous system
PPN	Painful peripheral neuropathy
pre-mRNA	Precursor messenger RNA
qPCR	Quantitative real time PCR
SFN	Small fibre neuropathy
SNI	Spared nerve injury
SNL	Spinal nerve ligation
SNT	Sciatic nerve transection
Th	Tyrosine hydroxylase

Tmem173	Transmembrane protein 173
Tmem8b	Transmembrane protein 8B
VGCC	Voltage-gated calcium channel
VGSC	Voltage-gated sodium channel
WT	Wildtype
Zfhx2	Zinc finger homeobox 2

FUNDING

I would like to thank the following for funding the projects.

I would also like to thank Honjo International Scholarship Foundation for supporting my finance during the study.

PUBLICATION

Habib, A.M.*, **Matsuyama, A**.*, Okorokov, A.L.*, Santana-Varela, S.*, Bras. J.T.*, Aloisi, A.M.*, Emery, E.C. *, Bogdanov, Y.D., Follenfant, M, Gossage, S.J., Gras, M., Humphrey. J., Kolesnikov, A., Le Cann, K., Li, S., Minett, M.S., Pereira, V., Ponsolles, C., Sikandar, S., Torres, J.M., Yamaoka, K., Zhao, J., Komine, Y., Yamamori, T., Maniatis, N., Panov, K.I., Houlden, H., Ramirez, J.D., Bennett, D.L.H., Marsili, L., Bachiocco, V., Wood, J.N., Cox, J.J. 2017. A novel human pain insensitivity disorder caused by a point mutation in *ZFHX2*. *Brain*, awx326

Kanellopoulos, A. H.*, **Matsuyama, A**.* 2016. Voltage-gated sodium channels and pain-related disorders. *Clinical Science*, 130 (24), 2257-2265

Minett, M. S.*, Pereira, V.*, Sikandar, S., **Matsuyama, A.**, Lolignier, S., Kanellopoulos, A. H., Mancini, F., Iannetti, G. D., Bogdanov, Y. D., Santana-Varela, S., Millet, Q., Baskozos, G., Macallister, R., Cox, J. J., Zhao, J. & Wood, J. N. 2015. Endogenous opioids contribute to insensitivity to pain in humans and mice lacking sodium channel Nav1.7. *Nat Commun,* 6, 8967-8967

* ; co-first author

ACKNOWLEDGEMENTS

First and foremost, I would like to thank Professor John Wood for giving me this precious opportunity to undertake a Ph.D. in his lab where I have learnt so much under his guidance. I truly appreciate his unwavering support, and respect his ideas, thoughts, and enthusiasm for science.

I would like to express my gratitude to Dr. Jing Zhao for his patience, thoughtful advice, and dedication to proofreading my thesis- thank you very much for guiding me throughout my studies. I would also like to show great appreciation to Dr. James Cox for his generous support, and for the wonderful advice he has given me on my thesis- I am grateful to him for giving me an opportunity to work with him on these projects.

Thank you to all members of the Molecular Nociception Group (past and present) and the people who have kindly helped these projects, for being so warm and considerate. You all made my study wonderful and special! I enjoyed working with you all - Abdella, Alex, Alice, Ana, Anna, Donald, Ed, Jack, Jenny, Kenji, Larissa, Liam, Mike, Queeni, Ran, Roman, Sam, Skip, Shengnan, Stephane, Sunny, Toru, Vanessa and Yury. In particular, massive thanks to Dr. Andrei Okorokov for his passionate guidance on molecular works. Many thanks to Jane for always helping me with my English and also for proofreading my thesis and her general advice. I would also like to thank Sonia for her great help with behaviour tests. Special thanks to all members in the 'fun office' and lunch members for giving me many happy moments and encouragement- I will never forget this valuable time!

I would like to extend my sincere thanks to Honjo International Scholarship Foundation for their generous support towards my Ph.D. study. I could not have started the study and obtained this amazing opportunity without their help. I would also like to express my gratitude to Professor Kenichi Hatanaka at University of Tokyo for his help towards my studentship award.

Thank you to all my former colleagues at Konica Minolta Inc. for sending me off with encouragement and seeing me even after I left the company- your success and active roles always cheer me up. Special thanks to Mr. Takeshi Yamamoto for his kind support throughout my stay in the UK. I'd like to say thank you to all my school and university friends in Japan- I'm always happy to see you and talk about what you have achieved, which motivates me and makes me feel positive! Thank you to all the friends I have met in London- you made my London life fabulous! I will certainly remember our incredible time together.

I would like to show my huge appreciation to Vlad for his enormous help with my English and for providing so many interesting thoughts on the studies. Thank you for your kind support and always believing I could do it throughout my Ph.D.

Finally, I would like to thank and send my love to my family. Thank you to my father for his generous understanding, my mother for always being on my side and encouraging me, and my sister and her husband for being cheerful and always listening to me. And finally, I would like to send my appreciation to my grandaunt, who passed away in 2015- without her kind support I would not have decided to come to the UK to do a Ph.D. where I have had such a splendid experience. I wish I could have shown her that I have now achieved it.

1 INTRODUCTION

1.1 INTRODUCTION

Pain perception is a crucial mechanism for survival that enables us to avoid injury. The International Association for the Study of Pain (IASP) defines pain as "an unpleasant sensory and emotional experience associated with actual or potential tissue damage, or described in terms of such damage". In mammals, the pathways responsible for pain operate at multiple levels of both the peripheral and central nervous systems and under both voluntary and involuntary control. Pain is a highly complex biological phenomenon which can promote recovery from an injured state. Pain, however, may remain even after recovery. Such chronic pain can significantly reduce quality of life, which is one of the major clinical issues for a number of patients. For example, 19% of people in European countries suffer from moderate to severe pain (Breivik et al., 2006) and an estimated 10 million people in Britain suffer from chronic pain almost daily (British Pain Society 2014). With an aging population this problem may become even more serious, especially in developed countries. The importance of increasing the quality of life by reducing unpleasant chronic pain may therefore become increasingly important. In the past few decades, some pain mechanisms have been revealed that are helping in the development of new analgesic drugs. This is important as currently available analgesics still do not relieve pain for all chronic pain patients. This thesis describes new potential routes to develop analgesic drugs from the study of genes that are mutated in patients with rare inherited pain disorders.

1.1.1 The nervous system and pain

I. The nervous system

The nervous system is divided into two main parts: the central nervous system (CNS) is composed of the brain and spinal cord and the peripheral nervous system (PNS) contains all neurons outside of the CNS and includes both motor and sensory components. The sensory component of the PNS consists of afferent neurons and conveys information to the CNS; the motor component combines somatic (involved in voluntary functions) and autonomic (involved in automatic functions) which consist of efferent neurons. Autonomic neurons are furthermore subdivided into sympathetic and parasympathetic nervous systems responsible for 'fight or flight' functioning and maintenance of normal 'at rest' functions, respectively.

II. Sensory neurons and pain

The primary afferent neurons of the PNS all have their cell bodies in dorsal root or trigeminal ganglia; they are pseudo-unipolar neurons projecting from these cell bodies to the periphery and to the dorsal horn of the spinal cord. Based on diameter, myelination and the corresponding conduction velocity, peripheral nerve axons were first classified by Erlanger and Gasser into three groups (A–C) and later by Lloyd into 4 types (I–IV) (Manzano et al., 2008). The differences in conduction velocity give rise to separate roles of conveying information. The sense of touch is conveyed by large diameter, myelinated and fast conducting Aβ (Type II) fibres (>35μm diameter, 10-30m/s) from cutaneous mechanoreceptors. Slower/thinner myelinated Aδ (Type III) fibres (25-35μm diameter, 1.2-10m/s) and the smallest unmyelinated C (TypeIV) fibres (<25μm diameter, <1.5m/s) are classically considered as 'nociceptors'. Aδ fibres conduct temperature information from cold thermoceptors, pressure from free nerve endings and pain from nociceptors of the neospinothalamic tract ("sharp pain"). C fibres provide warmth sense and pain from nociceptors (noxious chemicals) of the paleospinothalamic tract ("aching, throbbing or burning pain") (Almeida et al., 2004).

Primary afferent neurons can be also classified by specific molecular markers they express. Large-diameter DRG neurons convey low-threshold mechanoreception from the skin and express Ret and/or TrkB. TrkC is expressed in large proprioceptive neurons that sense limb movement and position. Noxious stimuli is primarily detected by small- and medium-diameter neurons, many of which express TrkA, Met and/or Ret (Lallemend and Ernfors, 2012) (Figure 1-4). Recently, single cell RNA transcriptome analysis have further helped to categorise sensory neurons based on gene expression (Usoskin et al., 2015). According to this study, primary sensory neurons can be classified into four main clusters; the first one is called the NF cluster, expressing neurofilament heavy chain (Nefh) and parvalbumin (Pvalb). This cluster was previously known to be correlated with myelinated DRG neurons. The second category is the PEP cluster and express substance P (Tac1), TRKA (Ntrk1) and calcitonin gene-related peptide (CGRP, also known as Calca), previously associated with peptidergic nociceptors. The third, the NP cluster, shows expression of Mrgprd and P2rx3. This cluster was previously described as nonpeptidergic nociceptors. The fourth category can be defined as the TH cluster, showing distinct expression of tyrosine hydroxylase (Th), and was previously described as a distinct subclass of unmyelinated neurons. The Ernfors group further subcategorised these clusters into 11 distinct subpopulations using several molecular markers (Figure 1-1b).

This RNA-seq study by Ernfors group enables us to understand subpopulation of elements in sensory neurons along with previous studies. Several important genes in pain

pathways are expressed in certain subpopulations of sensory neurons (Table 1-1). For example, *Trpa1*, which has been linked to noxious mechanical and chemical stimuli (see 1.1.2 I), is preferentially expressed in NP and TH clusters which are categorised as unmyelinated neurons. *Trpv1*, which has been connected to noxious heat sensitivity (see 1.1.2 I), is expressed in NP and PEP clusters. Of particular interest in this thesis are voltage-gated sodium channels. Among the genes encoding voltage-gated sodium channels alpha subunit, *Scn9a*, *Scn10a* and *Scn11a* have been linked to human heritable pain disorders (1.1.5V). These three channels are present in nociceptive neurons (Dib-Hajj et al., 2010). It has been previously reported that $Na_v1.7$ encorded by *Scn9a* is expressed in both large (>30 μm) and small diameter (<25 μm) DRG neurons (Black et al., 1996, Ho and O'Leary, 2011). $Na_v1.8$ encoded by *Scn10a* is predominantly expressed in small diameter unmyelinated nociceptive sensory neurons (Akopian et al., 1996). The expression of $Na_v1.8$ was thought to be exclusively confined to small and medium diameter nociceptive subsets of sensory neurons of the dorsal root ganglia (Akopian et al., 1996, Benn et al., 2001). However a recent study has suggested that 75% of dorsal root ganglion cells express $Na_v1.8$ with 90% of these expressing nociceptive markers and the presence of $Na_v1.8$ in around 40% of myelinated A fibres (Shields et al., 2012). $Na_v1.9$ is preferentially expressed in nociceptive dorsal root ganglia, exclusively in small neurons (Dib-Hajj et al., 2002, Dib-Hajj et al., 1998, Dib-Hajj et al., 2010). The RNA-seq study by Ernfors group supported these evidences of the expression patterns in DRG neurons (Figure 1-1, Table 1-1). The expression of five VGSCs including $Na_v1.7$, $Na_v1.8$ and $Na_v1.9$ in DRG neurons by immunofluorescence is shown in (Figure 1-2). Subpopulations of sensory neurons and expression patterns can be functionally essential to understand sensory roles and development of new pharmaceutical agents to treat pain.

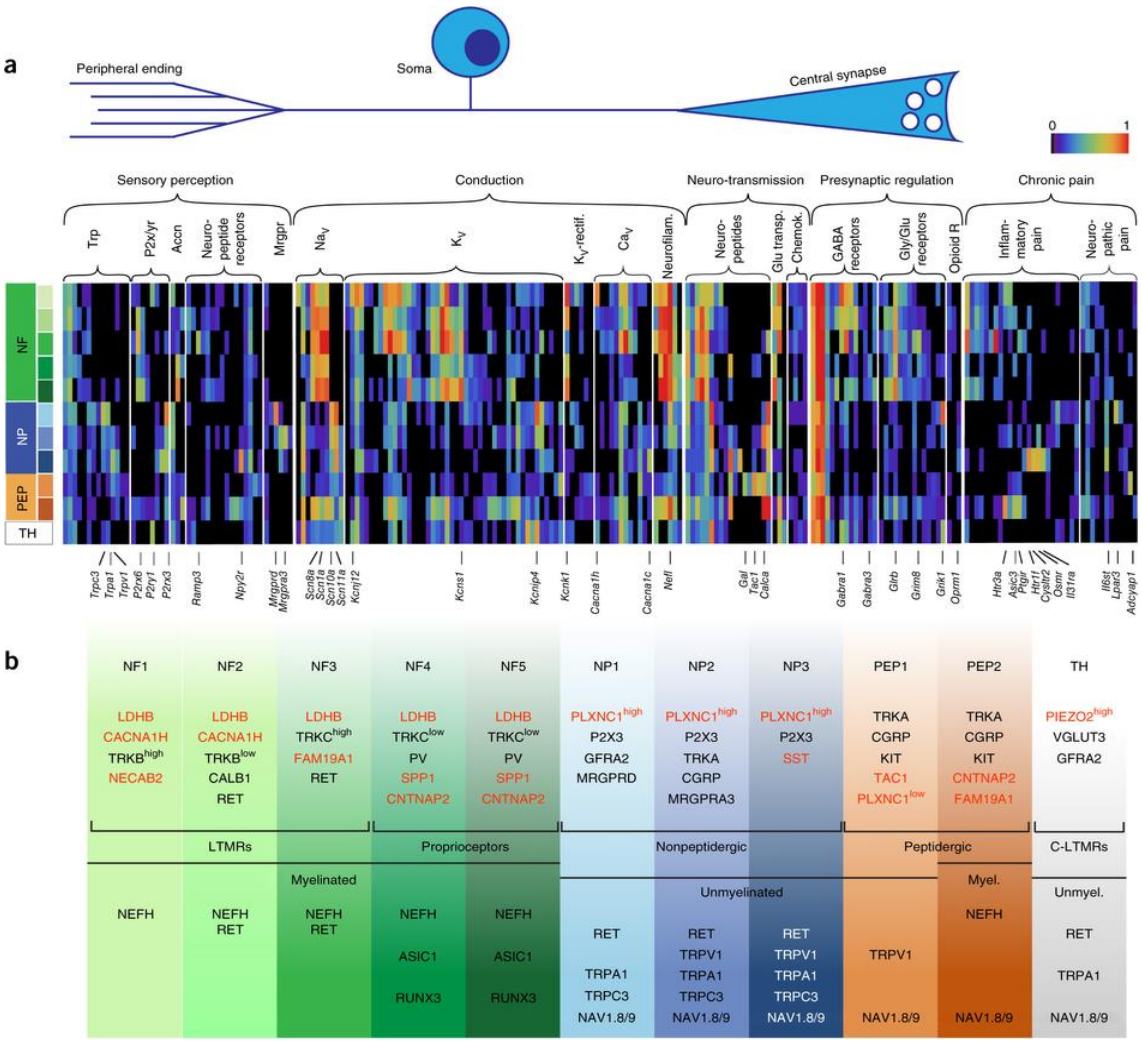

Figure 1-1. Heat map of expression patterns in distinct neuronal populations as classified by the Ernfors group. NF cluster, expressing neurofilament heavy chain (Nefh) and parvalbumin (Pvalb), was previously known to be correlated with myelinated DRG neurons. PEP cluster, expressing substance P (Tac1), TRKA (Ntrk1) and CGRP, was previously associated with peptidergic nociceptors. NP cluster, showing expression of Mrgprd and P2rx3, was previously described as nonpeptidergic nociceptors. TH cluster, showing distinct expression of Th, and was previously described as a distinct subclass of unmyelinated neurons. (a) Heat map of expression (fraction of positive cells) of the various operational components of sensory neurons in different classes of neurons. Neuronal identity is reflected by the unique combination of activation properties encoded by the specificity of transducer ion channels at peripheral terminals and presence of voltage-gated ion channels which are involved in conduction. This eventually results in release of neurotransmitters including glutamate, neuropeptides and other signaling molecules in the spinal cord. Trp, transient receptor potential cation channels; P2x/yr, purinergic receptor P2X or P2Y; Accn, amiloride-sensitive cation channels; K_V-rectif., open rectifier potassium channels (Kcnk), neurofilam., neurofilaments; Glu transp., glutamate transporters; chemok., chemokines; Opioid R., opioid receptors. (b) Proposed new sensory neuron classification based on unbiased full RNA transcriptome analyses. Gene products on top are suggested markers for identification of subtypes (red, new markers; black, selected previously used markers). Gene products at bottom are examples of a distribution of gene products. For example, $Na_V1.8$ and 1.9 are expressed in NP, PEP and TH cluster. LTMR, low-threshold mechanoreceptors; Myel., myelinated; Unmyel., unmyelinated. (Usoskin et al., 2015).

Table 1-1. Distinct expression patters of voltage-gated sodium channel alpha subunits and some TRP channels in mouse DRG neurons by RNA-seq study (Usoskin et al., 2015). *Trpa1* is preferentially expressed in NP and TH clusters which are categorised as unmyelinated neurons. *Trpv1* is expressed in NP and PEP clusters. *Scn10a* and *Scn11a* are expressed in NP, PEP and TH clusters which are mostly categorised in small unmyelinated neurons. On the other hands, *Scn9a* is expressed in both myelinated and unmyelinated neurons. The number in each column of these subpopulations represents the ratio of fraction of positive cells for different neuronal populations. Colour indicator; 0, green to 1, red.

		NH					NP			PEP		TH
		NF1	NF2/3		NF4/5		NP1	NP2/3		PEP1	PEP2	
			NF2	NF3	NF4	NF5		NP2	NP3			
Gene symbol	Channel											
Scn1a	$Na_v1.1$	0.581	0.854	1.000	0.773	0.885	0.032	0.063	0.083	0.125	0.471	0.215
Scn2a	$Na_v1.2$	0.097	0.208	0.000	0.136	0.192	0.096	0.156	0.083	0.094	0.000	0.129
Scn3a	$Na_v1.3$	0.032	0.000	0.083	0.045	0.038	0.032	0.031	0.000	0.078	0.000	0.116
Scn4a	$Na_v1.4$	0.000	0.021	0.000	0.000	0.000	0.072	0.031	0.083	0.000	0.059	0.039
Scn5a	$Na_v1.5$	0.677	0.021	0.000	0.000	0.000	0.008	0.000	0.000	0.031	0.000	0.069
Scn7a	NaX	0.903	0.688	0.917	0.455	0.192	0.232	0.125	0.250	0.391	0.588	0.708
Scn8a	$Na_v1.6$	0.742	0.896	0.833	0.818	0.923	0.064	0.063	0.000	0.109	0.706	0.270
Scn9a	$Na_v1.7$	0.387	0.521	0.667	0.227	0.000	0.544	0.656	0.750	0.391	0.765	0.777
Scn10a	$Na_v1.8$	0.000	0.000	0.000	0.000	0.000	0.760	0.625	0.417	0.281	0.588	0.227
Scn11a	$Na_v1.9$	0.000	0.000	0.000	0.000	0.000	0.904	0.781	0.833	0.313	0.176	0.330
Trpa1	Trpa1	0.000	0.000	0.000	0.000	0.000	0.512	0.219	0.167	0.063	0.000	0.176
Trpv1	Trpv1	0.000	0.000	0.000	0.045	0.000	0.032	0.281	0.583	0.313	0.059	0.000

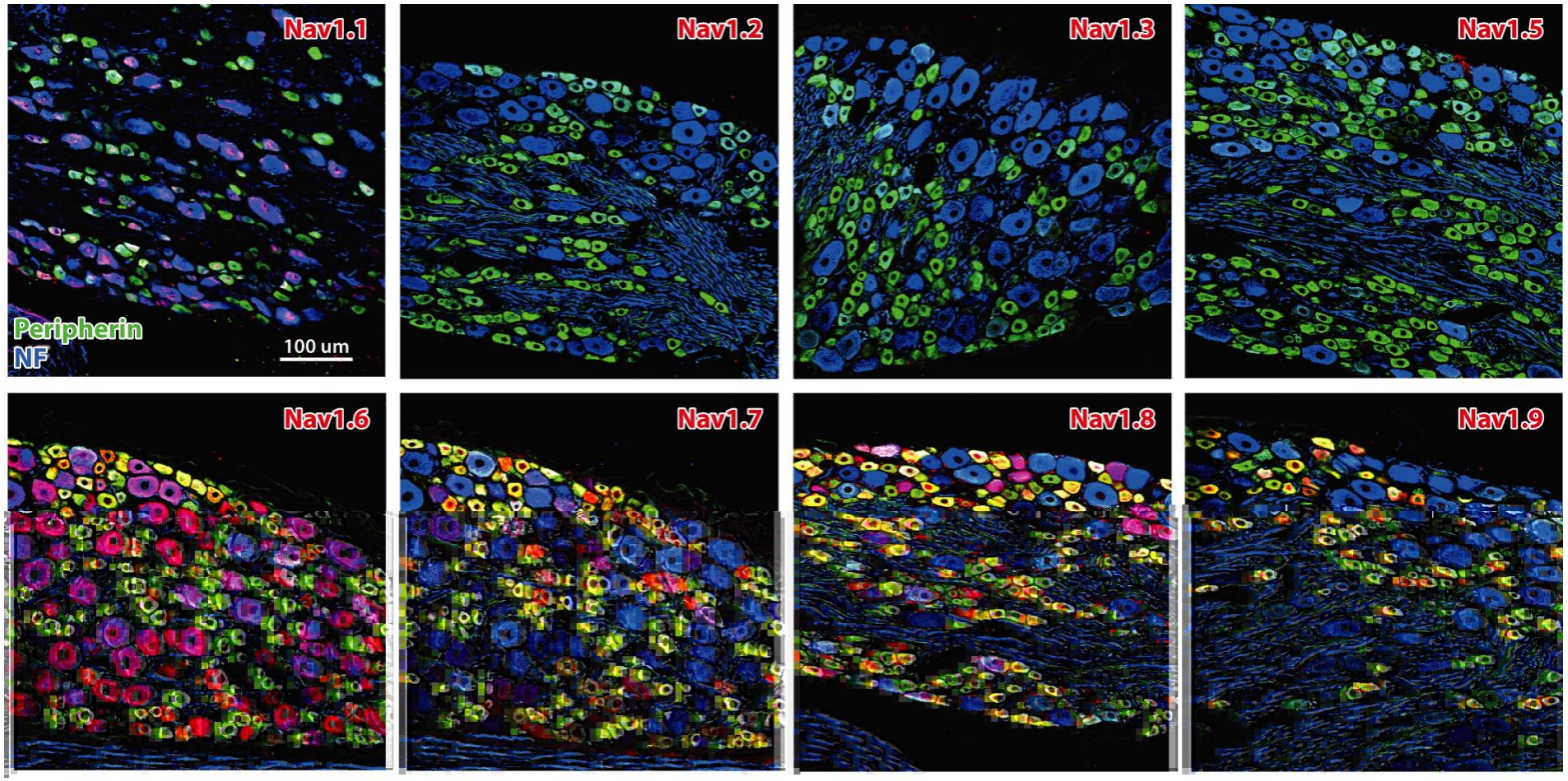

Figure 1-2. Expression of five voltage-gated sodium channels in adult DRG neurons. Sodium channel isoforms $Na_v1.1$, $Na_v1.6$, $Na_v1.7$, $Na_v1.8$, and $Na_v1.9$ (red) are colocalized in DRG neurons expressing peripherin (green), a specific small neuron marker, and neurofilament (blue), a marker of medium and large neurons. $Na_v1.1$ expression is largely confined to large neurons. $Na_v1.2$, $Na_v1.3$ and $Na_v1.5$ are undetectable in adult DRG neurons. $Na_v1.6$ generally has expression in all size classes of neurons. $Na_v1.7$ is highly expressed in small neurons, and is also present in some large neurons. $Na_v1.8$ is expressed preferentially in small and medium neurons, whereas $Na_v1.9$ is present exclusively in small neurons. Colocalization of sodium channels with peripherin is depicted in yellow and with neurofilament in magenta. (Dib-Hajj et al., 2010)

1.1.2 Pain pathways

Nociceptive neurons detect noxious thermal, mechanical, or chemical stimuli and transduce these noxious stimuli into action potentials that are transmitted to the afferent central termini resulting in the release of neurotransmitters (Basbaum and Jessell, 2000). Nociceptive information is then passed to a second order neuron within the spinal cord and then transmitted to the brain. Figure 1-3 shows key elements of transduction, transmission and neurotransmitter release in primary afferent neurons. Figure 1-4 illustrates a brief explanation for the ascending sensory pathway.

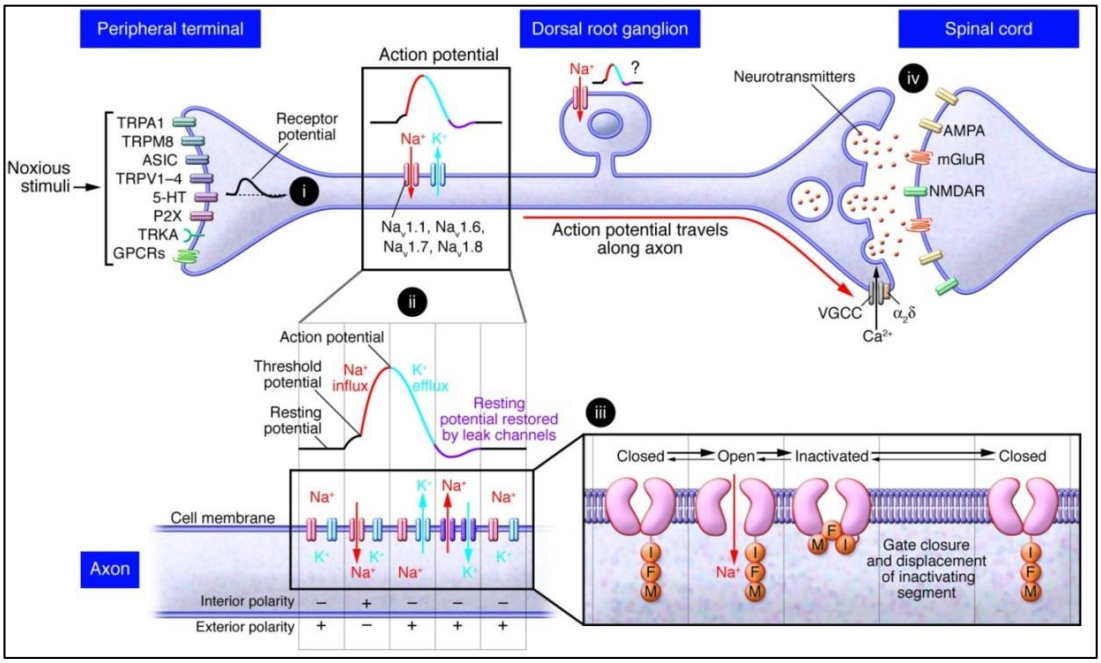

Figure 1-3. A brief illustration of the channels at their peripheral terminals in primary afferent neurons, such as TRP channels, transducing sensory stimuli including thermal, chemical and mechanical stimuli. Transmission of the action potential is conducted by voltage-gated sodium channels and potassium channels to the dorsal horn of the spinal cord and voltage-gated calcium channels trigger neurotransmitter release across the synapse. (Raouf et al., 2010)

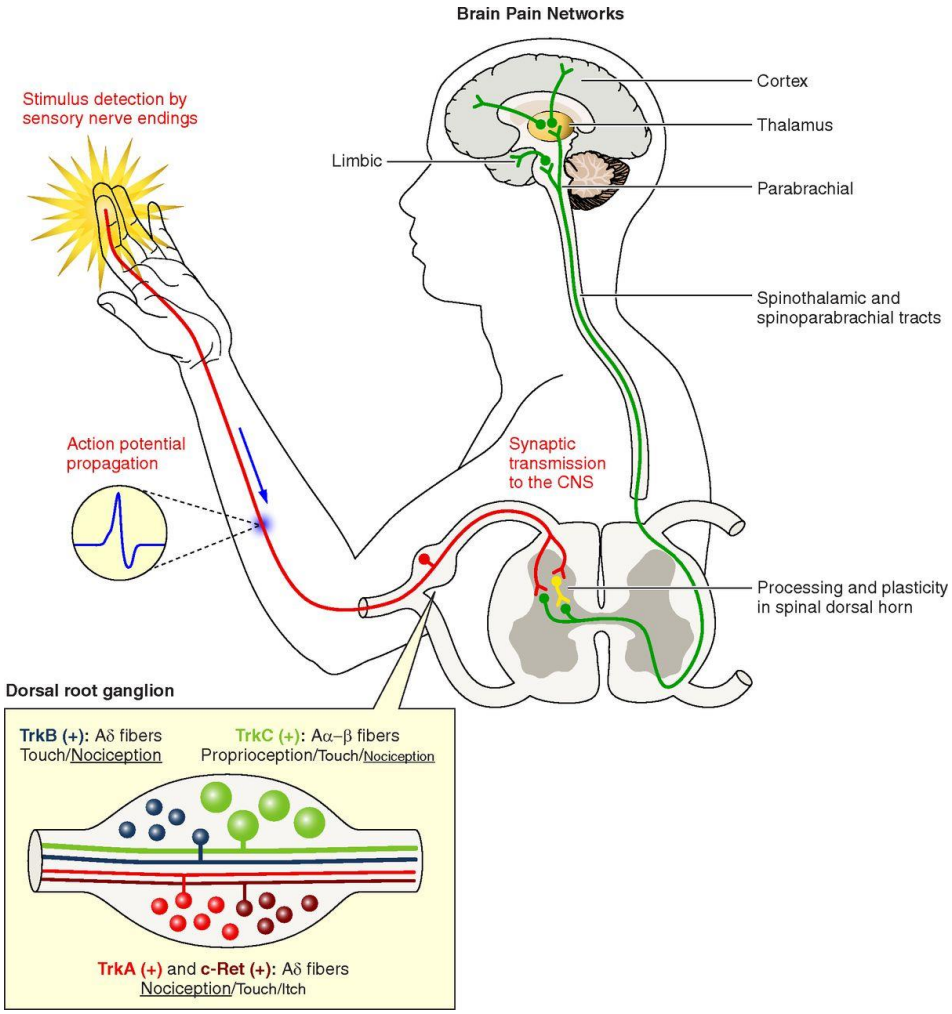

Figure 1-4. Ascending sensory pathway from peripherary to the brain. Nociceptive neurons in the peripheral nervous system have their soma located in the dorsal root ganglia (DRG). These neurons have a peripheral axon innervating the skin and viscera where they detect painful stimuli. The depolarization of the membrane by the stimulus leads to propagation of action potentials that travel along the fibers up to the DRG. Then the nociceptive information relays in the dorsal spinal cord. Sensory neurons within the DRGs can be classified based on the expression of several molecular markers. Small-diameter sensory afferents that correspond to unmyelinated C-fibers that are mainly involved in nociception express TrkA and Ret. TrkB- and TrkC-positive myelinated larger diameter afferents correspond to A-δ and A-α/β fibers, respectively. The sensory information is processed locally in neuronal circuitry within the dorsal horn of the spinal cord before being sent to the thalamus to convey nociceptive information. Following thalamic filtering, the information is sent to the cortical structures of the pain matrix. (Bourinet et al., 2014)

I. Transduction

Transduction, whereby a stimulus is converted into electrical signalling within a neuron, is key to understanding sensory systems and the detection of noxious stimuli. Transduction involves TRP channels (transient receptor potential cation channels), acid-sensing ion channels (ASICs), ATP receptors and G protein coupled receptors (GPCRs) among others, and distinct nociceptors require different types of thermal, chemical or mechanical stimuli (Raouf et al., 2010).

Multiple TRP channels are involved in detecting noxious thermal stimuli. For example, TRPV1 channels are considered to be activated by noxious heat; *Trpv1* null mice demonstrate deficits in response to acute noxious heat and thermal hyperalgesia, but responses to mechanical stimuli are normal (Caterina et al., 2000) (Figure 1-5). On the other hand, the TRPM8 channel which is menthol-sensitive with a thermal activation threshold of around 25°C (Basbaum et al., 2009) is involved in transduction of cold stimuli (Figure 1-5); *Trpm8* knockout mice show a loss of menthol and cold-evoked responses (Bautista et al., 2007, Dhaka et al., 2007). These mice do not have altered behavioural responses to noxious heat.

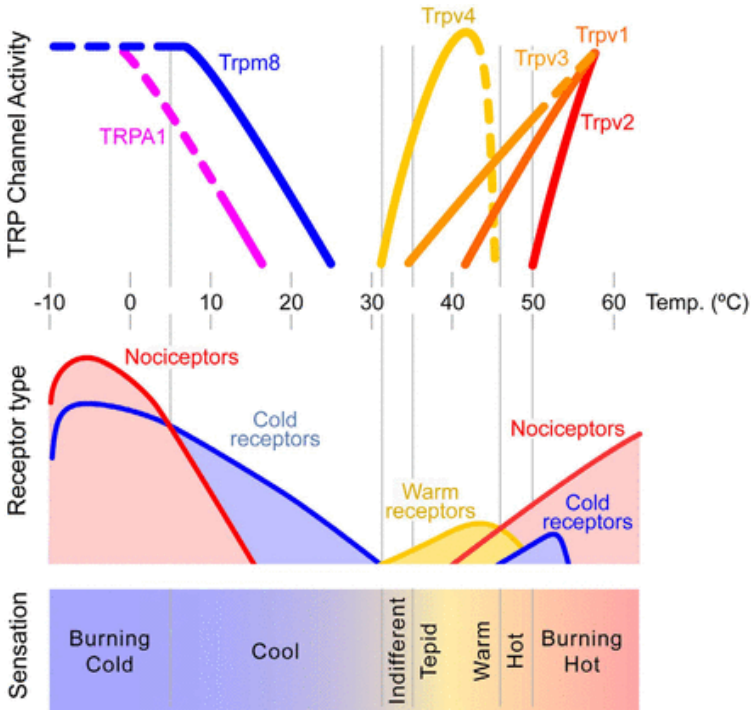

Figure 1-5. Hypothetical correspondence between activation of TRP channels, body surface temperature and evoked sensations. (Belmonte and Viana, 2008)

The molecular mechanisms behind mechanotransduction appear to be more complicated. Several candidate mechanotransducer molecules have been reported, such as TRP channels, potassium channels, Piezos and ASICs (acid sensing ion channels) (Basbaum et al., 2009, Raouf et al., 2012). *Trpa1* null mice demonstrate reduced responses to high-force innocuous and noxious mechanical stimuli (Kwan et al., 2006). Small diameter DRG neurons taken from *Trpa1* null mice show a lack of slowly and intermediately adapting currents associated with noxious mechanosensation (Brierley et al., 2011, Vilceanu and Stucky, 2010). However, some studies on *Trpa1* knockout mice show unaltered mechanical thresholds (Bautista et al., 2006) and knockdown of *Trpa1* by antisense oligonucleotides resulted in the mice that developed nerve injury induced mechanical allodynia normally (Obata et al., 2005). More recently, TRPC1, 3, 5, and 6 have been linked to mechanotransduction. Deletion of both *Trpc3* and *Trpc6* attenuated light touch sensitivities and silenced half of small-diameter sensory neurons expressing mechanically activated rapidly adapting currents (Quick et al., 2012). Double *Trpc3*/*Trpc6* knockout mice also showed a hearing impairment (Quick et al., 2012). Furthermore, the quadruple knockout mice demonstrated larger deficits of behavioural responses in light touch stimuli than the *Trpc3*/ *Trpc6* double knockouts (Sexton et al., 2016). These studies imply that TRP channels are required for mechanosensation in a combinatorial matter. Piezo protein 1 and 2 are also candidate molecules for mechanotransduction. Mechanically activated currents were shown to be dependent on Piezo1 expression in a mouse neuroblastoma cell line (Coste et al., 2010). Also, expression of Piezo2 appears to be essential to induce mechanically activated rapidly adapting currents. In addition, knockdown of Piezo2 in cultured DRG neurons reduced these kinetically distinct currents (Coste et al., 2010). The conditional Piezo2 KO mice, where *Piezo2* is deleted from all sensory neurons, significantly attenuated behavioural responses to a variety of innocuous mechanical stimuli (Ranade et al., 2014).

Chemical compounds are also a cause of acute pain. Again, TRP channels are important in transduction of chemo-nociception. For example, heat sensitive TRPV1 is activated in response to capsaicin, the active component in chili peppers (Caterina et al., 1997). TRPA1 is also involved in detecting noxious chemicals since *Trpa1* knockout mice show reduced sensitivity to several chemical compounds such as allyl isothiocyanates, found in wasabi, and allicin found in garlic (Macpherson et al., 2007, Hinman et al., 2006).

II. Conduction

Electrical signals transduced from noxious stimuli are transmitted along the length of a neuron to the central terminals. Voltage-gated sodium channels (VGSCs) and potassium channels are involved in this process. VGSCs serve as key elements in propagating action potentials while potassium channels shape action potentials and set the resting membrane potential. These channels' role in pain has been well documented. For example, both K2P4.1 and K2P2.1 knockout mice showed mechanical allodynia and heat hyperalgesia (Noël et al., 2009). Also, double knockout of these channels increased responses to acute noxious cold as well as causing cold hyperalgesia. VGSCs are particularly interesting and relevant to this thesis with the properties and functions of VGSCs and their roles in pain discussed in detail in section 1.1.5.

III. Transmission

The activation of VGSCs propagates action potentials and leads to the entry of calcium ions (Ca^{2+}); once the depolarizing signals reach at the terminal, voltage-gated calcium channels (VGCCs) are activated, mediating Ca^{2+} influx in response to action potentials and depolarizing signals. This process triggers neurotransmitter release in neurons. A number of VGCCs are expressed in nociceptive neurons, being involved in neurotransmitter(s) release through regulating calcium influx. Similarly to VGSCs (discussed in the following section, 1.1.3), tissue and cellular distribution of VGCCs subtypes are distinct allowing them to play a number of different roles in neuronal processing. They are categorised broadly into two groups based on their voltage dependence of activation: low voltage activated (LVA) and high voltage activated (HVA) channels (Bean, 1991, Bean, 1989, Nowycky et al., 1985). The HVA channel family is further subdivided, based on pharmacological and functional properties, into L-, N-, P/Q-, and R-types (Bean, 1991, Catterall et al., 2005). Several subtypes of VGCCs have well documented roles in pain. For instance, N-type calcium channels are enriched at presynaptic nerve terminals where they trigger the release of neurotransmitters (Wheeler et al., 1994, Westenbroek et al., 1992a); knockout of $Ca_v2.2$, which forms a N-type calcium channel, leads to hyposensitivity to pain (Westenbroek et al., 1992b, Saegusa et al., 2002, Saegusa et al., 2001, Kim et al., 2001). R-type calcium channels are known to be associated with the regulation of neuronal excitability in many neuronal cells including DRG neurons (Zaman et al., 2011, Park et al., 2010, Lirk et al., 2008). Mice lacking the expression of $Ca_v2.3$, which forms an R-type calcium channel, were less sensitive to inflammatory pain (Saegusa et al., 2000) through

alterations in both ascending and descending pathways (Saegusa et al., 2002). Similarly, young mice without functional expression of $Ca_v2.1$, which forms a P/Q-type calcium channel, showed impaired sensitivity to inflammatory pain as well as neuropathic pain, although they displayed increased acute thermal nociception (Luvisetto et al., 2006).

Another key element in nociceptive pathways is neurotransmitter release. The vesicular glutamate transporter family (VGLUT), which incorporates glutamate into synaptic vesicles (Lagerström et al., 2010), has an important function in pain. Global heterozygote VGLUT2-KO (Leo et al., 2009, Moechars et al., 2006) or homozygote VGLUT3-KO (Seal et al., 2009) mice showed reduced mechanical hypersensitivity to neuropathic pain following the spared nerve injury model (SNI). VGLUT3 knockout mice also showed impaired acute mechanical pain sensitivity, as well as deficits in inflammatory pain (Seal et al., 2009).

IV. Modulation and perception

The nociceptive information conveyed by primary afferent neurons is passed to a second order neuron within the spinal cord by neurotransmitter(s). Primary afferent neurons mostly terminate at laminae I-V (Figure 1-6) in the dorsal horn of the spinal cord with second order neurons (Todd, 2010). Then the nociceptive information ascends from the spinal cord to the brain though five major pathyways; the spinothalamic, spinoreticular, spinomesencephalic, spinocervical, and spinohypothalamic tracts (Basbaum and Jessell, 2000, Almeida et al., 2004)(Figure 1-7, Figure 1-8). These tracts consist of neurons originated from different lamina of the dorsal horn and terminate at different central destinations. The spinothalamic tract arises from the axons of nociceptive-specific and wide-dynamic-range neurons in laminae I and V-VII of the dorsal horn. The nociceptive information terminates at the thalamus through the contralateral side of the spinal cord and the anterolateral white matter. The spinoreticular tract consists of the axons of neurons from laminae VII and VIII. It terminates at both the reticular formation and the thalamus. The spinomesencephalic tract comprises the axons of neurons originating from laminae I and V. It projects in the anterolateral quadrant of the spinal cord to the mesencephalic reticular formation and periaqueductal grey matter and terminates at parabrachial nuclei via the spinoparabrachial tract. The spinocervical tract comprises neurons mostly from laminae III and IV, which receive input from Aβ and Aδ fibres. Most axons ascend in the brain stem to the midbrain and to the thalamus. Some axons terminate at the medulla. The spinohypothalamic tract comprises the axons of neurons in laminae I, V, and

VIII. It projects directly to the supraspinal autonomic control centre, thus is considered to activate neuroendocrine and cardiovascular responses (Basbaum and Jessell, 2000, Almeida et al., 2004).

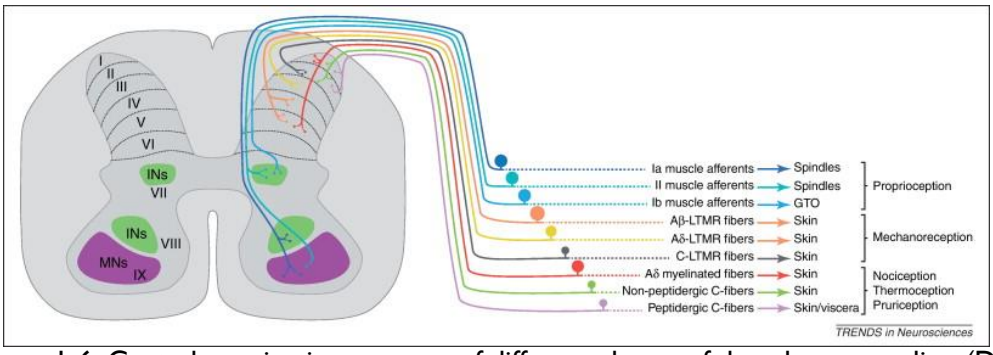

Figure 1-6. Central termination patterns of different classes of dorsal root ganglion (DRG) neuron (Lallemend and Ernfors, 2012).

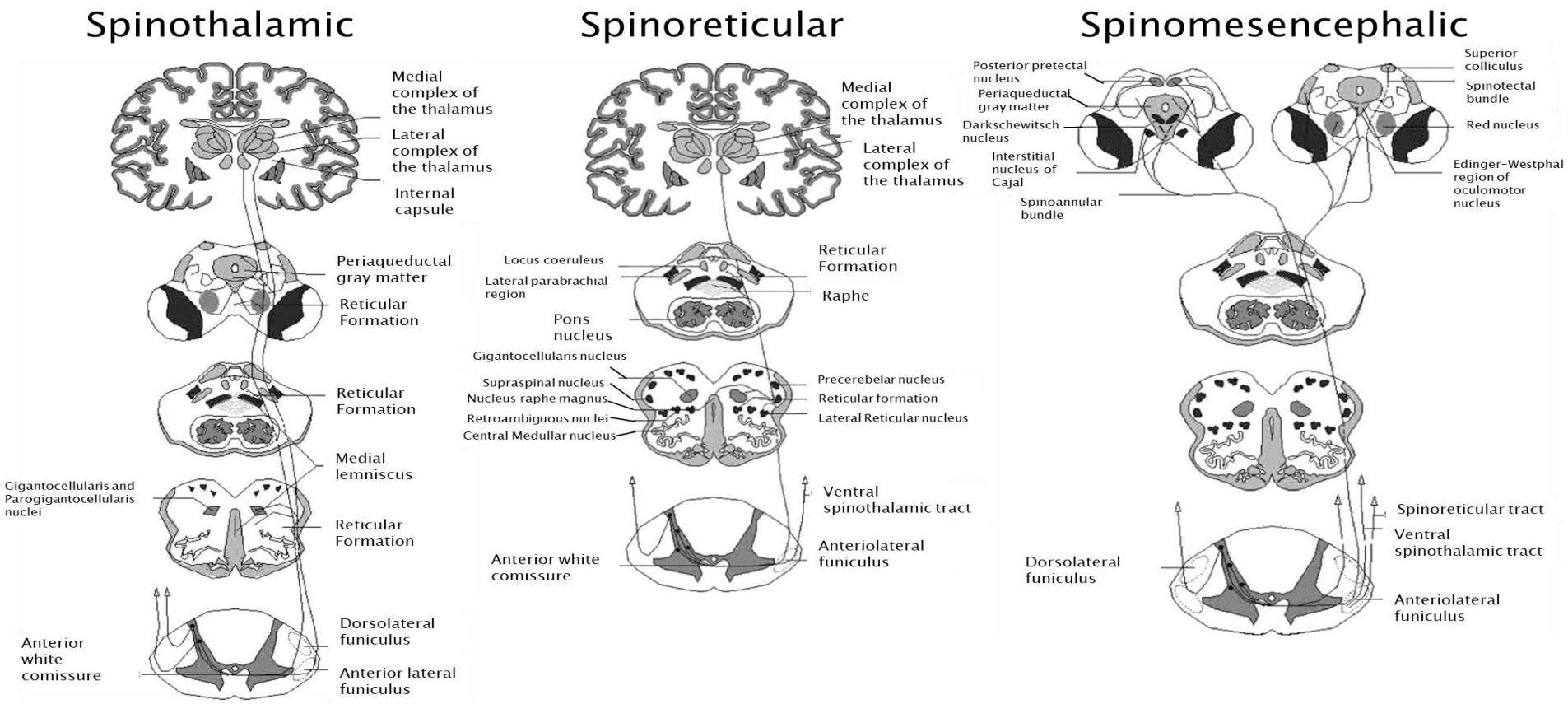

Figure 1-7. Spinothalamic, spinoreticular, and spinomesencephalic tracts. The spinothalamic tract arises from the axons of neurons in laminae I and V-VII of the dorsal horn. The nociceptive information terminates at the thalamus through the contralateral side of the spinal cord and the anterolateral white matter. The spinoreticular tract consists of the axons of neurons from laminae VII and VIII and terminates at both the reticular formation and the thalamus. The spinomesencephalic tract comprises the axons of neurons from laminae I and V. It projects in the anterolateral quadrant of the spinal cord to the mesencephalic reticular formation and periaqueductal grey matter and terminates at parabrachial nuclei via the spinoparabrachial tract. (Almeida et al., 2004)

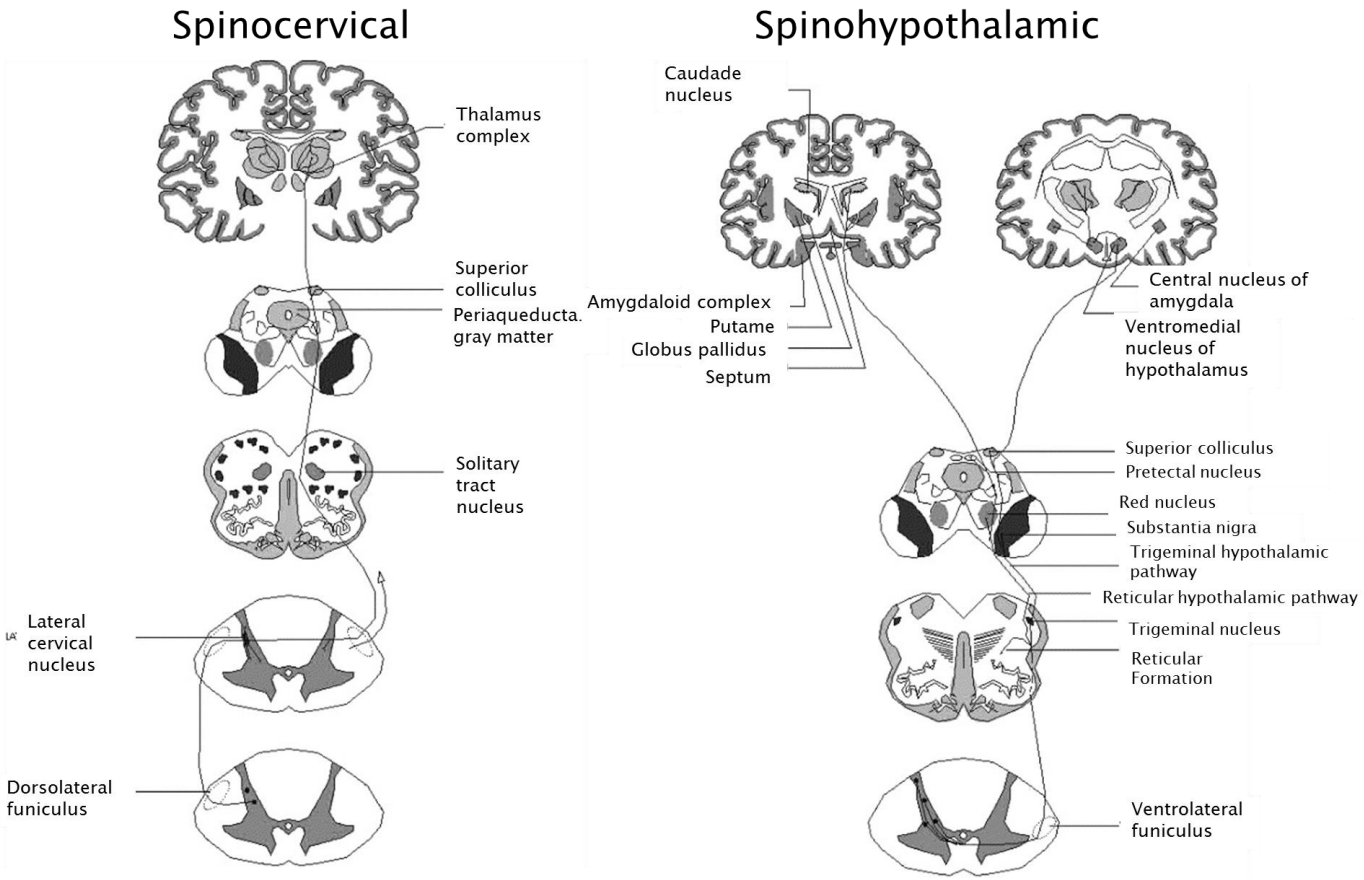

Figure 1-8. Spinocervical and spinohypothalamic tracts. The spinocervical tract comprises neurons mostly from laminae III and IV, which receive input from Aβ and Aδ fibres. Most axons ascend in the brain stem to the midbrain and to the thalamus and some axons terminate at the medulla. The spinohypothalamic tract comprises the axons of neurons in laminae I, V, and VIII. It projects directly to the supraspinal autonomic control centre, thus is considered to activate neuroendocrine and cardiovascular responses. (Almeida et al., 2004)

Neuronal activities in both the spinal cord and brain can modulate nociceptive information, thus altering the perception of pain. Great numbers of molecules and factors are associated with central processing in nociception and pain perception. For example, projection neurons, which are concentrated in lamina I in the dorsal horn, can modulate nociceptive information by regulating neurotransmitter release. The neurokinin 1 receptor (NK1R) is the main target for one of the neurotransmitters, substance P, and is predominantly expressed in lamina I. Ablation of NK1R-expressing cells with a substance P–saporin conjugate in rats showed that they did not develop hyperalgesia in neuropathic and inflammatory pain models (Mantyh et al., 1997, Nichols et al., 1999). Also, the descending pain modulatory system is a well-characterized anatomical network that can modulate nociceptive processing. It is known that some neurons in the periaqueductal grey (PAG) matter in the midbrain directly project to the rostral ventromedial medulla (RVM) and the doral horn of the spinal cord (Tracey et al., 2007). Direct microinjection of opioids into the PAG produces antinociception (Jacquet and Lajtha, 1976, Bodnar, 2000) by inhibiting the firing of nociceptive neurons in the dorsal horn (Basbaum and Jessell, 2000).

1.1.3 Overview of sodium channels

As discussed above, ion channels have an important role in neuronal processing. Investigating the function of ion channels can be essential to identify potential drug targets for specific diseases such as epilepsy, ataxia, seizure, as well as pain. In mammals, there are nine voltage-gated sodium channel genes (*SCN1A–SCN5A* and *SCN8A–SCN11A*) that encode molecularly and physiologically distinct α subunits ($Na_V1.1$-$Na_V1.9$) (Catterall et al., 2005). The association of the alpha subunits with beta auxiliary proteins, encoded by four genes (*SCN1B-SCN4B*), regulates channel gating and trafficking, allowing cell specific modulation of sodium channels in different cell types. With the exception of $Na_v1.4$, all voltage-gated sodium channels are expressed in the nervous system. The subtypes have been shown to be associated with different diseases (Table 1-2). Among the isoforms important in nociceptive transmission and pain, $Na_v1.7$, $Na_v1.8$ and $Na_v1.9$, are all preferentially expressed in the peripheral nervous system (Eijkelkamp et al., 2012)(Table 1-2). Some evidence showing an upregulation of $Na_v1.3$ in rodent DRG neurons following nerve injury has also suggested a potential role for this channel in pain (Waxman and Zamponi, 2014). There is strong evidence showing $Na_v1.7$, $Na_v1.8$ and $Na_v1.9$ are essential in pain sensation in both animal and human studies, as discussed in section 1.1.5.

Table 1-2. Expression patterns of VGSCs and their disease association (modified from (Eijkelkamp et al., 2012))

Channel	Gene	Tetrodotoxin sensitive	Major Expression	Channel disease association
$Na_v1.1$	*SCN1A*	+	CNS, PNS, Heart	Epilepsy, Migraine, Autism
$Na_v1.2$	*SCN2A*	+	CNS, PNS	Epilepsy, Autism, Episodic ataxia
$Na_v1.3$	*SCN3A*	+	CNS, PNS	Epilepsy
$Na_v1.4$	*SCN4A*	+	Skeletal muscle	Hyperkalaemic periodic paralysis, Paramyotonia congenital, Hypokalaemic periodic paralysis
$Na_v1.5$	*SCN5A*	-	Cardiac muscle	Brugada syndrome, Long QT syndrome 3, Atrial fibrillation
$Na_v1.6$	*SCN8A*	+	CNS, ONS, Smooth muscle	Mental retardation, Pancerebellar atrophy, Ataxia, Infantile Experimental encephalopathy
$Na_v1.7$	*SCN9A*	+	PNS	Congenital insensitivity to pain, Inherited primary erythromelalgia, Paroxysmal extreme pain disorder, Small fibre neuropathy, anosmia
$Na_v1.8$	*SCN10A*	-	PNS, Heart	Small fibre neuropathy
$Na_v1.9$	*SCN11A*	-	PNS	Congenital insensitivity to pain, Painful peripheral neuropathy, Familial episodic pain syndrome
NaX	*SCN7A*	+	Circumventricular organs	Unknown

1.1.4 Structure and functional states of voltage-gated sodium channels

As stated before, voltage-gated sodium channels are critical for pain perception. The structure and functional states of these channels is essential to understanding pain sensation. In this section, the structure and subtypes of these channels, and their functional states will be addressed.

The voltage-gated sodium channels (VGSCs) are heteromeric transmembrane proteins which open in response to alteration in membrane potential to provide selective permeability for sodium ions (Anger et al., 2001). There are at least three functional states of sodium channels. The "resting" (closed, activatable) state emerges from a conformational change that requires repolarization of the membrane (membrane potentials below -60 mV). In this state, the channels are ready to open. In response to membrane depolarization they become "open" (or "activated") and allow rapid influx of sodium ions. Then they are converted to "inactivated", when the channels undergo conformational changes in which isoleucine, phenylalanine, and methionine between domains III and IV play an important role. When inactivation takes a time of around 1 ms it is called "fast-inactivation" and channels shift into a

fast inactivated state. On the other hand, some channels undergo slow-inactivation, which takes considerably longer (seconds to minutes). As a result the "slow-inactivation" state, a fourth possible functional state is created (Anger et al., 2001, Kyle and Ilyin, 2007). Moreover, functional changes and increased permeability of sodium ions result in generation of sodium currents, which can be measured. These currents are responsible for the upstroke of the action potential. Many neurons possess two types of sodium currents: transient and persistent. Transient sodium currents (INaT) are related to the opening of the channel when sodium ions passively move through the channel on the basis of an electrochemical gradient (Sun et al., 2007). On the other hand, a persistent sodium current (INaP) is a small, slowly inactivating sodium current with relatively long kinetics of inactivation (tens of seconds), which appears when inactivation of channels is incomplete (Mantegazza et al., 2010). It activates as potentials close to or slightly more negative than resting membrane potential and it hardly inactivates. Its amplitude is relatively small, constituting about 1% of the peak amplitude of the transient sodium current (Sun et al., 2007, Hammarström and Gage, 2002).

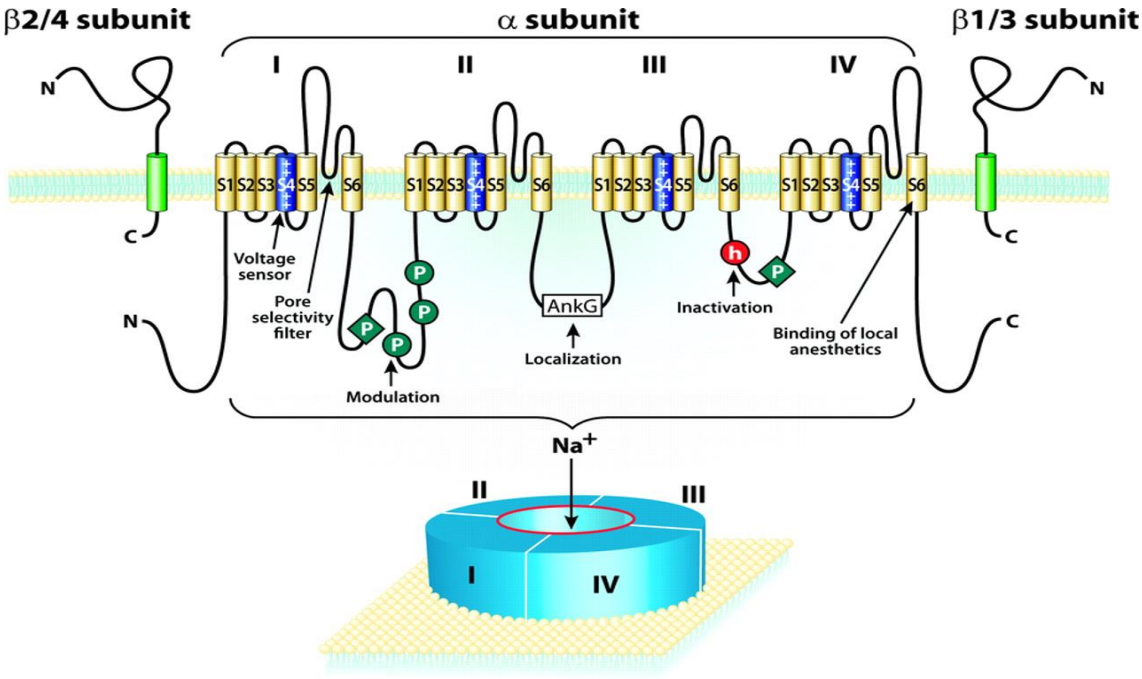

Figure 1-9. Primary structure of a voltage-gated sodium channel. Transmembrane segments are shown as cylinders. The main pore-forming and voltage-sensing α-subunit comprises four domains (labelled I–IV), each with six transmembrane segments. The β-subunits have a single transmembrane segment, a short intracellular domain and a single, extracellular immunoglobulin-like loop; β1 and β3 have non-covalent interactions with the α-subunit, whereas β2 and β4 are covalently linked to it with disulfide bridges. (Mantegazza et al., 2010, Benarroch, 2007)

Sodium channels consist of a pore-forming α subunit that is sufficient for functional expression, and β subunits that play an important role in channel localization and interaction with cell adhesion molecules, the extracellular matrix, and the intracellular cytoskeleton. The structure of mammalian VGSCs has yet been determined. However, the crystal structure of the homotetrameric bacterial sodium channel has provided insights into the atomic structure of mammalian sodium channels (Payandeh et al., 2011). Figure 1-9 shows the primary structure of VGSCs. These pore forming alpha subunits, each composed of a long polypeptide chain (1700-2000 amino acids), comprise four homologous domains (DI-DIV) with each domain broken down into six transmembrane alpha helical segments (SI-S6) with an additional membrane-reentrant pore loop between S5 and S6. The ion selective pore of the channel is formed by S5-S6 and the voltage sensor is located at S4. Domains are linked by three intracellular loops (LI-L3). There are 4 homologous domains (I–IV) with the N and C termini regions located intracellularly. The pore loops line the outer, narrow entry to the pore, whereas the S5 and S6 segments line the inner, wider exit from the pore. The S4 segments

which contain positively charged residues contribute to the voltage sensor. These positively charged residues are neutralized by interaction with negatively charged residues from the surrounding protein (principally the S2 and S3 segments). Depolarization of the membrane allows the S4 segments to move outward, leading to a conformation change which opens the pore. Additionally, a short loop connecting S3 and S4 serves as an inactivation gate, blocking the pore from inside upon sustained depolarization (Catterall, 2000).

By similarities between the amino acid sequences of the channels, $Na_v1.1$, $Na_v1.2$, $Na_v1.3$, and $Na_v1.7$ are most closely related. They are broadly expressed in neurons and they are sensitive to block by nanomolar concentrations of tetrodotoxin (TTX-S) found in puffer fish and other marine and terrestrial animals (Narahashi, 2008). $Na_V1.5$, $Na_V1.8$, and $Na_V1.9$ are also closely related. They are resistant to nanomolar concentration of tetrodotoxin (TTX-R). The other TTX-S isoforms $Na_v1.4$ (expressed primarily in skeletal muscle), and Na_V 1.6 (expressed primarily in the nervous system) are set apart from these other two closely related groups of sodium channel genes (Catterall et al., 2005). DRGs neurons express $Na_V\alpha$ subunits (Black et al., 1996) together with four isoforms ($\beta1$–$\beta4$) of β subunits; predominantly $\beta1$, $\beta4$ in large-diameter mechanoreceptors and $\beta3$ in small-diameter nociceptors (Chahine and O'Leary, 2011) presumably to help fine-tune the electrical properties to different sensory modalities. Adult rodent DRG neurons can express the TTX-S channels $Na_v1.1$, $Na_v1.6$, and $Na_v1.7$, and the TTX-R channels $Na_v1.8$ and $Na_v1.9$ as well as $Na_v1.5$ at low levels. $Na_v1.6$ is expressed in all size classes of neurons while $Na_V1.1$ is expressed only by large sensory neurons. $Na_v1.7$ is expressed in small sympathetic, myenteric and sensory neurons as well in some large sensory neurons. $Na_v1.8$ is considered to be expressed almost specifically in sensory nociceptive neurons, and $Na_v1.9$ is expressed in small myenteric and sensory neurons as well as motor neurons (Dib-Hajj et al., 2010).

These differences in localization and electrophysiological properties of the channels contribute to their distinct functions. For example, $Na_v1.7$ produces a rapidly activating and inactivating TTX sensitive current. $Na_v1.7$ contributes to low-frequency firing in C-fibres due to its slow repriming nature (Herzog et al., 2003, Rush et al., 2007). Also it is considered a threshold channel due to its ability to boost subthreshold stimuli and thereby increase action potential firing frequency (Dib-Hajj et al., 2007, Herzog et al., 2003). $Na_v1.8$, producing a TTX resistant current, acts as a major contributor to the upstroke of action potentials (Renganathan et al., 2001, Akopian et al., 1999). $Na_v1.8$ is the sole channel that generates electrical impulses acting to maintain nociceptor excitability under cold conditions, where slow inactivation is enhanced in TTX sensitive channels (Zimmermann et al., 2007). $Na_v1.9$ has

unique biophysical properties; this channel generates a persistent TTX-resistant current that has very slow gating kinetics and can be activated at potentials close to resting membrane potential (Dib-Hajj et al., 2002). Activation kinetics of this nature are unable to contribute to the up-stroke of action potentials and instead act as modulators of membrane excitability through persistent inward currents and the ability to activate at a strategic range that is negative to, and overlaps with, the voltage thresholds of other transient sodium channels. Figure 1-10 illustrates distinct electrophysiological properties of $Na_v1.7$, $Na_v1.8$ and $Na_v1.9$ in action potential generation (Momin and Wood, 2008).

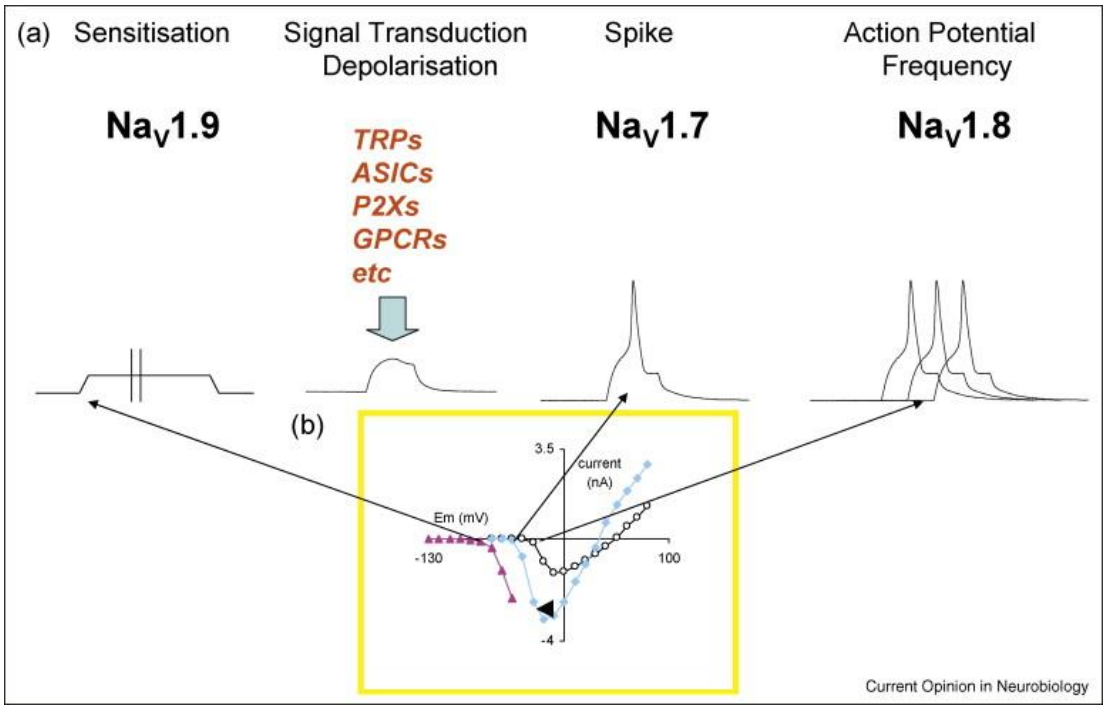

Figure 1-10. Three subtypes of voltage-gated sodium channels, $Na_v1.7$, $Na_v1.8$ and $Na_v1.9$ in action potential generation. (Momin and Wood, 2008)

1.1.5 Voltage-gated sodium channels and pain

$Na_v1.3$, $Na_v1.7$, $Na_v1.8$ and $Na_v1.9$ are ion channels that play important roles in pain pathways. In this section, properties and animal and human studies of these channels will be addressed (1.1.5 I-IV). Later human heritable sodium channelopathies (1.1.5 V) will be discussed.

I. $Na_v1.3$ (*SCN3A*)

$Na_v1.3$ is widely expressed in brain (Whitaker et al., 2001, Hains et al., 2003) and also reported to be expressed in skeletal muscle (Haimovich et al., 1987), and sensory neurons (Waxman et al., 1994). $Na_v1.3$ is a TTX-S channel which produces a persistent current and responds to small depolarizations close to resting potential thus amplifying small inputs. $Na_v1.3$ also demonstrates repetitive firing due to rapid recovery from inactivation (Cummins et al., 2001). While $Na_v1.7$, $Na_v1.8$ and $Na_v1.9$ have all been linked to human pain disorders, *SCN3A* mutations have yet to be found as a cause of a human pain syndrome. Animal studies of this channel are controversial: interest in $Na_v1.3$ as a pain target came from upregulation of this channel after nerve injury. $Na_v1.3$ expression, which was not detectable in the adult rodent nervous system, was upregulated in sensory neurons after peripheral nerve injury (Waxman et al., 1994, Dib-Hajj et al., 1999). Results from neuropathic pain models in rodents appeared to give some support to $Na_v1.3$ as a potential therapeutic target. Knockdown of $Na_v1.3$ expression using an antisense approach attenuated pain-related behaviour associated with spinal cord injury and chronic constriction injury (Hains et al., 2004). More recently, a knockdown of this channel by adeno-associated virus delivery of $Na_V1.3$ short hairpin RNA attenuated $Na_v1.3$ expression in a rodent neuropathic pain model. These rats showed reduced pain behavioural responses following nerve injury (Samad et al., 2013). However, another antisense study demonstrated that knockdown of $Na_v1.3$ did not reduce allodynia in the spared nerve injury model (Lindia et al., 2005). More evidence of an elusive role of $Na_v1.3$ in pain sensation has been searched for by analysis of $Na_v1.3$ knockout mice, where the gene was deleted globally or selectively in nociceptive neurons. However, these mice showed normal pain behaviour and normal development of neuropathic pain in the Chung model of neuropathic pain (Nassar et al., 2006). Further investigations are necessary to understand the role of $Na_v1.3$ in pain sensation and its potential as a therapeutic target.

II. $Na_v1.7$ (*SCN9A*)

$Na_v1.7$ was first found in somatosensory and sympathetic neurons and has since been detected in myenteric neurons, smooth myocytes, olfactory neurons and visceral sensory neurons. $Na_v1.7$ is preferentially expressed in a number of tissues including dorsal root ganglia (DRG), trigeminal ganglia, olfactory epithelia, and sympathetic neurons (Toledo-Aral et al., 1997, Weiss et al., 2011). Among DRG, $Na_v1.7$ is expressed in both large (>30 μm) and small

diameter (<25 μm) dorsal root ganglion neurons (Black et al., 1996, Ho and O'Leary, 2011). In the CNS, $Na_v1.7$ expression has been recently reported in the hypothalamus (Black et al., 2013), as well as in free nerve endings within superficial lamina of the dorsal horn in the spinal cord (Black et al., 2012). Functional mutations in *SCN9A*, the gene that encodes $Na_v1.7$, are known to be the underlying cause of a number of heritable disorders such as congenital insensitivity to pain (CIP) (Cox et al., 2006), inherited primary erythromelalgia (IEM) (Yang et al., 2004), paroxysmal extreme pain disorder (PEPD) (Fertleman et al., 2006), and small fibre neuropathy (SFN) (Faber et al., 2012a).

Several mouse studies have also highlighted the importance of $Na_v1.7$ in pain sensation. Interestingly, $Na_v1.7$ expression in different sets of mouse sensory and sympathetic neurons is essential for distinct types of pain sensation (Nassar et al., 2004, Minett et al., 2012). Conditional knockout mice of $Na_v1.7$ in $Na_v1.8$ positive nociceptors show a loss of acute noxious mechanosensation and inflammatory pain (Nassar et al., 2004)(Table 1-3) but normal hot-plate evoked responses (Minett et al., 2012). Ablating $Na_v1.7$ in all sensory neurons using an Advillin Cre abolishes mechanical pain, inflammatory pain and reflex withdrawal responses to heat. Ablation of $Na_v1.7$ in all DRG sensory neurons *and* sympathetic neurons is needed for insensitivity to the hot plate test and a surgical neuropathic pain model (Minett et al., 2012) (Table 1-3). Consistent with human findings, global $Na_v1.7$ KO mice displayed marked insensitivity to mechanical and thermal pain as well as anosmia but are otherwise phenotypically normal (Cox et al., 2006, Gingras et al., 2014, Weiss et al., 2011) (Table 1-3). These studies indicate the importance of $Na_v1.7$ in pain sensation and highlight it as an excellent drug target for pain therapies.

The crucial role of $Na_v1.7$ in pain sensation has accelerated the development of drugs targeting this channel. Considerable efforts have been made to develop new analgesic drugs which selectively block $Na_v1.7$ (Schmalhofer et al., 2008). Moreover, a recent study focussing on the natural antisense transcript (NAT) for *SCN9A* (Koenig et al., 2015), that is conserved in humans and mice, showed it can downregulate $Na_v1.7$ mRNA and protein levels and reduce $Na_v1.7$ peak sodium currents when overexpressed in human embryonic kidney cells (HEK293A) and human neuroblastoma (SH-SY5Y) cell lines. These results suggest that the *SCN9A* NAT can attenuate native sodium currents and regulate *SCN9A* post-transcriptionally, potentially altering pain thresholds and highlighting a new route to target $Na_v1.7$ function.

Aside from the generation and propagation of action potentials in sensory neurons, further functional roles for $Na_v1.7$ have been uncovered such as involvement of $Na_v1.7$ in itch (Lee et al., 2014, Devigili et al., 2014). Furthermore, in the olfactory system, deleting $Na_v1.7$ in

all olfactory sensory neurons caused the absence of postsynaptic responses and currents in olfactory bulb projection neurons. However, these neurons produced normal action potentials when depolarized via current injection through the patch pipette, linking $Na_v1.7$ to a role in neurotransmitter release (Weiss et al., 2011). Our group also reported that electrical stimulation of isolated sciatic nerve roots failed to induce increased substance P release in the dorsal horn of conditional $Na_v1.7$ KO mice, where $Na_v1.7$ was deleted in all sensory neurons (Minett et al., 2012).

III. $Na_v1.8$ (*SCN10A*)

$Na_v1.8$ is predominantly expressed in small diameter unmyelinated nociceptive sensory neurons (Akopian et al., 1996). Previously, the expression of $Na_v1.8$ was thought to be exclusively confined to small and medium diameter nociceptive subsets of sensory neurons of the dorsal root ganglia (Akopian et al., 1996, Benn et al., 2001). However it has subsequently been shown that 75% of dorsal root ganglion cells express $Na_v1.8$ with 90% of these expressing nociceptive markers (Shields et al., 2012). Evidence also suggests the presence of $Na_v1.8$ in around 40% of myelinated A fibres (Shields et al., 2012). The slowly TTX-R inactivating sodium channel, later identified as $Na_v1.8$, was described in an electrophysiological study using rat small DRG neurons (Rizzo et al., 1994); the predominant sodium conductance in the small neurons (18-25 μm diameter) to be resistant to TTX and slower than in many larger DRG neurons (44-50 μm diameter), while sodium conductance in the latter ones was kinetically faster and TTX sensitive.

This TTX-resistant sodium channel (IC50=60mM) (Akopian et al., 1999) is the main contributor to the upstroke of action potentials in nociceptive neurons (Renganathan et al., 2001, Akopian et al., 1999). $Na_v1.8$ also mediates the excitability of nociceptors at low temperatures, indicating its essential role in the propagation of cold stimuli. In mice, deleting $Na_v1.8$ in sensory neurons reduces the sensitivity to noxious mechanical stimuli as well as thermal stimuli and causes insensitivity to noxious cold (Abrahamsen et al., 2008, Akopian et al., 1999, Zimmermann et al., 2007) (Table 1-3). Engineered gain-of-function mutations in $Na_v1.8$ increase sensitivity to cold stimuli by enhancing $Na_v1.8$ sodium currents and show mechanically-evoked action potential firing in subclasses of Aβ, Aδ and C-fibers (Blasius et al., 2011, Garrison et al., 2014). This evidence cumulatively supports the role of $Na_v1.8$ in noxious cold stimuli sensation. In addition, multiple studies also support the role of $Na_v1.8$ in inflammatory pain; $Na_v1.8$ KO mice show reduced CFA-induced heat hypersensitivity (Leo et

al., 2010), and ablation of $Na_v1.8$-positive sensory neurons using diphtheria toxin reduces mechanical and heat hypersensitivity in carrageenan and CFA models (Abrahamsen et al., 2008). Furthermore, the administration of antisense oligodeoxynucleotides targeting $Na_v1.8$ in rats leads to a decrease in prostaglandin E2 (PGE2)-induced hyperalgesia (Khasar et al., 1998) and reverses (CFA)-induced heat and mechanical hypersensitivity in rats (Yu et al., 2011). In contrast, the role of $Na_v1.8$ in neuropathic pain is unclear. In some antisense studies, the knockdown of $Na_v1.8$ attenuates the development and maintenance of neuropathic pain in rats (Joshi et al., 2006, Lai et al., 2002). On the other hand, $Na_v1.8$ knockout mice, as well as $Na_v1.7$ and $Na_v1.8$ double knockout mice, show normal behaviour in neuropathic pain models (Kerr et al., 2001, Nassar et al., 2005).

In humans, gain-of-function mutations in $Na_v1.8$ in patients with small fibre neuropathies are known to cause mechanical hypersensitivity (Faber et al., 2012b, Huang et al., 2013), propounding that $Na_v1.8$ is a key contributor to pain sensation in peripheral neuropathies. Electrophysiology studies using $Na_v1.8$-null mouse DRG neurons, transfected with either $Na_v1.8$ WT or mutant constructs, have demonstrated that these mutations cause increased excitability of small DRG neurons that are characterised as nociceptors. These neurons have reduced current threshold, increased firing frequency and increased spontaneous firing (Faber et al., 2012b, Huang et al., 2013). It should be noted that a recent electrophysiological study has provided novel distinctions between properties of the human and rodent $Na_v1.8$ orthologues, including slower inactivation kinetics, larger persistent and ramp currents, as well as longer-lasting action potentials and increased firing frequency in human $Na_v1.8$ channels (Han et al., 2015a).

IV. $Na_v1.9$ (*SCN11A*)

$Na_v1.9$ is preferentially expressed in nociceptive dorsal root ganglia, trigeminal ganglia and motor neurons (Dib-Hajj et al., 2002, Dib-Hajj et al., 1998). $Na_v1.9$ is a TTX-resistant channel that activates at more hyperpolarising voltages in comparison to other VGSCs, which produces its characteristic persistent current (Herzog et al., 2001, Cummins et al., 1999). This feature enables $Na_v1.9$ to regulate resting membrane potentials and prolongs the depolarisation response to subthreshold stimuli (Herzog et al., 2001, Cummins et al., 1999) helping to lower the threshold for single action potentials and increasing repetitive firing (Maingret et al., 2008).

$Na_v1.9$ holds an important role in the generation of inflammatory pain (Table 1-3). Administration of inflammatory mediators such as Interleukin-1B, Bradykinin or PGE2 increases the current density of the channel, lowering the threshold for action potential generation in these neurons and thereby enhancing excitability of rodent DRG neurons (Maingret et al., 2008, Binshtok et al., 2008, Petho and Reeh, 2012). $Na_v1.9$KO mice showed reduced responses compared to WT mice in several inflammatory pain tests (Priest et al., 2005, Leo et al., 2010, Amaya et al., 2006, Lolignier et al., 2011) (Table 1-3): $Na_v1.9$KO mice did not develop thermal hyperalgesia after CFA (Priest et al., 2005, Amaya et al., 2006, Lolignier et al., 2011) or carrageenan injection (Priest et al., 2005) (Table 1-3). Mechanical hypersensitivity induced by CFA was also diminished in $Na_v1.9$KO mice (Lolignier et al., 2011) as well as having reduced responses after formalin-induced inflammation (Priest et al., 2005, Leo et al., 2010) (Table 1-3).

Several mutations in *SCN11A* have been described which cause a number of pain related diseases. Familial episodic pain (Zhang et al., 2013b) is known to be caused by two different missense mutations in $Na_v1.9$. Furthermore, other gain-of-function mutations in this channel are thought to be associated with peripheral neuropathy (Han et al., 2015b, Huang et al., 2014). Also, a recurrent mutation causing a heritable inability to experience pain has also been identified in this channel (Leipold et al., 2013).

Table 1-3. A summary of pain behaviour in $Na_v1.7$, $Na_v1.8$ and $Na_v1.9$ KO mice. (0: No change, -: Reduced responses) Modified from (Kanellopoulos and Matsuyama, 2016)

$Na_v1.7^{Na_v1.8}$: $Na_v1.7$ flox $Na_v1.8$ Cre ($Na_v1.7$ is deleted in $Na_v1.8$-positive sensory neurons), $Na_v1.7^{Advillin}$: $Na_v1.7$flox Advillin Cre ($Na_v1.7$ is deleted in all sensory neurons), $Na_v1.7^{Wnt1}$: $Na_v1.7$ flox Wnt1 Cre ($Na_v1.7$ is deleted in all sensory neurons and sympathetic neurons), $Na_v1.8^{DTA}$: Floxed stop DTA $Na_v1.8$ Cre ($Na_v1.8$-positive neurons are ablated with diphtheria toxin). Mechanical pain: Randall-Selitto test (RS), Light touch: Von Frey (vF), Thermal spinal reflex: Hargreaves' test (HG), Supraspinal thermal: Hot plate test, Noxious cold: Cold plate test, Noxious cooling: acetone test (Ac), Weight distribution to each hindpaw: Weight-bearing test (WB). CFA: complete Freund's adjuvant, SNT: spinal nerve transection, CCI: chronic constriction injury, SNI: spared nerve injury, WW: warm water

Transgenic mice	Acute Pain						Inflammatory Pain (F: Formalin, C; Carrageenan)				Neuropathic pain			Reference
	RS	vF	HG	Hot plate	Cold plate	Ac	F	CFA	C	Other	SNT	CCI	SNI	
$Na_v1.7$ KO	- (tail)	0	-	-			-	- (HG)		[1]				[1]
$Na_v1.7^{Na_v1.8}$	-	0	0/-	0	0	-	-	- (HG, vF)	- (HG)					[2] [3]
$Na_v1.7^{Advillin}$	-	0	-	0	0	-					0 (vF)			[3]
$Na_v1.7^{Wnt1}$	-	0	-	-	0	-					- (vF)			[3]
$Na_v1.8$ KO	-	0	0/-	0			0	- (HG), 0 (vF)	0/- (HG)			0 (vF)	0 (vF)	[4] [5]
$Na_v1.8^{DTA}$	-	0	0	0	-		0/-	- (vF, HG)			0 (vF, HG)			[4][6][7]
$Na_v1.9$ KO		0	0	0	0		-	- (Hot plate, WW, WB), 0 (vF),-/0 (HG)	-(vF, WW, WB), -/0 (HG)	- (PGE2, NGF, IL-1β, bradykinin; vF, Hot plate)		0 (vF, WB), - (Ac)	0 (vF, WB, Ac)	[5][8][9] [10]

[1] Gingras et al., 2014; [2] Nassar et al., 2004; [3] Minett et al., 2012; [4] Akopian et al. 1999; [5] Leo et al, 2010; [6] Zimmermann et al., 2007; [7] Abrahamsen et al., 2008; [8] Priest et al., 2005; [9] Amaya et al., 2006; [10] Lolignier et al., 2011

V. Human heritable sodium channelopathies

As briefy described above, mutations in $Na_v1.7$, $Na_v1.8$ and $Na_v1.9$ cause several inherited human pain disorders including IEM, PEPD, CIP, SFN, and FEP. Figure 1-11 demonstrates the structure of VGSC alpha subunit and the locations of some of the mutations that cause these disorders. Table 1-4 summarises these mutations and the associated diseases. Of note, the structure of mammalian VGSCs has not been determined as stated in 1.1.4. Thus the consequences of these mutations in the structural states of these channels are still open questions.

i. Inherited primary erythromelalgia (IEM) ($Na_v1.7$)

Mutations in *SCN9A* are known to be the underlying cause of Inherited Primary Erythromelalgia (IEM). IEM's symptoms include symmetrical burning pain accompanied by redness, increased skin temperature, oedema, and erythema. Symptoms usually appear in childhood or adolescence, but some infant or adult cases have also been reported (Waxman and Dib-Hajj, 2005). The phenotype can vary from mild to severe, even in the same family. The first IEM related mutations were identified in a Chinese family in 2004 (Yang et al., 2004) and more have been reported since then (Ahn et al., 2010, Dib-Hajj et al., 2010). Electrophysiological characterisation of IEM mutations in *SCN9A* has shown that these mutations cause a hyperpolarizing shift in the voltage dependence activation and increased persistent current of the channel (Dib-Hajj et al., 2010). Recent studies have also suggested that the mutations lead to a significant hyperpolarized shift in voltage dependent activation (Stadler et al., 2015), and a persistent current, which in turn, leads to a reduced current threshold and enhanced action potential firing probability (Vasylyev et al., 2014). Furthermore, along with the notable expression of $Na_v1.7$ in sensory neurons, sympathetic ganglion neurons, and olfactory neurons, it has been claimed that this channel is expressed in the smooth muscle cells of cutaneous arterioles, arteriole-venule shunts and endothelial cells in the skin, accounting for the redness of the skin seen in IEM (Rice et al., 2015). However, despite the evidence supporting *SCN9A* mutations in IEM, only 10% of IEM families are proven to have *SCN9A* mutations, implying that some other genetic mutations may be linked to this disorder (Goldberg et al., 2012).

ii. Paroxysmal extreme pain disorder (PEPD) ($Na_v1.7$)

Paroxysmal extreme pain disorder, originally named familial rectal pain syndrome, is a dominantly inherited condition with its common symptom being severe burning pain in the rectal, ocular and submandibular areas, which can last several hours. Pain attacks can also be accompanied by flushing of the skin, legs, eyelids, and buttocks (Hayden and Grossman, 1959, Fertleman et al., 2006). In 2006 Fertleman and colleagues described the first mutations associated with PEPD. The eight disease-causing mutations in *SCN9A* were mapped in 11 families and 2 sporadic cases (Fertleman et al., 2006). Electrophysiological analysis showed that the gain-of-function mutations in *SCN9A* are linked to neuronal hyperexcitability. Although both IEM and PEPD are caused by gain-of-function mutations in *SCN9A*, their electrophysiological profiles are distinct. In contrast to IEM, certain PEPD mutations shift the voltage dependency of steady-state fast-inactivation in a depolarizing direction and may make inactivation incomplete. This results in a persistent current entering the channel. Interestingly, one *SCN9A* mutation is associated with a mixed clinical phenotype, displaying characteristics of both IEM and PEPD (Estacion et al., 2008).

iii. Pain insensitivity ($Na_v1.7$ and $Na_v1.9$)

To date, there are two VGSC genes that cause pain insensitivity in humans: *SCN9A* and *SCN11A* encoding $Na_v1.7$ and $Na_v1.9$, respectively. The first description of a number of homozygous nonsense mutations in *SCN9A* causing a CIP phenotype were described in a number of patients originating from consanguineous families in northern Pakistan (Cox et al., 2006). Since this discovery, other loss-of-function mutations in *SCN9A* causing pain insensitivity have been reported in other families (Goldberg et al., 2007, Cox et al., 2010). Another phenotype caused by loss-of-function mutations in *SCN9A* was described in 2013 in two Japanese families (Yuan et al., 2013). In contrast to the Pakistani families, these patients demonstrated complete loss of temperature sensation, autonomic nervous dysfunctions, hearing loss, and hyposmia in addition to adolescent onset of a loss of pain sensation. The homozygous mutation was identified in exon 22 of *SCN9A* in these patients. However, the reason for the difference in phenotype in these individuals remains elusive.

Interestingly, pain insensitivity phenotypes are not solely generated by mutations confined to *SCN9A*. In 2013, a *de novo* missense mutation in *SCN11A*, the gene that encodes $Na_v1.9$, was found in two unrelated patients exhibiting a similar pain insensitive phenotype to that of CIP patients but with extra syndromal features (Leipold et al., 2013). These individuals

displayed signs of mild muscular weakness, delayed motor development, slightly reduced motor and sensory nerve conduction velocities with normal amplitudes, no intellectual disability, and a prominent hyperhidrosis together with gastrointestinal dysfunction. A mutation changing a highly conserved amino acid within the D2/S6 domain was identified in these patients. An investigation into the electrical properties of mouse DRG neurones bearing this mutation suggested that a gain-of-function mutation in this channel was the underlying cause of this pain insensitive phenotype.

iv. Small fibre neuropathies (SFN)/ Painful peripheral neuropathies (PPN) ($Na_v1.7$, $Na_v1.8$ and $Na_v1.9$)

Adult onset small fibre neuropathy (SFN) affects unmyelinated and thinly myelinated axons with patients displaying a reduced intraepidermal nerve fibre density. This disorder is often characterised by burning pain, allodynia and hyperesthesia. Large diameter axons are typically not damaged by SFN, resulting in normal tendon reflexes and vibration sense, and preservation of normal nerve conduction.

SCN9A, *SCN10A*, *SCN11A*, encoding $Na_v1.7$, $Na_v1.8$, and $Na_v1.9$ respectively, have been identified as the three VGSC genes that can cause SFN. Gain-of-function missense variants in $Na_v1.7$ have been reported in approximately one third of the individuals with small fibre neuropathies (Faber et al., 2012a). The phenotype of these individuals with *SCN9A* mutations is different from IEM. For instance, SFN patients have reported experiencing pain throughout the body, whereas in IEM pain tends to localise to the extremities. Furthermore, in contrast to the patients with IEM whose symptom is mostly relieved by cooling (Bennett and Woods, 2014), this treatment did not help for most of the patients with SFN caused by *SCN9A* mutations (Faber et al., 2012a). Functional profiling of the SFN mutant $Na_v1.7$ channels showed impaired slow inactivation, depolarised slow and fast inactivation, and increased resurgent currents. However, the hyperpolarizing shift in voltage dependence of activation and enhanced ramp responses that normally characterise IEM were not observed. In addition, the SFN mutant $Na_v1.7$ channels did not demonstrate the incomplete fast inactivation often found in PEPD (Faber et al., 2012a).

Gain-of-function mutations in $Na_v1.8$ have also been identified in patients with painful SFN (Faber et al., 2012b, Huang et al., 2013). These mutations caused enhanced ramp responses, recovery from inactivation and activation, and led to hyperexcitability of small neurons in DRG, characterised by reduced current thresholds, increased firing frequency, and

an increase in spontaneous activity.

More recently, mutation of *SCN11A* was also identified as a cause of painful peripheral neuropathy (PPN) (Huang et al., 2014) (Han et al., 2015b). The G699R mutation, located in the domain II S4-S5 linker region of the channel, causes a hyperpolarisation in channel activation, a depolarisation in steady-state fast inactivation along with enhancing ramp responses of $Na_v1.9$, leading to hyperexcitablility in dorsal root ganglion neurons.

v. Familial episodic pain syndrome (FEP) ($Na_v1.9$)

Familial episodic pain syndrome (FEP) is a Mendelian heritable trait resulting in severe pain and triggered by conditions such as fatigue, fasting, and cold. Three distinct types of this disease have so far been documented (Bennett and Woods, 2014). Type I, characterised by pain localised predominantly to the upper body, is linked to a gain-of-function missense mutation in *TRPA1* encoding the TRPA1 channel (Kremeyer et al., 2010). In contrast to type I, type II and type III have a distal distribution. Type II is also characterised as SFN caused by *SCN10A* mutations; clinical features of these patients are paroxysmal pain mainly affecting the distal lower extremities with reduced intraepidermal nerve fiber density or epidermal denervation (Faber et al., 2012b). The autosomal dominant type III disease form, first identified in two Chinese families, is characterised by pain in the distal parts of the body, more specifically localised to the hands and feet (Zhang et al., 2013b). In these patients, pain attacks usually occur late in the day with pain expanding simultaneously in different localisations, often triggered by intercurrent illness and fatigue after exercise. A combination of linkage analysis and whole-exome sequencing in both Chinese families revealed missense mutations in *SCN11A*, the gene encoding $Na_v1.9$. Electrophysiological analysis has shown these mutations cause hyperexcitability of dorsal root ganglia cells with increased peak current densities and enhanced action potential firing after current injection without changing the resting membrane potential.

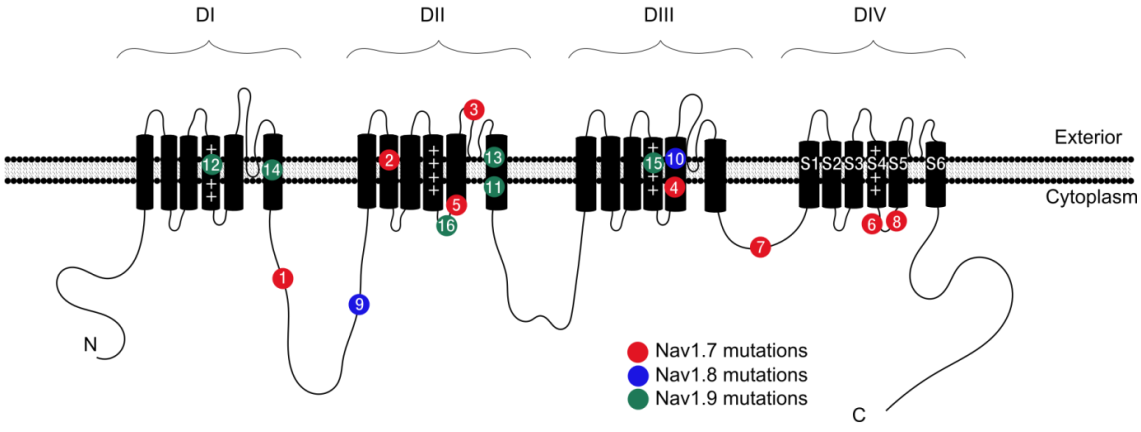

Figure 1-11. VGSC function and disease association. Schematic of a typical voltage-gated sodium channel. VGSCs are heteromeric transmembrane proteins complexes. Nine homologous members, *SCN1A-11A*, make up the voltage-gated sodium channel gene family. The pore forming alpha subunit encoded by these genes is comprised of four homologous domains (D1-D4). Each domain can be broken down into six transmembrane alpha helix segments (S1-S6) with the voltage sensor located at S4. The pore is formed by S5-S6. Numbered red dots designate the location of currently known mutations associated with major pain diseases summarised in Table 1-4. (Kanellopoulos and Matsuyama, 2016)

Table 1-4. VGSCs channelopathies and mutations. (Kanellopoulos and Matsuyama, 2016)

No. in Figure 1-11	VGSCs	Protein mutation	Disease	Functional effect	Reference
1	$Na_v1.7$	S459X	CIP	Loss-of-function	(Cox et al., 2006)
2	$Na_v1.7$	I767X	CIP	Loss-of-function	(Cox et al., 2006)
3	$Na_v1.7$	W897X	CIP	Loss-of-function	(Cox et al., 2006)
4	$Na_v1.7$	L1331P	CIP	Loss-of-function	(Yuan et al., 2013)
5	$Na_v1.7$	I848T/ L858H	IEM	Gain-of-function	(Yang et al., 2004)
6	$Na_v1.7$	M1627K	PEPD	Gain-of-function	(Fertleman et al., 2006)
7	$Na_v1.7$	I1461T/ T1464I	PEPD	Gain-of-function	(Fertleman et al., 2006)
8	$Na_v1.7$	A1632E	IEM/ PEPD	Gain-of-function	(Estacion et al., 2008)
9	$Na_v1.8$	L544P	SFN	Gain-of-function	(Faber et al., 2012b)
10	$Na_v1.8$	A1304T	SFN	Gain-of-function	(Faber et al., 2012b)
11	$Na_v1.9$	L811P	CIP	Gain-of-function	(Leipold et al., 2013)
12	$Na_v1.9$	R255C	FEP	Gain-of-function	(Zhang et al., 2013b)
13	$Na_v1.9$	A808G	FEP	Gain-of-function	(Zhang et al., 2013b)
14	$Na_v1.9$	I381T	PPN	Gain-of-function	(Huang et al., 2014)
15	$Na_v1.9$	L1158P	PPN	Gain-of-function	(Huang et al., 2014)
16	$Na_v1.9$	G699R	SFN	Gain-of-function	(Huang et al., 2014)

1.1.6 Project aims

This thesis is comprised of three overlapping parts, each with a common goal of better understanding pain pathways by studying the function of key genes that are mutated in inherited pain disorders. In chapter 2, I investigate the *SCN9A* gene and show that loss of function of the encoded $Na_v1.7$ channel causes dysregulation of genes within dorsal root ganglia from *Scn9a* knockout mice, helping to explain the observed analgesic phenotype. In chapter 3, I focus on a new gene that is mutated in a family with a pain-insensitive phenotype that segregates dominantly. This gene encodes a transcriptional regulator with enriched expression in nociceptive neurons. In chapter 4, I carry out an exome sequencing project with the aim of identifying the causal mutation in a patient with a painful small fibre neuropathy with symptoms that predominantly affect the knees.

2 VOLTAGE–GATED SODIUM CHANNEL AS A TRANSCRIPTIONAL REGULATOR

In this chapter, a novel function of an excellent analgesic drug target, one of the isoforms of the α-subunit of voltage-gated sodium channels (VGSCs) family, $Na_v1.7$, is explored; the importance of VGSCs in pain generation and pain related diseases is now well recognised. VGSCs are essential for electrical signalling in excitable cells. In the peripheral nervous system, these channels have an intrinsic role of conveying sensory information to the central nervous system, being involved in transmission of action potentials. Of a particular interest is $Na_v1.7$. Genetic, structural and functional studies have shown that $Na_v1.7$ regulates sensory neuron excitability and is a major contributor to several sensory modalities (Dib-Hajj et al., 2012, Eijkelkamp et al., 2012); the contribution of this sodium channel isoform to human pain disorders has also been established (Dib-Hajj et al., 2010). The human patients diagnosed with CIP due to loss-of-function of $Na_v1.7$ channels and $Na_v1.7$KO mice are normal apart from pain insensitivity and anosmia (Cox et al., 2006, Gingras et al., 2014), suggesting that there would be minimum adverse side effects by targeting $Na_v1.7$ therapeutically. However, despite considerable efforts, there are currently no drugs targeting $Na_v1.7$ on market and $Na_v1.7$ selective blockers with potent analgesic activity have proven elusive. For example, the $Na_v1.7$ antagonist Protoxin-II that has profound effects on electrical signalling in the peripheral nervous system is not an analgesic (Schmalhofer et al., 2008), and monoclonal antibodies blocking $Na_v1.7$ have short term effects on pain thresholds (Lee et al., 2014). Human IEM patients show pain relief following administration of some sodium channel blockers such as mexiletine or carbamazepine, however, the effect is restricted and these blockers cannot be used as a cure for all patients suffering from pain disorders (Choi et al., 2009, Fischer et al., 2009). Recently Convergence have conducted Phase II clinical trial using raxatrigine showing analgesia, and now it is in Phase III clinical trial (Lawrence, 2016, Convergence Pharmaceuticals, 2016). This compound is $Na_v1.7$ antagonist but less selective compared to the other selective antagonist such as Protoxin-II (Emery et al., 2016). This raises a question why more selective $Na_v1.7$ inhibitors exert less potent analgesic. Thus, we hypothesize that $Na_v1.7$ may have another function apart from the electrical signalling; this additional role of $Na_v1.7$ may be the key to developing effective pain treatments. This project will explore the novel function of $Na_v1.7$: recent studies from John Wood's group and the present data in this chapter suggest that $Na_v1.7$ mediates several gene expression changes (2.1, 2.3.1, 2.3.4). Pain behavioural tests indicated that the genes regulated by $Na_v1.7$ contribute to the pain sensation (2.3.2). The data also indicates a potential role of sodium ions acting as a second messenger to mediate gene expression (2.3.5). This novel function of $Na_v1.7$ may broaden the range of possibilities for targeted drug development and effective pain therapies.

2.1 AIMS OF THE PROJECT

The aim of this project is to explore a novel function of $Na_v1.7$ in nociception. Prior to starting the project, Wood's group examined the effects of deleting the genes encoding sodium channels $Na_v1.7$, $Na_v1.8$ and $Na_v1.9$ on transcriptional profiles in mouse sensory neurons using microarrays. We used conditional $Na_v1.7$ KO mice and global $Na_v1.8$ and $Na_v1.9$ KO mice. The conditional $Na_v1.7$ KO mice were generated by crossing floxed (Scn9a) $Na_v1.7$ mice with Advillin-Cre mice (Minett et al., 2012). In these mice, $Na_v1.7$ is deleted in all sensory neurons. Surprisingly, loss of $Na_v1.7$ expression has dramatic effects on gene expression (Figure 2-1). We found more marked alteration in gene expression in $Na_v1.7$ null mutant mice (194 genes which were dysregulated more than 1.5 fold) than $Na_v1.8$ (19 genes) and $Na_v1.9$ (64 genes) null mice. Some remarkable alterations of genes following $Na_v1.7$ deletion include upregulation of enkephalin precursors, *Penk* mRNA (fold change = 3.84) and *Tmem173*, transmembrane protein 173 (fold change = 2.82), and down regulation of *Ceacam10*, carcinoembryonic antigen-related cell adhesion molecule 10 (fold change = 18.94), and *Th*, tyrosine hydroxylase (fold change = 4.22) mRNA. This microarray data may support the theory of $Na_v1.7$ regulating gene expression, and furthermore, suggests that $Na_v1.7$ has an additional role apart from the known electrical signalling function.

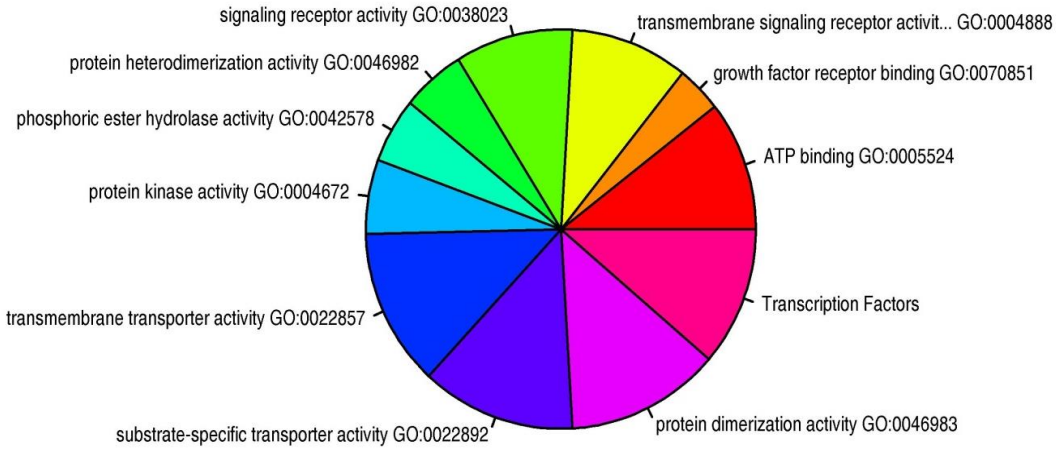

Figure 2-1. Deletion of $Na_v1.7$ leads to altered gene expression in DRG neurons in microarray analysis. The pie chart shows the ratio of significantly differentially expressed (DE) genes (ANOVA p-value < 0.01) between $Na_v1.7$ knockout mice (n=3) and littermates control (n=3), annotated with the top enriched Gene Ontology (GO) terms regarding the Biological Process (BP). For the enrichment analysis we used the classical Fisher test on genes counts to extract the GO terms in DE genes. Kolmogorov-Smirnov type tests were used on genes ranks and scores to compare the genes between $Na_v1.7$ knockout mice (n=3) and littermates control and simplify the number of GO terms. (Minett et al., 2015)

How $Na_v1.7$ regulates these gene expressions and whether these genes are associated with pain sensation, are critical questions to answer. We hypothesised that the dysregulated genes are associated with pain sensation and contribute to the CIP phenotype. Regarding the mechanism, we raised a question that $Na_v1.7$ may function as a transcriptional regulator and control gene expression at the transcriptional level, similar to the calcium channels; the association between transcription and ion channels is well documented in the case of closely related voltage-gated calcium channels (Gomez-Ospina et al., 2006, Barbado et al., 2009). We also considered if sodium ions mediate gene expression through $Na_v1.7$, since some studies suggested sodium ions act as a transcriptional mediator, or affect functional properties of GPCRs (Katritch et al., 2014, Popov et al., 2012). To investigate these matters further, this chapter focused on five aspects:

1. The mRNA expression level of four genes of interest was assessed using Real-time qRT-PCR in $Na_v1.7$ null mutant mice (KO) and littermates control. These genes, namely *Ceacam10*, *Penk*, *Th* and *Tmem173* (2.3.1), were dysregulated in the $Na_v1.7$ KO microarray so performing this qPCR allowed confirmation of this finding.

2. Pain behaviour assays were performed to see if the genes dysregulated in $Na_v1.7$ KO mice are associated with changes in sensory function. Two genes were of particular interest: *Ceacam10* and *Penk* (2.3.2).

3. Reporter assays in the presence or absence of $Na_v1.7$ were performed to explore if $Na_v1.7$ functions as a transcriptional regulator. To perform these assays, luciferase constructs controlled by the promoter region of the gene of interest were created. HEK293A and Neuro2A cell lines, and primary cultured mouse DRG neurons were assayed using these constructs. We hypothesised that the expression of the luciferase genes might be different in the presence or absence of $Na_v1.7$, if $Na_v1.7$ is a transcriptional regulator (2.3.3).

4. To evaluate further if $Na_v1.7$ affects gene expression at the transcriptional level, *Penk* pre-mRNA in DRG neurons was analysed with RT qRT-PCR (2.3.4).

5. Luciferase assays and pre-mRNA measurements were performed by altering intracellular sodium levels to investigate if sodium ions mediate gene expression (2.3.5).

Our results suggest that the novel function of $Na_v1.7$ can open a door for effective pain therapies helping patients with pain related diseases.

2.2 METHODS

2.2.1 Animals

Both female and male mice aged 6–12 weeks were kept on a 12-h light/ dark cycle and provided with food and water ad libitum. The conditional $Na_v1.7$ knockout mice were generated using the Cre-loxP system by crossing floxed (*Scn9a*) $Na_v1.7$ mice ($Na_v1.7^{fl/fl}$) (Nassar et al., 2004) with strains where Cre expression is driven by the Advillin promoter expressed in all DRG neurons ($Na_v1.7^{Adv}$ mice) (Minett et al., 2012). This method enables us to maintain conditional $Na_v1.7$ KO mice where $Na_v1.7$ is deleted in all sensory neurons. We used floxed $Na_v1.7$ mice as littermate control. Ceacam10 global null mutant mice on a BALBc background were supplied by EMMA (EM:00196 BALB/c-Ceacam10). The mice were maintained by Dr. Pereira in the Molecular Nociception Group, WIBR, UCL. All experiments were performed with approval from the United Kingdom Home Office according to guidelines set by personal and project licenses, as well as guidelines of the Committee for Research and Ethical Issues of IASP.

I. Genotyping

Genomic DNA was isolated from the ear. Ear punching samples were taken from mice of at least 3 weeks of age. Samples were digested in 30µl lysis buffer (see below) for 60 minutes at 55◦C then for 5 minutes at 95◦C to inactivate Proteinase K. Samples were vortexed, spun down and stored at -20◦C.

Lysis buffer: 10x GB Buffer 3.60ml, 25% TritonX-100 0.72ml, β-Mercaptoethanol 0.36ml, water 31.32ml. 1µl 19.7mg/ml Proteinase K (Roche) added per 499µl Lysis Buffer.

10X GB Buffer: 1.5M Tris pH8.8 4.47ml, 1.0M Ammonium Sulphate 1.66ml, 1.0M Magnesium Chloride 0.67ml, water 3.20ml.

$Na_v1.7$ was detected by PCR as described (Nassar et al., 2004). Advillin-Cre was also detected as described (Minett et al., 2012). The following primers were used:

Advillin wild-type (480 bp) and Advillin-Cre (180 bp) fragments

5'-CCCTGTTCACTGTGAGTAGG-3' (Advillin forward)

5'-AGTATCTGGTAGGTGCTTCCAG-3' (Advillin wild-type reverse)

5'-GCGATCCCTGAACATGTCCATC-3' (Advillin-Cre reverse).

$Na_v1.7$ wild-type fragment (317 bp), $Na_v1.7$ floxed fragment (461 bp) and $Na_v1.7$ knockout fragment (395 bp). The $Na_v1.7$ knockout fragment can detect the deletion of Exon 15 and 16 by using the primer pair designed to amplify segments of intron14-16 boundary.

5'-CAGAGATTTCTGCATTAGAATTTGTTC-3' ($Na_v1.7$ forward)

5'-AGTCTTTGTGGCACACGTTACCTC-3' ($Na_v1.7$ wild-type/floxed reverse)

5'-GTTCCTCTCTTTGAATGCTGGGCA-3' ($Na_v1.7$ knockout reverse).

2.2.2 Cell lines and primary cultured DRG neurons

Neuro2A cells or HEK293A cells were cultured in Dulbecco's modified Eagle's medium (DMEM) (Gibco, 31966-021 for Neuro2A cells and SIGMA, D5671 for HEK293A cells) with 10% fetal bovine serum (FBS).

6-12 week old $Na_v1.7$ floxed Advillin-Cre mice were killed by inhalation of a rising concentration of CO_2 followed by cervical dislocation, and whole thoracic and lumbar dorsal root ganglia were dissected. The DRG were kept in Ca^{2+}- and Mg^{2+}-free Hanks' balanced salt solution (HBSS) (Gibco, 14170-070) during the dissection and were subsequently digested for 25 min at 37°C in 1ml of Enzyme Mix (HEPES (Gibco 15630-049) at 5mM, Glucose at 10mM, Collagenase type XI (Sigma C7657) at 5 mg/ml and Dispase (Gibco 17105-041) at 10 mg/ml in Ca^{2+}- and Mg^{2+}-free Hanks' balanced salt solution (HBSS) (Gibco, 14170-070)). After digestion, ganglia were gently triturated in DMEM (Gibco, 31966-021) containing 10% FBS using fire-polished glass Pasteur pipettes. Cells were centrifuged for 5 min at 800RPM, following the transfection or harvesting. The cells were placed on poly-L-lysine laminin coated plates; the plates were incubated with poly-L-lysine (0.01mg/mL) for 30 min and rinsed with sterile water twice, Then the plates were air-dried at least for 30min and then incubated with laminin in PBS (0.02mg/ml) for 1-2 hour at 37°C. Regarding reagents treatment, the cells were cultured overnight in DMEM + 10% FBS with nerve growth factor (NGF) at 125ng/ml. The agents (monensin, tetrodotoxin (TTX) or ionomycin) were dissolved in ethanol to reach at 0.5 μM,

and 1 µl of the agents or ethanol were added into the cells with 1ml of the media. The final concentration of the agents was at 500nM. The cells were collected at appropriate time point.

2.2.3 Real-time qRT-PCR

To detect the gene expression at mRNA levels in DRG in $Na_v1.7$KO or littermate mice, total RNA was isolated from DRG. Briefly, DRGs were dissected from either KO mice or littermates control and suspended in RNA later (Ambion, AM7020) solution. DRG complements from several mice were pooled and homogenized in TRIzol reagent (Life Technologies, 15596018) using a homogenization kit with ceramic beads (PEQlab, 91-PCS-CKM). Then total RNA was purified using an RNasy Mini kit (QIAGEN, 74104). To measure mRNA levels of DRG treated with each agent, the cells were collected by 0.05% trypsin and 100µl of TRIzol reagent was added into the cell pellet. The samples were incubated at 20℃ for 30 min. To extract RNA, 80µl of chloroform was added into the each sample and the colourless phase was collected following centrifugation of samples for 10 minutes at 13000 RPM at 4℃. The total RNA was purified with 200µl of isopropanol and 70% ethanol. The quantity and quality were checked using a NanoDrop spectrometer (Thermo Scientific). Reverse transcription was performed by using the iScript Reverse Transcription Supermix for RT-qPCR (Bio-Rad, 170-8841). SYBR qPCR reactions were performed according to the manufacturer's instructions, using SsoAdvanced Universal SYBR Green Supermix (BioRad, 172-5270) and the following primers (Table 2-1). Taqman assays were also performed to measure mRNA levels of *Tmem173* and *Penk* using the following probes: *Penk*; Mm01212875_m1, *Tmem173*; Mm01158117_m1. BioRad CFX was used to amplify the selected genes from each sample in three parallel runs on a 96-well reaction plate using the following protocol: SYBR Green; 3min polymerase activation at 95°C, and 40 cycles of 15 sec denaturation at 95°C, 20sec annealing at 60°C and 20sec extension at 72°C. Taqman; 2min at 50°C, 10min polymerase activation at 95°C and 40 cycles of 15 sec denaturation at 95°C, 1min annealing and extension at 60°C. Melt-Curve analysis was performed following to the amplification for the SYBR Green assay under the following conditions: 1 min annealing at 65°C, 0.5°C increments (5 sec each) beginning at 65°C (data collection step) to 95°C. Relative expression of the target gene was calculated using the comparative $2^{\Delta\Delta CT}$ method (Livak and Schmittgen, 2001). Expression of the test gene was compared with that of *Gapdh* or *β-Actin* measured on the same sample, giving a CT difference (ΔCT) for *Gapdh* or *β-Actin* minus the test gene. The CT difference, ΔCT values of individual samples were compared to ΔCT of the control or WT

clones, giving ΔΔCT values of each clone. The relative expression was calculated as $2^{-\Delta\Delta CT}$. Mean, S.E.M. and statistics were calculated from the $2^{-\Delta\Delta CT}$. Data were analyzed using Microsoft Excel, and Student's t-test was performed with *p < 0.05, **p < 0.01, ***p < 0.001 as statistically significant.

Table 2-1. Primers for real-time qPCR

Primer	Sequence (5'-3)
mGapdh_qPCR_Fw	TGCGACTTCAACAGCAACTC
mGapdh_qPCR_Rev	CTTGCTCAGTGTCCTTGCTG
mPenk_qPCR_Fw	TTCAGCAGATCGGAGGAGTTG
mPenk_qPCR_Rev	AGAAGCGAACGGAGGAGAGAT
mTh_qPCR_Fw	GTCAGAGGAGCCCGAGGTC
mTh_qPCR_Rev	CGCTGGATACGAGAGGCATAG
mCeacam10_qPCR_Fw	AGAATTAAATGCAAGGGGGC
mCeacam10_qPCR_Rev	ATGAGGGAGCCTACGCACTA
mPenk pre-mRNA Ex2 Fwd	CCCAGATTTTGAAAGAAGGCAGC
mPenk pre-mRNA Int1 Rev	TCTCTTAACCACTCATCCCCTTGA
mβActin Fwd	GACGTTGACATCCGTAAAGA
mβActin Rev	AATCTCCTTCTGCATCCTGT

2.2.4 Luciferase assay

I. Introduction to the luciferase assay

Reporter gene assays are widely used for studying gene expression and regulation. They are frequently performed to explore transcriptional activity in cells. To investigate the transcriptional activity of the target element, the reporter genes are placed downstream of the promoter sequence of the target element. The expression of the reporter gene is associated with the transcriptional activity which depends on the promoter of interest. The most widely used genes for reporter gene assays are luciferase genes, which can give a sensitive and quick response by detecting enzymatic activity. The expression of luciferase genes is obtained after the cells of interest are transfected with the vector controlling the luciferase genes. The expression is simply detected by adding the corresponding substrate of the reporter protein to yield luminescence (Figure 2-2).

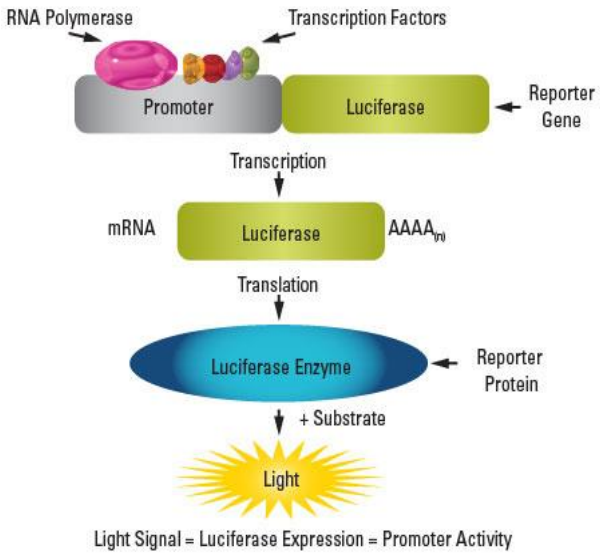

Figure 2-2. Schematic of the luciferase reporter assay (LifeTechnologies, 2015)

Ideally the reporter genes which yield luminescence should not be endogenously expressed in the cells of interest. In this project, we used four types of luciferase gene, none of which are endogenously expressed. There are many classes of luciferase genes derived though separate evolutionary histories. In this project, we chose four distinct types of luciferase; *Gaussia*, *Cypridina*, *Firefly* and *Renilla*. *Gaussia* luciferase is a recently discovered, naturally secreted protein by the copepod, *Gaussia princeps* requiring Coelenterazine in a reaction that produces luminescence (Figure 2-3). *Cypridina* luciferase is also a secreted protein from the marine ostracod, *Cyridina noctiluca,* requiring a specific luciferin, Vargulin, to yield light (Figure 2-4). On the other hand, Firefly and Renilla luciferase are intracellular luciferases, catalyzing a reaction with their substrates, Beetle Luciferin and Coelenterazine, respectively (Figure 2-5). These luciferases are not produced in the cells we are targeting; HEK cells to test the promoter activity of human genes of *GAPDH*, *PENK* and *TH*, Neuro2A cells for mouse genes, and mouse DRG cells to explore the mechanisms of pain pathways related to $Na_v1.7$. Thus, we can assay the transcriptional activity without any confounding issues of endogenous expression. In some luciferase assays, a second reporter is used to normalize results of the experimental reporter. This is because the luminescence signal corresponds to the cell number and transfection rate. Therefore the second reporter can be used for normalizing the cell numbers and transfection rate. We used *Cypridina* luciferase for an internal control for normalization of *Gaussia* luciferase expression, and *Renilla* luciferase to normalise *Firefly* luciferase expression. The result is given by the RLU (Relative Light Unit) ratio, *Gaussia* luciferase RLU divided by *Cypridina* luciferase RLU or *Firefly* luciferase RLU divided by *Renilla* luciferase RLU.

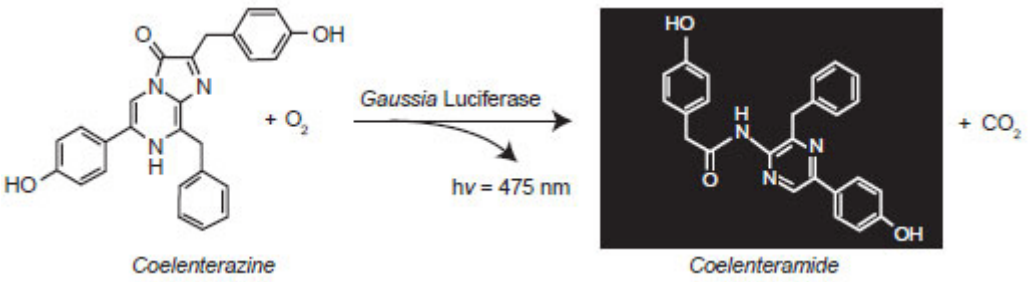

Figure 2-3. The photo-oxidation catalyzed by Gaussia Luciferase (NewEnglandBiolabs)

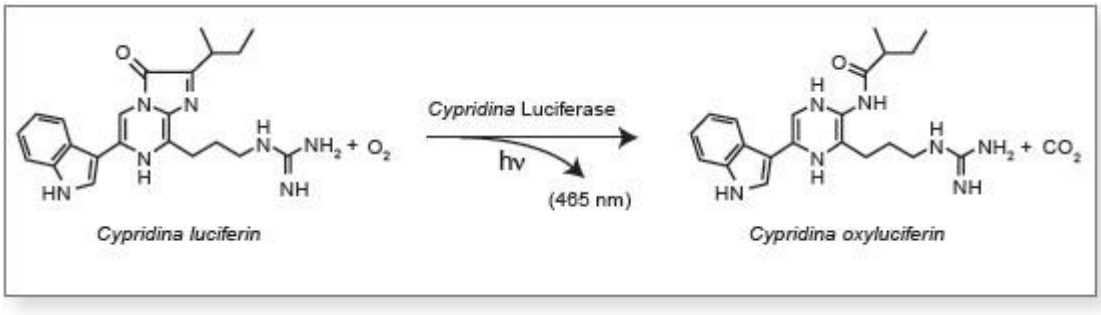

Figure 2-4. The photochemical reaction catalyzed by Cypridina Luciferase. (NewEnglandBiolabs)

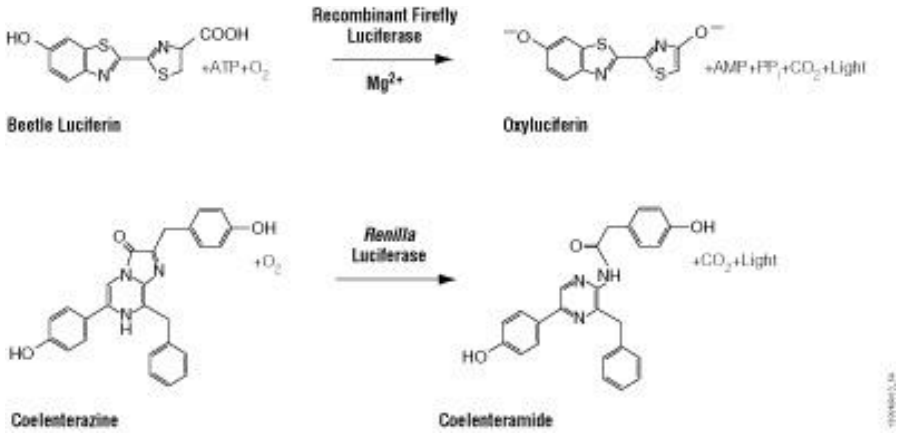

Figure 2-5. The photochemical reaction catalyzed by Firefly and Renilla Luciferase (Promega)

II. Luciferase reporter constructs

i. Gaussia and Cypridina luciferase constructs

The original plasmid pCMV-GLuc2 was obtained from New England Biolabs (NEB, Figure 2-6). We aimed to create seven constructs;

1. Gaussia luciferase construct without promoter as a negative control
2. Gaussia luciferase construct bearing 5kb upstream regions of mouse *Gapdh*
3. Gaussia luciferase construct bearing 5kb upstream regions of mouse *Penk*
4. Gaussia luciferase construct bearing 5kb upstream regions of mouse *Th*
5. Gaussia luciferase construct bearing 5kb upstream regions of human *GAPDH*
6. Gaussia luciferase construct bearing 5kb upstream regions of human *PENK*
7. Gaussia luciferase construct bearing 5kb upstream regions of human *TH*

Gaussia luciferase construct without promoter (1):

To create the negative control plasmid and to create a vector for cloning the amplified promoters we amplified the original plasmid with the following primers:

CMV_AscR- TAAGGCGCGCCGAAGCAGCGCAAAACGCCTAACCCTAAGC

CMV_PacF - GGCTACGACTCACTATAGGGAGACCCAAGC.

The amplification is performed by following PCR protocol: 30sec initial denaturation at 98°C, 20 cycles of 10 sec denaturation at 98°C, 20sec annealing at 69°C and 1min extension at 72°C, and 10min final extension at 72°C.

This deletes the CMV promoter and creates the unique AscI and PacI restriction sites. To create the negative control that lacks CMV promoter the amplified plasmid was phosphorylated by T4 polynucleotide kinase (NEB, M0201) and self-ligated.

Gaussia luciferase constructs bearing 5kb upstream regions of mouse and human *Gapdh*, *Penk* and *Th*(2-7):

To create the plasmids containing mouse and human *Gapdh*, *Penk* and *Th* promoters controlling the expression of the Gaussia luciferase, 5kb upstream regions of the each gene were amplified. These upstream regions were expected to cover the promoter sequence elements (putative promoter regions). The amplified plasmid and amplified genomic DNA fragments corresponding to these promoters were digested with AscI/PacI and ligated using T4 DNA Ligase (NEB, M0202). Amplification of the putative promoter regions for mouse and human *Gapdh*, *Penk* and *Th* genes was performed from genomic DNA using the the following primer pairs and Q5 polymerase (NEB, M0491). The amplification is performed by the following protocol: 30sec initial denaturation at 98°C, 20 cycles of 10 sec denaturation at 98°C, 20sec annealing at 69°C for mouse *Gapdh*, 65°C for mouse *Penk* and *Th*, 71°C for human *GAPDH*, 62°C for human *PENK* and 68°C for human *TH*, and 5min extension at 72°C, and 10min final extension at 72°C.

Mouse putative promoter regions:

Mouse *Gapdh* putative promoter region was amplified with the following primers giving 4907bp product from Chromosome 6 (positions 125165774 – 125170680; UCSC Genome Browser GRCm38/mm10)

MusGapdh_AscF - TAAGGCGCGCCTTAGGATGGATGGATGGATGGATGG

MusGapdh_PacR – TACTTAATTAATCCTCCCTCTCTTTGGACCCGCCTC

To amplify 4943 bp product from Chromosome 4 (positions 4138504-4143420; UCSC Genome Browser GRCm38/mm10) corresponding to putative *Penk* promoter region we used the following primers:

MusPenk_AscF - TAAGGCGCGCCAGGGTCTTTATCTATGTATCTTCAGC

MusPenk_PacR – TACTTAATTAAGAACACTGAAGTTCGCGGCTCGGGAGC

Mouse putative *Th* promoter was amplified with the following primers giving 4849bp product form Chromosome 7 (positions 142900015 – 142904863; UCSC Genome Browser GRCm38/mm10)

MusTh_AscF - TAAGGCGCGCCAGGAATAAGGCAGGCAGAG

MusTh_PacR – TACTTAATTAAGCCTCTTAAAGGCCAGGCTGACGTC

Human putative promoter regions:

Human *GAPDH* putative promoter region was amplified with the following primers. The product size is 4998bp from Chromosome 12 (positions 6528929 – 6533926; UCSC Genome Browser GRCh38/hg38).

HumGAPDH_AscF - TAAGGCGCGCCTCTCTCTGTCTTACAGGGCAACGCAATC

HumGAPDH_PacR - TACTTAATTAATCCCCATCTCCTGGCTCCTGGCATC

Human putative *PENK* promoter region was amplified with the following primers. The product size is 5040bp from Chromosome 8 (positions 56446735 – 56451774; UCSC Genome Browser GRCh38/hg38)

HumPENK_AscF - TAAGGCGCGCCGCTGTGAACTTTACATATGTTCTTAG

HumPENK_PacR - TACTTAATTAAGCCCTACGCCAGCCCCGCGCCGACGCCTTC

Human putative *TH* promoter region was amplified with the following primers. Product size is 5016bp from Chromosome 11 (positions 2171878 – 2176893; UCSC Genome Browser GRCh38/hg38).

HumTH_AscF - TAAGGCGCGCCGGTGTCCCTGGGAGCCAGGCTCTAG

HumTH_PacR – TACTTAATTAACCCACCTTCCCCTCCTTACATC

All restriction enzymes were purchased from NEB.

The resulting plasmids were verified by sequencing, using the following primers.

Table 2-2. Sequencing primers

construct	Sequence (5'-3)	Description
GLuc2 (without promoter)	TGTGCAGTCCACACACAGAT	gLuc-Rev1
	CCAGTTTGGAACAAGAGTCCA	gLuc-Rev2
	Rev3-CTGACAGCCGGAACACGG	gLuc-Rev3
	AGAAGGCGATAGAAGGCGAT	gLuc-Rev4
	CGCCTTTGAGTGAGCTGATA	gLuc-Rev5
	CTACCAGCGGTGGTTTGTTT	gLuc-Rev6
	CGAAGGAGCTAACCGCTTTT	gLuc-Rev7
MusPenk-GLuc2	TGGTCTGTATCACACATCTCTTCTG	mPenk-Fwd1
	TTTCCCTGTCTGAGAGATAAAGG	mPenk-Fwd2
	TTCTCAGAAACCTTACTGAACAGC	mPenk-Fwd3
	ACTGTCAACTGTTCGCTTGG	mPenk-Fwd4
	ACAAGCACTCCGCTCTCCT	mPenk-Fwd5
	AAAAAGATGAGCGCTTGGAG	mPenk-Fwd6
	TGCCTACTCTGTCCCTGGAT	mPenk-Fwd7
	ACGCTCTTCCAGTAACCTGC	mPenk-Fwd8
	GGGCAGAAGGACTAGAAGGC	mPenk-Rev1
MusTh-GLuc2	TCCTCAGACTTCCATCCACC	mTh-Fwd1
	TTGTGCGTGCATAGGTTTGT	mTh-Fwd2
	ATTACAGGGGTGCAAAGGG	mTh-Fwd3
	GTGCCCACAGATGCTTTAGA	mTh-Fwd4
	GGGCTGTGGAGAACACTCAG	mTh-Fwd5
	GCTCTGTCCTTTGGCACTTC	mTh-Fwd6
	CCAGTGCCAGCACATACACT	mTh-Fwd7
	TTATCCCTAAGTGTCTCCTATCGAC	mTh-Fwd8
	CACCCAGGAGACTGAGATGG	mTh-Rev1
MusGapdh-GLuc2	AAGAGAGAGTCCCTGGTGGC	mGapdh-Fwd1
	AGATTCCCCTGCCTCTGTCT	mGapdh-Fwd2
	GTCCCCTTGCCTTTCTTTTC	mGapdh-Fwd3
	TGGTTTTAACATGGAAATGGC	mGapdh-Fwd4
	TGCTGAGTCACTTGGAGCAG	mGapdh-Fwd5
	GGAGTGAAGAATCCCGGTCT	mGapdh-Fwd6
	CCTGGCATTTTCTTCCACTC	mGapdh-Fwd7
	ACAGCCCGGTATGCTCCAT	mGapdh-Fwd8
	CGCTCAGTTCTACAGGGAGG	mGapdh-Rev1
HumPENK-GLuc2	ATTCACCATCACTTGGGAGC	hPenk-Fwd1
	AATTTTTCATAATAGGACTTGCTTT	hPenk-Fwd2
	GGGCAGACAGAAATGGCTT	hPenk-Fwd3
	CTGTTTCTCTCTCCCCTGACA	hPenk-Fwd4
	TGTTTTCCTGCTCAGAGGGT	hPenk-Fwd5
	GGGAAAGCGTGTCTTAATGG	hPenk-Fwd6
	ATGCGGAGAAACTTGATCCT	hPenk-Fwd7
	CACAGCACAGATGTTTGCAC	hPenk-Rev1

HumTH-GLuc2	TACCTGTGTCATGGGTGCTC	hTH-Fwd1
	ACAGCAAGGGCTCCTCAGAC	hTH-Fwd2
	GGAAAGACCAGTGTCTTGGG	hTH-Fwd3
	ACTCACCTCCACAGGGGTC	hTH-Fwd4
	CTTTGGGGAACACTGTGGAG	hTH-Fwd5
	GGTTCTTCTCCAGGAGGGAC	hTH-Fwd6
	GCCCTCCTGGGACATTCT	hTH-Fwd7
	AATGCAGGCATCTGTGTGAG	hTH-Rev1
HumGAPDH-GLuc2	GGACAAGCAGACAGAGAGCC	hGapdh-Fwd1
	CAATTCTTGTTTGTTTGTTTTTAAT	hGapdh-Fwd2
	GTAAGGCAGCCTGTGCGG	hGapdh-Fwd3
	TGTTTCCCTTGTAAAATATTTGTCTG	hGapdh-Fwd4
	CCTGCACAGTGACCAGACAG	hGapdh-Fwd5
	TTTGCGGGGAGAAGACAGTA	hGapdh-Fwd6
	CCCAAGACCTCTTTTCCCAC	hGapdh-Fwd7
	GCTCAGCACAAAGAACCCTC	hGapdh-Rev1

Cypridina luciferase driven by SV40 as an internal control was purchased from NEB (N0318S, Figure 2-6).

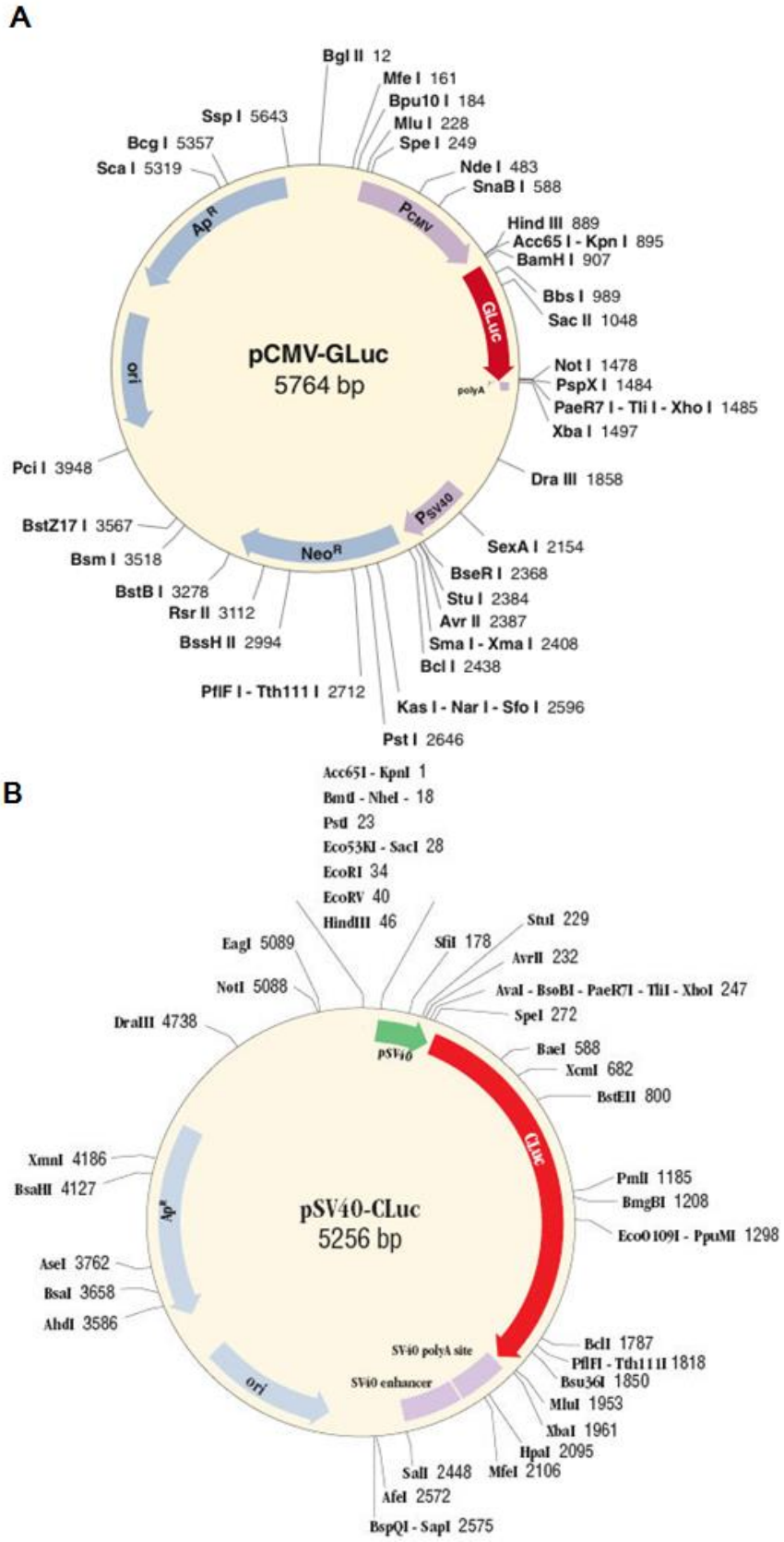

Figure 2-6. The maps of Luciferase reporter constructs purchased from NEB. (A) Gaussia luciferase construct bearing CMV promoter. (B) Cypridina luciferase construct bearing SV40 promoter. (NEB)

ii. Firefly and Renilla luciferase report constructs

The empty vectors were purchased from Promega; pGL4.14 for Firefly luciferase (FLuc) and pGL4.79 for Renilla luciferase (RLuc)(Figure 2-7). To insert the amplified promoter, the vectors were double digested with the following Restriction Enzymes (NEB) for each construct (Table 2-3). The vector digested with EcoRV (for mTh-Fluc) was used for the ligation straight after the digestion. The other digested vectors were dephosphorylated by Alkaline Phosphatase, Calf Intestinal (NEB, M0290).

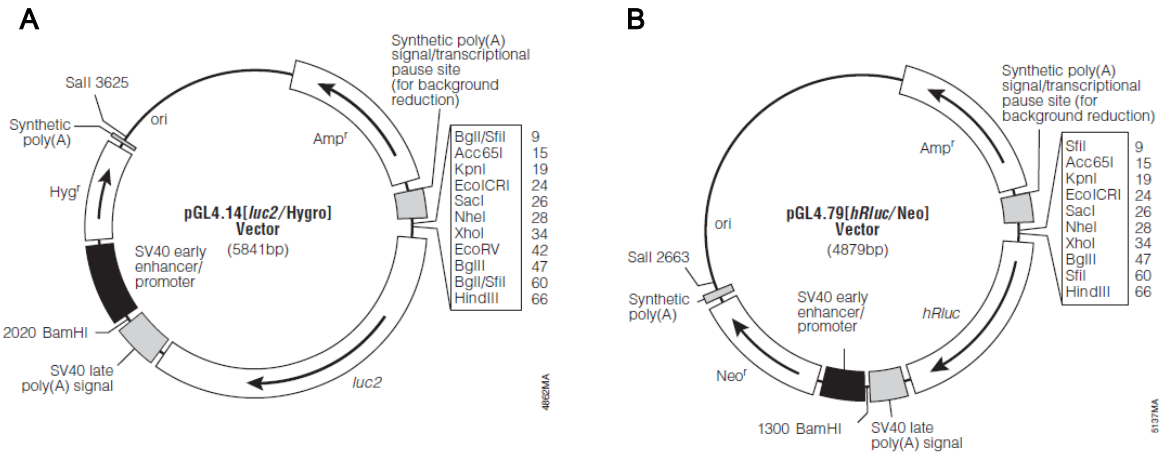

Figure 2-7. Firefly luciferase construct and Renilla luciferase construct purchased from Promega. (A) Firefly luciferase construct (B) Renilla luciferase construct (Promega)

Table 2-3. Restriction enzymes for Firefly and Renilla lucifase constructs

Target construct	Restriction Enzyme
SV40-RLuc	Kpn I / Bgl II
CMV-FLuc	Kpn I / Xho I
mPenk-FLuc	Nhe I / Xho I
mTh-FLuc	EcoRV
mGapdh-FLuc	Kpn I / Xho I

To create the plasmids containing CMV and mouse *Penk* and *Gapdh* promoters controlling the expression of the FLuc and SV40 promoter controlling the expression of RLuc, amplified genomic DNA fragments corresponding to these promoters were digested with the same restriction enzyme stated above (Table 2-3) and ligated with the digested vectors (Table 2-3) using T4 DNA Ligase (NEB, M0202). To create the plasmids containing mouse *Th* promoter controlling the expression of the FLuc, the genomic DNA fragments were ligated

straight after the amplification of the promoter region using Gibson Assembly Master Mix (NEB, E2611).

Amplification of the promoter regions for CMV, SV40 and mouse *Penk*, *Th* and *Gapdh* genes was performed from the plasmids which were created for Gaussia luciferase construct stated above or SV40-CLuc (NEB) using the primer pairs listed below and Q5 polymerase (NEB, M0491) for mouse Gapdh and SV40, KAPA HiFi DNA Polymerase (KAPA Biosystems, KK2602) for mouse Penk, and CMV, and Phusion High-Fidelity DNA Polymerase (NEB, M0530) for mouse *Th*. The amplification is performed using the following protocol: Q5 polymerase; 30sec initial denaturation at 98°C, 30 cycles of 10 sec denaturation at 98°C, 20sec annealing at 69°C for mouse Gapdh, 59°C for SV40, 5min extension for mouse Gapdh and 1min extension for SV40 at 72°C, and 10min final extension at 72°C. KAPA HiFi DNA Polymerase; 3min initial denaturation at 95°C, 30 cycles of 20 sec denaturation at 98°C, 15sec annealing at 67°C for mouse Penk, 71°C for CMV and 5min extension for mouse Penk and 2min extension for CMV at 72°C, and 5min for mouse Penk and 2min for CMV of final extension at 72°C. Phusion High-Fidelity DNA Polymerase; 30sec initial denaturation at 98°C, 30 cycles of 10 sec denaturation at 98°C, 30sec annealing at 72°C, 5min extension at 72°C, and 10min final extension at 72°C.

SV40_KpnIF- TAAGGTACCCCGATCGATCGCTAGCTGCA

SV40_BglIIR- TAAAGATCTGGTTCTACCTCCTACTAGTTTACCA

CMV_KpnIF- TAAGGTACCGCTTAGGGTTAGGCGTTTTGCGCTGCTTCG

CMV_XhoIR- TAACTCGAGGCTTGGGTCTCCCTATAGTGA

MusPenk_ NheIF - TAAGCTAGCAGGGTCTTTATCTATGTATCTTCAGC

MusPenk_ XhoIR - TAACTCGAGGAACACTGAAGTTCGCGGCTCGGGAGC

MusTh_GAF-
AGCTCGCTAGCCTCGAGGATTTTGGAAGGACCAGAGCACCTGAG

MusThpr_GAR-
CGCCGAGGCCAGATCTTGATCCTCTTAAAGGCCAGGCTGACGTC

MusGapdh_KpnIF- TAAGGTACCTTAGGATGGATGGATGGATGGATGG

mGapdh_XhoIR- TAACTCGAGTCCTCCCTCTCTTTGGACCCGCCTC

The resulting plasmids were verified by sequencing, using the above primers (Table 2-2. Sequencing primers).

2.2.5 Transient transfection

I. Cell lines

Regarding transient transfection in HEK293 and Neuro2A cells with *Gaussia* and *Cypridina* luciferase constructs, the cells were co-transfected with three constructs at about 80-95% confluency using lipofectamine 2000 (Thermo Fisher Scientific, 11668027); *Gaussia* luciferase reporter constructs, *Cypridina* luciferase construct, and $hNa_v1.7$ or IRES-DsRED2 in pcDNA3 as an empty vector (both plasmids were kindly provided by Dr. James Cox, see (Cox et al., 2006)). The *Cypridina* luciferase construct was used as an internal control for cell number and transfection efficiency and $hNa_v1.7$ or IRES-DsRED2 in pcDNA3 as an empty vector were used to assess whether $Na_v1.7$ affects the transcription of *Gaussia* luciferase driven by each promoter. A total of three micro grams of plasmid DNA (one micro gram per construct) was combined with 15 µl of lipofectamine 2000 in 500 µl of Opti-MEM (GIBCO 31985-062). The mixture of DNA and lipofectamine 2000 in Opti-MEM was added into the cells at 80-95% confluency in 35mm dish. The cells were kept 5 hours at 37°C in 5% CO_2 and 10% of cells were split into a well in 24 well plate.

Regarding the transient transfection with $hNa_v1.7$ in Neuro2A stable cell line, 0.5 µg of $hNa_v1.7$ or IRES-DsRED2 in pcDNA3 were combined with 2.5 µl of lipofectamine 2000 in 200 µl of Opti-MEM. The mixture of DNA and lipofectamine 2000 in Opti-MEM was added into the cells seeded one day before the transfection ($2x10^5$ cells/well) in 24 well plate. The cells were kept 5 hours at 37°C in 5% CO_2 and 20% of cells were split into a well in 96 well plate.

II. Primary cultured DRG neurons

Primary cultured DRG neurons were re-suspended in electroporation buffer (10 µl per reaction, Neon kit, Invitrogen, MPK1096) together with 0.6 µg of mPenk-Gaussia luciferase (mPenk-gLuc) or Empty-Gaussia luciferase construct (ϕ-cLuc) and 0.6 µg SV40-Cypridina luciferase construct (SV40-cLuc) as an internal control. Regarding the Firefly and Renilla luciferase constructs, 0.6 µg of mPenk-Firefly luciferase (mPenk-fLuc) and SV40-Renilla luciferase construct (SV40-rLuc) were re-suspended with DRG neurons in electroporation buffer. Neurons were subsequently electroporated using a 2 x 20 ms 1100V pulses protocol and immediately plated onto poly-L-lysine/laminin coated wells after electroporation, in DMEM containing 10% FBS and 125ng/ml nerve growth factor (NGF). Neurons were kept at 37°C in 5% CO_2 and luciferase assays were performed at 72 h after transfection.

2.2.6 Generation of Neuro2A stable cell line

We aimed to generate five stable cell lines: CMV-fLuc, φ-fLuc, mGapdh-fLuc, mPenk-fLuc and mTh-fLuc, which are all together with SV40-rLuc. The cells were co-transfected with each Firefly Luciferase construct and Renilla Luciferase driven by SV40 (SV40-rLuc) construct using Lipofectamin 2000. A total of two micro grams of plasmid DNA (one micro gram per construct) was combined with 20 µl of lipofectamine 2000 in 500 µl of Opti-MEM (GIBCO 31985-062). The cells were kept overnight at 37°C in 5% CO_2 and were split into a T75 flask. The cells were cultured with DMEM with 10% FBS for 3 days. Next, the cells were reseeded in DMEM FBS10% with 300 µg/ml Geneticin (GIBCO 10131-027) and 300 µg/ml Hygromycin B (Invivogen, ant-hg-1). This selection media was replaced twice a week for approximately 3 weeks. To generate stable cell lines derived from single cells, the cells were re-suspended in medium without serum and sorted into single cells using Flow Cytometry (BD FACSArray, SORP) with help from Dr Ayad Eddaoudi, UCL Institute of Child Health. Single cells were cultured in 96 well plates without Geneticin for 10 days, followed by media replacement with DMEM FBS10% with 300 µg/ml Geneticin and 300 µg/ml Hygromycin B twice a week for 3 weeks until the cells were around 70% confluent. The single clones were then detached with a pipette and transferred into 24 well plates and cultured with DMEM FBS10% with 300 µg/ml Geneticin and 300 µg/ml Hygromycin B with Antibiotic-Antimycotic (GIBCO 15240-062). The media was replaced twice a week for 1 week and the clones were validated by luciferase assay and immunostaining.

2.2.7 Immunocytochemistry

The immunocytochemistry on the cells were performed by muself. The spinial cord immunocytochemistry was performed by Dr. Vanessa Pereira at Molecular Nociception Group, WIBR, UCL.

The cells were cultured on glass coverslips coated with poly-L-Lysine (SIGMA P9155-5MG). At the appropriate confluency, cells were fixed with 4% PFA (paraformaldehyde) in PBS (Phosphate Buffered Saline) for 15min followed by permeabilization with 0.1% Triton X-100 for 5min at room temperature. The cells were blocked with 3% BSA (Bovine Serum Albumin, SIGMA A7906) in PBS for 1hr at room temperature and incubated with both anti-Firefly raised in goat (abcam ab181640, 1:750), anti-Renilla raised in rabbit (abcam ab185926, 1:750) in 3% BSA in PBS for overnight at 4°C. The cells were incubated with a corresponding secondary antibody for 45min at room temperature; Alexa488 Donkey anti-Goat (Invitrogen A11055, 1:1000) or Alexa594 Donkey anti-Rabbit (Invitrogen A21207, 1:1000) in 3% BSA in PBS. The stained cells were imaged using a Leica microscope (LEITZ DMRB, Germany).

Regarding the immunocytochemistry in the spinal cord section of mice, mice were anaesthetized with intraperitoneal pentobarbital and transcardially perfused with PBS (0.01% Heparin) and ice-cold paraformaldehyde (4% in PBS). Lumbar spinal cord fragments were dissected and post fixed for at least 1h in paraformaldehyde and transferred to a sucrose solution (0.3M) for cryoprotection. Tissues were embedded in optical coherence tomography mounting medium, frozen in liquid nitrogen and stored at -80°C. Free-floating sections (30mm) were blocked 1h in PBS with 10% goat serum (Sigma) and 0.1% Triton X-100, followed by overnight incubation at 4°C in Rabbit anti-met-enkephalin primary antibody (1:500 in PBS with 3% goat serum and 0.1% Triton X-100, AB5026, Millipore). Co-staining with Isolectin B4 biotin conjugate (IB4, Sigma) was used to label spinal cord lamina II. Corresponding monoclonal goat anti-rabbit met- enkephalin (1:1,000 Alexa Fluor 488, A11017, Life Technology, UK) or anti-biotin (1:1,000 Streptavidin Alexa Fluor 568 conjugate, S-11226, Life Technology) secondary antibodies were used. Spinal cord slices were imaged using a Leica TCS SP8 spectral confocal microscope (Leica Microsystems, Germany) using laser lines 488nm (Met-enk) and 552nm (IB4) at an acquisition frequency of 200Hz (1,024 x 1,024 format). The laser power and acquisition frequency was kept constant between all respective samples. The relative fluorescence for met-enkephalin was calculated by taking the mean fluorescence of the entire dorsal horn (indicated by IB4 staining) and subtracting background fluorescence (LAS AF 3

analysis software). The relative fluorescence for each animal was taken as an average of at least three spinal sections. Three animals were used per group.

2.2.8 Luminescence measurement

I. Gaussia and Cypridina Luciferase assay

Transfection of Gaussia luciferase, under the control of the mouse or human *Gapdh*, *Penk* and *Th* promoter or without promoter, and Cypridina luciferase, driven by SV40, was performed following the protocol described in the previous section (2.2.5). Luminescence obtained by Gaussia and Cypridina luciferase was performed with Gaussia and Cypridina Luciferase kits (NEB, E3300, E3309) according to manufacturer's instructions. Briefly, Gaussia and Cypridina assay solution was prepared immediately or 30min before performing the assay, respectively. The supernatant containing the secreted Gaussia and Cypridina luciferase was collected 72 h after the transfection and 20ul of the supernatant was transferred into 2 wells per sample in 96well white-bottom plate (Thermo Scientific, 136101). Bioluminescence was measured upon addition of 50ul of Gaussia or Cypridina assay solution. The activity was monitored immediately after the addition of the solution in a FLUOstar Omega microplate reader (BMG LABTECH GMBH, Germany). The relative light units of two different reporter cell clones in at least three independent experiments were measured for Gaussia luciferase and Cypridina activity. Gaussia relative light units were normalized to Cypridina and are presented as x-fold over mock and are presented as mean ± SEM. Student's t-test was performed with *$p < 0.05$, **$p < 0.01$, ***$p < 0.001$ as statistically significant.

II. Firefly and Renilla Luciferase assay

The Dual-Luciferase® Reporter Assay System (Promega E1910) was used for DRG neurons and selecting Neuro2A clones stably expressing Firefly and Renilla driven by each promoter according to manufacturer's instructions. Briefly, the cells were harvested in a 48 well plate and the growth media was removed prior to the measurement. The cells were washed with 1x PBS and lysis buffer (provided by the Dual-Luciferase® Reporter Assay System kit) was added. The cell lysate were gently shaken for 15min at room temperature and transferred into 96well white-bottom plate. To measure Firefly luciferase activity, the

luminescence was measured immediately after adding 100 µl of luciferase substrate in luciferase assay solution. Renilla luciferase activity was measured by adding 100 µl of Stop&Glo Reagents followed by the firefly measurement. Since the luminescence in this assay drops rapidly, automatic injector was used to measure both Firefly and Renilla luciferase activity; pump speed 300 µl/s, shaking for 1 sec at 100rpm, and measurement start time was 0.5 sec after shaking.

Dual-Glo® Luciferase Assay System (Promega E2920) was used for overexpressing $hNa_v1.7$ and monensin or TTX treatment in Neuro2A clones stably expressing Firefly and Renilla driven by each promoter, according to manufacturer's instructions. Briefly, for measuring the effect of monensin/TTX, Neuro2A stable clones were seeded at $2x10^4$ cells/well in 96 well plate one day before adding the agents. The agents were then added and the cells were cultured for appropriate time. For overexpressing $hNa_v1.7$ in Neuro2A stable cells, the cells were cultured in 96 well plate after the transfection for appropriate time. Some of the growing media was removed to have remaining media 75 µl/well. Then 75 µl of Dual-Glo Reagent that is equal volume to that of culture media was added. The cells were gently shaken for 10min at room temperature in foil to allow for cell lysis to occur, then the firefly luminescence was measured. Dual-Glo Stop & Glo Reagent equal to the original culture medium volume (75 µl) was added to each well and gently mixed by shaking in a rocker for 10min at room temperature in foil. Then Renilla luminescence were measured. All luciferase activities was monitored by FLUOstar Omega microplate reader. Student's t-test was performed with $*p < 0.05$, $**p < 0.01$, $***p < 0.001$ as statistically significant.

2.2.9 Behaviour tests

All behavioural experiments were performed by an experimenter blind to both genotype and treatment. Naloxone hydrochloride dihydrate ($2mgkg^{-1}$ intraperitoneally, Sigma) was administered 30 min before behavioural assessment.

I. Randall–Selitto test

This test was performed by Dr. Vanessa Pereira, Ms. Sonia Santana, Miss Queensta Millet at Molecular Nociception Group, WIBR, UCL and Dr. Michael Minett formerly at Molecular Nociception Group, WIBR, UCL.

The Randall Selitto test is used to assess noxious mechanical pain thresholds and the pressure can be applied on the tail and paw of animals. In this project, we used tail to assess the mechanical pain thresholds. The test was originally described by Randall and Selitto to measure inflammatory pain thresholds by application of increasing pressure on a rat paw (Randall and Selitto, 1957). Later this method was modified by Takesue et al. (Takesue et al., 1969). Prior to testing, animals were restrained in a clear plastic tube with an acclimatisation period of approximately 1-2 minutes. A 3 mm^2 blunt conical probe is applied to the tail with increasing pressure until the animal exhibits a painful response using a 500 g cutoff. The responses include struggling, withdrawal of tail or paw or vocalisation. The test was repeated 3 times for each animal.

II. Hargreaves' test

Performed by Dr. Vanessa Pereira, Ms. Sonia Santana, Miss Queensta Millet at Molecular Nociception Group, WIBR, UCL and Dr. Michael Minett formerly at Molecular Nociception Group, WIBR, UCL.

The Hargreaves' test was performed to assess spinal reflex responses to noxious thermal stimulation. This method was originally designed to assess thermal nociception in inflammatory pain states (Hargreaves et al., 1988). Animals were acclimatised in an enclosure with a glass base for a minimum of 60 minutes. A radiant heat light source at a ramp of 2.25 ℃ s^{-1} was applied to the plantar surface of the hind paw with a cut off time of 20 seconds. Urine and faeces were removed as much as possible from the glass floor of each test compartment. The stimulus was stopped when a painful response was observed (licking, lifting or shaking the paw) and the latency to paw withdrawal (in seconds) was recorded. Three recordings were made from each animal and an average taken.

III. Human behaviour

Performed by Dr. Flavia Mancini, Professor Giandomenico Iannetti, and Professor Raymond MacAllister at UCL

All participants gave written informed consent. The study was approved by the UCL Research Ethics Committee. The CIP patient was a 39-year-old woman. Healthy controls were age matched (N¼3, mean age±s.d.: 38.7±3.2). Perception of phasic and tonic radiant heat was assessed at baseline and during intravenous administration of saline or naloxone (12 mg), in a randomized order. Psychophysical assessment was carried out by an experimenter blind to the pharmacological condition. Radiant heat was generated by an infrared neodymium:yttrium-aluminum-perovskite laser with a wavelength of 1.34 mm (Electro- nical Engineering, Italy). This method was used to selectively activate free nerve endings in the superficial layers of the hairy skin. The laser fluency was 0.6 Jmm^2 and the duration of each laser pulse was 9 ms. After each of the ten pulses delivered at random intervals (15–40 s) to the forearm, participants were asked to verbally report whether they detected any stimulus. Tonic radiant heat was generated by a CO_2 laser, whose power is regulated using a feedback control based on an online measurement of skin temperature at the site of stimulation (Laser Stimulation Device, SIFEC, Belgium). On each trial, tonic radiant heat was delivered to the forearm for 25 s, at one of three possible temperatures: 42, 45 and 48 °C. Participants were asked to rate the intensity of the thermal sensation on a visual analogue scale throughout the trial (0=no sensation, 100=worst pain imaginable). Three trials per stimulus temperature were given on each session (baseline, saline and naloxone) in a randomized order.

2.2.10 Data analysis

Data were analyzed using Microsoft Excel, and Student's t-test was performed with *p < 0.05, **p < 0.01, ***p < 0.001 as statistically significant for real-time qRT-PCR and luciferase assay.

Statistical differences between KOs and littermates, as well as the effects of naloxone in each genotype group, were determined using a two-way analysis of variance using GraphPad Prism (GraphPad Software, Inc). Data are expressed as mean±s.e.m. *P<0.05, **P<0.01 and ***P<0.001 significance levels indicate differences between KOs and littermates using a

Student's t-test and $P<0.05, $$P<0.01 and $$$ P<0.001 indicate differences following naloxone administration using a paired t-test by GraphPad Prism (GraphPad Software, Inc).

2.3 RESULTS

2.3.1 Expression of *Penk*, *Ceacam10*, *Th* and *Tmem173* in $Na_v1.7$ knockout mice

Performed by Dr. Vanessa Peraira at Molecular Nociception Group, WIBR, UCL. and myself

As stated in the introduction, loss-of-function mutations in *SCN9A* encoding $Na_v1.7$ is linked to complete insensitivity to pain, indicating the essential role of $Na_v1.7$ in pain and an excellent drug target. However, there are not currently available drugs targeting this channel on markets and some studies have demonstrated that some selective $Na_v1.7$ blockers are not analgesic (Schmalhofer et al., 2008, Lee et al., 2014). Although a $Na_v1.7$ antagonist, raxatrigine, from Convergence are now in Phase lll clinical trial, the impression of some clinical trials' results is that selective $Na_v1.7$ inhibitors exert less potent analgesic (Emery et al., 2016, Lawrence, 2016, Convergence Pharmaceuticals, 2016). One of the possible reasons for this elusive effect may be that $Na_v1.7$ is correlated with other roles in nociceptive processing. Interestingly, calcium channels have been reported to function as a transcription factors, distinct from their role in neuronal excitability (Gomez-Ospina et al., 2006, Du et al., 2013, Tadmouri et al., 2012). Thus, we asked if $Na_v1.7$ has an additional role to that of propagating action potentials. Previously we analysed the pattern of gene expression in the sensory neurons of dorsal root ganglia (DRG) from $Na_v1.7$, $Na_v1.8$ and $Na_v1.9$ KO mice using microarrays. We used conditional $Na_v1.7$ KO mice and global $Na_v1.8$ and $Na_v1.9$ KO mice. The conditional $Na_v1.7$ KO mice where $Na_v1.7$ is deleted in all sensory neurons were generated by crossing floxed (Scn9a) $Na_v1.7$ mice with Advillin-Cre mice (Minett et al., 2012). Surprisingly, we found more marked alteration in gene expression in $Na_v1.7$ null mice than in $Na_v1.8$ or $Na_v1.9$ null mice. The most dramatically down-regulated gene in $Na_v1.7$ null mice was *Ceacam10*, carcinoembryonic antigen-related cell adhesion molecule 10 (fold change 18.94). The second down-regulated gene in $Na_v1.7$ null mice was *Hal*, histidine ammonia lyase (fold change 5.01). The mRNA levels of Tyrosine hydroxylase (*Th*), which catalyses the conversion of the amino acid L-tyrosine to L-3,4-dihydroxyphenylalanine (L-DOPA), were also significantly down-regulated (fold change 4.22). Interestingly, mRNA level of *Penk*, the precursor of Leu and Met-enkephalin was upregulated in $Na_v1.7$ null mice (fold change 3.84),

but not in $Na_v1.8$ and $Na_v1.9$ null mice. Also, mRNA level of *Tmem173*, *Transmembrane protein 173*, was also significantly up-regulated in $Na_v1.7$ null mice (fold change 2.82).

Among these top 5 dysregulated genes, we were interested in investigating the 4 genes further; two of each down- or up-regulated genes. *Ceacam10* is a little characterised gene; despite exclusive expression in the maternal placenta surrounding the implantation site, *Ceacam10* null mice are viable, fertile, and exhibit no obvious phenotype (Finkenzeller et al., 2003). We wondered if *Ceacam10* may play a role in pain sensation. Down-regulation of *Th* in $Na_v1.7$ null mice could be also interesting; several studies have supported that *TH* and L-DOPA may be linked to pain sensation (Skinner et al., 2011, Galbavy et al., 2013). Although *Hal* showed larger fold change than *Th*, we excluded this gene for the first selection. This selection came from two reasons. Firstly, this gene has not been studied in pain therefore *Th* would be more interesting target on analgesic effects due to loss of $Na_v1.7$ function. Secondly, targeting this gene for pain relief might cause some side effects. This gene is a cytosolic enzyme which play a role in histidine catabolism, catalyzing the nonoxidative deamination of L-histidine to trans-urocanic acid (Suchi et al., 1995). The mutations within this gene have been linked to histidinemia (Kawai et al., 2005); this disease is an autosomal recessive metabolic disorder characterized by increased levels of histidine in blood, urine, and cerebrospinal fluid, and decreased levels of the metabolite urocanic acid in blood, urine, and skin cells. Patients suffering from histidinemia often showed mental retardation and speech defects (Levy et al., 2001) and some clinical features demonstrated developmental disorders such as perinatal events (Ishikawa, 1987). We therefore chose *Th* instead of *Hal* for the first selection. Regarding the up-regulated genes, we selected *Tmem173,* also known as STING (STimulator of INterferon Genes) for the further analysis because it is the second up-regulated genes in DRG in conditional $Na_v1.7$ KO mice and has been well-documented in immunology; *Tmem173* activated both the NF-kappa-B and IRF3 (Interferon Regulatory Factor 3) transcription pathways to induce expression of IFN-alpha (Interferon, alpha-1) and IFN-beta (Interferon, beta-1) (Ishikawa and Barber, 2008). Also, *Tmem173* is required to initiate effective type I interferon (IFN) production in antigen presenting cells such as macrophages and dendritic cells after infection (Ishikawa et al., 2009). Although the role of Tmem173 in neuronal cells have not examined, we wondered if *Tmem173* could also have an essential role in inflammatory pain. Of particular interest of this result is up-regulation of *Penk*, the precursor of Met-enkephalin and Leu-enkephalin. Enkephalins are well-characterised opioid peptides. The importance of enkephalin in pain has been well documented (Chu Sin Chung and Kieffer, 2013). Up-regulation of endogenous opioids in loss of $Na_v1.7$ function could be an important factor to cause analgesia.

To confirm this microarray result in $Na_v1.7$ null mice, real-time qRT-PCR was performed to detect the expressions of *Ceacam10*, *Penk*, *Th* and *Tmem173* (Figure 2-8) in DRG of $Na_v1.7^{Adv}$ knockout mice. These $Na_v1.7$ floxed Advillin Cre mice enable us to knockout $Na_v1.7$ in all sensory neurons in DRG (Minett et al., 2012). Two points must be taken into consideration when measuring mRNA expression; age and sex. The mice we used were 6 to 12 weeks as we wanted to examine the expression level in adult mice since postnatal development may affect pain pathways (Tadros et al., 2015). In addition to developmental effects, several studies have suggested sex differences in pain (Mogil, 2012, Bastos et al., 2013). Therefore, female and male mice were separately analysed (Figure 2-8). The expression level of *Ceacam10* was dramatically down-regulated in $Na_v1.7$ KO mice compared to WT mice in both female and male mice (Figure 2-8A, fold change 16.7 for both female and male). This result is consistent with the microarray data. Up-regulation of *Penk* (fold change 3.47 for female and 3.04 for male) also corresponds to the microarray data (Figure 2-8B). However, the data showed no significant difference between male and female (Figure 2-8b). The mRNA levels of *Th* was down-regulated in qPCR results (fold change 5.26 for female and 4.17 for male), which was consistent to the microarray data (Figure 2-8C). Up-regulation of *Tmem173* was also observed; the fold change for female was 2.07, and for male was 2.82 (Figure 2-8D). These present real-time qPCR results supported the microarray data (Table 2-4).

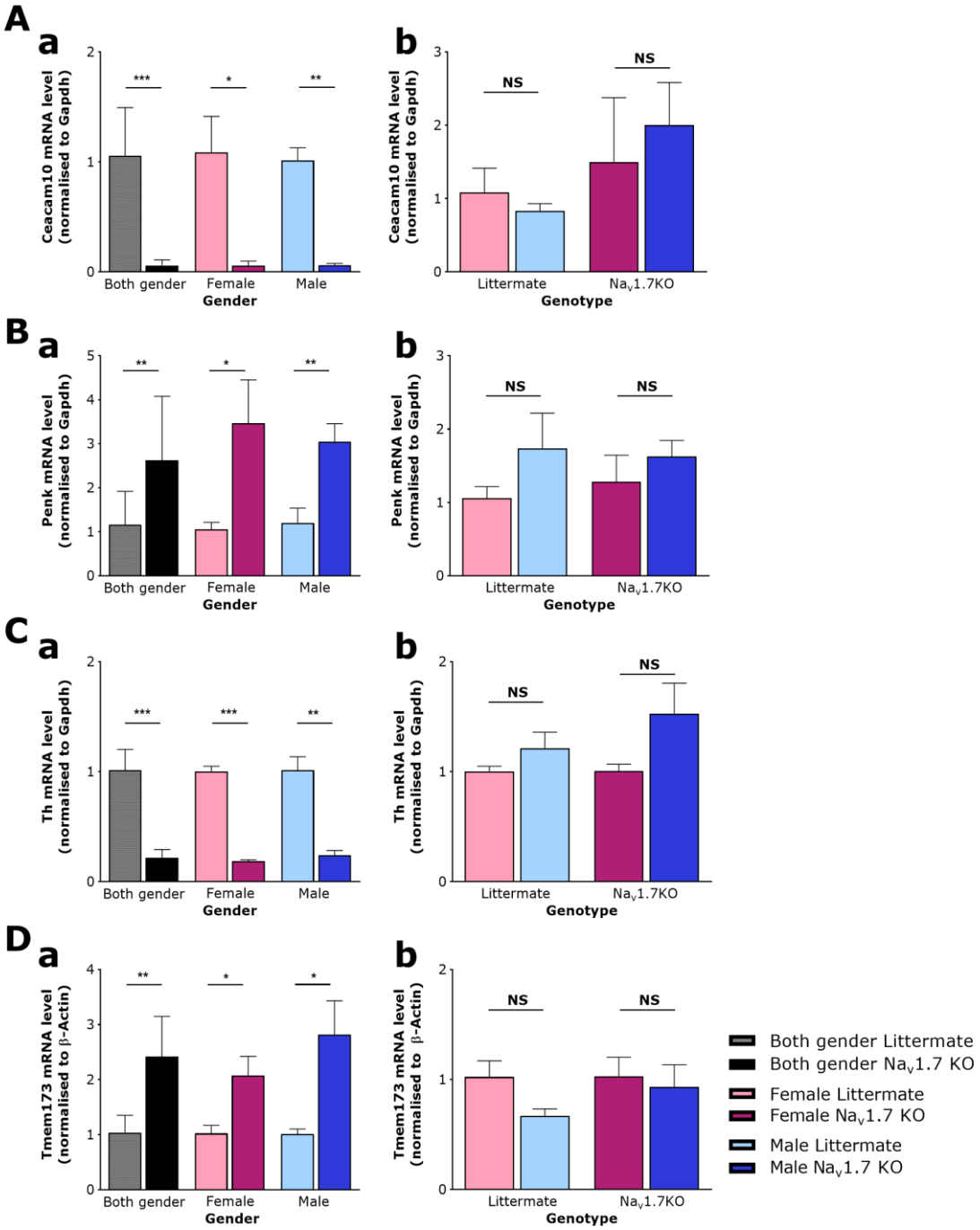

Figure 2-8. Real-time qRT-PCR analysis of mRNA expression in DRG in floxed Na$_v$1.7 littermates control relative to *Gapdh* or *β-Actin*. (a)Comparison between Na$_v$1.7KO and littermates. (b) Comparison between female and male mice.（A）The mRNA level of *Ceacam10* was markedly down-regulated in both gender (n=3 for each gender). (B) mRNA level of *Penk* was significantly up-regulated in both gender (n=6 for each gender). (C)(D)The mRNA levels of *Th* (C) and *Tmem173* (D) were down- or up- regulated, respectively (n=3 for each gender). Relative expression levels of mRNA were calculated using the comparative ΔΔCt (Ct) method. All results are shown as mean ± SEM. *P<0.05, **P<0.01 and ***P<0.001 significance levels indicate differences between KOs and littermates control using a Student's t-test. The data is collected by myself.

Table 2-4. Summary of microarray and real-time qPCR results in DRG of $Na_v1.7$ KO mice.

	Ceacam10	*Penk*	*Th*	*Tmem173*
Fold change in microarray	-18.94	+3.84	-4.22	+2.82
Fold change in Real-time qPCR (Female/Male)	-16.7/-16.7	+3.47/+3.04	-5.26/-4.17	+2.07/+2.82

As stated above, *Penk*, the precursor of Met-enkephalin and Leu-enkephalin could be one of the most interesting genes to explore further since the importance of enkephalin in pain has been well documented (Chu Sin Chung and Kieffer, 2013). The link between $Na_v1.7$ and endogenous opioids could provide a new insight into pain therapies. Therefore, we investigated if the protein levels of enkephalin were also up-regulated. In L5-L6 spinal cord, where the central terminals of primary afferents were located, Met-enkephalin immunoreactivity was strongly enhanced in $Na_v1.7$KO mice ($Na_v1.7^{Adv}$) compared with littermate control mice (Figure 2-9). The increase in immunoreactive Met-enkephalin was more than two fold (Figure 2-9B). This result suggested that Met-enkephalin levels were up-regulated as a result of the loss of $Na_v1.7$ function.

These real-time qPCR and immunohistochemistry data suggested that dramatic down-regulation of a little characterised gene, *Ceacam10*, and up-regulation of *Penk* due to the loss of *Scn9a* in DRG. The expression level of *Th* was markedly down-regulated and *Tmem173* was also up-regulated in DRG in $Na_v1.7$ null mice. The expression level of Met-enkephalin in the spinal cord was up-regulated in $Na_v1.7$ KO mice. The next question is if these genes are associated with pain behaviour. The first attempt was to narrow down the genes of interest to explore if they are associated with pain behaviour. Although dysregulation of *Th* and *Tmem173* might be important for pain therapies, *Penk* and *Ceacam10* were settled on for the further investigation in pain behaviour; *Penk* was selected since endogenous opioids have been reported to play a role in pain behaviour, and the link between $Na_v1.7$ and endogenous opioids could have an essential factor of analgesia in loss of $Na_v1.7$ function. *Ceacam10* was the most significantly dysregulated in $Na_v1.7$KO mice; however, little is known about this gene. This gave an idea that *Ceacam10* could be associated with pain sensation. Therefore the pain behaviour tests for these genes were examined, addressed in the next section (2.3.2).

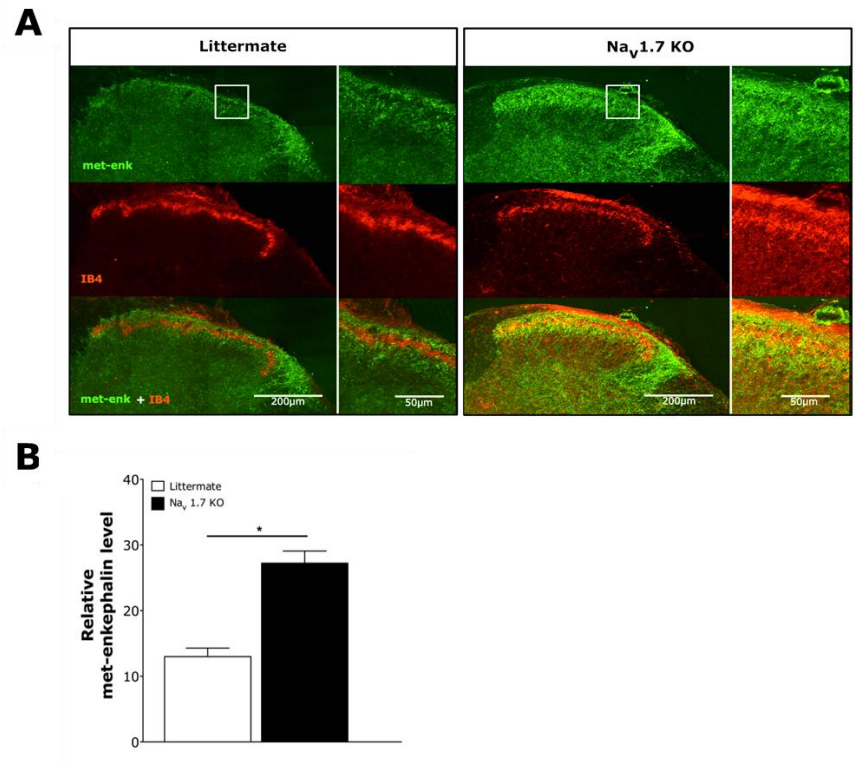

Figure 2-9. Met-enkephalin levels in L5–L6 spinal cord sections in floxed $Na_v1.7$ littermates control and $Na_v1.7$ KO ($Na_v1.7^{Adv}$) mice. (A) The sections were double-labelled with met-enkephalin (Green) and IB-4 (Red). Right panel insert shows higher magnification of lamina I and II within the dorsal horn. (B) Quantification of immunostaining signal shows less Met-enkephalin immunoreactivity in littermate dorsal horns (n=3) compared with the $Na_v1.7$ KO dorsal horn (n=3). Data are shown as mean±s.e.m. *P<0.05 significance levels indicate differences between KOs and littermates using a Student's t-test. This data is collected by Dr.Vanessa Pereira at Molecular Nocuception Group, WIBR, UCL. Cited from (Minett et al., 2015).

2.3.2 Pain behaviour

I. Pain behaviour test in mice

Performed by Dr. Vanessa Peraira, Ms. Sonia Santana, Miss Queensta Millet at Molecular Nociception Group, WIBR, UCL and Dr. Michael Minett formerly at Molecular Nociception Group, WIBR, UCL.

The data shown in the previous section (2.3.1) demonstrates that enkephalins are upregulated in $Na_v1.7$KO mice and *Ceacam10* was significantly down-regulated. We therefore explored the role of endogenous opioids in the loss of function of $Na_v1.7$ and *Ceacam10* in pain behaviour in mice. Firstly, we used the opioid antagonist naloxone to examine the role of endogenous opioids in pain behaviour in $Na_v1.7$-null mutant mice using $Na_v1.7^{Adv}$ mice. Recent

RNA sequencing data highlights the significance of the μ-opioid receptor in nociceptive $Na_v1.8$-expressing neurons that do not contain mRNA for κ- or δ-opioid receptors (Usoskin et al., 2015). Thus the target of naloxone on sensory neurons is likely to be the μ-opioid receptor. Notably, *Penk* is a precursor of Met-enkephalin and Leu-enkephalin. Met-enkephalin is a potent agonist of the δ-opioid receptor, and to a lesser extent the μ-opioid receptor. Leu-enkephalin has agonistic actions at both the μ- and δ-opioid receptors (Janecka et al., 2004). Met- and Leu-enkephalin could thus act as agonists for the μ-opioid receptor in nociceptive $Na_v1.8$-expressing neurons and naloxone could block this activity. Since thermal and mechanical analgesia in $Na_v1.7$KO mice were documented (Minett et al., 2012), we measured thresholds for acute pain using Hargreave's (thermal pain) and Randall-Selitto tests (mechanical pain). When naloxone was administered to $Na_v1.7$ KO mice, there was a dramatic reversal of analgesia and restoration of both thermal and mechanical pain thresholds (Figure 2-10). The reversal levels were close to that found in littermate controls. On the other hand, the dose of naloxone used had no effect on pain thresholds of littermate controls (Figure 2-10).

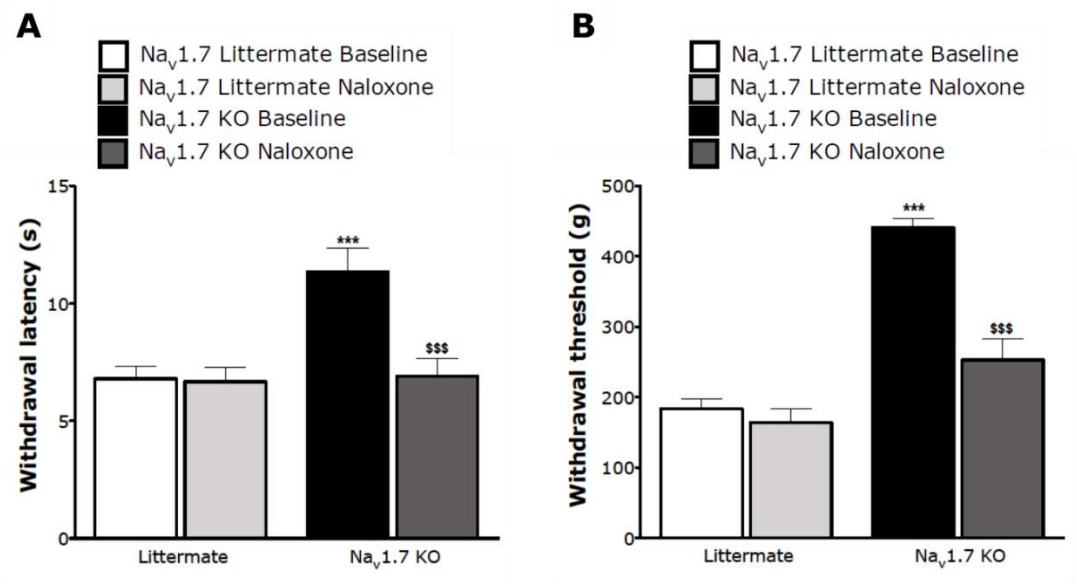

Figure 2-10. Pain behaviour tests on $Na_v1.7$ KO mice and littermate control injected with naloxone. (A) Hargreaves (n=6 female and n=6 male per genotype) and (B) Randall-Selitto (n=3 female and n=3 male per genotype) pain behavioural tests show higher pain thresholds of $Na_v1.7$ KO ($Na_v1.7^{Adv}$) mice compared with littermates. Systemic naloxone reduces thermal and pressure pain thresholds of male and female $Na_v1.7$ KO ($Na_v1.7^{Adv}$) mice but has no effect on littermates. White bar=$Na_v1.7$ littermate (WT) baseline, light grey bar= $Na_v1.7$ littermate naloxone infusion, Black bar=$Na_v1.7$ KO baseline, dark grey bar=$Na_v1.7$ KO naloxone infusion. Data are expressed as mean±s.e.m. * ***P<0.001 significance levels indicate differences between KOs and littermates using a Student's t-test and $$$ P<0.001 indicate differences following naloxone administration using a paired t-test. Cited from (Minett et al., 2015).

Secondly, the effects of gene deletion on pain behaviour using *Ceacam10*-null mice were examined. As mentioned, *Ceacam10* was the most downregulated transcript in the $Na_v1.7$ microarray analysis and thus we wondered if it contributes to pain behaviour. *Ceacam10*-null mutant mice have a limited analgesic phenotype to thermal stimuli in the Hargreaves test' and the heterozygous null mutant mice also show partial analgesia (Figure 2-11). We also administrated naloxone to these mice to see if the analgesia is opioid-dependent. However, naloxone does not reverse the analgesic phenotype of *Ceacam10*-null mice (Figure 2-11). This result can suggest that *Ceacam10* plays a role in pain sensation through a non-opioid-dependent mechanism.

These pain behaviour tests on mice indicate that up-regulation of *Penk* contributes to the CIP analgesic phenotype associated with loss of $Na_v1.7$ expression, and down-regulation of *Ceacam10* may also make a small contribution.

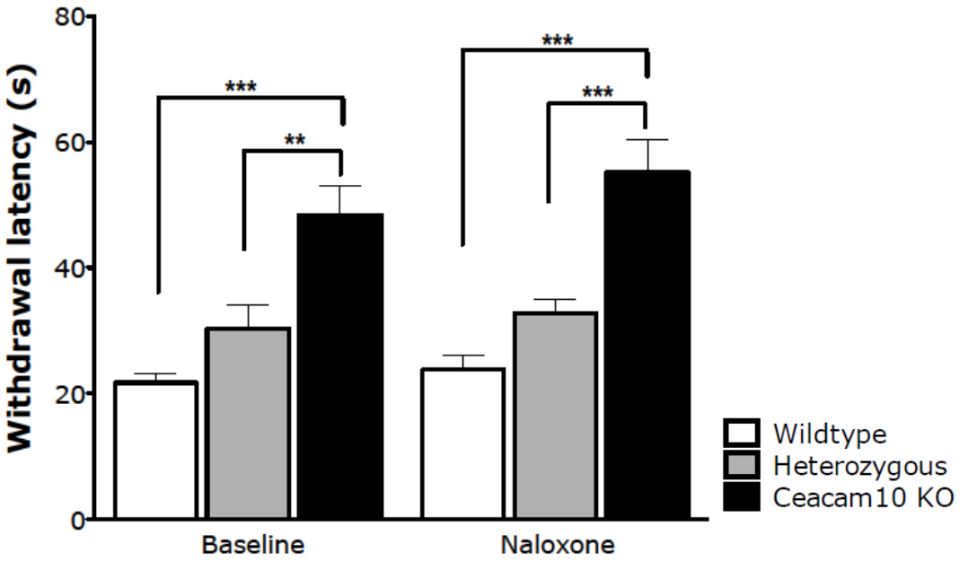

Figure 2-11. Hargreaves' pain behavioural test in global *Ceacam10* KO mice. *Ceacam10* KO and heterozygous KO mice show clear thermal analgesia in the Hargreaves' test and this is unaffected by naloxone administration (n=6 per genotype). White bar=wild type, grey bar=heterozygous KO mice, black bar=*Ceacam10* KO mice. Data are expressed as mean±s.e.m. **P<0.01 and ***P<0.001 significance levels indicate differences between KOs and littermates (wrote as Wildtype) using a Student's t-test. Cited from (Minett et al., 2015).

II. Pain threshold change in $Na_v1.7$–null CIP patient by administration of naloxone

Performed by Dr. Flavia Mancini, Professor Gian Iannetti, and Professor Raymond MacAllister at UCL

The present results of pain behaviour tests have demonstrated the endogenous opioid-contribution to the CIP analgesic phenotype associated with loss of Nav1.7 expression in mice. We then examined the effect of naloxone on pain thresholds in a rare human Nav1.7-null CIP individual (genotyped was described in detail in (Nilsen et al., 2009). In normal conditions, the Nav1.7- null subject was completely unaware of the phasic pain stimulus (Figure 2-12A). However, infusion of naloxone reversed analgesia dramatically in the Nav1.7-null CIP patient. The ability of the Nav1.7-null CIP individual to detect a single noxious heat stimulus in the presence of naloxone rose from 0 to 80% (Figure 2-12A). Ongoing thermal pain (tonic pain stimulus) could also be detected by the Nav1.7-null individual only in the presence of naloxone (Figure 2-12C). These results in the CIP patient were consistent with the Nav1.7 KO mouse data. On the contrary, there was no change in healthy control participants following infusion of naloxone in both phasic and tonic pain (Figure 2-12B, D). It should be noted that this pain test indicated opioid-dependent analgesia in only one Nav1.7-null patient; however, the mechanistic studies in mice seem to also explain aspects of the human Nav1.7-null CIP phenotype. It would be useful to examine larger numbers of the extremely rare CIP individuals to extend these studies.

These mice and human pain behaviour studies suggested that the loss of $Na_v1.7$ expression in *SCN9A*-null mice and humans leads to the upregulation of an endogenous opioid system that contributes substantially to the CIP pain-free state through inhibition of nociceptive sensory neuron input into the spinal cord. In addition, *Ceacam10* could contribute to the CIP analgesic phenotype associated with loss of $Na_v1.7$ expression. The next question is how the loss of a voltage-gated sodium channel alters mRNA levels. We attempted to examine the mechanisms of mRNA regulation of these 4 genes; *Penk*, *Th*, *Ceacam10* and *Tmem173*, addressed in the next section.

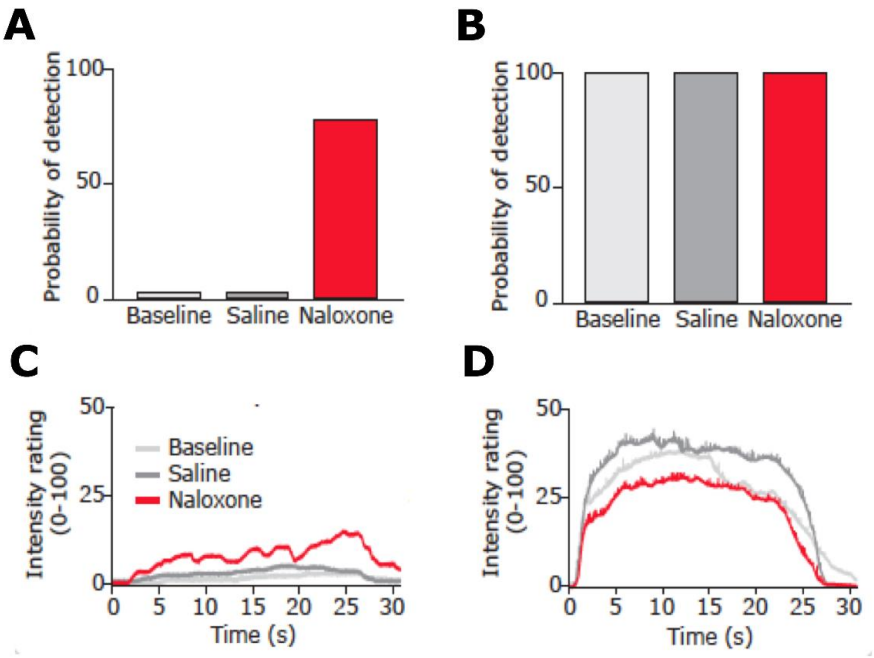

Figure 2-12. Perception of phasic and tonic pain in humans. (A)(B) Phasic pain test. The probability of detecting 9-ms radiant heat pulses was assessed in a $Na_v1.7$-null patient (A) and in three age-matched healthy controls (B). Neodymium:yttrium-aluminum-perovskite (Nd:YAP) laser pulses (El.En, Italy) selectively stimulate intra-epidermal free-nerve endings, thus providing a pure nociceptive input without touch. The human $Na_v1.7$ null did not detect any stimuli in baseline and saline conditions. The probability of detecting the stimulus dramatically increased to 80% of stimuli detected during the infusion of 12 mg naloxone, almost reaching the detection levels of matched healthy controls. (C)(D)Tonic pain was elicited by 25 s laser stimuli, whereas the participants rated online the intensity of the heat sensation on a visual analogue scale (0=no sensation, 100=worst pain imaginable) throughout the laser application. Again, naloxone strongly enhanced tonic pain sensations in the $Na_v1.7$-null patient (C) throughout the time course of the stimulation without effect in the control subjects (D). Cited from (Minett et al., 2015).

2.3.3 Luciferase reporter assay

Creating Gaussia and Cypridina luciferase constructs were performed by Dr. Yury Bogdanov formerly at Molecular Nociception Group, WIBR, UCL.and myself. All the other procedures were performed by myself.

As stated in the introduction section, the hypothesis of this project is that $Na_v1.7$ can function as a mediator of transcriptional activity. To address this question, we performed luciferase assays in the presence or absence of $Na_v1.7$. We assumed that the luciferase expression could be different if $Na_v1.7$ plays a role in transcriptional activity. We chose *Penk*

and *Th* to examine transcriptional activities of the genes mediated by $Na_v1.7$ using luciferase assays. *Penk* is of particular interest as our data strongly suggested up-regulation of endogenous opioids contributes to the CIP analgesic phenotype associated with loss of $Na_v1.7$. *TH* is also interesting to investigate further as; several studies have supported that *TH* and L-DOPA may be linked to pain sensation. Also transcriptional activity of *TH* using luciferase assay has been well documented (Jeong et al., 2006). We therefore explored the mechanisms of mRNA regulation for these 2 genes using luciferase assays. In this section, cell line results, using transiently transfected HEK cells (I) and Neuro2A cells (II) will be shown first, and then a luciferase assay in stable Neuro2A cell line will be addressed (III).

I. Luciferase assay in transiently transfected HEK cells

HEK293A cells are derived from human embryonic kidney cells, which have seen wide use in stably transfected forms to study a variety of cell-biological questions in neurobiology. Their features including quick and easy reproduction and maintenance, high efficiency of transfection and protein production, and the ability to carry out most of the post-translational folding and processing enabling us to study the function of channels, receptors and cell signaling pathways. Using this cell line, we aimed to explore the transcriptional activity for each protein, *Penk* and *Th*. First, we created a Gaussia luciferase construct driven by h*PENK*, h*TH* or h*GAPDH* putative promoter (Figure 2-13). The promotor region of these genes have not known, apart from *TH* promoter. Some studies indicated around 500kb upstream of human *TH* gene is sufficient to drive reporter expression (Gardaneh et al., 2000, Coker et al., 1988). Also another study used 3.3kb upstream of TH for a promoter construct which was active in neuroblastoma cell line (Kim et al., 2003). Therefore the regions which are 5kb upstream of the each gene were placed into upstream of the luciferase genes, assuming the regions are sufficient to drive reporter expression functioning as promoter. The vector of Gaussia luciferase gene under the control of *Gapdh* putative promoter was attempted to create in order to confirm the target genes are not regulated randomly. Firstly, I transfected these plasmids into HEK293A cells to test if the constructs worked (Figure 2-14).

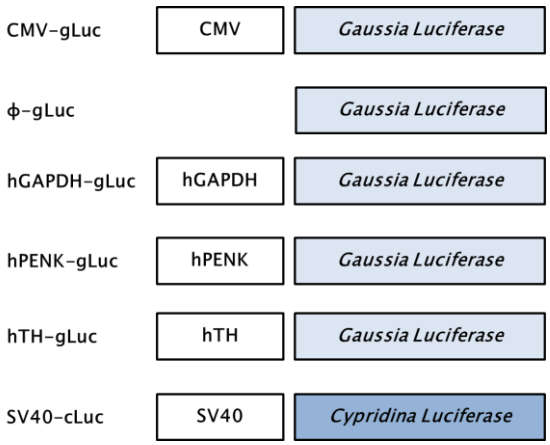

Figure 2-13. Construct of luciferase. Gaussia lucifearse driven by CMV and Gaussia luciferase without promoter are used for positive control or negative control, respectively.

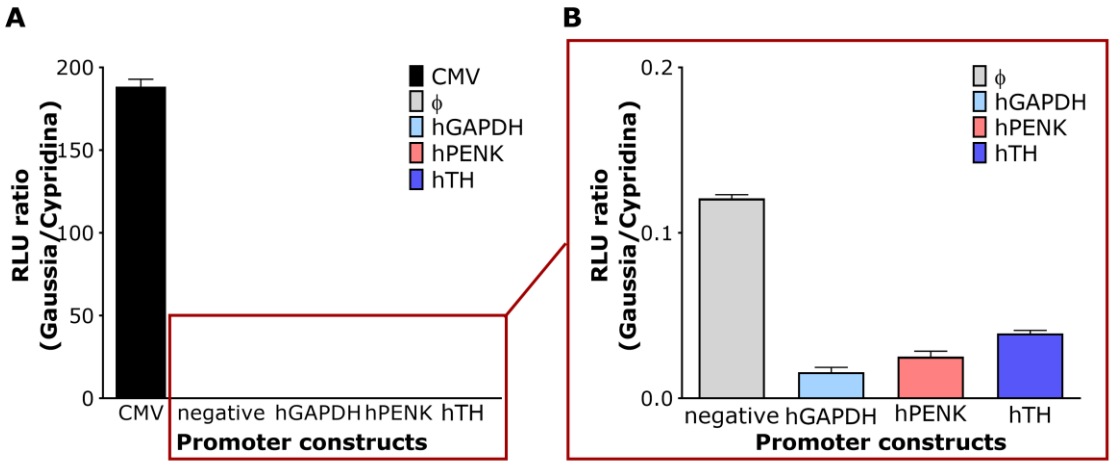

Figure 2-14. Luciferase assay in HEK293A cells. (A) (B) Cells were transfected with each construct of Gaussia luciferase together with Cypridina luciferase controlled by SV40. RLU of Gaussia luciferase indicating the activity of each promoter were divided by Cypridina luciferase RLU as an internal control to normalise cell numbers and transfection rate. Positive control (cells transfected with CMV-gLuc) showed high expression levels of Gaussia luciferase (A) while Gaussia RLU for h*GAPDH*, h*PENK* and h*TH* promoter represented lower signals than negative control (B). n=1, the results are shown as mean ± SEM for technical triplicates.

Unfortunately, the results indicated that Gaussia luciferase was not expressed under the control of each promoter, h*PENK*, h*TH* or h*GAPDH* in HEK293A cells because the ratio for each construct divided by internal control (SV40-cLuc) was lower than the negative control, which does not have promoter region. This result could be because HEK293A cells do not express *PENK* or *TH*; according to Human Protein Atlas (http://www.proteinatlas.org/)(Uhlen et al., 2015, Thul et al., 2017), the expression of these genes are not found in HEK293 cells.

Thus, another cell line which has closer environment to neuronal cells might be useful for this assay. We therefore performed this assay using neuronal cells as the second attempt, shown in the next section.

II. Luciferase assay in transiently transfected Neuro2A cells

Neuro2A cells are a mouse neural crest-derived cell line that has been extensively used to study neuronal differentiation, axonal growth and signaling pathways. Some studies described that *Penk* and *Th* are expressed in Neuro2A cells (Tremblay et al., 2010, Bamberger et al., 1995). Thus they could be a suitable model to explore the transcriptional activity of *Penk* or *Th* in the presence or absence of $Na_v1.7$.

Firstly, we created a Gaussia luciferase construct driven by m*Penk*, m*Th* or m*Gapdh* putative promoter. Similary to human gene promoter, promoter regions of m*Gapdh* and m*Penk* have not been well studied. On the other hand, there are several studies mentioning *Th* promoter in mouse. In a study, 68bp upstream of *Th* was placed into a reporter construct (Tanida et al., 2014), while some studies used 800bp to 4kb upstream of *Th* to identify the other elements in *Th* transcription (Hagerty et al., 2001, Lebel et al., 2001). Like the constructs bearing human putative promoter regions of each gene, we therefore placed 5kb upstream of each gene into the Gaussia luciferase construct.

In order to compare the effect of $Na_v1.7$, the cells are co-transfected with Gaussia luciferase driven by each promoter and $Na_v1.7$ or empty vector, together with the internal control, Cypridina luciferase controlled by SV40 (See Figure 2-13 for the construct; instead of the human gene promoter, we used the mouse promoter).

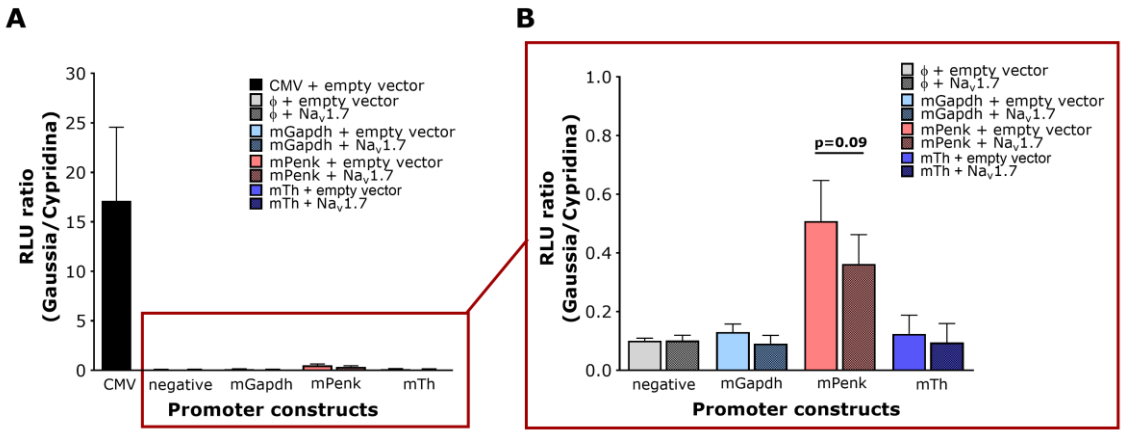

Figure 2-15. Luciferase assay in Neuro2A cells. Cells were transfected with each construct of Gaussia luciferase together with Cypridina luciferase controlled by SV40 (Figure 2-13, mouse promoter instead of human promoter) and human $Na_v1.7$ gene for presence of $Na_v1.7$ (+h$Na_v1.7$, dark colour bar) or empty plasmid for absence of $Na_v1.7$ (-h$Na_v1.7$, light colour bar). RLU of Gaussia luciferase indicating the activity of each promoter were divided by Cypridina luciferase RLU as an internal control to normalise cell numbers and transfection rate. (A) the results including positive control (CMV). The positive control represented the strong signal suggesting that the assay itself was performed properly. (B) the results without the positive control. RLU of Gaussia luciferase controlled by mPenk promoter has moderate signals while m*Gapdh* and m*Th* has the same RLU level as negative control. The transcription activity of m*Penk* was up-regulated in the absence of $Na_v1.7$. However, it was not statistically significant (p=0.09). n=3 for positive (CMV) and negative control, m*Gapdh* and m*Th*, and n=5 for m*Penk*. All results are shown as mean ± SEM.

Figure 2-15 shows the ratio of Gaussia luciferase expression measured by RLU divided by Cypridina luciferase expression as an internal control. The result indicates low luciferase expression controlled by *Th* and *Gapdh* promoters. Also, it may suggest that the expression controlled by the *Th* promoter did not give a marked difference between cells co-transfected with $Na_v1.7$ or without. However, the most interestingly, Gaussia luciferase expression controlled by the *Penk* promoter is higher in the cells without transfection of $Na_v1.7$ than in the cells where $Na_v1.7$ is overexpressed. However, there was no statistic significant difference between the transfection and non-transfection of $Na_v1.7$ (p=0.09). This result could be because endogenous $Na_v1.7$ might affect the transcriptional activity. In addition, the overexpression of $Na_v1.7$ might not be sufficient to produce significantly different levels of *Penk* in the cells transfected with or without $Na_v1.7$. A technical problem might be also the cause of the non-significant result. For example, we wondered if both Gaussia and Cypridina luciferase constructs are transfected into a positively transfected cell. If the transfected rate was different between Gaussia (test) and Cyprinida (internal control) luciferase, this difference may affect the RLU ratio. To solve this problem, stably expressing both test and internal control luciferase cells were generated, addressed in the next section (2.3.3III).

III. Luciferase assay in Neuro2A stable cell line

To generate a stable cell line, a luciferase construct carrying an antibiotic resistance gene was required. Since two different types of luciferase were needed, each gene should have distinct mechanism to be resistant to antibiotic. Two luciferase constructs were chosen; Firefly luciferase which bears the Hygromycin resistance gene (*Hyg*) and Renilla luciferase carrying Neomycin resistance gene (*neo*). These two luciferases are widely performed to examine promoter activities. One of commonly used antibiotic, Geneticin, also known as G418, blocks polypeptide synthesis by inhibiting the elongation step in both prokaryotic and eukaryotic cells. Resistance to Geneticin is conferred by the Neomycin resistance gene. On the other hand, *Hygromycin* affords resistance to Hygromycin B. Hygromycin B is an aminoglycosidic antibiotic that inhibits protein synthesis by disrupting translocation and promoting mistranslation at the 80S ribosome. Since it uses a different mode of action from Geneticin, it is suitable for dual-selection experiments when used in conjunction with Geneticin (Invitrogen, 2002). Therefore, Hygromycin B and Geneticin were attempted to use by adding it into the media to select the cells stably expressing both Firefly and Renilla luciferase.

Firstly, we created Firefly and Renilla luciferase constructs. Firefly was chosen as a test luciferase construct; each DNA fragment covering the promoter region was inserted upstream of Firefly luciferase gene. For an internal control, SV40 promoter was placed infront of Renilla luciferase gene in the plasmid. To create the construct, two methods were tested; firstly, the traditional method where both insert and vector are digested with the same restriction enzymes following ligation. The other method was Gibson Assembly, which has been recently developed by Gibson and colleagues (Gibson et al., 2009). It allows for successful assembly of multiple DNA fragments (Figure *2-17*). In this assembly, the insert needs to have overlapping fragments at its ends. Three different enzymatic activities in a single buffer enable us to create a new vector: first, the exonuclease create single-stranded 3´ overhangs that facilitate the annealing of fragments that share complementarity at one end (overlap region). Secondly, the polymerase fills in gaps within each annealed fragment. The final step is ligation. The DNA ligase seals nicks in the assembled DNA. Surprisingly, Gibson Assembly resulted in 100% positive clones by checking the plasmid size (Table 2-5). Compared to the traditional method, this assembly is easier to conduct because of one-step ligation in a short time (20min). Most importantly, it allows for creating a new construct efficiently.

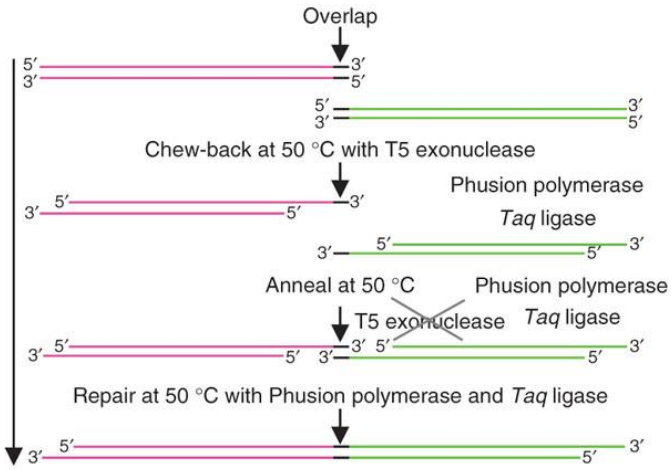

Figure 2-16. Overview of Gibson assembly. (Gibson et al., 2009)

Table 2-5. Comparison of Gibson assembly and conventional method.

	m*PENK*-fLuc	m*Th*-fLuc	m*Gapdh*-fLuc
Number of clones in Gibson Assembly (positive clone/pick up clone)	12/12	6/6	6/6
Number of clones in conventional method (positive clone/pick up clone)	2/20	4/6	2/6

Secondly, stable single clones expressing Firefly under the control of each promoter and Renilla luciferase were generated. The generated Firefly and Renilla luciferase constructs were transfected into Neuro2A cells. After a few weeks harvest with Geneticin and Hygromycin B, the cells were sorted into single clones using Flow Cytometry. The single cells were kept harvesting with Geneticin and Hygromycin B for another several weeks. Then, the single clones were verified if they express both Firefly and Renilla by measuring luminescence (Table *2-6*). Only 1 clone from 190 single cells transfected with CMV-fLuc, m*Gapdh*-fLuc, or m*Penk*-fLuc together with SV40-rLuc demonstrated both luminescence given by Firefly and Renilla luciferase. Also 1 clone from 190 single cells transfected with Φ-fLuc expressed Renilla luminescence. On the contrary, 6 clones from 190 single cells transfected with m*Th*-Fluc and SV40-Rluc showed signals conferred by both Firefly and Renilla luciferase.

Table 2-6. RLU in positive clones expressing Firefly and Renilla luciferase. The cells reached at 70-80% confluency in a well in a 48 well plate were used for luminescence measurement.

	Firefly RLU					
non-transfection	32	55	36			
CMV	4000000					
ϕ	11357					
m*Gapdh*	1563000					
m*Penk*	96970					
m*Th*	3466000	2030000	2714000	1371000	3276000	1279000
	Renilla RLU					
non-transfection	7327	3978	5763			
CMV	2287000					
ϕ	3983000					
m*Gapdh*	497086					
m*Penk*	443726					
m*Th*	3047000	1872000	1901000	1508000	3456000	1248000

Thirdly, the selected clones were also validated by immunofluorescence (Figure 2-17, Figure 2-18). Co-staining with anti-Firefly (green) and anti-Renilla (red) antibodies was performed. Anti-Firefly luciferase antibody showed green staining in the stable clones obtained from the cells transfected with CMV, m*Gapdh*, m*Penk*, or m*Th* -Fluc (Figure 2-17). However, the clone expressing Firefly luciferase under the control of m*Gapdh* putative promoter appeared to demonstrate weaker signals than the others (Figure 2-17). Among these clones, the ones expressing Firefly luciferase driven by m*Penk* and m*Th* promoter showed strong signals (Figure 2-17), although these clones also demonstrated weak green staining in negative control, no-primary-antibody treated cells (Figure 2-18). This staining in the negative control might be because of non-specific binding of the secondary antibody due to high expression of Firefly luciferase. Of note, the stable clone obtained from the cells transfected with CMV-Fluc did not show signals as strong as the ones from m*Th*- or m*Penk* -Fluc (Figure 2-17), although the RLU signals were high (Table 2-6). This could be alo because of the non-specific binding of the secondary antibody for the clones cobtained from m*Th*- or m*Penk* –Fluc. No obvious anti-Firefly luciferase staining was seen in a clone obtained from the cells transfected by Firefly luciferase without promoter construct. Staining in the cells without transfection was also not seen (Figure 2-17), suggesting that the green immunofluorescence in the clones apart from the ϕ–Fluc clone demonstrated expression of Firefly luciferase. Each stable clone showed red fluorescence stained by anti-Renilla luciferase antibody (Figure 2-17). However, weak red staining was observed in the clone expressing Renilla and Firefly luciferase driven by m*Gapdh*

promoter (Figure 2-17). Anti-Renilla luciferase antibody did not show marked fluorescence in non-transfected cells (Figure 2-17). These staining results suggest that all clones expressed Renilla luciferase although it seemed to be different levels of Renilla luciferase expression. All no-primary-antibody treated cells which were used as a negative control did not show red staining (Figure 2-18).

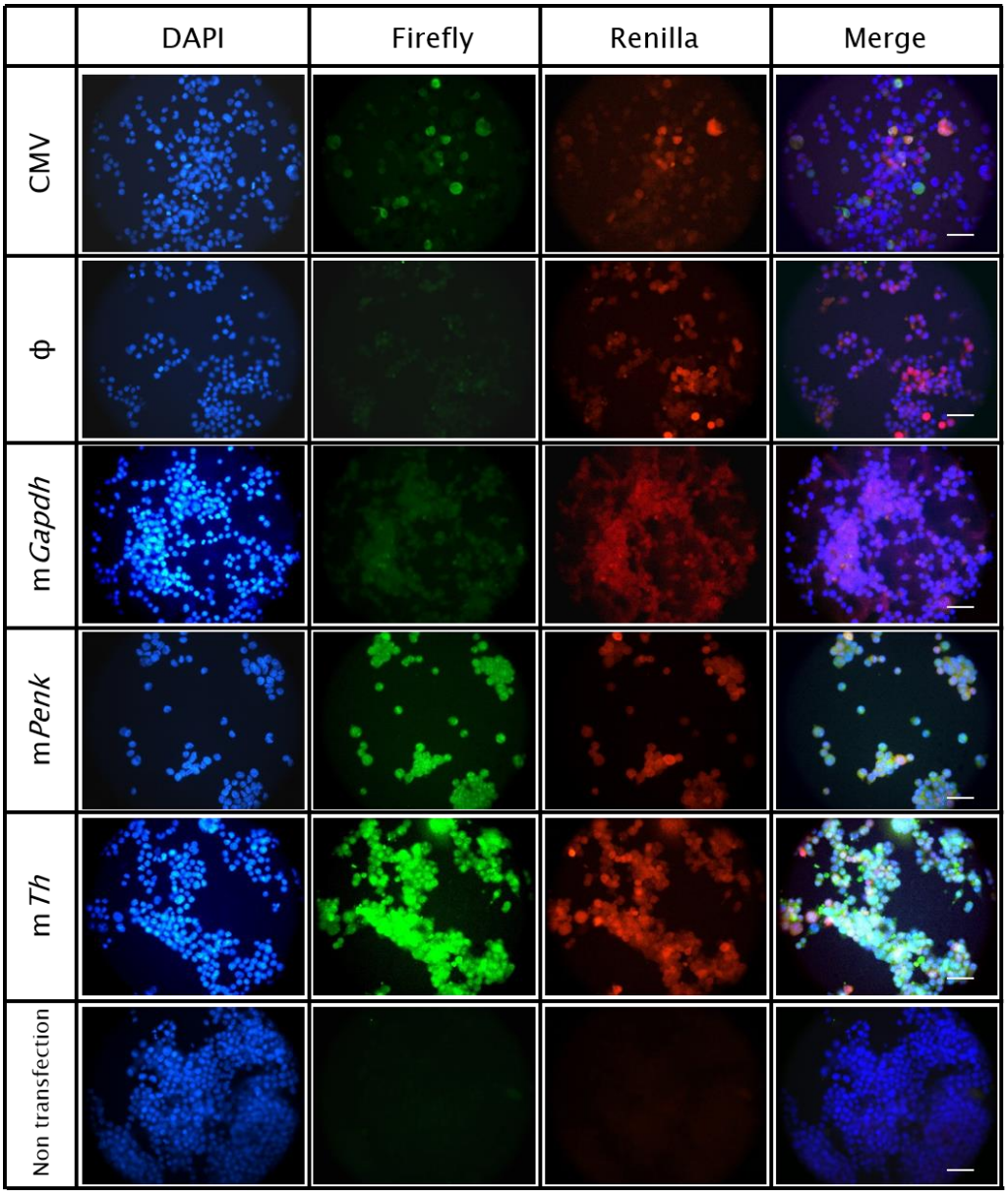

Figure 2-17. Immunofluorescence of Neuro2A stable cell line. Goat anti-Firefly (ab181640) and Rabbit anti-Renilla (ab185926) antibodies were used to stain the cells. Alexa 488 Donkey anti-Goat and Alexa 594 Donkey anti-Rabbitantibodies were used as secondary antibody. Each clone were from the transfected cells with SV40-rLuc and CMV; CMV-fLuc, ϕ; Fluc (no promoter), m*Gapdh*; m*Gapdh*-fLuc, m*Penk*; m*Penk*-fLuc, m*Th*; m*Th*-fLuc. Scale bar=60 μm.

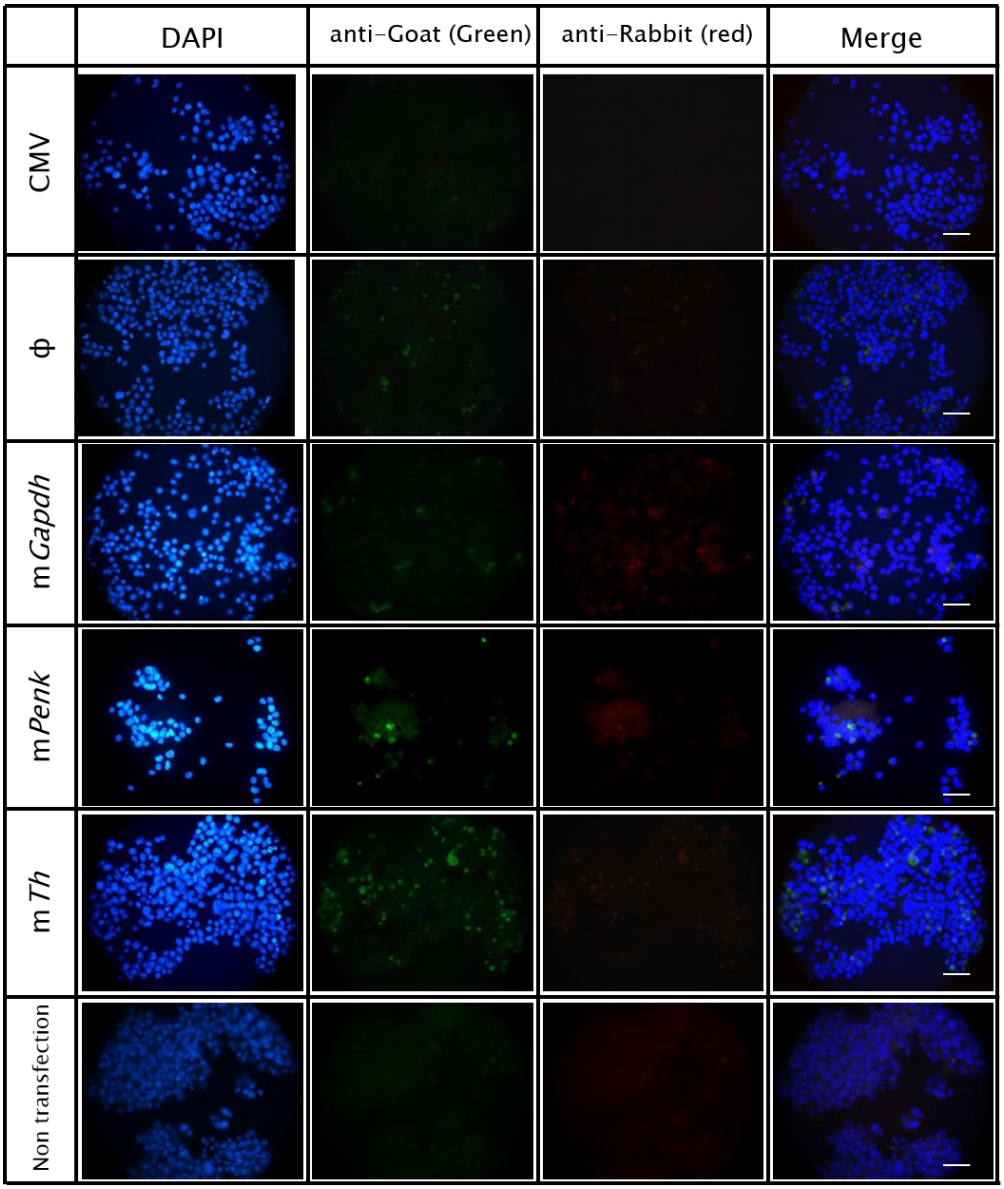

Figure 2-18. Immunofluorescence of Neuro2A stable cell line stained with secondary antibody only. Alexa 488 Donkey anti-Goat (used for Firefly luciferase) in green and Alexa594 Donkey anti-Rabbit (used for Renilla luciferase) in red. Each clone were from the transfected cells with SV40-rLuc and CMV; CMV-fLuc, ϕ; Fluc (no promoter), m*Gapdh*; m*Gapdh*-fLuc, m*Penk*; m*Penk*-fLuc, m*Th*; m*Th*-fLuc. Scale bar= 60 μm.

Generating Firefly and Renilla luciferase stable cell lines allowed us to resolve the issue that transient transfection might cause a different transfection rate between the test luciferase construct and the internal control. Finally, these stably expressing Firefly controlled by the each promoter and Renilla luciferase clones were tested to explore the effect of $Na_v1.7$ in transcriptional activity. Like in the previous experiments (II), each clone was transfected with $hNa_v1.7$ to overexpress or empty vector as a control. The RLU of Firefly luciferase given by the activity of each promoter was divided by that of Renilla luciferase to normalise cell

numbers. In the transient transfection (II), both cells transfected with m*Gapdh*-gLuc and m*Th*-gLuc demonstrated low signals similarly to the negative control (gLuc without promoter). Using the stable cell line enabled us to obtain higher signals than the negative control (φ-fLuc), however, significant difference between overexpression of $Na_v1.7$ and control (transfected with empty vector) was not observed in all clones (Figure 2-19).

These insignificant differences might be because of a technical limitation; overexpression of $Na_v1.7$ using lipofectamine might not be sufficient to see distinct transcriptional activity between the cells transfected with the vector bearing $Na_v1.7$ and the empty vector. Notably, moderate levels of mRNA expression of *Scn9a* as well as *Scn2a* and *Scn4a* are observed, while low expression of the other VGSCs are found in Neuro2A cell line according to BioGPS (http://biogps.org)(Wu et al., 2013, Wu et al., 2016). This endogenous expression of $Na_v1.7$ in Neuro2A might compensate the effect of $Na_v1.7$ overexpression. This limitation could bring an idea that the complete loss of $Na_v1.7$ functions might be able to display the difference in luciferase expression. Therefore, although the transcriptional activity of *Penk* and *Th* in Neuro2A cells did not show statistically significant differences, it could be interesting to test this assay in $Na_v1.7$ KO mice DRG neurons. In addition, transcriptional up- or down-regulation could be an important factor in dysregulation of those genes in mRNA levels in $Na_v1.7$ KO mice DRG neurons since mRNA levels were altered in DRG in $Na_v1.7$ KO mouse compared to littermate control mice (Figure 2-8). We further investigated this transcription activity of *Penk* and *Th* in mouse DRG neurons, addressed in the next section (IV).

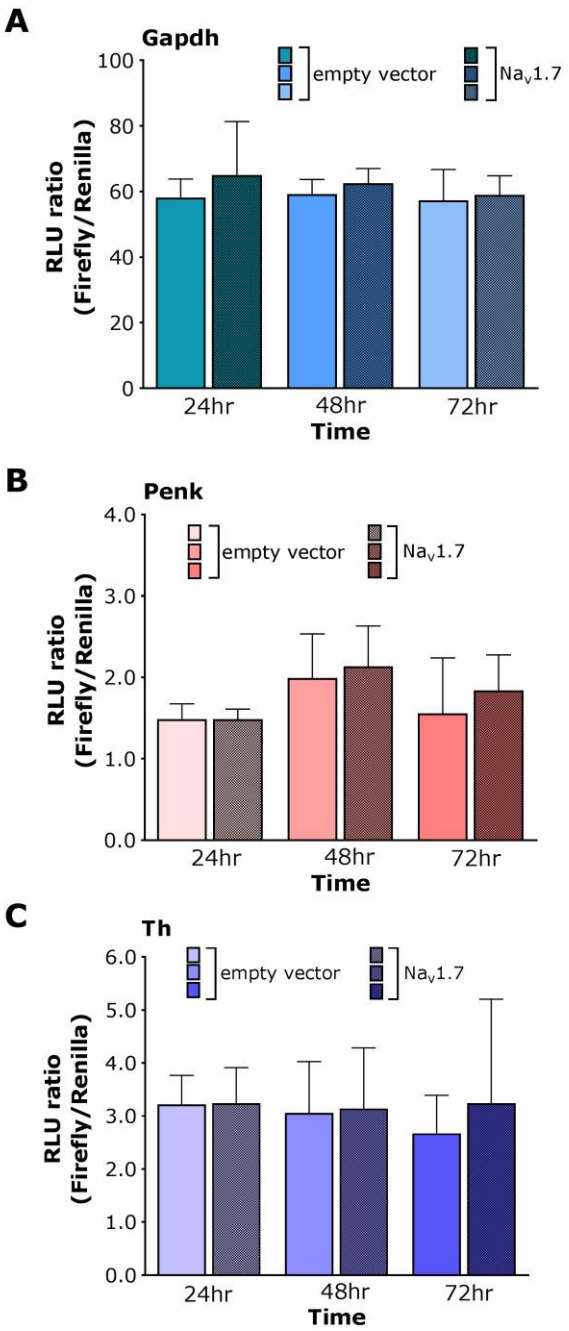

Figure 2-19. Luciferase assay in Neuro2A stable cell line with overexpression of hNa$_v$1.7. (A) The clone derived from cells transfected with mGapdh-fLuc and SV40-rLuc. (B) The clone derived from cells transfected with mPenk-fLuc and SV40-rLuc. (C) The clone derived from cells transfected with mTh-fLuc and SV40-rLuc. RLU of Firefly luciferase indicating the activity of each promoter were divided by Renilla luciferase RLU as an internal control to normalise cell numbers. The measurement was performed 24, 48, and 72hr post-transfection with hNa$_v$1.7. No significant differences were observed in all clones. n=3 for mGapdh, n=4 for mTh, and n=5 for mPenk. All results are shown as mean ± SEM.

IV. Luciferase assay with cultured DRG neurons

In order to measure transcriptional activity of each gene, we attempted to perform a luciferase assay in DRG from the conditional $Na_v1.7$KO mice ($Na_v1.7^{Adv}$). First, we tested Gaussia and Cypridina luciferase constructs using WT mice DRG neurons. Gaussia luciferase driven by *Gapdh* and *Th* were not expressed since RLU ratio of Gaussia and Cypridina luciferase was the same level as the one in negative control (Figure 2-20). Gaussia luciferase driven by *Penk* seemed to be expressed in DRG cells. However, it gave low signals since it is difficult to obtain many cells from mouse DRG comparing to cell lines such as Neuro2A.

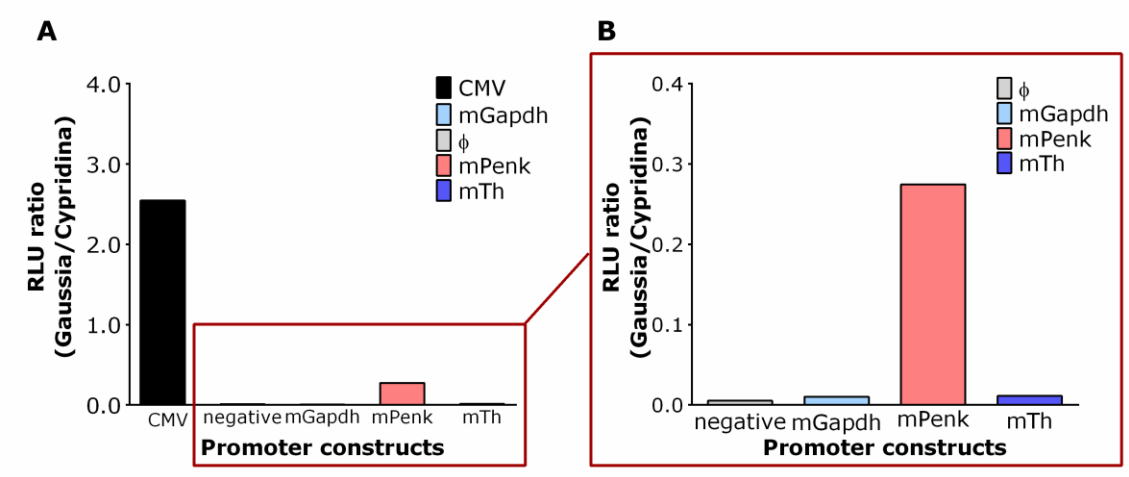

Figure 2-20. Luciferase assay in DRG taken from WT mouse. Cells were transfected with each construct of Gaussia luciferase together with Cypridina luciferase controlled by SV40 (Figure 2-13, mouse promoter instead of human promoter). RLU of Gaussia luciferase indicating the activity of each promoter were divided by Cypridina luciferase RLU as an internal control to normalise cell numbers and transfection rate. RLU of Gaussia luciferase controlled by mPenk promoter has moderate signals while mGapdh and mTh has the same RLU level as negative control. (n=1)

These low signals might lead to sizeable technical errors since slight changes of luminescence reading can cause large differences when shown as an RLU ratio. The luciferase kinetics should be also noted when considering the technical errors; the luminescence can drop down dramatically in a short period. Thus, we wondered if a different type of luciferase might allow us to obtain higher signals in order to reduce technical errors. Therefore, the new constructs carrying Firefly or Renilla luciferase genes were tested in mouse DRG. Since Gaussia luciferase controlled by m*Gapdh* and m*Th* promoter did not seem to express in DRG

neurons, we attempted to transfect with only m*Penk*-fLuc and negative control (φ-fLuc). In spite of our expectation, the luminescence given by Firefly luciferase was not high (Figure 2-21).

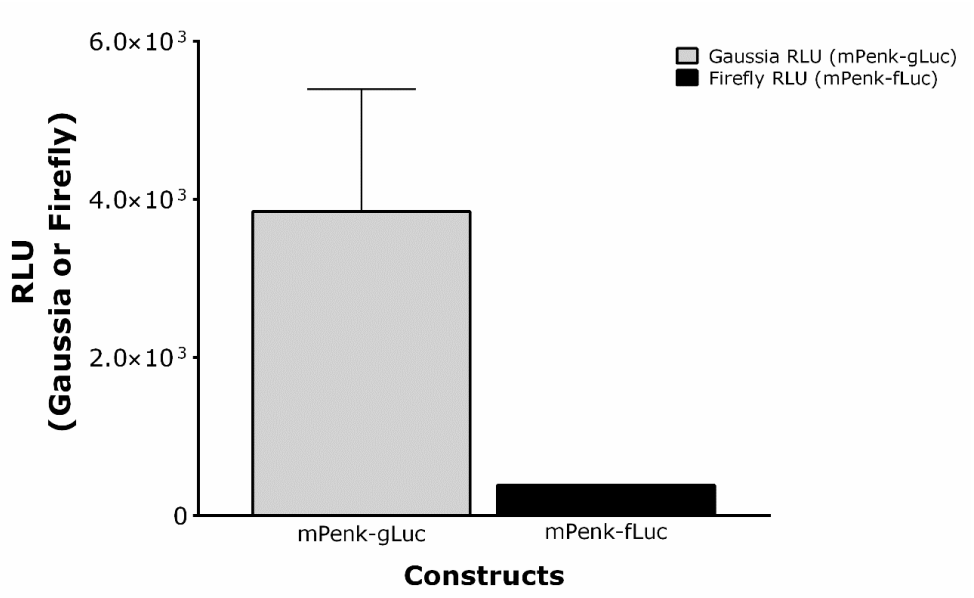

Figure 2-21. Gaussia or Firefly luciferase RLU in DRG taken from WT mouse. Cells were transfected with Gaussia luciferase or Firefly luciferase driven by mPenk promoter. (n=7 for Gaussia luciferase construct, n=1 for Firefly luciferase construct.)

We therefore tested $Na_v1.7$KO and littermate control mice measuring luminescence of Gaussia luciferase and Cypridina luciferase. Despite our hypothesis that $Na_v1.7$ can be a transcriptional regulator, RLU ratio of Gaussia luciferase driven by *Penk* and Cypridina luciferase under the control of SV40 did not show marked difference between $Na_v1.7$KO and littermate control mice (Figure 2-22). Since we could not obtain high signals due to small numbers of cells, there were sizeable differences of RLU between each trial, leading to notable technical errors. In addition, DRG neurons are considered to be difficult to transfect even using electroporation. Our primary data suggested approximately 5-10% of DRG neurons can be transfected in this method. We therefore attempted another method to measure transcriptional activity of *Penk*, addressed in the next section (2.3.4).

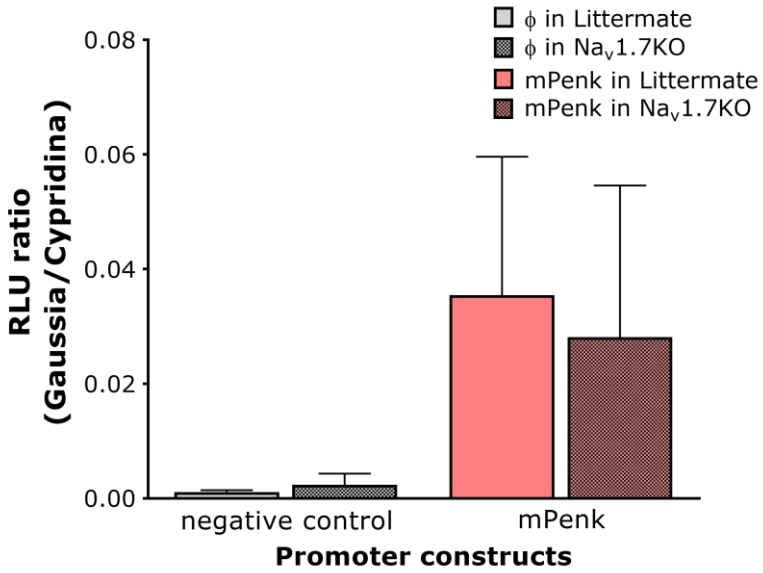

Figure 2-22. Luciferase assay in DRG in $Na_v1.7$KO mice or littermate control. Cells were transfected with each construct of Gaussia luciferase together with Cypridina luciferase controlled by SV40 (Figure 2-13, mouse promoter instead of human promoter). RLU of Gaussia luciferase indicating the activity of each promoter was divided by Cypridina luciferase RLU as an internal control to normalise cell numbers and transfection rate. There seems to be no obvious up-regulation of the transcriptional activity of *Penk*. (n=4 for *Penk*, n=5 for negative control)

2.3.4 Pre-mRNA levels of *Penk* in DRG neurons

Performed by myself

Since we could not conclude if $Na_v1.7$ regulates transcriptional activity of *Penk* in DRG using the luciferase assay (2.3.3IV), I tried to measure pre-messenger RNA levels of *Penk* in DRG neurons. In eukaryotic cells, initially transcription results in a pre-messenger RNA (pre-mRNA) molecule that is processed before it emerges as a mature mRNA ready for translation. Thereby measuring pre-mRNA could give an idea that $Na_v1.7$ mediates transcriptional activities of *Penk* and/or contributes to pre-mRNA stability leading to increased endogenous opioids due to loss of $Na_v1.7$ expression. The mechanisms of this gene expression mediated by $Na_v1.7$ might be beneficial to broaden potential analgesic targets for more effective pain therapies together with $Na_v1.7$. We designed a primer pair that amplified segments of intron-exon boundary. By performing RT-qPCR using the primer pair, we could measure pre-mRNA levels of *Penk* gene. First, we confirmed non-contamination of gDNA by performing non-RT samples. Amplification of non-RT samples was not observed, suggesting that there was no contamination by gDNA into total RNA samples. Secondly, we confirmed if mRNA levels of

Penk were up-regulated in $Na_v1.7$KO mice by performing RT-qPCR with another primer pairs. Again, we used $Na_v1.7^{Adv}$ knockout mice where $Na_v1.7$ is deleted in all sesory neurons and littermate control. Although we measured mRNA levels of *Penk* in DRG in both littermate control and $Na_v1.7$KO mice to confirm our microarray data (Figure 2-8), the primer pair we used overlaps the same exon. This primer pair overlapping the same exon can detect not only mRNA but also pre-mRNA, Therefore, we also tested amplification at a different exon boundary to confirm we measured mRNA, not with pre-mRNA. We used a Taqman assay as it provided a primer pair that amplified segments at a different exon boundary. The result demonstrated the same tendency as when performed using SYBR green with primers we designed; namely, up-regulation of mRNA levels of *Penk* in $Na_v1.7$KO mice (Figure 2-23A). Thirdly, we measured pre-mRNA of *Penk* in DRG to compare $Na_v1.7$KO and littermate control mice. Significant up-regulation of pre-mRNA levels of *Penk* in $Na_v1.7$KO mice was identified (Figure 2-23B). These results support our hypothesis that $Na_v1.7$ mediates transcriptional activity of *Penk*, leading to the up-regulation of mRNA and protein levels.

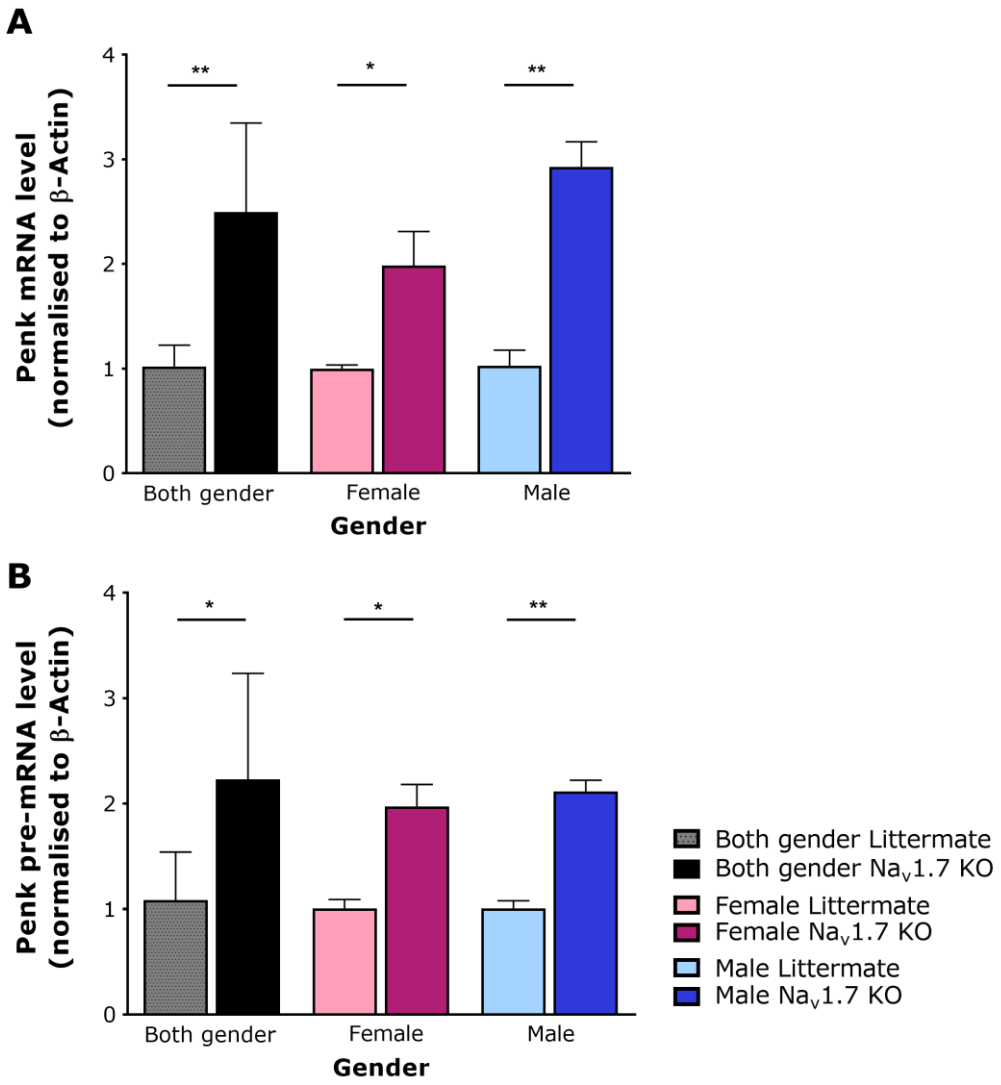

Figure 2-23. Real-time qRT-PCR results of mRNA and pre-mRNA levels of *Penk*. (A) mRNA levels of *Penk* was up-regulated in DRG in both female and male $Na_v1.7$KO mice . Taqman assay was used to amplify the segments of different exon boundary. (B) pre-mRNA levels of *Penk* was also up-regulated in DRG in both female and male $Na_v1.7$KO mice .

2.3.5 *Penk* expression mediated by intracellular sodium ions

Performed by Dr. Vanessa Peraira at Molecular Nociception Group, WIBR, UCL and myself

The next question is how the loss of $Na_v1.7$ can alter the mRNA expression of *Penk*. Several mechanisms can answer for this enigma; $Na_v1.7$ itself might serve as a transcription factor. This idea came from some studies in VGCCs that C-terminus of a subtype of VGCCs acts as a transcription factor (Gomez-Ospina et al., 2006, Barbado et al., 2009). Another idea is

that other elements may play a role in *Penk* transcription together with $Na_v1.7$ or downstream elements can be associated with transcriptional activities. A possibility of particular interest is that sodium ions may be involved in mediating gene expression. Increases in intracellular sodium ion concentration led to activation of salt-inducible kinase 1 that can activate myocyte enhancer factor 2 (MEF2)/transcription of nuclear factor of activated T cell (NFAT) transcriptional activity in a cardiac cell line (Popov et al., 2012). A related member of the NFAT family, TonEBP (Tonicity-responsive enhancers binding protein), appears to stimulate transcription by binding to TonE sequences (Miyakawa et al., 1999). TonE has been reported to serve a key role in transcriptional activation of sodium/*myo*-inositol cotransporter (Yamauchi et al., 1993) and sodium/chloride/betaine cotransporter (Uchida et al., 1993). NFAT5 is expressed in sensory neurons (Usoskin et al., 2015) and several copies of the NFAT5 consensus sequence 5'-TGGAAANYNY-3' (Esensten et al., 2005, Lopez-Rodriguez et al., 1999, Stroud et al., 2002) are also found upstream of the human *PENK* gene, indicating that NFAT5 could regulate *PENK* expression by binding to the promoter region. Taking these studies into account, sodium ions may play a role as a second messenger in sensory neurons to regulate gene expression, possibly via NFAT5 activities. Prior to investigating the link between NFAT5 and $Na_v1.7$, this thesis aimed to explore if increased levels of intracellular sodium ions impact on the transcriptional activity of *Penk* in DRG. Furthermore, if sodium ions play a role as a second messenger, other genes such as *Ceacam10* expression might be also altered through the increase of intracellular sodium ion levels. In this thesis, a possible role of sodium ions in transcriptional activities was explored. To address the effect of intracellular sodium ions on gene expression, we used three agents: firstly, monensin, a sodium ionophore that can elevate intracellular sodium levels. Secondly, the sodium channel-specific pore blocker tetrodotoxin (TTX). Thirdly, the calcium ionophore, ionomycin to explore the potential link between altered calcium levels and gene expression. We selected three genes to test this effect; *Ceacam10* which is the most down-regulated gene and *Penk* which appears to be the most interesting up-regulated gene. In addition to those genes, we tested another gene called *Tmem173*, which was also up-regulated in $Na_v1.7$KO mice. By measuring the effect of sodium ions on this gene, we expected to know sodium ion- mediated up-regulation could be *Penk*-specific or sodium ions could also affect the expression of *Tmem173*. The results will be addressed in the following sections.

I. Sodium-mediated mRNA upregulation of *Penk* in DRG

Firstly, we tested the effect of monensin that can increase intracellular sodium ion levels. We found that monensin (500nM) could downregulate the expression of *Penk* mRNA in DRG neurons derived from wild-type mice, whereas *Ceacam10* expression was enhanced a few-fold by monensin treatment (Figure 2-24AB). On the contrary, no significant down-regulation of *Tmem173* mRNA levels in monensin treated DRG neurons was observed although it appeared to be slightly down-regulated (Figure 2-24C). Secondly, to explore the mechanisms of the gene expression regulation by sodium ions further, we tested the effect of the sodium channel-specific pore blocker tetrodotoxin (TTX) on gene expression. The half-maximal inhibitory concentration (IC50) for TTX is 30nM for $Na_v1.7$; however, $Na_v1.8$ is defined as TTX insensitive with an IC50 of 60 mM (Nassar et al., 2004, Akopian et al., 1999). By using TTX at concentrations up to 500 nM, we could completely block the activity of $Na_v1.7$ and other TTX- sensitive sodium channels all known to be present in DRG, whereas $Na_v1.8$ would retain activity. Interestingly, *Penk* mRNA levels were up-regulated in TTX treated DRG neurons obtained from WT mice (Figure 2-25A), while mRNA levels of *Ceacam10* were not altered by TTX (Figure 2-25B). Also, *Tmem173* expression was not significantly up-regulated (Figure 2-25C). These results could indicate that *Penk* expression is altered by sodium ion mediated by main contributor of TTX-sensitive sodium channel, $Na_v1.7$. On the contrary, *Tmem173* expression does not seem to be mediated by sodium ions, and *Ceacam10* expression could be mediated by other factors through the elevation of intracellular sodium ion levels. Thirdly, we explored if sodium ions play a role directly on *Ceacam10* and *Penk* expression or other factors involved in gene expression. Calcium ions are likely candidates for mediating gene expression; calcium is the cation more usually linked to second messenger activity through interaction with a range of enzymes. Altered levels of intracellular sodium ions may result in changes in intracellular calcium through effects on pumps and exchangers (Kuroda et al., 2013). Moreover, at high concentrations, monensin is able to increase intracellular calcium levels in some cells (Gorczynska and Handelsman, 1993). We used the calcium ionophore ionomycin to explore the potential link between altered calcium levels and gene expression. Ionomycin (200 nM), unlike monensin, had no effect on *Penk* mRNA levels measured using qPCR in DRG neurons (Figure 2-26A). Interestingly, the increase in intracellular calcium caused by ionomycin led, as with monensin treatment, to enhanced expression of *Ceacam10* mRNA (Figure 2-26B). This result could indicate that calcium-mediated second messenger regulatory events are at play in *Ceacam10* expression in sensory neurons. However, as the increase in levels of intracellular calcium had no effect on *Penk*

mRNA levels, sodium rather than calcium seems to be a key second messenger in the regulation of opioid peptide expression.

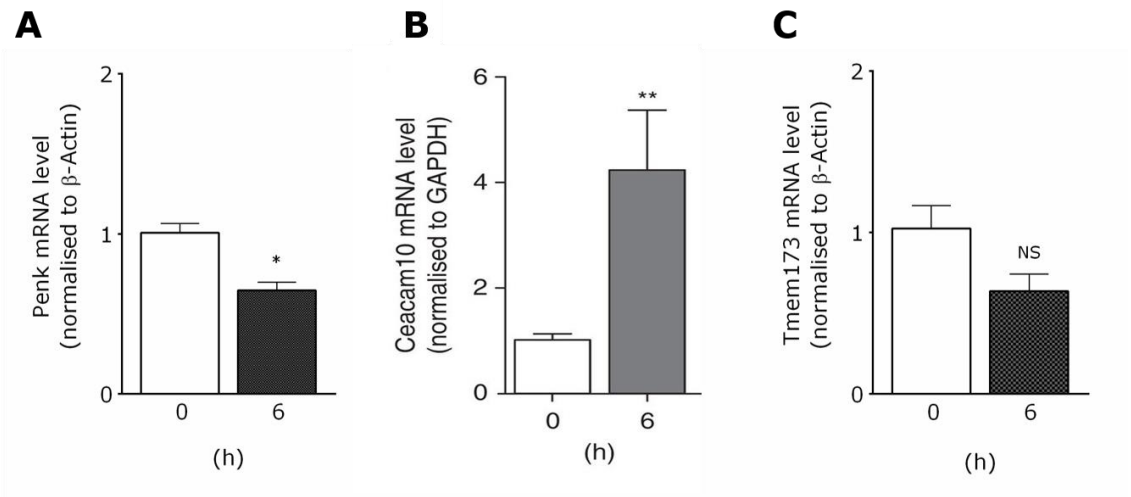

Figure 2-24. The mRNA levels of *Penk*, *Ceacam10* and *Tmem173* levels in DRG treated with monensin 500nM for 6 hours. mRNA levels of *Penk* was down-regulated (A) while *Ceacam10* mRNA level was up-regulated (B) by monensin administration. On the contrary, no significant dysregulation was observed in *Tmem173* mRNA level (C) although it seemed to be slightly down-regulated. n=3. The measurement for *Ceacam10* mRNA level was performed by Dr.Vanessa Pereira at Molecular Nocuception Group, WIBR, UCL and the others were performed by myself

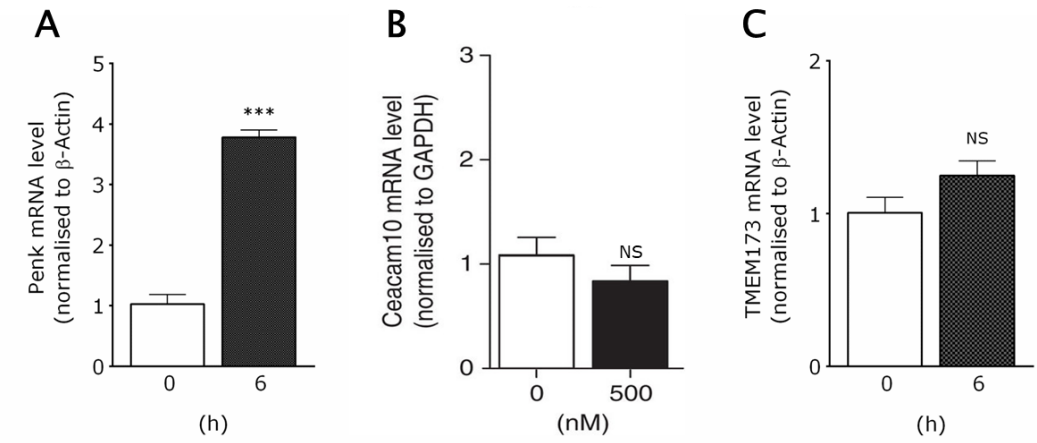

Figure 2-25. The mRNA levels of *Penk*, *Ceacam10* and *Tmem173* levels in DRG treated with TTX 500nM for 6 hours. The mRNA levels of *Penk* was strongly up-regulated (A) while both *Ceacam10* and *Tmem173* mRNA level was not altered by TTX administration (B) (C). n=3. The measurement for *Ceacam10* mRNA level was performed by Dr.Vanessa Pereira at Molecular Nocuception Group, WIBR, UCL and the others were performed by myself.

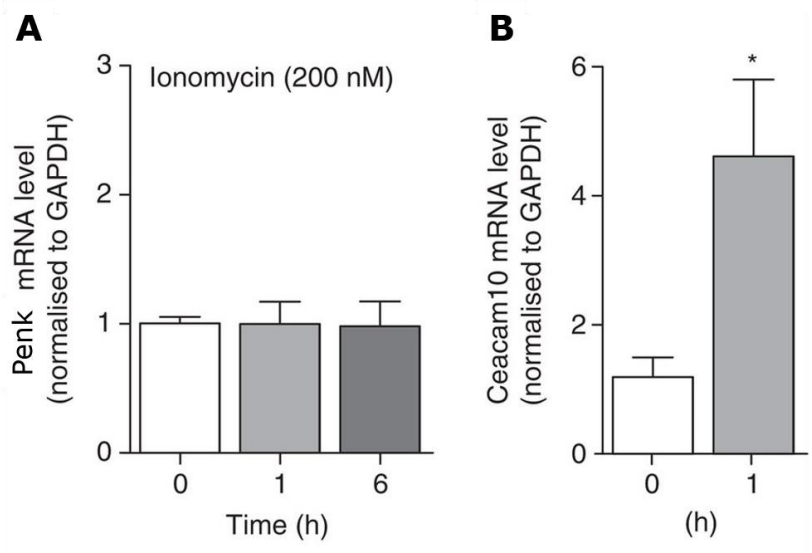

Figure 2-26. The mRNA levels of *Penk* and *Ceacam10* levels in DRG treated with ionomycin 200nM. The mRNA levels of *Penk* was not altered (A) while *Ceacam10* mRNA level was up-regulated in ionomycin treated DRG (B). These data was collected by Dr.Vanessa Pereira at Molecular Nocuception Group, WIBR, UCL.

II. Intracellular sodium levels did not alter transcriptional activity in Luciferase assay in Neuro2A stable cells

The present data suggest sodium seems to play a role in the regulation of *Penk* expression. We questioned if sodium mediates the transcriptional activity of *Penk*. To explore this question, we first attempted to test it on the Neuro2A cells stably expressing Firefly and Renilla luciferase. The same numbers of cells stably expressing Firefly and Renilla derived from the ones transfected with SV40-rLuc and m*Gapdh*-fLuc, m*Penk*-fLuc or φ-fLuc were treated with monensin, TTX or vehicle (ethanol) as a control. The RLU ratio of Firefly and Renilla did not show any marked difference between control and monensin or TTX treatment (Figure 2-27). We also analysed the data with RLU of Firefly luciferase since the cells were plated in the same numbers before treatment of the agents. Technically, the normalization of Renilla luciferase luminescence was not necessary if the cells were growing in the same manner. In addition, this experimental design could remove an effect on SV40 promoter activities due to agents' treatment. The luminescence of Firefly luciferase controlled by the m*Penk* promoter was significant down-regulated in monensin treated cells at 6hr and 24hr post-treatment while no dramatic difference was observed in TTX treated cells (Figure 2-28B). There were no significant differences in RLU of Firefly luciferase driven by the m*Gapdh* promoter between

monensin or TTX treatment and control cells (Figure 2-28A). However, monensin treated cells tended to show reduced levels of RLU of Firefly luciferase controlled by mGapdh promoter (Figure 2-28A). We therefore analysed the RLU of Firefly luciferase controlled by the m*Penk* promoter by normalising the RLU of Firefly luciferase driven by the m*Gapdh* promoter. Although Firefly signals given by *Penk* promoter activity were decreased in monensin treated cells, normalization by the signals controlled by m*Gapdh* promoter did not result in a marked decrease (Figure 2-29). This could be because sodium ions do not play a role in transcriptional activities of *Penk* or no role in transcriptional activities occurs in Neuro2A cells and the mechanisms are different from DRG neurons. We therefore aimed to measure pre-mRNA levels of *Penk* in DRG neurons to reveal if sodium ions mediate transcriptional activity of *Penk*, described in the next section (III).

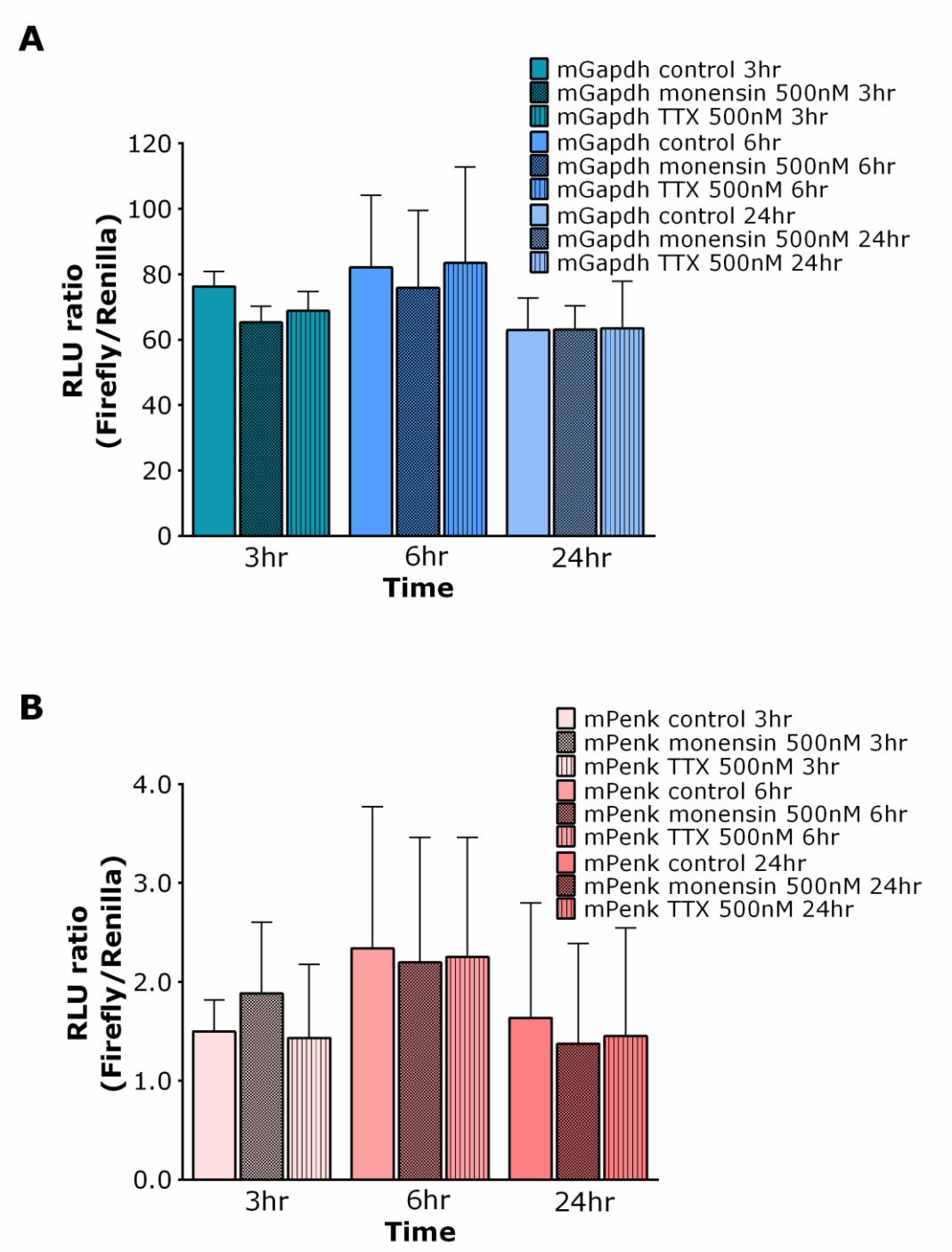

Figure 2-27. Luciferase assay in Neuro2A cells stably expressing Renilla luciferase driven by SV40 and Firefly luciferase driven by the promoter of m*Gapdh* (A) and m*Penk* (B), treated with monensin or TTX. RLU of Firefly luciferase indicating the activity of each promoter were divided by Renilla luciferase RLU as an internal control to normalise cell numbers. The measurement was performed at 3hr, 6hr and 24hr after the application of the agents. No significant difference was observed in both cell line stably expressing Firefly luciferase driven by m*Gapdh* and m*Penk*. (A) n=3 for 3hr and 24hr and n=8 for 6hr, (B) n=4 for 3hr and 24hr and n=5 for 6hr. The results are shown as mean ± SEM.

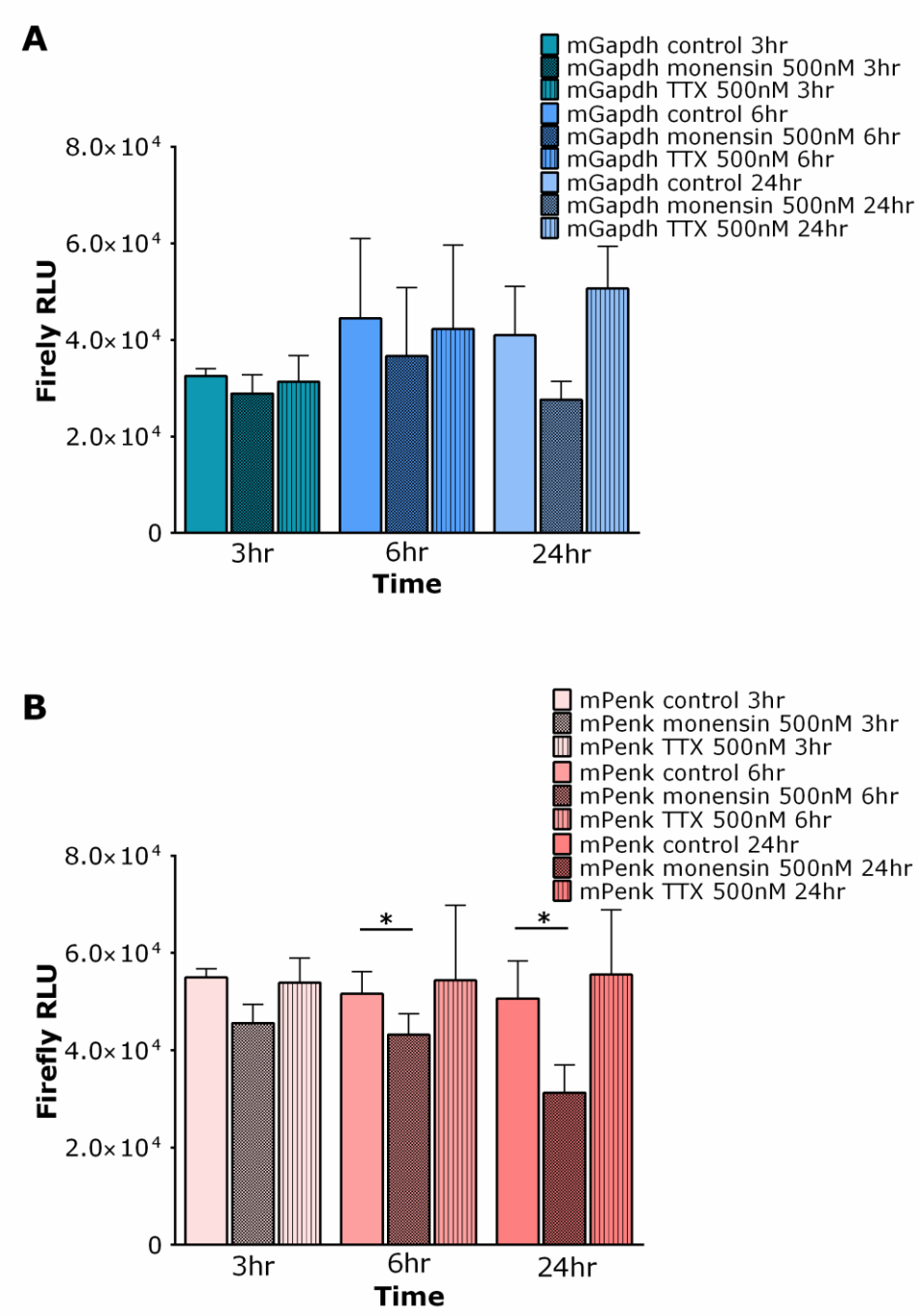

Figure 2-28. Luciferase assay in Neuro2A cells stably expressing Renilla luciferase driven by SV40 and Firefly luciferase driven by the promoter of m*Gapdh* (A) and m*Penk* (B), treated with monensin or TTX. RLU of Firefly luciferase indicating the activity of each promoter were shown. The measurement was performed at 3hr, 6hr and 24hr after the application of the agents. The significant difference was observed in only the cell line stably expressing Firefly luciferase driven by mPenk at 6hr and 24hr. (A) n=3 for 3hr and 24hr and n=8 for 6hr, (B) n=4 for 3hr and 24hr and n=5 for 6hr. The results are shown as mean ± SEM.

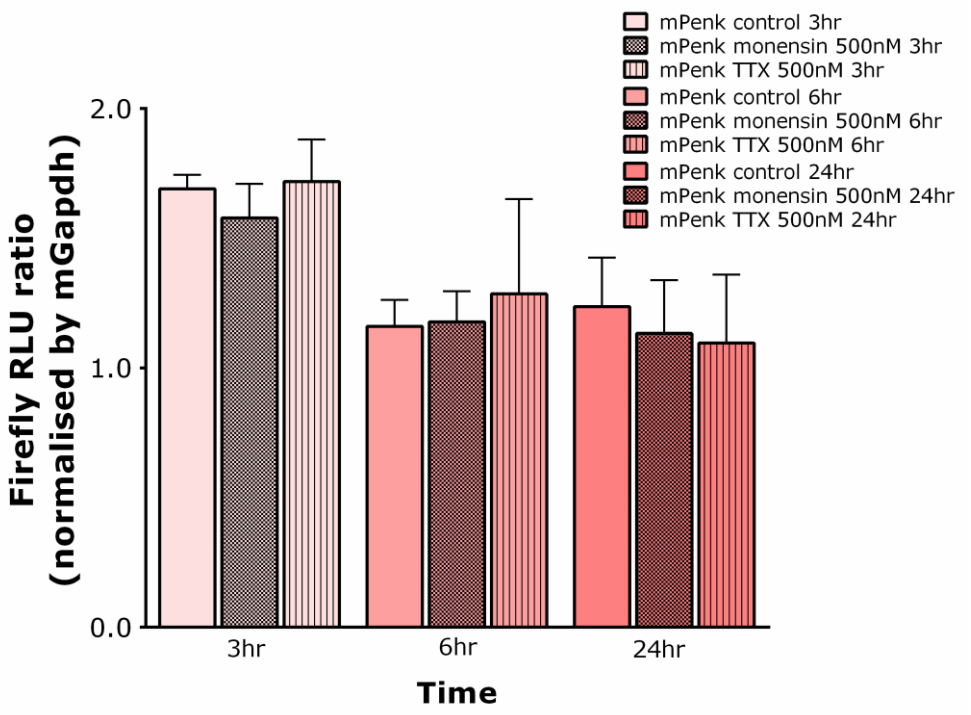

Figure 2-29. Luciferase assay in Neuro2A cells stably expressing Renilla luciferase driven by SV40 and Firefly luciferase driven by the promoter of m*Gapdh* and m*Penk*, treated with monensin or TTX. RLU of Firefly luciferase controlled by m*Penk* promoter was divided by that of m*Gapdh* promoter. The measurement was performed at 3hr, 6hr and 24hr after the application of the agents. No significant difference was observed. n=4 for 3hr and 24hr and n=5 for 6hr. The results are shown as mean ± SEM.

III. Intracellular sodium levels regulate Penk transcriptional activity in DRG neurons

To test whether sodium ions play a key role in the transcriptional activity of *Penk* in sensory neurons, cultured DRG neurons derived from WT mice were used. The same strategy was conducted; the effect of monensin, which acts to increase intracellular sodium ion levels, and TTX to block the activity of $Na_v1.7$ and other TTX- sensitive sodium channels. Down-regulation (Figure 2-30A) and up-regulation (Figure 2-30B) of pre-mRNA levels of *Penk* was observed in monensin and TTX application, respectively. These dysregulation of pre-mRNA levels of *Penk* was consistent with that of mRNA levels (Figure 2-24, Figure 2-25), suggesting that sodium ions mediate the transcriptional activities of *Penk* resulting in the regulation of endogenous opioid expression in DRG neurons.

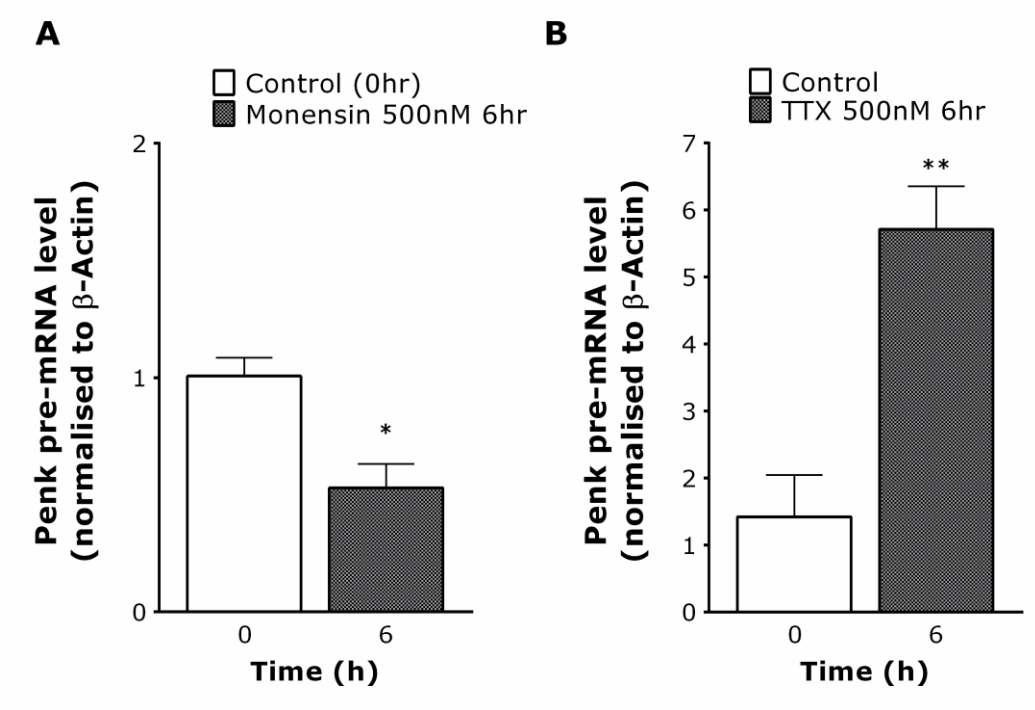

Figure 2-30. Pre-mRNA levels of *Penk* in monensin (A) and TTX (B) treated DRG neurons. Significant down-regulation and up-regulation of pre-mRNA levels in monensin (A) and TTX treated cells (B), respectively. n=3.

2.4 DISCUSSION

2.4.1 Summary of the results

In this study, we aimed to examine a novel role of $Na_v1.7$ in pain pathways. Our hypothesis came from previous microarray data showing that loss of $Na_v1.7$ function has dramatic effects on gene expression in DRG. Firstly, the data presented in this chapter confirmed the microarray analysis in DRG from $Na_v1.7$ null mice compared to littermate mice; significant down-regulation of *Ceacam10* and *Th*, and up-regulation of *Penk* and *Tmem173* in DRG of $Na_v1.7$ knockout mice (2.3.1). Secondly, the animal and human pain behaviour tests strongly support the hypothesis that the genes regulated by $Na_v1.7$ could contribute to the pain behaviour phenotype in $Na_V1.7$ knockout mice. The Hargreaves' test showed thermal deficits in *Ceacam10* KO mice (Figure 2-11), suggesting that *Ceacam10* plays a role in nociception. Application of the opioid antagonist, naloxone, to $Na_v1.7$ null mice restores their thermal and mechanical pain thresholds thus reversing the analgesia produced by loss of $Na_v1.7$ function without affecting pain thresholds in WT controls (Figure 2-10). Moreover, infusion of naloxone was able to reverse analgesia to a noxious heat stimulus in the $Na_v1.7$-null CIP

patient while there was no change in healthy control participants (Figure 2-12)(2.3.2). Thirdly, the results in this chapter demonstrated a possible role of sodium ions in *Penk* transcription though $Na_v1.7$ by measuring mRNA and pre-mRNA levels, but not the expression of *Ceacam10* or *Tmem173* (2.3.4, 2.3.5I, 2.3.5III). Of note, this mechanism was not clearly displayed by using luciferase assay (2.3.3, 2.3.5II).

The present data strongly suggests that dysregulated genes can be associated with pain and $Na_v1.7$ plays a key role in gene expression along with its well-known function of propagating action potentials. This novel activity of $Na_v1.7$ potentially broadens the possibilities for targeted drugs and moreover, effective treatments in pain therapy. The studies in this chapter would open more questions regarding this novel function of $Na_v1.7$ and its mechanisms. This section will discuss a role of the dysregulated genes in pain which this chapter focused on, several technical limitations and future work.

2.4.2 TH in pain pathways

TH is an enzyme which catalyses conversion of L-tyrosine to L-DOPA. L-DOPA is a precursor of dopamine, noradrenaline, and adrenaline which are known as catecholamines. *Th* may be deemed interesting to explore further in pain sensation. TH is expressed in a subpopulation of unmyelinated small DRG neurons (Brumovsky et al., 2006, Usoskin et al., 2015). We found dramatic down-regulation of *Th* in DRG of $Na_V1.7$ KO mice. Interestingly, correlation between dopamine receptors and sodium currents has been documented. An agonist of D1 dopamine receptor attenuated stimulated excitatory postsynaptic potential amplification in prefrontal cortex pyramidal neurons and TTX abolished this effect (Rotaru et al., 2007). In addition, dopamine itself appears to induce an increase in inward sodium current in prefrontal cortex pyramidal neurons in rat brain slices (Gorelova and Yang, 2000). Furthermore, in small DRG neurons, a study suggested that dopamine receptor activation inhibited the tetrodotoxin-resistant (TTX-R) sodium current (Galbavy et al., 2013). It is not solely sodium channels/ currents that are affected by dopamine or its receptors. The probability of calcium channel opening is strongly reduced by application of dopamine and noradrenaline and these catecholamines reduced single calcium channel activity at low membrane potentials in sensory and sympathetic neurons from chick embryo (Marchetti et al., 1986). A recent study suggested that dopamine or an agonist of D1/D5 dopamine receptors inhibited both inward and outward capsaicin-activated currents which are linked to TRPV1 channel activity in DRG neurons. This inhibition was calcium-calmodulin-dependent protein

kinase II (CaMKII) dependent (Chakraborty et al., 2016). Since TH is involved in synthesis of the dopamine, noradrenaline, and adrenaline precursor, L-DOPA, down-regulation of TH caused by loss of $Na_v1.7$ expression might alter the other channel functions leading to mediate pain phenotype. It would be interesting to investigate further the interaction between $Na_v1.7$ and TH, and this interaction may open other possibilities for developing drug targets to treat pain.

2.4.3 A role of *Ceacam10* in pain

Ceacam10 is a little characterised gene; despite exclusive expression in the maternal placenta surrounding the implantation site, Ceacam10 null mice are viable, fertile, and exhibit no obvious phenotype (Finkenzeller et al., 2003). In addition, Ceacam10 deficient mice showed no alterations in bone remodeling although Ceacam10 is expressed in bone marrow together with Ceacam1 (Heckt et al., 2014). However, the carcinoembryonic antigen (CEA) family, that Ceacam10 belongs to, has recently raised a great deal of interest; they play a number of roles in cell-to-cell recognition, tumour proliferation, and pathological processes (Kuespert et al., 2006). For example, Ceacam1 may induce proliferation of spleen T cells and cause inhibition of hypersensitivity (Nakajima et al., 2002). In this project, we found *Ceacam10* is expressed in DRG and the expression of *Ceacam10* was dramatically down-regulated in $Na_v1.7$KO mice. Interestingly, thermal deficits were found in *Ceacam10* KO mice in this study, suggesting that *Ceacam10* could play a role in thermal sensitivity. Notably, the RNA transcriptome analyses in the sensory neurons show *Ceacam10* is strongly expressed only in the TH cluster (Usoskin et al., 2015), which was previously described as subclass of unmyelinated neurons. Of note this TH cluster is considered to be low threshold mechanoreceptors which are involved in innocuous touch sensation (Li et al., 2011). However, these unmyelinated neurons are also categorised as nociceptors (see 1.1.1II). This high expression of *Ceacam10* in the unmyelinated sensory neurons supports the results of pain behaviour tests that the significant down-regulation of *Ceacam10* caused by loss of $Na_v1.7$ expression in the sensory neurons contributes to analgesic effects. Our present data shows an interesting link between *Ceacam10* in pain sensation and sodium channels.

The present results suggested the down-regulation of *Ceacam10* mediated by loss of $Na_v1.7$ expression could be linked to calcium regulatory events (2.3.5I). VGCCs constitute the predominant pathway for depolarization-mediated calcium entry into neurons (Bourinet et al., 2014). In sensory neurons, voltage-gated calcium channels (VGCCs) are activated once the

depolarizing signals reach, mediating Ca^{2+} influx in response to action potentials and depolarizing signals. Thereby, VGCCs might be involved in expression of *Ceacam10* along with $Na_v1.7$. The sodium-calcium exchanger (NCX) could be also one of the most likely elements involved in this. Sodium influx and NCX have been documented to play a role in neuronal injury and axonal degeneration related to pain: Sodium influx through voltage gated sodium channels affects recovery and the degree of anoxic injury in the optic nerve in rats, and NCX blockers significantly protected the optic nerve from anoxic injury (Stys et al., 1992). Several studies have also shown a link among $Na_v1.7$, NCX and intracellular calcium levels that leads to axonal degenerative disorders. SFN-associated variant $Na_v1.7$ channels, I228M, induced reduction in neurite length (Persson et al., 2013) and the application of sodium channel blocker carbamazepine and a blocker of reverse sodium-calcium exchange improved this reduction (Persson et al., 2013). The G856D mutation in $Na_v1.7$ identified in a multigenerational family with severe pain due to SFN displayed increased levels of both intracellular sodium and calcium levels following stimulation with high potassium levels compared with WT $Na_v1.7$-expressing neurons (Estacion et al., 2015). This G856D mutant $Na_v1.7$ channels demonstrate a time-dependent increase in intracellular calcium levels in DRG neurons (Rolyan et al., 2016). Blockade of reverse mode of the NCX or of sodium channels attenuates calcium ion transients evoked by high potassium levels in G856D-expressing DRG neurons (Estacion et al., 2015). NCX2, a subtype of NCX, is reported to be distributed in free nerve endings (Persson et al., 2010). These studies suggest that sodium influx though $Na_v1.7$ can be involved in NCX activities, altering intracellular calcium levels in the sensory neurons. Signalling pathways can be greatly affected by calcium ion induced by sodium influx; Veratridine, a sodium channel specific ionophore, induced increased calcium influx in adrenal chromaffin cells, and this sodium-calcium influx activated PKC- pathway elevating phosphorylation of extracellular signal-regulated kinase (ERK) and p38 (Nemoto et al., 2010). It has been well reported that calcium plays an important role in neuronal processes including gene expression (Bading, 2013). Alteration of calcium levels via loss of $Na_v1.7$ function therefore might affect expression of *Ceacam10*, contributing analgesic phenotype in the $Na_v1.7$ null mice and individual.

2.4.4 A possible role of *Tmem173* in pain

Tmem173, also known as STING (STimulator of Interferon Gene), plays an important role in innate immunity. It induces expression of IFN-α1 (Interferon alpha 1) and IFN-β (Interferon beta) by activating both the NFκB (Nuclear factor kappa B) and IRF3 (Interferon

regulatory factor 3) transcription pathways. This induction is considered to exert a potent antiviral effect (Ishikawa and Barber, 2008, Burdette and Vance, 2013). Several mutations in *TMEM173* have been liked to autoinflammatory vasculopathy causing severe skin lesions, particularly affecting the face, ears, nose, and digits (Liu et al., 2014). The clinical features also include ulceration, eschar formation, necrosis, and, in some cases, amputation and most of patients have interstitial lung disease (Liu et al., 2014). Tissue biopsy and *in vitro* assays showed a hyperinflammatory state, with evidence of increased IFN-β signalling (Liu et al., 2014). The TMEM173 signalling in innate immune responses has been well documented; an overview of these signalling pathways are shown in Figure 2-31 (Burdette and Vance, 2013); In response to dsDNA and cyclic dinucleotides, dimeric STING interacts with TBK1 (Tank-binding kinase 1) and relocalizes shown in myeloid cells or some cell lines such as HEK293 and HeLa. This STING-TBK1 complex is considered to serve a key role in three important signalling pathways. First, following the relocalization, TBK1 phosphorylates IRF3, which induces its dimerization and translocation to the nucleus. IRF3 along with other transcription factors bind to promoter elements to induce transcription of *Ifnb*. Secondly, STING can also interact with STAT6 (signal transducer and activator of transcription 6) after the relocalization. This interaction leads to TBK1- dependent phosphorylation of STAT6, leading to its dimerization and translocation to the nucleus, where it induces transcription of Ccl2 and Ccl20 (C-C motif chemokine ligand 2 and 20, respectively). This transcription appears to be independent from IRF3 and interferon. Thirdly, the STING-TBK1 complex can also recruit autophagy factors, which results in autophagy-like responses independently of *Ifnb* transcription (Burdette and Vance, 2013).

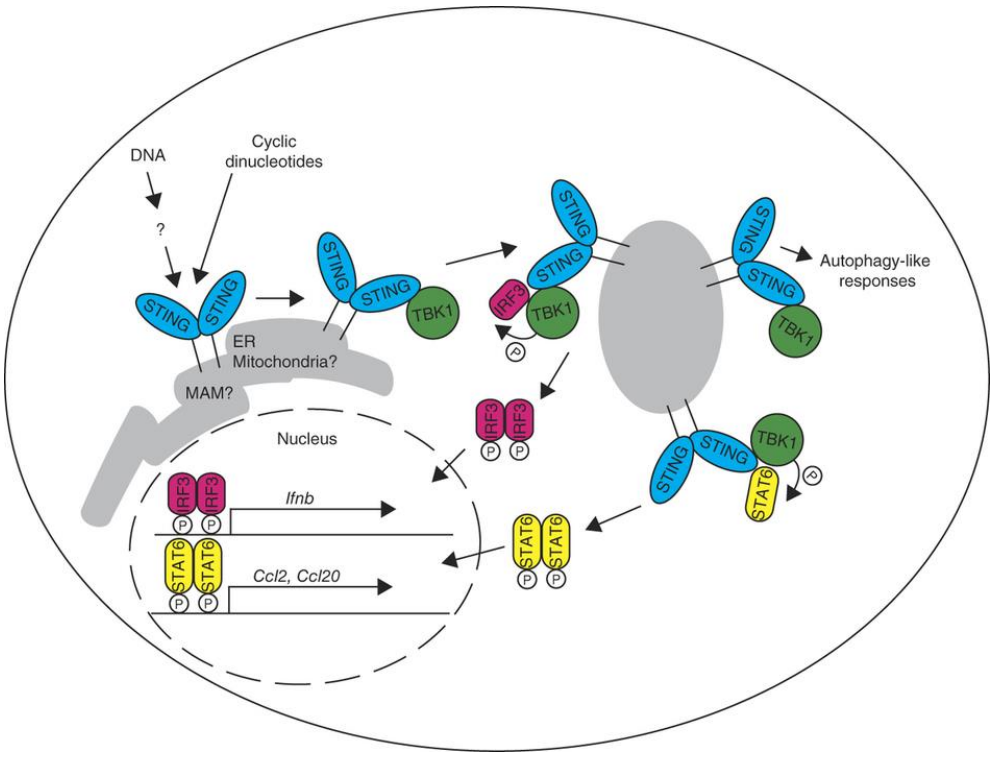

Figure 2-31. Overview of STING (TMEM173) signaling. ER, endoplasmic reticulum; MAM, mitochondria-associated membrane. (Burdette and Vance, 2013)

In this chapter, we found up-regulation of *Tmem173* in $Na_v1.7$ KO mice in microarray analysis which was confirmed by real-time qRT-PCR (Figure 2-8). Notably, the recent RNA sequencing data shows weak expression of *Tmem173* in the sensory neurons (Usoskin et al., 2015). This indicates that this gene may only have a small contribution to nociceptive processing. However, both the microarray and real-time qPCR analysis include the other cell types such as glial cells or fibroblast as well as sensory neurons. Therefore there is a possibility that loss of $Na_v1.7$ functions might alter the expression of *Tmem173* in both neuronal and non-neuronal cells, which may contribute to pain phenotype. Also, it should be noted that this gene may play a critical role in inflammatory pain rather than acute pain since Tmem173 is considered to be involved in innate immune responses. Interestingly, several studies have shown the low expression of TMEM173 in the patients suffering from chronic inflammation due to virus infection or cancer (Karimi-Googheri et al., 2015, Barber, 2015, Song et al., 2017). These studies indicate that the insufficient expression of TMEM173 might affect innate innmune responses from recovery. The up-regulation of *Tmem173* due to loss of functions of $Na_v1.7$ therefore may contribute to inflammatory pain. The downstream pathway of Tmem173 signalling might play a role in pain sensation, and non-neuronal cells might be involved in this event together with neurons. Some interesting studies indicate a link between interferons and

inflammatory pain (Tan et al., 2012, Liu et al., 2016). Intrathecal injection of IFN-α reduced CFA-induced mechanical allodynia (Tan et al., 2012, Liu et al., 2016) as well as heat hyperalgesia (Liu et al., 2016). This treatment also increased mechanical and noxious heat pain thresholds in naïve animals, and blocking endogenous IFN-α by a neutralizing antibody induced hyperalgesia (Liu et al., 2016). These results indicate an analgesic action of IFN-α. Interestingly, the study also demonstrated IFN-α was predominantly expressed in spinal cord astrocytes and to a lesser extent in microglial cells, but not in neurons in the dorsal horn (Liu et al., 2016). Application of IFN-α to spinal cord slices inhibited the frequency of sEPSCs (spontaneous excitatory postsynaptic current) without changing the amplitude of sEPSCs (Liu et al., 2016). This frequency change of sEPSC is considered to be caused by presynaptic mechanisms (Kohno et al., 2008, Yang et al., 1998, Kawasaki et al., 2008). Type I interferon receptors (IFN-α/β receptor) are expressed by primary afferent terminals in the superficial dorsal horn (Liu et al., 2016). Thus the results could indicate that the production of IFN-α by astrocytes in the dorsal horn inhibits excitatory synaptic transmission from presynaptic terminals. It would be interesting to explore the distribution of Tmem173 and downstream elements in sensory neurons as well as glial cells and the dorsal horn. $Na_v1.7$ KO mice have been documented to show reduced responses to inflammatory pain (Nassar et al., 2004). The up-regulation of *Tmem173* due to loss of $Na_v1.7$ functions therefore could contribute to this pain phenotype through stimulation of *Tmem173* downstream elements such as interferons. The studies of Tmem173 in sensory neurons do not appear to have been reported and this gene has not been linked with pain yet. Even so, the studies mentioned above would indicate a potential role of this gene in pain. Pain behaviour test on transgenic mice such as Tmem173 KO might be useful to address the correlation of this gene with pain. If this gene is proven to be associated with pain, this finding would be the first report in pain studies.

Whilst the mechanisms of induction of interferons stimulated by *Tmem173* have been well studied, research dedicated to factors upstream of this gene and regulation of gene expression are slim. Considering alteration of intracellular sodium levels by monensin or TTX did not affect the expression of *Tmem173* in primary cultured DRG neurons, other elements could be involved in the expression of this gene mediated by $Na_v1.7$. It would be also interesting to explore the link between $Na_v1.7$ and TMEM173, as this might contribute to development of therapeutic target to treat pain.

2.4.5 Endogenous opioids and $Na_v1.7$ in pain

Penk seems to be the most interesting gene which could be regulated by $Na_v1.7$. As stated before, *Penk* is a precursor of enkephalin, which is one of the well-characterised families of opioids. Opioid peptides are derived from four prepropeptide genes: the pro-opiomelanocortin (POMC), proenkephalin (PENK), prodynorphin (PDYN), and prepronociceptin (PNOC), encoding the precursors of endorphins, enkephalins, dynorphins, and nociceptin/orphanin, respectively (Vukojević et al., 2012). Also endomorphins have been discovered as opioid peptides although their precursors are yet to be found (Janecka et al., 2004). These opioids are the ligands for opioid receptors which are classified as μ, δ, and κ, and the non-classical nociceptin opioid receptor, denoted as MOP, DOP, KOP, and NOP, respectively (Vukojević et al., 2012). MOR is well-known for its high affinity to morphine, and endogenous ligands for this receptor is endomorphins. Other opioids such as endorphins, enkephalins and dynorphins bind to MOR at lower affinity (Koneru et al., 2009). DOR has high affinity for Leu- and Met-enkephalins which are its endogenous ligands. Notably, Met-enkephalin is a potent agonist of the δ-opioid receptor, and to a lesser extent the μ-opioid receptor. Leu-enkephalin has agonistic actions at both the μ- and δ-opioid receptors (Janecka et al., 2004). DOR is present in the dorsal horn of the spinal cord and analgesia mediated by DOR has been mainly documented in the spinal cord (Koneru et al., 2009). Naltrindole is considered to be a selective DOR antagonist (Koneru et al., 2009). KOR is defined by its high affinity for ketocyclazocine and Dynorphin A (Koneru et al., 2009). Norbinaltorphimine is a selective antagonist of KOR (Koneru et al., 2009). Table 2-7 shows these three receptors' endogenous ligands, agonists and antagonists, and Table 2-8 displays their selectivity. These three opioid receptors are classified as G-protein coupled receptors (GPCR).

Table 2-7. Opioid receptors-their agonists and antagonists and endogenous ligands. (Koneru et al., 2009, Janecka et al., 2004)

BNTX-7 benzylidenenaltroxone; EKC-ethylketocyclazosine; NTB-benzofuran analog of Naltrindole; nor-BNI-nor-binaltorphimine; DAMGO-[D-Ala 2, MePhe 4, Gly(ol) 5]enkephalin; DPDPE-[D-Pen 2, D-Pen 5]enkephalin; DSLET 0 [D-Ser 2, Leu 5]enkephalin-Thr 6; CTOP-D-Phe-Cys-Tyr-D-Trp Orn- Thr-Pen-Thr-NH2

Receptor Subtype	Endogenous Ligand		Selective Ligand		Nonselective Ligand	
		affinity for opioid receptors	Agonist	Antagonist	Agonist	Antagonist
μ	β-endorphins Endomorphins	μ, δ (μ=δ) μ	DAMGO Morphine Methadone Fentanyl Dermarphin	CTOP	Levorphanol Etorphine	Nalaxone Naltrexone β-funaltrexamine
κ	Dynorphin A, B	κ, μ, δ (κ>>μ and δ)	Spiradoline U50, 488	Nor-BNI	Levorphanol Etorphine EKC	Nalaxone Naltrexone
δ	Met- enkephalins Leu-enkephalins β-endorphins	δ, μ (δ>μ) μ, δ (μ=δ)	DPDPE Deltorphin DSLET	Naltrindole NTB BNTX	Levorphanol Etorphine	Nalaxone Naltrexone

Table 2-8. Ligands of opioid receptors and their selectivity. (Mannelli et al., 2011, Jordan et al., 2000, Chahl, 1996)

Ligand	Selectivity	Notes
Leu-enkephalins	δ, μ	Endogenous
Met-enkephalins	δ, μ	Endogenous
Dynorphin A	κ > μ > δ	Endogenous
β-endorphin	μ, δ > κ	Endogenous
Naloxone	μ, δ, κ (μ > δ, κ)	Universal antagonist
Naltrexone	μ >> κ > δ	Antagonist
β-funaltrexamine	μ > δ, μ_1?	Irreversible antagonist
Morphine	μ > δ > κ	Opiate
DPDPE	δ_1, δ_{cx}, δ_{ncx}	Selective agonist
DSLET	δ_2, δ_{cx}	Agonist
Deltorphin I	δ_1	Agonist
Deltorphin II	δ_2, δ_{cx}	Agonist
DAMGO	μ	Agonist

The role of these opioid receptors in pain has been well documented for decades (Koneru et al., 2009); Morphine analgesia via MOR has been well recognised (Matthes et al., 1996). Down-regulation of DOR in DRG contributes to surgery-induced nociception and increased enkephalin levels in the spinal cord and periphery reverse the postoperative pain (Cabanero et al., 2009). Importance of opioid receptors in pain has been also reported in genetic studies. For example, 118A>G polymorphism in μ-opioid receptor gene, *OPRM1*, showed reduced effects to μ-opioid analgesics (Lötsch et al., 2002), and decreased sensitivities to mechanical stimuli (Fillingim et al., 2005). As discussed above, in this chapter, both microarray analysis and qRT-PCR showed up-regulation of *Penk* levels in $Na_v1.7$ null mice as well as increased Met-enkephalin levels in the spinal cord. We also found the up-regulation of pre-mRNA of *Penk* in DRG from $Na_v1.7$ null mice. This indicates that $Na_v1.7$ is involved in transcription of *Penk*, therefore mRNA levels of *Penk* and Met-enkephalin level could be up-regulated in $Na_v1.7$ null mice. The correlation between opioids and $Na_v1.7$ in pain is supported by behaviour tests we have performed; systemic administration of the opioid antagonist, naloxone, to the conditional $Na_v1.7$ null mice where $Na_v1.7$ is deleted in all sensory neurons restores thermal and mechanical pain thresholds to reverse the analgesia of $Na_v1.7$ null mice, as well as detection of thermal pain by the CIP individual following naloxone infusion (Figure 2-10, Figure 2-12). The importance of opioids and pain in the CNS is well studied (Koneru et al., 2009). There could be another possibility that loss of $Na_v1.7$ function in sensory neurons might lead to alteration of opioids pathways in the CNS; if the upregulation of endogenous opioids is observed in the distant region of the CNS from sensory neurons such as in the brain,

the transcription activity of *Penk* is not likely to be mediated by $Na_v1.7$ but another mechanism could be involved in this upregulation. Therefore it would be important to investigate the correlation between this upregulation in the CNS and loss of $Na_v1.7$ function in sensory neurons. Even so, our behaviour tests on mice could support the idea that upregulation of endogenous opioids in sensory neurons, not in the CNS, could contribute to pain insensitive phenotype since systemic injection of littermate control did not alter the pain threshold.

The recent RNA sequencing data highlights the significance of the MOR in nociceptive $Na_v1.8$-expressing DRG neurons that do not contain mRNA of the KOR or DOR (Usoskin et al., 2015). Therefore, the target of naloxone on sensory neurons in this behaviour tests is thus likely to be the MOR. Of note naloxone did not reverse analgesic effects on *Ceacam10* KO mice (Figure 2-11), indicating that this mechanism is opioid-independent. On the contrary, a study showed IFN-α-induced anti-allodynia effect was reversed by naloxone (Tan et al., 2012), indicating that Tmem173 mediated analgesia would be opioid-dependent. The present behaviour results suggest that opioids may be responsible for the analgesia in mice and humans with loss of $Na_v1.7$ function, and support a strong correlation between opioids and $Na_v1.7$. The further study of link between opioids signalling and $Na_v1.7$ could be supported by pain behaviour tests using MOR / $Na_v1.7$ double KO mice. MOR / $Na_v1.7$ double KO mice by crossing MOR and $Na_v1.7$ KO mice might exhibit normal pain behaviour if loss of $Na_v1.7$ functions contributes to analgesic effects by altered opioids signalling through MOR. This opioids- $Na_v1.7$ correlation also indicates that use of selective $Na_v1.7$ channel blockers in combination with presently available opioid drugs could produce a synergetic effect for pain treatments and broaden the possibility of effective therapies.

2.4.6 A potential role of $Na_v1.7$ as a transcriptional factor

The hypothesis that $Na_v1.7$ could play a role in transcriptional regulator came from two aspects; the microarray results demonstrating $Na_v1.7$ has dramatic effects on gene expressions (described in 2.1) and VGCCs serving as a transcription factor (Gomez-Ospina et al., 2006, Barbado et al., 2009). For example, C-terminal fragment of a subunit of L-type VGCCs (Cav1.2) translocated to the nucleus in neurons in the brain regulating Connexin 31.1 gene and the other neuronal genes expression (Gomez-Ospina et al., 2006). Considering these studies dedicating a role of VGCCs in transcription factor, a fragment of $Na_v1.7$ can also play an important role serving as a transcription factor. This thesis did not explore a possibility of $Na_v1.7$ as a transcription factor, although aiming to explore the role of $Na_v1.7$ in

transcriptional regulator together with another element, sodium ions (addressed in the next section, 2.4.7). However, a role of $Na_v1.7$ serving as a transcription factor is still open question. Since we found a possible role of sodium ions mediating *Penk* transcription, expression of *Ceacam10* and *Tmem173* did not seem to be directly mediated by sodium ions (2.3.5I). Furthermore, there are large numbers of other dysregulated genes due to loss of $Na_v1.7$ functions in mouse sensory neurons. These genes might be directly regulated by $Na_v1.7$ as a transcription factor. To address this possible role, nucleus localization of $Na_v1.7$ should be tested. Since $Na_v1.7$ is a large protein, it is likely that a fragment of $Na_v1.7$ might play a role in transcription factor similarly to C-terminus of VGCCs. To determine which fragments and where they are located in the cells, first it would be required to develop antibodies to a peptide in the target fragments. Immunofluorescence on the cells and western blotting by purifying nuclear, cytoplasmic, and membrane fractions would be useful.

Once a fragment of $Na_v1.7$ is found in the nucleus, it would be interesting to identify what proteins it could bind to. Immunopreticipation and analysing binding proteins by mass spectrometry would help to answer this question. ChIP-seq could be also beneficial to identify which gene expression could be controlled by $Na_v1.7$. Together with the microarray data, these binding proteins could strengthen mechanisms of downstream gene expression regulated by $Na_v1.7$. Moreover, they might also give insight into why loss of $Na_v1.7$ expression has dramatic effects on gene expression compared to that of $Na_v1.8$ or $Na_v1.9$.

A number of potential mechanisms could be involved in gene expression regulated by $Na_v1.7$. Interestingly, several studies support transcriptional activities mediated by neuronal depolarization by VGCCs. For example, activation of NFATc4 (nuclear factor of activated T-cells 4) was inhibited by blockers of L-type channels. Of note, those of N- and P/Q-type channels have no effect on this activation (Graef et al., 1999). A further study suggested that activation of calcineurin, a Ca^{2+}- calmodulin-dependent phosphatase, led to phosphorylation of NFATc4, allowing its translocation from cytoplasmic to nucleus (Beals et al., 1997). In addition, calcineurin anchoring to $Ca_v1.2$ via A-kinase anchoring proteins AKAP79/150 is required to activate the NFATc4- dependent gene regulation pathway; AKAP150 specific RNAi inhibits depolarization-induced NFATc4 nuclear translocation (Oliveria et al., 2007). Effect on gene expression by neuronal depolarization led by VGSCs would be also interesting to explore, Selective blockers of $Na_v1.7$ and $Na_v1.8$ or $Na_v1.9$ when available, might be useful to uncover distinct mechanisms and downstream gene expression.

2.4.7 A possible role for sodium ions in opioid-mediated analgesia

It is still uncertain if $Na_v1.7$ plays a role as a transcription factor as discussed. How the loss of $Na_v1.7$ function can alter the expression of *Penk*, and moreover, what elements can be involved in together with $Na_v1.7$ to contribute to pain phenotypes, are interesting questions to explore. We raised a hypothesis that sodium ions may be involved in mediating gene expression. This idea came from several studies regarding sodium ions playing a role in gene expression. Increases in intracellular sodium ion concentration led to activation of salt-inducible kinase 1 that can activate myocyte enhancer factor 2 (MEF2)/transcription of nuclear factor of activated T cell (NFAT) transcriptional activity in a cardiac cell line (Popov et al., 2012). In addition, several copies of the NFAT5 consensus sequence 5'-TGGAAANYNY-3' (Esensten et al., 2005, Lopez-Rodriguez et al., 1999, Stroud et al., 2002) are also found upstream of the human *PENK* gene, indicating that NFAT5 could regulate *PENK* expression by binding to the promoter region. Taking these reports into account, sodium ions may play a role as a second messenger in sensory neurons to regulate gene expression mediated by NFAT5. In this chapter, we aimed to address if sodium ions influence gene expression. We found pre-mRNA of *Penk* were up-regulated in DRG collected from $Na_v1.7$ KO mice (Figure 2-23) and in TTX treated mice DRG neurons where TTX sensitive sodium channels were blocked (Figure 2-25). On the other hand, monensin treated DRG neurons in which intracellular sodium levels are increased showed reduced pre-mRNA levels of *Penk* (Figure 2-24). These results indicate that intracellular sodium ion levels through $Na_v1.7$ can mediate transcriptional activity of *Penk*. The link between gene regulation of *Penk* by $Na_v1.7$ and NFAT5 would be a key element to understanding a role of $Na_v1.7$ in gene regulation and their molecular mechanisms. If $Na_v1.7$ but not $Na_v1.8$ nor $Na_v1.9$ is associated with NFAT5 activities, this would explain why loss of $Na_v1.7$ functions can alter *Penk* expression. Knockdown or overexpression of NFAT5 in sensory neurons from $Na_v1.7$ might alter *Penk* expression. Measuring *Penk* expression levels in DRG neurons and performing behaviour test using $Na_v1.7$/NFAT5 double KO mice by crossing them might be also useful to answer this question.

It should also be noted that sodium ions could also interact to opioid receptors. GPCRs including DOR have altered functional properties due to allosteric changes caused by occupation of a sodium binding site (Katritch et al., 2014) (Figure 2-32). Sodium ions tend to negatively modulate agonist binding to the opioid receptors, without significantly affecting the binding affinity of antagonists, while the other cations such as magnesium and manganese and enhanced opioid agonist binding (Pasternak et al., 1975, Snyder and Pasternak, 2003). In addition, increased intracellular sodium uncouples opioid receptors from $G\alpha_i$ and increases the

constitutive signaling activity (Fenalti et al., 2014, Katritch et al., 2014). Taking these into accout, sodium influx via $Na_v1.7$ might lead to allosteric change that negatively affects opioid receptors functions. This also might indicate that blocked sodium influx due to loss of function of $Na_v1.7$ could result in increased opioid agonist binding ability, contributing to pain insensitive phenotype. Notably, a recent study from Hucho and Wood group suggested that nociceptive neurons of $Na_v1.7$ KO mice demonstrated decreased pronociceptive serotonergic signalling through the 5-HT_4 receptors, which are $G\alpha_s$-coupled GPCRs (Isensee et al., 2017). On the other hand, the efficacy of antinociceptive opioid signaling mediated by the $G\alpha_i$-coupled mu opioid receptors was enhanced in $Na_v1.7$ (Isensee et al., 2017). These effects were absent in the neurons of $Na_v1.8$ KO mice (Isensee et al., 2017). Moreover, opioids inhibited more efficiently TTX-resistant sodium currents (Isensee et al., 2017), Taking the modulation of functional properties of GPCRs by sodium ions into account, lacking $Na_v1.7$ might lead to altered sodium levels to result in altered pro- and antinociceptive GPCR signalling.

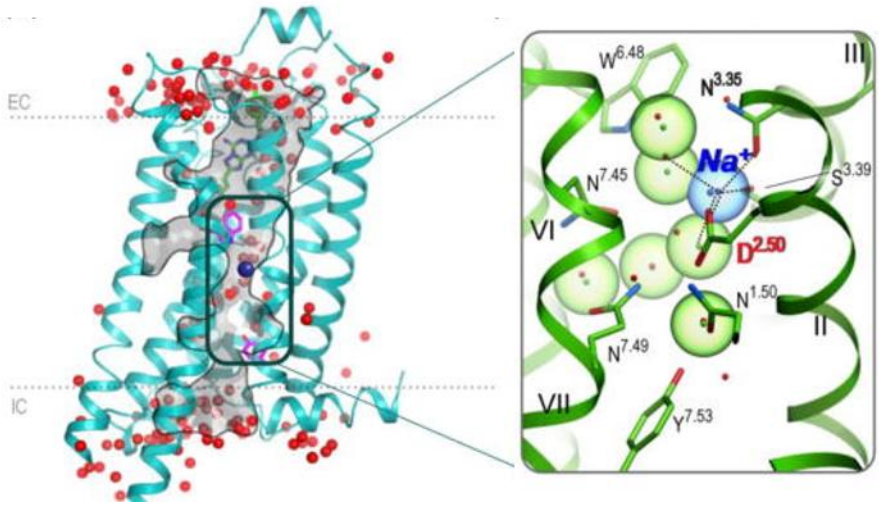

Figure 2-32. Na^+ and water cluster detected in GPCR structures and close-up of the δ-opioid receptor allosteric pocket. Modified from Katritch et al., 2014.

This possible role of sodium ions as a second messenger raises another question; $Na_v1.7$ rather than other subtypes of sodium channels might play a significant role in controlling the intracellular sodium level, contributing to gene expression. Preliminary studies in Wood's lab have recently been undertaken to investigate this question using HEK293 cells which are stably expressing $Na_v1.7$. The studies demonstrated that intracellular sodium levels were two-times higher compared with parentalHEK293 cells in their resting state (preliminary data from Wood's lab). The results indicated that $Na_v1.7$ may contribute substantially to the

intracellular concentration of sodium ions. Furthermore, this can suggest that the ablation of $Na_v1.7$ significantly decreases intracellular sodium ion levels in the cytoplasm, which could influence opioid signalling. Further investigation would be needed to uncover the correlation between sodium ions and $Na_v1.7$ or the other types of VGSCs. The understanding of this correlation may unravel the question why DRGs of $Na_v1.7$ KO mice showed greater numbers of dysregulated genes than $Na_v1.8$ KO or $Na_v1.9$ KO.

The loss of function of $Na_v1.7$ causes congenital insensitivity to pain; the patients never felt what pain like. This thesis showed up-regulation of endogenous opioids possibly though intracellular sodium levels in DRG neurons from $Na_v1.7$KO mice. In these experiments, this up-regulation demonstrated short-time effects since the measurements were conducted at 6hours after treatments. This could raise another issue regarding the time frame between human patients and this cell based analysis. The mice and human pain behaviour test demonstrated up-regulation of endogenous opioids due to loss of $Na_v1.7$ function could contribute pain insensitive phenotype (2.3.2). In these mice and the human CIP individual, intracellular sodium levels in sensory neurons could be less than WT control or individuals not carrying the mutation in $Na_v1.7$. If so, this could be consistent to high levels of intracellular sodium levels in HEK293 cells stably expressing $Na_v1.7$ as mentioned. Measuring intracellular sodium levels using DRG neurons of $Na_v1.7$KO mice would be useful to address this question. Even if no significant difference between $Na_v1.7$KO and control mice is observed, alteration of intracellular sodium levels might be local effects. The local and short-time effects might lead to trigger increased levels of endogenous opioids, and these effects might occur intermittently in $Na_v1.7$KO or CIP individual. Another question is correlation between sodium ions in gene expression and selective $Na_v1.7$ blockers. Why some selective $Na_v1.7$ blockers have not been proven as analgesic if sodium ions play a role in gene expression although less selective antagonist is effective? The clues may come from several elements; less selective antagonist might block sodium influx through the other subtypes of sodium channels more efficiently. Or the $Na_v1.7$ antagonist exhibiting potent analgesic might affect activity of downstream elements such as NFAT5 resulting in altered expression of endogenous opioids along with intracellular sodium levels. It has been already addressed that there could be several factors associated with $Na_v1.7$ and opioids. For example, vector-mediated enkephalin production resulted in reduction of $Na_v1.7$ levels in DRG, which may correlate with inhibition of phosphorylation of p38 MAPK (mitogen-activated protein kinase) and protein kinase C (PKC) (Chattopadhyay et al., 2008). Together with NFAT5, these elements might be essential to understanding the molecular mechanisms of gene regulation mediated by $Na_v1.7$. It would be also interesting to compare endogenous opioids levels in application of several $Na_v1.7$ blockers and their association with

the downstream elements together with intracellular sodium levels. These might uncover the conundrum why some blockers are less potent analgesic. Furthermore, this would broaden a possibility that these blockers may display analgesia if they are applied with opioids drugs. A deeper understanding of these mechanisms may give a new insight into nociceptive processing.

2.4.8 Limitations of the luciferase assay

Although pre-mRNA levels of *Penk* were up-regulated in DRG, we could not find clear evidence of transcriptional activity of $Na_v1.7$ using luciferase assays in either cell lines (HEK293 and Neuro2A cells) or DRG primary culture (2.3.3). The use of luciferase assays in this study demonstrated several technical limitations; 1) Difficulty of measuring luciferase signals. 2) Low transfection rate and limitation of overexpression of $Na_v1.7$. 3) Problem of stable cell line. 4) Selection of promoter regions. 5) Natures of cell types.

Fistly, since luminescence signals drop rapidly during the measurement in the assay using Gaussia and Cypridina luciferase, it could be difficult to see a significant difference between the effect of presence or absence of $Na_v1.7$, unless it strongly regulates the transcriptional activity of *Penk*. In the assay in DRG neurons, the DRG primary cell culture includes non-neuronal cells such as glial cells and fibroblasts that might have led to no significant difference in the culture between $Na_v1.7$ KO and littermate control mice. Dual-Luciferase Reporter Assay System using Firefly and Renilla luciferase can solve this problem. However, the signals were weaker than the assay using Gaussia and Cypridina luciferase in DRG neurons (Figure 2-21). Besides, the cell numbers in the DRG culture might not have been sufficient to obtain strong signals, having led to sizeable technical errors in each trial.

Secondly, the low transfection rate for DRG neurons might also lead to this sizeable technical errors; our primary data displayed that the transfection rate using electroporation on DRG is less than 10%. Transient transfection rate on cell lines are considered to be typically higher than DRG neurons. However, we observed approximately 20% positive cells. This transfection rate could bring another issue in this assay; technical limitation of overexpression of $Na_v1.7$. Although stable cell lines were expected to solve the problem of the different transfection rates between two types of luciferase constructs may cause. However, considering the transfection rate, overexpression of $Na_v1.7$ using lipofectamine might not be sufficient to see significant differences of transcriptional activities between the cells transfected with the vector bearing $Na_v1.7$ and the empty vector. In addition, functional expression of

$Na_v1.7$ should be also necessary to address if $Na_v1.7$ mediate the transcriptional activities. Since $Na_v1.7$ is a large protein, transient expression of $Na_v1.7$ might not be sufficient for its translation or transportation to sublocalise properly leading to the functional expression, Testing electrophysiological property and immunostaining would help to confirm this functional expression of $Na_v1.7$. The endogenous expression of $Na_v1.7$ in Neuro2A cells (BioGPS; http://biogps.org, (Wu et al., 2013, Wu et al., 2016)) might also compensate the difference between these two groups in the luciferase assay. In contrast to these elusive results of luciferase assay, pre-mRNA levels of *Penk* in DRG in $Na_v1.7$ null mice displayed significant up-regulation compared to littermate control. Taking these into account, complete loss of $Na_v1.7$ expression could be required to see the effect of transcriptional activities of *Penk* mediated by $Na_v1.7$. Knockdown of $Na_v1.7$ expression might be useful for this assay to solve this technical limitation of overexpression.

Thirdly, there is a limitation in the assay using the stable cell lines. Stable cell lines were created to solve the problem that low signals in DRG neurons and the different transfection rates between two types of luciferase constructs may cause. However, each clone has a different expression level of luciferase, which might lead to insignificant results between presence and absence of $Na_v1.7$.

Another technical problem in this experiment is that limited studies of promoter sequences in the genes we selected. As described in the result section, the studies of the promotor sequences of *Gapdh* and *Penk* are slim. Some studies indicated used 500kb to 3.3kb upstream of human *TH* gene is sufficient to drive reporter expression (Gardaneh et al., 2000, Coker et al., 1988, Kim et al., 2003). Of note, the construct bearing 3.3kb upstream of *TH* was active in neuroblastoma cell line although this construct did not drive reporter expression in immnature neural stem cells (Kim et al., 2003). One of the reasons why the Gaussia luciferase construct bearing putative *TH* promoter was not active in HEK cells might be each cell type might require different elements functioning as promoter. In addition, the 5kb upstream of *TH* might not be sufficient or repressor elements might be included leading to inhibition of the reporter expression. Since HEK293 cell line is a kidney derived cell line, it would be interesting to test on human neuronal cell line such as SH-SY5Y.

Finally, nature of the cell types could give these questionable results of luciferase assay in Neuro2A cells and pre-mRNA levels of DRG neurons. Similarly to the result using overexpression of $Na_v1.7$, luciferase assays in the stable Neuro2A cell line also did not show strong evidence that sodium ions can be involved in *Penk* transcription. The luciferase assay results shown in this chapter demonstrated that cells treated with monensin decreased Firefly

luciferase signals controlled by the Penk promoter but no change in TTX treated cells (Figure 2-28). Also the Firefly signals normalised by internal control (Cypridina luciferase driven by SV40) or *Gapdh* promoter did not display statistical significance (Figure 2-27, Figure 2-29). This elusive result could be because of some of the technical liminations of the luciferase assay as discussed above. Also, this may be due to different cell types; natures of DRG neurons and Neuro2A cell line, which was derived from neuroblastoma cells, can exhibit distinct properties. It is noteworthy that sensory neurons derived cell line could be useful to test this assay. Neuro2A is a neuroblastoma cell line, thereby the transcriptional activities of the target genes could be different from sensory neurons. There is a cell line called ND7/23 which is a hybrid cell line derived from neonatal rat DRG neurons fused with mouse neuroblastoma (Wood et al., 1990). This cell line exhibits properties of sensory neurons which are not displayed by neuroblastoma (Wood et al., 1990). We created the luciferase constructs driven by mouse putative promoter in order to be able to perform on both mouse DRG neurons and neuronal cell line. Since ND7/23 cells displayed sensory neuron-like properties derived from rat DRG neurons, the luciferase constructs were not tested in this thesis. However, the luciferase assay on ND7/23 might support the idea that transcriptional activity of *Penk* is mediated by $Na_v1.7$. As stated the limitation of overexpression, not only testing overexpression but also knock-down of $Na_v1.7$ expression might give a clear indication of this transcriptional activity. A possibility leading to the elusive results due to different natures of the cell types could be distinct expression of proteins between DRG and Neuro2A cells. These distinct proteins might be needed for activation of transcription of *Penk*, which might lead to the controversial results. Therefore, understanding of binding proteins with $Na_v1.7$ in DRG would be necessary to explore these mechanisms more effectively. Like the above discussion (2.4.6), these binding proteins might also give an idea of why $Na_v1.7$ KO has dramatic numbers of dysregulated genes compared to $Na_v1.8$ KO and $Na_v1.9$ KO.

2.4.9 Future work

The aim of this project was to explore a novel function of $Na_v1.7$. The data presented in this chapter showed significant down-regulation of *Ceacam10* and *Th*, and up-regulation of *Penk* and *Tmem173* in DRG of $Na_V1.7$ KO mice. The behavioural tests on $Na_v1.7$ null mice with administration of naloxone and *Ceacam10* KO mice suggest that *Ceacam10* and endogenous opioids could contribute to the pain insensitive phenotype in $Na_v1.7$ null mice; increased expression of endogenous opioids in DRG caused by the loss of $Na_v1.7$ function

could be also associated with the CIP phenotype in a human patient. We also found that the expression of Met-enkephalin is increased in the dorsal horn of the spinal cord in $Na_v1.7$ null mice compared to WT. However, in order to uncover whether the other genes of interest are important in pain sensation along with $Na_v1.7$, studying the alteration of protein levels is also essential. Immunohistochemistry and western blot can be used to confirm the altered expression levels of Th, enkephalin, Ceacam10 and Tmem173 in $Na_v1.7$ KO mice compared to $Na_v1.7$ WT mice. Investigating the distribution of these proteins not only in PNS, but also in CNS may also be essential to understand the mechanisms underlying $Na_V1.7$ mediated analgesia. Opioid receptors are abundantly expressed in the spinal cord and downstream elements of *Th* and *Tmem173* are also found in the CNS including the spinal cord. This indicates that dysregulation of these genes in sensory neurons could modulate pain pathways in the CNS along with the PNS. Investigating alteration of nociceptive transmission in the spinal cord mediated by activities of these dysregulated genes would be also interesting to explore.

Targeting Tmem173 could contribute to the development of a new drug since historically the research in this gene has been limited to immunological studies. The downstream elements of this gene such as interferons seem to be closely related to inflammatory pain. Pain behaviour tests in animals such as mice lacking Tmem173 expression would be useful to investigate whether Tmem173 is linked to pain. Also, it would be interesting to test knock-down effects of *Tmem173* in $Na_v1.7$ KO mice in inflammatory pain models; it may shed some light on the gene's association with analgesia caused by loss of $Na_v1.7$ function. Exploring activities of downstream elements such as interferons, NFκB and IRF3 in these animal models may provide an insight into mechanisms of the $Na_V1.7$ null phenotype. As mentioned above, since analgesic effects of IFN-α appear to be opioid-dependent, the link between opioids and Tmem173 could also open a door to better understand the complicated mechanisms of gene regulation mediated by $Na_v1.7$.

Further understanding of *Penk* transcription mechanisms mediated by $Na_v1.7$ can be intrinsic for pain treating drug development. The present results suggest a possible role for sodium ions as a second messenger. As discussed above, NFAT5 activities via alteration of intracellular sodium levels might be involved in *Penk* transcription. It is critical to investigate the expression levels of NFAT5 in $Na_v1.7$ KO mice compared to WT mice and to test whether sodium influx alters the expression of NFAT5 in order to understand the NFAT5-mediated *Penk* transcription. Measuring *Penk* expression levels in DRG neurons and performing behaviour test using $Na_v1.7$/NFAT5 double KO mice might be also useful to unravel the link between $Na_v1.7$, NFAT5 and endogenous opioids expression.

It would be also interesting to explore if $Na_v1.7$ itself could be a transcription factor. Like C-terminus of VGCCs, a fragment of $Na_v1.7$ might be localised in nucleus in the sensory neurons regulating several of downstream genes. Developing antibodies and performing immunofluorescence or western blotting could address if a fragment of $Na_v1.7$ is located in nucleus. Immunopreticipation and ChIP-seq could be also interesting to perform to address binding proteins and mechanisms of gene expressions controlled by $Na_v1.7$.

The reasons for a drastic difference between the numbers of genes regulated by $Na_v1.7$ and its counterparts, $Na_v1.8$ and $Na_v1.9$, remain unclear. A clue may come from investigating $Na_v1.7$ specific binding proteins and associated elements. It would be also noted that we used TTX to block TTX-sensitive sodium channel including $Na_v1.7$ to explore effects of the gene expression. $Na_v1.7$ or $Na_v1.8$ selective blockers would give clearer answer for these effects. There may be a number of factors mediating the relationship between the gene expression and $Na_v1.7$; as addressed above, enkephalin production resulted in reduction of $Na_v1.7$ levels in DRG and this reduction appears to be linked to the inhibition of phosphorylation of p38 MAPK and PKC. Exploring these factors further is necessary to evaluate the novel function of $Na_v1.7$, and furthermore, may lead to the development of a new, effective pain therapy.

2.5 CONCLUSION

In this project, we aimed to explore a novel function of $Na_v1.7$ in pain pathways. Prior to the study, using microarray analysis Wood's group found large numbers of genes have been dysregulated in DRG from $Na_v1.7$ null mice compared to littermate control mice. The data presented in this chapter confirmed significant down-regulation of *Ceacam10* and *Th*, and up-regulation of *Penk* and *Tmem173* in DRG of $Na_v1.7$ knockout mice. The pain behaviour tests suggest that *Ceacam10* and endogenous opioids could contribute to the pain insensitive phenotype in $Na_v1.7$ null mice. In addition, applying naloxone reversed analgesia in a CIP human individual, which indicates that up-regulation of endogenous opioids caused by loss of $Na_v1.7$ function can contribute to pain insensitive phenotype in humans too. These results strongly suggest that these dysregulated genes may be associated with the analgesia produced by loss of $Na_V1.7$ function, and that $Na_v1.7$ plays a key role in regulating gene expression along with its well-known function of propagating action potentials. The molecular biochemistry studies suggest that $Na_v1.7$, through alteration of intracellular sodium ion levels in DRG neurons, can influence the transcriptional activity of *Penk*, but not the expression of *Ceacam10*

or *Tmem173*. Further understanding the molecular mechanisms of gene expression mediated by $Na_v1.7$ and functions of dysregulated genes in pain may broaden the range of possibilities for targeted drug development and effective pain therapies. Moreover, they may provide some insight into why some more selective $Na_V1.7$ blocking molecules have failed to produce effective analgesia in the clinic.

3.1 INTRODUCTION

Over the last couple of decades numerous genes have been shown to be mutated in inherited pain disorders or have been linked to pain conditions through association studies (Table 2-1) (Diatchenko et al., 2007, Bennett and Woods, 2014). Although the functions of these genes are still under investigation, their identification are already contributing to the development of novel drugs for pain therapies (Eijkelkamp et al., 2012). A novel gene associated with a human pain insensitivity disorder could broaden the possibilities of further analgesic drug development. In this chapter, the function and pathological mechanism of a novel gene in pain studies is explored. The gene, called *ZFHX2* (zinc finger homeobox 2), has not yet been documented as being involved in regulating pain sensitivity. A potential causative mutation in *ZFHX2*, resulting in an amino acid change R1913K, was found from an analysis of genomic DNA from patients in a family who were diagnosed as being pain insensitive. In this chapter, the following topics will be explored; 1. Pathological mechanism of the ZFHX2 missense mutation, including subcellular localization (3.4.1) and arginine methylation (3.4.1) studies. 2. Association of *Zfhx2* with pain behaviour in global *Zfhx2* KO mice (V) and mutant BAC transgenic mice bearing the orthologous mutation identified in the human patients (3.4.3). 3. Functional studies of ZFHX2, exploring genes that are regulated by ZFHX2 and which potentially cause pain insensitivity via their altered expression. Microarray studies (3.4.4) and ChIP analyses (3.4.5) are also described. These experiments confirm the importance of ZFHX2 in pain perception.

3.1.1 Human monogenic pain disorders

The study of human inherited pain disorders can identify new genes that are important in pain pathways. As described in chapter 1 (1.1.5II), the genes encoding VGSCs are excellent examples that demonstrate how missense mutations can result in pain related disorders. For example, *SCN9A* encoding $Na_v1.7$ is known to underlie a number of heritable disorders such as congenital insensitivity to pain (CIP) (Cox et al., 2006), inherited primary erythromelalgia (IEM) (Yang et al., 2004), paroxysmal extreme pain disorder (PEPD) (Fertleman et al., 2006), and small fibre neuropathy (SFN) (Faber et al., 2012a). Also, mutations in *SCN10A* causing a gain-of-function in $Na_v1.8$ are considered to be associated with SFN (Faber et al., 2012b). Missense

mutations in *SCN11A* encoding $Na_v1.9$ are linked to painful peripheral neuropathies (Huang et al., 2014), familial episodic pain syndrome (FEP) (Zhang et al., 2013b), and have been recently associated with pain insensitivity (Leipold et al., 2013). Aside from the mutations in VGSCs, a heterozygous mutation in *TRPA1* encoding a transient receptor potential cation channel, has been reported to be a cause of FEP (Kremeyer et al., 2010). Several mutations in *CACNA1A,* that encodes the voltage-gated calcium channel α1A, are linked to familial hemiplegic migraine (Riant et al., 2010).

Mutations associated with pain related disorders are not only restricted to the genes encoding ion channels. For example, several mutations in a transcription factor, PR homology domain-containing member 12 (PRDM12), were found in patients with autosomal recessive congenital insensitivity to pain and hereditary sensory and autonomic neuropathy (HSAN) (Chen et al., 2015b). Indeed, the functions of HSAN genes are diverse, ranging from neurotrophic functions (TRK-A and NGF), sphingolipid metabolism (SPTLC1 and SPTLC2), structural integrity of the endoplasmic reticulum (ATL1) and Golgi apparatus (FAM134B) and vesicular trafficking (RAB7A and KIF1A) (Rotthier et al., 2012).

Table 3-1. Genetic variants implicated in human pain conditions. Modified from (Diatchenko et al., 2007)

Abbreviations: BM, basilar migraine; BMS, burning mouth syndrome; CIP, congenital insensitivity to pain; CFS, chronic fatigue syndrome; FEM, Familial episodic pain syndrome; FHM, familial hemiplegic migraine; FMS, fibromyalgia syndrome; HSAN, hereditary sensory and autonomic neuropathy; IBS, irritable bowel syndrome; LBP, low back pain; M6G, morphine-6-glucuronide; MA, migraine with aura; MO, migraine without aura; NGF, nerve growth factor; OA, osteoarthritis; PE, primary erythromelalgia; PEPD, paroxysmal extreme pain disorder; PTSD, posttraumatic stress disorder; SFN, small fibre neuropathy; TMJD, temporomandibular joint disorder; VA, vasospastic angina; VNTR, variable number tandem repeat; VVS, vulvar vestibulitis syndrome; 5-HTTLPR, 5-HTT gene-linked polymorphic region.

Functional class	Gene	Condition	Genetic polymorphism
Transporters	*SLC6A3, or DAT1*	PTSD	3′ Untranslated region VNTR
	SLC6A4, or 5-HTT, or SERT	FMS, CFS, D-IBS	5-HTTLPR
		Migraine	VNTR and 5-HTTLRP
		TMJD	VNTR in intron 2
	ABCB1, or MDR1	Efficacy of mu-opioid analgesia	C3435T silent polymorphism in exon 26 changes substrate specificity.
Metabolic genes and transcription regulators	*COMT*	TMJD, analgesia, migraine, FMS	Val158Met
			Three major haplotypes determine COMT activity.
	CYP2D6	Opioid analgesia	More than 75 alleles code for distinct metabolizer phenotypes.
	GCH1	LBP	A haplotype of the GCH1 gene was associated with less pain following diskectomy for persistent radicular LBP.

	MTHFR	MA	C677T
	ACE	MA	287-bp deletion in intron 16.
	SPTLC1, or SPT1	HSAN I	Autosomal dominant mutations Cys133Tyr, Cys133Trp, Val144Asp and Gly387Ala resulted in reduced SPT activity and impaired sphingolipid synthesis.
	HSN2	HSAN II	Autosomal recessive mutations led to truncated forms of deduced HSN2 protein with unknown function.
	IKBKAP, or IKAP	HSAN III	Mutation in intron 20 produced truncated protein. Arg696Pro in exon 19 disrupted phosphorylation.
	NGFB	HSAN V	Autosomal recessive mutation Trp211Arg A homozygous mutation resulting in frame-shift (V232fs)
Receptors	*NTRK1, or TRKA*	HSAN IV	43 known autosomal recessive mutations led to inability to transduce NGF into growing neurons and their death.
	ADRA2A, ADRA2C	C-IBS	α_{2C}Del322–325 and α_{2A}C-1291G polymorphisms were associated with constipation-predominant IBS.
	ADRB2	TMJD	3 major haplotypes were identified.
	DRD2	MA	His313His (*NcoI* restriction site polymorphism C/T)
		PTSD	3′ -UTR polymorphism
	DRD4	MO, FMS	Exon III tandem repeat polymorphism
	MC1R	Opioid analgesia	Arg151Cys, Arg160Tyr and Asp294Asn
	OPRM1, or MOR	Mu-opioid analgesia	A118G (Asn40Asp)
	5-HTR2A	MA,TMJD	T102C
Cytokines	*IL1A, IL1B, and IL1RN*	LBP	IL-1α C889T, IL-1β C3954T, and IL-1RN G1812A
	IL1RN	VVS	Second intron VNTR
	IL1B	VVS, BMS	C3954T
	IL6	LBP	T15A (Asp162Glu)
	IL10	IBS	Promoter polymorphism G-1082A
	TNF	IBS	Promoter polymorphism G-308A
	LTA	MO	A higher frequency of TNFB*2 allele in MO patients.
Ion channels	*ATP1A2*	BM	Arg548His mutation was found in BM family.
		FHM type 2	Missense mutations and deletions led to loss-of-function or alteration of the kinetics of Na^+/K+-ATPase pump.
	CACNA1A	MA	Significantly increased sharing of CACNA1A marker alleles in siblings with MA.
		FHM type 1	Missense mutations in a pore-forming α1A subunit of neuronal Ca_v2.1 channels.
	SCN1A	FHM type 3	Gln1489Leu mutation led to a faster Na_v1.1 channel recovery from fast inactivation.
	SCN9A	PE	Mutations enhanced activation of Na_v1.7 channels.
		PEPD	Mutations impaired inactivation of Na_v1.7 channels.
		CIP	Homozygous nonsense mutations caused loss-of-function of Na_v1.7 channels.
		SFN	Patients with small fiber neuropathies carried gain-of-function mutations in Na_v1.7 channels.
	SCN10A	SFN	Painful SFNs were caused by gain-of-function mutations in Na_v1.8 channels encoded by *SCN10A*.

	SCN11A	CIP	*de novo* missense mutations in *SCN11A* caused gain-of-function of $Na_v1.9$ channels.
		FEP type 3	Missense mutations in *SCN11A* led to gain-of-function of $Na_v1.9$ channels.
	TRPA1	FEP type 1	A mutation in *TRPA1* caused gain-of-function of TRPA1 channels.

3.1.2 Pain insensitivity

As described in the introduction in Chapter 1 (1.1.5V) and the section above (3.1.1), several genes causing human pain disorders have been identified. This chapter is dedicated to the pain insensitivity disorders (Table 3-2). Such disorders can be caused by degeneration of sensory neurons, or a congenital failure of nociceptor development or by dysfunction of VGSCs in intact neurons. For example, nerve growth factor (NGF) is essential for growth and differentiation of sympathetic and sensory neurons, and particularly critical for the survival of nociceptors (Crowley et al., 1994). In 2004, a large family from Sweden was reported with a mutation in NGF and an associated pain insensitive phenotype associated with an absence of nociceptive neurons (Einarsdottir et al., 2004). Another recent example is mutation of the PRDM12 gene which is associated with a severe peripheral neuropathy and pain insensitivity (Chen et al., 2015b). In 2006, the first cause of pain insensitivity was reported that was not associated with a peripheral neuropathy when loss of function mutations in *SCN9A* were identified (Cox et al., 2006). More recently, gain-of-function of *SCN11A*, encoding $Na_v1.9$, has been also reported as a cause of inability to experience pain with a normal nerve biopsy result (Leipold et al., 2013).

In this project we report a potential causative point mutation in *ZFHX2*, zinc finger homeobox 2, in a family diagnosed with pain insensitivity (see 3.1.3). Neither a mutation of *ZFHX2* or *ZFHX2* itself have been previously reported as a cause of pain insensitivity or associated with pain sensation. This could mean that exploring this gene further has a huge potential for novel pain therapies.

Table 3-2. Genes responsible for developmental and non-functional nociceptor-related painlessness. Modified from (Nahorski et al., 2015).

Name of Disorder	Gene	Protein	Inheritance	Phenotype	Pathogenic Mechanism	Notes
Hereditary autonomic and sensory neuropathy 4 (HSAN4)	NTRK1	TRKA	Recessive	No pain and temperature sensing No sweating Learning difficulties	Null	Susceptibility to Staphylococcal infection
Hereditary autonomic and sensory neuropathy 5 (HSAN5)	NGF	NGFβ	Recessive	No pain and temperature sensing No sweating Learning difficulties	Null	Susceptibility to Staphylococcal infection
Navajo neurohepatop-athy	MPV17	MPV17	Recessive	Progressive, often fatal, encephalopathy, hepatitis and neuropathy	Null	Other mitochondrial phenotypes cause by hypomorphic mutations
Channelopathy insensitivity to pain	SCN9A	Nav1.7	Recessive	Congenital anosmia	Null	
Hereditary autonomic and sensory neuropathy 7 (HSAN7)	SCN11A	Nav1.9	De novo dominant	Intestinal hypoperistalsis, hypotonia and mild weakness, hyperhidrosis, itching, altered temperature sensing	Hyperactivati ng	Phenotype may be restricted to one mutation, p.L811P HSAN7 may be a misnomer because there is no neuropathy on nerve biopsy
Hereditary autonomic and sensory neuropathy 8 (HSAN8)	PRDM12	PRDM12	Recessive	No pain- and temperature-sensing neurons Reduced sweating and tearing	Null	The most recently found gene causing CIP. The patients are unable to feel acute, inflammatory, or chronic pain from birth.

3.1.3 Patients with pain insensitivity carrying a point mutation in ZFHX2

In this project, we are focusing on patients in a family who have pain insensitivity. The phenotype of the patients in this family was first described in 2008 (Spinsanti et al., 2008). The five patients from this family were diagnosed as suffering from hyposensitivity to painful thermal and capsaicin stimulation. According to the publication (Spinsanti et al., 2008), the clinical features were described as follows: 'The subjects, belonging to the same family (3 women and 2 boys from 3 generations), were a 75-year-old woman, her two daughters (40-

year- old and 34-year-old sisters) and two nephews (two brothers, 14 and 11 years old). All these subjects were apparently healthy, with normal mental performance and high performance in physical activities, with an apparently normal quality of life. The main clinical data were: absence of pain in response to usual painful stimuli (all subjects), low sensitivity to capsaicin (all subjects), history of clinical autonomic disability plus several episodes of hyperthermia, increased warm and cold thresholds, recurrent infections (3 subjects), absence of corneal reflex (all subjects), rare episodes of orthostatic hypotension (3 subjects).' Subsequent to this paper being published, an additional 6th member of the family was identified as having the same phenotype.

Although the individuals suffer from pain insensitivity, the clinical features showing they are generally healthy subjects indicated that identification of the mutant gene could highlight a useful new analgesic drug target. Prior to my involvement in this project, a distal skin biopsy was taken from the proband and also genomic DNA was isolated from all 6 affected members from blood samples. The biopsy stained by anti-Pgp9.5 demonstrated a normal nerve fibre density for age and gender (Figure 3-1) (Data from Prof Bennett, University of Oxford). The gDNA of 6 individuals (shown in red arrow in Figure 3-2) were analysed by exome sequencing. A potential causative mutation was found in *ZFHX2*, zinc finger homeobox 2, at position 1913, resulting in an amino acid change from arginine to lysine (NM_033400:c.G5738A:p.R1913K). Sanger sequencing confirmed the point mutation and that all affected individuals were heterozygotes (Figure 3-3). This mutation was absent from 394 healthy controls and also from public polymorphism and exome databases. ZFHX2 consists of 2572 amino acids, and the mutation was found in one of the homeobox domains (Figure 3-4). The mouse homolog, Zfhx2, has previously been described as being highly expressed in mouse brain tissue such as thalamus, hypothalamus, midbrain and pontine area (Komine et al., 2006), and recent RNA-seq data has highlighted a relatively high expression of *ZFHX2* in small diameter DRG neurons (Usoskin et al., 2015). We considered if the point mutation resulting in the R1913K amino acid change in ZFHX2 could be the pathogenic mutation causing the human pain insensitivity.

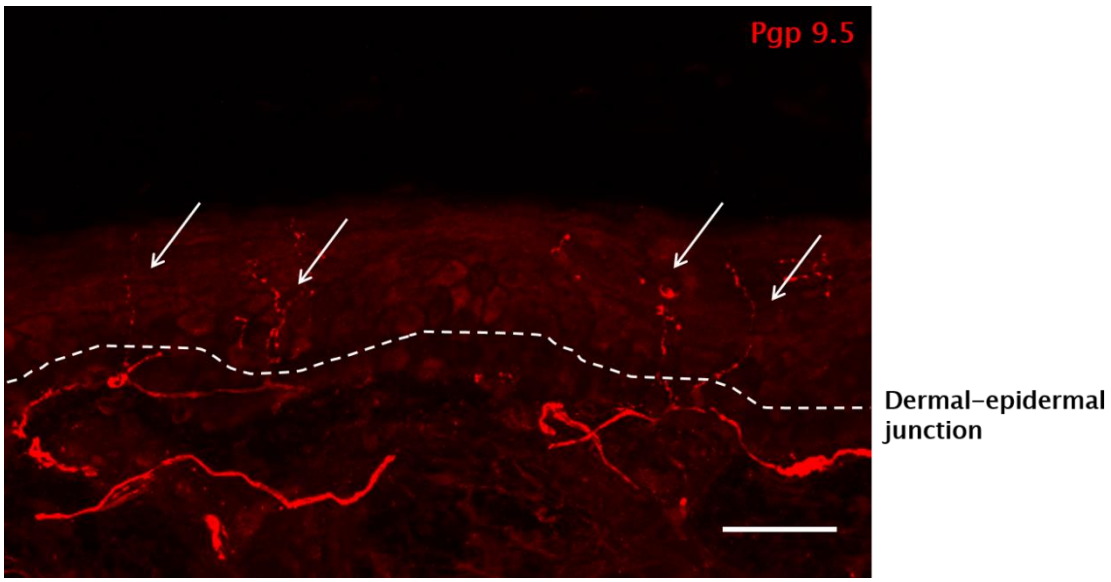

Figure 3-1. A patient (the individual II-4 in Figure 3-2) skin biopsy from lower leg. The sample was stained with anti-Pgp9.5. The white dots indicate dermal-epidermal junction. The white arrows show nerve fibres. Data from Prof Bennett, University of Oxford.

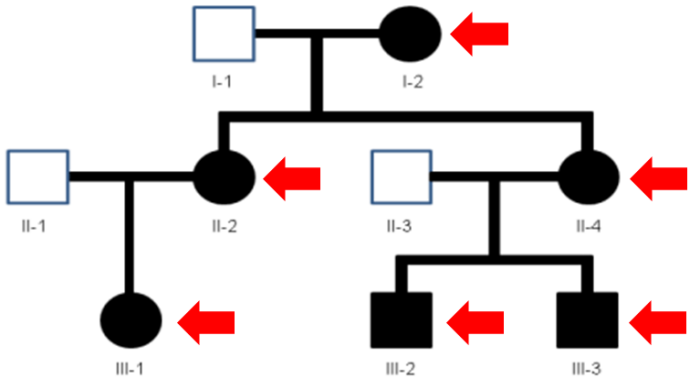

Figure 3-2. The individuals affected by pain insensitivity in the family (shown in black). The red arrows indicate that the samples from them were used for exome sequencing to identify potential causative mutations.

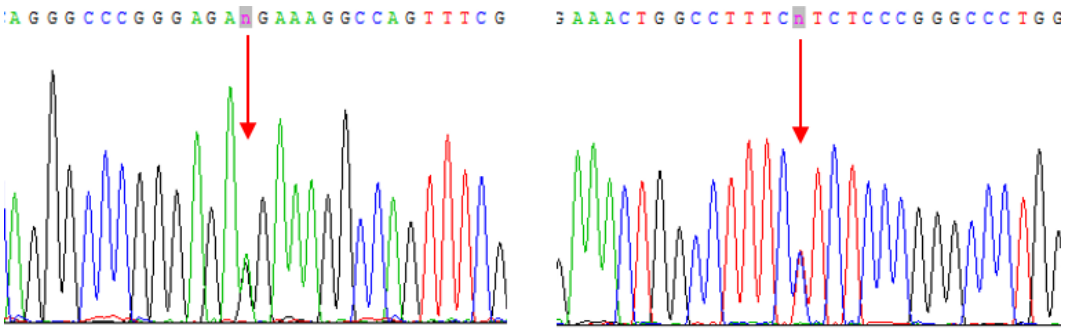

Figure 3-3. DNA sequence chromatograms of the patients showed a heterozygous mutation (c.G5738A: all patients showed the same mutation). The red arrows show the position of the mutation.

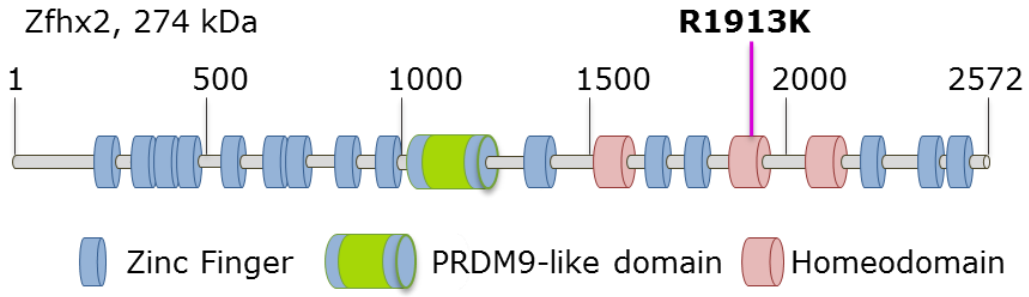

Figure 3-4. The structure of ZFHX2. The point mutation resulting in the amino acid change R1913K is in a Hox domain.

I. A potential causative mutation in a HOX domain in ZFHX2 that is evolutionally conserved across species

Exome sequencing showed that all 6 affected patients carry a potential causative point mutation in a homeobox (Hox) domain in ZFHX2, resulting in the amino acid change R1913K. Hox domains are 60 amino acid protein domains demonstrating a conserved structure which consists of three helical regions folded into a tight globular structure (Qian et al., 1989). Hox domains bind to DNA in a sequence-specific manner, regulating downstream gene expression and function (D'Elia et al., 2001). For example, homeodomain-containing transcriptional regulators can operate differential genetic programs along the anterior-posterior axis of animal bodies (Alonso, 2002). Since the Hox domain has a rigid structure and binds DNA in a sequence-specific manner, a missense mutation can easily change the structure and/or alter its function and downstream gene expression (D'Elia et al., 2001). In fact, missense mutations in

human HOX domains have been reported as a cause of various diseases (D'Elia et al., 2001): Septooptic dysplasia, which is defined by any combination of optic nerve hypoplasia, pituitary gland hypoplasia, and midline abnormalities of the brain, have been known to be associated with mutations in a homeobox gene, *HESX1* (Dattani et al., 1998). Also, several mutations in the HOX domain of *POU3F4* (POU class 3 homeobox 4), have been linked to deafness (Bitner-Glindzicz et al., 1995, de Kok et al., 1995, Schild et al., 2011, Choi et al., 2013). Some of these mutations alter the localization of POU3F4 from the nucleus to the cytoplasm and cause subsequent proteosomal degradation due to structural aberrations, leading to transcriptional inactivity (Choi et al., 2013). Taking these into account, a missense mutation in Hox domain has the potential to be pathogenic. Thus we hypothesised that the point mutation within the *HOX* domain in ZFHX2 might alter the functions of ZFHX2, leading to pain insensitivity.

To assess the likely pathogenicity of the ZFHX2 mutation, it is important to know how conserved the mutated residue is across species. Hox domains are known to be evolutionarily conserved (Gehring, 1992), indicating that the R1913K is likely to be a missense mutation that could lead to pain insensitivity. However, it was been reported that the position 57 (p57) in Hox domains where R1913K is located is often interchangeable between arginine and lysine (Figure 3-5).

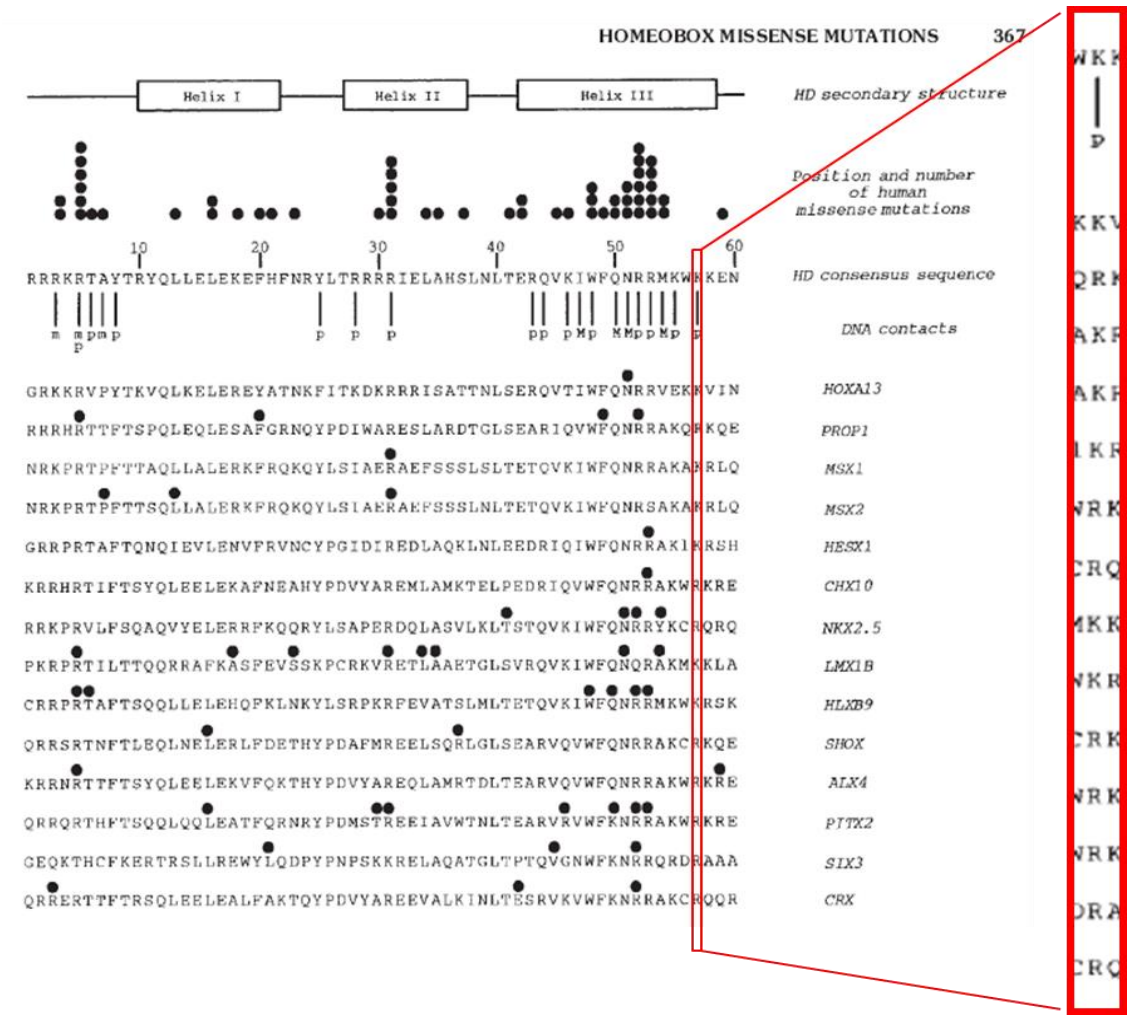

Figure 3-5. Protein sequence of Hox domain in different genes. Position 57 (highlighted in red) is interchangeable between Arginine (R) and Lysine (K). The black dots demonstrate positions and number of amino acid changed by missense mutations in human Hox domains. This figure is modified from (D'Elia et al., 2001).

Although position 57 in Hox domains is often interchangeable between arginine and lysine, it is still essential to understand how conserved the specific arginine 1913 residue is in ZFHX2. By analysing the genomes of all species that are accessible in the UCSC Genome Browser (UC Santa Cruz, University of California) we discovered that every ZFHX2 homolog had arginine 1913 conserved at the corresponding residue (Figure 3-6). This highly conserved R1913 and the several studies suggesting missense mutations in HOX domains lead to Mendelian disorders could indicate that R1913K is a potential causal mutation, warranting further studies.

Figure 3-6. Protein sequence of ZFHX2 homolog across species. Arginine 1913 (R1913) is highly conserved at the corresponding residue.

II. Transcription factor activation: involvement of arginine methylation in pathological mechanisms

We hypothesised that the point mutation in the Hox domain in ZFHX2 resulting in the amino acid change R1913K leads to pain insensitivity and we considered what could be the pathological mechanism. As mentioned, ZFHX2 is a transcription factor and activation of transcription factors is an important step for downstream gene expression. The activity of transcription factors has previously been shown to be affected by post-translational modifications. Several types of modification in transcription factors have been documented such as phosphorylation, acetylation, methylation, ubiquitylation, sumoylation and neddylation (Kruse and Gu, 2009). One of the well-characterised transcription factors, tumour protein 53 (p53), is well known for its highly regulated transcriptional activities by post-translational modification. This gene is a key factor involved in an appropriate cellular response to a variety of cellular stresses such as DNA damage. There are more than 100 genes controlled by p53 (Wei et al., 2006). Post-translational modifications of p53 including phosphorylation, acetylation and methylation contribute to its highly regulated activities (Kruse and Gu, 2009). For instance, phosphorylation of serine and tyrosine residues are considered to be essential to

stabilise p53 transcriptional activities (Donehower and Lozano, 2009, Kruse and Gu, 2009). Acetylation of lysine residues in p53 plays an important role in p53-dependant gene expression in embryonic cells and also the expression of proapoptotic genes in thymocytes (Kruse and Gu, 2009). It is not only phosphorylation and acetylation that contribute to transcriptional activities of p53; methylation of lysine and arginine residues also regulate transcriptional activation of p53. For example, monomethylation at K370 by SMYD2 (SET and MYND domain containing 2) was shown to repress p53-mediated transcription. This repression correlated with decreased p53 binding to the promoter of its target genes, including *p21*, *CDK-inhibitor 1A*, which is a well-known gene to play a role in the cell cycle (Huang et al., 2006, Terzi et al., 2016). More recently, arginine methylation in p53 has highlighted its essential role in the p53 response. Arginine methylation of p53, catalysed by PRMT5 (protein arginine methyltransferase 5), altered binding properties to promoters of several genes including *p21* (Jansson et al., 2008). In addition, depletion of PRMT5 caused a decreased progression of the cell-cycle, suggesting that arginine methylation mediated by PRMT5 underlies regulation of the p53 response (Jansson et al., 2008).

Methylation of lysine and arginine residues in transcription factors has raised much attention in the past decade. For a brief introduction to lysine and arginine methylation, their chemical structures are shown in Figure 3-7: Lysine specific methyltransferases (KMTs) can mono-, di- or trimethylate the amino group of lysine in an S-Adenosylmethionine (SAM)-dependent manner (Figure 3-7a). On the other hand, arginine can be mono- or dimethylated on its side chain by protein arginine methyltransferases (PRMTs) using SAM as the methyl donor (Figure 3-7b). Dimethylation of arginine is distinct from the one of lysine; two methyl groups can be added to a single guanidino nitrogen atom in asymmetrical dimethylation, or two nitrogen atoms in symmetrical dimethylation (Biggar and Li, 2014).

Alteration of transcriptional activities mediated by methylation are not limited to p53; methylation of lysine and arginine residues in transcription factors such as NFκB and HOXA9 have been reported to play an essential role in their functions of the promoter of E-selectin in tumor necrosis factor alpha (TNF-α) treated cells (Bandyopadhyay et al., 2012)(Table 3-3, Table 3-4). Of particular interest in this project is arginine methylation as we noticed that the region surrounding R1913 is an arginine and glycine -rich sequence motif (Figure 3-8). This sequence motif is similar to the ones in other transcription factors, such as p53, p65 subunit of NFκB and HOXA9, where arginine residues are methylated by PRMT5 (Jansson et al., 2008, Wei et al., 2013, Bandyopadhyay et al., 2012) (Figure 3-8).

In addition to the arginine methylation study in p53 mentioned above (Jansson et al., 2008), the arginine residue at position 30 in the p65 subunit of NFκB is dimethylated by PRMT5 and the mutants such as R30A and R30K showed reduced binding ability of NFκB to downstream genes (Wei et al., 2013). Furthermore, HOXA9 has been considered to be crucial in the cytokine induction of E-selectin, which is a mediator of initial adhesion of leukocytes to the endothelium in inflammatory responses (Bandyopadhyay et al., 2012). A role of arginine methylation was revealed to require this induction; the arginine methylation at position 140 (R140) in HOXA9 by PRMT5 influenced binding abilities to the promoter of E-selectin in tumor necrosis factor alpha (TNF-α) treated cells (Bandyopadhyay et al., 2012).

Table 3-3. Transcription factors which undergo lysine methylation. PKMT; protein lysine methyltransferase. (Carr et al., 2015)

Transcription factor	Site	Monomethylation or dimethylation	PKMT	Demethylase	Function
pRB	K873	Mono	SET7/9		Inhibits E2F-1-dependent transcriptior
pRB	K810	Mono	SET7/9	JMJD3	Inhibits pRB phosphorylation and E2F-1-dependent transcription, stimulates DNA repair
pRB	K810	Mono	SMYD2		Drives pRB phosphorylation and E2F-1-dependent transcription
pRB	K860	Mono	SMYD2		Inhibits E2F-1-dependent transcriptior
E2F-1	K185	Mono	SET7/9	LSD1	Conflicting reports (see text)
NFκB (p65, RelA)	K218/221	Mono/di	NSD1	FBXL11	Activates transcription of a subset of target genes
NFκB (p65, RelA)	K314/315	Mono/mono	SET7/9		Represses transcription of target genes, increases NFκB turnover
NFκB (p65, RelA)	K37	Mono	SET7/9		Activates transcription of a subset of target genes
NFκB (p65, RelA)	K310		SETD6		Represses transcription of target genes
PDX1	K123/131	Mono	SET7/9		Activates transcription of target genes
STAT3	K49		EZH2		Activates transcription of Il-6-dependent target genes
SOX2	K119	Mono	SET7/9		Represses transcription of target genes, increases SOX2 turnover
p53	K372	Mono	SET7/9		Stabilizes p53 during the DNA damage response
p53	K370	Mono	SMYD2	LSD1	Decreases binding to promoters, represses transcription
p53	K370	Di		LSD1	Increases binding to promoters, activates transcription
p53	K382	Mono	SET8		Decreases binding to promoters, alters target gene specificity
p53	K382	Di			Increases binding to promoters, activates transcription
p53	K373	Di	G9a, GLP1		Represses transcription
p53	K386	Mono/di			Unknown

Table 3-4. Transcription factors which undergo arginine methylation. SDMA; symmetric dimethylarginine, ADMA; asymmetric dimethylarginine, PRMT; protein arginine methyltransferase. (Carr et al., 2015)

Transcription factor	Site	SDMA/ADMA	PRMT	Function
E2F-1	R111/113	SDMA	PRMT5	Growth promoting
E2F-1	R109	ADMA	PRMT1	Upregulates apoptotic target genes
p53	R333/335/337	SDMA	PRMT5	Targets p53 to target genes associated with cell cycle arrest
TWIST1	R34	ADMA	PRMT1	Represses E-cadherin expression
NFκB (p65, RelA)	R30	SDMA	PRMT5	Upregulates NFκB-dependent transcription
FOXO1	R248/250	ADMA	PRMT1	Inhibits AKT-dependent phosphorylation, enhances sensitivity to apoptosis
RACO1	R98/109	ADMA	PRMT1	Enables association with c-Jun and upregulated transcription
GATA3	R261			Alters target gene specificity
HOXA9	R140	SDMA	PRMT5	Upregulates E-selectin during inflammatory response
RUNX1	R206/210	ADMA	PRMT1	Activates transcription of target genes
p/CIP		ADMA	PRMT4	Represses transcription
ER	R260	ADMA	PRMT1	Facilitates interaction with PI3K and Src during hormone response
pRB	R787	ADMA	PRMT4	Increases phosphorylation of pRB, to drive E2F-1-dependent transcription

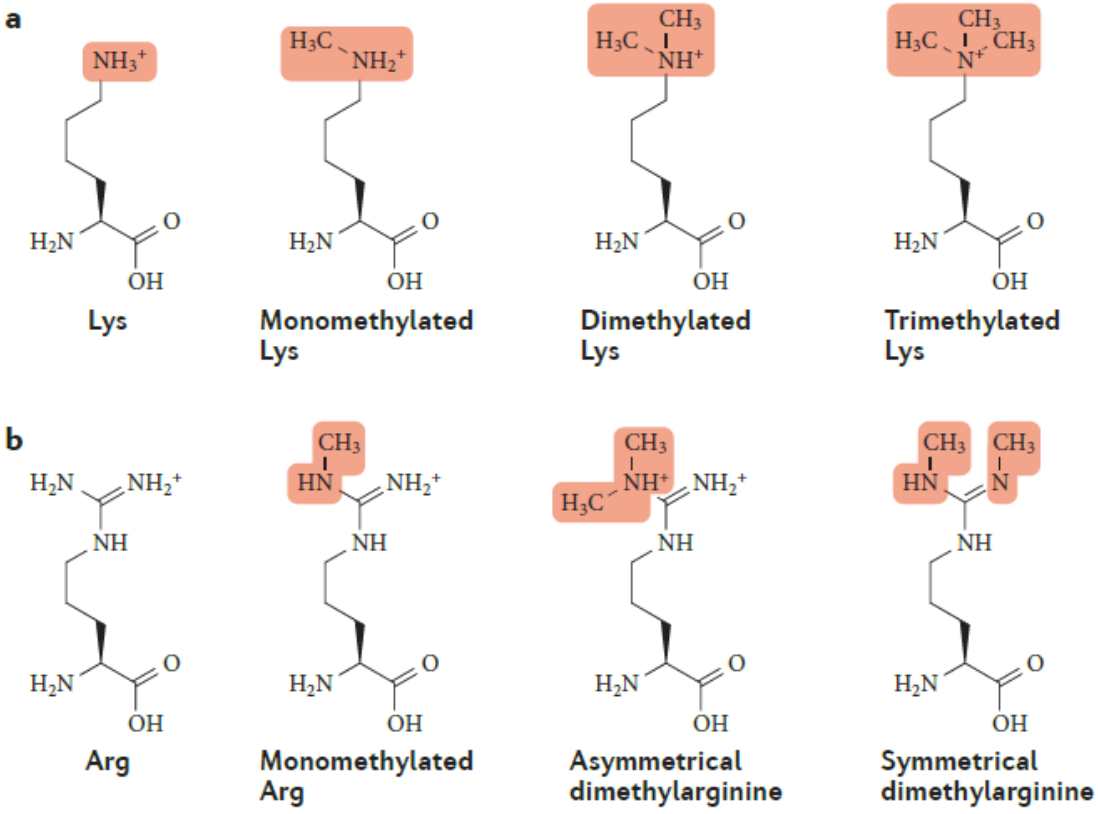

Figure 3-7. Lysine and Arginine methylation (Biggar and Li, 2014)

ZFHX2	1907	NTRARERKG	1915
p53		QIRGRERFE	
p65		KQRGMRFRY	
HOXA9		SARRGDCPT	

Figure 3-8. Sequence of ZFHX2 over R1913 and other transcription factors where arginine residues are methylated (Jansson et al., 2008, Wei et al., 2013, Bandyopadhyay et al., 2012)

Taking these important roles of arginine methylation in transcription factors into account, we raised the hypothesis that arginine methylation(s) in the motif over R1913 could be important in regulating the transcriptional activity of ZFHX2. The mutation resulting in the amino acid change R1913K could affect the arginine methylation status leading to an alteration in ZFHX2 function, and furthermore, this pathological mechanism could help explain the pain insensitive phenotype.

3.2 AIMS OF THIS PROJECT

The principal aim of this project was to prove whether the R1913K mutation in ZFHX2 was the cause of the human pain insensitivity. We planned to study (1) How the mutation might alter the function of ZFHX2; (2) the role of the Zfhx2 gene in pain processing using mouse models; (3) the genes regulated by Zfhx2 and understand whether the R1913K mutation causes changes in gene expression. To address the first question, we expressed ZFHX2 in cell lines and studied the subcellular localization and methylation status around residue 1913 using mass spectrometry. To investigate the second question, we performed pain behavioural tests on both global Zfhx2 KO mice and also BAC transgenic mice bearing the orthologous mutation. To explore the third question, we performed microarray and ChIP-seq (chromatin immunoprecipitation sequencing) assays.

3.3 METHODS

3.3.1 Mammalian expression constructs

The original R1913 wild-type (WT) and K1913 missense mutation (Mut) constructs (i.e. FLAG-ZFHX2 in pcDNA3 (Invitrogen) and FLAG-ZFHX2-IRES-eGFP in pcDNA3) were generated by Dr. James Cox at WIBR, UCL.

I generated several constructs based on these backbones to analyse the function of the *ZFHX2* gene:

1. WT FLAG-ZFHX2-IRES-td Tomato
2. Mut FLAG-ZFHX2-IRES-td Tomato
3. WT FLAG-ZFHX2-V5-IRES-eGFP
4. Mut FLAG-ZFHX2-V5-IRES-eGFP

FLAG-ZFHX2-IRES-td Tomato (1, 2):

The Gibson Assembly method (Gibson et al., 2009) was used to generate these constructs. Firstly, the IRES-td Tomato fragment was amplified from an IRES2-tdTomato plasmid derived from a pIRES2-AcGFP1 backbone (previously generated by Dr Yury Bogdanov, Molecular Nociception Group) using the following primer pairs and KAPA HiFi DNA Polymerase (KAPA Biosystems, KK2602). The amplified fragment size was 2082 bp:

GIB IRES2-td FWD;

TACACTTCTAGCTTTATAACTACCGCGGGCCCGGGATC

GIB IRES2-td REV;

CCCTCTAGATGCATGCTCGAGGCCGCTCATTACTTGTACAGCTC

The thermal cycling conditions were: 1min initial denaturation at 95°C, 30 cycles of 20 sec denaturation at 98°C, 15sec annealing at 61°C and 2min10sec extension at 72°C, and 2min10sec final extension at 72°C.

Next, the WT and Mut FLAG-ZFHX2 in pcDNA3 vectors were digested with *Xho*I (New England Biolabs). These linearised vectors (13176 bp) were gel-purified using a gel

purification kit (Qiagen, 28606) according to the manufacturer's instructions. Phusion High-Fidelity DNA Polymerase (NEB, M0530) was used to create blunt ends: HF Phusion Buffer 5µl, 10mM dNTPs 0.5µl, plasmid 19.25µl, and Phusion Polymerase 0.2 µl were incubated at 72°C for 10min. The linearised vectors were ligated with the gel purified IRES-tdTomato PCR products (3:1 insert:*vector molar ratios*) using Gibson Assembly Master Mix (NEB, E2611) at 50°C for 20min. Then, 2µl of assembled products were transformed into XL10-Gold Ultracompetent Cells (Agilent, 200315), clones picked and amplified in LB containing 100 µg/ml ampicillin and DNA isolated using a miniprep kit (Qiagen, 27104). The resulting plasmids were verified by Sanger sequencing using the following primers (Table 3-5). To obtain large quantities of DNA, the plasmids were amplified in SURE2 supercompetent cells (Agilent, 200152) and a maxiprep protocol was followed according to the manufacturer's conditions (Qiagen). All plasmids were then verified by Sanger sequencing (Source Bioscience).

Table 3-5. Sequence primers for FLAG-ZFHX2-IRES-tdTomato or FLAG-ZFHX2-V5-IRES-eGFP

Description	Sequence (5'-3)	Coverage region
FLFWD	GGTGGGAGGTCTATATAAGCAGA	ZFHX2
SEQ1FWD	GGCATCAAGGAAGAGCCCAGTCTG	ZFHX2
SEQ2FWD	CCCTTGACAACAGCAGCACAG	ZFHX2
SEQ3FWD	ACATGCGAGAGAAGCACCCTGAG	ZFHX2
SEQ4FWD	CCTGAACTCTTCCAGTACTTTG	ZFHX2
SEQ5FWD	TGCTCAGAAGTACCAGCTGGCAG	ZFHX2
SEQ6FWD	TGAGAAAGATGCCCAGAACAAGAC	ZFHX2
SEQ7FWD	TCCCAGACAAACCCTCAGGAAGC	ZFHX2
SEQ8FWD	CCACATGCGGTCAGTTCTGCATC	ZFHX2
SEQ9FWD	AGCCCTTCTAGAAAACTTTGGC	ZFHX2
SEQ10FWD	AGTTCCAGACCCAAGCCCTGCAG	ZFHX2
SEQ11FWD	CCATACCTGTGACCAGTGTGC	ZFHX2
SEQ12FWD	AGTTCAACCTCTTATTAGGCAAG	ZFHX2
SEQ13FWD	TCTGGTTCCAGAATGCTCGTG	ZFHX2
SEQ14FWD	ACCACAGTGGTCCAGACTGCTG	ZFHX2
SEQ15FWD	GAGGTTGATGAGCTGCTGACAG	ZFHX2
IRES2 td SEQ A FWD	CGTTACTGGCCGAAGCCGCTTG	IRES-tdTomato
IRES2 td SEQ B FWD	CGTGGTTTTCCTTTGAAAAACACG	IRES-tdTomato
IRES2 td SEQ C FWD	CCTCGGTACACATGCTTTACAT	IRES-tdTomato
pcDNA3 SEQ REV	GTG GCACCTTCCAGGGTCAAGGA	IRES-tdTomato

FLAG-ZFHX2-V5-IRES-eGFP (3, 4):

The Gibson Assembly method (Gibson et al., 2009) was used to generate these constructs. Firstly, the PCR product containing the V5 tag was PCR amplified with KAPA HiFi DNA Polymerase (KAPA Biosytems, KK2602) using FLAG-ZFHX2-IRES-EGFP as template and the following primer pairs (315 bp):

ZFHX2 V5 FWD;

GTGCCCATCTGCACCTACCACTGC

ZFHX2 V5 REV;

TTTAAGATCTTCCCGCTCGAGTTACGTAGAATCGAGACCGAGGAGAGGGTTA
GGGATAGGCTTACCTAAAGCTAGAAGTGTAGAGGTAG

Next, the WT and Mut FLAG-ZFHX2-IRES-eGFP constructs in pcDNA3 were double-digested with *XhoI* and *PflM*I. The fragments with the size of 14426 bp were isolated using the Qiagen gel purification kit (28606). Phusion High-Fidelity DNA Polymerase (NEB, M0530) was used to create blunt ends for the vectors. The linearised vectors were ligated with the gel-purified PCR products using Gibson Assembly Master Mix (NEB, E2611) at 50°C for 20min. Then, 2µl of assembled products were transformed into XL10-Gold Ultracompetent Cells (Agilent, 200315), clones picked and amplified in LB containing 100 µg/ml ampicillin and DNA isolated using a miniprep kit (Qiagen). The resulting plasmids were verified by Sanger sequencing using the following primers (Table 3-5). To obtain large quantities of DNA, the plasmids were amplified in SURE2 supercompetent cells (Agilent, 200152) and a maxiprep protocol was followed according to the manufacturer's conditions (Qiagen). All plasmids were then verified by Sanger sequencing (Source Bioscience).

3.3.2 Cell culture

AD293 and HEK293 cells were cultured in DMEM (GIBCO 31966-021) with 10% fetal bovine serum (GIBCO 10270-106). SH-SY5Y cells were cultured in DMEM / F12 (GE

Healthcare Cell Culture, SH30026) 1:1 with 10% FBS. All cells were kept at 37°C in 5% CO_2 and passaged at 70-80% confluency.

3.3.3 Transfection

I. Transient transfection using Lipofectamine

FLAG-ZFHX2-IRES-tdTomato (WT or Mut) constructs were transfected into HEK293 cells at about 80-95% confluency on the day of transfection in 35mm dishes using Lipofectamine 2000 (Thermo Fisher Scientific, 11668027) according to the manufacturer's conditions. Two µg of DNA was combined with 10 µl of lipofectamine 2000 in 500 µl of Opti-MEM (GIBCO 31985-062). The cells were kept overnight at 37°C in 5% CO_2 and then split into 65mm dishes. The cells were collected 48 h after transfection.

II. Nucleofection

The SF Cell Line 4D-Nucleofector® X Kit L (LONZA, V4XC-2024) and 4D-Nucleofector® System (LONZA) were used for nucleofection, following the manufacturer's instructions. Briefly, 2-3 x 10^6 cells were re-suspended in Nucleofector Solution with the provided supplement and 2 µg of plasmid. The cell suspension was transferred into a Nucleocuvette Vessel following the Nucleofection process. After nucleofection, the cells were immediately re-suspended with warm media and kept in flasks or dishes at 37°C in 5% CO_2. The cells were cultured with antibiotic 72h post-transfection to generate the stable cell lines, as described in 3.3.4.

3.3.4 Stable cell lines

I. SH-SY5Y stable cell line

We aimed to generate three stable cell lines: WT FLAG-ZFHX2-V5-IRES-eGFP, Mut FLAG-ZFHX2-V5-IRES-eGFP, and IRES-eGFP as a control. Firstly, the constructs were linearised overnight using the restriction enzyme *Pvu*I, which has a single restriction site within the ampicillin gene. The cells were transfected with either circular DNA or gel-purified

linearized constructs using Nucleofection (as described in 1.3.3.2), and cultured with DMEM / F12 (1:1) with 10% FBS for 3 days. Next, the cells were reseeded in DMEM / F12 (1:1) FBS10% with 500 µg/ml Geneticin (GIBCO 10131-027). This selection media was replaced twice a week for 16 days. To generate stable cell lines derived from single cells, the cells were re-suspended in medium without serum and sorted into single cells using Flow Cytometry (BD FACSArray, SORP) with help from Dr Ayad Eddaoudi, UCL Institute of Child Health. Positive cells were selected by green fluorescence signals excited at 488 nm. Single cells were cultured in 96 well plates without Geneticin for 10 days, followed by media replacement with DMEM / F12 (1:1) FBS10% with Geneticin at 500 µg/ml twice a week for 2 weeks until the cells were around 70% confluent. The single clones were then detached with a pipette and transferred into 24 well plates and cultured with DMEM / F12 (1:1) FBS10% with Geneticin 500 µg/ml and Antibiotic-Antimycotic (GIBCO 15240-062). The media was replaced twice a week for 1 week and the clones were validated by immunostaining, Sanger sequencing of genomic DNA and cDNA, and *ZFHX*2 expression levels were measured by qPCR.

II. AD293 stable cell line

Generated by Dr. Abdella Habib, WIBR, UCL.

Briefly, circular DNA was transfected into AD293 cells using Lipofectamine 2000, as described above. Stable cells were firstly selected in DMEM FBS 10% with Geneticin at 1500 µg/ml for 2 weeks, followed by single cell selection by flow cytometry. Stable clones were maintained in DMEM FBS 10% with Geneticin at 750 µg/ml.

3.3.5 Immunofluorescence

The cells were cultured on glass coverslips coated with poly-L-Lysine (SIGMA P9155-5MG). At the appropriate confluency, cells were fixed with 4% PFA (paraformaldehyde) in PBS (Phosphate Buffered Saline) for 15min followed by permeabilization with 0.1% Triton X-100 for 5min at room temperature. The cells were blocked with 3% BSA (Bovine Serum Albumin, SIGMA A7906) in PBS for 1hr at room temperature and incubated with either anti-FLAG raised in mouse (SIGMA F1804, 1:500), anti-FLAG raised in rabbit (SIGMA F7425, 1:400), rabbit anti-V5 (SIGMA V8137, 1:500) or a custom rabbit anti-ZFHX2 (Eurogentec, 1:200) in 3%

BSA in PBS for 1hr at room temperature. The cells were incubated with a corresponding secondary antibody for 45min at room temperature; Alexa594 goat anti-mouse (Invitrogen A11032, 1:1000) or Alexa546 goat anti-rabbit (Invitrogen A11035, 1:1000) in 3% BSA in PBS. The stained cells were imaged using a Leica microscope (LEITZ DMRB, Germany) to validate stable cell lines (3.4.2I, 3.4.2II) or cells were visualized using a Leica SP8 confocal microscope to explore alteration of subcellular localization by Mut ZFHX2 (3.4.1).

3.3.6 RNA extraction

RNA extraction from cell lines was performed by myself, and DRG RNA extraction was performed by Dr. Abdella Habib at WIBR, UCL.

The cells were cultured in a T75 flask and 5-8 million cells detached at roughly 70% confluency using trypsin. For DRG RNA extraction, the mice were killed by inhalation of a rising concentration of CO_2 followed by cervical dislocation, and whole lumbar dorsal root ganglia were dissected. The DRG were suspended in RNA later (Ambion, AM7020) solution. The collected cells were dissolved in 1ml of Trizol (Ambion 15596018) and total RNA was isolated using PureLink RNA Micro Kit (Invitrogen 12183-016), following the manufacturer's instructions.

3.3.7 Sequencing for SH-SY5Y stable cell line

Total RNA (1000 ng) was reverse transcribed to obtain cDNA using iScript™ Reverse Transcription Supermix (BioRad 170-8840). The cDNA was amplified using the following primer pair and 2x PremixJ (epicentre FSP995J) using the cycling conditions: 2 min at 95°C, 35 cycles of 30 sec at 95°C, 1min at 56.1°C and 40 sec at 72°C and 5 min at 72°C for final extension.

ZFHX2 SEG 2 FWD: CATCTTGCCTGAGCAGCTAGAG

ZFHX2 SEG REV: TAGGGAAAAGCAGGTGCTTCCCTC

To remove and dephosphorylate unused primers and dNTPs, 0.25 µl of exonuclease I and 0.5 µl of Shrimp Alkaline Phosphatase were added into the PCR products and incubated for 30

min at 37°C and 20 min at 80°C. Following this clean-up step, the PCR products were Sanger sequenced to verify the mutation using SEQ11FWD primer stated above (Table 3-5).

3.3.8 Real-time qPCR

Total RNA (1000 ng) was reverse transcribed as in 1.3.7. To check for contamination of genomic DNA in RNA samples, non-reverse transcriptase reactions were also included. We used Taqman analysis to measure mRNA levels of the target genes. The Taqman (Thermo Fisher Scientific) reactions were performed according to the manufacturer's instructions, using TaqMan Universal Master Mix II, with UNG (Thermo Fisher Scientific 4440038). The following probes were used: hActB; Hs01060665_g1, hSCN9A; Hs01081006_m1, hClusterin; Hs00156548_m1, hNAV2; Hs01093707_m1.

Amplification of the selected genes from each sample was performed in three parallel runs on a 96-well reaction plate using BioRad CFX with the following protocol: 2min at 50°C, 10min polymerase activation at 95°C and 40 cycles of 15 sec denaturation at 95°C, 1min annealing and extension at 60°C.

Relative expression of the target gene was calculated using the comparative $2^{\Delta\Delta CT}$ method (Livak and Schmittgen, 2001). Expression of the test gene was compared with that of b-Actin measured on the same sample, giving a CT difference (ΔCT) for b-Actin minus the test gene. The CT difference, ΔCT values of individual samples were compared to ΔCT of the control or WT clones, giving $\Delta\Delta$CT values of each clone. The relative expression was calculated as $2^{-\Delta\Delta CT}$. Mean, S.E.M. and statistics were calculated from the $2^{-\Delta\Delta CT}$. Data were analyzed using Microsoft Excel, and Student's t-test was performed with *$p < 0.05$, **$p < 0.01$, ***$p < 0.001$ as statistically significant.

3.3.9 Immunoprecipitation

AD293 or SH-SY5Y cells stably expressing FLAG-ZFHX2-V5 and eGFP (WT or Mut) or eGFP (control) were cultured in DMEM FBS10% with Geneticin at 750µg/ml or DMEM / F12 (1:1) FBS10% with Geneticin at 500µg/ml, respectively. The cells were washed with PBS and transferred into 1.5ml Eppendorf tube with 10 µl of 50x Protease Inhibitor EDTA free (Roche 04 693 132 001) per 1 million cells. The collected cells were kept in -80°C until performing the next procedure. The cells were lysed with RIPA buffer with 300mM salt (Table

3-6, 350µl per 10 million cells) on ice for 45min. After the lysis proteins were separated into a soluble and pellet fraction and another RIPA buffer with 150mM salt (Table 3-6, 350µl per 10 million cells) was added into the soluble fraction to reduce salt concentration. Either anti-FLAG M2 magnetic beads (SIGMA, M8823, 20µl slurry per 10 million cells) or anti-V5 sepharose beads (abcam, ab1229, 30µl slurry per 10 million cells) or anti-V5 magnetic beads (MBL, M167-11, 50µl slurry per 10 million cells) was washed with RIPA buffer 150mM salt three times and then added into the soluble fraction. The cell lysates were rotated overnight at 15rpm at 4 °C. Protein complexes were washed three times with RIPA buffer 150mM salt, and then boiled at 95 °C for 3 minutes with Loading Buffer (NEB, B7709S) with Reducing Agent (NEB, B7709S) to elute proteins. The elution was performed for electrophoresis for either Western Blot, silver staining or coomassie staining.

Table 3-6. RIPA buffer component

RIPA buffer	Component	Concentration
RIPA 300mM salt	Tris-HCl	50mM
	Sodium chloride	300mM
	SDS	0.1%
	Sodium deoxycholate	1%
	IGEPAL	1%
	EDTA	1mM
RIPA 150mM salt	Tris-HCl	50mM
	Sodium chloride	150mM
	SDS	0.1%
	Sodium deoxycholate	1%
	IGEPAL	1%
	EDTA	1mM

3.3.10 Protein electrophoresis

Two to 5 µl of the cell lysis samples were loaded onto the polyacrylamide gels following dilution with Loading Buffer and 1µl of 30x DTT (*Dithiothreitol)* (NEB, B7709S reducing agent). One µl of 30x DTT was also added into immunopurified proteins. Each sample was boiled at 98°C for 3 minutes before loading onto either 4–15% precast polyacrylamide gels (BioRad 456-1085) or 4-12% Bis-Tris protein gels (NuPAGE NP0321 or NP0335). Tris- Glycine running buffer (Table 3-7) or MOPS SDS Running Buffer (NuPAGE NP0001) was used for the 4–15% precast polyacrylamide gels or 4-12% Bis-Tris protein gels, respectively. Electrophoresis for the 4–15% precast polyacrylamide gels was performed at 90V for 10-15min and 120V for 1.5hr-2hr at room temperature. The 4-12% Bis-Tris Protein Gels

were run at 120V for 10-15min and 150V for 1.5-2hr at room temperature. To separate the target protein for mass spectrometry analysis, 4-12% Bis-Tris protein gels were run at 120V for 10-15min and 150V for 3hr on ice.

Table 3-7. Tris-Glycine running buffer for electrophoresis

Running Buffer	Component	Amount per 1 litre
Tris-Glycine	Tris-Base Glycine SDS	3.03g 14.4g 1.5g

3.3.11 Western Blot

After the proteins were separated on the gel by electrophoresis (3.3.10), proteins were transferred by either wet-transfer (for 4–15% precast polyacrylamide gel) or semi-wet transfer method (for 4-12% Bis-Tris protein gels) following the conditions outlined below (Table 3-8). The immunoblots were incubated with rabbit anti-V5 (Sigma V8137, 1:500) or mouse anti-FLAG (Sigma F1804, 1:500) or rabbit anti-Zfhx2 (Eurogentic, 1:200) overnight at 4°C. Following 4 times wash with PBS, the immunoblots were incubated with the corresponding secondary antibodies for 1hr at room temperature: Goat Anti-Mouse Immunoglobulins/HRP (Dako P0447) or Goat Anti-Rabbit Immunoglobulins/HRP (Dako P0448). The immunoblots were washed 4 times with PBS with 0.1% Tween20 and once with PBS. The proteins were detected by chemilluminescence followed by incubation with ECL (Pierce 80196).

Table 3-8. Transfer conditions

Transfer method	Membrane	Buffer	Running time and voltage
Wet transfer	Polyvinylidene Difluoride (PVDF)	Tris-Glycine buffer: Glycine 28.8g, Tris-Base 6g, Methanol 400ml, Water up to 2000ml	100V 1hr at 4°C
Semi-wet transfer	nitro-cellulose	Tris-CAPS buffer: Tris-Base 3.63g, CAPS 0.221g, SDS 20mg, Methanol 20ml, Water up to 100ml	15V 1hr at room temperature

3.3.12 Silver Staining

The separated proteins after the electrophoresis (3.3.10) were detected by silver staining (Invitrogen, Silver Quest LC6070), following the manufacturer's instructions. Fixation time was 40min at room temperature, and was developed for 4min 30sec.

3.3.13 Coomassie Staining

To separate the target proteins for mass spectrometry analysis, the separated proteins after electrophoresis (3.3.10) were stained by Instant Blue (Expedeon, ISB1L) for 1hr at room temperature by gentle shaking.

3.3.14 Mass spectrometry

The protein isolation was performed by myself with help from Dr. Andrei Okorokov at UCL. All the other procedures were performed by Dr. Honglei Huang at University of Oxford.

The size of the target ZFHX2 proteins were expected to be ~274kDa. The bands just above 270kDa marker in the gel stained by Coomassie were detected from WT or Mut samples, and there were no visible bands of the same size in control samples. The bands were excised and kept in clean 1.5ml Eppendorf tubes at -80°C. The mass spectrometry analysis was performed by Dr. Honglei Huang at University of Oxford. The gel bands were detained in Eppendorf tubes filled with 50% ethanol, 5% acetic acid until the coomassie blue have completely gone by vortexing. The protein were then reduced in 20 mM dithiothreitol (DTT) for 30mins at 37°C, then alkylated in 100 mM iodoacetamide (IAA) for 30mins at room temperature in the dark. Each gel band were split into two half, one half of the samples was digested with chymotrypsin (Promega, UK) at protein:chymotrypsin ration 50:1 overnight at room temperature. Another half of the sample was digested with elastase (Promega, UK) at protein:elastase ration 50:1 overnight at 37°C. The peptides were extracted from gel using 50% acetonitrile (ACN), 0.1% formic acid (FA), the peptides were dried in a Speedvac and resuspended in 10µl of 2% ACN 0.1% FA. Peptides digested by chymotrypsin and elastase were pooled and 5ul of mixed

peptides were injected into Orbitrap Fusion Lumos mass spectrometry (Thermo) coupled to a UPLC (Dionex).

Peptide were analyzed by nano-UPLC− MS/MS using a Dionex Ultimate 3000 nano-UPLC with EASY-Spray column (75 µm × 500 mm, 2 µm particle size, Thermo Scientific) with a 60 min gradient of 0.1% formic acid in 5% DMSO to 0.1% formic acid to 35% acetonitrile in 5% DMSO. MS scans were acquired at a resolution of 120 000 between 400 and 1500 m/z and an AGC target of 4.0E5. MS/MS spectra were acquired in the linear ion trap (rapid scan mode) after collision-induced dissociation (CID) fragmentation at a collision energy of 35% and an AGC target of 4.0E3 for up to 250 ms, employing a maximal duty cycle of 3s. Selected precursor masses were excluded for 30s.

The acquired raw LC-MS/MS data were searched against UPR *homo sapiens* database (retrived 15.10.2014). The protein identification score threshold was adjusted to achieve a protein FDR of ~1% using Peaks 7.5 software using the default target decoy approach with 20 ppm mass error tolerance for the precursor and 0.5 Da for fragment masses. Two miss cleavage sites and nonspecific enzyme cleavage was allowed, carboxymethylation was set as fixed modification, and variable modification on arginine methylation, lysine and N-termini, Deamidation (N,Q) and Oxidation (M) and maximal 1 variable modification per peptide in the de novo and database searches (three variable PTMs for PTM search nodes.

3.3.15 Microarray

Performed by AROS Applied Biotechnology. The analysis was performed by myself.

Total RNA samples obtained from three clones per condition were sent to AROS Applied Biotechnology A/S for analysis using the Human Transcriptome Array. The data was normalised by ST-RMA method using Expression Console Software (version 1.4.1, Affymetrix), and analysed using the Transcriptome Analysis Console (version3.0, Affymetrix).

3.3.16 Chromatin Immunoprecipitation sequencing (ChIP-seq)

Cell culture was performed by myself. All the other procedures were performed by Dr. Andrei Okorokov at University College London and Dr. Konstantin Panov at Queen's University Belfast

WT and Mut stable SH-SY5Y cell lines were used for ChIP-seq (SBC3 and SBL3 for WT, and SDC2 and SDL1 for Mut (see the result section II for the name of the clones). The cells were cultured on 150mm dishes (10-13 plates per clone). Freshly made 37% PFA was directly added to the cells at a final concentration of 1% (540 µl per 20ml media). The cells were incubated at room temperature for 10min by a gentle rocking at 20-25rpm. To quench the reaction, 1.25M of glycine at a final concentration of 0.125M was added (2ml per 20ml media) and the cells were incubated by rocking at room temperature for 5min. The plates were then placed on ice and media was removed. The cells were collected with cold PBS by a cell scraper, and then span at 200g for 10min at 4℃. The cells were transferred into two 2ml Eppendorf tubes and span again. Following the removal of PBS, the cells were frozen by liquid nitrogen and kept in -80℃ until the next step. The cells were lysed with FA buffer (Table 3-9), and this cell lysis was sonicated for 60min in total (6 cycles of 10min sonication) at 4-6℃ using 'High' power on Bioraptor (diagenode) to yield approximately 200bp DNA fragments. Following reverse cross-linking by adding sodium chloride to a final concentration of 0.2M, the sheared chromatin was treated with RNAase and purified with a PureLink PCR purification kit (Invitrogen) following the manufacturer's instructions. The sheared chromatin was diluted with 225µl of ChIP IP and dilution buffer (Table 3-9) to a final volume of 550µl per 1 million cells. To obtain antibody-chromatin complexes, the sheared chromatin was incubated with the respective antibodies on a plate at 500rpm with a cycle of 5sec on and 10sec off for overnight at 4°C (Table 3-10). To block unspecific binding, Dynabeads Sheep anti-rabbit IgG (M-280) were washed and re-suspended with ChIP dilution buffer, and incubated with BSA to final concentration of 5mg/ml for overnight at 4°C on a rotating wheel. After the Dynabeads were blocked by BSA they were washed with ChIP dilution buffer and resuspended. The Dynabeads were added into the samples containing the antibodies and the sheared chromatin to obtain antibody-chromatin-beads complexes (Table 3-10). Following RNase digestion, the antibody-chromatin-beads complexes were then washed with RIPA buffer and TE buffer using Precipitor (Abnova) and DNA was eluted with 100 µl of Elution buffer1 and then 100 µl of Elution buffer 2 (Table 3-9). After reversal of the crosslinking and proteinase K digestion, the DNA was purified using ChargeSwitch Nucleic Acid Purification (Thermoscientific). The purified DNA was then sequenced at Diagenode (Belgium). Analysis was performed using SeqMonk on the human genome GRCh37.

Table 3-9. Buffer components used in ChIP

Buffer	Components
FA Buffer	50 mM Tris-HCl, pH8.0 140 mM NaCl 1 mM EDTA pH8 1% Triton X-100 0.1% Sodium Deoxycholate 0.5% SDS Roche Complete Protease Inhibitors
ChIP IP Buffer	20mM Tris-HCl, pH7.5 150mM NaCl 1.2mM EDTA 1.4% Triton X100
ChIP dilution Buffer	20 mM Tris-HCl, pH 7.5 150 mM NaCl 1 mM EDTA pH8 0.5mM EGTA 1% Triton X-100 0.1% Sodium Deoxycholate 0.1% SDS
RIPA buffer	HEPES 50mM pH 8.0 EDTA 1mM pH 8.0 Np-40 1% DOC 0.7% LiCl 0.5 M
Elution Buffer 1	0.1M NaHCO3 1% SDS
Elution Buffer 2	0.2M Tris-HCl , pH 6.5 250mM NaCl Proteinase K

Table 3-10. Conditions of immunoprecipitation. Anti-V5; Anti-V5 tag antibody - ChIP Grade, Rabbit polyclonal (ab15828, abcam), Anti-TBP; Anti-TATA binding protein TBP antibody - ChIP Grade, Rabbit polyclonal (ab28175, abcam)

Clones	Numbers of cells used	Antibody	Antibody concentration (mg/ml)	Volume of antibody	Volume of Dynabeads
SBC3	$60x10^6$	Anti-V5	0.75	130µl	1.6ml
SBL3	$60x10^6$	Anti-V5	0.75	130µl	1.6ml
SBL3	$60x10^6$	Anti-IgG	1.08	90µl	1.6ml
SDC2	$74x10^6$	Anti-V5	0.75	130µl	1.6ml
SDC2	$74x10^6$	Anti-IgG	1.08	90µl	1.6ml
SDC2	$60x10^6$	Anti-TBP	0.65	150µl	1.6ml
SDL1	$55x10^6$	Anti-V5	0.75	130µl	1.6ml

3.3.17 Behaviour tests

I. Animals

Global Zfhx2 KO mice were kindly offered by Dr. Yuriko Komine, National Institute for Basic Biology, Okazaki, Japan (Komine et al., 2006). BAC transgenic mice bearing the orthologous R1907K mutation were generated by Cyagen.

All genotyping were performed by Dr. James Cox and Dr. Abdella Habib at WIBR, UCL from genomic DNA isolated from the ear.

All behaviour tests were approved by the United Kingdom Home Office Animals (Scientific Procedures) Act 1986. Animals were acclimatised for an appropriate amount of time for each test (specified below). Mice analysed were 6-12 weeks old. Data on different groups of animals were analysed usingGraphPad Prism (GraphPad Software, Inc), and Student's t-test was performed with *$p < 0.05$, **$p < 0.01$, ***$p < 0.001$ as statistically significant.

II. Von Frey test

The von Frey test is a behavioural paradigm designed to investigate sensitivity to an innocuous mechanical stimulus. In order to complete the test, animals were kept in a mesh bottomed enclosure in which they were acclimatised for at least 60 minutes prior to testing. A set of 20 nylon hairs of weights ranging from 0.008g – 300g were used to apply pressure to the plantar surface of the paw. A hair of 0.4g was always used first and the up-down method (Chaplan et al., 1994) to determine the 50% paw withdrawal threshold: A von Frey filament is applied to the paw; if a positive response was obtained (lifting, flinching or licking), a filament of lesser force was applied next. If no response was seen a filament of greater strength was applied. A positive response consists of lifting, flinching or licking of the paw during or immediately after stimulus application. A von Frey filament is applied until a different response is seen and then the application was continued until another 5 responses were obtained.

III. Randall–Selitto test

The Randall Selitto test is used to assess noxious mechanical pain thresholds and can be used on the tail and paw of animals. In this project, we used tail to assess the mechanical pain thresholds. The test was originally described by Randall and Selitto to measure inflammatory pain thresholds by application of increasing pressure on a rat paw (Randall and Selitto, 1957). Later this method was modified by Takesue et al. (Takesue et al., 1969). Prior to testing, animals were restrained in a clear plastic tube with an acclimatisation period of approximately 1-2 minutes. A blunt probe is applied to the tail with increasing pressure until the animal exhibits a painful response. The responses include struggling, withdrawal of tail or vocalisation. The test was repeated 3 times for each animal and averaged values were used for statistical analysis.

IV. Hargreave's test

The Hargreave's test was performed to assess spinal reflex responses to noxious thermal stimulation. This method was originally designed to assess thermal nociception in inflammatory pain states (Hargreaves et al., 1988). Animals were acclimatised in an enclosure with a glass base for a minimum of 60 minutes. Urine and faeces were removed as much as possible from the glass floor of each test compartment. A radiant heat light source was applied to the plantar surface of the hind paw with a cut off time of 30 seconds. The stimulus was stopped when a painful response was observed (licking, lifting or shaking the paw) and the latency to paw withdrawal (in seconds) was recorded. Three recordings were made from each animal and an average taken.

V. Hot Plate and Cold Plate test

In contrast to the Hargreave's test, which is a spinal response, the hot plate test seems to represent a supraspinal thermal assay. The most commonly used version of the hot plate test was originally described by Woolfe and Macdonald (Macdonald et al., 1946) and later modified by Eddy and Leimbach (Eddy and Leimbach, 1953). Temperatures used were 50°C and 55°C (±0.2°C). Once the plate was heated to the desired temperature, mice were placed on the plate and the time until the first distinctive pain behaviour (licking or fluttering of hind

paw) was recorded, at which point mice were removed from the plate. Each temperature was performed in separate sessions.

The cold plate test is designed to assess behavioural responses to noxious cold. Several ways have been described (Zimmermann et al., 2007, Abrahamsen et al., 2008, Lee et al., 1999), however, all versions involve observing hind paw nociceptive behaviours of mice placed onto a surface maintained at a temperature between 0°C to 4°C. In this project, we used 0°C to measure noxious cold thresholds. Like the hot plate test, once the plate is reached at the target temperature, mice were placed on the plate and the latency to the first response (licking or fluttering of hind paw) was recorded, at which point mice were removed from the plate.

VI. Thermal Place Preference

Thermal place preference is another method to assess noxious cold sensitivity. Temperatures under 15°C can be considered to be at a noxious level of cold. For this project, cold sensitivity was also assessed using a place preference test. Two adjacent plates were placed next to each other to allow animals to move freely between the two plates. A plate named as control was held at 20°C while the other one was held at the test temperature; 0°C, 5°C, 13°C, 15°C, 17°C and 30°C. Animals were placed onto the middle of these two plates and allowed to explore for 120 seconds. The time spent on the test plate was recorded using BIOSEB cold hot plate test software (BIOSEB). The test plate and second plate were switched in order that environmental effects did not bias the time spent on the test plate and the times spent on the test temperature plate in each trial were averaged.

VII. Acetone test

The acetone test is designed to assess cold sensitivity in the 10°C to 15°C range by application of acetone on the paw of animals. The application causes a rapid decrease in temperature (of~10°C). This can be used to examine sensitivity to cooling. Animals were kept in a mesh bottomed enclosure in which they were acclimatised for at least 60 minutes prior to testing. Acetone was filled in the syringe at the open end (without the needle) and gently applied onto the hind paw by pressuring the syringe. The amount of time the mice displayed

nocifensive behavior such as hindpaw fluttering and licking was measured for 1min and this application was repeated 3 times. The averaged value was used for statistical analysis.

VIII. Open field

The Open Field Test (Walsh and Cummins, 1976) provides simultaneous measures of locomotion, exploration and anxiety. The apparatus consists of a box with 72 x 72 cm grid with 36 cm high walls. The arena is virtually divided into 16 squares. To initiate testing, mice were placed in one corner of the enclosure and their exploratory behaviours were recorded for 5 min across the arena. Parameters measured were the number of entries in the centre of the arena (4 virtual central squares) and the total numbers of crossing of the grid lines (Brown et al., 1999). The number of line crosses are usually used as measures of locomotor activity, but are also measures of exploration and anxiety. A high frequency of these behaviours indicates increased locomotion and exploration and/or a lower level of anxiety. The number of central square entries is also a measure of exploratory behaviour and anxiety. A high frequency/duration of these behaviours indicates high exploratory behaviour and low anxiety levels. In pain studies, it seems to be considered that suffering from pain causes anxiety-related phenotypes by a decrease in the percentage of the number of entries and line crossing (Parent et al., 2012). An entry in a square and line crossing occurred when the animal's both front and hind paws crossed a frontier.

IX. Rotarod test

The rotarod test is a behavioural paradigm to assess motor coordination. This test was first described in the late 1960s (Jones and Roberts, 1968). Mice are given two consecutive trials with a maximum trial length of 5 min prior to the measurements. The animal is placed on top of an accelerating rod over the length of the trial. The rotation speed was set at 4rpm and increased up to 40rpm. The time spent on the rod was recorded when mice fell from the rod. The recording lasted up to 5min and repeated 3 times. The averaged time was used for statistical analysis.

X. Cotton Swab test

Performed by Ms. Sonia Santana-Varela at WIBR, UCL.

The cotton swab test is another measure of innocuous mechanical sensitivity. It uses a dynamic stimulus; a cotton swab puffed out to 15mm diameter (3x normal size) was moved across the glabrous skin of the paw in a ~1 second sweep (Garrison et al., 2012). The cotton swab stimulus was applied 5 times to each animal with a break of ≥60 seconds and the number of responses was recorded to produce a score out of 5.

XI. Inflammatory pain tests

In this project, we have used the formalin test and Complete Freund's adjuvant test. The formalin test was first modified for mice in order to provide a model of continuous, moderate pain which allowed non-invasive assessment of pain behaviour (Hunskaar et al., 1985). Animals were acclimatised to a Perspex box for at least 1 hour prior to testing when a 20μl intraplantar injection of 5% Formalin was given in the hind paw. Animals were observed for the next 60 minutes and the time spent licking, shaking or biting the affected paw was measured in five minute blocks. The test involves an early acute phase, which is believed to involve direct activation of C fibres via TRPA1 (McNamara et al., 2007) and occurs around 5-10 minutes after injection. The second, inflammatory phase begins around 20 minutes after injection and believed to result from the action of prostaglandins and other inflammatory mediators as well as spinally mediated changes (Coderre et al., 1990). The early acute phase (Phase I, 0-10min) and the latter inflammatory phase (Phase II, 10-60min) were separately analysed. The time spent licking, shaking or biting in every 5 min was also analysed.

Complete Freund's adjuvant (CFA) has been used as a reliable model of persistent inflammatory hyperalgesia since the 1980s (Larson et al., 1986). The thermal and mechanical hyperalgesia observed is linked to TNF-α and cytokine release in the periphery (Cunha et al., 1992), develops approximately 24 hr after injection, and remains for up to 2 weeks. In this project, we performed both the von Frey and Hargreave's tests before the injection to measure the baseline mechanical and thermal sensitivities. 20μl of CFA (SIGMA, F4258) was injected intraplantarly in the right hind paw. Von Frey and Hargreave's tests were performed 1, 3 and 6 days post-injection. The Hargreave's test was also conducted at 2 and 5 days post-injection.

3.4 RESULTS

3.4.1 Subcellular localization of ZFHX2 is not altered by the mutation

Mutations altering the subcellular localization of proteins have previously been reported to be associated with human diseases. For example, loss of nuclear localization signals due to missense mutations have been shown to be the cause of amyotrophic lateral sclerosis and frontotemporal lobar degeneration (Neumann et al., 2006). In patients with these diseases, affected neurons exhibit a striking redistribution of TAR (trans-activation response element) DNA-binding protein or the ALS (amyotrophic lateral sclerosis)-associated protein, fused in sarcoma, from the nucleus to the cytoplasm (Neumann et al., 2006). Subcellular localization is also important in pain related diseases. Several mutations in a transcription factor, PR homology domain-containing member 12 (PRDM12), were found in patients with autosomal recessive congenital insensitivity to pain and hereditary sensory and autonomic neuropathy. These mutations caused subcellular localization changes (Chen et al., 2015b, Nagy et al., 2015). PRDM12 with a polyalanine expansion mutation formed aggregates in the nucleus and cytoplasm that may potentially lead to reduced ability of PRDM12 to function correctly in the nucleus (Chen et al., 2015b). Another study also indicated that some PRDM12 mutations found in human hereditary sensory and autonomic neuropathies formed clusters of large aggregates in the nucleus and another mutation caused a loss of nuclear staining and was localized primarily in the cytoplasm (Nagy et al., 2015). This subcellular localization change is predicted to alter expression of downstream genes, and consequently change nociceptive behaviour (Nagy et al., 2015).

As mentioned in the introduction section, the patients described here carry a point mutation which resulted in the amino acid change R1913K in ZFHX2. We considered whether this mutation could lead to subcellular localization changes and this, in turn, alter downstream transcriptional activity. In order to test this hypothesis, we stained HEK293T cells transfected with either WT (R1913) or Mut (K1913) FLAG-ZFHX2 in pcDNA3 using an anti-FLAG antibody (Figure 3-9). Clear nuclear localization was observed in cells expressing either WT FLAG-ZFHX2 or Mut FLAG-ZFHX2 (Figure 3-9). This nuclear staining suggests that the mutation did not alter subcellular localization in transfected HEK293T cells.

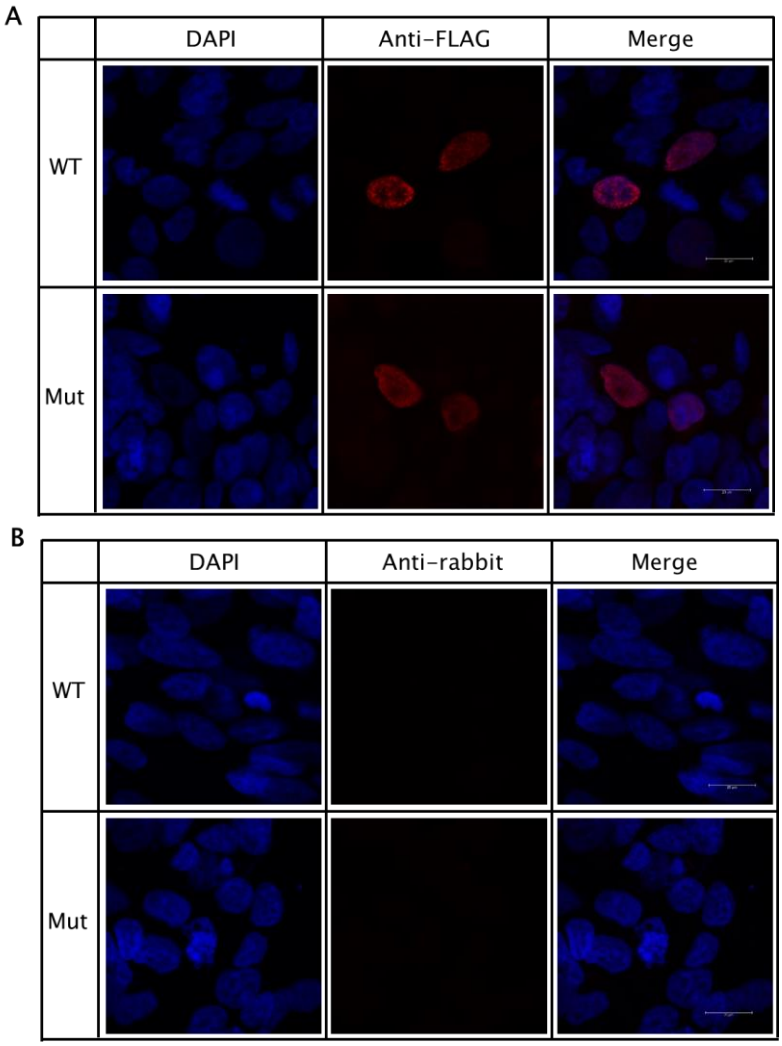

Figure 3-9. Subcellular localization of overexpression of WT (R1913) and Mut (K1913) FLAG-ZFHX2 in HEK293T cells. (A) Stained with anti-FLAG (SIGMA F7425). (B) Stained with secondary antibody only (Alexa 546 goat anti-rabbit). Clear nuclear localization was seen in both WT and Mut transfected cells. Scale bar=20 μm

Next, we tested two constructs that were created for the further study of ZFHX2 function: FLAG-ZFHX2-IRES-tdTomato and FLAG-ZFHX2-V5-IRES-eGFP (each construct has a WT (R1913) or Mut (K1913) ZFHX2 version) (Figure 3-10). IRES (internal ribosome entry site) allows for translation initiation in a cap-independent manner, This element was inserted since the ZFHX2 is a large protein. We expected the cells transfected with these constructs to express FLAG-ZFHX2 or FLAG-ZFHX2-V5 and also tdTomato or eGFP from an internal ribosome entry site. Firstly, we tested the FLAG-ZFHX2-IRES-tdTomato constructs in transfected HEK cells. The red fluorescence from the IRES-driven tdTomato was observed for both the WT and Mut constructs (Figure 3-11). FLAG tagged ZFHX2 protein was observed

within the nucleus in these transfected cells. Since FLAG tag signals were detected in the nucleus in cells expressing either WT or Mut FLAG-ZFHX2, the mutation did not seem to alter subcellular localization (Figure 3-11). These constructs were also transfected into mouse cultured DRG neurons with strong tdTomato fluorescence detected, indicating that transfected DRG neurons could be used as a model to further study ZFHX2 function (Figure 3-12).

Next, WT and Mut FLAG-ZFHX2-V5-IRES-EGFP constructs were generated and tested. The V5 tag is useful not only for immunofluorescence to verify subcellular localization, but also for immunoprecipitation (IP) and chromatin immunoprecipitation (ChIP) experiments (Rai et al., 2010). The FLAG and V5 tags are fused onto the N-terminus and C-terminus, respectively, of ZFHX2. The constructs were transfected into HEK293T cells and immunostaining was performed using anti-FLAG and anti-V5 antibodies (Figure 3-13). Both FLAG and V5 tagged protein was well stained and the fluorescence showed nuclear localization for both WT and Mut FLAG-ZFHX2-V5 constructs. Again, no obvious subcellular localization difference was observed between WT and Mut (Figure 3-13). The positive staining was verified with non-transfected cells stained with anti-FLAG and anti-V5 antibodies, which showed no obvious fluorescence (Figure 3-14).

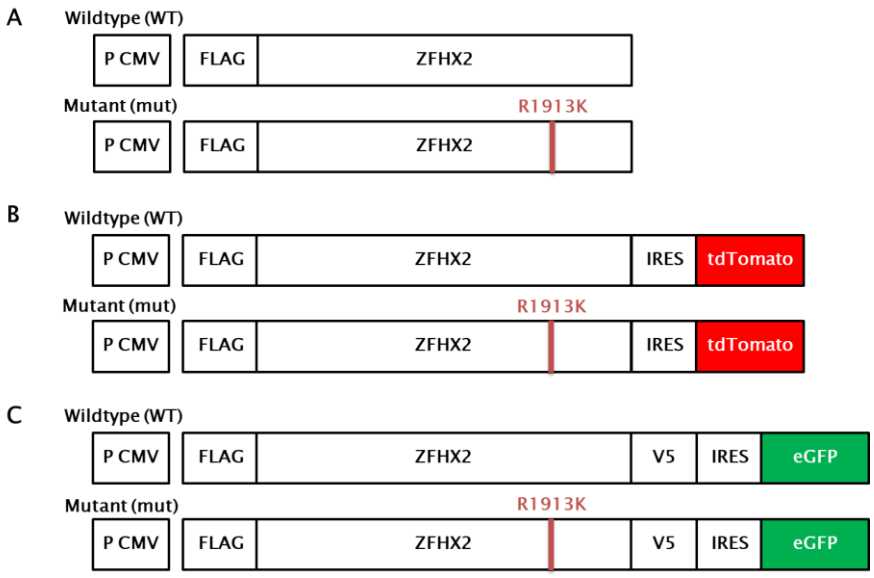

Figure 3-10. Created constructs. (A) FLAG-ZFHX2. (B) FLAG-ZFHX2-IRES-tdTomato. (C) FLAG-ZFHX2-V5-IRES-EGFP.

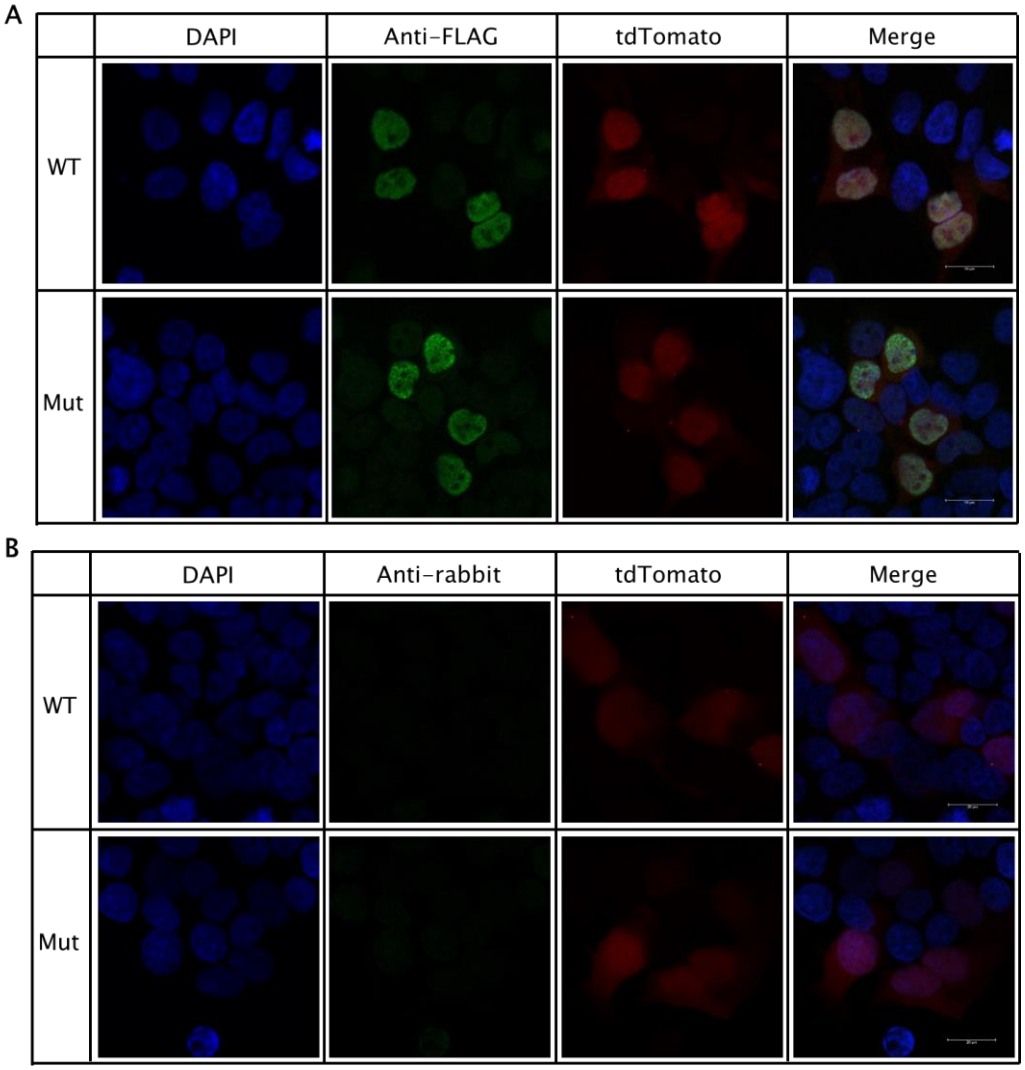

Figure 3-11. Subcellular localization of overexpression of WT (R1913) and Mut (K1913) FLAG-ZFHX2-IRES-tdTomato in HEK293T cells. (A) Stained with anti-FLAG (SIGMA F7425). (B) Stained with secondary antibody only (Alexa 488 goat anti-rabbit). FLAG staining shows clear nuclear localization in both WT and Mut transfected cells. Scale bar=20 μm

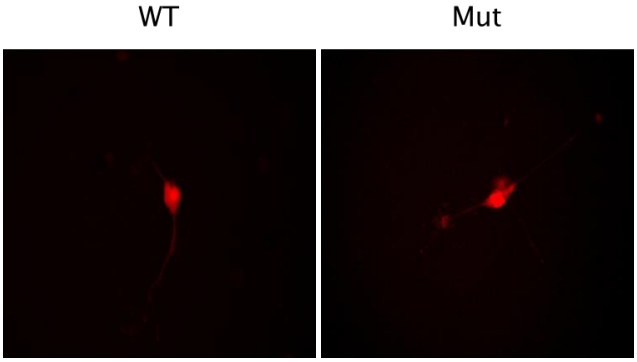

Figure 3-12. Mouse DRG cells expressing WT (R1913) and Mut (K1913) FLAG-ZFHX2-IRES-tdTomato. Both WT and Mut FLAG-ZFHX2-IRES-tdTomato were transfected into mouse DRG.

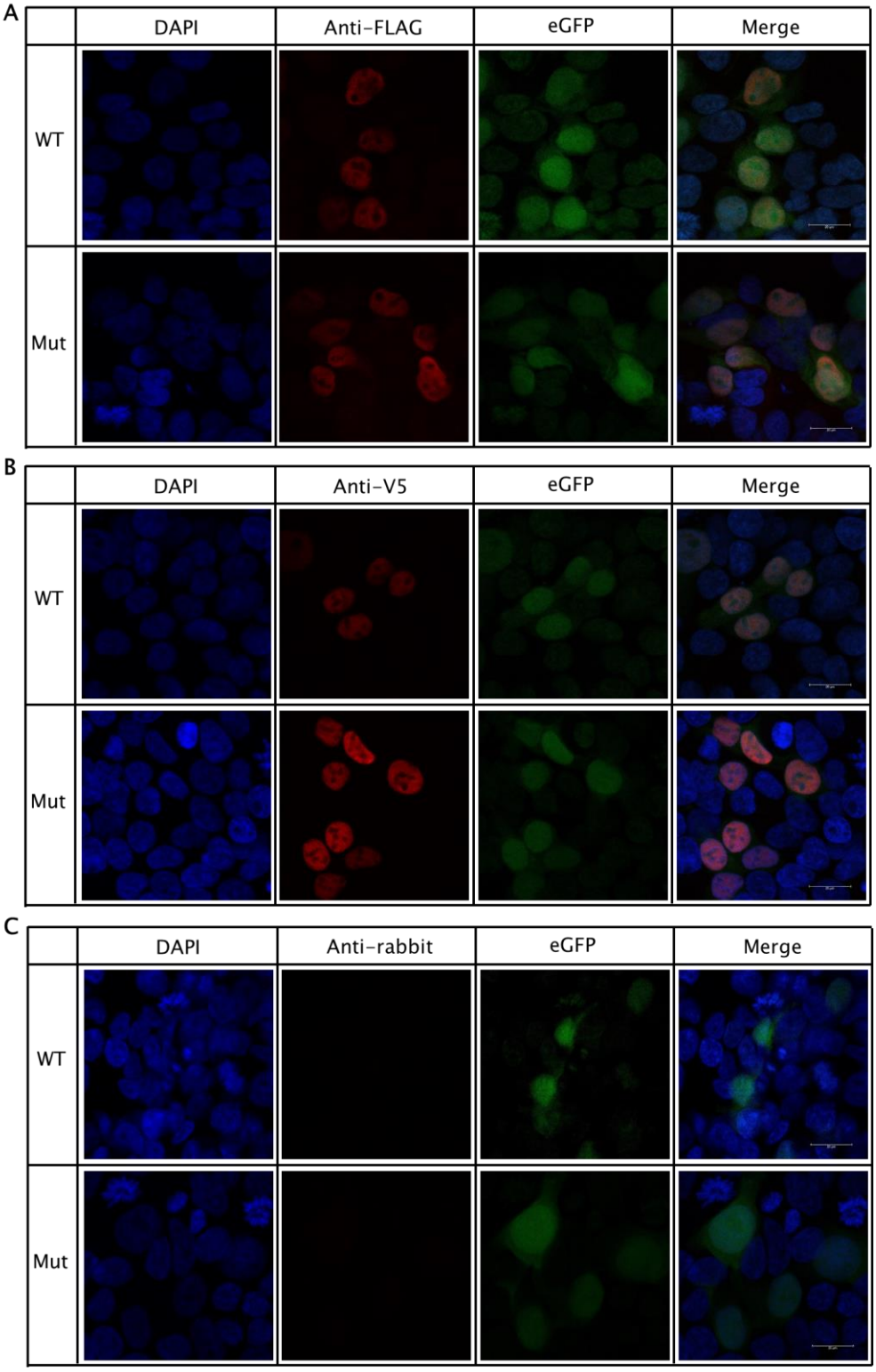

Figure 3-13. Subcellular localization of overexpression of WT (R1913) and Mut (K1913) FLAG-ZFHX2-V5-IRES-EGFP in HEK293T cells. (A) Stained with anti-FLAG (SIGMA F7425). (B) Stained with anti-V5 (SIGMA V8137) (C) Stained with secondary antibody only (Alexa 546 goat anti-rabbit). FLAG and V5 staining shows clear nuclear localization in both WT and Mut transfected cells. Scale bar=20 μm

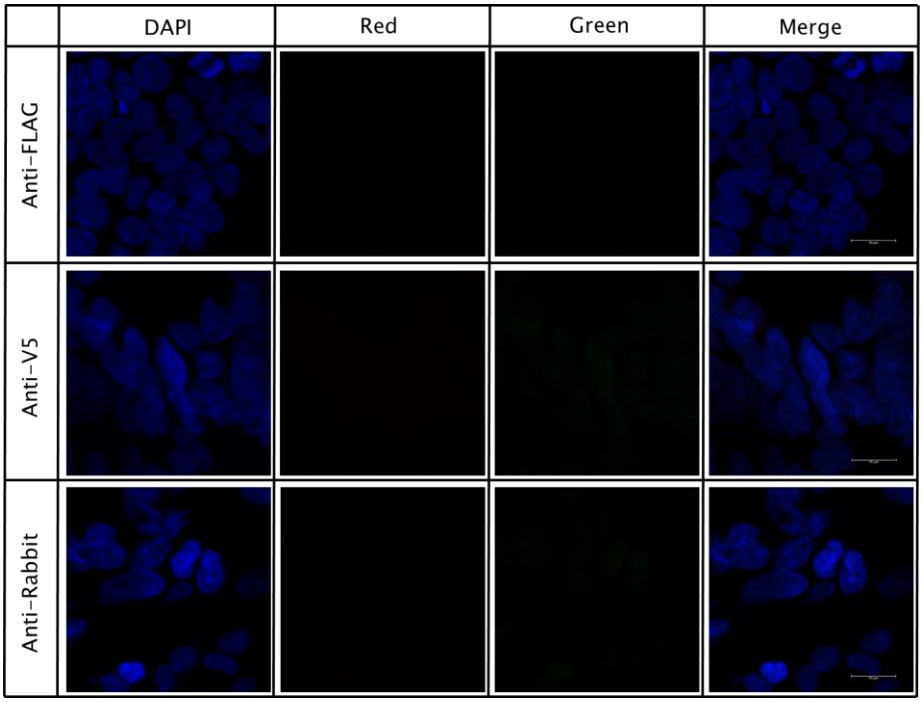

Figure 3-14. Non-transfected HEK293T cells incubated with anti-FLAG (SIGMA F7425) or anti-V5 (SIGMA V8137) or secondary antibody (Alexa 546 goat anti-rabbit) only. No obvious red and green fluorescence was observed. Scale bar=20 μm

3.4.2 Arginine methylation hypothesis

The patients carry a potential causative point mutation in a homeobox (Hox) domain in ZFHX2, resulting in the amino acid change R1913K. As discussed in 3.1.3, we hypothesized that R1913K in ZFHX2 could be a causative mutation, by altering the methylation status of the mutant ZFHX2 protein. Figure 3-15 shows the structure of the second Hox domain in ZFHX2 that is predicted to bind to DNA, with R1911 and R1913 in close proximity to the DNA strands.

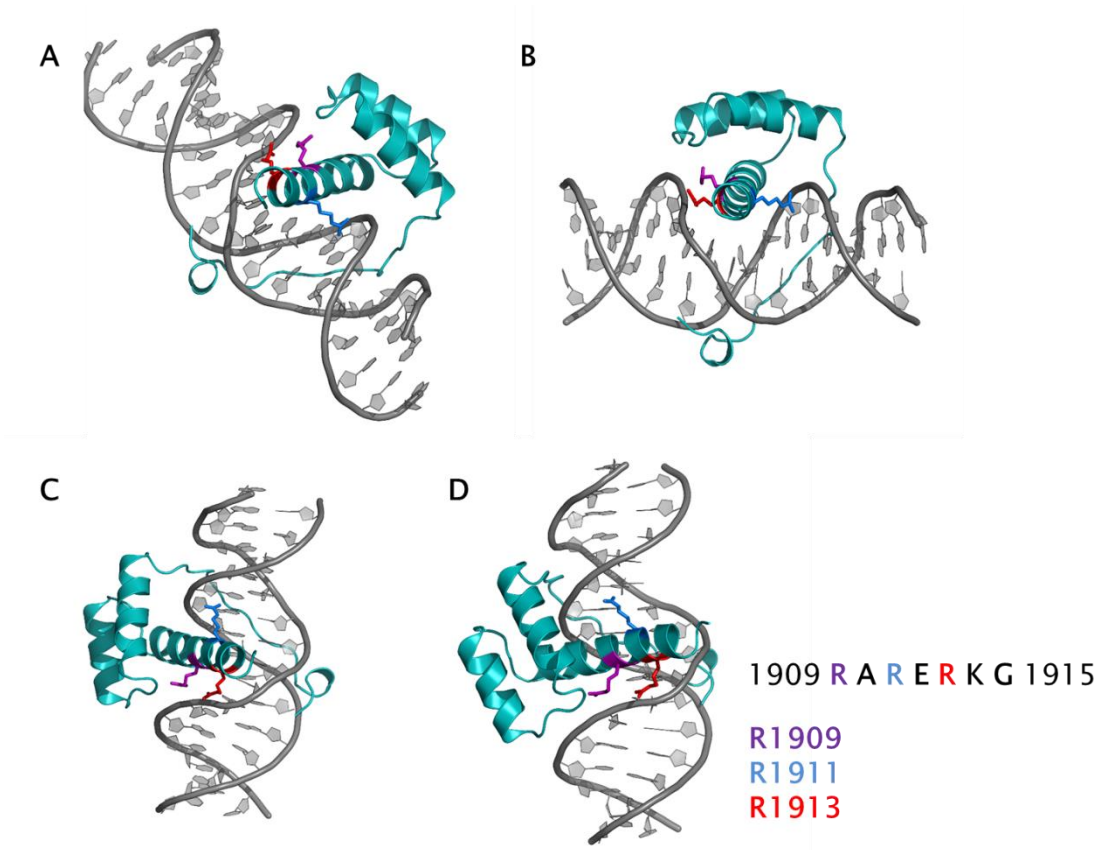

Figure 3-15. Interaction between DNA and Hox in ZFHX2. R1909 in purple, R1911 in blue, R1913 (where the mutation is) in red. (A)(B) DNA-Hox structure over the R1913 regions. (B)(C)(D) R1911 appears to face toward inside of DNA, while R1909 and R1913 toward outside of DNA. R1911 might interact/bind with DNA. Since R1913 seems to be close to DNA strand, it might also interact with DNA. This structure model is created by Dr. Andrei Okorokov at UCL.

To explore this methylation hypothesis, we aimed to immunoprecipitate both WT and Mut ZFHX2 proteins and analyse the R1913K regions to see the arginine methylation status using mass spectrometry. Firstly, we attempted a transient transfection into HEK293 cells (I). Secondly, AD293 cells that stably express FLAG-ZFHX2-V5 protein were generated and used to try to obtain enough protein for mass spectrometry analysis (I). Thirdly, SH-SY5Y stable cell lines which express FLAG-ZFHX2-V5 were generated to obtain larger amounts of protein (II, III). Mass spectrometry analysis was performed to identify the protein sequence and any modification over the mutation regions (IV).

I. Transient transfection in HEK293 cells

Firstly, we attempted to obtain ZFHX2 protein from HEK293 cells following transient transfection using Lipofectamine 2000. HEK293 (human embryonic kidney) cells were chosen as they are human cells that are relatively easy to transfect with high efficiency and also endogenously express the arginine methyltransferase PRMT5 which could potentially methylate ZFHX2 (Ren et al., 2010).

Following transfection we attempted to immunopurify and then detect protein on a western blot using an anti-FLAG tag antibody. The expected size of the protein is 274kDa and we anticipated the protein should be expressed in both transfected cells (WT and Mut) but not in non-transfected cells. However, the protein was not detected in the 250-300kDa range in both WT and Mut. In addition, there did not seem to be an additional band in WT or Mut which did not appear in non-transfected cells (Figure 3-16).

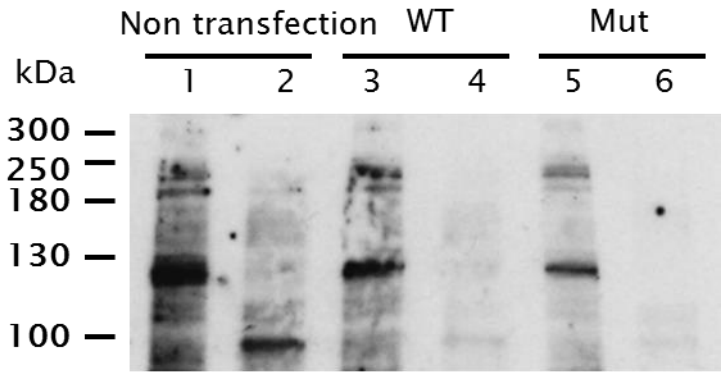

Figure 3-16. Western blotting for immunoprecipitation with anti-FLAG in HEK293 cells transfected with FLAG-ZFHX2-IRES-tdTomato. Anti-FLAG magnetic beads (SIGMA M8823) were used for immunoprecipitation. Tris-Glycine gel and anti-FLAG was used for Electrophoresis and primary antibody in western blot, respectively. Lane1: Cell lysis (non transfection), 2: Elution (non transfection), 3: Cell lysis (WT), 4: Elution (WT), 5: Cell lysis (Mut), 6: Elution (Mut). No bands were observed at the estimated size (274kDa).

We could not detect the protein in both lysis (input) and elution after immunoprecipitation and we considered that this could be due to either poor transfection efficiency or suboptimal anti-FLAG binding. We therefore tried immunoprecipitations using an alternative anti-V5 tag antibody. FLAG-ZFHX2-V5-IRES-EGFP or IRES-EGFP constructs were transfected into HEK293 cells, and anti-V5 was used to immunoprecipitate the proteins followed by western blotting (Figure 3-17). While we did not detect the target proteins using

anti-FLAG, using anti-V5 antibody gave a band between 250-300kDa in the cell lysis in WT and not in negative controls (the cells transfected with the IRES-eGFP plasmid) (Figure 3-17). However, the immunoprecipitated eluate did not show a clear band (Figure 3-17), suggesting that the larger amount of the target protein could be needed for immunoprecipitation experiments. We thought the transient transfection did not give enough numbers of positively transfected cells, which might have led to insufficient amount of ZFHX2 protein. Therefore, we aimed to generate a stable cell line expressing ZFHX2 to obtain a larger amount of protein (3.4.2I).

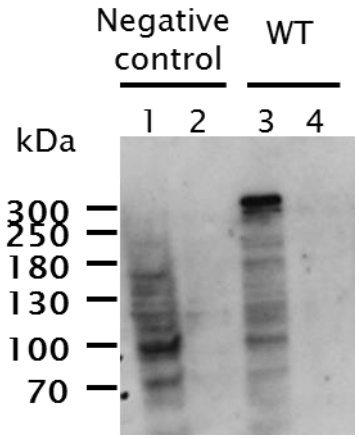

Figure 3-17. Western blotting for immunoprecipitation with anti-V5 in HEK293 cells transfected with FLAG-ZFHX2-V5-IRES-EGFP. Anti-V5 agarose beads (SIGMA A7345) were used for immunoprecipitation. Tris-Glycine gel and anti-V5 was used for electrophoresis and primary antibody in western blot, respectively. Lane1: Cell lysis (negative control, cells transfected with IRES-EGFP), 2: Elution (negative control, cells transfected with IRES-EGFP), 3: Cell lysis (WT FLAG-ZFHX2-V5-IRES-EGFP), 4: Elution (WT FLAG-ZFHX2-V5-IRES-EGFP). The approximate 300kDa protein was observed in cell lysis in WT although no protein was detected in immunoprecipitated eluate.

II. Immunoprecipitation using AD293 stable cell line

AD293 cells are derived from HEK293 cells to improve adhesion ability. This cells were chosen as they have no endogenous resistance to geneticin, human cells like HEK293 cells are and also endogenously express the arginine methyltransferase PRMT5 (Ren et al., 2010) which could potentially methylate ZFHX2. AD293 cells were transfected with the following constructs and stable cell lines selected (these lines were generated by Dr Abdella Habib, UCL):

1. WT FLAG-ZFHX2-V5-IRES-EGFP (named 'AB')

2. WT FLAG-ZFHX2-IRES-EGFP (named 'AC')

3. Mut FLAG-ZFHX2-V5-IRES-EGFP (named 'AD')

4. Mut FLAG-ZFHX2-IRES-EGFP (named 'AE')

5. IRES-EGFP (named 'AF')

The backbone of the plasmids was pcDNA3 which bears the Neomycin resistance gene (*neo*). Geneticin (also known as G418) blocks polypeptide synthesis by inhibiting the elongation step in both prokaryotic and eukaryotic cells and resistance to Geneticin is conferred by the Neomycin resistance gene. Following ~ 4 weeks of Geneticin selection we performed immunostaining to check for stable ZFHX2-expressing cells. Although the signals of immunofluorescence using anti-FLAG antibody were weak, all AB, AC, AD and AE lines showed anti-FLAG staining while no clear staining was observed in the negative control AF line (Figure 3-18). Clear signals of immunofluorescence were exhibited in AB and AD line using an anti-V5 antibody whilst there is no obvious fluorescence in AC, AE and AF line which did not carry the FLAG-ZFHX2-V5 construct (Figure 3-18). The immunofluorescent signals using anti-FLAG and anti-V5 antibodies were verified by the cells incubated with anti-mouse or anti-rabbit secondary antibody only, showing no obvious staining (Figure 3-18). Approximately 20% of cells expressed FLAG- or FLAG- and V5-tagged ZFHX2 (Figure 3-18).

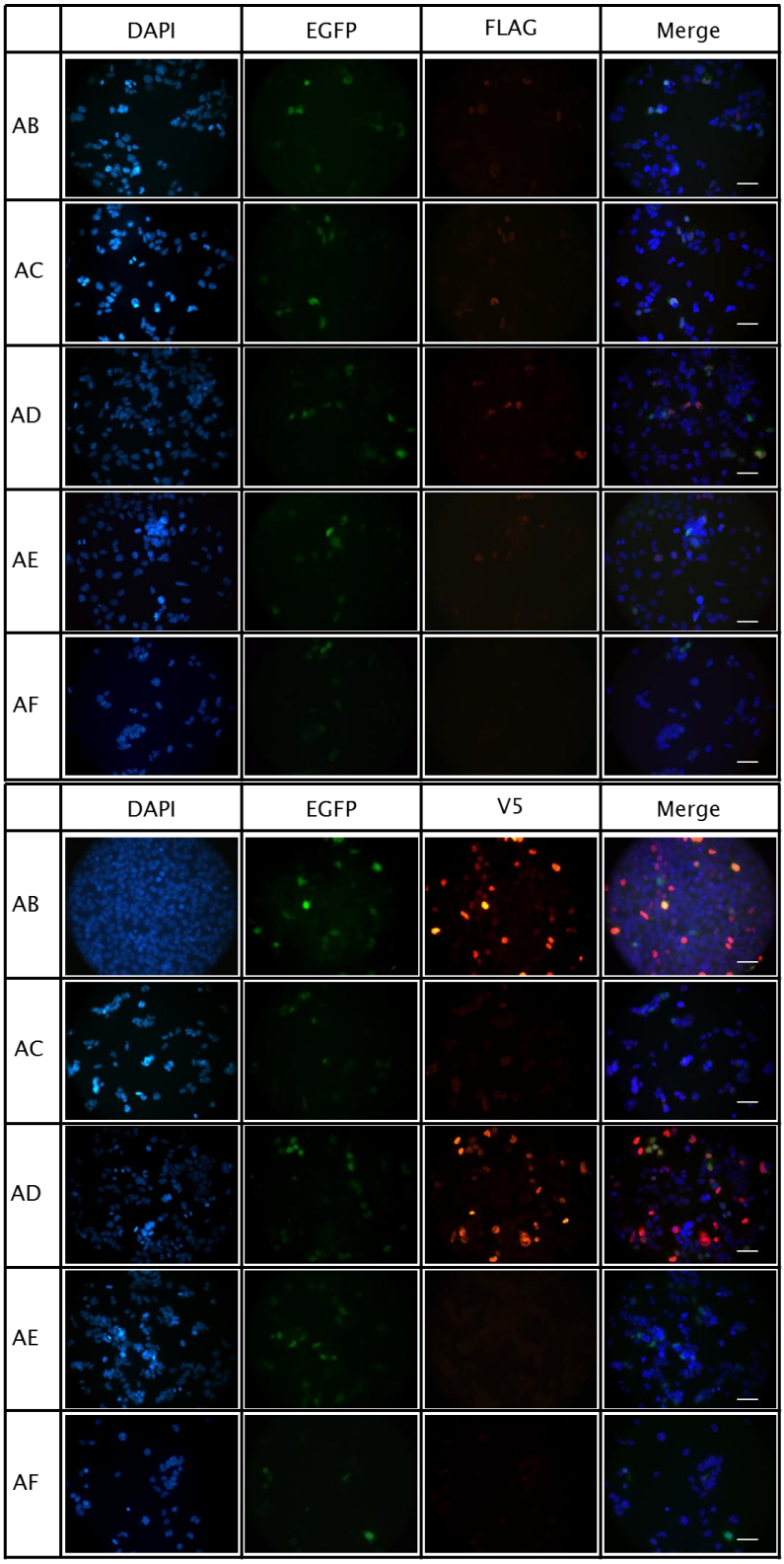
DAPI
EGFP
FLAG
Merge
AB
AC
AD
AE
AF
DAPI
EGFP
V5
Merge
AB
AC
AD
AE
AF

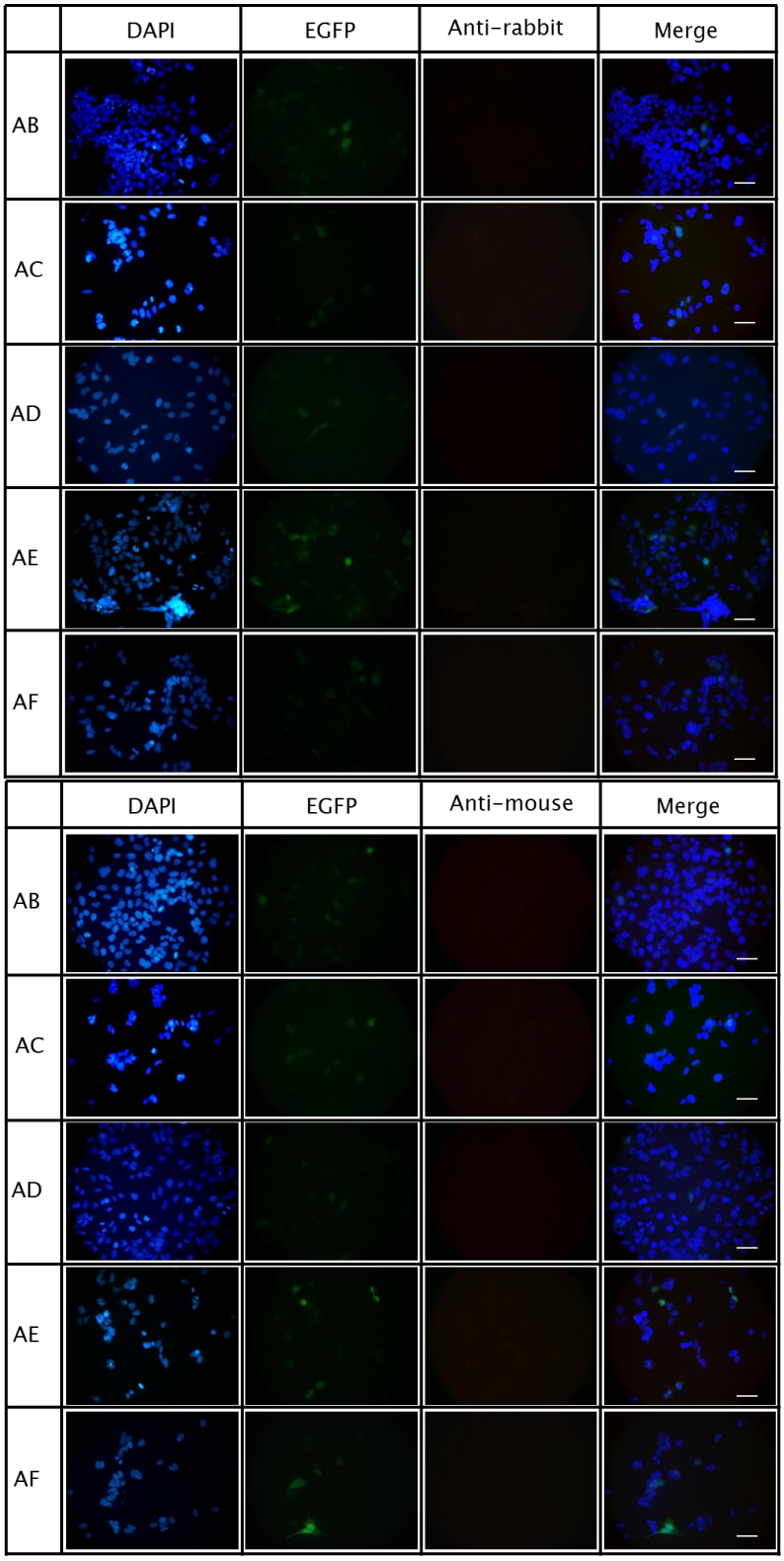

Figure 3-18. Immunocytochemical images for AD293 stable cell line. The cells were transfected with either of the constructs; AB; WT FLAG-ZFHX2-V5-IRES-EGFP, AC; WT FLAG-ZFHX2-IRES-EGFP, AD; Mut FLAG-ZFHX2-V5-IRES-EGFP, AE; Mut FLAG-ZFHX2-IRES-EGFP, AF; IRES-EGFP and incubated with Geneticin for a few weeks to select cells stably expressing ZFHX2. DAPI (Blue), eGFP (Green), FLAG or V5 (Red). Mouse anti-FLAG (SIGMA F1804) or Rabbit anti-V5 were used. Scale bar=60 μm

Since we generated cells that stably expressed FLAG-ZFHX2-V5, we attempted to perform immunoprecipitation and western blotting to detect ZFHX2 protein using an anti-FLAG antibody (Figure 3-19). No bands were detected in the immunoprecipitated eluate, although a band around 300kDa was observed in the AB, AC and AD lines (Figure 3-19A) for the cell lysis input samples. The poor detection of the protein might have been caused by poor binding ability of the antibody against the FLAG tagged protein. To explore if other antibodies could better detect ZFHX2, anti-ZFHX2 (Figure 3-19B) and anti-V5 antibodies were used (Figure 3-19C). The blot using rabbit anti-ZFHX2 (a custom antibody from Eurogentec) showed a band around 300kDa in all conditions, AB, AC, AD, AE, and AF line, suggesting that these cell lines expressed ZFHX2, although we cannot exclude non-specificity of the antibody detecting a different protein of the same size. However, the blot using anti-V5 demonstrated strong signals around 300kDa in AB and AD line, but not in the negative control AC, AE and AF lines which do not express V5 tagged protein. This result suggested that the V5 tag may be a suitable target to purify and detect ZFHX2 protein because the antibody against V5 may have high and specific binding ability.

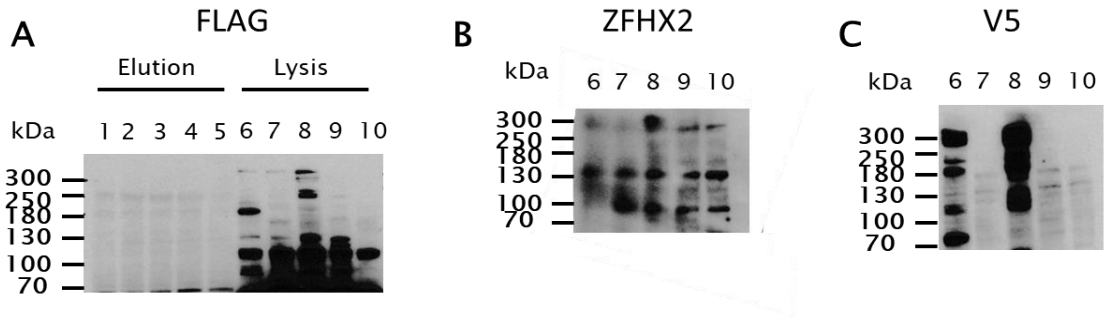

Figure 3-19. Western blotting for immunoprecipitation with anti-FLAG in AD293 stable cell line. Tris-Glycine gel was used for electrophoresis. Lanes 1and 6; AB line (WT FLAG-ZFHX2-V5-IRES-eGFP), Lanes 2 and 7; AC line (WT FLAG-ZFHX2-IRES-eGFP), Lanes 3 and 8; AD line (Mut FLAG-ZFHX2-V5-IRES-eGFP), Lanes 4 and 9; AE line (Mut FLAG-ZFHX2-IRES-eGFP), Lanes 5 and 10; AF line (IRES-eGFP). Lanes 1-5; immunoprecipitated eluate, Lanes 6-10; cell lysis. (A) Anti-FLAG magnetic beads (SIGMA M8823) were used for immunoprecipitation. The protein is detected by mouse anti-FLAG as a primary antibody in western blotting. (B)(C) cell lysis samples were loaded and anti-ZFHX2 (B) and anti-V5 (C) were used as a primary antibody in western blotting.

Prior to immunoprecipitation experiments, we checked the stable batch culture lines AB (WT), AD (Mut) and AF (IRES-eGFP) by immunostaining using an anti-ZFHX2 antibody (Figure 3-20). Both AB and AD cell lines stained by anti-ZFHX2 antibody showed fluorescence

(red), but no strong signals were observed in the control AF cell line. Together with the western blot data (Figure 3-19), these results indicated that these cells express V5-tagged ZFHX2.

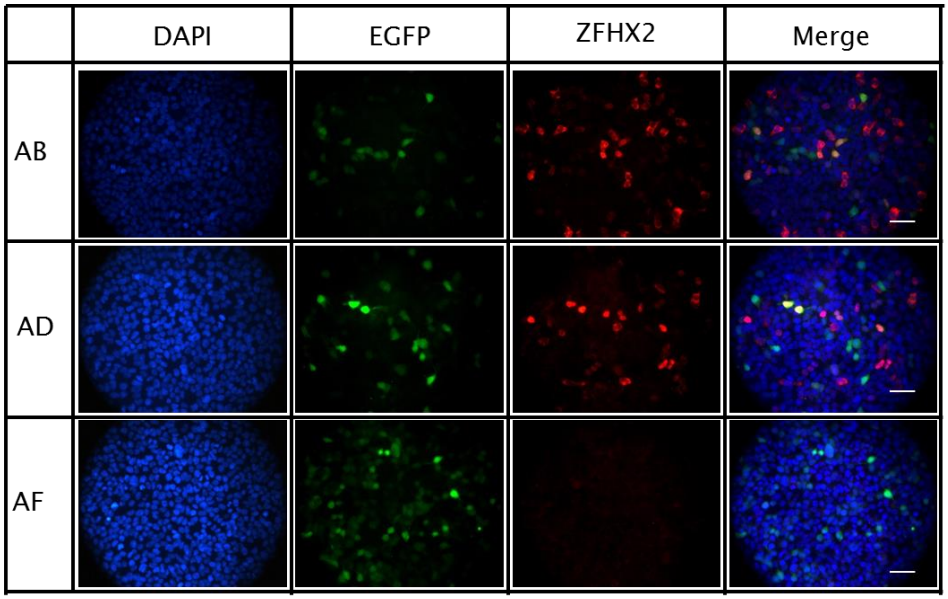

Figure 3-20. Immunostaining for AD293 stable cell line using anti-ZFHX2. AB (WT FLAG-ZFHX2-V5-IRES-EGFP), AD (Mut FLAG-ZFHX2-V5-IRES-EGFP), AF (IRES-EGFP) were stained by rabbit anti-ZFHX2 (red). No bright signals were observed from AF line while a proportion of cells showed red nuclear fluorescence in AB and AD lines. Scale bar=60 μm

We therefore conducted immunoprecipitation experiments using the AB, AD and AF cell lines. The cell lysis samples obtained from each of the cell lines were immunoprecipitated using anti-V5 agarose beads. To confirm if these cell lines express full length of ZFHX2 and use this immunoprecipitated ZFHX2 for mass spec analysis, the protein level was checked by western blotting using either anti-V5 or anti-FLAG antibodies. The blot incubated with the anti-V5 antibody showed strong signals around 300kDa in both the input cell lysis samples and the immunoprecipitated eluate samples from the AB and AD cell lines (Figure 3-21A). Protein with the size of approximately 300kDa was also detected by the anti-ZFHX2 antibody in both the input and immunoprecipitated samples from the AB, AD and AF cell lines (Figure 3-21C). Faint bands of the expected size were observed in the blot using the anti-FLAG antibody for the AB and AD immunoprecipitated samples (Figure 3-21B). This faint staining with anti-FLAG antibody might be because of the antibody's weak activity or insufficient translation of FLAG tag since another downstream initiation codon exists close to the FLAG tag start codon. Since we could obtain strong signals using the anti-V5 antibody, we expected there might be enough

protein to conduct mass spectrometry. Therefore, we performed Coomassie staining using for the immunoprecipitated samples. Despite the strong signal seen in western blotting using the anti-V5 antibody, we could not find a clear band in the AB and AD lines compared to the control cell line (AF) by Coomassie staining (Figure 3-22).

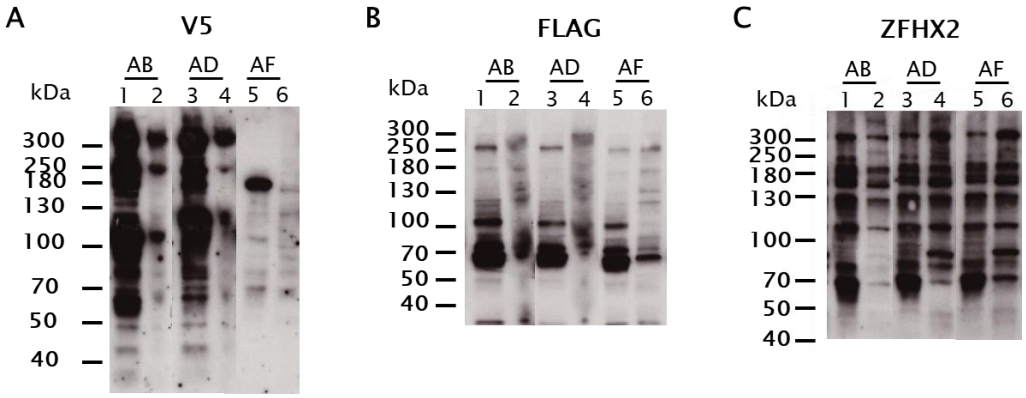

Figure 3-21. Western blots following immunoprecipitation using an anti-V5 antibody in AD293 stable cell lines. Tris-Glycine gel was used for electrophoresis. Anti-V5 agarose beads (abcam ab1229) were used for immunoprecipitation. Lanes 1 and 2; AF line (IRES-eGFP), Lanes 3 and 4; AD line (Mut FLAG-ZFHX2-V5-IRES-eGFP), Lanes 5 and 6; AB line (WT FLAG-ZFHX2-V5-IRES-eGFP). Lanes 1,3,5; Cell lysis, Lanes 2,4,6; immunoprecipitated eluate. The blot was incubated with (A) anti-V5or (B) anti-FLAG antibody or (C) anti-ZFHX2.

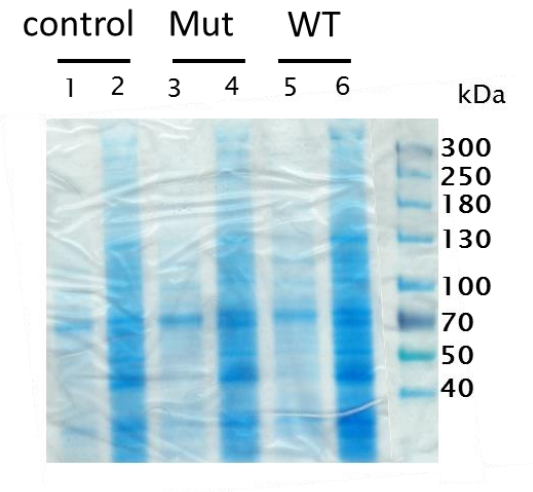

Figure 3-22. Coomassie staining using immunoprecipitated samples from the AD293 stable cell lines. Tris-Glycine gel was used for electrophoresis. Lanes 1 and 2; AF line (IRES-EGFP), Lanes 3 and 4; AD line (Mut FLAG-ZFHX2-V5-IRES-EGFP), Lanes 5 and 6; AB line (WT FLAG-ZFHX2-V5-IRES-EGFP). Lanes 1,3,5; Cell lysis, Lanes 2,4,6; immunoprecipitated eluate.

To obtain a larger amount of the target protein, we aimed to generate stable cell lines derived from single cells (as opposed to the batch stable cell lines described above which contain a mixed population of ZFHX2-expressing and non-expressing cells). In order to generate these cell lines, the antibiotic selected cell lines (AB, AD, AF line) were sorted into single cells using flow cytometry by selecting for green fluorescence. The single cells were grown in Geneticin-containing media and clones verified by immunostaining, qRT-PCR and western blotting. Firstly, to select the single clones that stably express V5 tagged ZFHX2 and eGFP, the cells were stained with anti-V5 antibody. Among the WT and Mut clones, the ones which showed bright immunofluorescence staining against the V5 tag were selected for further analysis. The AF clones which showed green fluorescence and were negative for anti-V5 staining were selected as the control clones. Four clones from each line were selected. Secondly, the mRNA levels of *ZFHX2* were measured by quantitative RT-PCR in the selected clones. The single clones from AB line, named AB5, AB7, AB10 and AB12, and the AD line, named AD1, AD2, AD4 and AD14 expressed approximately the same mRNA levels of *ZFHX2* i.e. 4 to 117 fold more than control single clones from the AF line, named AF5, AF11, AF12, AF14 (Figure 3-23). Finally, we performed western blotting to check protein levels. We could see high protein levels (a band around 300kDa) in AB10 and AD2, and moderate to low target protein levels in AB5, AD1 and AD14 (Figure 3-24). None of the protein is observed in controls using anti-V5, suggesting that V5 tag is specific and it is highly likely that the band around 300kDa is the target protein, V5 tagged ZFHX2 (Figure 3-24). It should be noted that AB5 and AD1 expressed high levels of mRNA although they did not show strong expression in protein levels. This could be because the samples were not properly kept and degrated or the protein was not fully translated in these clones.

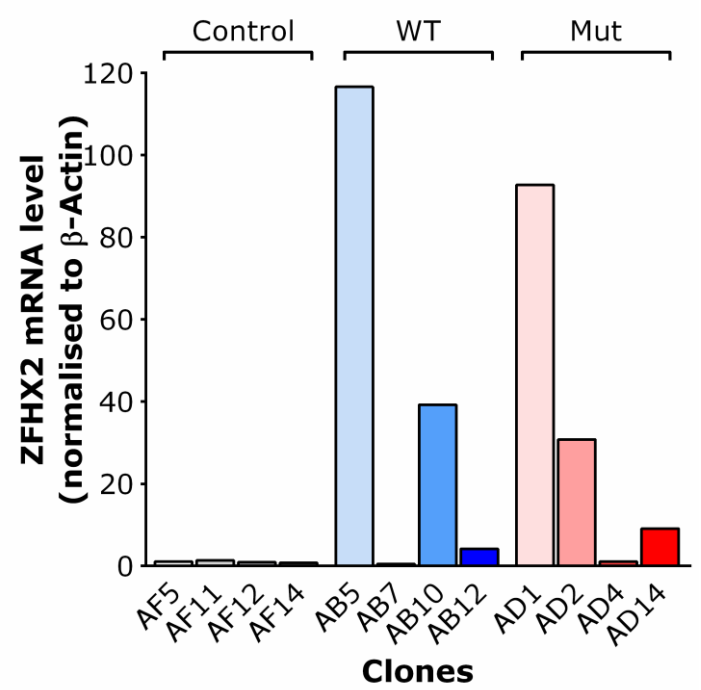

Figure 3-23. Real-time qRT-PCR analysis of ZFHX2 mRNA expression in AD293 stable clones relative to β-Actin. Relative expression levels of mRNA were calculated using the comparative ΔΔCt (Ct) method and normalised by control clones (AF).

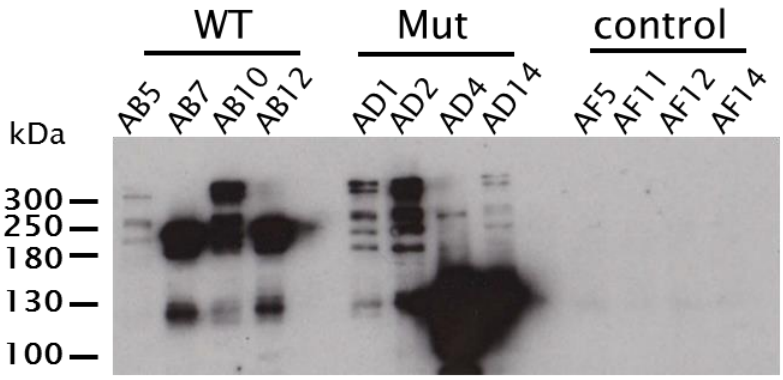

Figure 3-24. Western blotting for AD293 single clones. Tris-Glycine gel was used for electrophoresis and anti-V5 was used to detect the proteins. A ~300kDa protein was detected in some of the WT and Mut clones; AB5, AB10, AB12, AD1, AD2 and AD14. No anti-V5 bands were detected from the control clones (AF line).

Next, we performed immunoprecipitation to purify V5 tagged ZFHX2 protein using anti-V5 magnetic beads. Magnetic beads are easy to handle and the loss of proteins during immunoprecipitation is less than with agarose beads. We used AB5 and AB10 for WT, AD2 and AD14 for Mut, and AF11 for control. The strong signal around 300kDa was observed in AB10 and AD2 (Figure 3-25). The immunofluorescent staining in these clones also indicated the overexpression of V5 tagged ZFHX2 (Figure 3-26). Thus we performed Coomassie staining using the immunoprecipitated eluate from AB10, AD2 and AF11 (Figure 3-27). However, no bands of the target protein were observed.

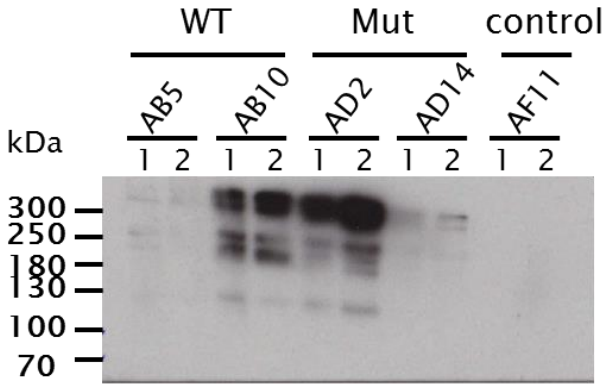

Figure 3-25. Western blot following immunoprecipitation with anti-V5 magnetic beads in samples derived from the AD293 single clone stable cell lines. Tris-Glycine gel was used for electrophoresis. Anti-V5 magnetic beads (MBL) and rabbit anti-V5 were used for immunoprecipitation and detection of the proteins, respectively. AB5 and AB10; WT, AD2 and AD14; Mut, AF11; control clone.

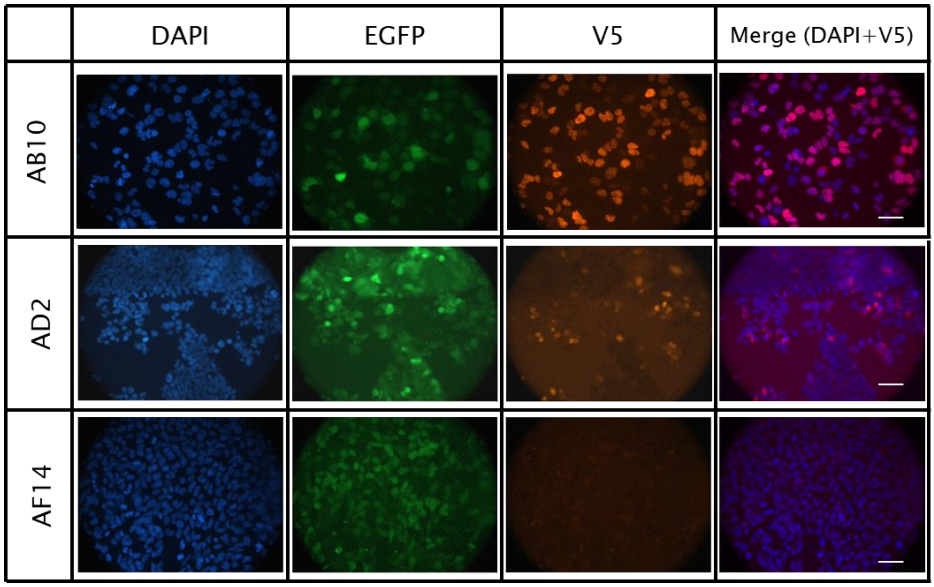

Figure 3-26. Immunostaining for AD293 stable single clones using anti-V5. AB10 (WT FLAG-ZFHX2-V5-IRES-EGFP), AD2 (Mut FLAG-ZFHX2-V5-IRES-EGFP), AF14 (IRES-EGFP) were stained using rabbit anti-V5 (SIGMA V8137 in red). No bright signals were observed for AF14 while the cells in AB5 and AD2 clone showed red nuclear fluorescence. Scale bar=60 μm.

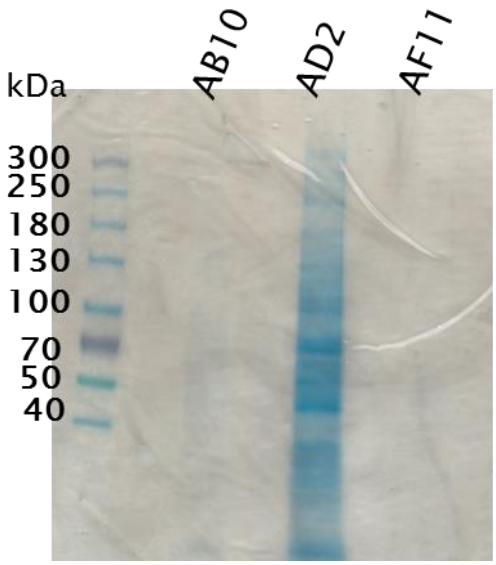

Figure 3-27. Coomassie staining for the AD293 single clone stable cell lines. Anti-V5 magnetic beads were used for immunoprecipitation. AB10; WT, AD2; Mut, AF11; Control clone. Several very faint bands were observed in AB10 and AF11. No clear bands were observed around 300kDa.

III. Generating SH−SY5Y stable cell lines

The SH-SY5Y cell line is a human neuroblastoma cell line, which is a thrice cloned subline of SK-N-SH cells. SK-N-SH cells were originally obtained from a bone marrow biopsy of a neuroblastoma patient with sympathetic adrenergic ganglial origin in the early 1970's (Biedler et al., 1973). SK-N-SH cells were subcloned first to SH-SY, then to SH-SY5, finally to SH-SY5Y which could be differentiated to a more mature neuron-like phenotype (Kovalevich and Langford, 2013). This cell line has been also reported that it expresses PRMT5 (Park et al., 2015, Uhlen et al., 2015, Thul et al., 2017). The primary goals of generating the SH-SY5Y cells that stably express FLAG-ZFHX2-V5 were: 1. To obtain large amounts of FLAG/V5 tagged ZFHX2 for mass spectrometry analysis. 2. To explore pathological mechanisms in neuronal-like cells. 3. To perform microarrays to explore downstream targets of ZFHX2 in neuronal-like cells (described in 3.4.4).

To generate the stable cell lines we followed a similar method to the one described for the AD293 cells. However, this time we also linearized the plasmids prior to the transfection to limit the chance of the open reading frame of *ZFHX2* being disrupted when it became inserted into the cell's genome (Figure 3-28). The plasmids were linearized with a

restriction enzyme that cut within the ampicillin resistance gene, whose expression is not essential for generation of the stable cell line (Figure 3-28). The following 6 constructs were prepared for transfection into the SH-SY5Y cells:

1. Circular (non-linearized) WT FLAG-ZFHX2-V5-IRES-eGFP (named SBC)
2. Linear WT FLAG-ZFHX2-V5-IRES-eGFP (named SBL)
3. Circular (non-linearized) Mut FLAG-ZFHX2-V5-IRES-eGFP (named SDC)
4. Linear Mut FLAG-ZFHX2-V5-IRES-eGFP (named SDL)
5. Circular (non-linearized) IRES-eGFP (named SFC)
6. Linear IRES-eGFP (named SFL)

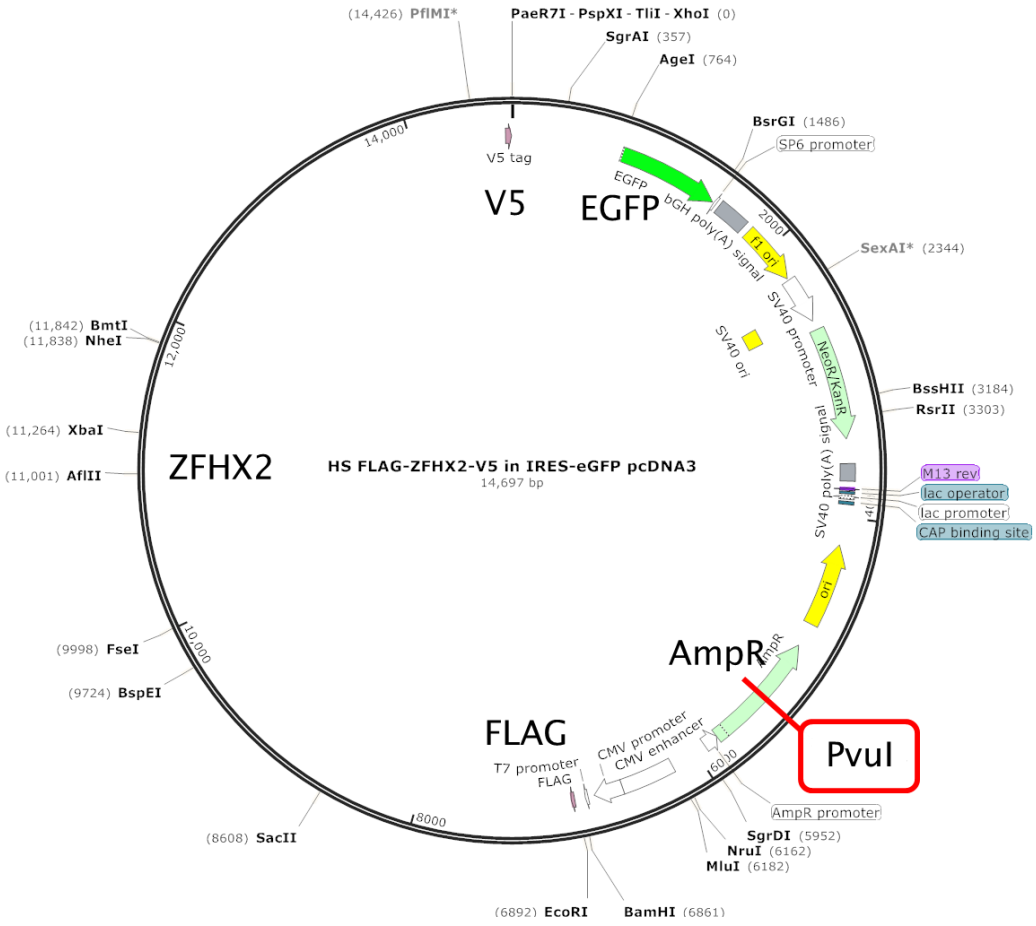

Figure 3-28. FLAG-ZFHX2-V5-IRES-eGFP construct map. To linearize the plasmid, PvuI was used which has a single restriction site within the ampicillin resistance gene.

After Geneticin-selection lasting a few weeks, immunofluorescent staining was performed to check for positive cells using an anti-V5 antibody (Figure 3-29). Some cells

expressed V5 tagged ZFHX2 in the nucleus in SBC, SBL, SDC and the SDL lines. However, there did not appear to be marked numbers of positive cells. Therefore, we aimed to select single clones which expressed FLAG-ZFHX2-V5 by selecting for green fluorescence using flow cytometry.

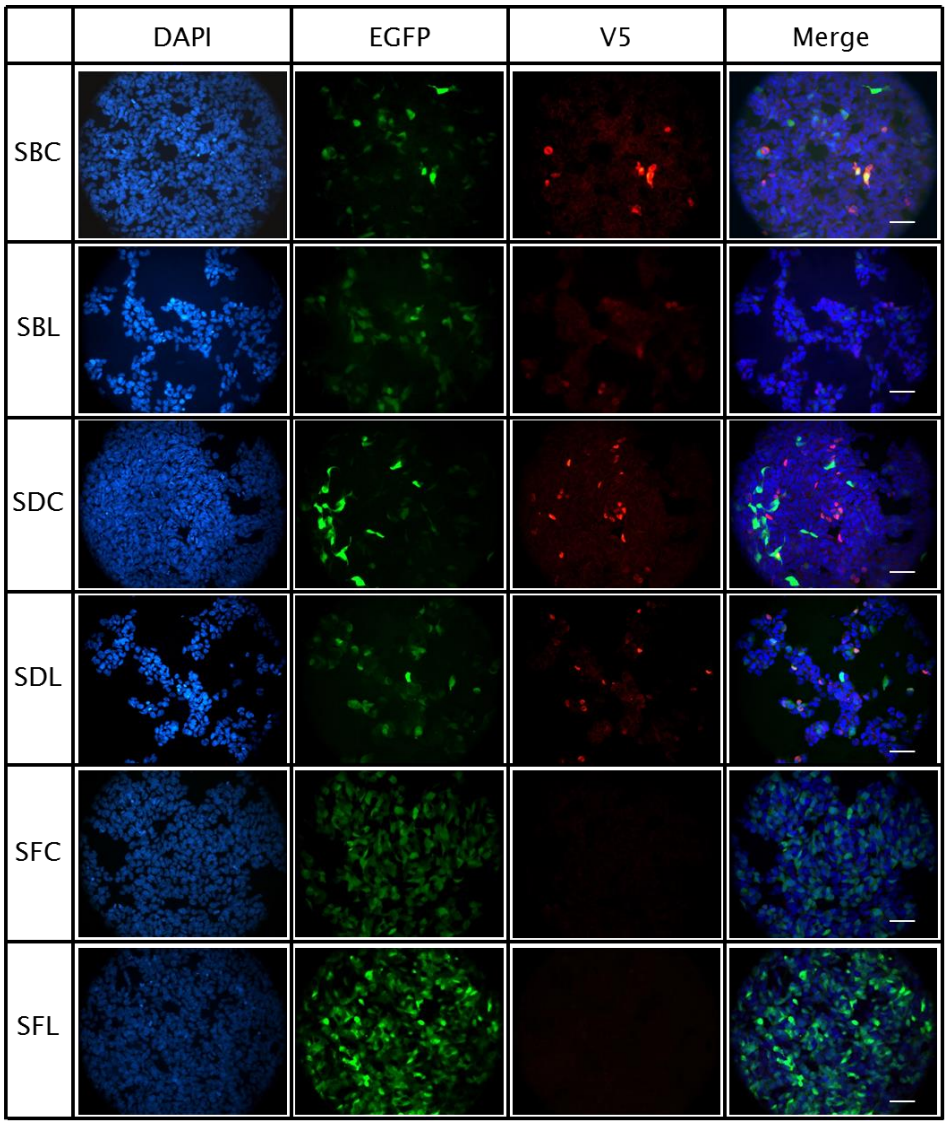

Figure 3-29. Immunostaining images for SH-SY5Y stable cell lines. SBC (Circular WT FLAG-ZFHX2-V5-IRES-eGFP), SBL (Linear WT FLAG-ZFHX2-V5-IRES-eGFP), SDC (Circular Mut FLAG-ZFHX2-V5-IRES-eGFP), SDL (Linear Mut FLAG-ZFHX2-V5-IRES-eGFP), SFC (Circular IRES-eGFP), SFL (Linear IRES-eGFP). Anti-V5 (Sigma V8137) was used to stain the cells. Scale bar=60 μm

Single eGFP-expressing cells were sorted by flow cytometry into 96 well plates and grown for several weeks in Geneticin-containing media. Single clones were verified by the

following steps: immunostaining using anti-V5 antibody to select for positive cells, qRT-PCR to verify *ZFHX2* mRNA levels, sequencing over the mutation regions, and western blotting to check for protein levels. Firstly, immunofluorescent staining was performed with an anti-V5 antibody to select the clones expressing V5 tagged ZFHX2. We could select several clones from the SBC, SBL, SDC, SDL, SFC and SFL lines (Table 3-11) (Figure 3-30, Figure 3-31, Figure 3-32). Clear and strong immunofluorescence staining by anti-V5 was observed from several WT and Mut clones; SBC3, SBL3 (Figure 3-30), SDC2, SDL1, SDL2, and SDL9 (Figure 3-31). Some WT and Mut clones also showed moderate signals; SBL7, SBL9, SBL12 (Figure 3-30), SDC13 and SDL7 (Figure 3-31). Only background levels of fluorescence were seen in the control cell lines, SFC and SFL (Figure 3-32). Secondly, total mRNA of these clones was isolated and RT-qPCR was conducted to measure the *ZFHX2* mRNA levels. All positive clones showed higher mRNA levels of *ZFHX2* compared to the control cell lines (SFC and SFL). However, each clone demonstrated different mRNA levels of *ZFHX2*, ranging from 6 to 96 fold change compared to the control clones (SFC and SFL) (Figure 3-33). Thirdly, all clones were sequenced to identify if the point mutation was present in the mutant clones (SDC and SDL lines), and whether it was absent in wild type (SBC and SBL lines) and control clones (SFC and SFL lines). The mutation was present in all mutant clones, and absent in all wild type and control clones. Finally, western blotting was performed with an anti-V5 antibody to check if protein was translated. The protein levels of ZFHX2 seemed to differ for each clone. However, the expression levels of V5 tagged ZFHX2 showed a similar tendency to the mRNA levels seen in the qRT-PCR results (Figure 3-33, Figure 3-34). WT clones, SBC3 and SBL3 showed high levels of the protein as well as mRNA levels while SBL7, SBL9, SBL12 indicated low levels of proteins and mRNA levels. The Mut clones SDC2, SDL1, SDL2 and SDL7 tended to express higher levels of protein whilst SDC13 and SDL9 showed lower levels. No bands around 270kDa were observed in control clones, suggesting that the observed band around 270kDa was likely to be V5 tagged ZFHX2. Most of the WT and Mut clones demonstrated several smaller sized proteins; these could be degraded proteins of V5 tagged ZFHX2, or potentially, proteins which were translated from another downstream start codon. We chose some of the clones from each cell line to proceed with immunoprecipitation to purify the protein for mass spectrometry, as shown in the next section (3.4.2III).

Table 3-11. Summary of stably expressing FLAG-ZFHX2-V5 SH-SY5Y clones from each line.

	SBC	SBL	SDC	SDL	SFC	SFL
Numbers of clones sorted by flow cytometry	95	190	95	190	95	190
Numbers of clones by antibiotic selection	4	12	14	11	11	15
Numbers of clones selected by immunofluorescence	1	4	2	4	4	4

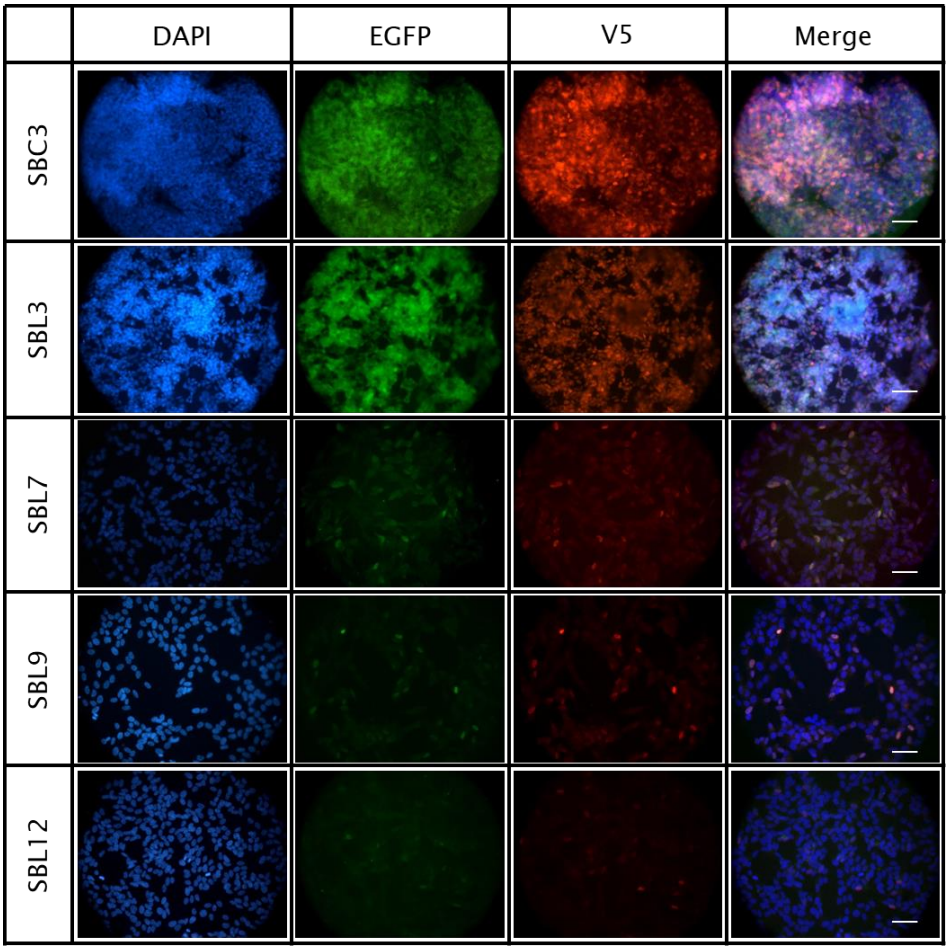

Figure 3-30. Immunofluorescence images for WT SH-SY5Y stable clones. SBC (Circular WT FLAG-ZFHX2-V5-IRES-eGFP), SBL (Linear WT FLAG-ZFHX2-V5-IRES-eGFP). Anti-V5 (Sigma V8137) was used to stain the cells. Scale bar=60 μm.

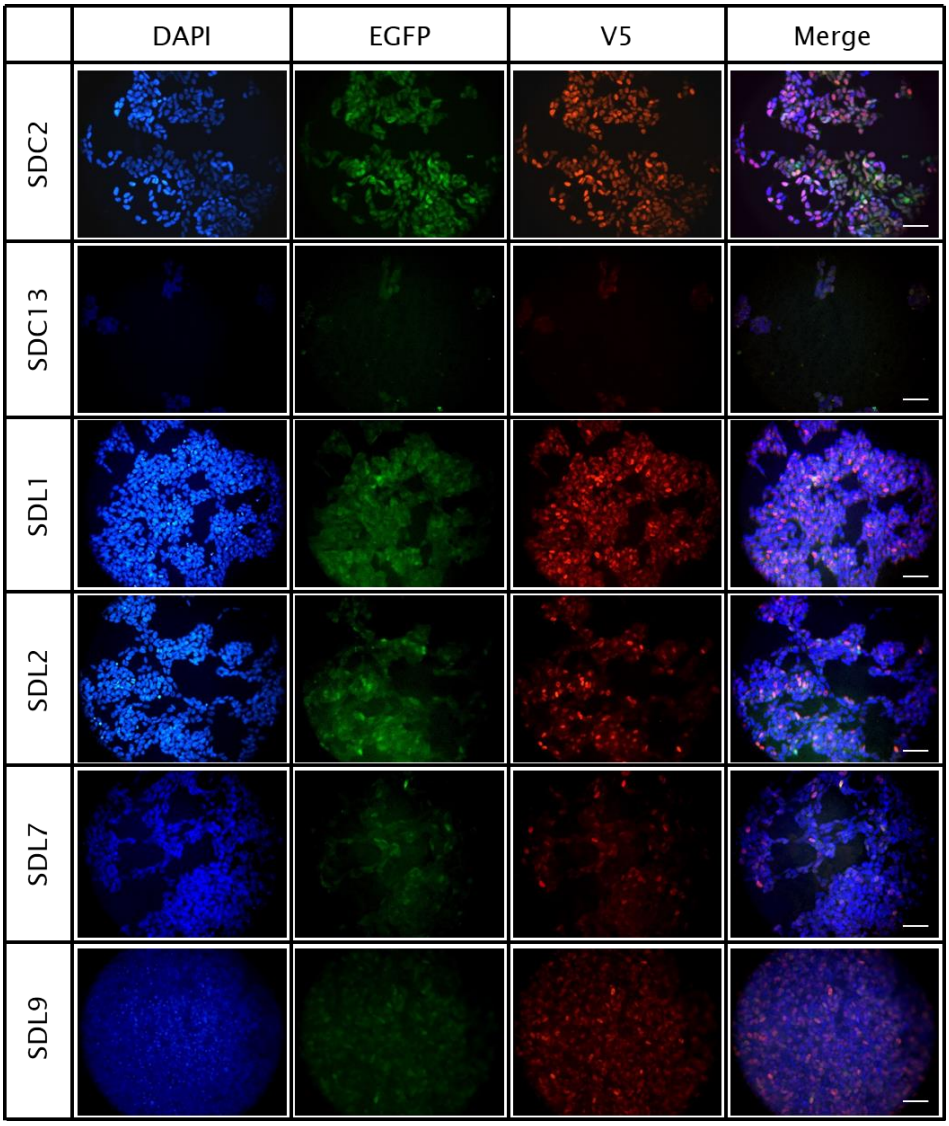

Figure 3-31. Immunofluorescence images for Mut SH-SY5Y stable clones. SDC (Circular Mut FLAG-ZFHX2-V5-IRES-eGFP), SDL (Linear Mut FLAG-ZFHX2-V5-IRES-eGFP). Rabbit anti-V5 was used to stain the cells. Scale bar=60 μm.

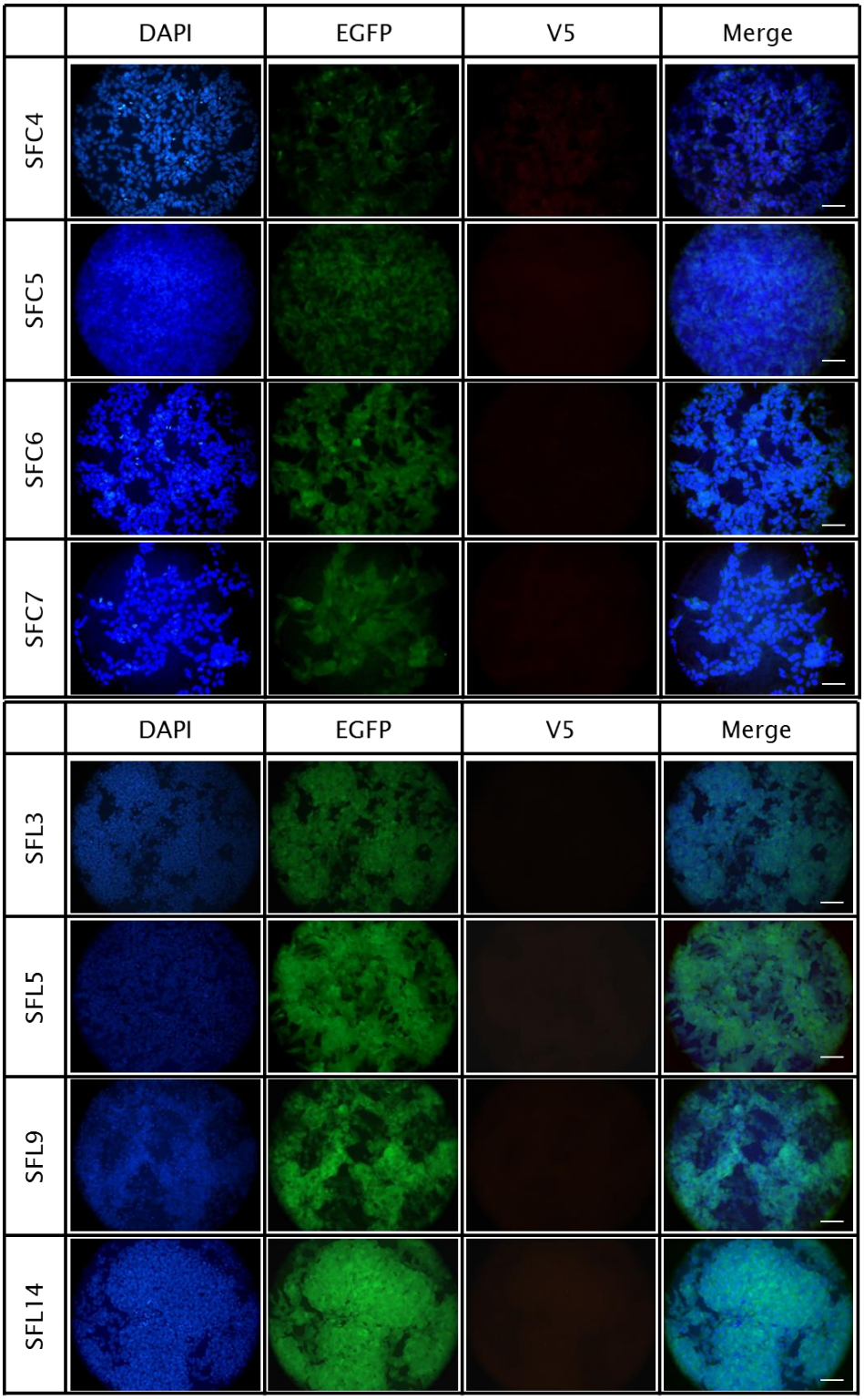

Figure 3-32. Immunofluorescence images for control SH-SY5Y stable clones. SFC (Circular IRES-eGFP), SFL (Linear IRES-eGFP). Rabbit anti-V5 was used to stain the cells. Scale bar=60 μm.

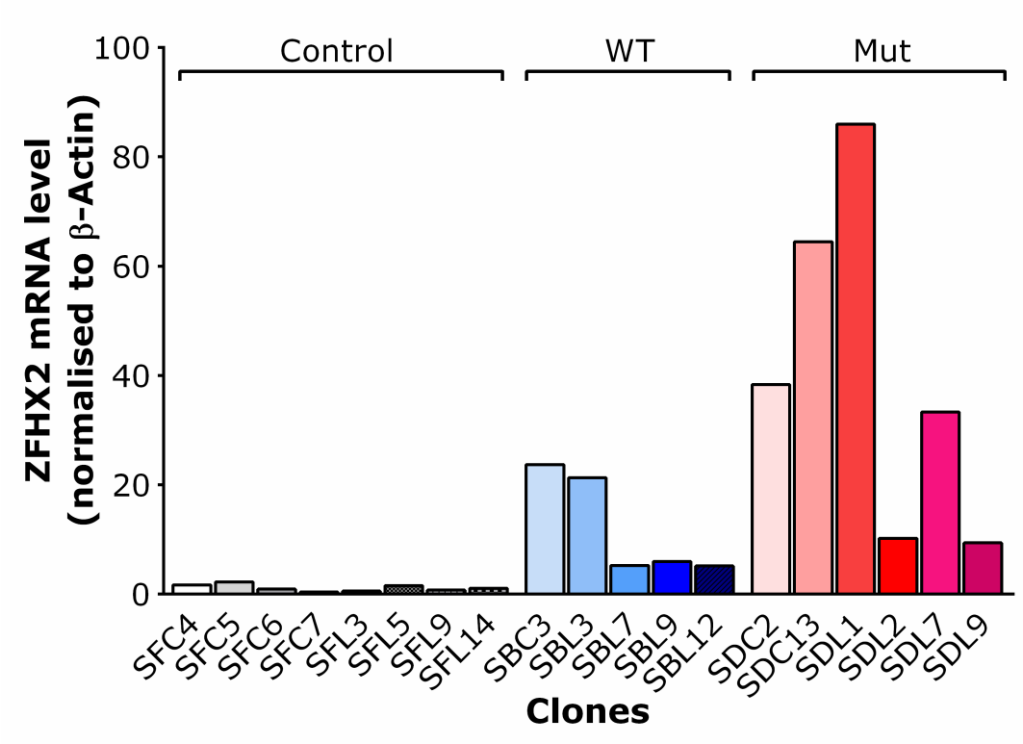

Figure 3-33. Real-time qRT-PCR analysis of ZFHX2 mRNA expression in SH-SY5Y stable clones relative to β-Actin. Relative expression levels of mRNA were calculated using the comparative ΔΔCt (Ct) method and normalised by control clones (SF).

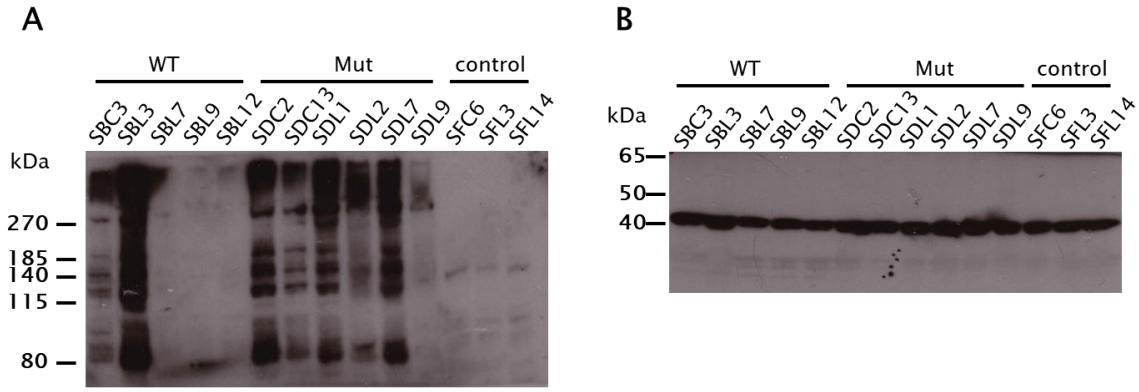

Figure 3-34. Western blotting for SH-SY5Y single clone stable cell lines. Bis-Tris gel was used for electrophoresis and (A) anti-V5 and (B) anti- β-Actin were used to detect the proteins. (A) High levels of ~270kDa protein was detected in SBL3, SDC2, SDL1. This band was absent in the control clones (AF line). (B) β-Actin was detected with approximately same level in each clone.

IV. Immunoprecipitation in SH−SY5Y stable cell lines

In the previous section, SH-SY5Y stable cell lines were generated that overexpressed ZFHX2. We aimed to perform immunoprecipitation to purify ZFHX2 protein for mass spectrometry analyses. In order to obtain a large amount of ZFHX2, we chose several clones from each line. Two WT and three Mut clones, which expressed higher levels of protein and mRNA were selected; SBC3 and SBL3 for WT, SDC2, SDL1, and SDL7 for Mut. In addition, SBL7 (WT) and SDL9 (Mut) were chosen because they showed less degraded proteins by western blotting. Antibody against V5 tagged protein was used for immunoprecipitation, and western blotting with anti-V5 (Figure 3-35A) and anti-ZFHX2 (Figure 3-35B) was performed to detect and identify the protein. Strong signals around 270kDa from the immunoprecipitated eluate were detected by western blotting with anti-V5 antibody for clones SBC3, SBL3, SDC2 and SDL1, whilst no clear signals were seen in the control clone, SFL3 (Figure 3-35A). To identify if the protein shown around 270kDa marker was ZFHX2, western blotting with anti-ZFHX2 was also performed (Figure 3-35B). The band around 270kDa is barely seen in SBC3; however, SBL3, SDC2 and SDL1 showed the band which was absent in the control clone (SFL3). No visible bands were observed for SBL7 and SDL9. The immunoprecipitated eluate from 7 clones was used for silver staining to check if the amount of protein could be enough for mass spectrometry analysis (Figure 3-36A). A clear ~270 kDa band was observed in SBC3, SBL3, SDC2 and SDL1 (Figure 3-36A, indicated by the red arrow). This band was not visible in the control clone, SFL3 (Figure 3-36A), suggesting that this band was the overexpressed ZFHX2-V5. The same band was also observed, but was fainter, in SBL7 and SDL9 (Figure 3-36A, indicated by the red arrow). These low protein levels could be a reason why it was not detected by western blotting with anti-ZFHX2. Next, we combined SBC3 and SBL3, and SDC2 and SDL1 to conduct coomassie staining (Figure 3-36B). A band around 270kDa was visible in these WT and Mut clones, but not from the negative control clone (Figure 3-36B, indicated by the red arrow). The bands were carefully isolated and sent for mass spectrometry analysis, described in the next section (3.4.2IV).

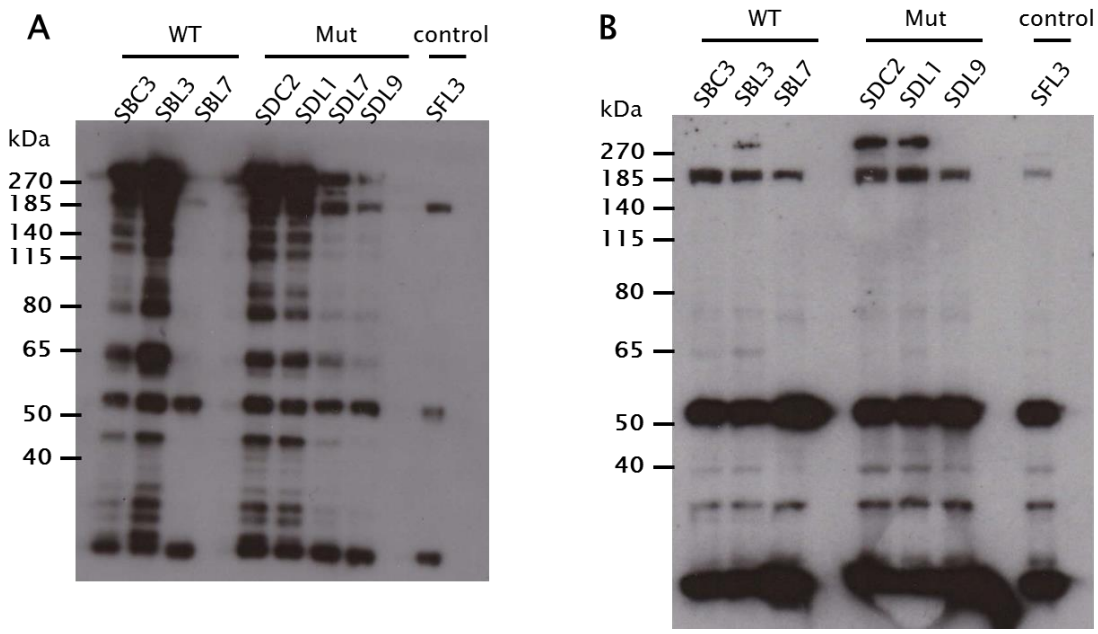

Figure 3-35. Western blotting following immunoprecipitation with anti-V5 antibody in SH-SY5Y single clone stable cell lines. Bis-Tris protein gel was used for electrophoresis. Anti-V5 agarose beads (MBL) were used for immunoprecipitation. The blot was incubated with (A) anti-V5 or (B) anti-ZFHX2.

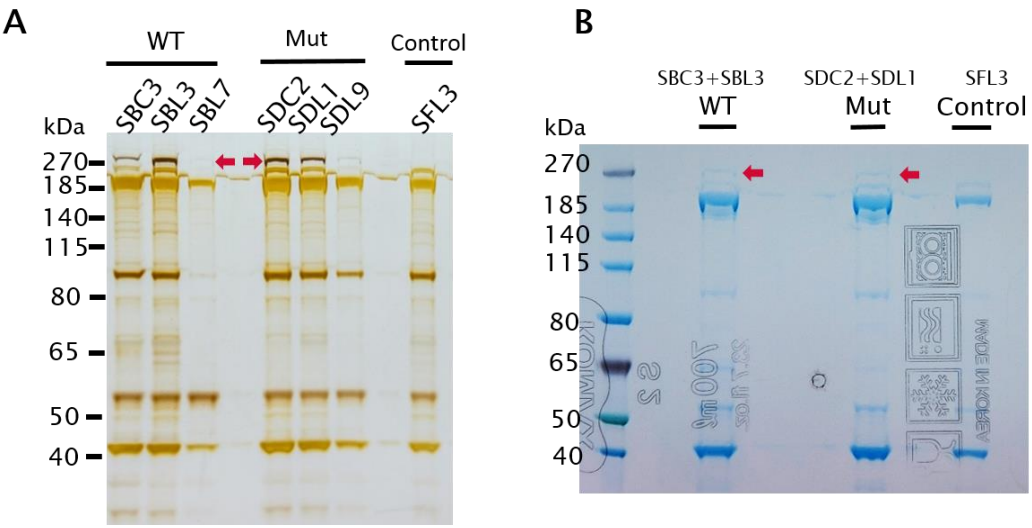

Figure 3-36. Silver staining and Coomassie staining of immunoprecipitated eluates prior to mass spectrometry analysis. Bis-Tris protein gel was used for electrophoresis. (A) Silver staining. A clear band around 270kDa (indicated by the red arrow) was observed SBC3, SBL3, SDC2 and SDL9, and a faint band of the same size was also seen in SBL7 and SBL9. No visible bands around 270kDa were observed for the control clone, SFL3. (B) Coomassie staining of WT clones (combination of SBC3 and SBL3), Mut clones (combination of SDC2 and SDL1), and control clone, SFL3. A faint band around 270kDa (indicated by the red arrow) was observed in WT and Mut clones but not in the control clone. These bands were isolated for mass spectrometry analysis.

V. Mass spectrometry analysis

Protein isolation by Coomassie staining was perfomed by myself with help from Dr. Andrei Okorokov at WIBR, UCL. All the other experimental procedures were performed by Dr. Honglei Huang at University of Oxford.

The mass spectrometry analysis of the protein isolated from the bands around 270kDa shown in Figure 3-36 identified 242 peptides for the WT band and 366 peptides for the Mut band. This equated to 54% and 66% ZFHX2 sequence coverage for WT and Mut proteins, respectively, indicating that the band isolated from around 270kDa was ZFHX2. Unfortunately, the fragments detected in this analysis did not cover the R1913 mutation region (Figure 3-37). Therefore another immunoprecipitation was performed to obtain ~10 times more protein. The coomassie staining of immunoprecipitated eluates from approximately 70 million cells displayed thicker bands around 270kDa (Figure 3-38). The bands were carefully isolated and sent for mass spectrometry analysis.

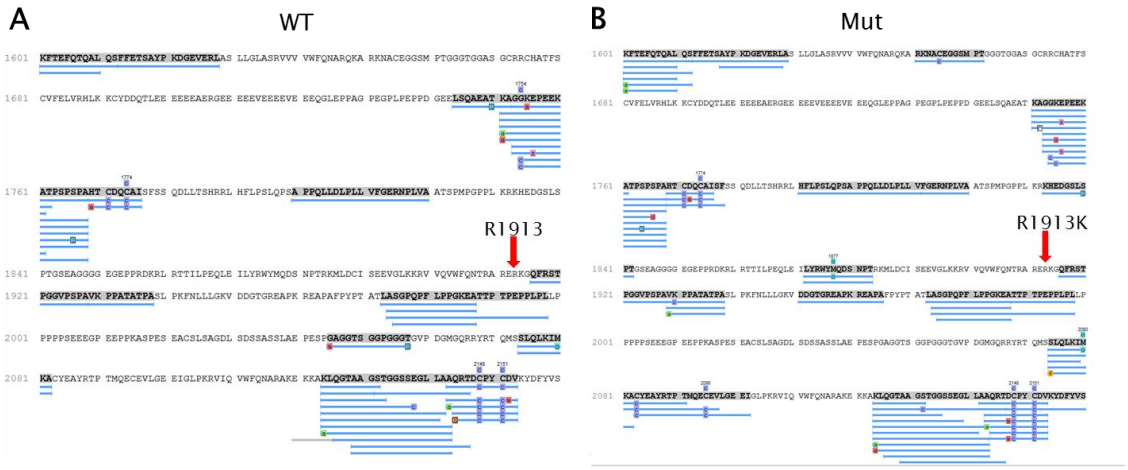

Figure 3-37. The fragments detected in mass spectrometry analysis and ZFHX2 sequence. Both fragments from (A) WT and (B) Mut did not include amino acid 1913, indicated by the red arrows. Blue lines show the detected peptide fragments.

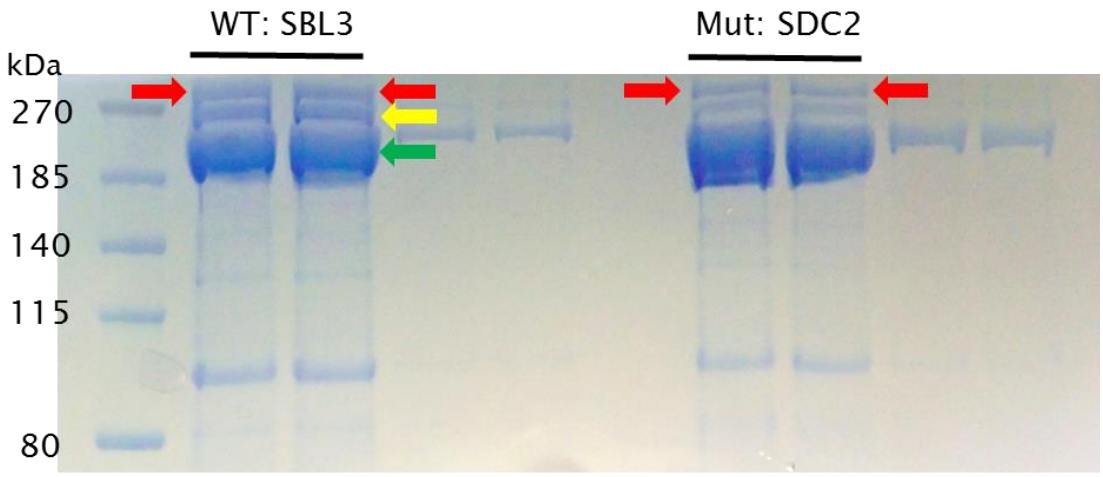

Figure 3-38. Coomassie staining of immunoprecipitated eluates prior to mass spectrometry analysis. Bis-Tris protein gel was used for electrophoresis. Approximately 70 million cells of SBL3 and SDC2 were used for WT and Mut clones, respectively. The bands around 270kDa (indicated by the red arrow) was observed in WT and Mut clones were isolated for mass spectrometry analysis to evaluate arginine methylation around amino acid 1913. The two bands below 270kDa (indicated by the yellow and green arrows) were also separated for mass spectrometry analysis to test if these are ZFHX2 associated protein.

The mass spectrometry analysis of the immunoprecipitated eluates with high numbers of cells detected 1772 and 1487 peptides from WT and Mut clones, respectively, with 97% ZFHX2 sequence coverage for both clones. The fragments of detected peptides showed R1913K in the mutant protein (Figure 3-39B), indicating the isolated band from immunoprecipitated elutes is over expressed Mut ZFHX2. Both R1913 in WT ZFHX2 and K1913 in Mut ZFHX2 were not methylated although only 1 peptide was detected for WT, and 2 peptides were detected for Mut (Figure 3-39). We also found R1911 in the Mut ZFHX2 is not methylated in 2 peptide fragments (Figure 3-39B). However, although the higher amount of protein was analysed in this attempt, R1911 in WT ZFHX2 is not detected (Figure 3-39A). We also analysed two other bands; the band just below 270kDa (indicated in the yellow arrow in Figure 3-38, named WT1) and around 180kDa (indicated in the green arrow in Figure 3-38, named WT2). The fragments of WT1 and WT2 mainly demonstrates the trace of myosin and spectrin, respectively. Of note, the mass spectrometry analysis shows some fragments carry the trace of ZFHX2 for both WT1 and WT2, indicating that these proteins could be a part of ZFHX2 due to degradation or translation from another downstream start codon.

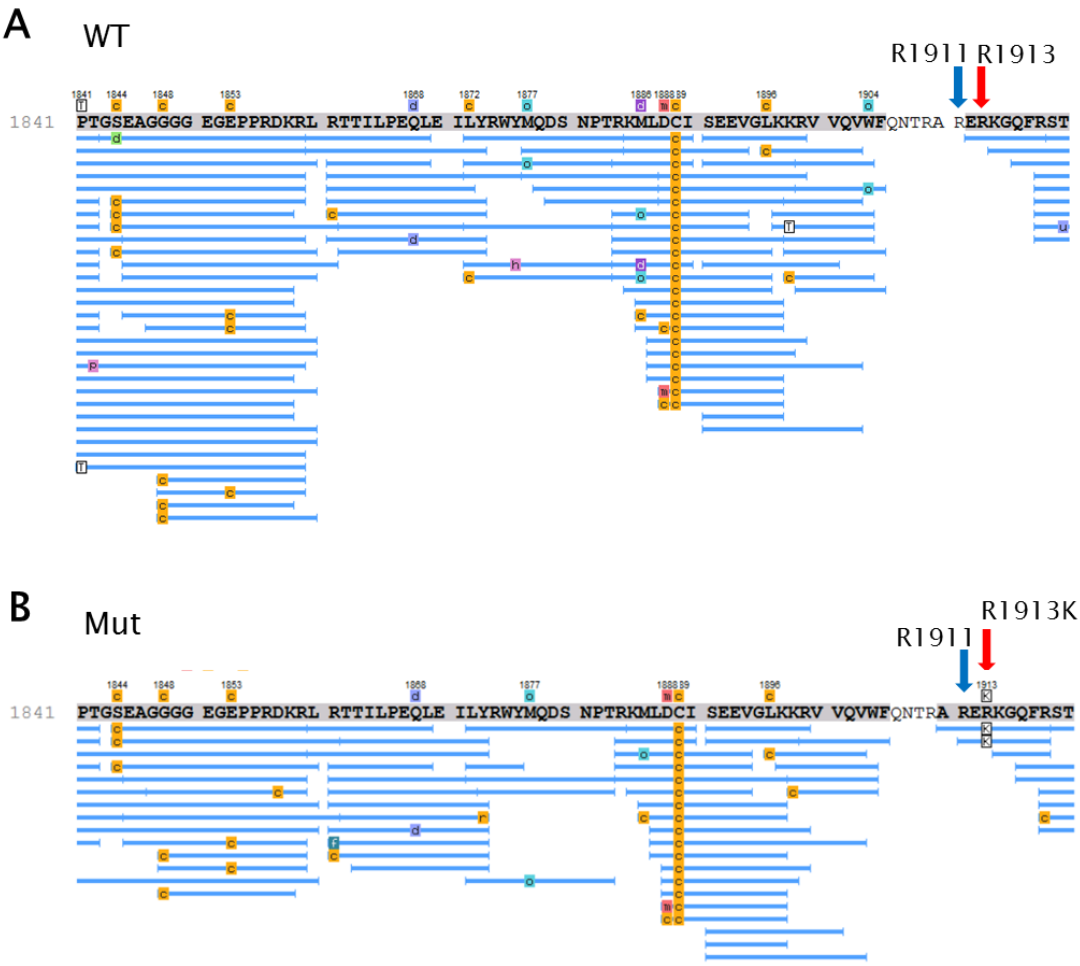

Figure 3-39. The fragments detected in mass spectrometry analysis using higher amounts of ZFHX2 protein. (A) WT ZFHX2. R1913 was detected (indicated by the red arrow), however, fragments that cover R1911 (indicated by the blue arrow) were not found. (B) Mut ZFHX2. R1911 (indicated by the blue arrow) and R1913K (indicated by the red arrow) were detected without methylation. Blue lines show the detected fragments.

Although the mass spectrometry analysis did not show any differences between WT and Mut ZFHX2 around position 1913 (Figure 3-39), post-translational modifications at other sites were identified (Table 3-12). For example, the methylation on aspartic acid at the position 1772 is relatively strong in WT (one third of aspartic acid residues were methylated) whilst it seems to be weak in Mut (approximately one tenth of them were methylated) (Table 3-13). The residues on R1961, E2019 and E2021 demonstrate weak methylated status in Mut while none of methylated fragments are observed in WT (Table 3-13). In addition, approximately 20% of residues on S2020 are methylated in WT, whilst no methylation is found on this residue in Mut (Table 3-13). Arginine and lysine are two major residues where methylation occurs predominantly, although methylation can take place on other amino acids.

These include histidine, aspartic acid, and glutamic acid, and on the carboxyl groups of proteins (Stallcup, 2001, Sprung et al., 2008, Aletta et al., 1998, Alam et al., 2015). However, methylation on serine residues has not seemed to be reported yet. Since the methylations are found at the position 2019, 2020 and 2021, it might be due to a technical analysis error that the methylation was found on serine residue at the position 2020. Even so, the methylation on D1772, E2019 and E2021 might be affected by the R1913K mutation, and these methylations may play a role in the functions of ZFHX2. The methylation on R1961 would be also interesting, although it does not seem to be strongly methylated. Along with structural analysis to understand if these residues are likely to be interact with DNA, more evidences would be necessary to understand if these modifications regulate functions of ZFHX2 and if the R1913K mutation alters the modifications.

Table 3-12. Modification in WT or Mut ZFHX2 around the region over R1913(K). Numbers of peptide fragments which detected as a corresponding modification were shown. No notable modification changes were seen between WT and Mut in contiguous residues over R1913(K).

Post-translational modifications	**Position**	**Numbers of fragments showing the modifications in WT**	**Numbers of fragments showing the modifications in Mut**
Phosphorylation	1764	8	5
Phosphorylation	1766	0	1
Carbamidomethylation	1769	1	1
Methylation	1770	7	8
Carbamidomethylation	1771	32	21
Methylation	1772	10	1
Ethylation	1772	1	2
Carbamidomethylation	1774	32	21
Methylphosphonylation	1777	1	0
Carbamidomethylation	1791	2	1
Carbamidomethylation	1792	1	1
Carbamidomethylation	1812	2	2
Carbamidomethylation	1813	1	1
Carbamidomethylation	1814	1	0
Carbamidomethylation	1821	1	0
Carbamidomethylation	1822	1	1
Oxidation	1825	5	4
Dethiomethyl	1825	2	1
Carbamidomethylation	1833	1	1
Carbamidomethylation	1834	1	1
Phosphorylation	1838	6	2
Phosphorylation	1840	13	6
Phosphorylation	1842	1	0

Carbamidomethylation	1844	4	3
2,3-dihydro-2,2-dimethyl-7-benzofuranol N-methyl carbamate	1844	1	0
Carbamidomethylation	1848	3	2
Carbamidomethylation	1853	3	2
Carbamidomethylation	1861	1	1
Formylation		0	1
Deamidation	1868	1	1
Carbamidomethylation	1872	1	0
Hydroxylation	1876	1	0
Oxidation	1877	1	1
Dethiomethyl	1886	1	0
Carbamidomethylation	1886	1	1
Oxidation	1886	2	1
Methylation	1888	1	1
Carbamidomethylation	1888	2	1
Carbamidomethylation	1889	22	16
Carbamidomethylation	1896	1	1
Carbamidomethylation	1898	1	1
Oxidation	1904	1	0
Carbamidomethylation	1918	0	1
Ubiquitin	1920	1	0
Carbamidomethylation	1929	1	1
Carbamidomethylation	1930	1	0
Glycidamide adduct	1939	1	0
Carbamidomethylation	1939	1	1
Methyl ester	1940	1	0
Carbamidomethylation	1942	1	0
Deamidation	1944	1	0
Carbamidomethylation	1947	1	1
Carbamidomethylation	1949	3	1
Carbamidomethylation	1952	1	1
Methylation	1956	0	1
Methylation	1957	1	
Carbamidomethylation	1957	0	1
Methylation	1960	1	2
Methylation	1961	0	2
Carbamidomethylation	1962	1	4
Methylphosphonylation	1968	1	2
Methylphosphonylation	1970	1	1
Carbamidomethylation	1974	1	1
Carbamidomethylation; Methylation	1975	2	2
Methylation	1985	1	3
Carbamidomethylation	1986	1	3
Methyl ester; Carbamidomethylation	1986	0	1
Phosphorylation	1988	2	1
Phosphorylation	1989	4	4
Phosphorylation	2017	1	0

Methylation	2019	0	3
Carbamidomethylation	2019	0	1
Methylation	2020	2	0
Methyl ester; Carbamidomethylation	2021	2	1
Carbamidomethylation	2021	0	1
Methylation	2021	0	2
Carbamidomethylation	2023	4	3
Carbamidomethylation	2050	1	0
Carbamidomethylation	2052	1	0
Carbamidomethylation	2059	2	0
Carbamidomethylation	2061	0	1
Oxidation	2063	3	3

Table 3-13. Modifications changes which might be correlated with the mutation. Numbers of peptide fragments with modification and total numbers of detected fragments were shown for both WT and Mut ZFHX2.

Post-translational modifications	Position	Numbers of fragments showing the modifications in WT	Numbers of detected fragments in WT	Numbers of fragments showing the modifications in Mut	Numbers of detected fragments in Mut	Amino acid
Methylation	1772	10	30	1	21	D (Aspartic acid)
Methylation	1961	0	25	2	27	R (Arginine)
Methylation	2019	0	5	3	10	E (Glutamic acid)
Methylation	2020	2	9	0	10	S (Serine)
Methylation	2021	0	9	2	10	E (Glutamic acid)

In summary, the arginine methylation status in the motif around amino acid 1913 is still unknown since we could not detect many fragments covering the motif over R1913. Even so, we found arginine residue at position R1911 is unlikely to be methylated in Mut ZFHX2. Further investigation with higher protein levels will be needed to understand arginine status in WT and Mut ZFHX2.

3.4.3 Pain behaviour assay in *Zfhx2* knockout mice

An essential question for this project is whether *ZFHX2* is involved in pain behaviour and furthermore, does the mutation in this gene cause pain insensitivity. Prior to evaluating the pain behavioural responses caused by the mutation, we investigated if *Zfhx2* is involved in pain behaviour using *Zfhx2* global KO mice and a battery of behavioural tests: the rotarod test to assess motor coordination, acetone test to evaluate noxious cooling, thermal place preference to assess noxious cold sensitivity, Hargreaves's test and hot plate test to assess noxious thermal sensitivity, von Frey and cotton swab test to evaluate innocuous mechanical sensitivity, Randall-Selitto test to assess noxious mechanical pain thresholds and formalin tests to evaluate inflammatory pain.

Firstly, we performed the acute pain tests. We could not see a difference in phenotype in the rotarod test (Figure 3-40A), suggesting that *Zfhx2* is not essential for normal motor coordination in mice. There was no marked difference between WT and KO mice in the acetone test and thermal place preference test (Figure 3-40B, C), suggesting that *Zfhx2* is not involved in noxious cooling and cold sensitivity. We also did not observe a significant difference between WT and KO mice in von Frey and cotton swab tests (Figure 3-40E, F), indicating that *Zfhx2* is not associated with innocuous mechanical sensitivity in mice. However, *Zfhx2* seemed to be associated with noxious thermal (heat) and mechanical sensitivity. We found higher sensitivity in *Zfhx2* KO mice in the hot plate test in both female and male mice at 50℃ and males at 55℃ (Figure 3-41) although no significant differences were observed in the Hargreave's test (Figure 3-40D). The hot plate test represents a supraspinal thermal assay while the Hargreave's test is designed to assess spinal reflex responses to noxious thermal stimulation. The results indicated that *Zfhx2* appeared to be involved in noxious thermal sensitivity via supraspinal thermal pathways. We also found a phenotype in noxious mechanical sensitivity; in the Randall-Selitto test, *Zfhx2* KO mice demonstrated a significant deficit in mechanical sensitivity in both male and female mice, suggesting that *Zfhx2* is associated with detecting noxious mechanical pain.

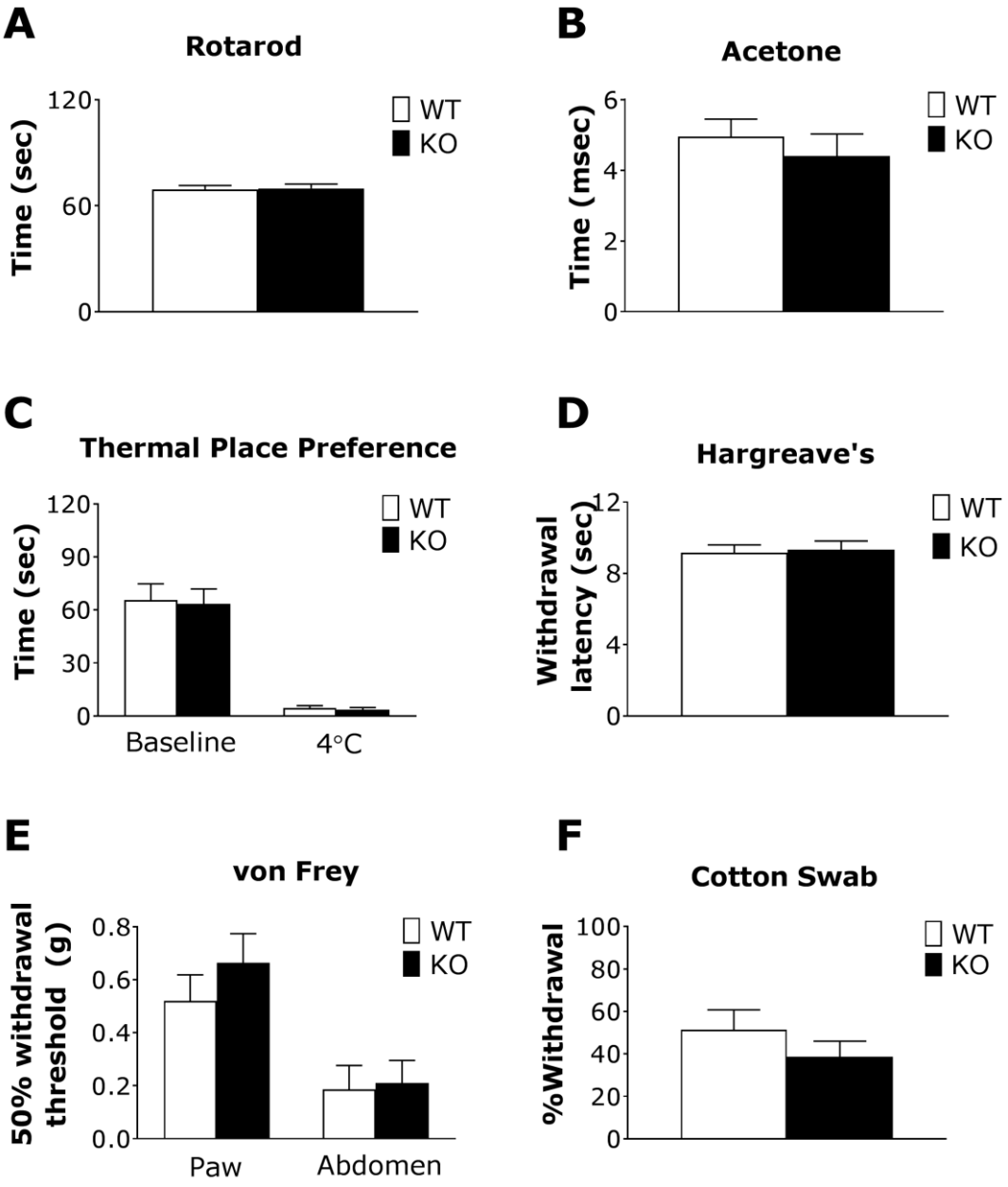

Figure 3-40. Behaviour test in *Zfhx2* global KO mice. (A) Rotarod, (B) Acetone, (C) Thermal Place Preference, (D) Hargreaves, (E) von Frey, (F) Cotton Swab test. WT; n=8, KO; n=10 for (A)-(E), WT; n=14, KO; n=14 for (F). All data analysed by t-test. The results are presented as mean ± SEM. These experiments were performed by Dr. Michael Minett and Ms. Sonia Santana-Valera.

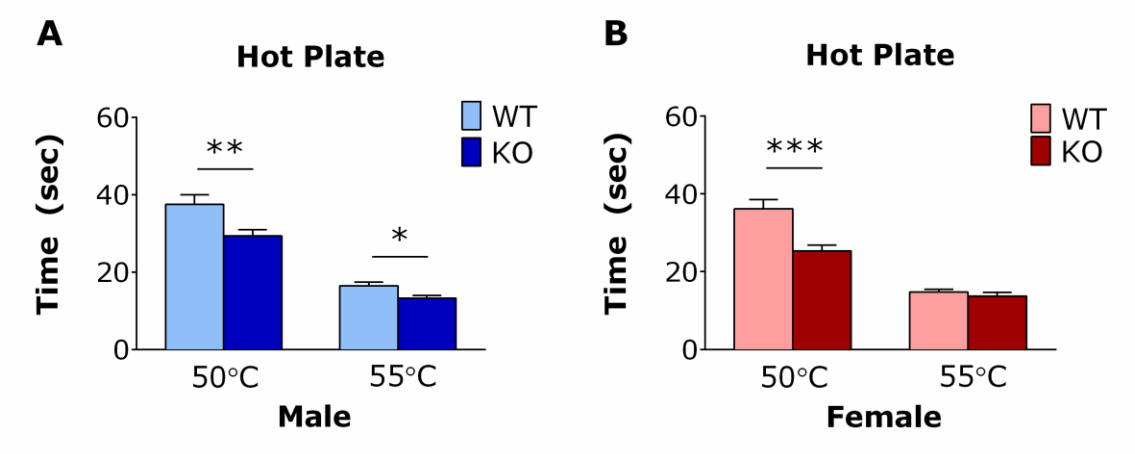

Figure 3-41. Hot plate test in *Zfhx2* global KO mice. Both male (A) and female (B) KO mice showed higher sensitivity than WT. n=20 (WT) and n=20 (KO) for (A) male, and n=12 (WT) and n=10 (KO) for (B) female. The data analysed by t-test. The results are presented as mean ± SEM. * $p < 0.05$, ** $p < 0.01$, *** $p < 0.001$.This test was performed by Dr. Michael Minett, Ms. Sonia Santana-Valera and myself.

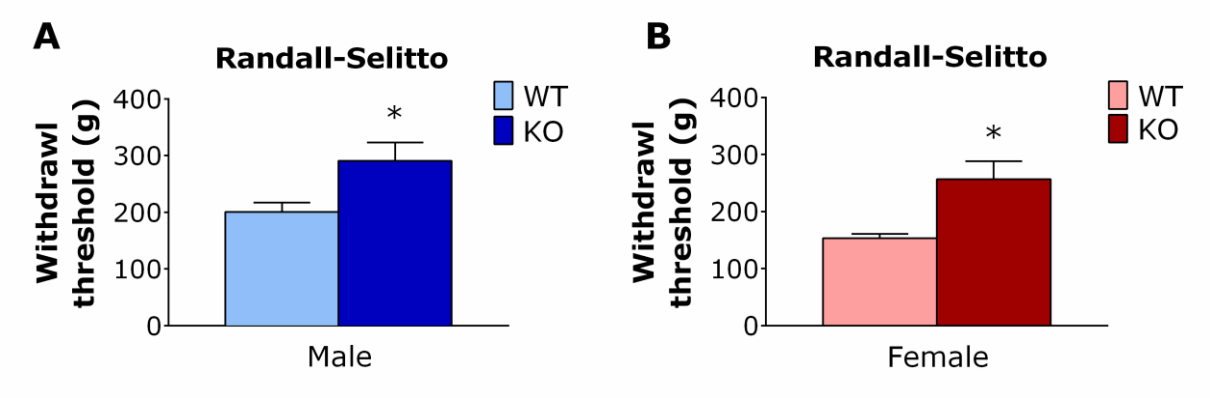

Figure 3-42. Randall-Selitto test in *Zfhx2* global KO mice. Both male (A) and female (B) KO mice showed a deficit in the behavioural response to the noxious mechanical stimulus compared to WT mice. n=8 (WT) and n=10 (KO) for (A) male, and n=5 (WT) and n=5 (KO) for (B) female. The data was analysed by t-test. The results are presented as mean ± SEM. * $p < 0.05$, ** $p < 0.01$, *** $p < 0.001$.This test was performed by Dr. Michael Minett, Ms. Sonia Santana-Valera and myself.

Next, we assessed inflammatory pain in *Zfhx2* KO mice. We performed formalin tests on both female and male mice by measuring the behavioural responses (licking, shaking or biting of paw) following intraplantar injection of 20 μl of 5% formalin. The test involves an early acute phase, which is believed to involve direct activation of C fibres via TRPA1 (McNamara et al., 2007) and occurs around 5-10 minutes after injection. The second, inflammatory phase

begins around 20 minutes after injection and is believed to result from the action of prostaglandins and other inflammatory mediators as well as spinally mediated changes (Coderre et al., 1990). The early acute phase (Phase I, 0-10min) and the latter inflammatory phase (Phase II, 10-60min) were separately analysed. Female mice tended to show decreased behavioural responses in the first phase, whilst no significant difference was observed in the second phase (Figure 3-43E). On the other hand, male mice did not appear to show any significant change between WT and KO mice although they seemed to show a slight deficit in responses in phase I (Figure 3-43C, D). These results indicate that *Zfhx2* might be involved in the acute phase of the formalin test and these responses could be different between female and male mice.

In summary, we found *Zfhx2* was involved in noxious mechanical and thermal sensitivities, and might be associated with inflammatory pain. The next question is if the mutation resulting in the amino acid change R1913K alters pain behaviour. In the next section, the results of behavioural tests using BAC transgenic mice carrying the point mutation will be described.

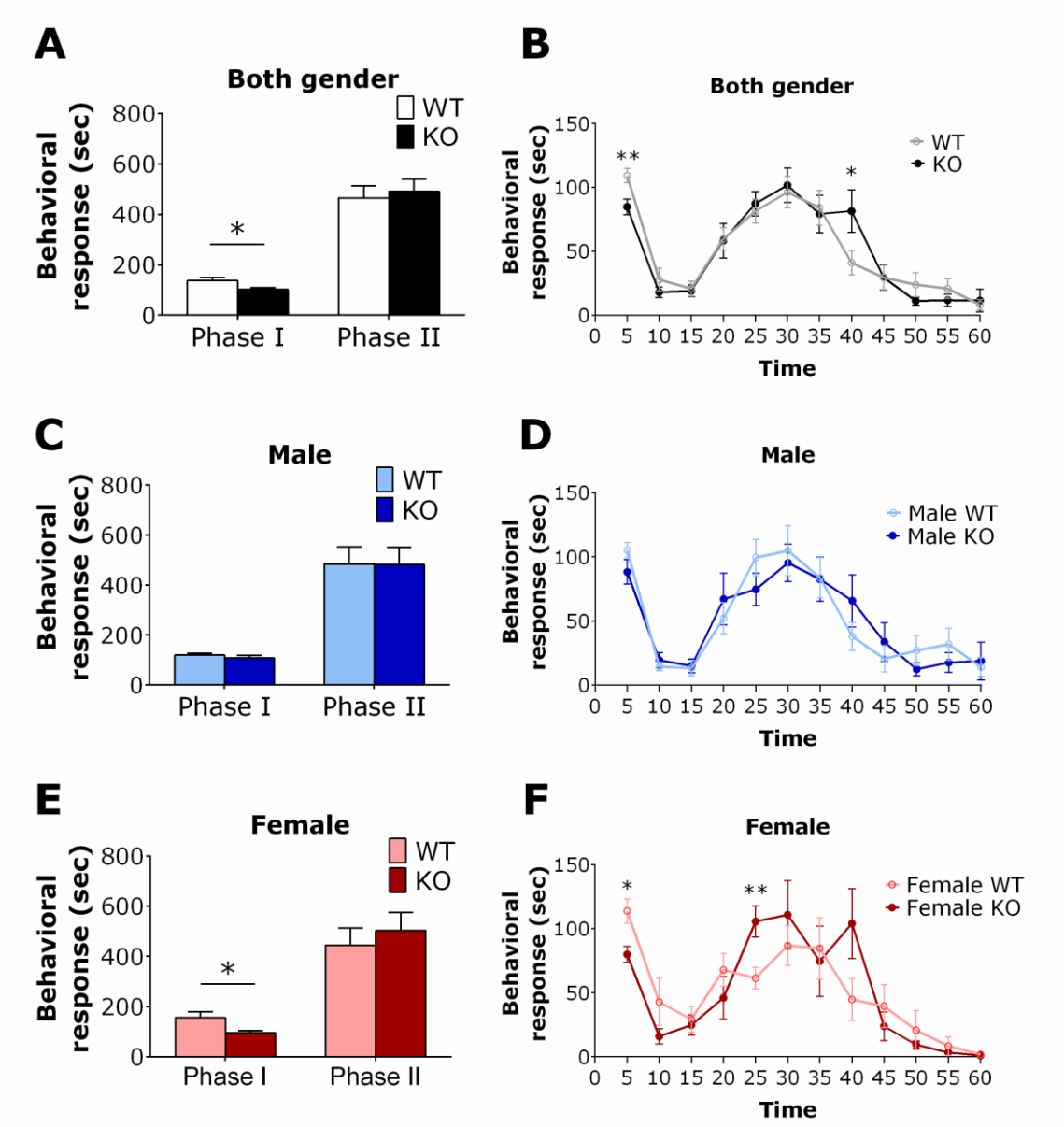

Figure 3-43. Formalin test in *Zfhx2* global KO mice. The time the mice spent licking, shaking and biting their paw is recorded and Phase I =5-10 min and Phase II = 10-60 min were separately analysed (A, C, E). The responses with 5 min block were shown in B,D,F. (A)(B) both male and female data was combined. A reduced pain response was shown in KO mice in phase I. (C)(D) The responses in male mice. No statistical significance was seen in both phases. (E)(F) The responses in female mice. A reduced response was shown in KO mice in phase I. n=8 (WT) and n=10 (KO) for (A) male, and n=9 (WT) and n=7 (KO) for (B) female. The data analysed by t-test. The results are presented as mean ± SEM. * $p < 0.05$, ** $p < 0.01$, *** $p < 0.001$.This test was performed by Ms. Sonia Santana-Valera and myself.

3.4.4 Pain behaviour assay on BAC transgenic mice bearing the orthologous mutation

The next question was whether the point mutation R1913K leads to a pain insensitive phenotype. To address this question, we aimed to perform pain behaviour tests on BAC transgenic mice bearing the orthologous mutation (R1907K). We obtained three founders of BAC transgenic mice bearing this orthologous mutation, named Founders A, B and C (Cyagen Biosciences). We first performed acute pain behaviour tests and an inflammatory pain test using a CFA model on the BAC transgenic mice bred from all these three founders.

Despite our hypothesis of mutant mice showing pain insensitive phenotypes, we could not find any acute pain phenotypes on these particular BAC transgenic mice. No marked differences were observed in light touch (von Frey and cotton swab test), mechanical stimuli (Randall-Selitto test), thermal stimuli (hot plate and Hargreave's test), noxious cold stimuli (cold plate test) and noxious cooling (acetone test) (Figure 3-44A-G). However, we found a statistically significant difference in the place preference test at 15℃; WT mice tended to avoid staying at 15℃which was lower than the baseline (20℃), whilst mutant mice spent a longer time at 15℃ than WT mice (Figure 3-44 I). Also we found higher frequencies of centre/corner entries and total numbers of crosses in the mutant mice during the open field test. These results indicate high exploratory behaviour and low anxiety levels of the mutant mice (Figure 3-44H). Interestingly, it was previously shown that global *Zfhx2* KO mice have a hyperactive phenotype (Komine et al., 2012).

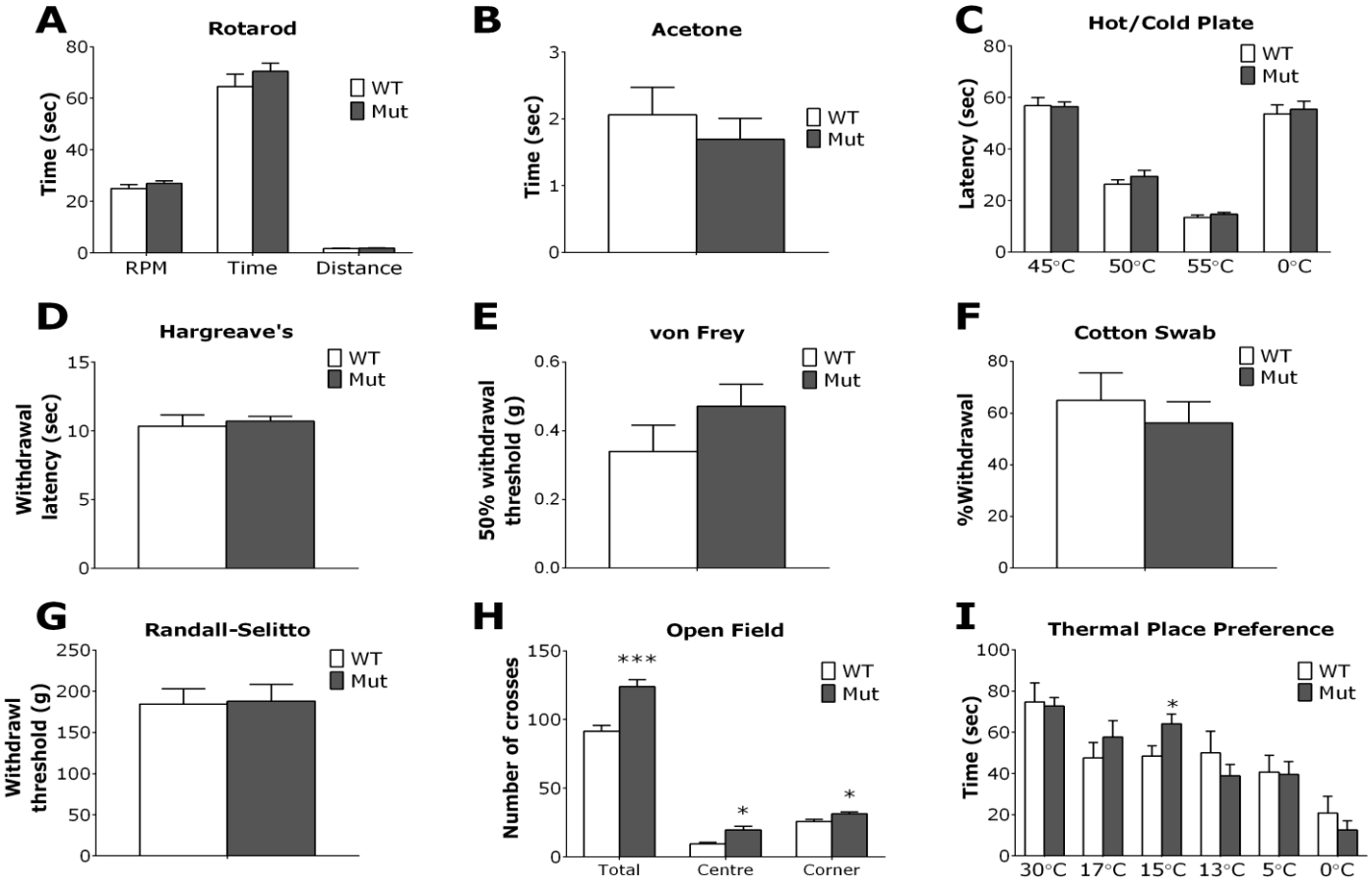

Figure 3-44. Behaviour test in BAC transgenic mice (derived from founders A, B and C) bearing the orthologous mutation. Founder A; n=2 for WT female, n=6 for Mut female, n=0 for male mice. FounderB; n=2 for WT female, n=6 for Mut female, n=0 for male mice. FounderC; n=4 for WT female, n=4 for Mut female, n=0 for male mice. (A) Rotarod, (B) Acetone, (C) Hot and cold plate, (D) Hargreave's, (E) von Frey, (F) Cotton Swab, (G) Randall-Selitto, (H) Open field, (I) Thermal Place Preference test. WT; n=8, Mut; n=16. All data analysed by t-test. *P<0.05, **P<0.01 and ***P<0.001. The results are presented as mean ± SEM. These experiments were performed by Ms. Sonia Santana-Valera and myself.

Although we could not observe a clear acute pain phenotype, we considered if the mutant mice would show decreased responses in inflammatory pain since the global *Zfhx2* KO mice appeared to indicate *Zfhx2* might be involved in inflammatory pain (Figure 3-43). We performed von Frey and Hargreave's tests to assess mechanical allodynia and thermal hyperalgesia, respectively, on the BAC transgenic mice before and 1, 3, and 7 days after CFA (Complete Freund's adjuvant) injection. There were no dramatic effects on the baseline (before the injection) and both 1 and 3 days post-injection. However, the mutant mice showed significantly reversed responses in the von Frey test on Day 7 compared to WT mice. There were no marked differences between the mutant and WT mice in the Hargreave's test.

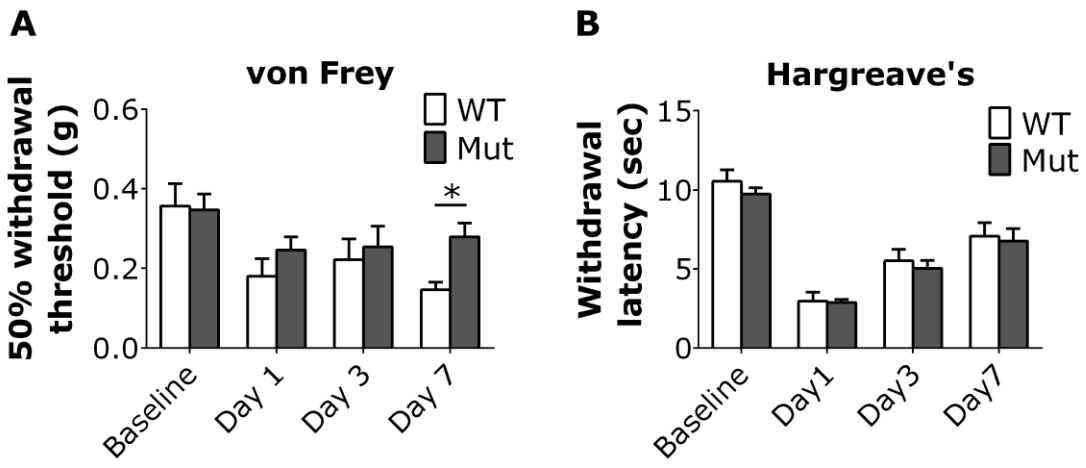

Figure 3-45. Inflammatory pain test using CFA model in BAC transgenic mice (including all founders) bearing the orthologous mutation. CFA was injected intraplantarly in the right hind paw and (A) von Frey, (B) Hargreave's test were performed 1, 3 and 7 days post-injection. WT; n=8, Mut; n=16 (All female mice. Founder A; n=2 for WT female, n=6 for Mut female. FounderB; n=2 for WT female, n=6 for Mut female. FounderC; n=4 for WT female, n=4 for Mut female.). All data analysed by t-test. *P<0.05, **P<0.01 and ***P<0.001. The results are presented as mean ± SEM. These experiments were mainly performed by Ms. Sonia Santana-Valera with a small contribution from myself.

The BAC transgenic mouse data described above did not prove pathogenicity of the mutation. However, we considered if the presence of 2 WT alleles in this model could be masking the effects of the mutation. We decided to investigate the BAC copy number in each of the founder mice, showing 4 for Founder A, 1 for Founder B, and 5 for Founder C (measured by Dr. Abdella Habib, WIBR, UCL). We also measured mRNA levels of *Zfhx2* in DRG in mice derived from these founders (Figure 3-46). All mice derived from each founder demonstrated higher expression of Zfhx2 than littermate controls (WT); however, the fold

change was lower than 2 times (Figure 3-46). Considering these BAC transgenic mice carry 2 wild type alleles, the expression levels of the mutant Zfhx2 in these BAC transgenic mice could be lower than if we had a heterozygous knockin animal. Since the human patients carry a heterozygous mutation, these low expression levels of mutant Zfhx2 could explain the elusive pain insensitive phenotypes.

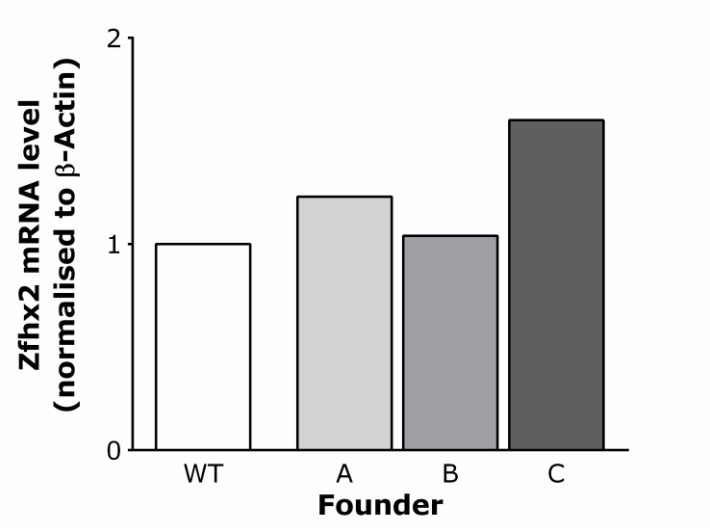

Figure 3-46. Real-time qRT-PCR analysis of *Zfhx2* mRNA expression in DRG relative to β-Actin. Relative expression levels of mRNA were calculated using the comparative ΔΔCt (Ct) method and normalised by a WT mouse. N=1 for each founder. This data was collected by Dr. Abdella Habib at WIBR, UCL.

We therefore aimed to perform pain behaviour tests using the mutant mice bred from Founder C to obtain high BAC copy numbers that can result in high expression of the mutant *Zfhx2*. Using these mice we could see thermal pain phenotypes (Figure 3-47); the mutant mice with high copy numbers had markedly reduced sensitivity to noxious thermal stimuli in the hot plate and Hargreave's tests (Figure 3-47A, B), although no significant difference was observed at high temperature, 55℃, in the hot plate test (Figure 3-47A). Mechanical pain thresholds in von Frey and Randall-Selitto test were not altered in the mutant mice (Figure 3-47C, D), although global *Zfhx2* KO mice demonstrated a deficit in the behavioural response to the noxious mechanical stimulus compared to WT mice in the Randall-Selitto tests (Figure 3-42). The present data suggests that the mutation leads to a thermal pain insensitive phenotype. Further investigations are needed to confirm the pain phenotype in the mutant mice and to understand the difference between human and mice pain insensitive phenotypes.

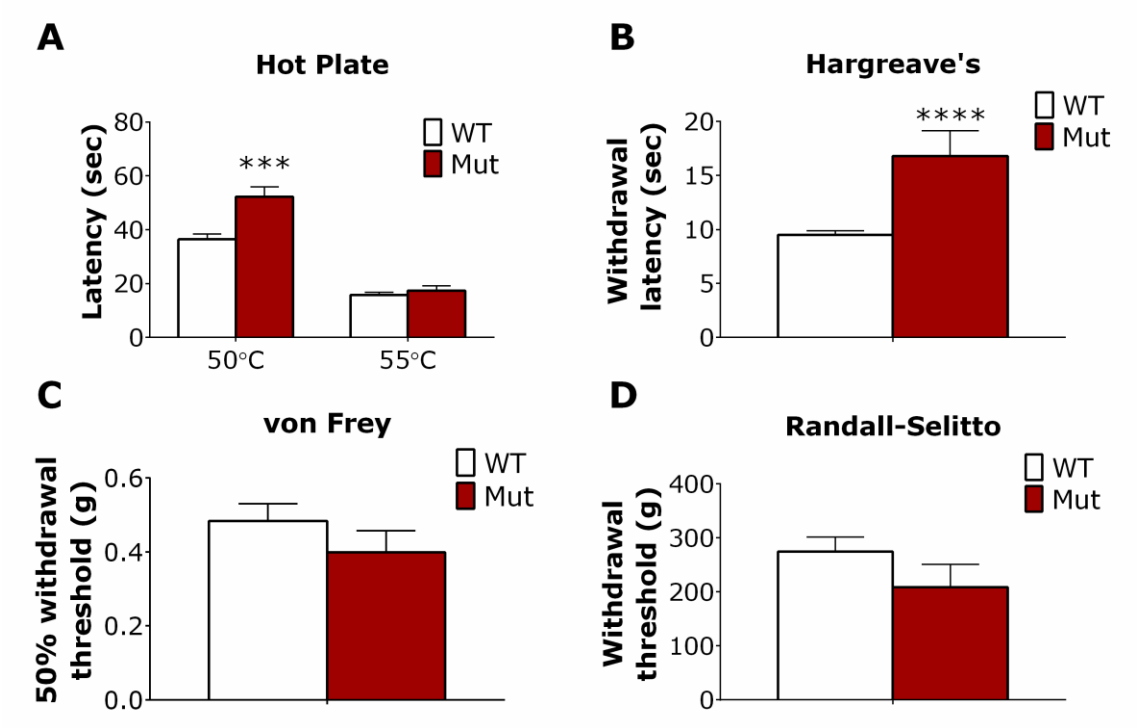

Figure 3-47. Acute pain behaviour test on BAC transgenic mice bearing the orthologous mutation with high copy number. WT; n=16, Mut; n=5. All data analysed by t-test. *P<0.05, **P<0.01 and ***P<0.001. The results are presented as mean ± SEM. These experiments were performed by Ms. Sonia Santana-Valera and Miss Shengnan Li.

3.4.5 Microarray

In order to identify genes regulated by ZFHX2 and potentially causing pain insensitivity via their altered expression, we aimed to perform microarray analyses using SH-SY5Y stable cell lines generated in the above section (3.4.2II). We performed microarrays using all clones we obtained; 5 clones from WT (SBC3, SBL3, SBL7, SBL9 and SBL12), 6 clones from Mut (SDC2, SDC13, SDL1, SDL2, SDL7 and SDL9) and 8 clones from control (i.e. IRES-eGFP) (SFC4, SFC5, SFC6, SFC7, SFL3, SFL5, SFL9, and SFL14). Many genes showed significant expression changes for the Mut clones compared to WT or control clones (505 and 208 genes which were dysregulated more than 1.5 fold, respectively, and ANOVA p-value < 0.05; Table 3-14). Also, significant numbers of genes were dysregulated in WT clones compared to control clones (179 genes which were dysregulated more than 1.5 fold and ANOVA p-value < 0.05; Table 3-14). Figure 3-48 demonstrates a heat map of expression of the dysregulated genes (>3 fold) for Mut clones against control clones. We also analysed the data by including the differentially expressed genes with ANOVA p-value < 0.1 between each group of clones (instead of a <0.05 cut-off) (Table 3-14). Volcano plots show numbers of genes dysregulated in

each comparison (ANOVA p-value < 0.1, fold change >1.5) (Figure 3-49A-C). The functional classification by Gene Ontology (GO) terms regarding the Biological Process suggested that the functions of the dysregulated genes were mostly related to metabolism, development, signal transduction, transport and cell communications (Figure 3-49D-F). Several GO terms were not included such as transcriptional/ translation regulator activities and protein/ DNA/ RNA binding.

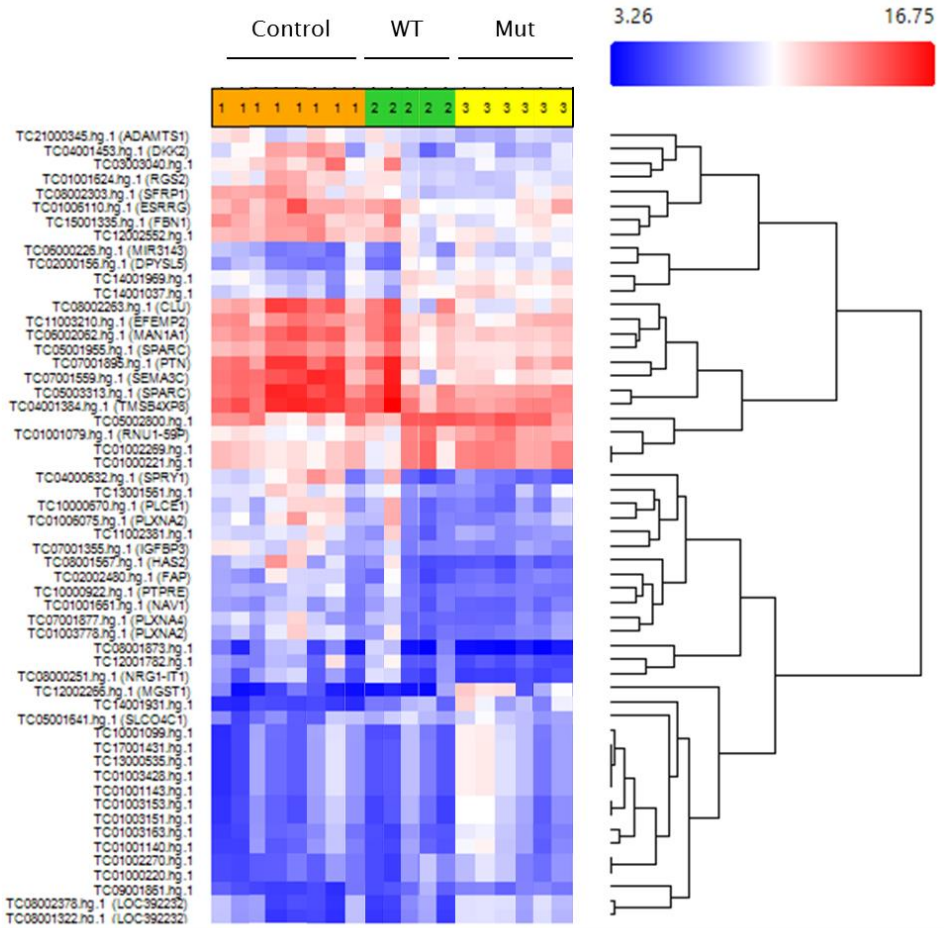

Figure 3-48. Heat map of expression of the dysregulated genes in Mut clones against control clones with more than 3 times fold change (ANOVA p-value <0.05). Control; control clones (SF), WT; wild type clones (SB), Mut; mutant clones (SD). Probe signal intensity is indicated in colours; 3.26 in blue to 16.75 in red.

Table 3-14. Numbers of dysregulated genes in SH-SY5Y stable cell lines

	Mut vs Control	Mut vs WT	WT vs Control
ANOVA p-value < 0.05, Fold change >1.5 or <-1.5	505	208	179
ANOVA p-value < 0.1, Fold change >1.5 or <-1.5	694	359	305

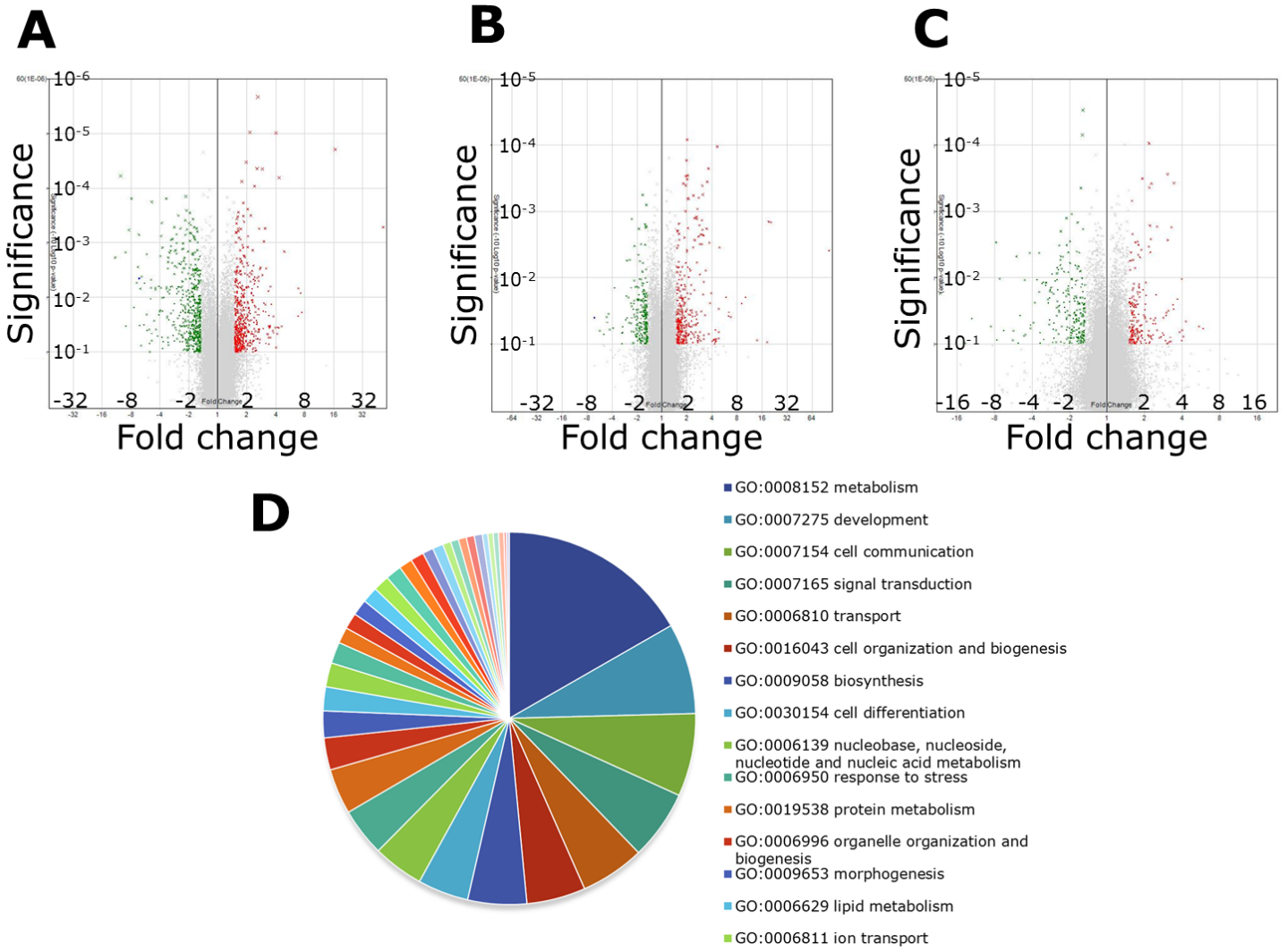
A
B
C
Significance
Fold change
-32 -8 -2 2 8 32
-16 -8 -4 -2 2 4 8 16
D
GO:0008152 metabolism
GO:0007275 development
GO:0007154 cell communication
GO:0007165 signal transduction
GO:0006810 transport
GO:0016043 cell organization and biogenesis
GO:0009058 biosynthesis
GO:0030154 cell differentiation
GO:0006139 nucleobase, nucleoside, nucleotide and nucleic acid metabolism
GO:0006950 response to stress
GO:0019538 protein metabolism
GO:0006996 organelle organization and biogenesis
GO:0009653 morphogenesis
GO:0006629 lipid metabolism
GO:0006811 ion transport

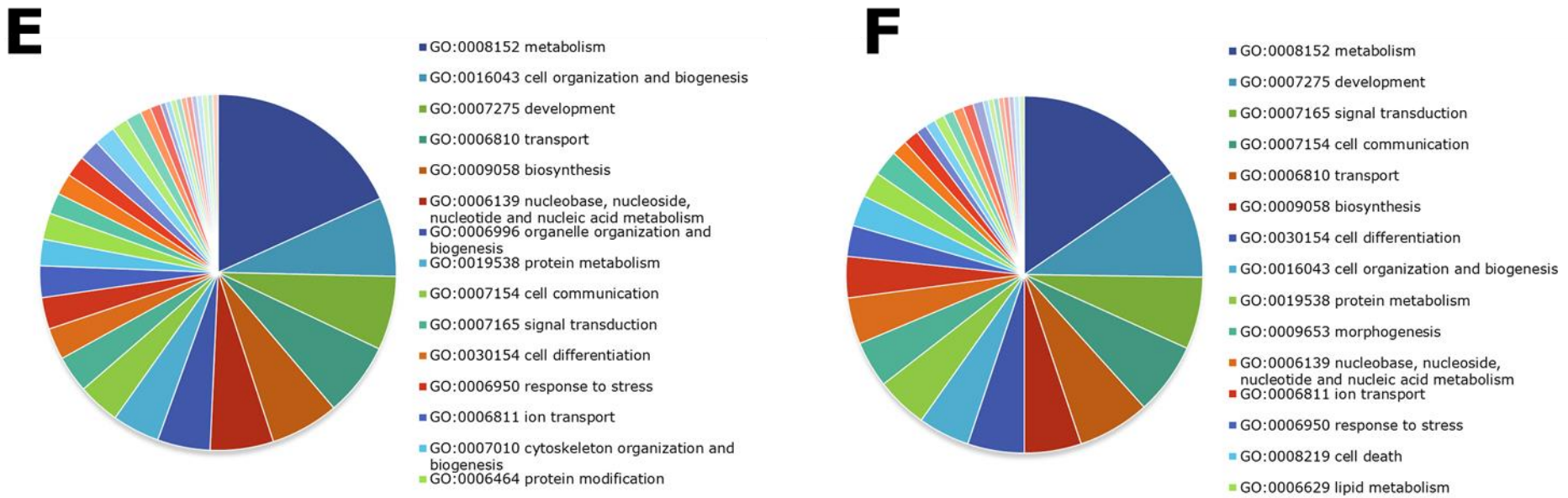

Figure 3-49. Volcano plots and pie charts of differentially expressed genes annotated with Gene Ontology (GO) terms regarding the Biological Process (analysis of variance P-value <0.1, fold change >1.5 or <-1.5). (A) volcano plots of significantly differentially expressed genes between Mut and control clones. Green and red dots indicate up-regulated and down-regulated in Mut vs control clone, respectively. (B) Volcano plots of significantly differentially expressed genes between Mut and WT clones. Green and red dots indicate up-regulated and down-regulated in Mut vs WT clone, respectively. (C) Volcano plots of significantly differentially expressed genes between WT and control clones. Green and red dots indicate up-regulated and down-regulated in WT vs control clone, respectively. (D) Pie chart of significantly differentially expressed genes between Mut and control clones annotated with GO Biological Process terms. (E) Pie chart of significantly differentially expressed genes between Mut and WT clones annotated with GO Biological Process terms. (F) Pie chart of significantly differentially expressed genes between WT and control clones annotated with GO Biological Process terms. In all pie chart, the top15 enriched GO biological process terms were shown in the legend. GO Biological Process terms were classified with GO_slim2 by single count by CateGOrizer (Hu et al., 2008)

Genes regulated by ZFHX2 and dysregulated by the mutant form are likely to be involved in the pain insensitive phenotype. Table 3-15, Table 3-16 and Table 3-17 show the 10 most significantly differentially expressed genes (either up- or down-regulated) in each comparison (ANOVA p-value < 0.05). The expression levels of all genes which were differentially expressed in each comparison more than 1.5 fold change with ANOVA p-value < 0.1 were referred using the mouse sensory neurons RNA-seq study (Usoskin et al., 2015). Since Zfhx2 is expressed in NP, PEP and TH clusters (Usoskin et al., 2015), the genes which are expressed in these clusters were checked if they have been linked to pain studies. In addition to these, the dysregulated genes showing more than 5 fold change in each comparison were also searched in pain studies.

Several genes are worth to be noted in relation to pain. For example, clusterin (*CLU*), which is highly down-regulated in Mut against control clones (fold change 8.43), is known to be involved in tumor progression as well as neurodegenerative disorders (Zhang et al., 2005b, Shuai et al., 2015, Přikrylová Vranová et al., 2016). A clinical trial of custirsen, a CLU inhibitor, shows dramatic pain relief effects along with increased survival rates (Saad et al., 2011). This suggests the altered expression of this gene by R1913K mutant ZFHX2 might contribute to pain insensitivity. Protein kinase C alpha (*PRKCA*) has also been documented in the pain literature. Knock-out of this gene in mice showed increased mechanical allodynia in a neuropathic pain model (Zhao et al., 2011). The expression level of this gene is significantly down-regulated in both Mut and WT clones compared to control clones (fold change 5.5 and 5.73, respectively), indicating that ZFHX2 could regulate the expression of *PRKCA*, which might be involved in pain sensitivity. Dihydropyrimidinase-like 5 (*DPYSL5*, also known as *CRMP5*) might also be controlled by ZFHX2. CRMP2 belongs to the same family as CRMP5 and binds to $Ca_V2.2$ and inhibiting this binding reduced the channel function resulting in supressed inflammatory and neuropathic hypersensitivity (Brittain et al., 2011). The expression level of *DPYSL5* is markedly up-regulated in Mut compared to control clones (fold change 4.91). Considering *CRMP2* plays a role in a pain phenotype by mediating VGCC function, *DPYSL5* might also have a key role in disturbing ion channel functions and hence regulate nociceptive pathways.

Genes that are involved in neuronal development and axonal growth are also interesting to explore; Neuron navigator 2 (*NAV2*) has been documented to play a role in neuronal development (McNeill et al., 2010). This gene is down-regulated in both Mut and WT compared to control clones (fold change 2.17 and 2.9, respectively). Mutant mice that carry a hypomorphic allele of this gene showed less sensitivity to thermal noxious stimuli in the hot

plate test (Peeters et al., 2004). Semaphorins and their receptors are also interesting to note. Semaphorins including SEMA3A, SEMA3C and SEMA3D are secreted or transmembrane proteins that are known to regulate cell motility and attachment in axon guidance, vascular growth, immune cell regulation and tumour progression (Kruger et al., 2005). The main receptors of semaphorins are plexins (Kruger et al., 2005) and most of the effects of semaphorins are mediated by plexins (Worzfeld and Offermanns, 2014). Neuropilins are also required as co-receptors to stabilize the semaphorin–plexin interaction in secreted class 3 semaphorins, including Sema3A, Sema3C and Sema3D (Worzfeld and Offermanns, 2014). We found 3 subtypes of semaphorin, SEMA3A, SEMA3C and SEMA3D, were down-regulated in Mut compared to control clones in the microarray analyses. Similarly, some subtypes of plexins, PLXNA2 and PLXNA4, and neuropilin 1 (*NRP1*) were also down-regulated in Mut compared to control clones. One of the well-studied semaphorins, Sema3A, has been documented to restrict sensory axon projections during development (Messersmith et al., 1995). Sema3A is also thought to serve a key role in the establishment of an appropriate pattern of innervation within the dorsal horn of the spinal cord during its development (Messersmith et al., 1995, Pasterkamp et al., 2000). This key role in development appears to be associated with neuropathic pain. Coexpression of Sema3A and NGF at moderate to low concentrations (but not high concentrations) within the adult spinal cord reduced sprouting of calcitonin gene-related peptide and substance P-containing axons (Tang et al., 2004). Sema3A coexpression with NGF reduced mechanical allodynia in the von Frey test compared to the sole expression of NGF (Tang et al., 2004). Interestingly, another study suggests Sema3A and neuropilin1 (Npr1) interaction in neuropathic pain; intrathecal administration of Sema3A, in the spinal cord of chronic constriction injury (CCI) model rat attenuated mechanical allodynia and heat hyperalgesia (Hayashi et al., 2011). This reduction was accompanied by increased protein levels of Npr1, but not PlexinA, in the dorsal spinal cord (Hayashi et al., 2011). The microarray data using SH-SY5Y stable cell lines showed down-regulation of *SEMA3A*, *SEMA3D* and *PLXNA2* only in Mut clones compared to control clones. On the contrary, expression levels of *SEMA3C* and *PLXNA4* are down-regulated in both Mut and WT clones compared to control clones. Considering these, the alteration of semaphorin signalling along with plexins and neuropilins controlled by ZFHX2 may be involved in pain pathways, and moreover, subtypes of semaphorins and plexins could be important clues to understand semaphorin signalling altered by Mut ZFHX2.

The other genes listed above which are involved in the development and cell differentiation could also be beneficial to explore further. In addition to these genes, Dickkopf WNT signalling pathway inhibitor 2 (*DKK2*) might be involved in pain. *DKK2* is a Wnt inhibitor

that binds to Wnt receptors/co-receptors (Arenas, 2014). Wnts are a well-studied highly conserved family of lipid-modified glycoproteins serving a key role in regulating multiple cellular functions and cell systems, such as the neuron development processes (Arenas, 2014). Wnt signalling in pain has been described in several studies. For example, intrathecal administration of WNT inhibitors and WNT–Frizzled–β-catenin pathway inhibitors attenuated allodynia and hyperalgesia in both neuropathic pain model using rat CCI and cancer pain model (Zhang et al., 2013c, Harrison, 2013). Intraplantar injection of recombinant Wnt3a increased mechanical and thermal sensitivity in wild-type mice (Simonetti et al., 2014, Ferrarelli, 2014). Of note the microarray analysis in SH-SY5Y stable cell lines displayed that both Mut and WT clones decreased expression of *DKK2* comparing to control clones, indicating that an overexpression of ZFHX2 could regulate DKK2 expression. It should be also mentioned that the expression of this gene in mouse sensory neurons appears to be low (Usoskin et al., 2015), indicating that ZFHX2 might be involved in this gene expression in the CNS rather than sensory neurons. Although direct evidences showing that DKK2 is associated with pain do not seem to be reported, this gene might mediate neuronal development processes and pain pathways.

Furthermore, the differentially expressed genes with an analysis of ANOVA p-value < 0.1 indicate another interesting therapeutic target for pain. Surprisingly, we found expression of *SCN9A* is markedly decreased in Mut compared to control clones (fold change 5.12). Loss-of-function of $Na_v1.7$ channel encoded by *SCN9A* leads to pain insensitivity (Cox et al., 2006). Several studies in mice also suggested that deleting *Scn9a* resulted in a pain insensitive phenotype (Nassar et al., 2004, Minett et al., 2012, Gingras et al., 2014). The results indicate that the mutant R1913K ZFHX2 could suppress the expression of $Na_v1.7$ which might result in the pain insensitive phenotype seen in the patients. The fold changes of these genes between each comparison are shown in Table 3-18.

Table 3-15. Top20 dysregulated genes in Mut clones compared to control clones

Fold Change (linear) (Mut vs. Control)	ANOVA p-value (Mut vs. Control)	Gene Symbol	Description
-11.7	0.001864	SPRY1	sprouty homolog 1, antagonist of FGF signaling (Drosophila)
-10.31	0.00006	SEMA3C	sema domain, immunoglobulin domain (Ig), short basic domain, secreted, (semaphorin) 3C
-9.13	0.001497	HAS2	hyaluronan synthase 2
-9.11	0.033559	SPARCL1	SPARC-like 1 (hevin)
-8.43	0.000584	CLU	Clusterin
-7.95	0.000155	RELN	Reelin
-7.46	0.015178	SEL1L3	sel-1 suppressor of lin-12-like 3 (C. elegans)

-6.99	0.005431	PLCE1	phospholipase C, epsilon 1
-6.8	0.002784	SFRP1	secreted frizzled-related protein 1
-6.61	0.000717	IGFBP3	insulin-like growth factor binding protein 3
3.8	0.04493	MIR127	microRNA 127
3.96	0.03542	MIR433	microRNA 433
4.03	0.00001	RNU1-59P	RNA, U1 small nuclear 59, pseudogene
4.14	0.046124	MIR432	microRNA 432
4.61	0.03416	MIR431	microRNA 431
4.91	0.001451	DPYSL5	dihydropyrimidinase-like 5
6.83	0.021887	DLK1	delta-like 1 homolog (Drosophila)
6.84	0.006867	LOC392232	transient receptor potential cation channel, subfamily A, member 1 pseudogene
7.25	0.008308	LOC392232	transient receptor potential cation channel, subfamily A, member 1 pseudogene
52.59	0.000521	MGST1	microsomal glutathione S-transferase 1

Table 3-16. Top20 dysregulated genes in Mut clones compared to WT clones

Fold Change (linear) (Mut vs. WT)	ANOVA p-value (Mut vs. WT)	Gene Symbol	Description
-4.69	0.039338	NRG1-IT1	NRG1 intronic transcript 1 (non-protein coding); novel transcript
-4.55	0.047926	EGR1	early growth response 1
-3.73	0.014253	SLC16A4	solute carrier family 16, member 4; solute carrier family 16, member 4 (monocarboxylic acid transporter 5)
-2.74	0.043168	LOC728755	uncharacterized LOC728755
-2.69	0.01881	TLCD1	TLC domain containing 1
-2.65	0.005533	SNORD116-29	small nucleolar RNA, C/D box 116-29
-2.54	0.020157	AP1G2	adaptor-related protein complex 1, gamma 2 subunit
-2.49	0.047855	PLCXD3	phosphatidylinositol-specific phospholipase C, X domain containing 3
-2.44	0.005403	SNORD116-27	small nucleolar RNA, C/D box 116-27
-2.38	0.049101	TGFB1	transforming growth factor, beta 1
3.09	0.000556	MTMR8; ASB12	myotubularin related protein 8; ankyrin repeat and SOCS box containing 12
3.12	0.018086	RASL11B	RAS-like, family 11, member B
3.19	0.011545	ARHGEF9	Cdc42 guanine nucleotide exchange factor (GEF) 9
3.31	0.036829	MGST1	microsomal glutathione S-transferase 1
3.45	0.001821	SMC1A	structural maintenance of chromosomes 1A
3.5	0.000354	HUWE1	HECT, UBA and WWE domain containing 1, E3 ubiquitin protein ligase
3.73	0.00295	ZC4H2	zinc finger, C4H2 domain containing
3.93	0.017245	PDGFRA	platelet-derived growth factor receptor, alpha polypeptide
4.61	0.000105	SPIN4	spindlin family, member 4
19.23	0.001425	LOC392232	transient receptor potential cation channel, subfamily A, member 1 pseudogene

Table 3-17. Top20 dysregulated genes in WT clones compared to control clones

Fold Change (linear) (WT vs. Control)	ANOVA p-value (WT vs. Control)	Gene Symbol	Description
-21.84	0.017546	LOC650226	ankyrin repeat domain 26 pseudogene
-13.82	0.098211	SPRY1	sprouty homolog 1, antagonist of FGF signaling (Drosophila)
-12.23	0.041342	PTPRK	protein tyrosine phosphatase, receptor type, K
-8.57	0.054573	SEMA3C	sema domain, immunoglobulin domain (Ig), short basic domain, secreted, (semaphorin) 3C
-7.78	0.002932	SFRP1	secreted frizzled-related protein 1
-7.69	0.086846	HAS2	hyaluronan synthase 2
-7.29	0.010473	IGFBP3	insulin-like growth factor binding protein 3
-6.75	0.063094	DKK2	dickkopf WNT signaling pathway inhibitor 2; dickkopf homolog 2 (Xenopus laevis)
-5.73	0.08808	PRKCA	protein kinase C, alpha
-5.65	0.064101	PLXNA4	plexin A4
2.97	0.036949	FEV	FEV (ETS oncogene family)
2.99	0.033987	MIR2682	microRNA 2682
3.01	0.098775	SLC18A1	solute carrier family 18 (vesicular monoamine transporter), member 1; solute carrier family 18 (vesicular monoamine), member 1
3.06	0.002714	FAM155A-IT1	FAM155A intronic transcript 1 (non-protein coding)
3.08	0.031687	SLCO4C1	solute carrier organic anion transporter family, member 4C1
3.14	0.093461	HSPA1B; HSPA1A	heat shock 70kDa protein 1B; heat shock 70kDa protein 1A
3.22	0.080882	MIR137HG; MIR137; MIR2682	MIR137 host gene (non-protein coding); microRNA 137; microRNA 2682
3.38	0.025874	ABCC9	ATP-binding cassette, sub-family C (CFTR/MRP), member 9
3.96	0.010474	ZNF804A	zinc finger protein 804A
4.09	0.077406	GPR64	G protein-coupled receptor 64

Table 3-18. Fold change and ANOVA p-value of dfferentially expressed genes between each group of clones that might be involved in pain insensitive phenotype

Gene Symbol	Description	Fold Change (linear) / ANOVA p-value (Mut vs. Control)	Fold Change (linear) / ANOVA p-value (WT vs. Control)
CLU	Clusterin	-8.13 / 0.000584	
PRKCA	protein kinase C alpha	-5.5 / 0.020846	-5.73 / 0.08808
DPYSL5	dihydropyrimidinase-like 5	4.91 / 0.001451	
NAV2	neuron navigator 2	-2.17 / 0.018829	-2.9 / 0.020318
SEMA3A	semaphorin 3A	-2.24 / 0.088998	
SEMA3C	semaphorin 3C	-10.31 / 0.00006	-8.57 / 0.054573
SEMA3D	semaphorin 3D	-4.45 / 0.006687	

PLXNA2	plexin A2	-6.17 / 0.006293	
PLXNA4	plexin A4	-4.98 / 0.004769	-5.65 / 0.064101
NRP1	neuropilin 1	-2.36 / 0.04868	
DKK2	dickkopf WNT signaling pathway inhibitor 2	-5.19 / 0.038431	-6.75 / 0.063094
SCN9A	voltage-gated sodium channel alpha subunit 9	-5.12 / 0.070101	

The genes listed in Table 3-18 could be regulated by ZFHX2 and potentially causing pain insensitivity via their altered expression. Figure 3-50 shows the signal intensity of the probes of these genes in microarray analysis, giving an initial idea of the expression levels in each clone. The data suggested that each clone demonstrated different levels of expression. To validate the microarray data, we performed RT-qPCR to measure gene expression levels. We selected three genes to verify; *CLU*, *NAV2* and *SCN9A* (Figure 3-51). All these three genes have been linked with clinical data or animal studies showing they are associated with pain as discussed above. In addition to this, *CLU* is one of the most significantly dysregulated genes. $Na_v1.7$ encoded by *SCN9A* has been well known for pain insensitivity (Cox et al., 2006), which can raise an interesting idea that the down-regulation of this gene by Mut ZFHX2 might contribute to pain free state. Although *NAV2* did not display large fold change in the microarray analysis, this gene is chosen because it is associated with thermal sensitivity (Peeters et al., 2004), which are consistent with pain behaviour test (Figure 3-47) and all of both WT and Mut clones appears to be downregulated (Figure 3-50). The results support the microarray data; mRNA levels of *CLU* are significantly decreased in Mut comparing to control clones (fold change 3.95, p=0.03), but neither against WT clones nor WT clones against control clones, which is consistent with the microarray data. Mut clones tend to show decreased mRNA levels of *NAV2* compared to control clones; however, no statistical significance was observed although microarray analysis showed ANOVA p-value <0.05. On the contrary, mRNA levels of this gene were significantly down-regulated in WT against control clones (fold change 2.28, p=0.0067), which supports the microarray data. The fold change of *NAV2* expression levels in Mut clones versus control clones was relatively small in the microarray data, which might give a slightly different result. The supressed mRNA levels of *SCN9A* were also observed in Mut compared to control clones albeit it was not statistically significant (fold change 1.95, p=0.08), which is also consistent with the microarray data, although fold change was smaller than the microarray analysis. In summary, the RT-qPCR results basically appear to support the microarray analysis, and they tend to be consistent with the microarray data, especially for the highly dysregulated genes.

CLU

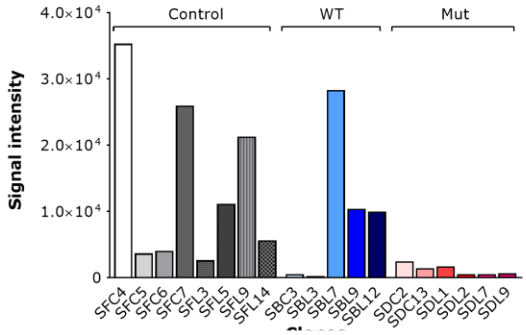

PRKCA

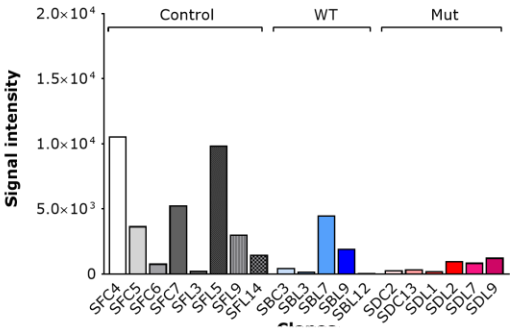

DPYSL5

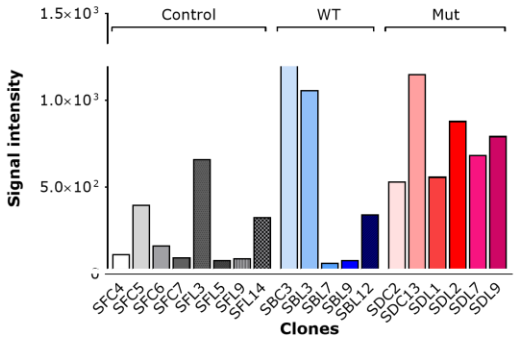

NAV2

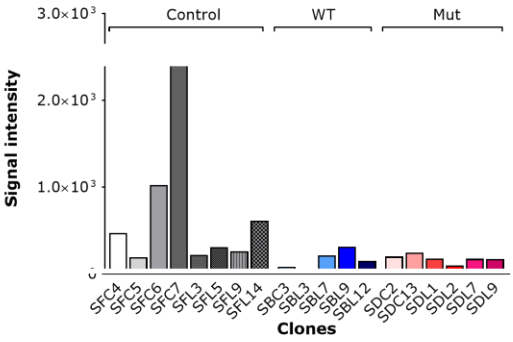

SEMA3A

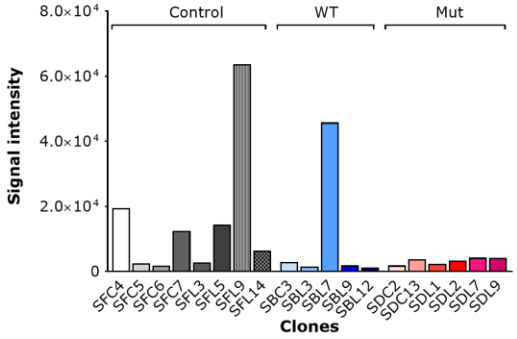

SEMA3C

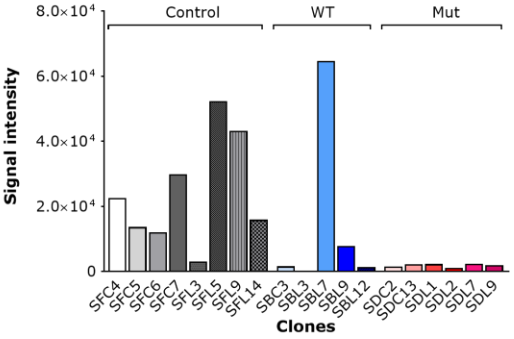

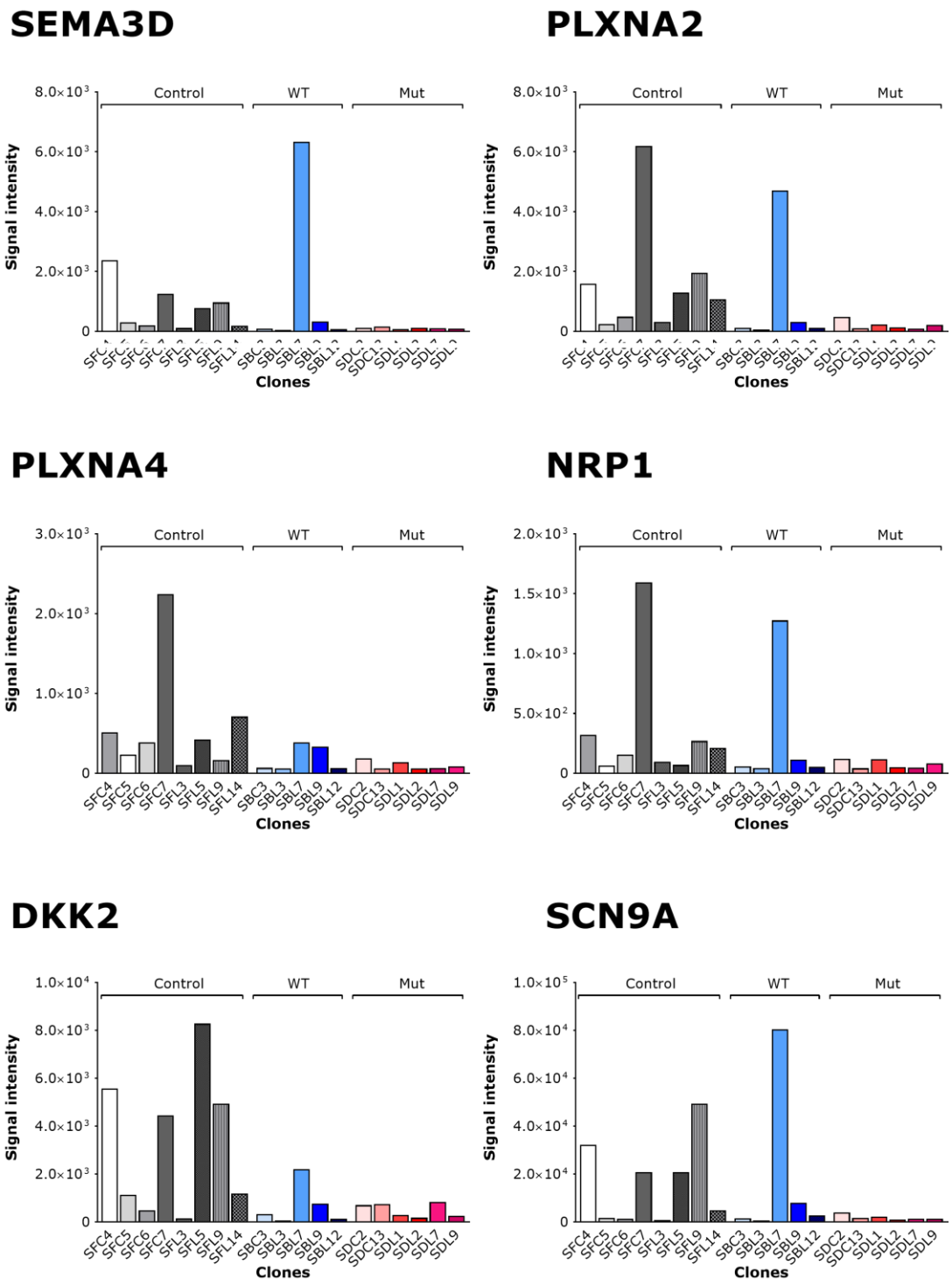

Figure 3-50. Signal intensity of the genes listed in Table 3-18 for each SH-SY5Y stable clone in microarray analysis.

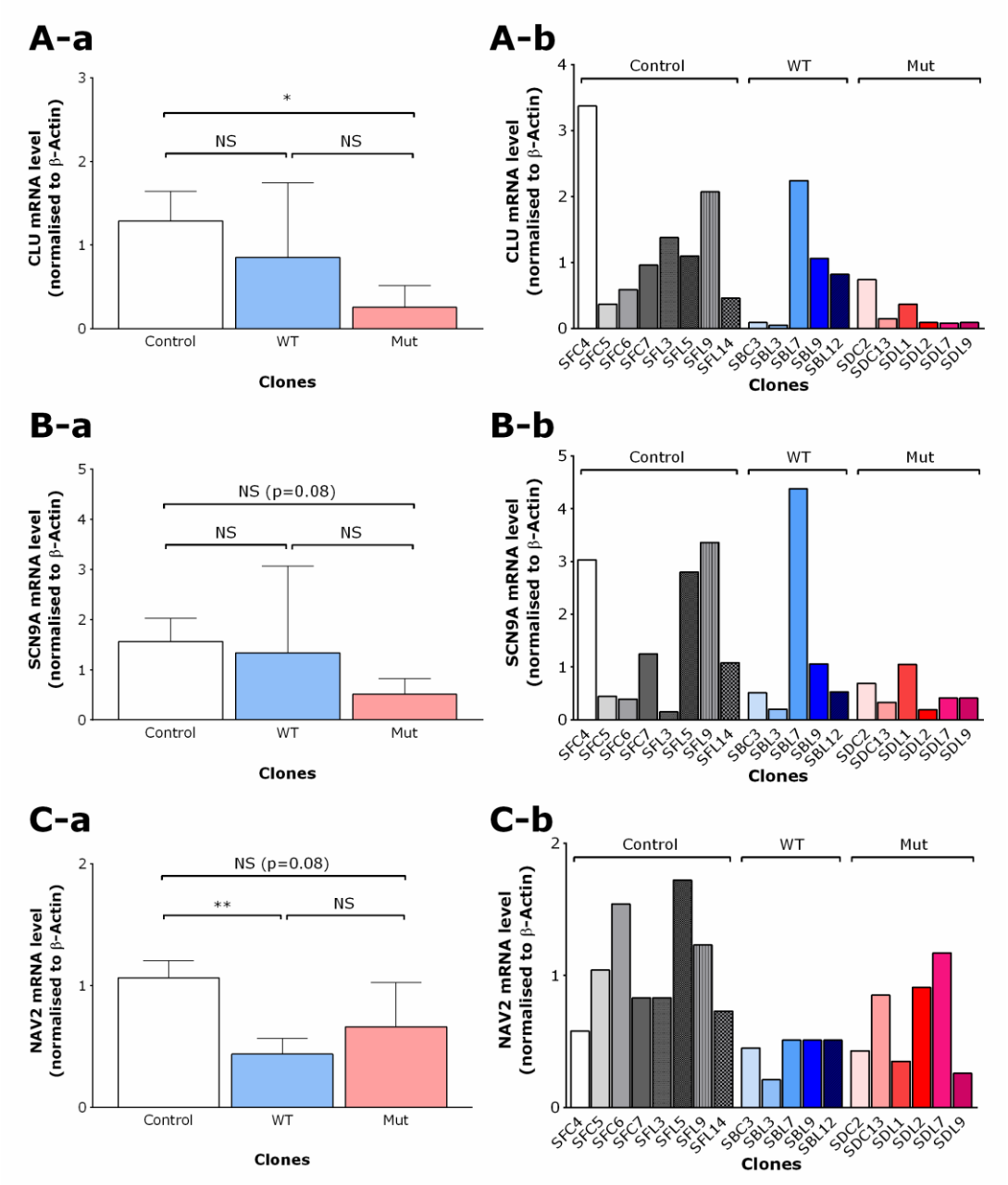

Figure 3-51. Real-time qRT-PCR analysis of (A) *CLU*, (B) *SCN9A* and (C) *NAV2* mRNA expression in SH-SY5Y stable clones relative to β-Actin. Relative expression levels of mRNA were calculated using the comparative ΔΔCt (Ct) method and normalised by control clones (SF). (b) shows the expression in each clone.

We also performed microarray analyses using DRG in global Zfhx2 KO mice to explore the downstream genes further. The data indicated 44 genes are down-regulated and 26 genes were up-regulated (fold change >1.5, ANOVA p-value <0.1) in KO mice compared to WT. The differentially expressed genes between KO and WT mice include *Trpv1* (transient receptor potential cation channel, subfamily V, member 1; down-regulated in KO mice, fold change 1.51), *Penk* (preproenkephalin; down-regulated in KO mice, fold change 1.47), *Htr3a* (5-hydroxytryptamine (serotonin) receptor 3A, down-regulated in KO mice, fold change 1.42), *Htr3b* (5-hydroxytryptamine (serotonin) receptor 3B, down-regulated in KO mice, fold change 1.42) and *Tac1* (tachykinin 1; down-regulated in KO; fold change 1.39). There is another gene which might contribute to pain behavioural phenotype although it is not a dramatic change; *Lrp1* (low density lipoprotein receptor-related protein 1) is up-regulated in KO (fold change 1.33). The fold change and ANOVA p-value of these genes are summarised in Table 3-19.

Table 3-19. Several dysregulated genes in DRG in global Zfhx2 KO mice compared to WT mice which are relevant to pain

Gene Symbol	Description	Fold Change (linear) (KO vs. WT)	ANOVA p-value (KO vs. WT)
Trpv1	transient receptor potential cation channel, subfamily V, member 1	-1.51	0.05494
Penk	Preproenkephalin	-1.47	0.096282
Htr3a	5-hydroxytryptamine (serotonin) receptor 3A	-1.42	0.055527
Htr3b	5-hydroxytryptamine (serotonin) receptor 3B	-1.32	0.047314
Tac1	tachykinin 1	-1.39	0.00993
Lrp1	low density lipoprotein receptor-related protein 1	1.33	0.06918

The genes described above have been documented in pain studies. TRPV1 is a well-known channel that is activated in response to capsaicin and serves a key role in noxious heat sensitivity (Caterina et al., 2000, Caterina et al., 1997). As addressed in Chapter2 (2 Voltage-gated sodium channel as a transcriptional regulator), *Penk* is the precursor of Met-enkephalin and Leu-enkephalin. Enkephalins are well-characterised opioid peptides and are some of the most studied innate pain-relievers, and the importance of enkephalin in pain has been well documented (Chu Sin Chung and Kieffer, 2013). 5-hydroxytryptamine receptor 3A (5-HT_{3A}) and 5-hydroxytryptamine receptor 3B (5-HT_{3B}) are receptors for 5-hydroxytryptamine (5-HT,

known as serotonin). 5-HT is a neurotransmitter in both the CNS and PNS and has a role in many physiological processes including nociception and pain. The role of 5-HT and its receptor in the CNS in pain has been well documented for decades such as in descending pain pathways (Eide and Hole, 1993). For example, electrical stimulation in the periaqueductal gray (PAG) leads to 5-HT release in the dorsal horn that excites inhibitory interneurons through 5-HT3 receptors, resulting in inhibited responses to mechanical stimuli (Peng et al., 1996). In the PNS, several subtypes of 5-HT receptors are considered to be involved in nociceptive responses (Sommer, 2004). These include 5-HT_{3A} and 5-HT_{3B} encoded by *HTR3A* and *HTR3B*, respectively. Antagonist of 5-HT_3 receptors or 5-HT_3 KO mice demonstrated inhibited inflammatory pain responses (Zeitz et al., 2002, Giordano and Rogers, 1989, Giordano and Dyche, 1989, Eschalier et al., 1989, Doak and Sawynok, 1997). Notably, transcripts of *HTR3B* were reduced in WT SH-SY5Y stable cell lines compared to control clones (fold change 1.94), indicating that overexpression of ZFHX2 might also alter the expression of *HTR3B*, which might modulate nociception and pain perception. Another down-regulated gene, *Tac1*, encodes substance P and neurokinin A (Krause et al., 1987). By deleting *Tac1,* mice demonstrated decreased noxious thermal and mechanical sensitivity and reduced responses to capsaicin-induced pain and formalin-induced inflammatory pain in Phase I (Cao et al., 1998). The immunoreactivity of substance P and neurokinin A were detected in the WT mice but not in the *Tac1* deleted mice (Cao et al., 1998), suggesting that *Tac1* plays a role in the pain phenotype by mediating the expression of substance P and neurokinin A. Similarly, in targeted deletion of *Tac1*, the mice showed a deficit in noxious thermal sensitivity in the hot plate test together with significantly decreased expression of substance P expression in brain extracts (Zimmer et al., 1998). However, these mutant mice react normally in the tail flick assay and acetic acid-induced writhing tests (Zimmer et al., 1998). *Lrp1* (low density lipoprotein receptor-related protein 1) is up-regulated in KO (fold change 1.33), and this up-regulation might also contribute to pain behaviour. Injection of a soluble or shed form of LRP1with an intact alpha-chain directly to sciatic nerves prior to chronic constriction injury (CCI) inhibited p38 MAPK activation that can induce inflammatory cytokines such as TNF-α and IL-1β (Gaultier et al., 2008). The expression of TNF-α and IL-1 β were decreased after CCI in mice with the injection compared to mice without the injection (Gaultier et al., 2008). These mice with the injection had decreased CCI-induced neuropathic pain, suggesting that this gene could be involved in neuropathic pain by mediating induction of inflammatory cytokines via activation of p38 MAPK (Gaultier et al., 2008). Notably, the expression of this gene is slightly supressed in the Mut SH-SY5Y stable cell line compared to control clones (fold change 1.33), indicating that mutant *Zfhx2* mice and global *Zfhx2* KO mice would lead to different effects on pain behaviour.

In summary, these microarray results suggest several downstream genes that are potentially regulated by ZFHX2 and which could be involved in pain perception. The alteration of the expression of these genes caused by the R1913K mutation could contribute to the observed pain phenotypes. Of note the analysis also showed that the differentially dysregulated genes in SH-SY5Y stable cell lines and *Zfhx2* global KO mice were largely different. Microarray analysis of mutant *Zfhx2* mice and WT mice may shed some further light on important genes regulated by mutant Zfhx2.

3.4.6 ChIP–seq assays

Performed by Dr. Konstantin Panov at Queen's University Belfast and Dr. Andrei Okorokov at University College London

In order to explore the downstream genes further, we aimed to perform ChIP-seq assays using SH-SY5Y stable cell lines to identify genomic binding sites of WT and Mut ZFHX2. We used SBC3 and SBL3, and SDC2 and SDL1 to analyse WT and Mut ZFHX2, respectively. Approximately 60 million cells per sample were used to perform ChIP and 730-1450ng of DNA was obtained for ChIP-seq. The numbers of genes detected in the assay is shown in Table 3-20. The ChIP-seq analysis showed Mut ZFHX2 has many genomic binding sites. However, WT ZFHX2 did not seem to display as many as Mut ZFHX2, indicating that overexpression of WT ZFHX2 may affect binding abilities to DNA or the assay for WT ZFHX2 was not well conducted. Even so, the assay from Mut clones appears to demonstrate several genes in which Mut ZFHX2 can bind. We selected several genes which were detected in the ChIP-seq analysis and also found in differentially expressed genes between Mut and control clones with more than 1.5 fold in microarray analysis. The functions of these genes annotated with Gene Ontology (GO) terms regarding the Biological Process highlighted an association between Mut ZFHX2 and genes playing a role in development and cell differentiation; in the genes which are categorised in the top10 enriched GO biological process terms, approximately 30% of genes were annotated with development or cell differentiation (Figure 3-52). These include *SEMA3A, SEMA3C*, *SEMA3D*, *PLXNA2*, *PLXNA4*, *DKK2*, and *NAV2*, which all seem to be associated with pain as addressed in the previous section. Table 3-21 shows the downstream genes addressed in the previous section (3.4.4) and presence or absence of peaks within these genes in ChIP-seq in Mut clones.

Table 3-20. Numbers of genes detected in ChIP-seq assay in each condition.

Clone	Antibody	Numbers of genes detected
SBC3	Anti-V5	254
SBL3	Anti-V5	62
SDC2	Anti-V5	1942
SDL1	Anti-V5	324
SBL3	Anti-IgG (negative control)	110
SDC2	Anti-IgG (negative control)	62
SDC2	Anti-TBP (positive control)	6040

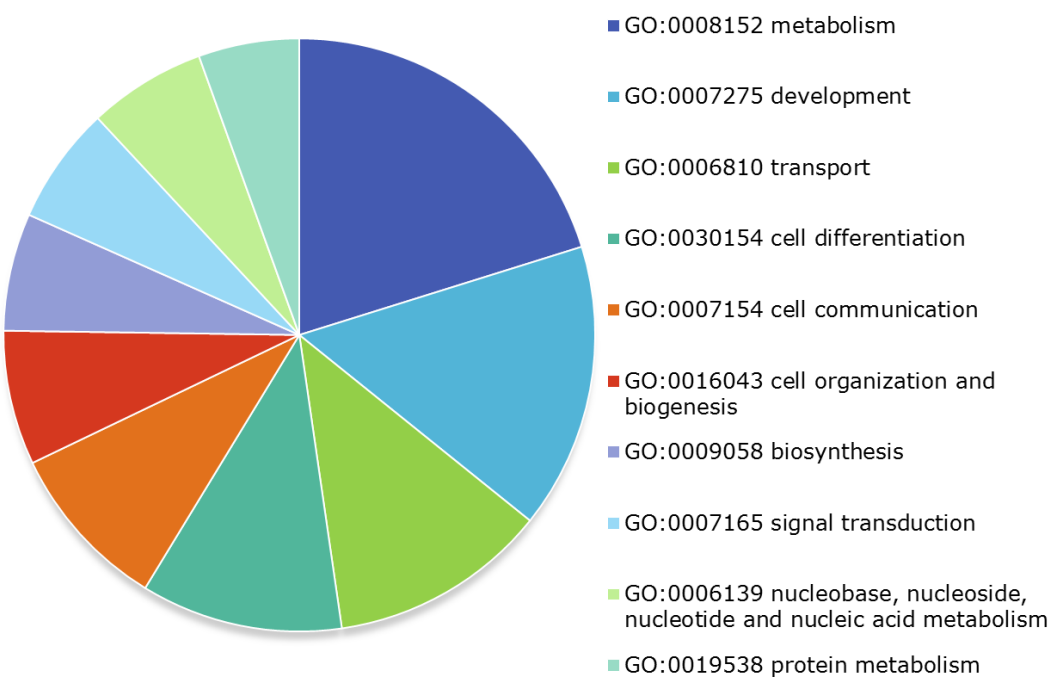

Figure 3-52. Pie charts of genes to which Mut ZFHX2 binds, annotated with Gene Ontology (GO) terms regarding the Biological Process. The top10 enriched GO biological process terms were shown. GO Biological Process terms were classified with GO_slim2 by single count by CateGOrizer (Hu et al., 2008).

Table 3-21. The downstream genes found in microarray analysis which can be associated with pain pathways and detection in ChIP-seq. -; the gene is not detected in ChIP-seq in Mut clones. +; the gene is detected in ChIP-seq in Mut clones

Gene Symbol	Microarray		Detected in ChIP-seq in Mut clones	Note
	Fold Change (linear) / ANOVA p-value (Mut vs. Control)	Fold Change (linear) / ANOVA p-value (WT vs. Control)		
CLU	-8.13 / 0.000584		-	
PRKCA	-5.5 / 0.020846	-5.73 / 0.08808	+	High peaks in 5' ends
DPYSL5	4.91 / 0.001451		-	
NAV2	-2.17 / 0.018829	-2.9 / 0.020318	+	
SEMA3A	-2.24 / 0.088998		+	
SEMA3C	-10.31 / 0.00006	-8.57 / 0.054573	+	High peaks in 5' ends
SEMA3D	-4.45 / 0.006687		+	High peaks in 5' ends
PLXNA2	-6.17 / 0.006293		+	High peaks in 5' ends
PLXNA4	-4.98 / 0.004769	-5.65 / 0.064101	+	
NRP1	-2.36 / 0.04868		-	
DKK2	-5.19 / 0.038431	-6.75 / 0.063094	+	High peaks in 5' end
SCN9A	-5.12 / 0.070101		+	High peaks in 5' ends

In summary, this ChIP-seq analysis helps further to identify genes that are directly regulated by ZFHX2. Further analysis could be beneficial to identify consensus binding sites or recognition motifs within the ChIP-seq peaks.

3.5 DISCUSSION

3.5.1 Summary of the results

The principal aim of this project was to find whether the R1913K mutation in ZFHX2 was the cause of the human pain insensitivity. We investigated: (1) how the mutation might alter the function of ZFHX2; (2) the role of the *Zfhx2* gene in pain processing using mouse models; (3) ZFHX2 regulated genes and whether the R1913K mutation causes any changes in downstream gene expression compared to WT ZFHX2.

To address the first question, we expressed ZFHX2 in cell lines and studied the subcellular localization (3.4.1) and methylation status around residue 1913 using mass spectrometry (3.4.2). The HEK293 cells transfected with WT or Mut *ZFHX2* constructs did not display any alteration of subcellular localization; both WT and Mut ZFHX2 were expressed within the nucleus (3.4.1). We successfully generated AD293 and SH-SY5Y stable cell lines to obtain large amounts of ZFHX2 protein (3.4.2II, 3.4.2III, 3.4.2IV). We then performed mass spectrometry analysis following the immunoprecipitation in the SH-SY5Y stable cell lines (3.4.2V). In spite of large amounts of ZFHX2 protein isolated from the stable cell line, we could not detect enough peptide fragments around residue 1913 to reveal the methylation status. Even so, the analysis showed R1913 in WT, and R1911 and K1913 in Mut did not appear to be methylated. Further analysis with higher amounts of protein is necessary to determine if the R1913K mutation alters the methylation status around the region.

Next, we performed pain behavioural tests on both global *Zfhx2* KO mice (3.4.3) and also BAC transgenic mice bearing the orthologous mutation (3.4.4). Behaviour tests on global *Zfhx2* KO mice indicated that *Zfhx2* is involved in pain perception; KO mice demonstrated a deficit in noxious mechanical sensitivity, but were more sensitive to thermal stimuli in the hot plate test. In addition, female KO mice tended to show less sensitivity to inflammatory pain in the formalin test. Behaviour tests on BAC transgenic mice bearing the orthologous mutation suggested the mutation could lead to the pain insensitive phenotype; the mice with high expression of mutant *Zfhx2* displayed reduced sensitivity to thermal stimuli in both the hot plate and Hargreaves' tests.

For the third question, we performed microarray and ChIP-seq (chromatin immunoprecipitation sequencing) assays (3.4.5, 3.4.6). Differentially expressed genes in SH-SY5Y stable cell lines or DRG from global *Zfhx2* KO mice using microarray analyses identified numerous candidate genes that may contribute to the pain phenotype. ChIP-seq analysis using SH-SY5Y stable cell lines supported the involvement of some of these genes in pain pathways.

Our results confirm that ZFHX2 is involved in pain pathways and that R1913K is a causative mutation that leads to a pain insensitive phenotype. ZFHX2 can regulate downstream gene expression and the R1913K mutation can alter the expression level of downstream genes. However, the pathological mechanism of the ZFHX2 missense mutation has not been fully uncovered yet.

3.5.2 Pain behaviour in animal model

In this project, we used global *Zfhx2* KO mice to study the role of Zfhx2 in pain and BAC transgenic mice bearing the orthologous mutation to explore whether R1913K is a causative point mutation leading to a pain insensitive phenotype. Table 3-22 shows the behaviour results addressed in this chapter. The global *Zfhx2* KO mice showed a deficit in noxious mechanical sensitivity in the Randall-Selitto test, but they were more sensitive to noxious thermal (heat) stimuli compared to WT mice in the hot plate test. The BAC transgenic mice bearing the orthologous mutation with low copy numbers did not display any distinct acute pain behaviour from WT control. However, the mutant BAC transgenic mice with high copy numbers of the mutant BAC had markedly reduced sensitivity to noxious thermal stimuli in the hot plate (50℃) and Hargreaves' tests. On the other hand, these mice did not show altered mechanical pain thresholds in the von Frey and Randall-Selitto tests. The present data indicates that *Zfhx2* plays a role in pain pathways and the missense mutation could lead to pain insensitive phenotype. The open field test on the mutant BAC transgenic mice displayed high exploratory behaviour and low anxiety levels of the mutant mice, which are of the same tendency as global *Zfhx2* KO mice (Komine et al., 2012). This may confirm Mut Zfhx2 is likely to function in the CNS and leads to low anxiety behaviour. Interestingly, it has been clinically experienced that anxiety exacerbate pain (Von Graffenried et al., 1977, Ploghaus et al., 2001). The low anxiety levels due to Mut Zfhx2 might also contribute to pain insensitive phenotype in mice, and furthermore, human patients might not claim pain partly because of this contribution.

The pain behaviour tests showed that the global *Zfhx2* KO mice and mutant BAC transgenic mice have different pain phenotypes and may be explained by the missense mutation conferring a gain-of-function. Although the BAC transgenic mice were hyposensitive to heat, they displayed normal mechanical pain thresholds (unlike the human patients). There could be several reasons for why the mutant BAC transgenic mice did not show reduced sensitivity to mechanical stimuli. First, BAC transgenic mice have 2 wild-type alleles and the mutant *Zfhx2* expression relies on the BAC copy number in the mouse genome. Knock-in mice would have a more similar background to that of the human patients. Pain behaviour tests in knock-in mice may help to answer this technical issue. Secondly, downstream genes or expression of these genes altered by the mutant ZFHX2 could be different between mice and humans. The microarray data shows several genes appear to be controlled by ZFHX2 implying multiple genes contribute to the pain phenotype. Certain subtle differences in gene expression between mice and humans could lead to distinct effects on pain behaviour. Similarly, the dysregulation of

the downstream genes might require higher expression of mutant Zfhx2 than human mutant ZFHX2, leading to a distinct pain phenotype. Thirdly, considering several genes associated with neuronal development were dysregulated in the microarray analysis, the pain insensitive phenotype could develop at a later stage. The development might differ between mice and humans. In this study we have used the mice aged 8-15 weeks, but it might be interesting to test pain behaviour in older mice. Fourthly, the tissue distribution of Zfhx2 in mice and humans might affect the pain phenotype. Zfhx2 expression in the subpopulations of sensory neurons might differ between species. Recent RNA-seq data has highlighted a relatively high expression of *Zfhx2* in small diameter DRG neurons in mice (Usoskin et al., 2015). Whether the same population of human neurons express ZFHX2 remains to be clarified. It is also worth noting that Zfhx2 is expressed in CNS regions, such as the thalamus (Komine et al., 2006). The thalamus is an important region for pain processing with the nociceptive information ascending from the spinal cord to the brain though several pathways and some of these pathways terminate at the thalamus (Basbaum and Jessell, 2000, Almeida et al., 2004). Several studies have suggested that gene expression in the thalamus may mediate pain perception; the expression of the several markers such as c-fos, IL-1β and VGLUT2 that are considered to be closely related to pain are altered followed by surgeries that induce neuropathic pain (Wang et al., 2015, Vania Apkarian et al., 2006, Üçeyler et al., 2008, Narita et al., 2003). Taking these facts into account, we may presume the gene expression controlled by Zfhx2 in the thalamus could be involved in the pain phenotype.

Table 3-22. A summary of pain behaviour in global *Zfhx2* KO mice and BAC transgenic mice bearing the orthologous mutation (BAC mutant).
0: No change, -: Reduced responses (less sensitive to stimuli), +; Increased responses (more sensitive to stimuli)
Mechanical pain: Randall-Selitto test (RS), Light touch: Von Frey (vF) and Cotton Swab (CS), Thermal spinal reflex: Hargreaves' test (HG), Supraspinal thermal: Hot plate test, Noxious cold: Cold plate test, Noxious cooling: acetone test (Ac), CFA: complete Freund's adjuvant, TPP; Thermal Place Preference, RR; Rotarod, OF; Open Field

Transgenic mice	Acute Pain							Inflammatory Pain		Other			Results
	RS	vF	CS	HG	Hot plate	Cold plate	Ac	Formalin	CFA	TPP	RR	OF	
Zfhx2 KO mice	-	0	0	0	+ (0; female at 55℃)		0	- (Phase I, female)		0 (4℃)	0	+	(Figure 3-40, Figure 3-41, Figure 3-42, Figure 3-43) OF; (Komine et al., 2012)
BAC mutant (low copy numbers)	0	0	0	0	0	0	0		- (vF Day7), 0 (HG)	- (15℃)	0	+	(Figure 3-44, Figure 3-45)
BAC mutant (high copy numbers)	0	0		-	-								(Figure 3-47)

3.5.3 Downstream genes regulated by ZFHX2 and their role in pain

The pain behaviour tests in global *Zfhx2* KO and BAC transgenic mice suggested that *Zfhx2* is involved in pain and the mutation could contribute to analgesic effects. Since ZFHX2 can act as a transcription factor we aimed to understand which genes were regulated by ZFHX2 using microarray and ChIP-seq analyses. Table 3-23 is a summary of the genes addressed in the results section which are potentially associated with the pain phenotype in global *Zfhx2* KO mice, mutant *Zfhx2* mice or the human patients. These genes have been documented in pain studies; however, it should be also noted that some genes markedly regulated by *ZFHX2* or *Zfhx2,* but not previously reported in the pain literature may also contribute to the pain behaviour.

I. Association of downstream genes and pain behavioural phenotype

Some of the genes addressed in Table 3-23 are interesting candidates that may help to explain the pain insensitivity. For example, a CLU inhibitor has been reported to relieve pain in patients with metastatic castration-resistant prostate cancer (Saad et al., 2011). The down-regulation of CLU in Mut SH-SY5Y clones compared to control clones (eGFP) could support the idea that reduced expression of CLU by mutant ZFHX2 may contribute to the pain insensitive phenotype. Another down-regulated gene, *NAV2*, could also be important as mutant mice that carry a hypomorphic allele of *Nav2* show attenuated thermal noxious sensitivity (Peeters et al., 2004). Of note, WT clones also showed marked down-regulation of *NAV2*, indicating that high levels of ZFHX2 itself might act like a gain-of-function mutation and alter the expression of *NAV2*. Another downregulated gene in the mutant cell lines, *SCN9A*, is also another obvious candidate (Minett et al., 2012, Gingras et al., 2014, Cox et al., 2006, Nassar et al., 2004).

The microarray analyses in global KO mice and WT littermates also supports the idea of differentially expressed genes influencing the pain phenotype in KO mice. For example, decreased expression of *Penk*, a precursor of Leu- and Met-enkephalins, which are endogenous ligands of the δ-opioid receptor and μ-opioid receptor and well-studied innate pain-relievers (Chu Sin Chung and Kieffer, 2013), in KO mice might contribute to the thermal hypersensitivity observed.

Table 3-23. Potential downstream genes of ZFHX2 which could be involved in pain pathways.

Gene Symbol (Description)	Fold Change in microarray analysis			Gene function in pain study
	SH-SY5Y stable cell line		Mice DRG	
	Mut vs. Control	WT vs. Control	KO vs. WT	
CLU (clusterin)	-8.13			CLU inhibitor custirsen shows pain relief effect in clinical trial
PRKCA (protein kinase C alpha)	-5.5	-5.73		·*Prkca* KO mice showed increased mechanical allodynia in neuropathic pain model · PRKCA is required for TRPV1 activation
DPYSL5 (dihydropyrimidinase-like 5)	4.91			Inhibiting the binding of CRMP2 (the same family of DPYSL5) to $Ca_V2.2$ results in supressed inflammatory and neuropathic hypersensitivity
NAV2 (neuron navigator 2)	-2.17	-2.9		Less sensitivity to thermal noxious stimuli in hot plate test in mutant mice that carry a hypomorphic allele of *Nav2*
SCN9A (voltage-gated sodium channel alpha subunit 9)	-5.12			·*Scn9a* KO mice show deficits in mechanical and thermal stimuli, inflammatory and neuropathic pain. · Loss-of-function mutations cause CIP.
SEMA3A (semaphorin 3A)	-2.24			·Sema3A overexpression attenuated NGF-induced mechanical allodynia in von Frey test. · Plexins are receptors of semaphorins. · Intrathecal administration of Sema3A, in the spinal cord in CCI model attenuated mechanical allodynia and heat hyperalgesia, being accompanied by increased levels of Npr1.
SEMA3C (semaphorin 3C)	-10.31	-8.57		
SEMA3D (semaphorin 3D)	-4.45			
PLXNA2 (plexin A2)	-6.17			
PLXNA4 (plexin A4)	-4.98	-5.65		
NRP1 (neuropilin 1)	-2.36			
DKK2 (dickkopf WNT signalling pathway inhibitor 2)	-5.19	-6.75		· DKK2 is a Wnt inhibitor · Wnt signalling in pain; eg. WNT–Frizzled–β-catenin pathway inhibitors attenuated allodynia and hyperalgesia in CCI model

Trpv1 (transient receptor potential cation channel, subfamily V, member 1)			-1.51	· Trpv1 is activated in response to capsaicin. · Trpv1 is responsible for noxious heat sensitivity.
Penk (preproenkephalin)			-1.47	· Precursor of opioid peptides, enkephalins, which are well studied innate pain-relievers
Htr3a (5-hydroxytryptamine (serotonin) receptor 3A)			-1.42	· Receptors for 5-HT (serotonin). ·Antagonist of 5-HT_3 receptors or 5-HT_3 KO mice inhibited inflammatory pain responses
Htr3b (5-hydroxytryptamine (serotonin) receptor 3B)		-1.94	-1.32	
Tac1 (tachykinin 1)			-1.39	Deleting *Tac1* in mice led to decreased noxious thermal and mechanical sensitivity and reduced responses to capsaicin-induced pain and formalin-induced inflammatory pain in Phase I
Lrp1 (low density lipoprotein receptor-related protein 1)	-1.33		1.33	The mice with the injection of a soluble or shed form of LRP1 showed decreased CCI-induced neuropathic pain, by inhibiting induction of inflammatory cytokines.

II. Technical limitations in the microarray and ChIP–seq analyses

(1) Using cell lines for microarrays to explore dysregulated genes.

We performed microarrays using SH-SY5Y stable cell lines to identify the genes dysregulated by Mut ZFHX2. The SH-SY5Y cells are a human neuronal cell line, which is a thrice cloned subline of SK-N-SH cells. SK-N-SH cells were originally obtained from a bone marrow biopsy of a neuroblastoma patient with sympathetic adrenergic ganglial origin (Biedler et al., 1973). Since this cell line is human derived, it may be beneficial to explore the downstream genes of human ZFHX2. However, a major disadvantage is that is not a sensory-neuron derived cell line, and the gene expression changes may not be representative to those that may be observed in, for example, DRG tissue from knockin mice.

(2) Diverse expression of ZFHX2 in each clone of SH-SY5Y stable cell line.

Another limitation of the SH-SY5Y cell line work is that each clone showed different levels of ZFHX2 overexpression. The results of the real-time RT-qPCR to measure mRNA levels indicated that the expression levels ranged from 5 to 24 fold change for WT vs control clones and from 9 to 86 fold change for Mut vs control clones (Figure 3-33). Of note, even control clones (eGFP) express *ZFHX2* at different levels, approximately 4 fold change between the lowest and highest expressing clones. This distinct expression may be problematic for analyses when it comes to selecting candidate genes as we may observe false positive results from ectopic activity. In this chapter all clones were included to analyse microarray data to help reduce the number of false positive results.

(3) Using cell lines and tagged protein (V5) in ChIP-seq analyses.

We also used the SH-SY5Y stable cell lines for ChIP-seq analyses. The advantages were that they were a human cell line in which we could purify high amounts of ZFHX2 using a ChIP-grade anti-V5 antibody. However, the major disadvantage of this strategy is that the ectoptic overexpression of ZFHX2 could have led to false-positive binding. In the future we plan to carry out ChIP-seq in DRG neurons from mutant mice, when a ChIP-grade anti-ZFHX2 antibody has been developed. Of note since ChIP-seq needs large amount of cells and numbers of cells from mice are limited, ChIP-seq using DRG neurons might be difficult to perform. Some techniques have developed to solve this problem, such as ultra-low-input (ULI) micrococcal nuclease-based native ChIP (NChIP) (Brind'Amour et al., 2015). In this method,

approximately as few as 10^3-10^5 cells are required. It might be useful to test these scaled-down procedures of ChIP-seq when using DRG neurons from mice.

Some genes listed in the microarray analysis and ChIP-seq using SH-SY5Y stable cell line might be affected by characteristic features of the cell line. For example, some genes have been documented in cancer studies. Clusterin has been well-known for its role in carcinogenesis and tumour progression (Shannan et al., 2006, Zhang et al., 2005a, Xiu et al., 2015). Semaphorins and their receptors have been also well documented in cancer diseases (Sakurai et al., 2012, Neufeld and Kessler, 2008, Worzfeld and Offermanns, 2014). These genes could be an excellent drug target for pain as well as cancer therapy. Moreover, further development of these drug targets could be useful for cancer pain treatment. It should be also noted, however, that these genes might be dysregulated significantly due to the nature of the neuroblastoma derived cell. Further analysis using DRG neurons would be required for deeper understanding of downstream genes and pathological pathways of ZFHX2.

3.5.4 Pathological mechanism of ZFHX2 missense mutation

In this project, we aimed to investigate exactly how the missense mutation alters the function of ZFHX2. We explored two potential mechanisms: subcellular localization and arginine methylation. Immunofluorescence by FLAG and/or V5 tags fused onto ZFHX2 did not exhibit alteration of subcellular localization between the cells transfected with WT and Mut constructs. This result can indicate that subcellular localization was not a pathological mechanism capable of altering ZFHX2 function, although subtle differences in chromatin binding cannot be excluded. Secondly, we aimed to explore another potential cause, the alteration of arginine methylation(s) status. This idea is based on two factors: the importance of methylation on arginine and lysine residues in transcriptional activities, and the sequence motif over R1913. The structure of the Hox domain in ZFHX2 that binds to DNA also supports this hypothesis; arginine residues at R1911 and R1913 tend to be in proximity to DNA (Figure 3-15). This proximity suggests these arginine residues are likely to interact with the DNA. To explore this hypothesis, we successfully obtained sufficient amount of ZFHX2 protein for mass spectrometry analysis using the WT and Mut SH-SY5Y stable cell line. In spite of having enough proteins to perform mass spectrometry, fragments around position 1913 were not well detected; only 1 peptide and 2 peptides that cover position 1913 were detected from WT, and Mut clones, respectively (Figure 3-39). Only two fragments and none of the peptides were detected at the position 1911 in the Mut and WT clones, respectively (Figure

3-39). None of R1913(K) and R1911 detected in WT or Mut clones were methylated according to the analysis.

Interestingly, a protein methylation prediction tool called MeMo illustrates altered methylation status in the motif over R1913. MeMo is based on all annotated methylated residues in SWISS-PROT version 48 (Chen et al., 2006). A prediction using MeMo indicates that R1911 can be methylated in the motif of R1913 (WT) whilst R1911 cannot be methylated in the motif of K1913 (Mut) (Figure 3-53). This prediction is consistent with our hypothesis that R1913K mutation may alter arginine methylation(s) status over the motif. The alteration of methylation status on R1911 appears to be also corresponding to its proximity to DNA (Figure 3-15). Lack of methylation due to the missense mutation R1913K could alter transcriptional activity of ZFHX2. Although the prediction seems to strengthen our hypothesis, we could not conclude if the methylation(s) status over the motif R1913, particularly R1911, was altered. The mass spectrometry analysis demonstrated that the methylation did not occur at R1911 in Mut clones. However, we could not detect any fragments over R1911 in WT clones. In this thesis, approximately ~70 million cells were used and 1-2 fragments over the mutation region were detected. Therefore 10 times more cells might give 10-20 fragments which would be sufficient to show the hypothesis. Further analysis using these higher amounts of protein is required.

Another potential problem for few fragments around the mutation regions to could be selection of digestion enzymes. We divided the sample into two and used elastase and chymotrypsin respectively. Elastase is a nonspecific protease which preferentially cleaves at hydrophobic residues (Saveliev et al., 2012). In a study using *Halobacterium* and *Corynebacterium* peptides, over 82% for cleavage of alanine, valine, leucine, isoleucine, serine, and threonine in the P_1 position by elastase (Rietschel et al., 2009). Chymotrypsin, whose structure is similar to trypsin and catalyses peptide bond cleavage by identical mechanisms to trypsin (Perona et al., 1995), is a protease with a preference for aromatic and other hydrophobic residues (Saveliev et al., 2012). It has been reported that trypsin did not cleave C-terminally to methylated lysine or arginine (Ong et al., 2004). The cleavage sites for chymotrypsin have been reported as C-terminal of phenylalanine, tyrosine, leucine, tryptophan and methionine (Giansanti et al., 2016). These insights suggested that chymotrypsin would be ideal for detecting arginine methylation, and elastase is not likely to disturb the regions over R1913K. However, the regions around the position 1900 have highly hydrophobic residues such as valine, tryptophan, phenylalanine and threonine where either of the protease we chose can cleave. Thereby one of the reasons why less numbers of fragments were detected around the mutation region could be high chance of

cleavage around the regions. It would be worthy to try combination of the other enzymes such as Glu-C which cleaves C-terminal of aspartic or glutamic acid residues (Giansanti et al., 2016), in order to increase the coverage of fragments around the target regions.

Figure 3-53. Prediction of arginine/ lysine methylation using MeMo. R1911 is predicted to be methylated in WT while no methylation is predicted on R1911 in Mut.

Pathological mechanisms of the missense mutation cannot be limited to arginine methylation(s) or the other post-translational modifications. The mutation R1913K is found in Hox domain which consists of three helical regions folded into a tight globular structure (Qian et al., 1989). This rigid structure enables Hox domains to bind DNA in a sequence-specific manner (D'Elia et al., 2001). Even without any post-translational modification changes, the missense mutation itself can change the structure and/or alter its function and downstream gene expression (D'Elia et al., 2001). The ChIP-seq analysis performed in this chapter could be useful to explore sequence motifs which WT or Mut are likely to bind, and distinct sequence motifs between WT and Mut might explain the pathological mechanisms if any differences are observed. Also, the mutation might alter the binding abilities to coactivators and/or corepressors which can influence transcription of downstream genes. The combination of mass spectrometry technologies with co-immunoprecipitation may allow discovering discrete protein complexes with ZFHX2 potentially involved in transcription of downstream genes. Deeper understanding of pathological mechanisms may lead to discovering novel therapeutic targets and contributing to effective pain therapies.

3.5.5 Future studies

Several areas remain to be investigated further, for instance: (1) some additional pain behaviour tests in mice; (2) pathological mechanisms of the mutation; (3) target genes for future pain therapies.

We have used BAC transgenic mice to explore if the mutation is the cause of pain insensitive phenotype. In this model, the pain phenotype strongly depended on the expression levels of the mutant Zfhx2 since the mice with low copy numbers did not show any acute pain phenotype whilst the mutant mice with high copy numbers demonstrated reduced sensitivity to noxious thermal stimuli. On the contrary, no significant change was observed in mechanical stimuli in these mice. This pain phenotype does not seem to be consistent with the pain behaviour in human patients. Additional tests using knock-in mice would be needed to explore this matter. Also, inflammatory and neuropathic pain models would be interesting to investigate. Considering the results of the formalin test on global *Zfhx2* KO and CFA models on the mutant BAC transgenic mice, *Zfhx2* seems to be involved in inflammatory pain. More evidences using knock-in mice or BAC transgenic mice with high expression of Mut *Zfhx2* are needed to confirm the association of *Zfhx2* and the mutation on inflammatory pain.

Pathological mechanisms still remain terra incognita. We found no subcellular localization change in the Mut ZFHX2. However, the alteration of arginine methylation(s) status over the motif R1913K was elusive since the peptides around the R1913K region were not well detected. Another analysis with higher amount of protein would be necessary to confirm our arginine methylation hypothesis. It will also be interesting to perform a detailed analysis of the sequence motifs which WT or/and Mut ZFHX2 bind to in the ChIP-seq analysis. Further investigations of any transcriptional coregulators by coimmunoprecipitation will also be useful.

The microarray and ChIP-seq analysis performed in this project provided downstream genes which ZFHX2 can regulate, some of which may be useful analgesic drug targets, although possibly more than one gene could be involved. To refine this list, further experiments are needed. First, microarray analysis of DRG from mutant BAC transgenic mice or knock-in mice should be performed to understand dysregulated genes by the mutant *Zfhx2* in DRG. Secondly, it would be interesting to explore the downstream genes in the CNS, such as the thalamus or midbrain. Thirdly, ChIP-seq analysis using mutant and WT mice DRG and Zfhx2 antibodies would be useful to explain the mechanisms, although it is technically difficult.

3.6 CONCLUSION

The principal aim of this project was to prove whether the R1913K mutation in ZFHX2 was the cause of the human pain insensitivity. We investigated (1) How the mutation might alter the function of ZFHX2; (2) the role of *Zfhx2* gene in pain processing using mouse models; (3) the genes regulated by ZFHX2 and whether the R1913K mutation resulted in changes in gene expression. We discovered that: (1) subcellular localization of wildtype and mutant ZFHX2 is the nucleus; (2) *Zfhx2* is involved in pain and the mutation reduces noxious thermal sensitivity; (3) several downstream genes may contribute to the pain phenotype. However, several matters are still unclear. We could not confirm if the arginine methylation status over R1913K is altered; further analysis is required to clarify this. Although we found the mutant mice showed attenuated noxious thermal sensitivity, mechanical sensitivity was not altered. This phenotype is not consistent with the one in human patients; further behavioural tests using knock-in mice would be useful to answer this question. Although a deeper understanding of functions and mechanisms of ZFHX2 is still necessary, the present data suggests this gene plays a critical role in pain perception.

4 IDENTIFICATION OF A NOVEL PAINFUL SMALL FIBRE NEUROPATHY GENE

4.1 INTRODUCTION

Neurodegenerative disorders, in which there is damage or death to specific subsets of neurons, are often closely correlated with pain (Przedborski et al., 2003, Borsook, 2012). Peripheral neuropathies, which are examples of neurodegenerative disorders, are one of the major causes of chronic pain or, conversely, pain insensitivity (Bennett and Woods, 2014). Some of these are hereditary peripheral neuropathies which are classified into three groups; hereditary motor neuropathies, hereditary motor and sensory neuropathies, and hereditary sensory and autonomic neuropathies (HSANs) (Rotthier et al., 2012). Several genes have been linked to HSANs; these include *SCN11A* encoding $Na_v1.9$ (Leipold et al., 2013, Woods et al., 2015), *NGF* encoding nerve growth factor beta (Einarsdottir et al., 2004, Carvalho et al., 2011), and *ATL1* encoding atlastin GTPase1 (Guelly et al., 2011), associated with HSAN VII, HSAN V, HSAN I, respectively (Table 4-1).

HSANs comprise a heterogeneous group of inherited neuropathies that disproportionately affect small- and large-fibre sensory neurons. Small fibre neuropathies (SFNs) are restricted to the thinly myelinated Aδ-fibres and unmyelinated C-fibres (Hoeijmakers et al., 2012). Patients diagnosed with SFN experience multiple types of pain, described predominantly as a burning sensation, shooting pains, prickling or itching (Gorson et al., 2008, Holland et al., 1998). In general, the diagnosis should be considered in the presence of symptoms and/or clinical signs of small-fibre damage and in the absence of large-fibre involvement. Symptoms include neuropathic pain, autonomic dysfunction, loss of pinprick sensation, thermal sensory loss, allodynia, or hyperalgesia. Large fibre involvement can cause muscle weakness, loss of light touch and/or proprioceptive or vibratory sensation, hypoflexia, or areflexia (Hoeijmakers et al., 2012). Table 4-2 demonstrates the symptoms seen in the SFNs (Hoeijmakers et al., 2012). Some of the well-known causes underlying SFNs are diabetes and alcohol abuse. On the contrary, ion channel dysfunctions are also linked to SFNs; dysfunctions of VGSCs caused by mutations within *SCN9A*, *SCN10A*, and *SCN11A* encoding $Na_v1.7$, $Na_v1.8$ and Nav1.9 respectively have been documented to be associated with SFNs (Faber et al., 2012a, Faber et al., 2012b, Huang et al., 2013, Han et al., 2015).

Table 4-1. Overview of HSAN subtypes and genes linked to HSANs. ‡Congenital onset in one patient with hypotonia, cataracts, microcephaly and vocal cord paralysis. §Childhood onset in one patient. Abbreviations: CMT2B, Charcot–Marie–Tooth syndrome type 2B; HSAN, hereditary sensory and autonomic neuropathy. (Rotthier et al., 2012)

Subtype	**Gene or locus**	**Clinical features**	**Age at onset**
Diseases showing autosomal dominant inheritance			
HSAN-I	*SPTLC1*	Loss of pain and temperature sensation; lancinating pain; ulcerative mutilations; variable distal motor involvement	Adolescence‡
HSAN-I	*SPTLC2*	Loss of pain and temperature sensation; lancinating pain; ulcerative mutilations; variable distal motor involvement	Adulthood§
HSAN-I	*ATL1*	Severe distal sensory loss and amyotrophy in lower limbs; trophic skin and nail changes; ulcerative mutilations	Adulthood
CMT2B	*RAB7A*	Loss of all somatosensory modalities; ulcerative mutilations; prominent distal motor involvement	Adulthood
HSAN-I with dementia and hearing loss	*DNMT1*	Loss of all somatosensory modalities; lancinating pain; ulcerative mutilations; sensorineuronal hearing loss, dementia	Adulthood
HSAN-IB	3p24–p22	Sensory loss with cough and gastroesophageal reflux; foot ulcerations (rare)	Adulthood
Diseases showing autosomal recessive inheritance			
HSAN-II	*WNK1*	Loss of pain, temperature and touch sensation; mutilations in hands and feet; acropathy	Childhood
HSAN-II	*FAM134B*	Impaired nociception and progressive mutilating ulceration of hands and feet with osteomyelitis and acro-osteolysis	Childhood
HSAN-II	*KIF1A*	Impaired position and vibration senses; ulcerative mutilations; minor distal weakness	Childhood to adolescence
HSAN-III	*IKBKAP*	No response to painful stimuli and temperature changes; alacrima; absence of fungiform papillae of the tongue; vasomotor instability and hyperhidrosis	Congenital
HSAN-IV	*NTRK1*	No (or reduced) response to painful stimuli; anhidrosis; episodic fever; mild mental retardation; skin and corneal lesions; joint deformities	Congenital
HSAN-V	*NGFB*	Insensitivity to pain; severe loss of deep pain perception; painless fractures; joint deformities	Congenital
HSAN with spastic paraplegia	*CCT5*	Loss of all somatosensory modalities; mutilating acropathy; spastic paraplegia	Early childhood

Table 4-2. Symptoms of small-fibre neuropathy. For the diagnosis of small-fibre neuropathy, at least two of the following symptoms, not otherwise explained, are required (Hoeijmakers et al., 2012).

Sensory	Autonomic
■Pain (burning, shooting, prickling or itching) ■Paraesthesias ■Allodynia ■Thermal sensory loss ■Pinprick loss ■Sheet or sock intolerance ■Restless legs syndrome	■Sicca syndrome ■Accommodation problems ■Hyperhidrosis or hypohidrosis ■Micturition disturbances ■Impotence and/or diminished ejaculation or lubrication ■Bowel disturbances (constipation, diarrhoea, irritability, gastroparesis, cramps) ■Hot flushes ■Orthostatic dizziness ■Cardiac palpitations

This project aims to find a possible pathological cause of pain in a patient suffering from swollen red burning knees after exposition to heat (Figure 4-1). Skin biopsy of the knee in this patient showed reduced nerve fibres whereas nerve fibres in a skin biopsy from the back were within the normal range. The patient also suffers from a secondary erythromelalgia-like (EM) phenotype, with redness of the skin associated with the burning pain in the knee (1.1.5V.i). We also found similar symptoms in the family members of the patient; the patient's father does report pain, swelling and redness of both knees upon physical exertion such as walking downhill.The symptoms started in adult age. The patient's grandmother (the father's mother) does also report pain, swelling and occasionally also redness of both knees upon exertion. The symptom started at a relatively young age. The symptoms of these relatives appear to be similar to those reported by the patient but less distinct. Also, the cousin (the father's sister's son) is reported to have a recurring red ear syndrome (swelling and pain of the right ear). Of note, he is suffering from severe intractable epilepsy and mental retardation after encephalitis of unknown etiology at the age of 3 years. As discussed above, several genes are already known to be the underlying cause of SFNs, peripheral neuropathies and EM. We therefore aimed to investigate if this disorder is caused by a mutation within a gene, leading to SFNs and EM. We first attempted to identify whether any mutations are linked to *SCN9A* since this gene has been known to be a major cause of SFNs and IEM (1.1.5V.i, 1.1.5V.iv). Secondly, exome sequencing was performed to identify any potential causative mutations in other genes. We found three novel point mutations which are likely to be pathogenic; in *CWC22*, *TMEM8B* and *ATL3* (atlastin GTPase 3). These mutations result in an amino acid change, aspartic acid to tyrosine in CWC22, proline to serine at position 148 in TMEM8B and proline to leucine in

ATL3, respectively. We confirmed these mutations in the proband by Sanger sequencing. These findings, if proven to be the causative mutation, is the first report of *CWC22*, *TMEM8B* or *ATL3* as a cause of painful small fibre neuropathy.

Figure 4-1. A picture of the patient's knee (taken by Dr. Thomas Tölle and Dr. Isabel Voth at Universität München in Germany)

4.2 AIMS OF THE PROJECT

The aim of this project is to identify a causative mutation in a patient who was diagnosed with SFN and an associated EM-like phenotype. To investigate the potential causative mutation, the coding exons and intronic splice sequences of *SCN9A* were firstly screened by Sanger sequencing. Secondly, whole-exome sequencing was performed. Thirdly, further analysis was performed to rank the novel variants in terms of their likely pathogenicity. Finally, Sanger sequencing was conducted to validate the existence of the novel mutations identified in *CWC22*, *TMEM8B* and *ATL3*.

4.3 METHOD

4.3.1 Subject and clinical phenotype

A male patient (born in 1988) was referred to the Wood lab by Dr. Thomas Tölle and Dr. Isabel Voth (Universität München in Germany) after complaining of swollen red burning knees (on the left more than on the right side) after being exposed to heat. The symptoms first started in 2009/10 (left knee) and 2011/12 (right knee) respectively with an oedema after hard physical work. Due to retropatellar cartilage damage, the patient received an autologous cartilage transplantation in the left knee in January 2010. This did not lead to a clinical improvement although the left knee MRI scan result eleven months later was unremarkable. The MRI of the right knee in December 2013 also revealed marked cartilage damage without signs of arthritis and without contrast medium uptake. Laboratory parameters including leukocytes, CRP, blood count were within the normal range including no signs of lyme disease. A skeletal scintigraphy in January 2014 and an examination in the Rheumatological department were inconspicuous. Skin biopsy (left knee and paravertebral Th8 on the right side) revealed reduced nerve fibres in the knee whereas nerve fibres in the back were within the normal range. The knees were the unique manifestation areas. Family history of the phenotype was negative and there were no pre-existing diseases and the patient did not take regular medications apart from omeprazol 20 mg/d because of oesophageal reflux disease. Intravenous lidocaine ameliorated the pain from Numerical rating scale (NRS) 5/10 to 1-2/10. There was a questionable weak response to carbamazepine. Medication with oral corticoids, ibuprofen, voltaren, pregabalin, amitriptylin, lidocaine patch or ASS 100 mg/d remained ineffective. Application of cold and Swedish bitters lead to an improvement of pain for 2-3 hours.

4.3.2 gDNA extraction

Performed by Dr. James Cox, WIBR, UCL

Informed consent was taken from the patient prior to genetic analysis at UCL. A blood sample from the patient was collected and stored in dry ice by Dr. Isabel Voth at Universität München in Germany and shipped to the UK. The gDNA was extracted using a QIAamp Blood Midi Kit (Qiagen, 51183), according to the manufacturer's instructions. The extracted gDNA was kept at 80℃ for long-term and -20℃ for short-term storage.

4.3.3 Mutation detection for *SCN9A*

We initially aimed to find mutations in *SCN9A* since it is known to be a major cause of small fibre neuropathy (1.1.5V.iv). Total genomic DNA (gDNA) isolated from the patient's blood sample was used to screen for mutations. The gDNA was amplified using the following primer pairs (Table 4-3) and mixtures: 5 µl of 5x colourless GoTaq buffer (Promega, M7801), 2.5 µl of 25mM magnesium chloride (Promega, M7801), 0.5 µl of 10mM dNTPs (KAPA Biosystems, KK1017), 0.125 µl of GoTaq G2 Flexi DNA Polymerase (Promega, M7801) and 1ul of 25 ng/µl gDNA (or 1 µl of water as a negative control), 0.5 µl of each forward and reverse primer (10 µM) and nuclease free water to fill up to 25 µl/ reaction. The cycling conditions were: 3 min at 95°C, 35 cycles of 30 sec at 94°C, 30 sec at 55°C and 30 sec at 72°C and 5 min at 72°C for final extension. The PCR products were checked with agarose gel electrophoresis. To remove and dephosphorylate unused primers and dNTPs, 0.25 µl of exonuclease I and 0.5 µl of Shrimp Alkaline Phosphatase were added into the PCR products and incubated for 30 min at 37°C and 20 min at 80°C. Following this clean-up step, the PCR products were Sanger sequenced to screen for mutations using the primers stated in Table 4-3.

Table 4-3. Primer pairs for *SCN9A* mutation screening. (Cox et al., 2006)

Coding Exon	Forward primer (5'-3')	Reverse primer (5'-3')	PCR products (bp)
1	CCTTTCTTGGCAGGCAAAT	AAGCCAACAGAAACTGACCA	400
2	AGATGCGTTGATGACATTGG	CCAGAGTCTTTCAAGGTGCAA	377
3	TTCAAAGAGACAAAATAGTCTACAAGC	CTGGCAGGAAAAGGAAAGG	295
4	AAGTTATAAAGATTTACATGGTGGTTG	ACCCCAGAGGTTTGCTGTTA	283
5	GAAGCCCCAAACGTAGAAAA	TCTTTCTTTCAAAAGATCAAAGTCA	444
6	AGGTTACTTAAGGTCATTGATTTGA	AAAAGAGAGCAATGTTTTTAGCA	390
7	GGACCAGGCCTGAATTTGTA	TGCAAACTGACTGAACATTCTTT	247
8	TCCCCCTATAGAAGAAACCTTGA	GAGTTTCCTCCATTCTCAAATAAA	353
9	CAGATTTGCTCATGCCTGTC	TCTAGCTGGAGAAGGCCAAG	386
10	TCATTGTGTAAAGAAAACGATCA	AAGACATTTTTCTCTAGCATTCTGC	498
11	GCCAGTGGGTTCAGTGGTAT	GCCATGCCTGAGCTATGTAA	488
12	TTGAACCCAGCAATCTAGGC	TGTGCCTATTTAAGGTTGACCA	330
13	TTTCAATATTAGAATGCCTGACTGA	TGAAATGACAATGATGACAACTAAAA	396
14	TGATGAGCACTGACAGGACA	TGCAAAACCAAAGAAATACCC	467
15	TGCTTTACCCTTTGAACAAAAA	CATCACAAAATAATTTCCACAGAGA	500
16	CCTGTCTCCCTATTTCTCTACCC	TGCAATGTTAAGAAGAACTTATGACAA	621
17	TTTTTCATAATACTTTGCATGAGTCTG	CGTTAAGACAAACCCCAGAA	291
18	TGAGGGAGTATCACAGAAAGCA	AGGTAAAACAACTTGCCATGA	348
19	CAGCTGGCCCATGTCAATA	TTCACAACACACAGTAAGAATAAATCC	356
20	TGTTGAGTTGCTTTTAGTGAGTTT	TCATAATTTCTACATACCCATTGTTTT	300
21	TGTCTGCATGGCATTTCTTT	AAGAATAACTTATATCCTTCGTCCAA	431
22	CAGACAAAACTCTGTTTATGGCTATT	TGAGTCCCAAGGGCTTCAT	228
23	CCTCAACAATGCTATGGCTTC	TTGTTTTCTGTGCAAAAATGAAT	463
24	CTGTGTTTGGAGACCCATGTT	TCCAGAAATTAAAGATGTGCATT	378
25	ATTCCTCGACCAGGGGTAAA	TTCAGCATATACTTCCTTGAGCA	498
26A	TTGAATTCATAAGAAATGAGTTGACA	CAGTCGGGTGGCTTACTGTT	476
26B	GACCTTTGGCAACAGTATGATT	TTTGGAAGGATTTGCAGACA	577
26C	ACCGGATCCATTGTCTTGA	ACAGGCTGTAAACAATATATCAAAAA	500

4.3.4 Whole-exome sequencing

Whole-exome sequencing was carried out by BGI TECH SOLUTIONS (HONGKONG) CO., LIMITED using the Agilent SureSelect Human All Exon 50Mb V5 kit with sequencing performed on the Illumina HiSeq4000 with a 100x mean depth coverage. Sequencing data was analysed according to a custom pipeline in the laboratory of Dr Jose Bras (Institute of Neurology, UCL) with the aim of identifying novel variants not previously identified in public polymorphism databases. Briefly, sequence alignment and variant calling was performed against the reference human genome assembly (hg19) by using the Burrows-Wheeler Aligner (Li and Durbin, 2009) and the Genome Analysis Toolkit (DePristo et al., 2011, McKenna et al., 2010). Format conversion and indexing were performed with the Picard software. Single nucleotide variants and small insertions and deletions were checked against established databases (1000 Genomes Project and dbSNP v.142). Then, variants were further checked using the ExAC browser, dbSNP v.147 and Kaviar (http://db.systemsbiology.net/kaviar/). The protein coding effects of variants was predicted using SIFT (http://sift.jcvi.org/www/SIFT_enst_submit.html), Polyphen2 (http://genetics.bwh.harvard.edu/pph2/), Provean (http://provean.jcvi.org/seq_submit.php) and M-CAP (http://bejerano.stanford.edu/mcap/)(Jagadeesh et al., 2016). The location of the amino acid was predicted using SMART (http://smart.embl-heidelberg.de/). Splicing changes were analysed using the NNSPLICE Splice Site Predictor (http://www.fruitfly.org/seq_tools/splice.html). Novel variants were verified by Sanger sequencing (4.3.5).

4.3.5 Mutation detection for *ATL3*, *CWC22* and *TMEM8B*

To verify the exome sequencing results, the *ATL3* and *CWC22* mutation regions were amplified with the above protocol (4.3.3) using the following primers and cycling conditions:

ATL3 Forward; GAATACTTTGCTAAAAAGGCCATAG

ATL3 Reverse; CACAGAGCTTACTTTTTAAGCGATT

CWC22 Forward; CCCTACTCATTTCATTTAGATAGCA

CWC22 Reverse; TGAAGAGGAAGAGGATGGG

3 min at 95°C, 35 cycles of 30 sec at 94°C, 30 sec at 53.4°C (*ATL3*) or 52°C (*CWC22*) and 30 sec at 72°C and 5 min at 72°C for final extension. To verify the mutation within *TMEM8B*, the region was amplified using the following primer pair and mixture; 12.5 µl of 2x PremixJ (epicentre FSP995J), 0.125 µl of GoTaq G2 Flexi DNA Polymerase (Promega, M7801) and 1ul of 25 ng/µl gDNA (or 1 µl of water as a negative control), 0.5 µl of forward and reverse primer (10 µM) and nuclease free water to fill up to 25 µl/ reaction. The cycling condition was: 2 min at 95°C, 35 cycles of 30 sec at 95°C, 1min at 63.5°C and 40 sec at 72°C and 5 min at 72°C for final extension.

TMEM8B Forward; CTGCGCACTCCCCTACTCCC

TMEM8B Reverse; GATGGAATGGAGGAATGATAGGC

The PCR product (~450bp for *ATL3*, ~470bp for *CWC22* and ~550bp for *TMEM8B*) was checked with QIAxcel Screen gel (Qiagen) and cleaned-up using the EXOSAP protocol described above (4.3.3). The PCR product was Sanger sequenced to verify the mutation using the same primer pairs for amplification stated above.

4.4 RESULTS

4.4.1 Novel variants are absent in *SCN9A*

gDNA extraction was performed by Dr. James Cox at Molecular Nociception Group, WIBR, UCL. All the other procedures were performed by myself.

We considered that the cause of small fibre neuropathy with associated erythromelalgia at the knee in this patient could be linked to a mutation in *SCN9A,* since this gene is known to be associated with IEM and SFN (Faber et al., 2012a, Yang et al., 2004) (1.1.5II). We therefore attempted to perform Sanger sequencing for this gene. Genomic DNA was used as template to amplify all the coding exons and flanking intronic splice site sequences. A single band was observed by electrophoresis from each reaction, but not in the negative control in which gDNA was not added (Figure 4-2). These PCR products were Sanger sequenced and compared to reference sequence using BLAST2sequences (https://www.ncbi.nlm.nih.gov/blast). No novel variants were identified.

Another potential causative mutation could be in *SCN10A* and *SCN11A* encoding $Na_v1.8$ and $Na_v1.9$ respectively since these genes are also linked to SFN (Faber et al., 2012b, Huang et al., 2013, Han et al., 2015b) (see 1.1.5V.iv). In addition, several genes have been documented as a cause of peripheral neuropathies (Bennett and Woods, 2014, Rotthier et al., 2012) (see 4.1), indicating that a potential causative mutation might be linked to not only VGSCs, but also other genes. We therefore decided to perform whole-exome sequencing to identify the causative mutation in this patient.

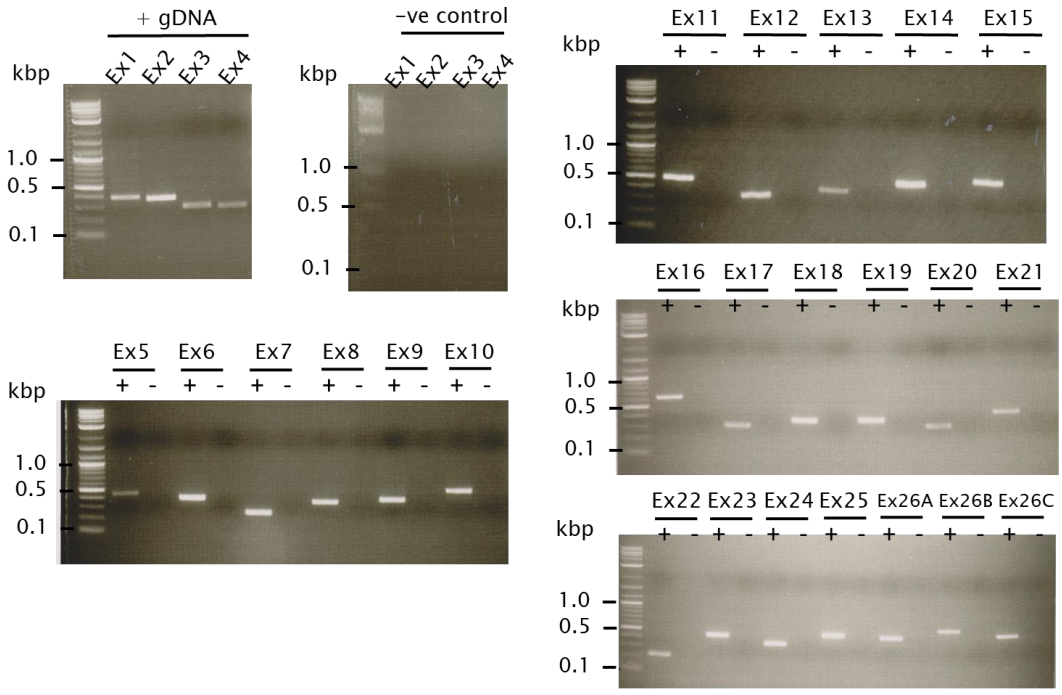

Figure 4-2. Agarose gel electrophoresis of PCR products using *SCN9A* primer pairs. Ex1 stands for PCR products using the primer pair to amplify exon 1. +/+ gDNA; gDNA was added to amplify. -/ -ve control; negative control without gDNA.

4.4.2 Three potential causative mutations identified by exome sequencing

Whole-exome sequencing was carried out by BGI TECH SOLUTIONS (HONGKONG) CO., LIMITED. The exome sequence data was initially analysed by Dr. Jose Bras (Institute of Neurology, UCL). Further checking the variants in established database and shortlisting the novel variants were performed by myself.

Whole-exome sequencing was performed to identify potential mutations that could be causing this painful phenotype. The exome sequence data was analysed by Dr Jose Bras according to a custom pipeline and several novel variants were identified (seeTable 4-4).

Table 4-4. The list of potential novel variants identified by whole-exome sequencing.

Chromosome	Position	REF	ALT	Gene name	Full name	Annotation	Accession number	cDNA change	Protein change
1	32678146	C	T	DCDC2B	doublecortin domain containing 2B	missense_variant	ENST00000409358	c.583C>T	p.His195Tyr
1	55182327	A	G	TTC4	tetratricopeptide repeat domain 4	missense_variant	ENST00000371281	c.166A>G	p.Arg56Gly
1	55525220	C	T	PCSK9	proprotein convertase subtilisin/kexin type 9	missense_variant	ENST00000302118	c.1565C>T	p.Ala522Val
1	94344698	C	T	DNTTIP2	deoxynucleotidyltransferase, terminal, interacting protein 2	missense_variant	ENST00000436063	c.7G>A	p.Val3Ile
2	27726455	A	G	GCKR	glucokinase (hexokinase 4) regulator	missense_variant	ENST00000264717	c.719A>G	p.Gln240Arg
2	31152344	C	G	GALNT14	UDP-N-acetyl-alpha-D-galactosamine:polypeptide N-acetylgalactosaminyltransferase 14	missense_variant	ENST00000324589	c.1083G>C	p.Lys361Asn
2	44507970	A	C	SLC3A1	solute carrier family 3 (amino acid transporter heavy chain), member 1	missense_variant	ENST00000260649	c.546A>C	p.Glu182Asp
2	88890379	A	G	EIF2AK3	eukaryotic translation initiation factor 2-alpha kinase 3	missense_variant	ENST00000303236	c.959T>C	p.Met320Thr
2	125622894	G	T	CNTNAP5	contactin associated protein-like 5	missense_variant	ENST00000431078	c.3226G>T	p.Val1076Phe
2	180815616	C	A	CWC22	CWC22 spliceosome-associated protein homolog (S. cerevisiae)	missense_variant	ENST00000295749	c.1855G>T	p.Asp619Tyr
2	233498472	G	A	EFHD1	EF-hand domain family, member D1	missense_variant	ENST00000264059	c.58G>A	p.Glu20Lys
3	49041656	G	T	P4HTM	prolyl 4-hydroxylase, transmembrane	stop_gained	ENST00000343546	c.850G>T	p.Glu284*

3	183756161	C	A	HTR3D	5-hydroxytryptamine (serotonin) receptor 3D, ionotropic	missense_variant	ENST00000382489	c.884C>A	p.Ala295Glu
4	39558151	A	G	SMIM14	small integral membrane protein 14	missense_variant	ENST00000295958	c.164T>C	p.Met55Thr
4	88535521	T	A	DSPP	dentin sialophosphoprotein	missense_variant	ENST00000282478	c.1707T>A	p.Ser569Arg
6	16327911	G	T	ATXN1	ataxin 1	missense_variant	ENST00000244769	c.631C>A	p.His211Asn
6	16327914	G	T	ATXN1	ataxin 1	missense_variant	ENST00000244769	c.628C>A	p.Gln210Lys
6	16327917	G	T	ATXN1	ataxin 1	missense_variant	ENST00000244769	c.625C>A	p.His209Asn
6	17601035	A	G	FAM8A1	family with sequence similarity 8, member A1	missense_variant	ENST00000259963	c.395A>G	p.His132Arg
6	17601040	G	A	FAM8A1	family with sequence similarity 8, member A1	missense_variant	ENST00000259963	c.400G>A	p.Gly134Ser
6	17601041	G	T	FAM8A1	family with sequence similarity 8, member A1	missense_variant	ENST00000259963	c.401G>T	p.Gly134Val
6	17601044	T	C	FAM8A1	family with sequence similarity 8, member A1	missense_variant	ENST00000259963	c.404T>C	p.Leu135Pro
6	17601058	G	A	FAM8A1	family with sequence similarity 8, member A1	missense_variant	ENST00000259963	c.418G>A	p.Ala140Thr
7	781078	A	C	HEATR2	HEAT repeat containing 2	missense_variant	ENST00000297440	c.1000A>C	p.Thr334Pro
7	100616336	G	A	MUC12	mucin 12, cell surface associated	stop_gained	ENST00000379442	c.299G>A	p.Trp100*
7	100616338	A	G	MUC12	mucin 12, cell surface associated	missense_variant	ENST00000379442	c.301A>G	p.Met101Val
7	100616344	G	A	MUC12	mucin 12, cell surface associated	missense_variant	ENST00000379442	c.307G>A	p.Gly103Arg
7	150934746	A	T	CHPF2	chondroitin polymerizing factor 2	missense_variant	ENST00000035307	c.1298A>T	p.Tyr433Phe
8	55541954	C	T	RP1	retinitis pigmentosa 1 (autosomal dominant)	missense_variant	ENST00000220676	c.5512C>T	p.Arg1838Cys
8	77618788	A	G	ZFHX4	zinc finger homeobox 4	missense_variant	ENST00000521891	c.2465A>G	p.Gln822Arg
9	12695536	T	A	TYRP1	tyrosinase-related protein 1	stop_gained	ENST00000388918	c.407T>A	p.Leu136*
9	35846323	C	T	TMEM8B	transmembrane protein 8B	missense_variant	ENST00000377988	c.442C>T	p.Pro148Ser

9	132571650	A	C	TOR1B	torsin family 1, member B (torsin B)	missense_variant	ENST00000259339	c.799A>C	p.Lys267Gln
9	140130633	T	C	SLC34A3	solute carrier family 34 (type II sodium/phosphate contransporter), member 3	missense_variant	ENST00000361134	c.1565T>C	p.Val522Ala
10	30653870	A	C	MTPAP	mitochondrial poly(A) polymerase	missense_variant	ENST00000358107	c.312T>G	p.Cys104Trp
11	1017024	T	A	MUC6	mucin 6, oligomeric mucus/gel-forming	missense_variant	ENST00000421673	c.5777A>T	p.His1926Leu
11	1018248	G	A	MUC6	mucin 6, oligomeric mucus/gel-forming	missense_variant	ENST00000421673	c.4553C>T	p.Thr1518Ile
11	1018272	C	G	MUC6	mucin 6, oligomeric mucus/gel-forming	missense_variant	ENST00000421673	c.4529G>C	p.Ser1510Thr
11	1018281	C	A	MUC6	mucin 6, oligomeric mucus/gel-forming	missense_variant	ENST00000421673	c.4520G>T	p.Ser1507Ile
11	1018303	G	A	MUC6	mucin 6, oligomeric mucus/gel-forming	missense_variant	ENST00000421673	c.4498C>T	p.Pro1500Ser
11	13408154	C	G	ARNTL	aryl hydrocarbon receptor nuclear translocator-like	missense_variant	ENST00000403290	c.1732C>G	p.His578Asp
11	22364859	A	T	SLC17A6	solute carrier family 17 (vesicular glutamate transporter), member 6	missense_variant	ENST00000263160	c.406A>T	p.Ile136Phe
11	62288795	T	C	AHNAK	AHNAK nucleoprotein	missense_variant	ENST00000378024	c.13094A>G	p.Asp4365Gly
11	63413986	G	A	ATL3	atlastin GTPase 3	missense_variant	ENST00000332645	c.692C>T	p.Pro231Leu
11	64056685	A	C	GPR137	G protein-coupled receptor 137	missense_variant	ENST00000411458	c.1276A>C	p.Thr426Pro
11	64693249	T	C	PPP2R5B	protein phosphatase 2, regulatory subunit B', beta	missense_variant	ENST00000164133	c.43T>C	p.Ser15Pro
11	78387405	C	T	TENM4	teneurin transmembrane protein 4	missense_variant	ENST00000278550	c.5288G>A	p.Gly1763Glu
11	85437941	T	A	SYTL2	synaptotagmin-like 2	missense_variant	ENST00000359152	c.1131A>T	p.Glu377Asp
12	27933640	G	A	KLHL42	kelch-like family member 42	missense_variant	ENST00000381271	c.377G>A	p.Arg126Gln

12	65456282	C	T	WIF1	WNT inhibitory factor 1	missense_variant	ENST00000286574	c.805G>A	p.Glu269Lys
12	132476749	C	T	EP400	E1A binding protein p400	missense_variant	ENST00000333577	c.2819C>T	p.Ala940Val
13	25457398	C	G	CENPJ	centromere protein J	missense_variant	ENST00000381884	c.3934G>C	p.Gly1312Arg
13	32747570	G	A	FRY	furry homolog (Drosophila)	missense_variant	ENST00000380250	c.2218G>A	p.Ala740Thr
13	41943395	A	C	NAA16	N(alpha)-acetyltransferase 16, NatA auxiliary subunit	missense_variant	ENST00000379406	c.1923A>C	p.Glu641Asp
14	59931032	G	T	GPR135	G protein-coupled receptor 135	missense_variant	ENST00000395116	c.913C>A	p.Arg305Ser
14	103986810	G	C	CKB	creatine kinase, brain	missense_variant	ENST00000348956	c.773C>G	p.Thr258Ser
15	80743305	T	G	ARNT2	aryl-hydrocarbon receptor nuclear translocator 2	missense_variant	ENST00000303329	c.116T>G	p.Met39Arg
15	85438282	G	A	SLC28A1	solute carrier family 28 (concentrative nucleoside transporter), member 1	missense_variant	ENST00000286749	c.389G>A	p.Arg130Gln
15	89395171	G	A	ACAN	Aggrecan	missense_variant	ENST00000439576	c.2173G>A	p.Glu725Lys
16	2287501	T	C	DNASE1L2	deoxyribonuclease 1-like 2	missense_variant	ENST00000320700	c.442T>C	p.Ser148Pro
16	2287505	G	C	DNASE1L2	deoxyribonuclease 1-like 2	missense_variant	ENST00000320700	c.446G>C	p.Arg149Pro
16	66511573	G	A	BEAN1	brain expressed, associated with NEDD4, 1	missense_variant	ENST00000536005	c.400G>A	p.Ala134Thr
16	84199443	A	T	DNAAF1	dynein, axonemal, assembly factor 1	missense_variant	ENST00000378553	c.918A>T	p.Arg306Ser
17	17722734	G	C	SREBF1	sterol regulatory element binding transcription factor 1	missense_variant	ENST00000355815	c.836C>G	p.Ser279Trp
17	38445704	C	T	CDC6	cell division cycle 6	missense_variant	ENST00000209728	c.32C>T	p.Thr11Ile
17	47284159	T	C	GNGT2	guanine nucleotide binding protein (G protein), gamma transducing activity polypeptide 2	missense_variant	ENST00000503070	c.170A>G	p.Lys57Arg

17	77111776	C	G	RBFOX3	RNA binding protein, fox-1 homolog (C. elegans) 3	missense_variant	ENST00000583458	c.22G>C	p.Ala8Pro
19	9000169	C	T	MUC16	mucin 16, cell surface associated	missense_variant	ENST00000397910	c.40588G>A	p.Gly13530Ser
19	9000187	C	T	MUC16	mucin 16, cell surface associated	missense_variant	ENST00000397910	c.40570G>A	p.Val13524Ile
19	9000205	C	A	MUC16	mucin 16, cell surface associated	missense_variant	ENST00000397910	c.40552G>T	p.Val13518Leu
19	9009652	C	T	MUC16	mucin 16, cell surface associated	missense_variant	ENST00000397910	c.39074G>A	p.Gly13025Glu
19	9406273	G	C	ZNF699	zinc finger protein 699	missense_variant	ENST00000308650	c.1807C>G	p.Arg603Gly
19	10335016	T	C	S1PR2	sphingosine-1-phosphate receptor 2	missense_variant	ENST00000590320	c.566A>G	p.His189Arg
19	13192535	A	G	NFIX	nuclear factor I/X (CCAAT-binding transcription factor)	missense_variant	ENST00000592199	c.1120A>G	p.Thr374Ala

To shortlist the most likely pathogenic mutations we used the following strategy; 1. The 74 variants (Table 4-4) were further checked using the ExAC browser and dbSNP v.147 (Table 4-5) to exclude newly reported polymorphic variants. 2. Remaining novel variants were further analysed by several algorithms to predict the protein coding effects of the mutations. Mendelian disorders associated with each gene were also searched (Table 4-6). 3. The variants which showed pathogenic effects predicted by the algorithms were further checked by using other tools to analyse how the mutation was likely to alter the gene product. The expression levels of the genes in mouse DRG were also considered (Table 4-7).

Firstly, the 74 variants were checked using the ExAC browser and dbSNP v.147 and we found that 35 variants do not have any polymorphisms at the position of the novel variants (Table 4-5). Next, we narrowed the search to these 35 variants to rank the novel variants in terms of their likely pathogenicity. The protein coding effects of these 35 variants were predicted using Polyphen2, Provean and SIFT for missense mutations. For the stop codon variants, we checked the numbers of known loss of function (LoF) mutations (nonsense, splice acceptor, and splice donor variants caused by single nucleotide changes) within the gene and the pLI score offered by ExAc. According to ExAc, pLI stands for probability of LoF intolerance and the closer pLI is to one, the more LoF intolerant the gene appears to be. ExAc considers pLI >= 0.9 as an extremely LoF intolerant set of genes. In addition to these predictions, another three analyses were performed in order to strengthen the possibility of the selected variants as being novel pathogenic mutations; SMART prediction, Mendelian disorders and functions of the genes. SMART was used to identify if the variants were within a domain; the variants within a domain can be more likely to alter the function of the protein leading to gain- or loss-of-function mutations. Mendelian disorders of the gene were checked to compare with the clinical features of the patient. Functions of the mutated gene were searched to support the initial selection of possible pathogenic variants. These analyses are shown in Table 4-6. Among the 35 variants listed in Table 4-6, we settled on three variants for future initial functional studies by using these two criteria; 1. All Polyphen2, Provean and SIFT predictions are 'Damaging' or equivalent. 2. A variant is not within a gene which is associated with Mendelian disorders apart from the patient's clinical phenotype. The three variants we settled on are within CWC22, TMEM8B and ATL3. Of note, since the pLI score of *P4HTM* (prolyl 4-hydroxylase, transmembrane) and *TYRP1* (tyrosinase-related protein 1) are 0.02 and 0.00, respectively, we excluded the two variants within P4HTM and TYRP1 from this initial selection. Then, splicing changes were analysed using the NNSPLICE Splice Site Predictor and M-CAP was also used to predict the protein coding effects of these three variants within *CWC22* (CWC22 spliceosome-associated protein homolog), *TMEM8B* (transmembrane protein 8B)

and *ALT3* (atlastin GTPase 3). Kaviar was used to verify again if there are no known variants at the position. Splicing changes were not predicted for all three variants and M-CAP showed they are possibly pathogenic (Table 4-7). Kaviar also demonstrated these three variants were novel (Table 4-7). The recent RNA-seq data (Usoskin et al., 2015) has highlighted a relatively high expression of the three genes in DRG neurons (Table 4-7). The expression of these genes in DRG showed medium to high levels among different tissues in mice (Figure 4-3), suggesting that these genes may play an important role in sensory neurons.

Table 4-5. Variants shortlisted from the whole-exome sequencing by dbSNP v147 and ExAC.

Gene name	cDNA change	Protein change	dbSNP 147	EVS variants	ExAC (UCSC)	ExAC browser	Genome variants
DCDC2B	c.583C>T	p.His195Tyr	No	No	No	No	No
TTC4	c.166A>G	p.Arg56Gly	No	No	No	No	No
PCSK9	c.1565C>T	p.Ala522Val	No but p.55525219 is rs777300852 G>A/G	No	No but p.55525219 G>A/G	No but p.55525219 G>A; p.Ala522Thr	No
DNTTIP2	c.7G>A	p.Val3Ile	Not same SNP but rs748109096; C>A/C	No	Not same but C>A	Not same but C/A; p.Val3Phe	No
GCKR	c.719A>G	p.Gln240Arg	No but p.27726454; rs764135777 C>C/T	No	No but p.27726454 C>C/T	No but p.27726454 C>T; p.Gln240Ter	No
GALNT14	c.1083G>C	p.Lys361Asn	No	No	No	No	No
SLC3A1	c.546A>C	p.Glu182Asp	No but p.44507968; rs549909989 G>A/G	No	No but p.44507968 G>A/G	No but p.44507968 G>A; p.Glu182Lys	No
EIF2AK3	c.959T>C	p.Met320Thr	No	No	No	No	No
CNTNAP5	c.3226G>T	p.Val1076Phe	No	No	No	No	No
CWC22	c.1855G>T	p.Asp619Tyr	No	No	No	No	No
EFHD1	c.58G>A	p.Glu20Lys	No	No	No	No	No
P4HTM	c.850G>T	p.Glu284*	No	No	No	No	No
HTR3D	c.884C>A	p.Ala295Glu	Not same SNP but rs745457011; C>T, p.183756162 rs370039191; G>A (Ala>Ala)	No	Not same but p. 3:183756161 C/T	Not same but missense C/T; p.Ala295Val, p.183756162 synonymous G/A; p.Ala295Ala	No
SMIM14	c.164T>C	p.Met55Thr	No	No	No	No	No
DSPP	c.1707T>A	p.Ser569Arg	rs765730532; chr4:88535503-88535550 frame indel	No	No	No	No

ATXN1	c.631C>A	p.His211Asn	Not same SNP but rs745595519 is H>Y; region very polymorphic with numerous indels	No	Not same SNP but region very polymorphic with numerous indels	Not same SNP but region very polymorphic with numerous indels	No
ATXN1	c.628C>A	p.Gln210Lys	Not same SNP but rs751377396 is -/TGA deletion; region very polymorphic with numerous indels	No	Not same SNP but region very polymorphic with numerous indels	Not same SNP but region very polymorphic with numerous indels	No
ATXN1	c.625C>A	p.His209Asn	Not same SNP but rs769636450 is -/TGCTGATGC deletion, rs775260870 is -/TGCTGATGCTGCTGCTGC deletion; region very polymorphic with numerous indels	No	Not same SNP but region very polymorphic with numerous indels	Not same SNP but region very polymorphic with numerous indels	No
FAM8A1	c.395A>G	p.His132Arg	No	No	No	No	No
FAM8A1	c.400G>A	p.Gly134Ser	No but p.17601041; rs748609966 is G>A	No	No but p.17601041 G>A	No but p.17601041 G>A; p.Gly134Asp	No
FAM8A1	c.401G>T	p.Gly134Val	Not same SNP but rs748609966 is G>A	No	Not same but G>A	Not same but G>A; p.Gly134Asp	No
FAM8A1	c.404T>C	p.Leu135Pro	No	No	No	No	No
FAM8A1	c.418G>A	p.Ala140Thr	No	No	No	No	No
HEATR2	c.1000A>C	p.Thr334Pro	No	No	No	No	No
MUC12	c.299G>A	p.Trp100*	rs796345412	No	No	No	No
MUC12	c.301A>G	p.Met101Val	rs796961768	No	No	No	No
MUC12	c.307G>A	p.Gly103Arg	rs796198853	No	No	No	No
CHPF2	c.1298A>T	p.Tyr433Phe	Not same SNP but rs764967022 is A>G, p. 150934745; rs754765489 T>C	No	Not same but A>G, p. 150934745 is T>C	Not same but A>G; p.Tyr433Cys, p. 150934745 is T>C; p.Tyr433His	No

RP1	c.5512C>T	p.Arg1838Cys	No but p. 55541955; rs576959220 G>A	No	No but p.55541955 G/A	No but p.55541955 G>A; p.Arg1838His	No
ZFHX4	c.2465A>G	p.Gln822Arg	No	No	No	No	No
TYRP1	c.407T>A	p.Leu136*	Not same but rs749735228; chr9:12695536-12695535 insertion -/TAAG frameshift, rs780407909; chr9:12695535-12695534 insertion -/TT frameshift, rs769074792; chr9:12695537-12695541 deletion -/AAGTA frameshift	No	Not same but 9:12695534 C/CTT, 9:12695535 T/TTAAG, 9:12695536 TAAGTA/T	Not same but 9:12695534 C / CTT; p.Leu136PhefsTer2 frameshift, 9:12695535 T / TTAAG; p.Glu139Ter frameshift, 9:12695536 TAAGTA / T; p.Ser137ArgfsTer42 frameshift	No
TMEM8B	c.442C>T	p.Pro148Ser	No. Synonymous SNP at chr9:35846325 resulting in Pro148Pro (rs557315408 G>A)	No	No. Synonymous SNP at chr9:35846325 resulting in Pro148Pro	No. Synonymous SNP at chr9:35846325 resulting in Pro148Pro	No
TOR1B	c.799A>C	p.Lys267Gln	No	No	No	No	
SLC34A3	c.1565T>C	p.Val522Ala	No but chr9:140130632; rs149912630 G>T, chr9:140130634; rs182451910 G>A/T	No but chr9:140130632 G>T	No but 9:140130632 G>T; p.Val522Leu, 9:140130634 G>T/A; p.Val522Val	No but 9:140130632 (rs149912630) G>T; p.Val522Leu, 9:140130634 (rs182451910) G>T/A; p.Val522Val	
MTPAP	c.312T>G	p.Cys104Trp	No but chr10:30653871; rs749557978 C>G	No	No but chr10:30653871 C>G; p.Cys104Ser	No but 10:30653871 C>G; p.Cys104Ser	
MUC6	c.5777A>T	p.His1926Leu	rs796211588	No	No	No	No
MUC6	c.4553C>T	p.Thr1518Ile	Not same SNP but chr11:1018245-1018249; rs777137413 is TTTGT deletion frameshift		Not same but 11:1018244 GTTTGT/G	No	No

MUC6	c.4529G>C	p.Ser1510Thr	rs796397888	No	No	No	No
MUC6	c.4520G>T	p.Ser1507Ile	rs796398923	No	No	No	No
MUC6	c.4498C>T	p.Pro1500Ser	rs796770803	No	No	No	No
ARNTL	c.1732C>G	p.His578Asp	No. Synonymous SNP at chr11:13408156 resulting in p.His578His (rs150333072)	No	No. Synonymous SNP at chr11:13408156 resulting in p.His578His	No	No
SLC17A6	c.406A>T	p.Ile136Phe	Not same SNP but rs779921521 is A>G	No	Not same but 11:22364859 A/G	Not same but 11:22364859 A / G; p.Ile136Val (VQSRTrancheSNP99.80to99.90)	No
AHNAK	c.13094A>G	p.Asp4365Gly	No	No	No	No	No
ATL3	c.692C>T	p.Pro231Leu	No	No	No	No	No
GPR137	c.1276A>C	p.Thr426Pro	No	No	No	No	No
PPP2R5B	c.43T>C	p.Ser15Pro	No	No	No	No	No
TENM4	c.5288G>A	p.Gly1763Glu	No but chr11:78387406; rs201995608 C>T		No but chr11:78387406 C / T; p.Gly1763Arg	No but 11:78387406 C / T; p.Gly1763Arg	No
SYTL2	c.1131A>T	p.Glu377Asp	No	No	No	No	No
KLHL42	c.377G>A	p.Arg126Gln	No	No	No	No	No
WIF1	c.805G>A	p.Glu269Lys	No but chr12:65456280; rs772563432 C>A		No but chr12:65456280 C / A; p.Glu269Asp	No but 12:65456280 C / A; p.Glu269Asp	No
EP400	c.2819C>T	p.Ala940Val	No	No	No	No	No
CENPJ	c.3934G>C	p.Gly1312Arg	Not same SNP but rs201508087 is C>T	No	Not same but chr13:25457398 C / T ; p.Gly1312Ser	Not same but 13:25457398 C / T ; p.Gly1312Ser	No

FRY	c.2218G>A	p.Ala740Thr	Not same but rs767370919 is G>T, rs575491413 (chr13:32747572) is T>A synonymous	No	Not same but chr13:32747570 G / T; p.Ala740Ser, chr13:32747572 T/A; p.Ala740Ala	Not same but 13:32747570 G / T; p.Ala740Ser, 13:32747572 T / A; p.Ala740Ala	No
NAA16	c.1923A>C	p.Glu641Asp	No. Synonymous SNP rs200001978 A>G	No	No. Synonymous SNP chr13:41943395 A / G; p.Glu641Glu	No. Synonymous SNP 13:41943395 A / G; p.Glu641Glu	No
GPR135	c.913C>A	p.Arg305Ser	No but chr14:59931031; rs763301840 is ?>C/G, synonymous SNP chr14:59931030; rs773281044 is ?>G/T	No	No but chr14:59931031 C / G; p.Arg305Pro, chr14:59931030 G / T; p.Arg305Arg synonymous	No but 14:59931031 C / G; p.Arg305Pro, 14:59931030 G / T; p.Arg305Arg synonymous	No
CKB	c.773C>G	p.Thr258Ser	No. Synonymous SNP chr14:103986809; rs781402849 G>A	No	No. Synonymous SNP chr14:103986809 G / A; p.Thr258Thr	No. Synonymous SNP 14:103986809 G / A; p.Thr258Thr	No
ARNT2	c.116T>G	p.Met39Arg	Not same SNP but rs757807661 is T>C, chr15:80743304; rs752021030 A>G	No	Not same but chr15:80743305 T/C; p.Met39Thr, chr15:80743304 A/G; p.Met39Val	Not same but 15:80743305 T/C; p.Met39Thr, 15:80743304 A/G; p.Met39Val	No
SLC28A1	c.389G>A	p.Arg130Gln	No but chr15:85438281; rs2277577 G>A/C/G	No	No but chr15:85438281 C/T; p.Arg130Trp	No but 15:85438281 C/T; p.Arg130Trp, 15:85438283 GC / G; p.Leu131PhefsTer6 frameshift	No
ACAN	c.2173G>A	p.Glu725Lys	No. Synonymous SNP chr15:89395173; rs774473524 G>A	No	No. Synonymous SNP chr15:89395173 G / A; p.Glu725Glu	No. Synonymous SNP 15:89395173 G / A; p.Glu725Glu	No

DNASE1L2	c.442T>C	p.Ser148Pro	No	No	No	No	No
DNASE1L2	c.446G>C	p.Arg149Pro	No	No	No	No	No
BEAN1	c.400G>A	p.Ala134Thr	No	No	No	No	No
DNAAF1	c.918A>T	p.Arg306Ser	No but chr16:84199442; rs766716060 G>C	No	No but chr16:84199442 G / C; p.Arg306Thr	No but 16:84199442 G / C; p.Arg306Thr	No
SREBF1	c.836C>G	p.Ser279Trp	Not same SNP but rs779049810 is G>A, synonymous SNP chr17:1772273; rs746795124 C>T	No	Not same but chr17:17722734 G / A; p.Ser279Leu, synonymous chr17:17722733 C / T; p.Ser279Ser	Not same but 17:17722734 G / A; p.Ser279Leu, synonymous 17:17722733 C / T; p.Ser279Ser	No
CDC6	c.32C>T	p.Thr11Ile	No but chr17:38445703; rs756261747 A>G	No	No but chr17:38445703 A / G; p.Thr11Ala	No but 17:38445703 A / G; p.Thr11Ala	No
GNGT2	c.170A>G	p.Lys57Arg	No	No	No	No	No
RBFOX3	c.22G>C	p.Ala8Pro	rs745729398; chr17:77111774-77111776 GGC>- deletion (chr17:77111777-9 is GGG)	No	chr17:77111773 GGGC/G	17:77111773 GGGC / G; p.Ala8del inframe deletion, 17:77111776 C / CGGGGGG; p.Pro6_Pro7dup inframe insertion, 17:77111776 C / CGGGGGGG; p.Ala8ProfsTer128 frameshift (all 'VQSRTrancheINDEL99.50to99.90')	No
MUC16	c.40588G>A	p.Gly13530Ser	No	No	No	No	No
MUC16	c.40570G>A	p.Val13524Ile	No	No	No	No	No

MUC16	c.40552G>T	p.Val13518Leu	Not saeme SNP but rs4994076 is C>T, Synonymous SNP chr19:9000203; rs773395274 C>T	No	Not same but chr19:9000205 C / T (rs4994076); p.Val13518Met, synonymous SNP chr19:9000203 C / T; p.Val13518Val	Not same but 19:9000205 C / T (rs4994076); p.Val13518Met, synonymous SNP 19:9000203 C / T; p.Val13518Val	No
MUC16	c.39074G>A	p.Gly13025Glu	rs796671806; C>T	No	No	No	No
ZNF699	c.1807C>G	p.Arg603Gly	Not same SNP but rs748599521 is G>A, chr19:9406272; rs781574708 C>T	No	Not same but chr19:9406273 G / A; p.Arg603Ter, chr19:9406272 C / T; p.Arg603Gln	Not same but 19:9406273 G / A; p.Arg603Ter stop gained, 19:9406272 C / T; p.Arg603Gln	No
S1PR2	c.566A>G	p.His189Arg	No but chr19:10335017; rs150504911 G>C	No but chr19:10335017; rs150504911 G>C	No but chr19:10335017 G / C (rs150504911); p.His189Asp	No but 19:10335017 G / C (rs150504911); p.His189Asp	No
NFIX	c.1120A>G	p.Thr374Ala	No	No	No	No	No

Table 4-6. Protein coding effects by SMART, Polyphen2, Provean and SIFT, Mendelian disorders described in OMIM, and functions of the genes where the variants are located.

Gene name	cDNA change	Protein change	In domain (SMART)	Polyphen2	Provean	SIFT	OMIM	Other notes
DCDC2B	c.583C>T	p.His195Tyr	In Doublecortin (DCX) domain; p.124 to 211	Benign (0.372)	Deleterious (-3.397)	Damaging (0.03)	Deafness, autosomal recessive 66, Nephronophthisis 19	The conserved polymorphic purine-rich STR in intron 2 of the DCDC2 gene (BV677278) can modify DCDC2 expression to various degrees, which may link to changes in neural migration in the central nervous system; Pubmed: 21042874. Dcdc2B is expressed in the developing neocortex; PMID: 16869982
TTC4	c.166A>G	p.Arg56Gly	No	Benign (0.003)	Neutral (-0.247)	Tolerated (0.4)	No Mendelian disorder	TTC4 often mediates protein-protein interactions and chaperone activity. The encoded protein interacts with heat shock proteins 70 and 90. This gene is often mutated in cancer cells.
GALNT14	c.1083G>C	p.Lys361Asn	In Glycosyltransferase like family 2 domain; p.116 to 364	Probably Damaging (0.994) Possibly Damaging (0.847); HumVar	Deleterious (-3.115)	Tolerated (0.11)	No Mendelian disorder	The encoded Golgi proteins catalyze the transfer of N-acetyl-D-galactosamine (GalNAc) to the hydroxyl groups on serines and threonines in target peptides. Playing a role in invasion and migration of cancer cells.
EIF2AK3	c.959T>C	p.Met320Thr	No	Possibly Damaging (0.561) BENIGN (0.109); HumVar	Neutral (-1.254)	Tolerated (0.13)	Wolcott-Rallison syndrome	Wolcott-Rallison syndrome is a rare autosomal recessive disorder characterized by permanent neonatal or early infancy insulin-dependent diabetes. A female patient had pain in many joints and short-trunk dwarfism with normal facies; PubMed: 7094931

CNTNAP5	c.3226G>T	p.Val1076Phe	In LamG domain; p.1036 to 1173	Possibly Damaging (0.942) Possibly Damaging (0.543); HumVar	Deleterious (-3.013)	Tolerated (0.2)	No Mendelian disorder	CNTNAP5 microdeletion in the patients with Autism spectrum disorders; PMID: 20346443. Microdeletion disrupting CNTNAP5 in Autism spectrum disorders family; PMID: 20346443. Cntnap2 KO mice showed ASD related behaviour and neurodevelopmental disorders such as hyperactivity and epileptic seizures; PMID: 21962519
CWC22	c.1855G>T	p.Asp619Tyr	No	Probably Damaging (1) Probably Damaging (0.940); HumVar	Deleterious (-8.579)	Damaging (0)	No Mendelian disorder	CWC22 is required for the exon junction complex assembly that is involved in pre-mRNA splicing, mRNA transport, translation, and nonsense-mediated mRNA decay; PMID: 22961380. CWC22 was aberrantly upregulated in diabetic DRG, and impaired neuronal function. CWC22 attenuated sensory neuron plasticity. Knockdown in vitro enhancing their neurite outgrowth. Axonal delivery of CWC22 siRNA unilaterally to locally knock down the aberrant protein in diabetic nerves improved aspects of sensory function in diabetic mice; PMID: 28250049
EFHD1	c.58G>A	p.Glu20Lys	Low complexity region; p.4-21	Benign (0.062)	Neutral (-0.702)	Tolerated (0.52)	No Mendelian disorder	Increased expression during neuronal differentiation (Tominaga and Tomooka, 2002; PubMed: 12270117). EFHD1 functions as a mitochondrial Ca(2+) sensor underlying Ca(2+)-dependent activation of mitochondrial flashes; PMID: 26975899
P4HTM	c.850G>T	p.Glu284*	In P4Hc (Prolyl 4-hydroxylase alpha subunit homologues) domain; p. 142 to 520	LoF (stop-gained and essential splice sites): 17.7 (Expected no. variants) 6 (Observed no. variants) pLI = 0.02 (The closer pLI is to one, the more LoF intolerant the gene appears to be. ExAc considers pLI >= 0.9 as an extremely LoF intolerant set of genes.)			No Mendelian disorder	P4HTM belongs to a family of enzymes that downregulates expression of hypoxia-induced transcription factors under normoxic conditions. Hypoxia-induced transcription factors play an essential role in cellular and systemic homeostatic responses to hypoxia; PubMed: 12163023

SMIM14	c.164T>C	p.Met55Thr	In Protein of unknown function (DUF2615) domain; p.2 to 98	Benign (0.081)	Deleterious (-3.919)	Tolerated (0.16)	No search results; SMIM1-Blood group, Vel system. SMIM3; No mendelian disorder	SMIM14 is an endoplasmic reticulum (ER) resident type I transmembrane protein, involving in ER retention; PMID: 24499674
FAM8A1	c.395A>G	p.His132Arg	No	Possibly Damaging (0.915) Benign (0.164); HumVar	Neutral (-1.233)	Tolerated (0.46)	No search results	Uncharacterised gene. FAM8A1 was captured by a retrovirus, followed by multiple retrotransposition events, during primate evolution; PMID: 11707071
FAM8A1	c.404T>C	p.Leu135Pro	No	Probably Damaging (1) Probably Damaging (0.972); HumVar	Neutral (-2.482)	Tolerated (0.3)		
FAM8A1	c.418G>A	p.Ala140Thr	No	Benign (0.005)	Neutral (-0.719)	Tolerated (0.26)		
HEATR2	c.1000A>C	p.Thr334Pro	Low complexity region; p.332-345	Benign (0)	Neutral (1.246)	Tolerated (0.28)	Ciliary dyskinesia, primary, 18	Knockdown of Htr2 expression in C. reinhardtii resulted in flagella that lacked outer dynein arms. Htr2-knockdown flagella also showed reduced beat frequency and reduced cell velocity. Knockdown of HEATR2 expression in primary human airway epithelial cells resulted in cilia that lacked outer dynein arms and had truncated or possibly absent inner dynein arms, and caused reduced motility; PubMed: 23040496

ZFHX4	c.2465A>G	p.Gln822Arg	No	Probably Damaging (0.981) Probably Damaging (0.969); HumVar	Deleterious (-3.120)	Tolerated (0.16)	?Ptosis, congenital	The chromosome breakpoints in a male patient with congenital bilateral isolated ptosis and a de novo balanced translocation t(1;8)(p34.3;q21.12); PubMed: 11935336. Zfhx4 was expressed transiently in differentiating P19 embryonal carcinoma cells and C2C12 myoblasts, and ZFHX4 transcripts were expressed in adult human brain, liver and muscle; PMID: 16946494
TYRP1	c.407T>A	p.Leu136*	No	LoF (stop-gained and essential splice sites): 14.5 (Expected no. variants) 25 (Observed no. variants) pLI = 0.00	Albinism, oculocutaneous, type III. Skin/hair/eye pigmentation, variation in, 11 (Melanesian blond hair)			TYRP1 protein is a catalase and is identical to a known human melanosomal protein; PubMed: 1693779. Tyrp1 displayed enriched expression in DRG and a null mutant were more resistant to thermal nociception; PMID: 20633051
TMEM8B	c.442C>T	p.Pro148Ser	No	Probably Damaging (1) Probably Damaging (0.992); HumVar	Deleterious (-7.111)	Damaging (0.02)	No Mendelian disorder	TMEM8B is a negative regulator of cell growth; PubMed: 25378401. Overexpression of TMEM8B reduced cancer cell growth; PubMed: 11565907. Expression of NGX6 was significantly downregulated in colorectal cancers; PubMed: 12918109
TOR1B	c.799A>C	p.Lys267Gln	No	Benign (0.034)	Neutral (-1.170)	Tolerated (0.15)	No Mendelian disorder	TOR1A; Dystonia-1, torsion (involuntary, sustained muscle contractions affecting one or more sites of the body) Tor1b KO mice had lack of phenotype; PMID: 27653693. SNP within TOR1A and TOR1B are found in

								idiopathic dystonia patients; PMID: 17130424
ARNTL	c.1732C>G	p.His578Asp	No	Possibly Damaging (0.651) Benign (0.214); HumVar	Neutral (-0.635)	Tolerated (0.11)	No Mendelian disorder	Significantly reduced ARNTL in human knee osteoarthritis cartilage and Arntl ablation in mouse chondrocytes abolished their circadian rhythm and caused progressive degeneration of articular cartilage; PMID: 26657859. Arntl deletion caused the degeneration of synaptic terminals and impaired cortical functional connectivity, as well as neuronal oxidative damage and impaired expression of several redox defense genes; PMID: 24270424 Null mice lose circadian rhythmicity; PubMed: 17124323. KO mice had significantly reduced levels of B lymphocytes in spleen, blood, and bone marrow; PubMed: 16925591.
AHNAK	c.13094A>G	p.Asp4365Gly	internal repeat; p.3322 to 5465	Probably Damaging (0.999) Probably Damaging (0.958); HumVar	Deleterious (-3.467)	Tolerated (0.21)	No Mendelian disorder	Disruption of Ahnak gene in mice showed no obvious phenotype; PubMed: 15007166. Ahnak1 -/- mice were highly susceptible to infection with Leishmania major; PubMed: 18191595. Ahnak binds to L-type Ca2+ channel β2 subunit and alters Cav1.2 channel conductance (ICaL); PMID: 17045254. S100A10 (Annexin II) binds to AHNAK; PMID: 22834835
ATL3	c.692C>T	p.Pro231Leu	In GBP domain; p.69 to 337	Probably Damaging (1) Probably Damaging (1); HumVar	Deleterious (-9.266)	Damaging (0)	Neuropathy, hereditary sensory, type IF; Autosomal dominant (AD)	Y192C within ATL3 was found in HSN1F patients. This muation caused mislocalization of the protein; Y192C ATL3 accumulated in condensed structures near the nucleus and localized to unbranched tubules but not in 3-way junctions in the

								endoplasmic reticulum; PubMed: 24459106
GPR137	c.1276A>C	p.Thr426Pro	Low complexity region; p.413-436	Benign (0)	Neutral (0.315)	*DAMAGING - Low confidence predictions with Median conservation above 3.25 (0.01)	No search result	Knockdown/inhibition/downregulation of GPR137 inhibits cancer prolification; PMID: 26669804, PMID: 25524330, PMID: 25301753.
PPP2R5B	c.43T>C	p.Ser15Pro	Low complexity region; p.6-25	Possibly Damaging (0.939) Benign (0.363); HumVar	Neutral (-0.35)	Tolerated (0.11)	No Mendelian disorder *VARIANT OF UNKNOWN SIGNIFICANC: autosomal dominant mental retardation with tall stature (a de novo heterozygous, S161).	PPP2R5B, PPP2R5D and PPP2R5E are highly expressed in the brain and the expression of the PPP2R5B and PPP2R5D increases when neuroblastoma cells are induced to differentiate with retinoic acid; PubMed: 7592815. KLHL15 (mutations cause mental retardation) controls PP2A holoenzyme composition and downstream phosphorylation events by directing degradation of B-prime-beta and promoting its exchange with other regulatory B subunits; PubMed: 23135275. A 23-year-old Caucasian man with severe intellectual disability, behavioral problems, dysmorphic features, dysphagia, gastroesophageal reflux, and skeletal abnormalities associated with a heterozygous 1.6-Mb deletion including PPP2R5B, NRXN2 and CDCA5.A 23-year-old Caucasian man with severe intellectual disability, behavioral problems, dysmorphic features, dysphagia, gastroesophageal reflux, and skeletal abnormalities associated with a heterozygous 1.6-Mb deletion

								including PPP2R5B, NRXN2 and CDCA5.
SYTL2	c.1131A>T	p.Glu377Asp	No	Benign (0.001)	Neutral (-0.148)	Tolerated (0.27)	No Mendelian disorder	SYTL2 is involved in RAB27A (nontransforming monomeric GTP-binding proteins). Mutations cause Griscelli syndrome, type 2 which results in results in pigmentary dilution of the skin and hair)-dependent vesicle transport and secretion in several types of secretory cells; PubMed: 15543135, 17182843, 18812475.
KLHL42	c.377G>A	p.Arg126Gln	Low complexity region; p.112 - 127	Probably Damaging (0.976) Benign (0.364); HumVar	Neutral (-0.430)	Tolerated (0.27)	No search result	A large genome-wide association study (GWAS) in 7410 unrelated and retrospectively and prospectively selected patients with severe osteoarthritis showed significant loci between KLHDC5 (KLHL42) and PTHLH; PMID: 22763110
EP400	c.2819C>T	p.Ala940Val	No	Benign (0.003)	Neutral (-2.026)	Tolerated (0.26)	No Mendelian disorder	EP400 is involved in histone acetyltransferase by forming complex; PubMed: 14966270, 18614019. Decreased p400 expression was associated with advanced tumor stage; PMID: 23982490. EP400 is recruited to DNA double-strand breaks and is required for the ubiquitination of chromatin, indicating p400 as a DNA damage response protein; PMID: 20876283
NAA16	c.1923A>C	p.Glu641Asp	Low complexity region; p.616-	Benign (0.045)	Neutral (-0.769)	Tolerated (1)	No search result	The hNaa16p-hNaa10p complex acetylates a major N-terminal acetyltransferase, NatA type N-termini in vitro; PMID: 19480662

			641.					
CKB	c.773C>G	p.Thr258Ser	In ATP:guanidophosphotransferases domain; p.120 to 367	Benign (0.0053)	Neutral (0.276)	Tolerated (0.24)	No Mendelian disorder	The C-terminal domain of K+/Cl- co-transporter 3 (KCC3, SLC12A6), which causes agenesis of the corpus callosum with peripheral neuropathy, directly interacted with CKB. Functional studies in Xenopus oocytes showed that an inhibitor of CKB reduced KCC3 transport activity; PMID: 18566107 CKB activates K+-Cl- co-transporter 2. The GABA reversal potential was shifted in the depolarizing direction in primary cortical neurons expressing CKB; PMID: 16336223
ACAN	c.2173G>A	p.Glu725Lys	No	Possibly Damaging (0.558) Benign (0.050); HumVar	Neutral (-1.533)	Tolerated (0.66)	Osteochondritis dissecans, short stature, and early-onset osteoarthritis. Spondyloepimetaphyseal dysplasia, aggrecan type. Spondyloepiphyseal dysplasia, Kimberley type	In the CNS, ACAN is considered to play a role in securing high-rate synaptic transmission in the perineuronal net-associated neurons. Mechanical stabilization of synaptic contacts. Neuroprotective actions by reducing oxidative stress through scavenging redox-active cations; reviewed in PMID: 22297263. Patients with human intervertebral disk degeneration claim pain; PMID: 21948754, PMID: 21689646. The homozygotes (-/-) died just after birth because of respiratory failure. The heterozygotes (+/-) exhibit spastic gait caused by misalignment of the cervical spine and die because of starvation with a high incidence of herniation and degeneration of vertebral discs and disc chondrocytes; PMID: 9192671

DNASE1L2	c.442T>C	p.Ser148Pro	In DNaseIc (deoxyribonuclease I) domain; p.5 to 296	Benign (0)	Neutral (0.004)	Tolerated (0.21)	No Mendelian disorder	Inflammatory cytokines, TNF-α and IL-1β, induce DNAS1L2 expression through activation of NF-κB in keratinocytes; PMID: 15203207
DNASE1L2	c.446G>C	p.Arg149Pro	In DNaseIc (deoxyribonuclease I) domain; p.5 to 296	Benign (0)	Neutral (-0.107)	Tolerated (0.2)		
BEAN1	c.400G>A	p.Ala134Thr	No	Possibly Damaging (0.720) Benign (0.275); HumVar	Neutral (-2.118)	Tolerated (0.09)	Spinocerebellar ataxia 31	A 2.5- to 3.8-kb insertion containing pentanucleotide repeats in all 160 affected individuals from 98 families with Spinocerebellar ataxia type 31 which is an adult-onset autosomal-dominant neurodegenerative disorder showing progressive cerebellar ataxia mainly affecting Purkinje cells; PMID: 19878914. BEAN-NEDD4 binding occurs via the 2 PY motifs of BEAN and the WW2 and WW3 domains of NEDD4; PubMed: 11042109
GNGT2	c.170A>G	p.Lys57Arg	No	Benign (0.067)	Neutral (-1.487)	Damaging (0.04)	No Mendelian disorder	G-protein βγ subunits bind to a potassium channel (Kir2.3) and suppressed Kir2.3 currents; PMID: 8943291. G protein beta2gamma2 subunits inhibited T-type Ca2+ channel activities by reducing channel open probability; PMID: 16973746
MUC16	c.40588G>A	p.Gly13530Ser	In SEA domain; p.13471 to 13604	Probably Damaging (0.995) Probably Damaging (0.991); HumVar	Neutral (-1.806)	Tolerated (0.053)	No Mendelian disorder	A tumor antigen widely used in monitoring ovarian cancer. KO mice showed activated Stat3 signal, affected JunB signal, upregulated the expression of IL-6 in the conjunctiva, increased proliferation and accelerated the wound healing of the corneal epithelium; PMID: 24812549

MUC16	c.40570G>A	p.Val13524Ile	In SEA domain; p.13471 to 13604	Possibly Damaging (0.884) Possibly Damaging (0.889); HumVar	Neutral (-0.204)	Tolerated (0.691)		
NFIX	c.1120A>G	p.Thr374Ala	In Nuclear factor I (NF-I) or CCAAT box-binding transcription factor (CTF) ; p. 213 to 502	Benign (0.120)	Neutral (-1.564)	Tolelated (0.118)	Marshall-Smith syndrome. Sotos syndrome 2	Nfix -/- mice newborns appeared normal but nearly all died before 1 month of age. Heterozygous mice showed no obvious anatomic or behavioural defects. Hydrocephalus was associated with partial agenesis of the corpus callosum in Nfix -/- and Nfix +/- mice; PubMed: 17353270

Table 4-7. Further analysis for the variants within *CWC22*, *TMEM8B* and *ATL3* by splicing change prediction, M-CAP and Kaviar and the expression levels of these genes in mouse DRG by RNA-seq study (Usoskin et al., 2015). Sensory neurons were classified into four main clusters and further subcategorised these clusters into 11 distinct subpopulations using several molecular markers; NF cluster, expressing neurofilament heavy chain (Nefh) and parvalbumin (Pvalb). NP cluster, showing expression of Mrgprd and P2rx3. PEP cluster expressing substance P (Tac1), TRKA (Ntrk1) and calcitonin gene-related peptide (CGRP, also known as Calca). TH cluster, showing distinct expression of tyrosine hydroxylase (Th). The number in each column of these subpopulations represents the ratio of fraction of positive cells for different neuronal populations. Colour indicator; 0, green to 1, red. (Usoskin et al., 2015)

Gene name	cDNA change	Protein change	Splice site prediction	M-CAP	Kaviar	NH					NP			PEP		TH
						NF1	NF2/3		NF4/5		NP1	NP2/3		PEP1	PEP2	
							NF2	NF3	NF4	NF5		NP2	NP3			
CWC22	c.1855G>T	p.Asp619Tyr	No difference between WT and Mut	Possibly Pathogenic (0.054)	no known variants	0.161	0.063	0.250	0.182	0.115	0.056	0.094	0.083	0.031	0.059	0.124
TMEM8B	c.442C>T	p.Pro148Ser	No difference between WT and Mut	Possibly Pathogenic (0.096)	no known variants	0.032	0.125	0.167	0.045	0.192	0.112	0.188	0.167	0.031	0.000	0.086
ATL3	c.692C>T	p.Pro231Leu	No difference between WT and Mut	Possibly Pathogenic (0.507)	no known variants	0.226	0.271	0.583	0.182	0.115	0.336	0.188	0.083	0.203	0.353	0.343

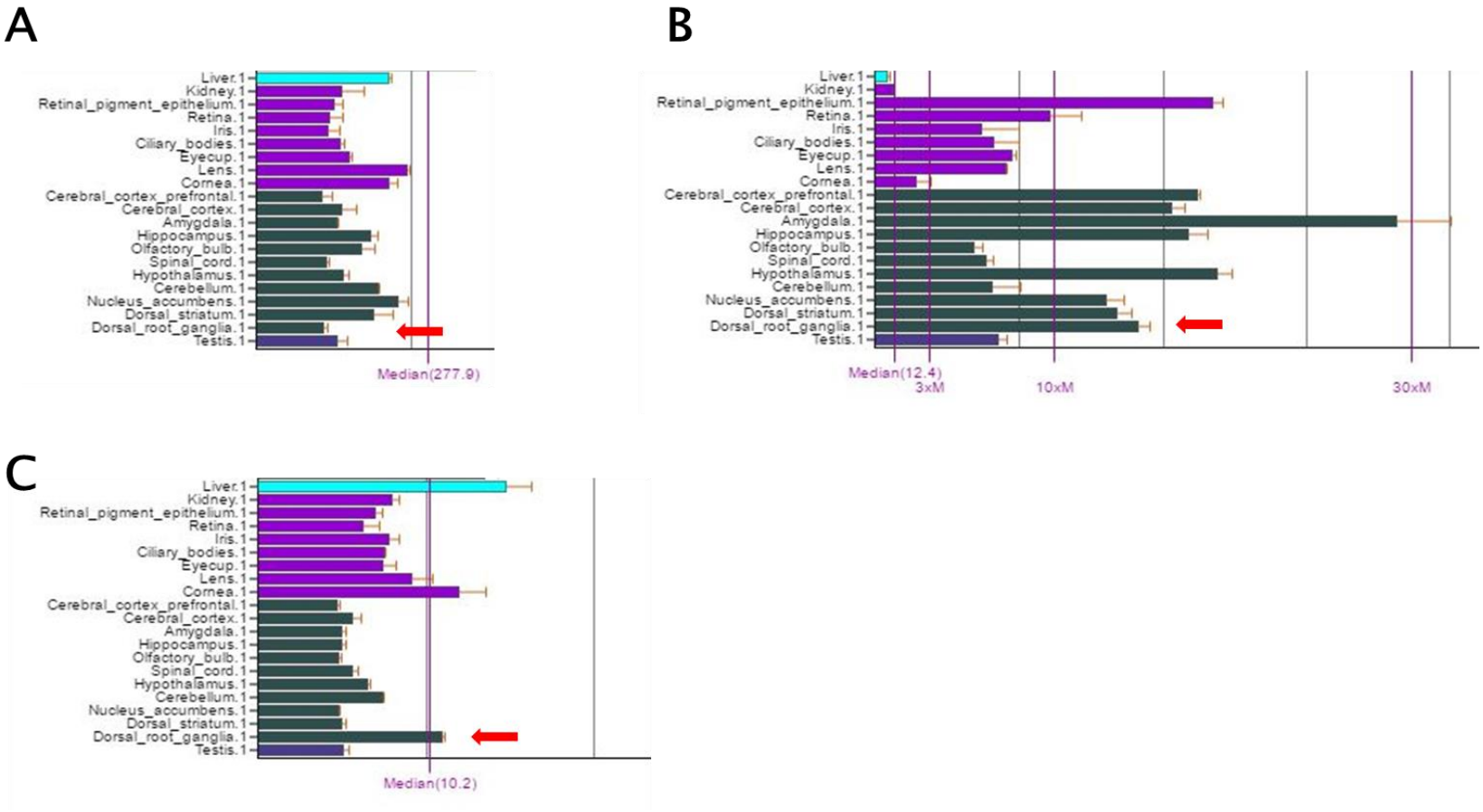

Figure 4-3. Gene expression in different tissues in mice. (A) *Cwc22* (B) *Tmem8b* (C) *Atl3*. Expression values from Affymetrix chips relate to fluorescence intensity in microarray are shown. (modified from BioGPS; http://biogps.org (Wu et al., 2013, Wu et al., 2016))

We settled on the point mutations in *CWC22*, *TMEM8B* and *ATL3* as the focus of future initial functional studies; the mutation in *CWC22* (NM_020943) is c.1855G>T and results in the amino acid change, aspartic acid to tyrosine at position 619 (D619Y). The mutation in *TMEM8B* (NM_001042590) is c.442C>T resulting in the amino acid change proline to serine at position 148 (P148S). The mutation in *ATL3* (NM_015459) is c.692C>T and results in the amino acid change, proline to leucine at position 231 (P231L). TMEM8B has been documented as a negative regulator of cell growth (Wang et al., 2014) and several studies have shown its potential as a drug target to treat cancer (Li et al., 2001, Zhang et al., 2003). More interestingly, association of *CWC22* and *ATL3* with neuropathy have recently been reported; CWC22 was aberrantly upregulated in diabetic DRG and axonal delivery of CWC22 siRNA to locally knock down the aberrant protein in diabetic nerves improved aspects of sensory function in diabetic mice (Kobayashi et al., 2017). Mutations in *ATL3* have previously been reported to be the cause of a painless neuropathy (Kornak et al., 2014); a heterozygous missense mutation (c.575A>G) in *ATL3*, resulting in amino acid substitution, tyrosine to cysteine (Y192C) at a highly conserved residue in the GTPase domain was identified in patients in a 4 generation German family and 2 generation Spanish family.

To confirm these three mutations, gDNA was amplified (Figure 4-4A, Figure 4-5A and Figure 4-6A) and Sanger sequenced. All three were heterozygous mutations (c.1855G>T in *CWC22*, c.442C>T in *TMEM8B* and c.692C>T in *ATL3*) resulting in an amino acid change D619Y, P148S and P231L, respectively, as the exome sequencing indicated (Figure 4-4B, Figure 4-5B and Figure 4-6B).

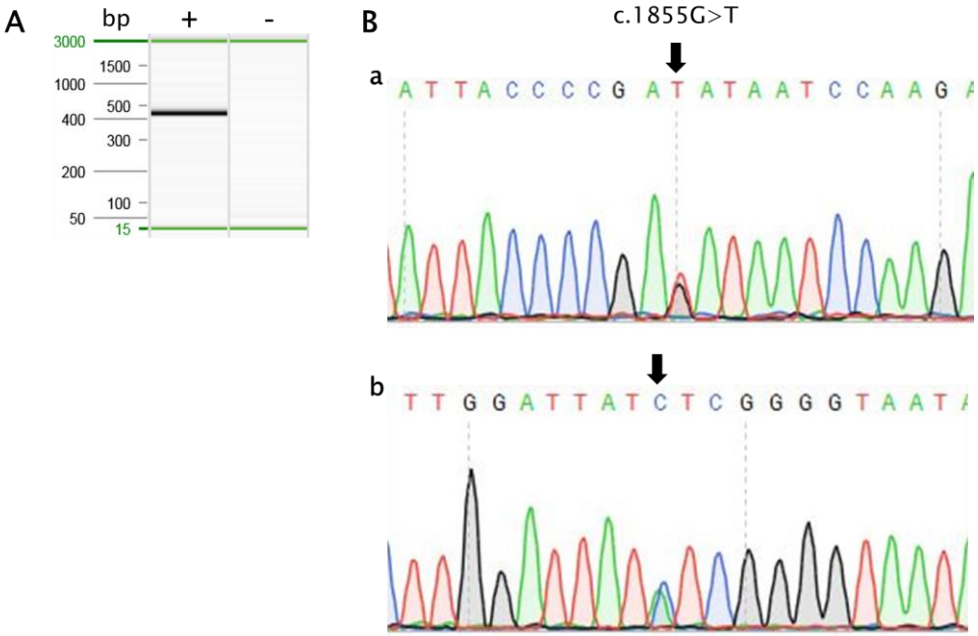

Figure 4-4. The PCR product of *CWC22* checked by QIAxcel Screen gel (A) and Sanger sequence chromatogram (B). (A) A single band shows the PCR product of *CWC22* with the expected size of 470bp (+) while no bands were observed in negative control (-). (B) (a) Sanger sequence chromatogram indicates the patient carries a heterozygous mutation (c.1855G>T) resulting in an amino acid change Asp619Tyr. (b) Sequencing using the reverse primer also shows a heterozygous mutation.

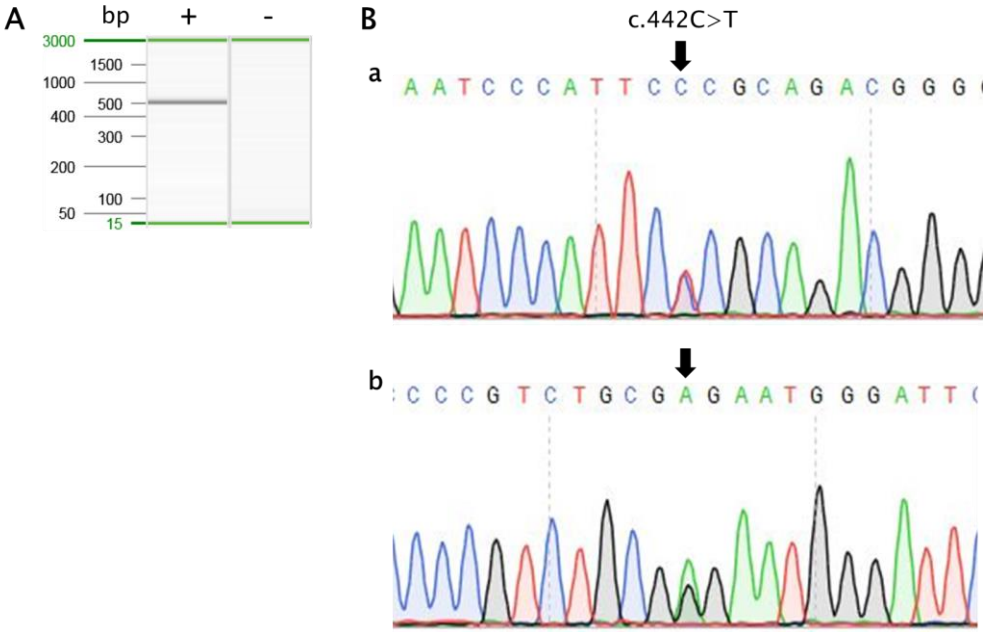

Figure 4-5. The PCR product of *TMEM8B* checked by QIAxcel Screen gel (A) and Sanger sequence chromatogram (B). (A) A single band shows the PCR product of *TMEM8B* with the expected size of 557bp (+) while no bands were observed in negative control (-). (B) (a) Sanger sequence chromatogram indicates the patient carries a heterozygous mutation (c.442C>T) resulting in an amino acid change Pro148Ser. (b) Sequencing using the reverse primer also shows a heterozygous mutation.

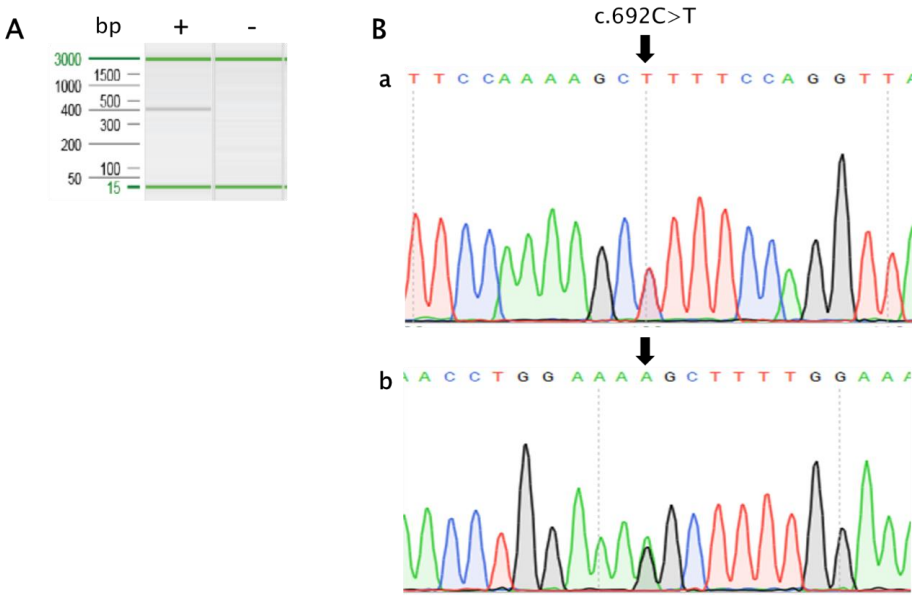

Figure 4-6. The PCR product of *ATL3* checked by QIAxcel Screen gel (A) and Sanger sequence chromatogram (B). (A) A single band shows the PCR product of *ATL3* with the expected size of 450bp (+) while no bands were observed in negative control (-). (B) (a) Sanger sequence chromatogram indicates the patient carries a heterozygous mutation (c.692C>T) resulting in an amino acid change Pro231Leu. (b) Sequencing using the reverse primer also shows a heterozygous mutation.

It is important to confirm if these mutations are evolutionally conserved. By analysing the genomes of species that are accessible in the UCSC Genome Browser (UC Santa Cruz, University of California), we discovered that aspartic acid 619 in CWC22 is evolutionarily conserved in every sequenced orthologue including ncm (nucampholin) in Drosophila (Figure 4-7). Likewise, TMEM8B and ATL3 orthologues had proline (Figure 4-8, Figure 4-9) at the corresponding residue at position 148 and 231, respectively. The residues of proline at the position 148 in TMEM8B and 231 in ATL3 are also conserved within the human homologs of these genes (Figure 4-10). Hence *CWC22*, *TMEM8B* and *ATL3* are the three lead candidate genes for future studies.

Figure 4-7. Sequence alignment around mutation site for orthologue CWC22 proteins across species.

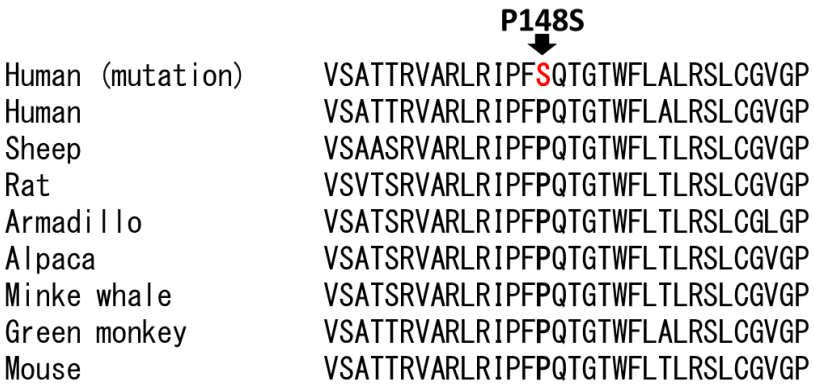

Figure 4-8. Sequence alignment around mutation site for orthologue TMEM8B proteins across species.

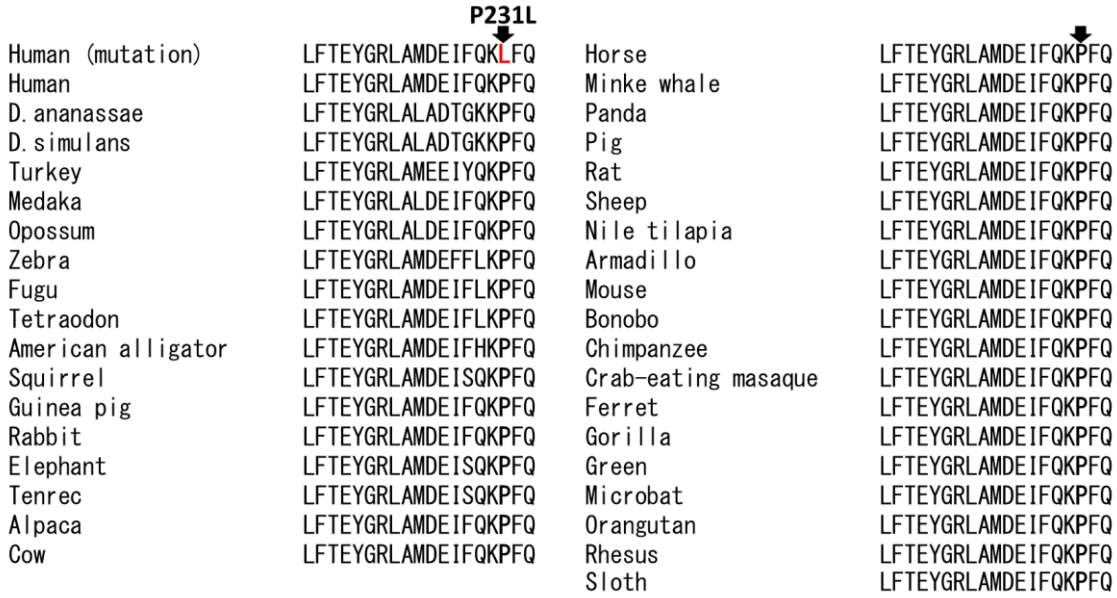

Figure 4-9. Sequence alignment around mutation site for orthologue ATL3 proteins across species.

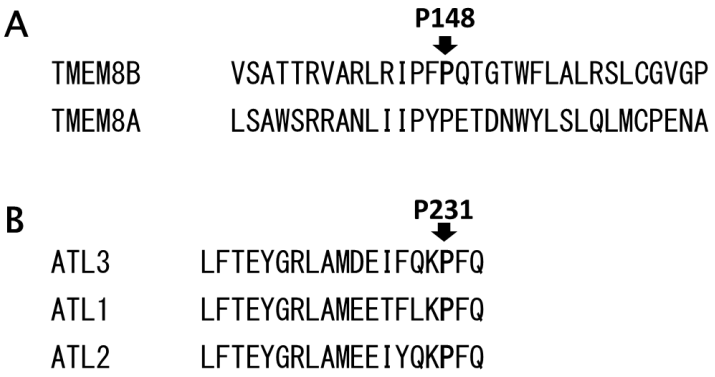

Figure 4-10. Sequence alignment around mutation site for human homologs of TMEM8B (A) and ATL3 (B) proteins.

4.5 DISCUSSION

In this project we attempted to identify the potential causative mutation(s) in a patient with a small fibre neuropathy and associated erythromelalgia-like symptoms which are restricted to the knees. We found three novel variants by exome sequencing and further analyses ranked the novel variants in terms of their likely pathogenicity. These three potential

causative mutations are all heterozygous point mutations; c.1855G>T in *CWC22*, c.442C>T in *TMEM8B* and c.692C>T in *ATL3*, resulting in the amino acid change D619Y, P148S and P231L, respectively. These mutations were confirmed by Sanger sequencing in the proband. These residues are evolutionally conserved and are present in the human homologues of TMEM8B or ATL3, highlighting the likely functional importance of these residues.

CWC22 (CWC22 spliceosome associated protein homolog) is known to have a critical function in splicing (Barbosa et al., 2012, Alexandrov et al., 2012, Steckelberg et al., 2012). CWC22 forms large protein complexes with eIF4A3 (eukaryotic translation initiation factor 4A3) (Barbosa et al., 2012). EIF4A3 is a component of the exon junction complex (EJC), which assembles near exon-exon junctions of mRNAs as a result of splicing (Chan et al., 2004). Pre-mRNA splicing is impaired in CWC22-depleted cells and CWC22 directly interacts with the core EJC component eIF4A3 *in vitro* and *in vivo* (Alexandrov et al., 2012, Steckelberg et al., 2012). In addition, depletion of CWC22 *in vivo* led to a splicing defect, resulting in decreased levels of mature cellular mRNAs (Alexandrov et al., 2012). More relevant to this project, a recent study has suggested its association with peripheral neuropathy. *Cwc22* was significantly upregulated in DRGs from diabetic mice demonstrating neuropathy and knockdown of *Cwc22* in sensory neurons by siRNA enhanced neurite outgrowth (Kobayashi et al., 2017). Thermal sensitivity analysed by the Hargreaves' test was impaired in diabetic mice, and this effect was reversed by administration of *Cwc22* siRNA. Of note, exposure of *Cwc22* siRNA in diabetic mice did not alter mechanical sensitivity in the von Frey test (Kobayashi et al., 2017). Taking these into account, the missense mutation in CWC22 in a patient may alter proper functions of CWC22 protein leading to painful neuropathy. It would be interesting to explore if the D619Y mutation alters interaction with eIF4A3 and affect splicing in sensory neurons.

TMEM8B, also known as NGX6, is considered to be a negative regulator of cell growth and a tumour suppressor (Wang et al., 2014). Roles of this gene in cell growth, proliferation, migration and metastasis have been well documented in multiple types of cancer (Li et al., 2001, Zhang et al., 2003, He et al., 2016). Although studies of this gene in pain do not seem to have been explored, the expression of this gene appears to be relatively high in DRG neurons (Table 4-7, Figure 4-3). Besides, a study indicated a high expression level of TMEM8B in human nervous tissue such as spinal cord and cerebellum (Wang et al., 2010). The expression pattern of this gene could imply that TMEM8B serves a key role in the nervous system including sensory neurons.

ATL3 encodes atlastin GTPase 3 (Atlastin-3), a member of a family of dynamin-like, integral membrane GTPases. Atlastin molecules consist of GTPase domains, three-helix bundle

(3HB), transmembrane (TM) segments and the C-terminal tail in the cytosol (Bian et al., 2011). Figure 4-11 shows the structure of human ATL1 (Atlastin-1). Unlike the other variants in CWC22 or TMEM8B which we found in the patient, the P231L mutation in ATL3 is predicted in a domain which can affect proper functions of ATL3. This domain is the GTPase domain that is evolutionally conserved across species (Figure 4-9) and is present in all three human atlastin GTPase homologs (Bian et al., 2011, Kornak et al., 2014)(UniProt)(Figure 4-10B), suggesting that the P231L mutant protein may affect the proper function of ATL3.

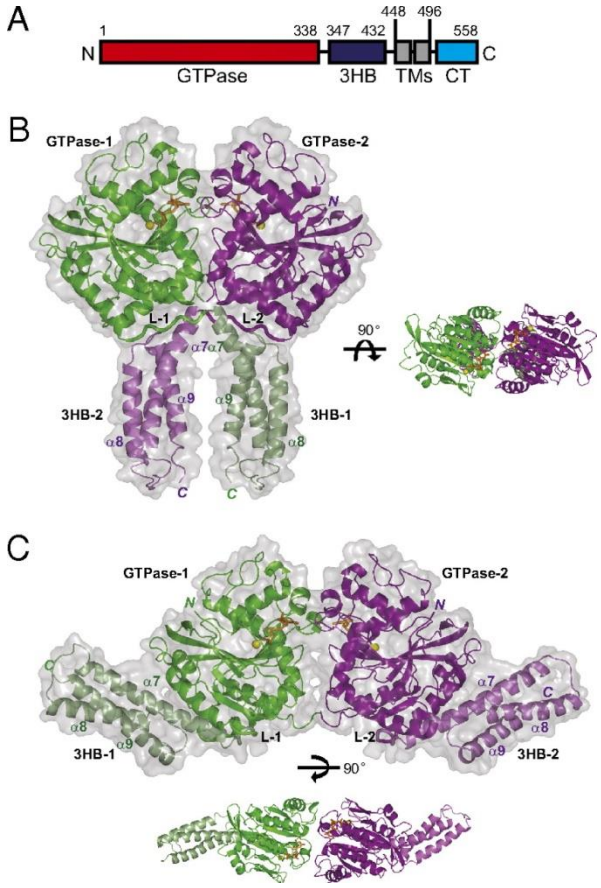

Figure 4-11. Structures of the cytosolic domain of human ATL1. (A) Scheme showing the domains of ATL1. 3HB, three-helix bundle; TMs, TM segments; CT, cytosolic tail. (B) Structure of the GDP-bound form of ATL1, corresponding to the postfusion state. The protomers in the dimer are shown in green and purple cartoon representation, superimposed on a space-filling model. The linkers (L-1 and L-2) between the GTPase domains and 3HBs (in pale colours) are highlighted. GDP is shown in orange stick representation, and magnesium ion is shown as a yellow sphere. The α-helices of the 3HBs are numbered. Right shows a different view of the dimer. (C) Structure of ATL1 crystallized with GDP and Pi, corresponding to the prefusion state. Lower shows a different view of the dimer (Bian et al., 2011).

The Atlastin family of proteins is considered to be intrinsic to the proper formation of the network of interconnected tubules of the endoplasmic reticulum (Hu et al., 2015,

Rismanchi et al., 2008). The endoplasmic reticulum is a large, membrane-bounded organelle responsible for a number of critical cellular processes in eukaryotic cells such as the synthesis of membrane lipids, membrane and secretory proteins, and the regulation of intracellular calcium (Baumann and Walz, 2001). Typically, the endoplasmic reticulum forms a continuous polygonal membrane network composed of interconnected sheets and tubules that spread throughout the cytoplasm. The endoplasmic reticulum forms three-way junctions by sliding along microtubules to fuse with the adjacent endoplasmic reticulum regions that it contacts during endoplasmic reticulum dynamics. These three-way junctions contribute to the overall "reticular" appearance of the endoplasmic reticulum. The factors that regulate homotypic endoplasmic reticulum membrane fusion are essential to maintain cellular processes; these factors should be endoplasmic reticulum specific since the endoplasmic reticulum is closely apposed and potentially connected to nearly every membrane-bound compartment in the cell. (English and Voeltz, 2013). Several proteins contributing to this formation have been documented including Atlastin family members and more recently, Lunapark family members that play a role in stabilization of three-way junctions (Chen et al., 2015a). The potential causative mutation we found in the patient is in *ATL3* which belongs to the Atlastin family. One of the Atlastin family members, atlastin-1, is predominantly localized to vesicular tubular complexes and cis-Golgi cisternae, mostly in brain. On the other hand, atlastin-2 and -3 are found ubiquitously and localize to the endoplasmic reticulum (Rismanchi et al., 2008, Zhu et al., 2003). A proposed model for the Atlastin-mediated homotypic membrane fusion in the endoplasmic reticulum has been documented in an Atlastin-1 crystal structure study (Bian et al., 2011)(Figure 4-12). Firstly, two Atlastin molecules sitting in different membranes form a dimer following binding of GTP. This can connect the membranes together; the three-helix bundles of the two molecules are pointing in different directions. Second, GTP hydrolysis and inorganic phosphate (P_i) can be released, and both atlastin molecules undergo a conformational change; the interaction surface between the GTPase domain and the three-helix bundle can probably lead to switch of the two regions. The three-helix bundles would then be released, and the linkers may allow the dimer of GTPase domains to freely rotate. The resulting conformational change would pull the apposing membranes together, so that after fusion the two Atlastin molecules would be anchored in the same membrane (Figure 4-12).

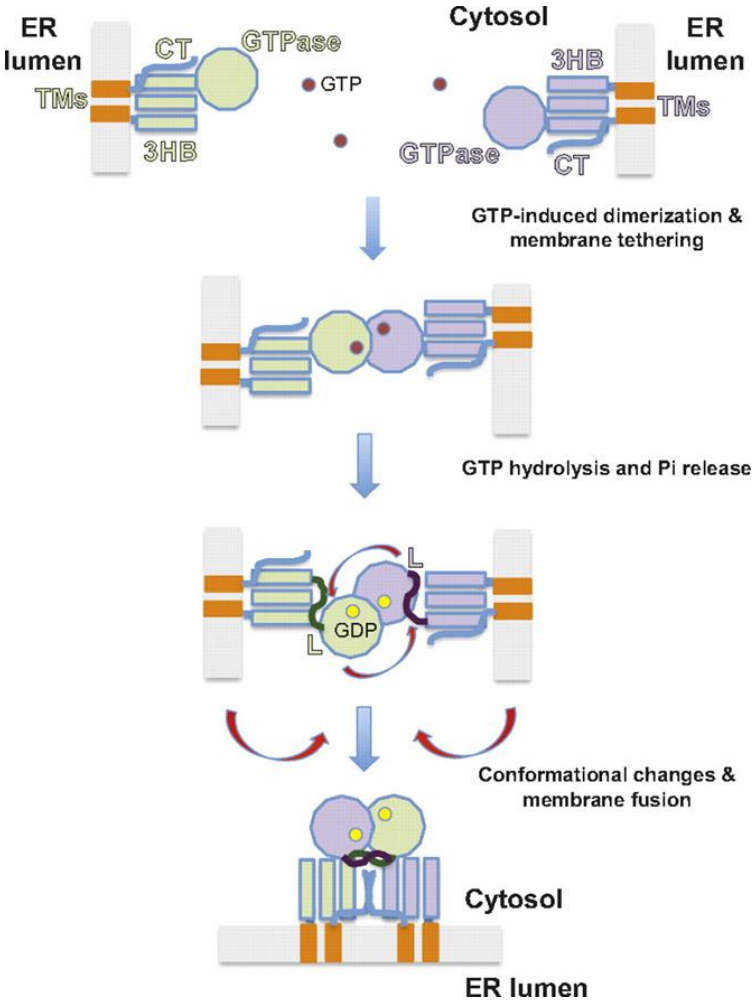

Figure 4-12. A proposed model for ATL-mediated homotypic membrane fusion in the endoplasmic reticulum (ER) (Bian et al., 2011).

Interestingly, a missense mutation in *ATL3* has been shown to be the cause of a painless neuropathy categorised as hereditary sensory neuropathy type IF (HSN 1F) by disruption of the endoplasmic reticulum network (Kornak et al., 2014). A heterozygous missense mutation (c.575A>G) in *ATL3*, resulting in amino acid substitution, tyrosine to cysteine (Y192C) at a highly conserved residue in the GTPase domain was identified in patients in a 4 generation German family and 2 generation Spanish family (Kornak et al., 2014). Clinical features of these patients are described in Table 4-8 (Kornak et al., 2014). The examples of these are: abnormal calluses of the feet and valgus deformity of the great toe, which became apparent between 14 and 30 years of age, initially without any noticeable numbness in the German patients. These patients showed painless chronic ulcerations and fractures of the metatarsals developed, which showed delayed healing and occasionally resulted in bone destruction. Motor nerve conduction velocities were in the normal range, whereas sensory nerve conduction studies showed an

axonal sensory neuropathy in these patients. Bilateral hyperkeratosis and plantar ulcers were developed at 14 years and 16 years of age in the Spanish patients. These patients also showed distal impairment of sensory function affecting superficial touch, pain and temperature sensations. *In vitro* assays revealed that the Y192C mutation disrupted the endoplasmic reticulum network by mislocalization of the protein. ATL3 co-localizes with protein disulphide isomerase, a marker of the reticular endoplasmic reticulum network including peripheral tubules. While no alteration of the co-localization was found in cells expressing wild type ATL3, in cells overexpressing the Y192C mutant, distribution of protein disulphide isomerase was drastically altered. The association with three-way junctions was lost in the Y192C mutant protein and the distribution was restricted to the condensed area in proximity to the nucleus and localized to a few unbranched tubules throughout the cell (Kornak et al., 2014). This indicates that the endoplasmic reticulum structure collapsed upon the expression of the mutant protein, supporting an important role of ATL3 in the formation of three-way junctions in the endoplasmic reticulum. Several reports have suggested that atlastin-3 is expressed in the CNS as well as DRG neurons (Hawrylycz et al., 2012, Kornak et al., 2014) and relatively high expression of *Atl3* (Usoskin et al., 2015) was found in the RNA transcriptome analyses of mouse sensory neurons, supporting an idea that ATL3 can serve essential functions in sensory neurons. Considering these, the alteration of membrane-shaping proteins in sensory neurons by mutant ATL3 protein could be intrinsic to axonal degeneration and peripheral neuropathies.

Table 4-8. Clinical findings in the individuals harbouring the p.Tyr192Cys mutation in ATL3. Het = heterozygous; n.d. = not done; - = not present; + = present; ++ = prominent; +++ = severe. (Kornak et al., 2014)

Patient ID	**A-III-1**	**A-IV-1**	**A-III-3**	**A-IV-2**	**B-II-1**	**B-III-1**	**B-III-2**
Origin	Germany	Germany	Germany	Germany	Spain	Spain	Spain
Age at onset (years)	14	30	not known	33	35	14	16
Foot ulcers	+++	+	-	-	-	+	+
Hallux valgus	++	++	+	+	-	+	+
Foot arthropathy	+	+	+	+	+	-	-
Fractures Metatarsals	+++	++	-	+	-	+	+
Foot bone destruction	+++	++	++	+	-	+	+
Amputations	Lower legs	-	-	-	-	Second toe and metatarsal	Second toe and metatarsal
Disturbed touch sensitivity	++	+	n.d.	n.d.	-	+	+
Disturbed pain sensitivity	+	+	+	+	-	+	+
Autonomic dysfunction	-	-	-	-	-	-	-
Spasticity/brisk reflexes	-	-	-	-	-	-	-
NCS	Axonal sensory neuropathy	Sensory neuropathy	n.d.	n.d.	n.d.	Axonal sensory neuropathy	Axonal sensory neuropathy

Others	Nail necrosis	DXA T-score −1	Prominent entheses	Prominent entheses	-	Absent ankle jerks	Absent ankle jerks
Initial diagnosis	Familial acroosteolysis	Familial acroosteolysis	Familial acroosteolysis	Familial acroosteolysis	HSAN type I	HSAN type I	HSAN type I
State	Het	Het	Het	Het	Het	Het	Het
Mutation	c.575A>G	c.575A>G	c.575A>G	c.575A>G	c.575A>G	c.575A>G	c.575A>G
Consequence	p.Tyr192Cys	p.Tyr192Cys	p.Tyr192Cys	p.Tyr192Cys	p.Tyr192Cys	p.Tyr192Cys	p.Tyr192Cys

Another member of the Atlastin family, atlastin GTPase 1 (*ATL1*), has also been documented as an underlying cause of hereditary peripheral neuropathies, HSAN 1D (Guelly et al., 2011). Similarly to the study regarding the missense mutation in *ATL3* that is linked to HSN 1F (Kornak et al., 2014), some mutant ATL1 proteins found in individuals diagnosed as HSAN 1D disrupted the endoplasmic reticulum morphology including three-way junctions, with lack of GTPase activities. Another mutant ATL1 was localized diffusely throughout the cytoplasm with markedly reduced expression levels of the protein, which could be due to the decreased protein stability. However, the other mutant ATL1 showed no significant alteration of the endoplasmic reticulum morphology nor GTPase activities, indicating that the subcellular mislocation including formation of three-way junctions in the endoplasmic reticulum is not the only disease mechanism involved in these peripheral neuropathies.

Study of the endoplasmic reticulum morphology in cells expressing the mutant P231L ATL3 could provide some evidence to confirm that this is the pathogenic mutation. Interestingly, another causative molecule of neuropathies, RAB7, constitutively binds to the endoplasmic reticulum, serving an essential function in endosome maturation (Friedman et al., 2013, Rotthier et al., 2012). Rab7 can regulate axonal transport and the retrograde signalling of NGF and its TrkA receptor by binding NGF (Zhang et al., 2013a). As mentioned before, NGF mutations also cause a HSAN phenotype (Einarsdottir et al., 2004, Carvalho et al., 2011). Therefore it would be also interesting to explore if there is any association between RAB7 and ATL3 since this might potentially lead to a painful peripheral neuropathy. Our mutation in ATL3 might affect proper functions of the endoplasmic reticulum. For example, the endoplasmic reticulum plays an essential role in Ca^{2+} storage as well as Ca^{2+} release (Baumann and Walz, 2001). Disturbances in the endoplasmic reticulum Ca^{2+} homeostasis may be also closely related to several disorders such as brain ischemia and Alzheimer disease as well as neuropathies (Verkhratsky and Toescu, 2003). Protein-folding is also an important role of the endoplasmic reticulum. Protein misfolding is a common feature of several neurodegenerative diseases such as Parkinson's disease, Huntington's disease, amyotrophic lateral sclerosis and prion-related diseases (Hetz and Mollereau, 2014). These disorders related to endoplasmic reticulum functions strengthen the idea that a number of pathways could be affected by ATL3 mutant protein through dysfunctions of the endoplasmic reticulum. As discussed above, another mutation in ATL3 (Y192C) has been linked to painless neuropathies, HSN 1F. It would be also interesting to explore the functional difference in the endoplasmic reticulum caused by these mutations, Y192C and our mutation, P231L, to unravel why Y192C leads to a painless neuropathy whereas P231L could be causing a painful neuropathy. Furthermore, the stability of

the mutant protein and its GTPase activity could be measured and potentially mouse models that express the orthologous mutation could be generated.

In addition to experiments outlined above, it is also important to ascertain whether the mutations in the proband are heritable. In this project, we focused on three missense variants in *CWC22*, *TMEM8B* or *ATL3*. However, it is still uncertain that these variants are pathogenic mutations since this initial selection was performed by whole-exome sequencing from only one patient. If the mutations are absent in his unaffected parent, but present in the affected parent and grandparent, then this would give further strength to the hypothesis that these mutations are pathogenic. Also, it should be also mentioned that the variants which have been reported to carry any polymorphisms were excluded in this project. However, there might be a causative mutation in a gene bearing polymorphisms at the position of the novel variants. Further analysis would be needed to identify causative mutations.

4.6 CONCLUSION

In this project, three missense heterozygous point mutations were found in the patient diagnosed with a SFN and an EM-like phenotype in the knee; the mutation in *CWC22* (c.1855G>T), *TMEM8B* (c.442C>T) and *ATL3* (c.692C>T). These mutations resulted in the amino acid change, aspartic acid to tyrosine at position 619 (D619Y) in CWC22, proline to serine at position 148 (P148S) in TMEM8B and proline to leucine (P231L) in ATL3. These mutations are evolutionally conserved. Among these genes *CWC22* and *ATL3* have been associated with neuropathy. *Cwc22* was significantly upregulated in DRGs from diabetic mice demonstrating neuropathy and the impaired thermal sensitivity in these mice was reversed by knockdown of *Cwc22*. Another mutation in ATL3 (Y192C) has been described to be linked to a painless neuropathy categorised as hereditary sensory neuropathy type IF (HSN 1F) by disruption of the endoplasmic reticulum network. The P231L mutation in ATL3 is predicted to locate to the GTPase domain and the proline residues are present in all three human atlastin GTPase homologues, highlighting the likely functional importance of these residues. The P231L mutation might lead to a painful neuropathy perhaps by affecting the endoplasmic reticulum morphology. Further investigations are necessary to confirm if these mutations are pathogenic.

SUMMARY

This thesis focuses on investigating mechanisms of pain sensation which are not yet completely understood, as well as identifying novel analgesic drug targets by using molecular, genetic and transgenic approaches. The key findings in this thesis are: an additional novel function of $Na_v1.7$ in gene expression regulation (Chapter 2); the role of *ZFHX2* in pain and the effects of a point mutation that causes pain insensitivity (Chapter 3); and the finding of three novel missense mutations which are potentially pathogenic in a patient with painful small fibre neuropathy and erythromelalgia-like symptoms in the knees (Chapter 4).

In Chapter 2, we aimed to explore a novel function of one of the most important elements in pain signalling, $Na_v1.7$. We show that lack of $Na_v1.7$ results in significant gene dysregulation in dorsal root ganglia neurons. Pain behavioural tests confirmed that some of these dysregulated genes are likely to contribute to the pain-insensitive phenotype. These include one of the well-studied endogenous opioid family genes, *Penk*, and the uncharacterised gene, *Ceacam10*. Interestingly, human pain studies showed that up-regulation of endogenous opioids caused by loss of function $Na_v1.7$ mutations can contribute to pain insensitivity in a $Na_v1.7$ null patient. The molecular studies demonstrated the up-regulation of *Penk* at the transcriptional level may be triggered by the alteration of intracellular sodium levels, highlighting a possible role of sodium ions as a second messenger. Notably this mechanism is unlikely to influence the dysregulation of other genes, such as *Ceacam10* and *Tmem173*. The dysregulated genes and their involvement in pain may explain why potent selective antagonists of $Na_v1.7$ are weak analgesics. Taking their potential synergy into account, targeting $Na_v1.7$ in combination with the dysregulated genes may be the foundation of an effective pain treatment and may expand the arsenal of pain therapies.

Other key findings of this thesis are the role of *Zfhx2* in pain and the missense mutation in *ZFHX2* found in pain insensitive patients. This gene likely mediates pain sensitivity via dysregulation of downstream genes. By using animal models, we discovered that *Zfhx2* is involved in pain with both global knockout and BAC transgenic mice bearing the orthologous mutation displaying significant acute pain perception deficits. Using stable cell lines we found that the R1913K mutation in *ZFHX2* alters the expression of numerous downstream genes. However, the pathological mechanisms of this mutation are still unclear. Our findings highlight that *ZFHX2* and its downstream genes could be considered as potential novel targets for new analgesic drugs.

We also discovered three potential causal missense mutations in *CWC22*, *TMEM8B* and *ATL3* for a novel human phenotype of painful small fibre neuropathy and associated erythromelalgia-like symptoms that predominantly affect the knees. Importantly, this analysis is based on a single patient sample and hence further experiments are needed to determine which is the pathogenic mutation. Among the candidate genes, the mutations in *CWC22* and *ATL3* are particularly interesting in terms of their known links to neuropathies.

Pain is a highly complex biological phenomenon involving numerous genes and pathways. This thesis highlights that although pain insensitive individuals have mutations in single genes (e.g. *SCN9A* or *ZFHX2*), the analgesic effects of the mutations are likely to be related to the dysregulation of numerous genes. In the case of *SCN9A*, we show that loss of function of the encoded $Na_v1.7$ channel results in significant gene dysregulation in dorsal root ganglia neurons, including upregulation of preproenkephalin. For *ZFHX2*, the point mutation in this transcriptional regulator also leads to dramatic dysregulation of downstream genes. Hence although $Na_v1.7$ and ZFHX2 are attractive analgesic targets, effective pain relief may only be reached by a drug combination that works synergistically on multiple targets.

REFERENCES

ABRAHAMSEN, B., ZHAO, J., ASANTE, C. O., CENDAN, C. M., MARSH, S., MARTINEZ-BARBERA, J. P., NASSAR, M. A., DICKENSON, A. H. & WOOD, J. N. 2008. The cell and molecular basis of mechanical, cold, and inflammatory pain. *Science,* 321**,** 702-5.

AHN, H. S., DIB-HAJJ, S. D., COX, J. J., TYRRELL, L., ELMSLIE, F. V., CLARKE, A. A., DRENTH, J. P., WOODS, C. G. & WAXMAN, S. G. 2010. A new Nav1.7 sodium channel mutation I234T in a child with severe pain. *Eur J Pain,* 14**,** 944-950.

AKOPIAN, A. N., SIVILOTTI, L. & WOOD, J. N. 1996. A tetrodotoxin-resistant voltage-gated sodium channel expressed by sensory neurons. *Nature,* 379**,** 257-262.

AKOPIAN, A. N., SOUSLOVA, V., ENGLAND, S., OKUSE, K., OGATA, N., URE, J., SMITH, A., KERR, B. J., MCMAHON, S. B., BOYCE, S., HILL, R., STANFA, L. C., DICKENSON, A. H. & WOOD, J. N. 1999. The tetrodotoxin-resistant sodium channel SNS has a specialized function in pain pathways. *Nat Neurosci,* 2**,** 541-8.

ALAM, H., GU, B. & LEE, M. G. 2015. Histone methylation modifiers in cellular signaling pathways. *Cellular and molecular life sciences : CMLS,* 72**,** 4577-92.

ALETTA, J. M., CIMATO, T. R. & ETTINGER, M. J. 1998. Protein methylation: a signal event in post-translational modification. *Trends in biochemical sciences,* 23**,** 89-91.

ALEXANDROV, A., COLOGNORI, D., SHU, M. D. & STEITZ, J. A. 2012. Human spliceosomal protein CWC22 plays a role in coupling splicing to exon junction complex deposition and nonsense-mediated decay. *Proc Natl Acad Sci U S A,* 109**,** 21313-8.

ALMEIDA, T. F., ROIZENBLATT, S. & TUFIK, S. 2004. Afferent pain pathways: a neuroanatomical review. *Brain Research,* 1000**,** 40-56.

ALONSO, C. R. 2002. Hox proteins: sculpting body parts by activating localized cell death. *Curr Biol,* 12**,** R776-8.

AMAYA, F., WANG, H., COSTIGAN, M., ALLCHORNE, A. J., HATCHER, J. P., EGERTON, J., STEAN, T., MORISSET, V., GROSE, D., GUNTHORPE, M. J., CHESSELL, I. P., TATE, S., GREEN, P. J. & WOOLF, C. J. 2006. The voltage-gated sodium channel Na(v)1.9 is an effector of peripheral inflammatory pain hypersensitivity. *J Neurosci,* 26**,** 12852-12860.

ANGER, T., MADGE, D., MULLA, M. & RIDDALL, D. 2001. Medicinal chemistry of neuronal voltage-gated sodium channel blockers. *Journal of Medicinal Chemistry,* 44**,** 115-137.

ARENAS, E. 2014. Wnt signaling in midbrain dopaminergic neuron development and regenerative medicine for Parkinson's disease. *Journal of Molecular Cell Biology,* 6**,** 42-53.

BADING, H. 2013. Nuclear calcium signalling in the regulation of brain function. *Nat Rev Neurosci,* 14**,** 593-608.

BAMBERGER, A.-M., PU, L.-P., COOL, D. R. & LOH, Y. P. 1995. The Neuro-2a neuroblastoma cell line expresses [Met]-enkephalin and vasopressin mRNA and peptide. *Molecular and Cellular Endocrinology,* 113**,** 155-163.

BANDYOPADHYAY, S., HARRIS, D. P., ADAMS, G. N., LAUSE, G. E., MCHUGH, A., TILLMAAND, E. G., MONEY, A., WILLARD, B., FOX, P. L. & DICORLETO, P. E. 2012. HOXA9 methylation by PRMT5 is essential for endothelial cell expression of leukocyte adhesion molecules. *Molecular and cellular biology,* 32**,** 1202-13.

BARBADO, M., FABLET, K., RONJAT, M. & DE WAARD, M. 2009. Gene regulation by voltage-dependent calcium channels. *Biochimica et biophysica acta,* 1793**,** 1096-104.

BARBER, G. N. 2015. STING: infection, inflammation and cancer. *Nat Rev Immunol,* 15**,** 760-70.

BARBOSA, I., HAQUE, N., FIORINI, F., BARRANDON, C., TOMASETTO, C., BLANCHETTE, M. & LE HIR, H. 2012. Human CWC22 escorts the helicase eIF4AIII to spliceosomes and promotes exon junction complex assembly. *Nat Struct Mol Biol,* 19**,** 983-90.

BASBAUM, A. I., BAUTISTA, D. M., SCHERRER, G. & JULIUS, D. 2009. Cellular and Molecular Mechanisms of Pain. *Cell,* 139**,** 267-284.

BASBAUM, A. I. & JESSELL, T. M. 2000. The Perception of Pain (in Principles of neural science). *New York: McGraw-Hill,* 4th edition, Eric R Kandel, James H, Schwartz, & Thomas M Jessell (editors)**,** 472-491.

BASTOS, L. F. S., PRAZERES, J. D. M., GODIN, A. M., MENEZES, R. R., SOARES, D. G., FERREIRA, W. C., DUTRA, M. M. G. B., MACHADO, R. R. & COELHO, M. M. 2013. Sex-independent suppression of experimental inflammatory pain by minocycline in two mouse strains. *Neuroscience Letters,* 553**,** 110-114.

BAUMANN, O. & WALZ, B. 2001. Endoplasmic reticulum of animal cells and its organization into structural and functional domains. *Int Rev Cytol.,* 205**,** 149-214.

BAUTISTA, D. M., JORDT, S.-E., NIKAI, T., TSURUDA, P. R., READ, A. J., POBLETE, J., YAMOAH, E. N., BASBAUM, A. I. & JULIUS, D. 2006. TRPA1 Mediates the Inflammatory Actions of Environmental Irritants and Proalgesic Agents. *Cell,* 124**,** 1269-1282.

BAUTISTA, D. M., SIEMENS, J., GLAZER, J. M., TSURUDA, P. R., BASBAUM, A. I., STUCKY, C. L., JORDT, S.-E. & JULIUS, D. 2007. The menthol receptor TRPM8 is the principal detector of environmental cold. *Nature,* 448**,** 204-208.

BEALS, C. R., CLIPSTONE, N. A., HO, S. N. & CRABTREE, G. R. 1997. Nuclear localization of NF-ATc by a calcineurin-dependent, cyclosporin-sensitive intramolecular interaction. *Genes Dev,* 11**,** 824-34.

BEAN, B. P. 1989. Classes of Calcium Channels in Vertebrate Cells. *Annual Review of Physiology,* 51**,** 367-384.

BEAN, B. P. 1991. Pharmacology of calcium channels in cardiac muscle, vascular muscle, and neurons. *American journal of hypertension,* 4**,** 406S-411S.

BELMONTE, C. & VIANA, F. 2008. Molecular and cellular limits to somatosensory specificity. *Molecular pain,* 4**,** 14-14.

BENARROCH, E. E. 2007. Sodium channels and pain. *Neurology,* 68**,** 233-6.

BENN, S. C., COSTIGAN, M., TATE, S., FITZGERALD, M. & WOOLF, C. J. 2001. Developmental expression of the TTX-resistant voltage-gated sodium channels Nav1.8 (SNS) and Nav1.9 (SNS2) in primary sensory neurons. *J Neurosci,* 21**,** 6077-85.

BENNETT, D. L. H. & WOODS, C. G. 2014. Painful and painless channelopathies. *The Lancet. Neurology,* 13**,** 587-599.

BIAN, X., KLEMM, R. W., LIU, T. Y., ZHANG, M., SUN, S., SUI, X., LIU, X., RAPOPORT, T. A. & HU, J. 2011. Structures of the atlastin GTPase provide insight into homotypic fusion of endoplasmic reticulum membranes. *Proceedings of the National Academy of Sciences,* 108**,** 3976-3981.

BIEDLER, J. L., HELSON, L. & SPENGLER, B. A. 1973. Morphology and growth, tumorigenicity, and cytogenetics of human neuroblastoma cells in continuous culture. *Cancer Res,* 33**,** 2643-52.

BIGGAR, K. K. & LI, S. S. C. 2014. Non-histone protein methylation as a regulator of cellular signalling and function. *Nature Reviews Molecular Cell Biology,* 16**,** 5-17.

BINSHTOK, A. M., WANG, H., ZIMMERMANN, K., AMAYA, F., VARDEH, D., SHI, L., BRENNER, G. J., JI, R. R., BEAN, B. P., WOOLF, C. J. & SAMAD, T. A. 2008. Nociceptors are interleukin-1beta sensors. *J Neurosci,* 28**,** 14062-73.

BITNER-GLINDZICZ, M., TURNPENNY, P., HÖGLUND, P., KÄÄRIÄINEN, H., SANKILA, E. M., VAN DER MAAREL, S. M., DE KOK, Y. J., ROPERS, H. H., CREMERS, F. P. & PEMBREY, M. 1995. Further mutations in Brain 4 (POU3F4) clarify the phenotype in the X-linked deafness, DFN3. *Human molecular genetics,* 4**,** 1467-9.

BLACK, J., DIB-HAJJ, S., MCNABOLA, K., JESTE, S., RIZZO, M., KOCSIS, J. & WAXMAN, S. 1996. Spinal sensory neurons express multiple sodium channel alpha-subunit mRNAs. *Brain Res Mol Brain Res,* 43**,** 117-131.

BLACK, J. A., FREZEL, N., DIB-HAJJ, S. D. & WAXMAN, S. G. 2012. Expression of Nav1.7 in DRG neurons extends from peripheral terminals in the skin to central preterminal branches and terminals in the dorsal horn. *Molecular pain,* 8**,** 82-82.

BLACK, J. A., HOEIJMAKERS, J. G., FABER, C. G., MERKIES, I. S. & WAXMAN, S. G. 2013. NaV1.7: stress-induced changes in immunoreactivity within magnocellular neurosecretory neurons of the supraoptic nucleus. *Mol Pain,* 9**,** 39.

BLASIUS, A. L., DUBIN, A. E., PETRUS, M. J., LIM, B. K., NAREZKINA, A., CRIADO, J. R., WILLS, D. N., XIA, Y., MORESCO, E. M., EHLERS, C., KNOWLTON, K. U., PATAPOUTIAN, A. & BEUTLER, B. 2011. Hypermorphic mutation of the voltage-gated sodium channel encoding gene Scn10a causes a dramatic stimulus-dependent neurobehavioral phenotype. *Proc Natl Acad Sci U S A,* 108**,** 19413-19418.

BODNAR, R. J. 2000. Supraspinal circuitry mediating opioid antinociception: antagonist and synergy studies in multiple sites. *J Biomed Sci,* 7**,** 181-94.

BORSOOK, D. 2012. Neurological diseases and pain. *Brain : a journal of neurology,* 135**,** 320-44.

BOURINET, E., ALTIER, C., HILDEBRAND, M. E., TRANG, T., SALTER, M. W. & ZAMPONI, G. W. 2014. Calcium-Permeable Ion Channels in Pain Signaling. *Physiological Reviews,* 94**,** 81-140.

BREIVIK, H., COLLETT, B., VENTAFRIDDA, V., COHEN, R. & GALLACHER, D. 2006. Survey of chronic pain in Europe: prevalence, impact on daily life, and treatment. *Eur J Pain,* 10**,** 287-333.

BRIERLEY, S. M., CASTRO, J., HARRINGTON, A. M., HUGHES, P. A., PAGE, A. J., RYCHKOV, G. Y. & BLACKSHAW, L. A. 2011. TRPA1 contributes to specific mechanically activated currents and sensory neuron mechanical hypersensitivity. *The Journal of Physiology,* 589**,** 3575-3593.

BRIND'AMOUR, J., LIU, S., HUDSON, M., CHEN, C., KARIMI, M. M. & LORINCZ, M. C. 2015. An ultra-low-input native ChIP-seq protocol for genome-wide profiling of rare cell populations. *Nat Commun,* 6**,** 6033.

BRITTAIN, J. M., DUARTE, D. B., WILSON, S. M., ZHU, W., BALLARD, C., JOHNSON, P. L., LIU, N., XIONG, W., RIPSCH, M. S., WANG, Y., FEHRENBACHER, J. C., FITZ, S. D., KHANNA, M., PARK, C.-K., SCHMUTZLER, B. S., CHEON, B. M., DUE, M. R., BRUSTOVETSKY, T., ASHPOLE, N. M., HUDMON, A., MEROUEH, S. O., HINGTGEN, C. M., BRUSTOVETSKY, N., JI, R.-R., HURLEY, J. H., JIN, X., SHEKHAR, A., XU, X.-M., OXFORD, G. S., VASKO, M. R., WHITE, F. A. & KHANNA, R. 2011. Suppression of inflammatory and neuropathic pain by uncoupling CRMP-2 from the presynaptic Ca2+ channel complex. *Nature Medicine,* 17**,** 822-829.

BROWN, R. E., COREY, S. C. & MOORE, A. K. 1999. Differences in Measures of Exploration and Fear in MHC-Congenic C57BL/6J and B6-H-2K Mice. *Behavior Genetics,* 29**,** 263-271.

BRUMOVSKY, P., VILLAR, M. J. & HOKFELT, T. 2006. Tyrosine hydroxylase is expressed in a subpopulation of small dorsal root ganglion neurons in the adult mouse. *Exp Neurol,* 200**,** 153-65.

BURDETTE, D. L. & VANCE, R. E. 2013. STING and the innate immune response to nucleic acids in the cytosol. *Nat Immunol,* 14**,** 19-26.

CABANERO, D., CELERIER, E., GARCIA-NOGALES, P., MATA, M., ROQUES, B. P., MALDONADO, R. & PUIG, M. M. 2009. The pro-nociceptive effects of remifentanil or surgical injury in mice are associated with a decrease in delta-opioid receptor mRNA levels: Prevention of the nociceptive response by on-site delivery of enkephalins. *Pain,* 141**,** 88-96.

CAO, Y. Q., MANTYH, P. W., CARLSON, E. J., GILLESPIE, A.-M., EPSTEIN, C. J. & BASBAUM, A. I. 1998. Primary afferent tachykinins are required to experience moderate to intense pain. *Nature,* 392**,** 390-394.

CARR, S. M., POPPY ROWORTH, A., CHAN, C. & LA THANGUE, N. B. 2015. Post-translational control of transcription factors: methylation ranks highly. *FEBS Journal,* 282**,** 4450-4465.

CARVALHO, O. P., THORNTON, G. K., HERTECANT, J., HOULDEN, H., NICHOLAS, A. K., COX, J. J., RIELLY, M., AL-GAZALI, L. & WOODS, C. G. 2011. A novel NGF mutation

clarifies the molecular mechanism and extends the phenotypic spectrum of the HSAN5 neuropathy. *J Med Genet,* 48**,** 131-5.

CATERINA, M. J., LEFFLER, A., MALMBERG, A. B., MARTIN, W. J., TRAFTON, J., PETERSEN-ZEITZ, K. R., KOLTZENBURG, M., BASBAUM, A. I. & JULIUS, D. 2000. Impaired nociception and pain sensation in mice lacking the capsaicin receptor. *Science (New York, N.Y.),* 288**,** 306-13.

CATERINA, M. J., SCHUMACHER, M. A., TOMINAGA, M., ROSEN, T. A., LEVINE, J. D. & JULIUS, D. 1997. The capsaicin receptor: a heat-activated ion channel in the pain pathway. *Nature,* 389**,** 816-24.

CATTERALL, W. A. 2000. From Ionic Currents to Molecular Mechanisms: The Structure and Function of Voltage-Gated Sodium Channels. *Neuron,* 26**,** 13-25.

CATTERALL, W. A., GOLDIN, A. L. & WAXMAN, S. G. 2005. International Union of Pharmacology. XLVII. Nomenclature and Structure-Function Relationships of Voltage-Gated Sodium Channels. *Pharmacological Reviews,* 57**,** 397-409.

CHAHINE, M. & O'LEARY, M. E. 2011. Regulatory Role of Voltage-Gated Na(+) Channel β Subunits in Sensory Neurons. *Frontiers in Pharmacology,* 2**,** 70.

CHAHL, L. A. 1996. Experimental and Clinical Pharmacology: Opioids - mechanisms of action. *Australian Prescriber,* 19**,** 63-65.

CHAKRABORTY, S., REBECCHI, M., KACZOCHA, M. & PUOPOLO, M. 2016. Dopamine modulation of transient receptor potential vanilloid type 1 (TRPV1) receptor in dorsal root ganglia neurons. *J Physiol,* 594**,** 1627-42.

CHAN, C. C., DOSTIE, J., DIEM, M. D., FENG, W., MANN, M., RAPPSILBER, J. & DREYFUSS, G. 2004. eIF4A3 is a novel component of the exon junction complex. *Rna,* 10**,** 200-9.

CHAPLAN, S. R., BACH, F. W., POGREL, J. W., CHUNG, J. M. & YAKSH, T. L. 1994. Quantitative assessment of tactile allodynia in the rat paw. *J Neurosci Methods,* 53**,** 55-63.

CHATTOPADHYAY, M., MATA, M. & FINK, D. J. 2008. Continuous delta-opioid receptor activation reduces neuronal voltage-gated sodium channel (NaV1.7) levels through activation of protein kinase C in painful diabetic neuropathy. *J Neurosci,* 28**,** 6652-8.

CHEN, H., XUE, Y., HUANG, N., YAO, X. & SUN, Z. 2006. MeMo: a web tool for prediction of protein methylation modifications. *Nucleic Acids Research,* 34**,** W249-W253.

CHEN, S., DESAI, T., MCNEW, J. A., GERARD, P., NOVICK, P. J. & FERRO-NOVICK, S. 2015a. Lunapark stabilizes nascent three-way junctions in the endoplasmic reticulum. *Proc Natl Acad Sci U S A,* 112**,** 418-23.

CHEN, Y. C., AUER-GRUMBACH, M., MATSUKAWA, S., ZITZELSBERGER, M., THEMISTOCLEOUS, A. C., STROM, T. M., SAMARA, C., MOORE, A. W., CHO, L. T., YOUNG, G. T., WEISS, C., SCHABHUTTL, M., STUCKA, R., SCHMID, A. B., PARMAN, Y., GRAUL-NEUMANN, L., HEINRITZ, W., PASSARGE, E., WATSON, R. M., HERTZ, J. M., MOOG, U., BAUMGARTNER, M., VALENTE, E. M., PEREIRA, D., RESTREPO, C. M.,

KATONA, I., DUSL, M., STENDEL, C., WIELAND, T., STAFFORD, F., REIMANN, F., VON AU, K., FINKE, C., WILLEMS, P. J., NAHORSKI, M. S., SHAIKH, S. S., CARVALHO, O. P., NICHOLAS, A. K., KARBANI, G., MCALEER, M. A., CILIO, M. R., MCHUGH, J. C., MURPHY, S. M., IRVINE, A. D., JENSEN, U. B., WINDHAGER, R., WEIS, J., BERGMANN, C., RAUTENSTRAUSS, B., BAETS, J., DE JONGHE, P., REILLY, M. M., KROPATSCH, R., KURTH, I., CHRAST, R., MICHIUE, T., BENNETT, D. L., WOODS, C. G. & SENDEREK, J. 2015b. Transcriptional regulator PRDM12 is essential for human pain perception. *Nat Genet,* 47**,** 803-8.

CHOI, B. Y., KIM, D.-H., CHUNG, T., CHANG, M., KIM, E.-H., KIM, A. R., SEOK, J., CHANG, S. O., BOK, J., KIM, D., OH, S.-H. & PARK, W.-Y. 2013. Destabilization and mislocalization of POU3F4 by C-terminal frameshift truncation and extension mutation. *Human mutation,* 34**,** 309-16.

CHOI, J.-S., ZHANG, L., DIB-HAJJ, S. D., HAN, C., TYRRELL, L., LIN, Z., WANG, X., YANG, Y. & WAXMAN, S. G. 2009. Mexiletine-responsive erythromelalgia due to a new Nav1.7 mutation showing use-dependent current fall-off. *Experimental Neurology,* 216**,** 383-389.

CHU SIN CHUNG, P. & KIEFFER, B. L. 2013. Delta opioid receptors in brain function and diseases. *Pharmacol Ther,* 140**,** 112-20.

CODERRE, T. J., VACCARINO, A. L. & MELZACK, R. 1990. Central nervous system plasticity in the tonic pain response to subcutaneous formalin injection. *Brain Res,* 535**,** 155-8.

COKER, G. T., 3RD, VINNEDGE, L. & O'MALLEY, K. L. 1988. Characterization of rat and human tyrosine hydroxylase genes: functional expression of both promoters in neuronal and non-neuronal cell types. *Biochem Biophys Res Commun,* 157**,** 1341-7.

CONVERGENCE PHARMACEUTICALS, C., UK. 2016. *CNV1014802* [Online]. Available: http://www.convergencepharma.com/ index.asp?page_id=14 [Accessed Jan 2016].

COSTE, B., MATHUR, J., SCHMIDT, M., EARLEY, T. J., RANADE, S., PETRUS, M. J., DUBIN, A. E. & PATAPOUTIAN, A. 2010. Piezo1 and Piezo2 Are Essential Components of Distinct Mechanically Activated Cation Channels. *Science,* 330**,** 55-60.

COX, J. J., REIMANN, F., NICHOLAS, A. K., THORNTON, G., ROBERTS, E., SPRINGELL, K., KARBANI, G., JAFRI, H., MANNAN, J., RAASHID, Y., AL-GAZALI, L., HAMAMY, H., VALENTE, E. M., GORMAN, S., WILLIAMS, R., MCHALE, D. P., WOOD, J. N., GRIBBLE, F. M. & WOODS, C. G. 2006. An SCN9A channelopathy causes congenital inability to experience pain. *Nature,* 444**,** 894-898.

COX, J. J., SHEYNIN, J., SHORER, Z., REIMANN, F., NICHOLAS, A. K., ZUBOVIC, L., BARALLE, M., WRAIGE, E., MANOR, E., LEVY, J., WOODS, C. G. & PARVARI, R. 2010. Congenital insensitivity to pain: novel SCN9A missense and in-frame deletion mutations. *Hum Mutat,* 31**,** E1670-86.

CROWLEY, C., SPENCER, S. D., NISHIMURA, M. C., CHEN, K. S., PITTS-MEEK, S., ARMANINI, M. P., LING, L. H., MCMAHON, S. B., SHELTON, D. L., LEVINSON, A. D. & ET AL. 1994. Mice lacking nerve growth factor display perinatal loss of sensory and sympathetic neurons yet develop basal forebrain cholinergic neurons. *Cell,* 76**,** 1001-11.

CUMMINS, T. R., AGLIECO, F., RENGANATHAN, M., HERZOG, R. I., DIB-HAJJ, S. D. & WAXMAN, S. G. 2001. Nav1.3 sodium channels: rapid repriming and slow closed-state inactivation display quantitative differences after expression in a mammalian cell line and in spinal sensory neurons. *The Journal of neuroscience : the official journal of the Society for Neuroscience,* 21**,** 5952-61.

CUMMINS, T. R., DIB-HAJJ, S. D., BLACK, J. A., AKOPIAN, A. N., WOOD, J. N. & WAXMAN, S. G. 1999. A novel persistent tetrodotoxin-resistant sodium current in SNS-null and wild-type small primary sensory neurons. *J Neurosci,* 19**,** Rc43.

CUNHA, F. Q., POOLE, S., LORENZETTI, B. B. & FERREIRA, S. H. 1992. The pivotal role of tumour necrosis factor alpha in the development of inflammatory hyperalgesia. *Br J Pharmacol,* 107**,** 660-4.

D'ELIA, A. V., TELL, G., PARON, I., PELLIZZARI, L., LONIGRO, R. & DAMANTE, G. 2001. Missense Mutations of Human Homeoboxes : A Review. 374**,** 361-374.

DATTANI, M. T., MARTINEZ-BARBERA, J. P., THOMAS, P. Q., BRICKMAN, J. M., GUPTA, R., MÅRTENSSON, I. L., TORESSON, H., FOX, M., WALES, J. K., HINDMARSH, P. C., KRAUSS, S., BEDDINGTON, R. S. & ROBINSON, I. C. 1998. Mutations in the homeobox gene HESX1/Hesx1 associated with septo-optic dysplasia in human and mouse. *Nature genetics,* 19**,** 125-33.

DE KOK, Y. J., VAN DER MAAREL, S. M., BITNER-GLINDZICZ, M., HUBER, I., MONACO, A. P., MALCOLM, S., PEMBREY, M. E., ROPERS, H. H. & CREMERS, F. P. 1995. Association between X-linked mixed deafness and mutations in the POU domain gene POU3F4. *Science (New York, N.Y.),* 267**,** 685-8.

DEPRISTO, M. A., BANKS, E., POPLIN, R., GARIMELLA, K. V., MAGUIRE, J. R., HARTL, C., PHILIPPAKIS, A. A., DEL ANGEL, G., RIVAS, M. A., HANNA, M., MCKENNA, A., FENNELL, T. J., KERNYTSKY, A. M., SIVACHENKO, A. Y., CIBULSKIS, K., GABRIEL, S. B., ALTSHULER, D. & DALY, M. J. 2011. A framework for variation discovery and genotyping using next-generation DNA sequencing data. *Nat Genet,* 43**,** 491-8.

DEVIGILI, G., ELEOPRA, R., PIERRO, T., LOMBARDI, R., RINALDO, S., LETTIERI, C., FABER, C. G., MERKIES, I. S., WAXMAN, S. G. & LAURIA, G. 2014. Paroxysmal itch caused by gain-of-function Nav1.7 mutation. *Pain,* 155**,** 1702-1707.

DHAKA, A., MURRAY, A. N., MATHUR, J., EARLEY, T. J., PETRUS, M. J. & PATAPOUTIAN, A. 2007. TRPM8 Is Required for Cold Sensation in Mice. *Neuron,* 54**,** 371-378.

DIATCHENKO, L., NACKLEY, A. G., TCHIVILEVA, I. E., SHABALINA, S. A. & MAIXNER, W. 2007. Genetic architecture of human pain perception. *Trends in Genetics,* 23**,** 605-613.

DIB-HAJJ, S., BLACK, J. A., CUMMINS, T. R. & WAXMAN, S. G. 2002. NaN/Nav1.9: a sodium channel with unique properties. *Trends Neurosci,* 25**,** 253-9.

DIB-HAJJ, S. D., CUMMINS, T. R., BLACK, J. A. & WAXMAN, S. G. 2007. From genes to pain: Na v 1.7 and human pain disorders. *Trends Neurosci,* 30**,** 555-63.

DIB-HAJJ, S. D., CUMMINS, T. R., BLACK, J. A. & WAXMAN, S. G. 2010. Sodium Channels in Normal and Pathological Pain. *Annual Review of Neuroscience,* 33**,** 325-347.

DIB-HAJJ, S. D., FJELL, J., CUMMINS, T. R., ZHENG, Z., FRIED, K., LAMOTTE, R., BLACK, J. A. & WAXMAN, S. G. 1999. Plasticity of sodium channel expression in DRG neurons in the chronic constriction injury model of neuropathic pain. *Pain,* 83**,** 591-600.

DIB-HAJJ, S. D., TYRRELL, L., BLACK, J. A. & WAXMAN, S. G. 1998. NaN, a novel voltage-gated Na channel, is expressed preferentially in peripheral sensory neurons and down-regulated after axotomy. *Proceedings of the National Academy of Sciences of the United States of America,* 95**,** 8963-8.

DIB-HAJJ, S. D., YANG, Y., BLACK, J. A. & WAXMAN, S. G. 2012. The NaV1.7 sodium channel: from molecule to man. *Nature Publishing Group,* 14**,** 1-14.

DOAK, G. J. & SAWYNOK, J. 1997. Formalin-induced nociceptive behavior and edema: involvement of multiple peripheral 5-hydroxytryptamine receptor subtypes. *Neuroscience,* 80**,** 939-49.

DONEHOWER, L. A. & LOZANO, G. 2009. 20 years studying p53 functions in genetically engineered mice. *Nature reviews. Cancer,* 9**,** 831-41.

DU, X., WANG, J., ZHU, H., RINALDO, L., LAMAR, K.-M., PALMENBERG, ANN C., HANSEL, C. & GOMEZ, CHRISTOPHER M. 2013. Second Cistron in CACNA1A Gene Encodes a Transcription Factor Mediating Cerebellar Development and SCA6. *Cell,* 154**,** 118-133.

EDDY, N. B. & LEIMBACH, D. 1953. Synthetic analgesics. II. Dithienylbutenyl- and dithienylbutylamines. *J Pharmacol Exp Ther,* 107**,** 385-93.

EIDE, P. K. & HOLE, K. 1993. The role of 5-hydroxytryptamine (5-HT) receptor subtypes and plasticity in the 5-HT systems in the regulation of nociceptive sensitivity. *Cephalalgia,* 13**,** 75-85.

EIJKELKAMP, N., LINLEY, J. E., BAKER, M. D., MINETT, M. S., CREGG, R., WERDEHAUSEN, R., RUGIERO, F. & WOOD, J. N. 2012. Neurological perspectives on voltage-gated sodium channels. *Brain,* 135**,** 2585-2612.

EINARSDOTTIR, E., CARLSSON, A., MINDE, J., TOOLANEN, G., SVENSSON, O., SOLDERS, G., HOLMGREN, G., HOLMBERG, D. & HOLMBERG, M. 2004. A mutation in the nerve growth factor beta gene (NGFB) causes loss of pain perception. *Hum Mol Genet,* 13**,** 799-805.

EMERY, E. C., LUIZ, A. P. & WOOD, J. N. 2016. Nav1.7 and other voltage-gated sodium channels as drug targets for pain relief. *Expert Opin Ther Targets,* 20**,** 975-83.

ENGLISH, A. R. & VOELTZ, G. K. 2013. Endoplasmic reticulum structure and interconnections with other organelles. *Cold Spring Harbor perspectives in biology,* 5**,** a013227-a013227.

ESCHALIER, A., KAYSER, V. & GUILBAUD, G. 1989. Influence of a specific 5-HT3 antagonist on carrageenan-induced hyperalgesia in rats. *Pain,* 36**,** 249-55.

ESENSTEN, J. H., TSYTSYKOVA, A. V., LOPEZ-RODRIGUEZ, C., LIGEIRO, F. A., RAO, A. & GOLDFELD, A. E. 2005. NFAT5 binds to the TNF promoter distinctly from NFATp, c, 3

and 4, and activates TNF transcription during hypertonic stress alone. *Nucleic Acids Res,* 33**,** 3845-54.

ESTACION, M., DIB-HAJJ, S. D., BENKE, P. J., TE MORSCHE, R. H., EASTMAN, E. M., MACALA, L. J., DRENTH, J. P. & WAXMAN, S. G. 2008. NaV1.7 gain-of-function mutations as a continuum: A1632E displays physiological changes associated with erythromelalgia and paroxysmal extreme pain disorder mutations and produces symptoms of both disorders. *J Neurosci,* 28**,** 11079-11088.

ESTACION, M., VOHRA, B. P., LIU, S., HOEIJMAKERS, J., FABER, C. G., MERKIES, I. S., LAURIA, G., BLACK, J. A. & WAXMAN, S. G. 2015. Ca2+ toxicity due to reverse Na+/Ca2+ exchange contributes to degeneration of neurites of DRG neurons induced by a neuropathy-associated Nav1.7 mutation. *J Neurophysiol,* 114**,** 1554-64.

FABER, C. G., HOEIJMAKERS, J. G., AHN, H. S., CHENG, X., HAN, C., CHOI, J. S., ESTACION, M., LAURIA, G., VANHOUTTE, E. K., GERRITS, M. M., DIB-HAJJ, S., DRENTH, J. P., WAXMAN, S. G. & MERKIES, I. S. 2012a. Gain of function Nanu1.7 mutations in idiopathic small fiber neuropathy. *Ann Neurol,* 71**,** 26-39.

FABER, C. G., LAURIA, G., MERKIES, I. S., CHENG, X., HAN, C., AHN, H. S., PERSSON, A. K., HOEIJMAKERS, J. G., GERRITS, M. M., PIERRO, T., LOMBARDI, R., KAPETIS, D., DIB-HAJJ, S. D. & WAXMAN, S. G. 2012b. Gain-of-function Nav1.8 mutations in painful neuropathy. *Proc Natl Acad Sci U S A,* 109**,** 19444-19449.

FENALTI, G., GIGUERE, P. M., KATRITCH, V., HUANG, X. P., THOMPSON, A. A., CHEREZOV, V., ROTH, B. L. & STEVENS, R. C. 2014. Molecular control of delta-opioid receptor signalling. *Nature,* 506**,** 191-6.

FERRARELLI, L. K. 2014. Delineating Wnt Pathways in Pain. *Science Signaling,* 7**,** ec192-ec192.

FERTLEMAN, C. R., BAKER, M. D., PARKER, K. A., MOFFATT, S., ELMSLIE, F. V., ABRAHAMSEN, B., OSTMAN, J., KLUGBAUER, N., WOOD, J. N., GARDINER, R. M. & REES, M. 2006. SCN9A mutations in paroxysmal extreme pain disorder: allelic variants underlie distinct channel defects and phenotypes. *Neuron,* 52**,** 767-774.

FILLINGIM, R. B., KAPLAN, L., STAUD, R., NESS, T. J., GLOVER, T. L., CAMPBELL, C. M., MOGIL, J. S. & WALLACE, M. R. 2005. The A118G single nucleotide polymorphism of the mu-opioid receptor gene (OPRM1) is associated with pressure pain sensitivity in humans. *The journal of pain : official journal of the American Pain Society,* 6**,** 159-67.

FINKENZELLER, D., FISCHER, B., LUTZ, S., SCHREWE, H., SHIMIZU, T. & ZIMMERMANN, W. 2003. Carcinoembryonic antigen-related cell adhesion molecule 10 expressed specifically early in pregnancy in the decidua is dispensable for normal murine development. *Mol Cell Biol,* 23**,** 272-9.

FISCHER, T. Z., GILMORE, E. S., ESTACION, M., EASTMAN, E., TAYLOR, S., MELANSON, M., DIB-HAJJ, S. D. & WAXMAN, S. G. 2009. A novel Nav1.7 mutation producing carbamazepine-responsive erythromelalgia. *Annals of neurology,* 65**,** 733-41.

FRIEDMAN, J. R., DIBENEDETTO, J. R., WEST, M., ROWLAND, A. A. & VOELTZ, G. K. 2013. Endoplasmic reticulum-endosome contact increases as endosomes traffic and mature. *Mol Biol Cell,* 24**,** 1030-40.

GALBAVY, W., SAFAIE, E., REBECCHI, M. J. & PUOPOLO, M. 2013. Inhibition of tetrodotoxin-resistant sodium current in dorsal root ganglia neurons mediated by D1/D5 dopamine receptors. *Mol Pain,* 9**,** 60.

GARDANEH, M., GILBERT, J., HABER, M., NORRIS, M. D., COHN, S. L., SCHMIDT, M. L. & MARSHALL, G. M. 2000. Synergy between 5' and 3' flanking regions of the human tyrosine hydroxylase gene ensures specific, high-level expression in neuroblastoma cells. *Neurosci Lett,* 292**,** 147-50.

GARRISON, S. R., DIETRICH, A. & STUCKY, C. L. 2012. TRPC1 contributes to light-touch sensation and mechanical responses in low-threshold cutaneous sensory neurons. *J Neurophysiol,* 107**,** 913-22.

GARRISON, S. R., WEYER, A. D., BARABAS, M. E., BEUTLER, B. A. & STUCKY, C. L. 2014. A gain-of-function voltage-gated sodium channel 1.8 mutation drives intense hyperexcitability of A- and C-fiber neurons. *Pain,* 155**,** 896-905.

GAULTIER, A., ARANDJELOVIC, S., LI, X., JANES, J., DRAGOJLOVIC, N., ZHOU, G. P., DOLKAS, J., MYERS, R. R., GONIAS, S. L. & CAMPANA, W. M. 2008. A shed form of LDL receptor-related protein-1 regulates peripheral nerve injury and neuropathic pain in rodents. *The Journal of clinical investigation,* 118**,** 161-72.

GEHRING, W. J. 1992. The homeobox in perspective. *Trends Biochem Sci,* 17**,** 277-80.

GIANSANTI, P., TSIATSIANI, L., LOW, T. Y. & HECK, A. J. 2016. Six alternative proteases for mass spectrometry-based proteomics beyond trypsin. *Nat Protoc,* 11**,** 993-1006.

GIBSON, D. G., YOUNG, L., CHUANG, R. Y., VENTER, J. C., HUTCHISON, C. A., 3RD & SMITH, H. O. 2009. Enzymatic assembly of DNA molecules up to several hundred kilobases. *Nat Methods,* 6**,** 343-5.

GINGRAS, J., SMITH, S., MATSON, D. J., JOHNSON, D., NYE, K., COUTURE, L., FERIC, E., YIN, R., MOYER, B. D., PETERSON, M. L., ROTTMAN, J. B., BEILER, R. J., MALMBERG, A. B. & MCDONOUGH, S. I. 2014. Global Nav1.7 Knockout Mice Recapitulate the Phenotype of Human Congenital Indifference to Pain. *PLoS ONE,* 9**,** e105895.

GIORDANO, J. & DYCHE, J. 1989. Differential analgesic actions of serotonin 5-HT3 receptor antagonists in the mouse. *Neuropharmacology,* 28**,** 423-7.

GIORDANO, J. & ROGERS, L. V. 1989. Peripherally administered serotonin 5-HT3 receptor antagonists reduce inflammatory pain in rats. *European journal of pharmacology,* 170**,** 83-6.

GOLDBERG, Y. P., MACFARLANE, J., MACDONALD, M. L., THOMPSON, J., DUBE, M. P., MATTICE, M., FRASER, R., YOUNG, C., HOSSAIN, S., PAPE, T., PAYNE, B., RADOMSKI, C., DONALDSON, G., IVES, E., COX, J., YOUNGHUSBAND, H. B., GREEN, R., DUFF, A., BOLTSHAUSER, E., GRINSPAN, G. A., DIMON, J. H., SIBLEY, B. G., ANDRIA, G., TOSCANO, E., KERDRAON, J., BOWSHER, D., PIMSTONE, S. N., SAMUELS, M. E., SHERRINGTON, R. & HAYDEN, M. R. 2007. Loss-of-function mutations in the Nav1.7 gene underlie congenital indifference to pain in multiple human populations. *Clin Genet,* 71**,** 311-319.

GOLDBERG, Y. P., PIMSTONE, S. N., NAMDARI, R., PRICE, N., COHEN, C., SHERRINGTON, R. P. & HAYDEN, M. R. 2012. Human Mendelian pain disorders: a key to discovery and validation of novel analgesics. *Clin Genet,* 82**,** 367-373.

GOMEZ-OSPINA, N., TSURUTA, F., BARRETO-CHANG, O., HU, L. & DOLMETSCH, R. 2006. The C Terminus of the L-Type Voltage-Gated Calcium Channel CaV1.2 Encodes a Transcription Factor. *Cell,* 127**,** 591-606.

GORCZYNSKA, E. & HANDELSMAN, D. J. 1993. Requirement for transmembrane sodium flux in maintenance of cytosolic calcium levels in rat Sertoli cells. *Am J Physiol,* 264**,** E863-7.

GORELOVA, N. A. & YANG, C. R. 2000. Dopamine D1/D5 receptor activation modulates a persistent sodium current in rat prefrontal cortical neurons in vitro. *J Neurophysiol,* 84**,** 75-87.

GORSON, K. C., HERRMANN, D. N., THIAGARAJAN, R., BRANNAGAN, T. H., CHIN, R. L., KINSELLA, L. J. & ROPPER, A. H. 2008. Non-length dependent small fibre neuropathy/ganglionopathy. *J Neurol Neurosurg Psychiatry,* 79**,** 163-9.

GRAEF, I. A., MERMELSTEIN, P. G., STANKUNAS, K., NEILSON, J. R., DEISSEROTH, K., TSIEN, R. W. & CRABTREE, G. R. 1999. L-type calcium channels and GSK-3 regulate the activity of NF-ATc4 in hippocampal neurons. *Nature,* 401**,** 703-8.

GUELLY, C., ZHU, P. P., LEONARDIS, L., PAPIC, L., ZIDAR, J., SCHABHUTTL, M., STROHMAIER, H., WEIS, J., STROM, T. M., BAETS, J., WILLEMS, J., DE JONGHE, P., REILLY, M. M., FROHLICH, E., HATZ, M., TRAJANOSKI, S., PIEBER, T. R., JANECKE, A. R., BLACKSTONE, C. & AUER-GRUMBACH, M. 2011. Targeted high-throughput sequencing identifies mutations in atlastin-1 as a cause of hereditary sensory neuropathy type I. *Am J Hum Genet,* 88**,** 99-105.

HAGERTY, T., MORGAN, W. W., ELANGO, N. & STRONG, R. 2001. Identification of a glucocorticoid-responsive element in the promoter region of the mouse tyrosine hydroxylase gene. *J Neurochem,* 76**,** 825-34.

HAIMOVICH, B., SCHOTLAND, D. L., FIELES, W. E. & BARCHI, R. L. 1987. Localization of sodium channel subtypes in adult rat skeletal muscle using channel-specific monoclonal antibodies. *The Journal of neuroscience : the official journal of the Society for Neuroscience,* 7**,** 2957-66.

HAINS, B. C., KLEIN, J. P., SAAB, C. Y., CRANER, M. J., BLACK, J. A. & WAXMAN, S. G. 2003. Upregulation of sodium channel Nav1.3 and functional involvement in neuronal hyperexcitability associated with central neuropathic pain after spinal cord injury. *The Journal of neuroscience : the official journal of the Society for Neuroscience,* 23**,** 8881-92.

HAMMARSTRÖM, A. & GAGE, P. 2002. Hypoxia and persistent sodium current. *European Biophysics Journal,* 31**,** 323-330.

HAN, C., ESTACION, M., HUANG, J., VASYLYEV, D., ZHAO, P., DIB-HAJJ, S. D. & WAXMAN, S. G. 2015a. Human Na(v)1.8: enhanced persistent and ramp currents contribute to distinct firing properties of human DRG neurons. *Journal of neurophysiology,* 113**,** 3172-85.

HAN, C., YANG, Y., DE GREEF, B. T., HOEIJMAKERS, J. G., GERRITS, M. M., VERHAMME, C., QU, J., LAURIA, G., MERKIES, I. S., FABER, C. G., DIB-HAJJ, S. D. & WAXMAN, S. G. 2015b. The Domain II S4-S5 Linker in Nav1.9: A Missense Mutation Enhances Activation, Impairs Fast Inactivation, and Produces Human Painful Neuropathy. *Neuromolecular Med,* 17**,** 158-69.

HARGREAVES, K., DUBNER, R., BROWN, F., FLORES, C. & JORIS, J. 1988. A new and sensitive method for measuring thermal nociception in cutaneous hyperalgesia. *Pain,* 32**,** 77-88.

HARRISON, C. 2013. Analgesia: A new player in neuropathic pain pathogenesis. *Nature Reviews Drug Discovery,* 12**,** 422-423.

HAWRYLYCZ, M. J., LEIN, E. S., GUILLOZET-BONGAARTS, A. L., SHEN, E. H., NG, L., MILLER, J. A., VAN DE LAGEMAAT, L. N., SMITH, K. A., EBBERT, A., RILEY, Z. L., ABAJIAN, C., BECKMANN, C. F., BERNARD, A., BERTAGNOLLI, D., BOE, A. F., CARTAGENA, P. M., CHAKRAVARTY, M. M., CHAPIN, M., CHONG, J., DALLEY, R. A., DALY, B. D., DANG, C., DATTA, S., DEE, N., DOLBEARE, T. A., FABER, V., FENG, D., FOWLER, D. R., GOLDY, J., GREGOR, B. W., HARADON, Z., HAYNOR, D. R., HOHMANN, J. G., HORVATH, S., HOWARD, R. E., JEROMIN, A., JOCHIM, J. M., KINNUNEN, M., LAU, C., LAZARZ, E. T., LEE, C., LEMON, T. A., LI, L., LI, Y., MORRIS, J. A., OVERLY, C. C., PARKER, P. D., PARRY, S. E., REDING, M., ROYALL, J. J., SCHULKIN, J., SEQUEIRA, P. A., SLAUGHTERBECK, C. R., SMITH, S. C., SODT, A. J., SUNKIN, S. M., SWANSON, B. E., VAWTER, M. P., WILLIAMS, D., WOHNOUTKA, P., ZIELKE, H. R., GESCHWIND, D. H., HOF, P. R., SMITH, S. M., KOCH, C., GRANT, S. G. & JONES, A. R. 2012. An anatomically comprehensive atlas of the adult human brain transcriptome. *Nature,* 489**,** 391-9.

HAYASHI, M., KAMIYA, Y., ITOH, H., HIGASHI, T., MIYAZAKI, T., FUNAKOSHI, K., YAMASHITA, N., GOSHIMA, Y., ANDOH, T., YAMADA, Y. & GOTO, T. 2011. Intrathecally administered Sema3A protein attenuates neuropathic pain behavior in rats with chronic constriction injury of the sciatic nerve. *Neuroscience Research,* 69**,** 17-24.

HAYDEN, R. & GROSSMAN, M. 1959. Rectal, ocular, and submaxillary pain; a familial autonomic disorder related to proctalgia fugaz: report of a family. *AMA J Dis Child,* 97**,** 479-482.

HE, S., ZHONG, Y., SHUAI, C., GAO, D., WEI, P., LI, G. & PENG, S. 2016. Tumor suppressor NGX6 inhibits the growth and metastasis of multiple cancers. *Tumour Biol,* 37**,** 5751-60.

HECKT, T., BICKERT, T., JESCHKE, A., SEITZ, S., SCHULZE, J., ITO, W. D., ZIMMERMANN, W., AMLING, M., SCHINKE, T., HORST, A. K. & KELLER, J. 2014. Increased osteoclastogenesis in mice lacking the carcinoembryonic antigen-related cell adhesion molecule 1. *PLoS ONE,* 9**,** e114360.

HERZOG, R. I., CUMMINS, T. R., GHASSEMI, F., DIB-HAJJ, S. D. & WAXMAN, S. G. 2003. Distinct repriming and closed-state inactivation kinetics of Nav1.6 and Nav1.7 sodium channels in mouse spinal sensory neurons. *J Physiol,* 551**,** 741-50.

HERZOG, R. I., CUMMINS, T. R. & WAXMAN, S. G. 2001. Persistent TTX-resistant Na+ current affects resting potential and response to depolarization in simulated spinal sensory neurons. *J Neurophysiol,* 86**,** 1351-64.

HETZ, C. & MOLLEREAU, B. 2014. Disturbance of endoplasmic reticulum proteostasis in neurodegenerative diseases. *Nature Reviews Neuroscience,* 15**,** 233-249.

HINMAN, A., CHUANG, H. H., BAUTISTA, D. M. & JULIUS, D. 2006. TRP channel activation by reversible covalent modification. *Proceedings of the National Academy of Sciences,* 103**,** 19564-19568.

HO, C. & O'LEARY, M. E. 2011. Single-cell analysis of sodium channel expression in dorsal root ganglion neurons. *Mol Cell Neurosci,* 46**,** 159-66.

HOEIJMAKERS, J. G., FABER, C. G., LAURIA, G., MERKIES, I. S. & WAXMAN, S. G. 2012. Small-fibre neuropathies—advances in diagnosis, pathophysiology and management. *Nature Reviews Neurology,* 8**,** 369-379.

HOLLAND, N. R., CRAWFORD, T. O., HAUER, P., CORNBLATH, D. R., GRIFFIN, J. W. & MCARTHUR, J. C. 1998. Small-fiber sensory neuropathies: clinical course and neuropathology of idiopathic cases. *Ann Neurol,* 44**,** 47-59.

HU, X., WU, F., SUN, S., YU, W. & HU, J. 2015. Human atlastin GTPases mediate differentiated fusion of endoplasmic reticulum membranes. *Protein Cell,* 6**,** 307-11.

HU, Z.-L., BAO, J. & REECY, J. M. 2008. CateGOrizer: A Web-Based Program to Batch Analyze Gene Ontology Classification Categories. *Online Journal of Bioinformatics,* 9**,** 108-112.

HUANG, J., HAN, C., ESTACION, M., VASYLYEV, D., HOEIJMAKERS, J. G., GERRITS, M. M., TYRRELL, L., LAURIA, G., FABER, C. G., DIB-HAJJ, S. D., MERKIES, I. S., WAXMAN, S. G. & GROUP, P. S. 2014. Gain-of-function mutations in sodium channel Na(v)1.9 in painful neuropathy. *Brain,* 137**,** 1627-42.

HUANG, J., PEREZ-BURGOS, L., PLACEK, B. J., SENGUPTA, R., RICHTER, M., DORSEY, J. A., KUBICEK, S., OPRAVIL, S., JENUWEIN, T. & BERGER, S. L. 2006. Repression of p53 activity by Smyd2-mediated methylation. *Nature,* 444**,** 629-632.

HUANG, J., YANG, Y., ZHAO, P., GERRITS, M. M., HOEIJMAKERS, J. G., BEKELAAR, K., MERKIES, I. S., FABER, C. G., DIB-HAJJ, S. D. & WAXMAN, S. G. 2013. Small-fiber neuropathy Nav1.8 mutation shifts activation to hyperpolarized potentials and increases excitability of dorsal root ganglion neurons. *J Neurosci,* 33**,** 14087-14097.

HUNSKAAR, S., FASMER, O. B. & HOLE, K. 1985. Formalin test in mice, a useful technique for evaluating mild analgesics. *J Neurosci Methods,* 14**,** 69-76.

INVITROGEN 2002. Potent, reliable selection reagents for gene expression. *Invitrogen eBrochure,* 710-011094.

ISENSEE, J., KRAHE, L., MOELLER, K., PEREIRA, V., SEXTON, J. E., SUN, X., EMERY, E., WOOD, J. N. & HUCHO, T. 2017. Synergistic regulation of serotonin and opioid signaling contributes to pain insensitivity in Nav1.7 knockout mice. *Sci Signal,* 10.

ISHIKAWA, H. & BARBER, G. N. 2008. STING is an endoplasmic reticulum adaptor that facilitates innate immune signalling. *Nature,* 455**,** 674-8.

ISHIKAWA, H., MA, Z. & BARBER, G. N. 2009. STING regulates intracellular DNA-mediated, type I interferon-dependent innate immunity. *Nature,* 461**,** 788-92.

ISHIKAWA, M. 1987. Developmental disorders in histidinemia--follow-up study of language development in histidinemia. *Acta Paediatr Jpn,* 29**,** 224-8.

JACQUET, Y. F. & LAJTHA, A. 1976. The periaqueductal gray: site of morphine analgesia and tolerance as shown by 2-way cross tolerance between systemic and intracerebral injections. *Brain research,* 103**,** 501-13.

JAGADEESH, K. A., WENGER, A. M., BERGER, M. J., GUTURU, H., STENSON, P. D., COOPER, D. N., BERNSTEIN, J. A. & BEJERANO, G. 2016. M-CAP eliminates a majority of variants of uncertain significance in clinical exomes at high sensitivity. *Nat Genet,* 48**,** 1581-1586.

JANECKA, A., FICHNA, J. & JANECKI, T. 2004. Opioid Receptors and their Ligands. *Current Topics in Medicinal Chemistry,* 4**,** 1-17.

JANSSON, M., DURANT, S. T., CHO, E.-C., SHEAHAN, S., EDELMANN, M., KESSLER, B. & LA THANGUE, N. B. 2008. Arginine methylation regulates the p53 response. *Nature Cell Biology,* 10**,** 1431-1439.

JEONG, H., KIM, M. S., KIM, S. W., KIM, K. S. & SEOL, W. 2006. Regulation of tyrosine hydroxylase gene expression by retinoic acid receptor. *J Neurochem,* 98**,** 386-94.

JONES, B. J. & ROBERTS, D. J. 1968. A rotarod suitable for quantitative measurements of motor incoordination in naive mice. *Naunyn Schmiedebergs Arch Exp Pathol Pharmakol,* 259**,** 211.

JORDAN, B. A., CVEJIC, S. & DEVI, L. A. 2000. Opioids and Their Complicated Receptor Complexes. *Neuropsychopharmacology,* 23**,** S5-S18.

JOSHI, S. K., MIKUSA, J. P., HERNANDEZ, G., BAKER, S., SHIEH, C. C., NEELANDS, T., ZHANG, X. F., NIFORATOS, W., KAGE, K., HAN, P., KRAFTE, D., FALTYNEK, C., SULLIVAN, J. P., JARVIS, M. F. & HONORE, P. 2006. Involvement of the TTX-resistant sodium channel Nav 1.8 in inflammatory and neuropathic, but not post-operative, pain states. *Pain,* 123**,** 75-82.

KANELLOPOULOS, A. H. & MATSUYAMA, A. 2016. Voltage-gated sodium channels and pain-related disorders. *Clin Sci (Lond),* 130**,** 2257-2265.

KARIMI-GOOGHERI, M., DANESHVAR, H., KHALEGHINIA, M., BIDAKI, R. & KAZEMI ARABABADI, M. 2015. Decreased Expressions of STING but not IRF3 Molecules in Chronic HBV Infected Patients. *Arch Iran Med,* 18**,** 351-4.

KATRITCH, V., FENALTI, G., ABOLA, E. E., ROTH, B. L., CHEREZOV, V. & STEVENS, R. C. 2014. Allosteric sodium in class A GPCR signaling. *Trends Biochem Sci,* 39**,** 233-44.

KAWAI, Y., MORIYAMA, A., ASAI, K., COLEMAN-CAMPBELL, C. M., SUMI, S., MORISHITA, H. & SUCHI, M. 2005. Molecular characterization of histidinemia: identification of four missense mutations in the histidase gene. *Hum Genet,* 116**,** 340-6.

KAWASAKI, Y., ZHANG, L., CHENG, J. K. & JI, R. R. 2008. Cytokine mechanisms of central sensitization: distinct and overlapping role of interleukin-1beta, interleukin-6, and tumor necrosis factor-alpha in regulating synaptic and neuronal activity in the superficial spinal cord. *J Neurosci,* 28**,** 5189-94.

KERR, B. J., SOUSLOVA, V., MCMAHON, S. B. & WOOD, J. N. 2001. A role for the TTX-resistant sodium channel Nav 1.8 in NGF-induced hyperalgesia, but not neuropathic pain. *Neuroreport,* 12**,** 3077-3080.

KHASAR, S. G., GOLD, M. S. & LEVINE, J. D. 1998. A tetrodotoxin-resistant sodium current mediates inflammatory pain in the rat. *Neurosci Lett,* 256**,** 17-20.

KIM, C., JUN, K., LEE, T., KIM, S.-S., MCENERY, M. W., CHIN, H., KIM, H.-L., PARK, J. M., KIM, D. K., JUNG, S. J., KIM, J. & SHIN, H.-S. 2001. Altered Nociceptive Response in Mice Deficient in the α 1B Subunit of the Voltage-Dependent Calcium Channel. *Molecular and Cellular Neuroscience,* 18**,** 235-245.

KIM, T. E., PARK, M. J., CHOI, E. J., LEE, H. S., LEE, S. H., YOON, S. H., OH, C. K., LEE, B. J., KIM, S. U., LEE, Y. S. & LEE, M. A. 2003. Cloning and cell type-specific regulation of the human tyrosine hydroxylase gene promoter. *Biochem Biophys Res Commun,* 312**,** 1123-31.

KOBAYASHI, M., CHANDRASEKHAR, A., CHENG, C., MARTINEZ, J. A., NG, H., DE LA HOZ, C. & ZOCHODNE, D. W. 2017. Diabetic polyneuropathy, sensory neurons, nuclear structure and spliceosome alterations: a role for CWC22. *Dis Model Mech,* 10**,** 215-224.

KOENIG, J., WERDEHAUSEN, R., LINLEY, J. E., HABIB, A. M., VERNON, J., LOLIGNIER, S., EIJKELKAMP, N., ZHAO, J., OKOROKOV, A. L., WOODS, C. G., WOOD, J. N. & COX, J. J. 2015. Regulation of $Na_v1.7$: A conserved SCN9A natural antisense transcript expressed in dorsal root Ganglia. *PLoS ONE,* 10**,** 1-14.

KOHNO, T., WANG, H., AMAYA, F., BRENNER, G. J., CHENG, J. K., JI, R. R. & WOOLF, C. J. 2008. Bradykinin enhances AMPA and NMDA receptor activity in spinal cord dorsal horn neurons by activating multiple kinases to produce pain hypersensitivity. *J Neurosci,* 28**,** 4533-40.

KOMINE, Y., NAKAMURA, K., KATSUKI, M. & YAMAMORI, T. 2006. Novel transcription factor zfh-5 is negatively regulated by its own antisense RNA in mouse brain. *Molecular and Cellular Neuroscience,* 31**,** 273-283.

KOMINE, Y., TAKAO, K., MIYAKAWA, T. & YAMAMORI, T. 2012. Behavioral abnormalities observed in Zfhx2-deficient mice. *PLoS ONE,* 7**,** e53114.

KONERU, A., SATYANARAYANA, S. & RIZMAN, S. 2009. Endogenous Opioids : Their Physiological Role and Receptors. *Global Journal of Pharmacology,* 3**,** 149-153.

KORNAK, U., MADEMAN, I., SCHINKE, M., VOIGT, M., KRAWITZ, P., HECHT, J., BARVENCIK, F., SCHINKE, T., GIESSELMANN, S., BEIL, F. T., POU-SERRADELL, A., VILCHEZ, J. J., BEETZ, C., DECONINCK, T., TIMMERMAN, V., KAETHER, C., DE JONGHE, P., HUBNER, C. A., GAL, A., AMLING, M., MUNDLOS, S., BAETS, J. & KURTH, I. 2014. Sensory neuropathy with bone destruction due to a mutation in the membrane-shaping atlastin GTPase 3. *Brain,* 137**,** 683-92.

KOVALEVICH, J. & LANGFORD, D. 2013. Considerations for the use of SH-SY5Y neuroblastoma cells in neurobiology. *Methods Mol Biol,* 1078**,** 9-21.

KRAUSE, J. E., CHIRGWIN, J. M., CARTER, M. S., XU, Z. S. & HERSHEY, A. D. 1987. Three rat preprotachykinin mRNAs encode the neuropeptides substance P and neurokinin A. *Proc Natl Acad Sci U S A,* 84**,** 881-5.

KREMEYER, B., LOPERA, F., COX, J. J., MOMIN, A., RUGIERO, F., MARSH, S., WOODS, C. G., JONES, N. G., PATERSON, K. J., FRICKER, F. R., VILLEGAS, A., ACOSTA, N., PINEDA-TRUJILLO, N. G., RAMIREZ, J. D., ZEA, J., BURLEY, M. W., BEDOYA, G., BENNETT, D. L., WOOD, J. N. & RUIZ-LINARES, A. 2010. A gain-of-function mutation in TRPA1 causes familial episodic pain syndrome. *Neuron,* 66**,** 671-680.

KRUGER, R. P., AURANDT, J. & GUAN, K.-L. 2005. Semaphorins command cells to move. *Nature reviews. Molecular cell biology,* 6**,** 789-800.

KRUSE, J.-P. & GU, W. 2009. Modes of p53 regulation. *Cell,* 137**,** 609-22.

KUESPERT, K., PILS, S. & HAUCK, C. R. 2006. CEACAMs: their role in physiology and pathophysiology. *Curr Opin Cell Biol,* 18**,** 565-71.

KURODA, H., SOBHAN, U., SATO, M., TSUMURA, M., ICHINOHE, T., TAZAKI, M. & SHIBUKAWA, Y. 2013. Sodium-calcium exchangers in rat trigeminal ganglion neurons. *Mol Pain,* 9**,** 22.

KWAN, K. Y., ALLCHORNE, A. J., VOLLRATH, M. A., CHRISTENSEN, A. P., ZHANG, D.-S., WOOLF, C. J. & COREY, D. P. 2006. TRPA1 Contributes to Cold, Mechanical, and Chemical Nociception but Is Not Essential for Hair-Cell Transduction. *Neuron,* 50**,** 277-289.

KYLE, D. J. & ILYIN, V. I. 2007. Sodium Channel Blockers. *Journal of Medicinal Chemistry,* 50**,** 2583-2588.

LAGERSTRÖM, M. C., ROGOZ, K., ABRAHAMSEN, B., PERSSON, E., REINIUS, B., NORDENANKAR, K., ÖLUND, C., SMITH, C., MENDEZ, J. A., CHEN, Z.-F., WOOD, J. N., WALLÉN-MACKENZIE, Å. & KULLANDER, K. 2010. VGLUT2-Dependent Sensory Neurons in the TRPV1 Population Regulate Pain and Itch. *Neuron,* 68**,** 529-542.

LAI, J., GOLD, M. S., KIM, C. S., BIAN, D., OSSIPOV, M. H., HUNTER, J. C. & PORRECA, F. 2002. Inhibition of neuropathic pain by decreased expression of the tetrodotoxin-resistant sodium channel, NaV1.8. *Pain,* 95**,** 143-152.

LALLEMEND, F. & ERNFORS, P. 2012. Molecular interactions underlying the specification of sensory neurons. *Trends in Neurosciences,* 35**,** 373-381.

LARSON, A. A., BROWN, D. R., EL-ATRASH, S. & WALSER, M. M. 1986. Pain threshold changes in adjuvant-induced inflammation: a possible model of chronic pain in the mouse. *Pharmacol Biochem Behav,* 24**,** 49-53.

LAWRENCE, J. 2016. A new channel for pain treatment. *The Pharmaceutical Journal,* 296**,** online.

LEBEL, M., GAUTHIER, Y., MOREAU, A. & DROUIN, J. 2001. Pitx3 activates mouse tyrosine hydroxylase promoter via a high-affinity binding site. *J Neurochem,* 77**,** 558-67.

LEE, D. E., KIM, S. J. & ZHUO, M. 1999. Comparison of behavioral responses to noxious cold and heat in mice. *Brain Res,* 845**,** 117-21.

LEE, J.-H., PARK, C.-K., CHEN, G., HAN, Q., XIE, R.-G., LIU, T., JI, R.-R. & LEE, S.-Y. 2014. A Monoclonal Antibody that Targets a NaV1.7 Channel Voltage Sensor for Pain and Itch Relief. *Cell,* 157**,** 1393-1404.

LEIPOLD, E., LIEBMANN, L., KORENKE, G. C., HEINRICH, T., GIESSELMANN, S., BAETS, J., EBBINGHAUS, M., GORAL, R. O., STODBERG, T., HENNINGS, J. C., BERGMANN, M., ALTMULLER, J., THIELE, H., WETZEL, A., NURNBERG, P., TIMMERMAN, V., DE JONGHE, P., BLUM, R., SCHAIBLE, H. G., WEIS, J., HEINEMANN, S. H., HUBNER, C. A. & KURTH, I. 2013. A de novo gain-of-function mutation in SCN11A causes loss of pain perception. *Nat Genet,* 45**,** 1399-1404.

LEO, S., D'HOOGE, R. & MEERT, T. 2010. Exploring the role of nociceptor-specific sodium channels in pain transmission using Nav1.8 and Nav1.9 knockout mice. *Behav Brain Res,* 208**,** 149-157.

LEO, S., MOECHARS, D., CALLAERTS-VEGH, Z., D'HOOGE, R. & MEERT, T. 2009. Impairment of VGLUT2 but not VGLUT1 signaling reduces neuropathy-induced hypersensitivity. *European Journal of Pain,* 13**,** 1008-1017.

LEVY, H. L., TAYLOR, R. G. & MCINNES, R. R. 2001. Disorders of histidine metabolism. In: Scriver, C. R.; Beaudet, A. L.; Sly, W. S.; Valle, D. (eds.): The Metabolic and Molecular Bases of Inherited Disease. Vol. II. (8th ed.), New York: McGraw-Hill.

LI, H. & DURBIN, R. 2009. Fast and accurate short read alignment with Burrows-Wheeler transform. *Bioinformatics,* 25**,** 1754-60.

LI, J., TAN, C., XIANG, Q., ZHANG, X., MA, J., WANG, J. R., YANG, J., LI, W., SHEN, S. R., LIANG, S. & LI, G. 2001. Proteomic detection of changes in protein synthesis induced by NGX6 transfected in human nasopharyngeal carcinoma cells. *J Protein Chem,* 20**,** 265-71.

LI, L., RUTLIN, M., ABRAIRA, V. E., CASSIDY, C., KUS, L., GONG, S., JANKOWSKI, M. P., LUO, W., HEINTZ, N., KOERBER, H. R., WOODBURY, C. J. & GINTY, D. D. 2011. The functional organization of cutaneous low-threshold mechanosensory neurons. *Cell,* 147**,** 1615-27.

LIFETECHNOLOGIES. 2015. *Schematic of the luciferase reporter assay* [Online]. Available: https://www.lifetechnologies.com/uk/en/home/life-science/protein-biology/protein-biology-learning-center/protein-biology-resource-library/pierce-protein-methods/luciferase-reporters.html [Accessed].

LINDIA, J. A., KÖHLER, M. G., MARTIN, W. J. & ABBADIE, C. 2005. Relationship between sodium channel NaV1.3 expression and neuropathic pain behavior in rats. *Pain,* 117**,** 145-153.

LIRK, P., POROLI, M., RIGAUD, M., FUCHS, A., FILLIP, P., HUANG, C.-Y., LJUBKOVIC, M., SAPUNAR, D. & HOGAN, Q. 2008. Modulators of Calcium Influx Regulate Membrane Excitability in Rat Dorsal Root Ganglion Neurons. *Anesthesia & Analgesia,* 107**,** 673-685.

LIU, C.-C., GAO, Y.-J., LUO, H., BERTA, T., XU, Z.-Z., JI, R.-R. & TAN, P.-H. 2016. Interferon alpha inhibits spinal cord synaptic and nociceptive transmission via neuronal-glial interactions. *Scientific Reports,* **6,** 34356-34356.

LIU, Y., JESUS, A. A., MARRERO, B., YANG, D., RAMSEY, S. E., MONTEALEGRE SANCHEZ, G. A., TENBROCK, K., WITTKOWSKI, H., JONES, O. Y., KUEHN, H. S., LEE, C. C., DIMATTIA, M. A., COWEN, E. W., GONZALEZ, B., PALMER, I., DIGIOVANNA, J. J., BIANCOTTO, A., KIM, H., TSAI, W. L., TRIER, A. M., HUANG, Y., STONE, D. L., HILL, S., KIM, H. J., ST HILAIRE, C., GURPRASAD, S., PLASS, N., CHAPELLE, D., HORKAYNE-SZAKALY, I., FOELL, D., BARYSENKA, A., CANDOTTI, F., HOLLAND, S. M., HUGHES, J. D., MEHMET, H., ISSEKUTZ, A. C., RAFFELD, M., MCELWEE, J., FONTANA, J. R., MINNITI, C. P., MOIR, S., KASTNER, D. L., GADINA, M., STEVEN, A. C., WINGFIELD, P. T., BROOKS, S. R., ROSENZWEIG, S. D., FLEISHER, T. A., DENG, Z., BOEHM, M., PALLER, A. S. & GOLDBACH-MANSKY, R. 2014. Activated STING in a vascular and pulmonary syndrome. *N Engl J Med,* 371**,** 507-18.

LIVAK, K. J. & SCHMITTGEN, T. D. 2001. Analysis of relative gene expression data using real-time quantitative PCR and the 2(-Delta Delta C(T)) Method. *Methods,* 25**,** 402-8.

LOLIGNIER, S., AMSALEM, M., MAINGRET, F., PADILLA, F., GABRIAC, M., CHAPUY, E., ESCHALIER, A., DELMAS, P. & BUSSEROLLES, J. 2011. Nav1.9 channel contributes to mechanical and heat pain hypersensitivity induced by subacute and chronic inflammation. *PLoS One,* **6,** e23083-e23083.

LOPEZ-RODRIGUEZ, C., ARAMBURU, J., RAKEMAN, A. S. & RAO, A. 1999. NFAT5, a constitutively nuclear NFAT protein that does not cooperate with Fos and Jun. *Proc Natl Acad Sci U S A,* 96**,** 7214-9.

LÖTSCH, J., SKARKE, C., GRÖSCH, S., DARIMONT, J., SCHMIDT, H. & GEISSLINGER, G. 2002. The polymorphism A118G of the human mu-opioid receptor gene decreases the pupil constrictory effect of morphine-6-glucuronide but not that of morphine. *Pharmacogenetics,* 12**,** 3-9.

LUVISETTO, S., MARINELLI, S., PANASITI, M. S., D' AMATO, F. R., FLETCHER, C. F., PAVONE, F. & PIETROBON, D. 2006. Pain sensitivity in mice lacking the Cav2.1 α 1 subunit of P/Q-type Ca2+ channels. *Neuroscience,* 142**,** 823-832.

MACDONALD, A. D., WOOLFE, G., BERGEL, F., MORRISON, A. L. & RINDERKNECHT, H. 1946. Analgesic action of pethidine derivatives and related compounds. *Br J Pharmacol Chemother,* 1**,** 4-14.

MACPHERSON, L. J., DUBIN, A. E., EVANS, M. J., MARR, F., SCHULTZ, P. G., CRAVATT, B. F. & PATAPOUTIAN, A. 2007. Noxious compounds activate TRPA1 ion channels through covalent modification of cysteines. *Nature,* 445**,** 541-545.

MAINGRET, F., COSTE, B., PADILLA, F., CLERC, N., CREST, M., KOROGOD, S. M. & DELMAS, P. 2008. Inflammatory mediators increase Nav1.9 current and excitability in nociceptors through a coincident detection mechanism. *J Gen Physiol,* 131**,** 211-25.

MANNELLI, P., PEINDL, K. S. & WU, L.-T. 2011. Pharmacological enhancement of naltrexone treatment for opioid dependence: a review. *Substance Abuse and Rehabilitation,* 2**,** 113-123.

MANTEGAZZA, M., CURIA, G., BIAGINI, G., RAGSDALE, D. S. & AVOLI, M. 2010. Voltage-gated sodium channels as therapeutic targets in epilepsy and other neurological disorders. *The Lancet Neurology,* **9,** 413-424.

MANTYH, P. W., ROGERS, S. D., HONORE, P., ALLEN, B. J., GHILARDI, J. R., LI, J., DAUGHTERS, R. S., LAPPI, D. A., WILEY, R. G. & SIMONE, D. A. 1997. Inhibition of hyperalgesia by ablation of lamina I spinal neurons expressing the substance P receptor. *Science (New York, N.Y.),* 278**,** 275-9.

MANZANO, G. M., GIULIANO, L. M. P. & NÓBREGA, J. A. M. 2008. A brief historical note on the classification of nerve fibers. *Arq Neuropsiquiatr,* 66**,** 117-119.

MARCHETTI, C., CARBONE, E. & LUX, H. D. 1986. Effects of dopamine and noradrenaline on Ca channels of cultured sensory and sympathetic neurons of chick. *Pflugers Arch,* 406**,** 104-11.

MATTHES, H. W., MALDONADO, R., SIMONIN, F., VALVERDE, O., SLOWE, S., KITCHEN, I., BEFORT, K., DIERICH, A., LE MEUR, M., DOLLE, P., TZAVARA, E., HANOUNE, J., ROQUES, B. P. & KIEFFER, B. L. 1996. Loss of morphine-induced analgesia, reward effect and withdrawal symptoms in mice lacking the mu-opioid-receptor gene. *Nature,* 383**,** 819-23.

MCKENNA, A., HANNA, M., BANKS, E., SIVACHENKO, A., CIBULSKIS, K., KERNYTSKY, A., GARIMELLA, K., ALTSHULER, D., GABRIEL, S., DALY, M. & DEPRISTO, M. A. 2010. The Genome Analysis Toolkit: a MapReduce framework for analyzing next-generation DNA sequencing data. *Genome Res,* 20**,** 1297-303.

MCNAMARA, C. R., MANDEL-BREHM, J., BAUTISTA, D. M., SIEMENS, J., DERANIAN, K. L., ZHAO, M., HAYWARD, N. J., CHONG, J. A., JULIUS, D., MORAN, M. M. & FANGER, C. M. 2007. TRPA1 mediates formalin-induced pain. *Proc Natl Acad Sci U S A,* 104**,** 13525-30.

MCNEILL, E. M., ROOS, K. P., MOECHARS, D. & CLAGETT-DAME, M. 2010. Nav2 is necessary for cranial nerve development and blood pressure regulation. *Neural development,* 5**,** 6-6.

MESSERSMITH, E. K., LEONARDO, E. D., SHATZ, C. J., TESSIER-LAVIGNE, M., GOODMAN, C. S. & KOLODKIN, A. L. 1995. Semaphorin III can function as a selective chemorepellent to pattern sensory projections in the spinal cord. *Neuron,* 14**,** 949-59.

MINETT, M. S., NASSAR, M. A., CLARK, A. K., PASSMORE, G., DICKENSON, A. H., WANG, F., MALCANGIO, M. & WOOD, J. N. 2012. Distinct Nav1.7-dependent pain sensations require different sets of sensory and sympathetic neurons. *Nat Commun,* 3**,** 791.

MINETT, M. S., PEREIRA, V., SIKANDAR, S., MATSUYAMA, A., LOLIGNIER, S., KANELLOPOULOS, A. H., MANCINI, F., IANNETTI, G. D., BOGDANOV, Y. D., SANTANA-VARELA, S., MILLET, Q., BASKOZOS, G., MACALLISTER, R., COX, J. J., ZHAO, J. & WOOD, J. N. 2015. Endogenous opioids contribute to insensitivity to pain in humans and mice lacking sodium channel Nav1.7. *Nat Commun,* 6**,** 8967-8967.

MIYAKAWA, H., WOO, S. K., DAHL, S. C., HANDLER, J. S. & KWON, H. M. 1999. Tonicity-responsive enhancer binding protein, a rel-like protein that stimulates transcription in response to hypertonicity. *Proc Natl Acad Sci U S A,* 96**,** 2538-42.

MOECHARS, D., WESTON, M. C., LEO, S., CALLAERTS-VEGH, Z., GORIS, I., DANEELS, G., BUIST, A., CIK, M., VAN DER SPEK, P., KASS, S., MEERT, T., D'HOOGE, R., ROSENMUND, C. & HAMPSON, R. M. 2006. Vesicular Glutamate Transporter VGLUT2 Expression Levels Control Quantal Size and Neuropathic Pain. *Journal of Neuroscience,* 26**,** 12055-12066.

MOGIL, J. S. 2012. Sex differences in pain and pain inhibition: multiple explanations of a controversial phenomenon. *Nat Rev Neurosci,* 13**,** 859-866.

MOMIN, A. & WOOD, J. N. 2008. Sensory neuron voltage-gated sodium channels as analgesic drug targets. *Current Opinion in Neurobiology,* 18**,** 383-388.

NAGY, V., COLE, T., VAN CAMPENHOUT, C., KHOUNG, T. M., LEUNG, C., VERMEIREN, S., NOVATCHKOVA, M., WENZEL, D., CIKES, D., POLYANSKY, A. A., KOZIERADZKI, I., MEIXNER, A., BELLEFROID, E. J., NEELY, G. G. & PENNINGER, J. M. 2015. The evolutionarily conserved transcription factor PRDM12 controls sensory neuron development and pain perception. *Cell Cycle,* 14**,** 1799-808.

NAHORSKI, M. S., CHEN, Y. C. & WOODS, C. G. 2015. New Mendelian Disorders of Painlessness. *Trends Neurosci,* 38**,** 712-24.

NAKAJIMA, A., IIJIMA, H., NEURATH, M. F., NAGAISHI, T., NIEUWENHUIS, E. E., RAYCHOWDHURY, R., GLICKMAN, J., BLAU, D. M., RUSSELL, S., HOLMES, K. V. & BLUMBERG, R. S. 2002. Activation-induced expression of carcinoembryonic antigen-cell adhesion molecule 1 regulates mouse T lymphocyte function. *J Immunol,* 168**,** 1028-35.

NARAHASHI, T. 2008. Tetrodotoxin: a brief history. *Proc Jpn Acad Ser B Phys Biol Sci,* 84**,** 147-54.

NARITA, M., OZAKI, S., NARITA, M., ISE, Y., YAJIMA, Y. & SUZUKI, T. 2003. Change in the expression of c-fos in the rat brain following sciatic nerve ligation. *Neuroscience letters,* 352**,** 231-3.

NASSAR, M. A., BAKER, M. D., LEVATO, A., INGRAM, R., MALLUCCI, G., MCMAHON, S. B. & WOOD, J. N. 2006. Nerve injury induces robust allodynia and ectopic discharges in Nav1.3 null mutant mice. *Molecular pain,* 2**,** 33-33.

NASSAR, M. A., LEVATO, A., STIRLING, L. C. & WOOD, J. N. 2005. Neuropathic pain develops normally in mice lacking both Na(v)1.7 and Na(v)1.8. *Mol Pain,* 1**,** 24-24.

NASSAR, M. A., STIRLING, L. C., FORLANI, G., BAKER, M. D., MATTHEWS, E. A., DICKENSON, A. H. & WOOD, J. N. 2004. Nociceptor-specific gene deletion reveals a major role for Nav1.7 (PN1) in acute and inflammatory pain. *Proc Natl Acad Sci U S A,* 101**,** 12706-11.

NEMOTO, T., MIYAZAKI, S., KANAI, T., MARUTA, T., SATOH, S., YOSHIKAWA, N., YANAGITA, T. & WADA, A. 2010. Nav1.7-Ca2+ influx-induced increased phosphorylations of extracellular signal-regulated kinase (ERK) and p38 attenuate tau phosphorylation via glycogen synthase kinase-3beta: priming of Nav1.7 gating by ERK and p38. *Eur J Pharmacol,* 640**,** 20-8.

NEUFELD, G. & KESSLER, O. 2008. The semaphorins: versatile regulators of tumour progression and tumour angiogenesis. *Nature Reviews Cancer,* 8**,** 632-645.

NEUMANN, M., SAMPATHU, D. M., KWONG, L. K., TRUAX, A. C., MICSENYI, M. C., CHOU, T. T., BRUCE, J., SCHUCK, T., GROSSMAN, M., CLARK, C. M., MCCLUSKEY, L. F., MILLER, B. L., MASLIAH, E., MACKENZIE, I. R., FELDMAN, H., FEIDEN, W., KRETZSCHMAR, H. A., TROJANOWSKI, J. Q. & LEE, V. M.-Y. 2006. Ubiquitinated TDP-43 in Frontotemporal Lobar Degeneration and Amyotrophic Lateral Sclerosis. *Science,* 314**,** 130-133.

NEWENGLANDBIOLABS. *The photo-oxidation catalyzed by Gaussia Luciferase* [Online]. Available: https://www.neb.com/products/e3300-biolux-gaussia-luciferase-assay-kit [Accessed].

NEWENGLANDBIOLABS. *The photochemical reaction catalyzed by Cypridina Luciferase* [Online]. Available: https://www.neb.com/products/e3309-biolux-cypridina-luciferase-assay-kit [Accessed].

NICHOLS, M. L., ALLEN, B. J., ROGERS, S. D., GHILARDI, J. R., HONORE, P., LUGER, N. M., FINKE, M. P., LI, J., LAPPI, D. A., SIMONE, D. A. & MANTYH, P. W. 1999. Transmission of chronic nociception by spinal neurons expressing the substance P receptor. *Science (New York, N.Y.),* 286**,** 1558-61.

NILSEN, K. B., NICHOLAS, A. K., WOODS, C. G., MELLGREN, S. I., NEBUCHENNYKH, M. & AASLY, J. 2009. Two novel SCN9A mutations causing insensitivity to pain. *Pain,* 143**,** 155-8.

NOËL, J., ZIMMERMANN, K., BUSSEROLLES, J., DEVAL, E., ALLOUI, A., DIOCHOT, S., GUY, N., BORSOTTO, M., REEH, P., ESCHALIER, A. & LAZDUNSKI, M. 2009. The mechano-activated K+ channels TRAAK and TREK-1 control both warm and cold perception. *The EMBO Journal,* 28**,** 1308-1318.

NOWYCKY, M. C., FOX, A. P. & TSIEN, R. W. 1985. Three types of neuronal calcium channel with different calcium agonist sensitivity. *Nature,* 316**,** 440-3.

OBATA, K., KATSURA, H., MIZUSHIMA, T., YAMANAKA, H., KOBAYASHI, K., DAI, Y., FUKUOKA, T., TOKUNAGA, A., TOMINAGA, M. & NOGUCHI, K. 2005. TRPA1 induced in sensory neurons contributes to cold hyperalgesia after inflammation and nerve injury. *The Journal of clinical investigation,* 115**,** 2393-401.

OLIVERIA, S. F., DELL'ACQUA, M. L. & SATHER, W. A. 2007. AKAP79/150 anchoring of calcineurin controls neuronal L-type Ca2+ channel activity and nuclear signaling. *Neuron,* 55**,** 261-75.

ONG, S. E., MITTLER, G. & MANN, M. 2004. Identifying and quantifying in vivo methylation sites by heavy methyl SILAC. *Nat Methods,* 1**,** 119-26.

PARENT, A. J., BEAUDET, N., BEAUDRY, H., BERGERON, J., BERUBE, P., DROLET, G., SARRET, P. & GENDRON, L. 2012. Increased anxiety-like behaviors in rats experiencing chronic inflammatory pain. *Behav Brain Res,* 229**,** 160-7.

PARK, J.-Y., REMY, S., VARELA, J., COOPER, D. C., CHUNG, S., KANG, H.-W., LEE, J.-H. & SPRUSTON, N. 2010. A post-burst after depolarization is mediated by group i metabotropic glutamate receptor-dependent upregulation of Ca(v)2.3 R-type calcium channels in CA1 pyramidal neurons. *PLoS biology,* 8**,** e1000534-e1000534.

PARK, J. H., SZEMES, M., VIEIRA, G. C., MELEGH, Z., MALIK, S., HEESOM, K. J., VON WALLWITZ-FREITAS, L., GREENHOUGH, A., BROWN, K. W., ZHENG, Y. G., CATCHPOOLE, D., DEERY, M. J. & MALIK, K. 2015. Protein arginine methyltransferase 5 is a key regulator of the MYCN oncoprotein in neuroblastoma cells. *Mol Oncol,* 9**,** 617-27.

PASTERKAMP, R. J., GIGER, R. J., BAKER, R. E., HERMENS, W. T. & VERHAAGEN, J. 2000. Ectopic adenoviral vector-directed expression of Sema3A in organotypic spinal cord explants inhibits growth of primary sensory afferents. *Developmental biology,* 220**,** 129-41.

PASTERNAK, G. W., SNOWMAN, A. M. & SNYDER, S. H. 1975. Selective enhancement of [3H]opiate agonist binding by divalent cations. *Mol Pharmacol,* 11**,** 735-44.

PAYANDEH, J., SCHEUER, T., ZHENG, N. & CATTERALL, W. A. 2011. The crystal structure of a voltage-gated sodium channel. *Nature,* 475**,** 353-8.

PEETERS, P. J., BAKER, A., GORIS, I., DANEELS, G., VERHASSELT, P., LUYTEN, W. H. M. L., GEYSEN, J. J. G. H., KASS, S. U. & MOECHARS, D. W. E. 2004. Sensory deficits in mice hypomorphic for a mammalian homologue of unc-53. *Developmental Brain Research,* 150**,** 89-101.

PENG, Y. B., LIN, Q. & WILLIS, W. D. 1996. The role of 5-HT3 receptors in periaqueductal gray-induced inhibition of nociceptive dorsal horn neurons in rats. *J Pharmacol Exp Ther,* 276**,** 116-24.

PERONA, J. J., HEDSTROM, L., RUTTER, W. J. & FLETTERICK, R. J. 1995. Structural origins of substrate discrimination in trypsin and chymotrypsin. *Biochemistry,* 34**,** 1489-99.

PERSSON, A. K., BLACK, J. A., GASSER, A., CHENG, X., FISCHER, T. Z. & WAXMAN, S. G. 2010. Sodium-calcium exchanger and multiple sodium channel isoforms in intra-epidermal nerve terminals. *Mol Pain,* 6**,** 84.

PERSSON, A. K., LIU, S., FABER, C. G., MERKIES, I. S., BLACK, J. A. & WAXMAN, S. G. 2013. Neuropathy-associated Nav1.7 variant I228M impairs integrity of dorsal root ganglion neuron axons. *Ann Neurol,* 73**,** 140-5.

PETHO, G. & REEH, P. W. 2012. Sensory and signaling mechanisms of bradykinin, eicosanoids, platelet-activating factor, and nitric oxide in peripheral nociceptors. *Physiol Rev,* 92**,** 1699-775.

PLOGHAUS, A., NARAIN, C., BECKMANN, C. F., CLARE, S., BANTICK, S., WISE, R., MATTHEWS, P. M., RAWLINS, J. N. P. & TRACEY, I. 2001. Exacerbation of Pain by Anxiety Is Associated with Activity in a Hippocampal Network. *The Journal of Neuroscience,* 21**,** 9896-9903.

POPOV, S., VENETSANOU, K., CHEDRESE, P. J., PINTO, V., TAKEMORI, H., FRANCO-CERECEDA, A., ERIKSSON, P., MOCHIZUKI, N., SOARES-DA-SILVA, P. & BERTORELLO, A. M. 2012. Increases in intracellular sodium activate transcription and gene expression via

the salt-inducible kinase 1 network in an atrial myocyte cell line. *Am J Physiol Heart Circ Physiol,* 303**,** H57-65.

PRIEST, B. T., MURPHY, B. A., LINDIA, J. A., DIAZ, C., ABBADIE, C., RITTER, A. M., LIBERATOR, P., IYER, L. M., KASH, S. F., KOHLER, M. G., KACZOROWSKI, G. J., MACINTYRE, D. E. & MARTIN, W. J. 2005. Contribution of the tetrodotoxin-resistant voltage-gated sodium channel NaV1.9 to sensory transmission and nociceptive behavior. *Proc Natl Acad Sci U S A,* 102**,** 9382-9387.

PŘIKRYLOVÁ VRANOVÁ, H., HÉNYKOVÁ, E., MAREŠ, J., KAISEROVÁ, M., MENŠÍKOVÁ, K., VAŠTÍK, M., HLUŠTÍK, P., ZAPLETALOVÁ, J., STRNAD, M., STEJSKAL, D. & KAŇOVSKÝ, P. 2016. Clusterin CSF levels in differential diagnosis of neurodegenerative disorders. *Journal of the Neurological Sciences,* 361**,** 117-121.

PROMEGA. *The photochemical reaction catalyzed by Firefly and Renilla Luciferase* [Online]. Available: http://www.promega.co.uk/resources/product-guides-and-selectors/protocols-and-applications-guide/bioluminescent-reporters/ [Accessed].

PRZEDBORSKI, S., VILA, M. & JACKSON-LEWIS, V. 2003. Neurodegeneration: what is it and where are we? *The Journal of clinical investigation,* 111**,** 3-10.

QIAN, Y. Q., BILLETER, M., OTTING, G., MULLER, M., GEHRING, W. J. & WUTHRICH, K. 1989. The structure of the Antennapedia homeodomain determined by NMR spectroscopy in solution: comparison with prokaryotic repressors. *Cell,* 59**,** 573-80.

QUICK, K., ZHAO, J., EIJKELKAMP, N., LINLEY, J. E., RUGIERO, F., COX, J. J., RAOUF, R., GRINGHUIS, M., SEXTON, J. E., ABRAMOWITZ, J., TAYLOR, R., FORGE, A., ASHMORE, J., KIRKWOOD, N., KROS, C. J., RICHARDSON, G. P., FREICHEL, M., FLOCKERZI, V., BIRNBAUMER, L. & WOOD, J. N. 2012. TRPC3 and TRPC6 are essential for normal mechanotransduction in subsets of sensory neurons and cochlear hair cells. *Open Biol,* 2**,** 120068.

RAI, K., SARKAR, S., BROADBENT, T. J., VOAS, M., GROSSMANN, K. F., NADAULD, L. D., DEHGHANIZADEH, S., HAGOS, F. T., LI, Y., TOTH, R. K., CHIDESTER, S., BAHR, T. M., JOHNSON, W. E., SKLOW, B., BURT, R., CAIRNS, B. R. & JONES, D. A. 2010. DNA demethylase activity maintains intestinal cells in an undifferentiated state following loss of APC. *Cell,* 142**,** 930-42.

RANADE, S. S., WOO, S.-H., DUBIN, A. E., MOSHOURAB, R. A., WETZEL, C., PETRUS, M., MATHUR, J., BÉGAY, V., COSTE, B., MAINQUIST, J., WILSON, A. J., FRANCISCO, A. G., REDDY, K., QIU, Z., WOOD, J. N., LEWIN, G. R. & PATAPOUTIAN, A. 2014. Piezo2 is the major transducer of mechanical forces for touch sensation in mice. *Nature,* 516**,** 121-125.

RANDALL, L. O. & SELITTO, J. J. 1957. A method for measurement of analgesic activity on inflamed tissue. *Arch Int Pharmacodyn Ther,* 111**,** 409-19.

RAOUF, R., QUICK, K. & WOOD, J. N. 2010. Pain as a channelopathy. *The Journal of Clinical Investigation,* 120**,** 3745-3752.

RAOUF, R., RUGIERO, F., KIESEWETTER, H., HATCH, R., HUMMLER, E., NASSAR, M. A., WANG, F. & WOOD, J. N. 2012. Sodium channels and mammalian sensory mechanotransduction. *Molecular Pain,* 8**,** 21-21.

REN, J., WANG, Y., LIANG, Y., ZHANG, Y., BAO, S. & XU, Z. 2010. Methylation of ribosomal protein S10 by protein-arginine methyltransferase 5 regulates ribosome biogenesis. *J Biol Chem,* 285**,** 12695-705.

RENGANATHAN, M., CUMMINS, T. R. & WAXMAN, S. G. 2001. Contribution of Na(v)1.8 sodium channels to action potential electrogenesis in DRG neurons. *J Neurophysiol,* 86**,** 629-640.

RIANT, F., DUCROS, A., PLOTON, C., BARBANCE, C., DEPIENNE, C. & TOURNIER-LASSERVE, E. 2010. De novo mutations in ATP1A2 and CACNA1A are frequent in early-onset sporadic hemiplegic migraine. *Neurology,* 75**,** 967-72.

RICE, F. L., ALBRECHT, P. J., WYMER, J. P., BLACK, J. A., MERKIES, I. S., FABER, C. G. & WAXMAN, S. G. 2015. Sodium channel Nav1.7 in vascular myocytes, endothelium, and innervating axons in human skin. *Mol Pain,* 11**,** 26-26.

RIETSCHEL, B., ARREY, T. N., MEYER, B., BORNEMANN, S., SCHUERKEN, M., KARAS, M. & POETSCH, A. 2009. Elastase digests: new ammunition for shotgun membrane proteomics. *Mol Cell Proteomics,* 8**,** 1029-43.

RISMANCHI, N., SODERBLOM, C., STADLER, J., ZHU, P. P. & BLACKSTONE, C. 2008. Atlastin GTPases are required for Golgi apparatus and ER morphogenesis. *Hum Mol Genet,* 17**,** 1591-604.

RIZZO, M. A., KOCSIS, J. D. & WAXMAN, S. G. 1994. Slow sodium conductances of dorsal root ganglion neurons: intraneuronal homogeneity and interneuronal heterogeneity. *J Neurophysiol,* 72**,** 2796-2815.

ROLYAN, H., LIU, S., HOEIJMAKERS, J. G., FABER, C. G., MERKIES, I. S., LAURIA, G., BLACK, J. A. & WAXMAN, S. G. 2016. A painful neuropathy-associated Nav1.7 mutant leads to time-dependent degeneration of small-diameter axons associated with intracellular Ca2+ dysregulation and decrease in ATP levels. *Mol Pain,* 12.

ROTARU, D. C., LEWIS, D. A. & GONZALEZ-BURGOS, G. 2007. Dopamine D1 receptor activation regulates sodium channel-dependent EPSP amplification in rat prefrontal cortex pyramidal neurons. *J Physiol,* 581**,** 981-1000.

ROTTHIER, A., BAETS, J., TIMMERMAN, V. & JANSSENS, K. 2012. Mechanisms of disease in hereditary sensory and autonomic neuropathies. *Nature Reviews Neurology,* 8**,** 73-85.

RUSH, A. M., CUMMINS, T. R. & WAXMAN, S. G. 2007. Multiple sodium channels and their roles in electrogenesis within dorsal root ganglion neurons. *J Physiol,* 579**,** 1-14.

SAAD, F., HOTTE, S., NORTH, S., EIGL, B., CHI, K., CZAYKOWSKI, P., WOOD, L., POLLAK, M., BERRY, S., LATTOUF, J.-B., MUKHERJEE, S. D., GLEAVE, M. & WINQUIST, E. 2011. Randomized Phase II Trial of Custirsen (OGX-011) in Combination with Docetaxel or Mitoxantrone as Second-line Therapy in Patients with Metastatic Castrate-Resistant Prostate Cancer Progressing after First-line Docetaxel: CUOG Trial P-06c. *Clinical Cancer Research,* 17**,** 5765-73.

SAEGUSA, H., KURIHARA, T., ZONG, S., KAZUNO, A., MATSUDA, Y., NONAKA, T., HAN, W., TORIYAMA, H. & TANABE, T. 2001. Suppression of inflammatory and

neuropathic pain symptoms in mice lacking the N-type Ca2+ channel. *The EMBO journal,* 20**,** 2349-56.

SAEGUSA, H., KURIHARA, T., ZONG, S., MINOWA, O., KAZUNO, A. A., HAN, W., MATSUDA, Y., YAMANAKA, H., OSANAI, M., NODA, T. & TANABE, T. 2000. Altered pain responses in mice lacking alpha 1E subunit of the voltage-dependent Ca2+ channel. *Proceedings of the National Academy of Sciences,* 97**,** 6132-6137.

SAEGUSA, H., MATSUDA, Y. & TANABE, T. 2002. Effects of ablation of N- and R-type Ca(2+) channels on pain transmission. *Neuroscience research,* 43**,** 1-7.

SAKURAI, A., DOCI, C. & GUTKIND, J. S. 2012. Semaphorin signaling in angiogenesis, lymphangiogenesis and cancer. *Cell Research,* 22**,** 23-32.

SAMAD, O. A., TAN, A. M., CHENG, X., FOSTER, E., DIB-HAJJ, S. D. & WAXMAN, S. G. 2013. Virus-mediated shRNA Knockdown of Nav1.3 in Rat Dorsal Root Ganglion Attenuates Nerve Injury-induced Neuropathic Pain. *Molecular Therapy,* 21**,** 49-56.

SAVELIEV, S., ENGEL, L., STRAUSS, E., JONES, R. & ROSENBLATT, M. 2012. *The Advantages to Using Arg-C, Elastase, Thermolysin and Pepsin for Protein Analysis.* [Online]. Promega. Available: http://www.promega.co.uk/resources/pubhub/the-advantages-to-using-arg-c-elastase-thermolysin-and-pepsin-for-protein-analysis/ [Accessed 2017].

SCHILD, C., PRERA, E., LÜBLINGHOFF, N., ARNDT, S., ASCHENDORFF, A. & BIRKENHÄGER, R. 2011. Novel mutation in the homeobox domain of transcription factor POU3F4 associated with profound sensorineural hearing loss. *Otology & neurotology : official publication of the American Otological Society, American Neurotology Society [and] European Academy of Otology and Neurotology,* 32**,** 690-4.

SCHMALHOFER, W. A., CALHOUN, J., BURROWS, R., BAILEY, T., KOHLER, M. G., WEINGLASS, A. B., KACZOROWSKI, G. J., GARCIA, M. L., KOLTZENBURG, M. & PRIEST, B. T. 2008. ProTx-II, a Selective Inhibitor of NaV1.7 Sodium Channels, Blocks Action Potential Propagation in Nociceptors *Molecular Pharmacology,* 74**,** 1476-1484.

SEAL, R. P., WANG, X., GUAN, Y., RAJA, S. N., WOODBURY, C. J., BASBAUM, A. I. & EDWARDS, R. H. 2009. Injury-induced mechanical hypersensitivity requires C-low threshold mechanoreceptors. *Nature,* 462**,** 651-655.

SEXTON, J. E., DESMONDS, T., QUICK, K., TAYLOR, R., ABRAMOWITZ, J., FORGE, A., KROS, C. J., BIRNBAUMER, L. & WOOD, J. N. 2016. The contribution of TRPC1, TRPC3, TRPC5 and TRPC6 to touch and hearing. *Neuroscience Letters,* 610**,** 36-42.

SHANNAN, B., SEIFERT, M., LESKOV, K., WILLIS, J., BOOTHMAN, D., TILGEN, W. & REICHRATH, J. 2006. Challenge and promise: roles for clusterin in pathogenesis, progression and therapy of cancer. *Cell Death and Differentiation,* 13**,** 12-19.

SHIELDS, S. D., AHN, H.-S., YANG, Y., HAN, C., SEAL, R. P., WOOD, J. N., WAXMAN, S. G. & DIB-HAJJ, S. D. 2012. Nav1.8 expression is not restricted to nociceptors in mouse peripheral nervous system. *Pain,* 153**,** 2017-30.

SHUAI, P., LIU, Y., LU, W., LIU, Q., LI, T. & GONG, B. 2015. Genetic associations of CLU rs9331888 polymorphism with Alzheimer's disease: A meta-analysis. *Neuroscience Letters,* 591**,** 160-165.

SIMONETTI, M., AGARWAL, N., STÖSSER, S., BALI, KIRAN K., KARAULANOV, E., KAMBLE, R., POSPISILOVA, B., KUREJOVA, M., BIRCHMEIER, W., NIEHRS, C., HEPPENSTALL, P. & KUNER, R. 2014. Wnt-Fzd Signaling Sensitizes Peripheral Sensory Neurons via Distinct Noncanonical Pathways. *Neuron,* 83**,** 104-121.

SKINNER, G. O., DAMASCENO, F., GOMES, A. & DE ALMEIDA, O. M. 2011. Increased pain perception and attenuated opioid antinociception in paradoxical sleep-deprived rats are associated with reduced tyrosine hydroxylase staining in the periaqueductal gray matter and are reversed by L-dopa. *Pharmacol Biochem Behav,* 99**,** 94-9.

SNYDER, S. H. & PASTERNAK, G. W. 2003. Historical review: Opioid receptors. *Trends Pharmacol Sci,* 24**,** 198-205.

SOMMER, C. 2004. Serotonin in pain and analgesia: actions in the periphery. *Mol Neurobiol,* 30**,** 117-25.

SONG, S., PENG, P., TANG, Z., ZHAO, J., WU, W., LI, H., SHAO, M., LI, L., YANG, C., DUAN, F., ZHANG, M., ZHANG, J., WU, H., LI, C., WANG, X., WANG, H., RUAN, Y. & GU, J. 2017. Decreased expression of STING predicts poor prognosis in patients with gastric cancer. *Sci Rep,* 7**,** 39858.

SPINSANTI, G., ZANNOLLI, R., PANTI, C., CECCARELLI, I., MARSILI, L., BACHIOCCO, V., FRATI, F. & ALOISI, A. M. 2008. Quantitative Real-Time PCR detection of TRPV1-4 gene expression in human leukocytes from healthy and hyposensitive subjects. *Molecular pain,* 4**,** 51-51.

SPRUNG, R., CHEN, Y., ZHANG, K., CHENG, D., ZHANG, T., PENG, J. & ZHAO, Y. 2008. Identification and validation of eukaryotic aspartate and glutamate methylation in proteins. *Journal of proteome research,* 7**,** 1001-6.

STALLCUP, M. R. 2001. Role of protein methylation in chromatin remodeling and transcriptional regulation. *Oncogene,* 20**,** 3014-3020.

STECKELBERG, A. L., BOEHM, V., GROMADZKA, A. M. & GEHRING, N. H. 2012. CWC22 connects pre-mRNA splicing and exon junction complex assembly. *Cell Rep,* 2**,** 454-61.

STROUD, J. C., LOPEZ-RODRIGUEZ, C., RAO, A. & CHEN, L. 2002. Structure of a TonEBP-DNA complex reveals DNA encircled by a transcription factor. *Nat Struct Biol,* 9**,** 90-4.

STYS, P. K., WAXMAN, S. G. & RANSOM, B. R. 1992. Ionic mechanisms of anoxic injury in mammalian CNS white matter: role of Na+ channels and Na(+)-Ca2+ exchanger. *J Neurosci,* 12**,** 430-9.

SUCHI, M., SANO, H., MIZUNO, H. & WADA, Y. 1995. Molecular cloning and structural characterization of the human histidase gene (HAL). *Genomics,* 29**,** 98-104.

SUN, G.-C., WERKMAN, T. R., BATTEFELD, A., CLARE, J. J. & WADMAN, W. J. 2007. Carbamazepine and Topiramate Modulation of Transient and Persistent Sodium Currents Studied in HEK293 Cells Expressing the Nav1.3 α−Subunit. *Epilepsia,* 48**,** 774-782.

TADMOURI, A., KIYONAKA, S., BARBADO, M., ROUSSET, M., FABLET, K., SAWAMURA, S., BAHEMBERA, E., PERNET-GALLAY, K., ARNOULT, C., MIKI, T., SADOUL, K., GORY-FAURE, S., LAMBRECHT, C., LESAGE, F., AKIYAMA, S., KHOCHBIN, S., BAULANDE, S., JANSSENS, V., ANDRIEUX, A., DOLMETSCH, R., RONJAT, M., MORI, Y. & DE WAARD, M. 2012. *Cacnb4 directly couples electrical activity to gene expression, a process defective in juvenile epilepsy*.

TADROS, M. A., FARRELL, K. E., GRAHAM, B. A., BRICHTA, A. M. & CALLISTER, R. J. 2015. Properties of sodium currents in neonatal and young adult mouse superficial dorsal horn neurons. *Mol Pain,* 11**,** 17.

TAKESUE, E. I., SCHAEFER, W. & JUKNIEWICZ, E. 1969. Modification of the Randall-Selitto analgesic apparatus. *J Pharm Pharmacol,* 21**,** 788-9.

TAN, P. H., GAO, Y. J., BERTA, T., XU, Z. Z. & JI, R. R. 2012. Short small-interfering RNAs produce interferon-alpha-mediated analgesia. *British Journal of Anaesthesia,* 108**,** 662-669.

TANG, X.-Q., TANELIAN, D. L. & SMITH, G. M. 2004. Semaphorin3A inhibits nerve growth factor-induced sprouting of nociceptive afferents in adult rat spinal cord. *The Journal of neuroscience : the official journal of the Society for Neuroscience,* 24**,** 819-27.

TANIDA, T., TASAKA, K., AKAHOSHI, E., ISHIHARA-SUGANO, M., SAITO, M., KAWATA, S., DANJO, M., TOKUMOTO, J., MANTANI, Y., NAGAHARA, D., TABUCHI, Y., YOKOYAMA, T., KITAGAWA, H., KAWATA, M. & HOSHI, N. 2014. Fetal exposure to 2,3,7,8-tetrachlorodibenzo-p-dioxin transactivates aryl hydrocarbon receptor-responsive element III in the tyrosine hydroxylase immunoreactive neurons of the mouse midbrain. *J Appl Toxicol,* 34**,** 117-26.

TERZI, M. Y., IZMIRLI, M. & GOGEBAKAN, B. 2016. The cell fate: senescence or quiescence. *Molecular biology reports,* 43**,** 1213-1220.

THUL, P. J., AKESSON, L., WIKING, M., MAHDESSIAN, D., GELADAKI, A., AIT BLAL, H., ALM, T., ASPLUND, A., BJORK, L., BRECKELS, L. M., BACKSTROM, A., DANIELSSON, F., FAGERBERG, L., FALL, J., GATTO, L., GNANN, C., HOBER, S., HJELMARE, M., JOHANSSON, F., LEE, S., LINDSKOG, C., MULDER, J., MULVEY, C. M., NILSSON, P., OKSVOLD, P., ROCKBERG, J., SCHUTTEN, R., SCHWENK, J. M., SIVERTSSON, A., SJOSTEDT, E., SKOGS, M., STADLER, C., SULLIVAN, D. P., TEGEL, H., WINSNES, C., ZHANG, C., ZWAHLEN, M., MARDINOGLU, A., PONTEN, F., VON FEILITZEN, K., LILLEY, K. S., UHLEN, M. & LUNDBERG, E. 2017. A subcellular map of the human proteome. *Science,* 356.

TODD, A. J. 2010. Neuronal circuitry for pain processing in the dorsal horn. *Nature Reviews Neuroscience,* 11**,** 823-836.

TOLEDO-ARAL, J. J., MOSS, B. L., HE, Z. J., KOSZOWSKI, A. G., WHISENAND, T., LEVINSON, S. R., WOLF, J. J., SILOS-SANTIAGO, I., HALEGOUA, S. & MANDEL, G. 1997. Identification of PN1, a predominant voltage-dependent sodium channel expressed principally in peripheral neurons. *Proc Natl Acad Sci U S A,* 94**,** 1527-1532.

TRACEY, I., MANTYH, P. W., ALBE-FESSARD, D., BERKLEY, K. J., KRUGER, L., RALSTON, H. J., WILLIS, W. D., ALTIER, N., STEWART, J., APKARIAN, A. V., THOMAS, P. S., KRAUSS, B. R., SZEVERENYI, N. M., APKARIAN, A. V., SOSA, Y., KRAUSS, B. R., THOMAS, P. S., FREDRICKSON, B. E., LEVY, R. E., HARDEN, R. N., CHIALVO, D. R., APKARIAN, A. V., SOSA, Y., SONTY, S., LEVY, R. M., HARDEN, R. N., PARRISH, T. B., GITELMAN, D. R., APKARIAN, A. V., BUSHNELL, M. C., TREEDE, R. D., ZUBIETA, J. K., BALIKI, M. N., CHIALVO, D. R., GEHA, P. Y., LEVY, R. M., HARDEN, R. N., PARRISH, T. B., APKARIAN, A. V., BANATI, R. B., BANTICK, S. J., WISE, R. G., PLOGHAUS, A., CLARE, S., SMITH, S. M., TRACEY, I., BASBAUM, A. I., FIELDS, H. L., BECERRA, L., MORRIS, S., BAZES, S., GOSTIC, R., SHERMAN, S., GOSTIC, J., PENDSE, G., MOULTON, E., SCRIVANI, S., KEITH, D., AL, E., BEHRENS, T. E., JOHANSEN-BERG, H., WOOLRICH, M. W., SMITH, S. M., WHEELER-KINGSHOTT, C. A., BOULBY, P. A., BARKER, G. J., SILLERY, E. L., SHEEHAN, K., CICCARELLI, O., AL, E., BENEDETTI, F., MAYBERG, H. S., WAGER, T. D., STOHLER, C. S., ZUBIETA, J. K., BENTLEY, D. E., WATSON, A., TREEDE, R. D., BARRETT, G., YOUELL, P. D., KULKARNI, B., JONES, A. K., BLACKBURN-MUNRO, G., BOCCALON, S., SCAGGIANTE, B., PERISSIN, L., BONNEMAIN, B., BREFEL-COURBON, C., PAYOUX, P., THALAMAS, C., ORY, F., QUELVEN, I., CHOLLET, F., MONTASTRUC, J. L., RASCOL, O., BREIVIK, H., COLLETT, B., VENTAFRIDDA, V., COHEN, R., GALLACHER, D., et al. 2007. The cerebral signature for pain perception and its modulation. *Neuron,* 55**,** 377-91.

TREMBLAY, R. G., SIKORSKA, M., SANDHU, J. K., LANTHIER, P., RIBECCO-LUTKIEWICZ, M. & BANI-YAGHOUB, M. 2010. Differentiation of mouse Neuro 2A cells into dopamine neurons. *Journal of Neuroscience Methods,* 186**,** 60-67.

ÜÇEYLER, N., TSCHARKE, A. & SOMMER, C. 2008. Early cytokine gene expression in mouse CNS after peripheral nerve lesion. *Neuroscience Letters,* 436**,** 259-264.

UCHIDA, S., YAMAUCHI, A., PRESTON, A. S., KWON, H. M. & HANDLER, J. S. 1993. Medium tonicity regulates expression of the Na(+)- and Cl(-)-dependent betaine transporter in Madin-Darby canine kidney cells by increasing transcription of the transporter gene. *J Clin Invest,* 91**,** 1604-7.

UHLEN, M., FAGERBERG, L., HALLSTROM, B. M., LINDSKOG, C., OKSVOLD, P., MARDINOGLU, A., SIVERTSSON, A., KAMPF, C., SJOSTEDT, E., ASPLUND, A., OLSSON, I., EDLUND, K., LUNDBERG, E., NAVANI, S., SZIGYARTO, C. A., ODEBERG, J., DJUREINOVIC, D., TAKANEN, J. O., HOBER, S., ALM, T., EDQVIST, P. H., BERLING, H., TEGEL, H., MULDER, J., ROCKBERG, J., NILSSON, P., SCHWENK, J. M., HAMSTEN, M., VON FEILITZEN, K., FORSBERG, M., PERSSON, L., JOHANSSON, F., ZWAHLEN, M., VON HEIJNE, G., NIELSEN, J. & PONTEN, F. 2015. Proteomics. Tissue-based map of the human proteome. *Science,* 347**,** 1260419.

USOSKIN, D., FURLAN, A., ISLAM, S., ABDO, H., LONNERBERG, P., LOU, D. & HJERLING-LEFFLER, J. 2015. Unbiased classification of sensory neuron types by large-scale single-cell RNA sequencing. 18**,** 145-53.

VANIA APKARIAN, A., LAVARELLO, S., RANDOLF, A., BERRA, H. H., CHIALVO, D. R., BESEDOVSKY, H. O. & DEL REY, A. 2006. Expression of IL-1β in supraspinal brain regions in rats with neuropathic pain. *Neuroscience Letters,* 407**,** 176-181.

VASYLYEV, D. V., HAN, C., ZHAO, P., DIB-HAJJ, S. & WAXMAN, S. G. 2014. Dynamic-clamp analysis of wild-type human Nav1.7 and erythromelalgia mutant channel L858H. *J Neurophysiol,* 111**,** 1429-1443.

VERKHRATSKY, A. & TOESCU, E. C. 2003. Endoplasmic reticulum Ca 2+ homeostasis and neuronal death. *Journal of Cellular and Molecular Medicine,* **7,** 351-361.

VILCEANU, D. & STUCKY, C. L. 2010. TRPA1 Mediates Mechanical Currents in the Plasma Membrane of Mouse Sensory Neurons. *PLoS ONE,* **5,** e12177-e12177.

VON GRAFFENRIED, B., ADLER, R., ABT, K., NÜESCH, E. & SPIEGEL, R. 1977. The influence of anxiety and pain sensitivity on experimental pain in man. *Pain,* **4,** 253-263.

VUKOJEVIĆ, V., MING, Y. & TERENIUS, L. 2012. Opioid Receptors: Cellular and Molecular Mechanisms Underlying Opioid Receptor Function. *In:* CHOI, S. (ed.) *Encyclopedia of Signaling Molecules.* New York, NY: Springer New York.

WALSH, R. N. & CUMMINS, R. A. 1976. The Open-Field Test: a critical review. *Psychol Bull,* **83,** 482-504.

WANG, L., LI, X., XIANG, B., ZHOU, M., LI, X., XIONG, W., NIU, M., WEI, P., WANG, Z., WANG, H., CHEN, P., SHEN, S., PENG, S. & LI, G. 2014. NGX6a is degraded through a proteasome-dependent pathway without ubiquitination mediated by ezrin, a cytoskeleton-membrane linker. *J Biol Chem,* **289,** 35731-42.

WANG, L., XIANG, B., YI, M., ZHANG, W. L., YANG, J. B., PENG, S. P., LI, X. L. & LI, G. Y. 2010. Identification of a new seven-span transmembrane protein: NGX6a is downregulated in nasopharyngeal carcinoma and is associated with tumor metastasis. *J Histochem Cytochem,* **58,** 41-51.

WANG, Z.-T., YU, G., WANG, H.-S., YI, S.-P., SU, R.-B. & GONG, Z.-H. 2015. Changes in VGLUT2 expression and function in pain-related supraspinal regions correlate with the pathogenesis of neuropathic pain in a mouse spared nerve injury model. *Brain Research,* **1624,** 515-524.

WAXMAN, S. G. & DIB-HAJJ, S. D. 2005. Erythromelalgia: a hereditary pain syndrome enters the molecular era. *Ann Neurol,* **57,** 785-8.

WAXMAN, S. G., KOCSIS, J. D. & BLACK, J. A. 1994. Type III sodium channel mRNA is expressed in embryonic but not adult spinal sensory neurons, and is reexpressed following axotomy. *Journal of neurophysiology,* **72,** 466-70.

WAXMAN, S. G. & ZAMPONI, G. W. 2014. Regulating excitability of peripheral afferents: emerging ion channel targets. *Nat Neurosci,* **17,** 153-63.

WEI, C.-L., WU, Q., VEGA, V. B., CHIU, K. P., NG, P., ZHANG, T., SHAHAB, A., YONG, H. C., FU, Y., WENG, Z., LIU, J., ZHAO, X. D., CHEW, J.-L., LEE, Y. L., KUZNETSOV, V. A., SUNG, W.-K., MILLER, L. D., LIM, B., LIU, E. T., YU, Q., NG, H.-H., RUAN, Y., BERGH, J., NORBERG, T., SJOGREN, S., LINDGREN, A., HOLMBERG, L., BOYER, L. A., LEE, T. I., COLE, M. F., JOHNSTONE, S. E., LEVINE, S. S., ZUCKER, J. P., GUENTHER, M. G., KUMAR, R. M., MURRAY, H. L., JENNER, R. G., AL, E., CARROLL, J. S., LIU, X. S., BRODSKY, A. S., LI, W., MEYER, C. A., SZARY, A. J., EECKHOUTE, J., SHAO, W., HESTERMANN, E. V., GEISTLINGER, T. R., AL, E., CAWLEY, S., BEKIRANOV, S., NG, H. H., KAPRANOV, P., SEKINGER, E. A., KAMPA, D., PICCOLBONI, A., SEMENTCHENKO, V., CHENG, J., WILLIAMS, A. J., AL, E., CHEN, J., SADOWSKI, I., COATES, P. J., LORIMORE, S. A., LINDSAY, K. J., WRIGHT, E. G., CROSBY, M. E., OANCEA, M., ALMASAN, A., DEKKER, J., RIPPE, K., DEKKER, M., KLECKNER, N., EL-DEIRY, W. S.,

KERN, S. E., PIETENPOL, J. A., KINZLER, K. W., VOGELSTEIN, B., EL-DEIRY, W. S., TOKINO, T., VELCULESCU, V. E., LEVY, D. B., PARSONS, R., TRENT, J. M., LIN, D., MERCER, W. E., KINZLER, K. W., VOGELSTEIN, B., CONSORTIUM, E. P., FEI, P., WANG, W., KIM, S. H., WANG, S., BURNS, T. F., SAX, J. K., BUZZAI, M., DICKER, D. T., MCKENNA, W. G., BERNHARD, E. J., EL-DEIRY, W. S., et al. 2006. A global map of p53 transcription-factor binding sites in the human genome. *Cell,* 124**,** 207-19.

WEI, H., WANG, B., MIYAGI, M., SHE, Y., GOPALAN, B., HUANG, D.-B., GHOSH, G., STARK, G. R. & LU, T. 2013. PRMT5 dimethylates R30 of the p65 subunit to activate NF-κB. *Proceedings of the National Academy of Sciences of the United States of America,* 110**,** 13516-21.

WEISS, J., PYRSKI, M., JACOBI, E., BUFE, B., WILLNECKER, V., SCHICK, B., ZIZZARI, P., GOSSAGE, S. J., GREER, C. A., LEINDERS-ZUFALL, T., WOODS, C. G., WOOD, J. N. & ZUFALL, F. 2011. Loss-of-function mutations in sodium channel Na(v)1.7 cause anosmia. *Nature,* 472**,** 186-190.

WESTENBROEK, R. E., HELL, J. W., WARNER, C., DUBEL, S. J., SNUTCH, T. P. & CATTERALL, W. A. 1992a. Biochemical properties and subcellular distribution of an N-type calcium channel alpha 1 subunit. *Neuron,* 9**,** 1099-115.

WESTENBROEK, R. E., HELL, J. W., WARNER, C., DUBEL, S. J., SNUTCH, T. P. & CATTERALL, W. A. 1992b. Biochemical properties and subcellular distribution of an N-type calcium channel alpha 1 subunit. *Neuron,* 9**,** 1099-1115.

WHEELER, D. B., RANDALL, A. & TSIEN, R. W. 1994. Roles of N-type and Q-type Ca2+ channels in supporting hippocampal synaptic transmission. *Science,* 264**,** 107-11.

WHITAKER, W. R., FAULL, R. L., WALDVOGEL, H. J., PLUMPTON, C. J., EMSON, P. C. & CLARE, J. J. 2001. Comparative distribution of voltage-gated sodium channel proteins in human brain. *Brain research. Molecular brain research,* 88**,** 37-53.

WOOD, J. N., BEVAN, S. J., COOTE, P. R., DUNN, P. M., HARMAR, A., HOGAN, P., LATCHMAN, D. S., MORRISON, C., ROUGON, G., THEVENIAU, M. & ET AL. 1990. Novel cell lines display properties of nociceptive sensory neurons. *Proc Biol Sci,* 241**,** 187-94.

WOODS, C. G., BABIKER, M. O., HORROCKS, I., TOLMIE, J. & KURTH, I. 2015. The phenotype of congenital insensitivity to pain due to the NaV1.9 variant p.L811P. *Eur J Hum Genet,* 23**,** 561-3.

WORZFELD, T. & OFFERMANNS, S. 2014. Semaphorins and plexins as therapeutic targets. *Nature reviews. Drug discovery,* 13**,** 603-21.

WU, C., JIN, X., TSUENG, G., AFRASIABI, C. & SU, A. I. 2016. BioGPS: building your own mash-up of gene annotations and expression profiles. *Nucleic Acids Res,* 44**,** D313-6.

WU, C., MACLEOD, I. & SU, A. I. 2013. BioGPS and MyGene.info: organizing online, gene-centric information. *Nucleic Acids Res,* 41**,** D561-5.

XIU, P., DONG, X.-F., LI, X.-P. & LI, J. 2015. Clusterin: Review of research progress and looking ahead to direction in hepatocellular carcinoma. *World journal of gastroenterology,* 21**,** 8262-70.

YAMAUCHI, A., UCHIDA, S., PRESTON, A. S., KWON, H. M. & HANDLER, J. S. 1993. Hypertonicity stimulates transcription of gene for Na(+)-myo-inositol cotransporter in MDCK cells. *Am J Physiol,* 264**,** F20-3.

YANG, K., KUMAMOTO, E., FURUE, H. & YOSHIMURA, M. 1998. Capsaicin facilitates excitatory but not inhibitory synaptic transmission in substantia gelatinosa of the rat spinal cord. *Neurosci Lett,* 255**,** 135-8.

YANG, Y., WANG, Y., LI, S., XU, Z., LI, H., MA, L., FAN, J., BU, D., LIU, B., FAN, Z., WU, G., JIN, J., DING, B., ZHU, X. & SHEN, Y. 2004. Mutations in SCN9A, encoding a sodium channel alpha subunit, in patients with primary erythermalgia. *Journal of Medical Genetics,* 41**,** 171-174.

YU, Y. Q., ZHAO, F., GUAN, S. M. & CHEN, J. 2011. Antisense-mediated knockdown of Na(V)1.8, but not Na(V)1.9, generates inhibitory effects on complete Freund's adjuvant-induced inflammatory pain in rat. *PLoS One,* 6**,** e19865.

YUAN, J., MATSUURA, E., HIGUCHI, Y., HASHIGUCHI, A., NAKAMURA, T., NOZUMA, S., SAKIYAMA, Y., YOSHIMURA, A., IZUMO, S. & TAKASHIMA, H. 2013. Hereditary sensory and autonomic neuropathy type IID caused by an SCN9A mutation. *Neurology,* 80**,** 1641-1649.

ZAMAN, T., LEE, K., PARK, C., PAYDAR, A., CHOI, JEE H., CHEONG, E., LEE, C. J. & SHIN, H.-S. 2011. CaV2.3 Channels Are Critical for Oscillatory Burst Discharges in the Reticular Thalamus and Absence Epilepsy. *Neuron,* 70**,** 95-108.

ZEITZ, K. P., GUY, N., MALMBERG, A. B., DIRAJLAL, S., MARTIN, W. J., SUN, L., BONHAUS, D. W., STUCKY, C. L., JULIUS, D. & BASBAUM, A. I. 2002. The 5-HT3 subtype of serotonin receptor contributes to nociceptive processing via a novel subset of myelinated and unmyelinated nociceptors. *The Journal of neuroscience : the official journal of the Society for Neuroscience,* 22**,** 1010-9.

ZHANG, H., KIM, J. K., EDWARDS, C. A., XU, Z., TAICHMAN, R. & WANG, C.-Y. 2005a. Clusterin inhibits apoptosis by interacting with activated Bax. *Nature Cell Biology,* 7**,** 909-915.

ZHANG, H., KIM, J. K., EDWARDS, C. A., XU, Z., TAICHMAN, R. & WANG, C. Y. 2005b. Clusterin inhibits apoptosis by interacting with activated Bax. *Nat Cell Biol,* 7**,** 909-15.

ZHANG, K., FISHEL BEN KENAN, R., OSAKADA, Y., XU, W., SINIT, R. S., CHEN, L., ZHAO, X., CHEN, J. Y., CUI, B. & WU, C. 2013a. Defective Axonal Transport of Rab7 GTPase Results in Dysregulated Trophic Signaling. *Journal of Neuroscience,* 33**,** 7451-7462.

ZHANG, X. M., WANG, X. Y., SHENG, S. R., WANG, J. R. & LI, J. 2003. Expression of tumor related genes NGX6, NAG-7, BRD7 in gastric and colorectal cancer. *World J Gastroenterol,* 9**,** 1729-33.

ZHANG, X. Y., WEN, J., YANG, W., WANG, C., GAO, L., ZHENG, L. H., WANG, T., RAN, K., LI, Y., LI, X., XU, M., LUO, J., FENG, S., MA, X., MA, H., CHAI, Z., ZHOU, Z., YAO, J., ZHANG, X. & LIU, J. Y. 2013b. Gain-of-function mutations in SCN11A cause familial episodic pain. *Am J Hum Genet,* 93**,** 957-966.

ZHANG, Y.-K., HUANG, Z.-J., LIU, S., LIU, Y.-P., SONG, A. A. & SONG, X.-J. 2013c. WNT signaling underlies the pathogenesis of neuropathic pain in rodents. *Journal of Clinical Investigation,* 123**,** 2268-2286.

ZHAO, C., LEITGES, M., GEREAU, R. W. & IV 2011. Isozyme-specific effects of protein kinase C in pain modulation. *Anesthesiology,* 115**,** 1261-70.

ZHU, P. P., PATTERSON, A., LAVOIE, B., STADLER, J., SHOEB, M., PATEL, R. & BLACKSTONE, C. 2003. Cellular localization, oligomerization, and membrane association of the hereditary spastic paraplegia 3A (SPG3A) protein atlastin. *J Biol Chem,* 278**,** 49063-71.

ZIMMER, A., ZIMMER, A. M., BAFFI, J., USDIN, T., REYNOLDS, K., KONIG, M., PALKOVITS, M. & MEZEY, E. 1998. Hypoalgesia in mice with a targeted deletion of the tachykinin 1 gene. *Proceedings of the National Academy of Sciences,* 95**,** 2630-2635.

ZIMMERMANN, K., LEFFLER, A., BABES, A., CENDAN, C. M., CARR, R. W., KOBAYASHI, J., NAU, C., WOOD, J. N. & REEH, P. W. 2007. Sensory neuron sodium channel Nav1.8 is essential for pain at low temperatures. *Nature,* 447**,** 855-858.